Contact Stresses in Hip Replacements

Antonio Strozzi

Submitted in accordance with the requirements
for the degree of Doctor of Philosophy

University of Durham
School of Engineering & Applied Science
Durham DH1 3LE
England

March 1992

Nor are you to be called doctors ;
you have one doctor, Christ.

Nec vocemini magistri,
quia Magister vester unus est,
Christus.

Matthew, 23 . 10 .

Declaration

No material in this thesis has been previously submitted for a degree at the University of Durham or at any other University. Except where stated otherwise, this thesis reports individual research carried out by the author.

31th March 1992

Dedication

This work is dedicated to the memory of my father, Pietro Strozzi, whose hard work has enabled me to follow my own vocation.

Acknowledgements

I would like to express my sincere gratitude to my supervisor, Prof. Anthony Unsworth, for redirecting my experience in the mechanical analysis of elastomeric seals towards the more beneficial and rewarding field of elastomeric layer hip replacements. His experienced supervision and the indefatigable encouragement which he provided during the course of the present study are deeply appreciated.

Vital assistance in running the finite element package ABAQUS was provided by Eugenio Dragoni. The Lanczos σ smoothing method employed in Section 3 was suggested by Paolo Bariani. Valuable support in the experimental work was provided by Vittorio Ciavatti. Camillo Bandera was a patient tutor in the use of the graphical package AUTOCAD. The computational resources of the Laboratory for Computational Mechanics of the University of Bologna, Italy, were extensively employed.

Less technical, but equally valuable support came from the many friends who accepted my Italian outlook unquestioningly, providing an invariably warm welcome regardless of the weather inclemency. I would especially like to say thanks to Jill Unsworth, Paul Binnington, Graeme Willis, Ruth Hopkins, Peter Senior, Sally Craig, Lona Williams and Nick Kalita amongst many others.

I must also express my sincere thanks to those in Italy who demonstrated great understanding, in particular my mother, Alba Strozzi, and Maria Grazia Dalla Ca'.

Finally, the financial support given by the Italian Consiglio Nazionale delle Ricerche is greatly acknowledged (CT 86.02329.07 ; 86.02536.07 ; 87.01849.07 ; 87.02802.07 ; 88.02776.07 ; 88.02777.07 ; 89.03340.07 ; 90.01084.07 ; 92.03172.07).

Summary

This thesis presents a mechanical analysis of a particular type of hip replacement, characterized by the presence of an elastomeric layer firmly bonded to a metal cup, and compressed by a metal head during walking. Various theoretical-numerical models of increasing adherence to the actual geometry are either extended or developed, namely : a) a cylinder compressing a flat covering ; b) a cylinder penetrating a curved stratum ; c) a sphere indenting a flat cortex ; d) a sphere squeezing a spherical lining.

The theoretical solutions achieved are mainly of perturbation type, where various algebraic manipulators are exploited to perform the analytical passages. The numerical forecasts are obtained with the nonlinear finite element package ABAQUS, aimed at analysing configurations which appear too complex to be modelled analytically. To clarify the terminology employed in connection with the use of ABAQUS package, a complementary introduction to the theory of elasticity in finite deformations is also included.

The previous analytical-numerical tools are mainly employed to perform a systematic sensitivity analysis of the hip joint mechanical response to perturbations of the Poisson's ratio in the physically realistic range 0.49 - 0.5 . The effects of the layer thickness and of the initial gap between head and elastomeric layer on the peak contact pressure between head and lining and on the maximum shear stress at the interface between elastomeric stratum and cup are also explored.

In addition, an experimental study is undertaken for the configuration of a cylindrical indenter compressing a curved layer, as a support to the analytical analyses.

Experimental measurements of the Poisson's ratio are effected via a purposely built piston device. The influences of the device elastic distortions and of possible extrusions of the elastomeric specimen on the apparent Poisson's ratio are examined, and the corrections are evaluated with suitable theories.

Some robust analytical tools are developed, which are useful in the numerical solution of the stationary, plane, elastohydrodynamic lubrication problem for soft contacts, having in mind possible applications to the hip joint realm. In particular, a method is proposed for constructing closed form solutions to be used as test cases

in validating numerical codes. Secondly, an extended variational formulation is developed which possesses local minimum properties in the solution neighbourhood. Third, a mathematical justification of the possible appearance of spurious numerical undulations in the fluid film thickness is derived.

TABLE OF CONTENTS

3. ON THE CUBIC COMPRESSIBILITY OF ELASTOMERIC MATERIALS

4. THE PLANE STRAIN, FLAT ELASTOMERIC LAYER: THEORY

9. OVERALL CONCLUSIONS

10. REFERENCES

Nomenclature

a	Constant , contact semiwidth , contact radius , series coefficient
A	Constant , operator
A	Pure deformation matrix
b	Constant , layer thickness , series coefficient
B	Constant
c	Contact half width , series coefficient
C	Constant
d	Pitch of an infinite series of punches indenting a half plane , series coefficient , coefficient
D	Constant , domain
$\mathfrak{D}$	Denominator
E	Young's modulus , constant
E	Elliptic integral of the second kind
f	Deformation gradient component , function
F	Constant , function
F	Deformation gradient
g	Left Cauchy-Green strain tensor component , function
G	Left Cauchy-Green strain tensor
h	Tube half height , fluid film thickness , layer thickness
H	Constant , layer thickness
I	Strain invariant , integral
I_o	Modified Bessel function of the first kind
I_1	Modified Bessel function of the first kind
I	Identity matrix
J_o	Bessel function of the first kind
J_1	Bessel function of the first kind
k	Index
K	Bulk modulus , constant , kernel , foundation coefficient
K_o	Modified Bessel function of the second kind
K_1	Modified Bessel function of the second kind
K	Elliptic integral of the first kind

l	Seal height
L	Constant , kernel , foundation operator
M	Integer number
N	Constant
p	Pressure
P	Constant , load , normalized pressure , Péclet number
PI	Particular integral
q	Peak pressure
Q	Constant , discriminant coefficient , fluid flow , integer number
r	Coordinate
R	Constant , radius , equivalent radius , discriminant coefficient , range
R	Rigid rotation matrix
s	Constant , coordinate
S	Constant
t	Constant , coordinate , layer thickness
T	Function
u	Displacement vector component
$\boldsymbol{u}$	Displacement vector
U	Strain energy function , normalized displacement , sliding velocity
v	Displacement vector component
V	Volume , normalized displacement
w	Displacement vector component
x	Coordinate
$\boldsymbol{x}$	Coordinate vector in the deformed configuration
X	Coordinate vector component in the undeformed configuration , normalized coordinate
$\boldsymbol{X}$	Coordinate vector in the undeformed configuration
y	Coordinate
Y	Coordinate vector component in the undeformed configuration , normalized coordinate
Y_o	Bessel function of the second kind
Y_1	Bessel function of the second kind
z	Coordinate

Z	Coordinate vector component in the undeformed configuration
α	Eigenvalue , coefficient , material constant , piezoviscous viscosity coefficient
β	Eigenvalue , perturbation ratio
γ	Eigenvalue , material constant
δ	Kronecker delta , function , indentation depth
∂	Partial differentiation operator
Δ	Determinant , discretization pitch
ϵ	Perturbation ratio , linear elasticity strain , Gateaux correction
η	Viscosity
θ	Coordinate
λ	Material constant , Lame' constant
Λ	Determinant
μ	Lame' constant
ν	Poisson's ratio
ρ_b	Geometric ratio
π	Constant
σ	Normal stress
τ	Shear stress
φ	Function , slope
Φ	Stress function
Φ	Basis function
ψ	Function
ψ	Basis function
ω	Integration device

Indices

b
c
i
j
k
l
m
n
p_t
p_u
r
θ
z

Apices

e
o

CHAPTER1 . INTRODUCTION AND MOTIVATION

1.1 INTRODUCTION

1.2 GENERAL ASPECTS

1.2.1 On the sensitivity of the stress field to the cubic compressibility of the elastomer

1.2.2 On the effects of finite deformations

1.2.3 On the usefulness of algebraic manipulators

1.3 PARTICULAR ASPECTS

1.3.1 Problems connected to the experimental measurement of the Poisson's ratio

1.3.2 Problems related to the geometry of a cylinder penetrating a flat layer

1.3.3 Problems connected to the geometry of a cylinder indenting a curved layer

1.3.4 Aspects related to the geometry of a sphere compressing a flat, axisymmetric layer

1.3.5 Problems associated with the geometry of a sphere compressing a spherical cavity

1.3.6 Aspects connected with the elastohydrodynamic lubrication problem

1.4 CONCLUSIONS

1.1 INTRODUCTION

This thesis addresses a particular type of hip replacements, characterized by the presence of an elastomeric layer adherent to the cup, and compressed by the head during walking. Fig. 1.1.1 compares natural (left) and artificial (right) hip joints. The artificial joint consists of a metal cup to which the elastomeric lining adheres, and of a metal head connected to a metal stem. The cup is fixed to the acetabular socket of the patient's pelvis. The stem conforms to the diaphisary channel of the femur. The spherical pair thus obtained behaves kinematically as the replaced natural joint. Fig. 1.1.2 sketches the relevant elements of this joint, namely the cup to which the elastomeric lining adheres, and the spherical head.

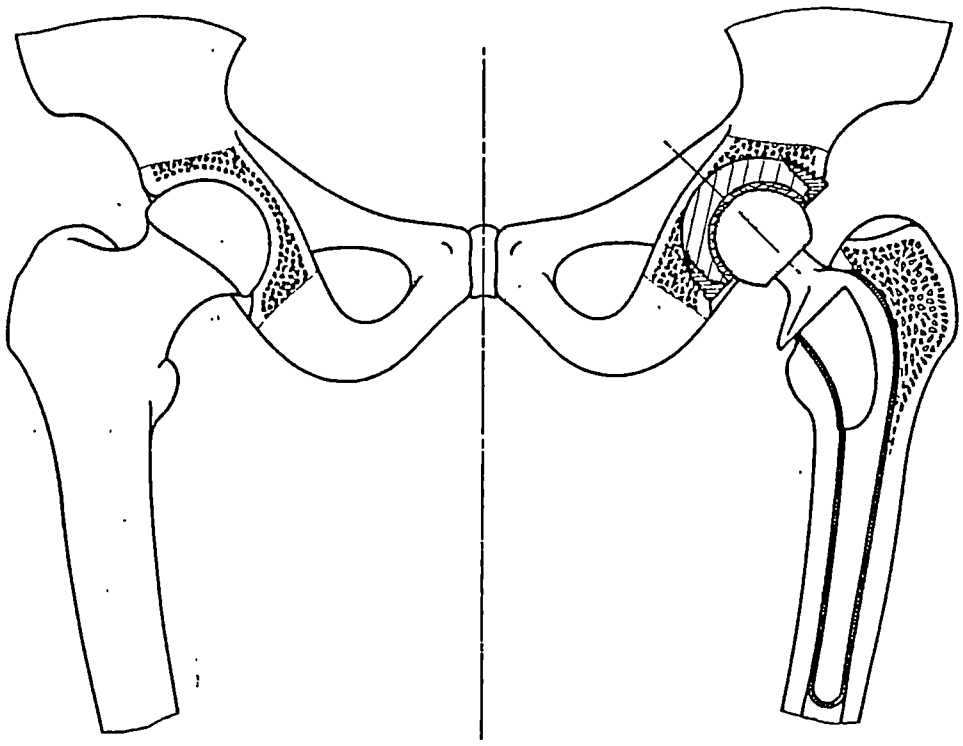

Fig. 1.1.1 : A comparison between natural (left) and artificial (right) hip joints.

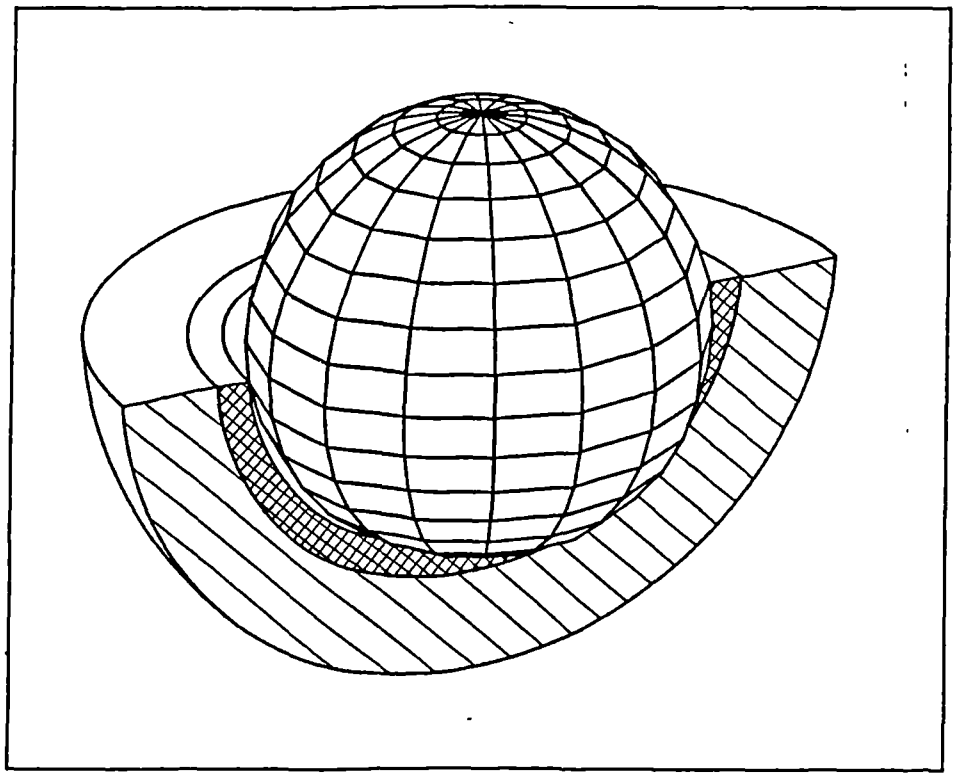

Fig. 1.1.2 : A sketch of the main elements of the hip joint, namely the cup to which the elastomeric lining adheres, and the head.

Current research supports the belief that such soft joints exhibit some benefits in comparison to hard prostheses, in terms of a) microelastohydrodynamic effects; b) possible increase in the squeeze film duration; c) less stringent mechanical tolerances; and d) more favourable stress distribution.

Depending on the desired degree of approximation, plane and axisymmetric models of this contact problem can be advocated. A cylinder and a sphere compressing a flat or curved, deformable stratum are therefore plausible, although idealized, descriptions of the hip configuration, and these geometries possess an extensive and distinguished literature, where such studies have often been spurred by practical problems totally extraneous to the biomechanical field. Due to its variety, the review of the pertinent literature is presented at the beginning of each Chapter.

Although especially in the last years a noticeable collection of studies have

flourished with direct reference to the hip joints possessing elastomeric layers, various relevant aspects do not appear to have been extensively investigated. The main open problems are summarized in the following Section, where the resolution of some of the controversial points constitutes the motivation of this thesis. The more general obscure subjects are listed first, followed by discussions addressing more particular enigmatic aspects. In the interest of higher conciseness, the critical discussions are not accompanied by bibliographic quotations which, as already remembered, are reviewed in the bibliographic apparatus at the beginning of each Section.

1.2 GENERAL ASPECTS

This Section briefly analyses the more general open problems. The following analysis aims at sampling some representative problems, more than at providing an exhaustive picture of the existing controversial points.

1.2.1 On the sensitivity of the stress field to the cubic compressibility of the elastomer

A variety of studies underlines the fact that, when a deformable layer adherent to a rigid foundation is compressed by a cylinder or by a sphere to such an extent that the contact width between indenter and elastic cortex is considerably larger than the lining thickness, the stress field in the deformable stratum is mainly hydrostatic and, consequently, it is particularly sensitive to perturbations of the Poisson's ratio. Normally the elastomers employed in this biomechanical application exhibit Poisson's ratios not lower than 0.49 , and often closely approaching the incompressibility upper limit 0.5 . The present author is unaware of studies systematically exploring a close sequence of Poisson's ratios ranging from 0.49 to 0.5 , and analyzing the dependence of the layer stress distribution on the cubic compressibility adopted. In addition, no papers in the hip joint field are known to the author which measure experimentally the cubic compressibility of the elastomer employed, and use this physical input in the mechanical analysis of hip joints endowed with elastomeric layers. Finally, the experimentally measured Poisson's ratio often depends, although moderately, upon the level of the hydrostatic pressure imposed (*i.e.*, it is not constant), and this non-linearity has never been mimicked in the mechanical analysis of hip joints.

Moving to head-layer contacts characterized by smaller contact widths, it is known that in this case the layer mechanical response exhibits a much lower sensitivity to Poisson's ratio perturbations. An exhaustive definition of the transition zone between contacts which are either sensitive or not sensitive to modifications of the cubic compressibility does not appear to be available.

1.2.2 On the effects of finite deformations

Various studies attribute to the effects of finite deformations in the elastomeric layer the responsibility for the mismatches often noticed between theoretical forecasts (normally obtained with a linear elasticity approach) and experimental measurements. The results available are not sufficient to clarify the relevance of the effects of finite deformations.

1.2.3 On the usefulness of algebraic manipulators

No closed form solutions are accessible for the geometry of a layer compressed by an indenter, however simple its profile is. Various perturbation-type solutions have been developed, especially in times when the numerical solutions were not feasible. The related computations are generally particularly awkward, and practical errors are inevitably likely to affect the formulations presented. Various algebraic manipulators capable of performing algebraic and analytical operations in a formal way have been extensively used in this thesis, in assessing many existing formulations. Various analytical inaccuracies have been signalled and corrected, and several formal calculations, impossibly lengthy if performed manually, have been confidently developed with the aid of these symbolic algebra packages.

1.3 PARTICULAR ASPECTS

This Section briefly ranks some open problems related to particular aspects or geometries encountered in the hip joint realm.

1.3.1 Problems connected to the experimental measurement of the Poisson's ratio

The Poisson's ratio is often measured via a piston device, where the deformability of the metal hollow cylinder which contains the cylindrical elastomeric specimen affects the readings to an unknown extent.

1.3.2 Problems related to the geometry of a cylinder penetrating a flat layer

A perturbation solution is available for small contact widths, but a detailed analysis of the influence of the perturbation order on the solution accuracy is not available. In addition, some misprints obscure the published analytical formulae. In the interest of mathematical simplicity, the punch is generally assumed to possess a parabolic profile, but the errors incurred in mimicking a cylindrical indenter with a parabolic curve have not been thoroughly explored in the case of appreciable contact widths.

1.3.3 Problems connected to the geometry of a cylinder indenting a curved layer

The curvature effects have been only partially explored, since the errors detected are often superimposed to the inaccuracies deriving from the simplifications adopted in describing the indenter profile. In addition, a Green function (case of concentrated transverse force), which would permit any distributed pressure profile to be easily mimicked, does not appear to have been derived.

1.3.4 Aspects related to the geometry of a sphere compressing a flat, axisymmetric layer

A perturbation solution parallel to that available for the analogous plane case has been developed only at an abstract stage, but the corresponding manipulations have not been performed in detail. An iterative analytical solution is also available, but the exactness of the formulae presented is suspect.

1.3.5 Problems associated with the geometry of a sphere compressing a spherical cavity

For this geometry, which closely simulates the actual joint, an open problem is the border effect, connected to the circumstance that in the real hip joint the layer is not a complete spherical stratum, since it covers only the half-spherical cavity of the cup, so that it is in fact a half-spherical cortex. When the contact between head and lining terminates sufficiently close to the layer border, it is not known to what degree this event influences the pressure distribution with respect to an idealized, completely spherical layer.

1.3.6 Aspects connected with the elastohydrodynamic lubrication problem

The theoretical simulation of the lubrication in hip replacements requires a correct model to be adopted for the deformability of the lubricated profiles. When the Poisson's ratio of the elastomer approaches the incompressibility figure 0.5 , the reliability of a simple column model declines, so that considerably more complex descriptions need to be selected. In addition, when the foundation becomes softer, numerical troubles manifesting themselves in convergence and regularity problems may appear.

1.4 CONCLUSIONS

Some of the open problems encountered in the mechanical analysis of hip joints with elastomeric coverings and examined in this thesis have been described. At the risk of excessive synthesis, the two main ingredients characterizing this thesis are a) an exploitation of some algebraic manipulators in developing analytical solutions capable of resolving some controversial aspects, and b) a sensitivity analysis of the hip joint mechanical behaviour to perturbations of the Poisson's ratio.

CHAPTER 2 . ASPECTS OF THE THEORY OF ELASTICITY IN FINITE DEFORMATIONS

Chapter 2 Theory of Elasticity in Finite Deformations 2.2

2.1 INTRODUCTION

The elastomeric layer covering the cup in the hip replacements analyzed in this thesis can undergo finite deformations during walking. In fact, due to the limited cubic compressibility of the elastomers adopted, the rubber lining flows laterally under the head penetration, so that sufficiently large distortions may occur in the elastomeric stratum. In addition, the head compresses the rubber cortex unilaterally, so that the extent of the contact zone must be evaluated in the deformed condition. With this regard, the finite element package ABAQUS (1989) can practically handle unilateral contact problems only by formulating the contact via a nonlinear elasticity approach. These aspects show that an infinitesimal elasticity theory may be inadequate (or numerically inapplicable) in mimicking hip joints with elastic layers, so that tests on the consequences of finite deformations on the solution accuracy in comparison to a more traditional linear elastic approach are advisable.

Some practically relevant concepts of the theory of elasticity in finite deformations are introduced in the following Sections. Such elements of finite elasticity are necessary to interpret unequivocally the terminology used in Chapters 3, 6 and 7, where the nonlinear finite element package ABAQUS (1989) is extensively employed to retrieve information on the layer stress field, and to assess the relative importance of the finite deformations in some test cases.

2.2 SOME ASPECTS OF THE THEORY OF ELASTICITY IN FINITE DEFORMATIONS

This Section possesses an essentially bibliographic character, and it addresses three main aspects : a) to introduce the definitions of finite strains, b) to comment upon the definition of strain invariants, and c) to discuss the fundamental aspects of the stress-strain relationships in finite deformations.

2.2.1 On the definition of strain in finite deformations

Following Mase (1970), if x denotes the coordinate vector of a point in the deformed configuration (whose entries are x_1 , x_2 , x_3), while X indicates the coordinate vector (whose entries are X_1 , X_2 , X_3) of the same point before deformation and referring to the same Cartesian coordinate system, the displacement vector, u (whose entries are u_1 , u_2 , u_3) is :

$$u = x - X \qquad \text{or} \qquad u_i = x_i - X_i \quad (i = 1 , 2 , 3) \tag{2.2.1.1}$$

According to a Lagrangian description, the coordinate, x , of a generic point of the deformed configuration is expressed as a function of the undeformed coordinate, X :

$$x = x (X) \qquad \text{or} \qquad x_j = f_j (X_1 , X_2 , X_3) \qquad (j = 1 , 2 , 3) \tag{2.2.1.2}$$

The expressions for the strains must be freed from rigid translations and rotations, since rigid movements do not generate deformations. The rigid displacements are eliminated from (2.2.1.2) by considering, instead of eqns (2.2.1.2), their derivatives, which define the Jacobian matrix (also named deformation gradient) $F = [f_{i,j}]$, where :

$$f_{i,j} = \frac{\partial f_i}{\partial X_j} \tag{2.2.1.3}$$

Such derivatives are useful in expressing, say, d x_1 :

$$d\,x_1 = \frac{\partial\, x_1}{\partial\, X_1}\,\mathrm{d}\,X_1 + \frac{\partial\, x_1}{\partial\, X_2}\,\mathrm{d}\,X_2 + \frac{\partial\, x_1}{\partial\, X_3}\,d\,X_3 =$$

$$\frac{\partial\, f_1}{\partial\, X_1}\,\mathrm{d}\,X_1 + \frac{\partial\, f_1}{\partial\, X_2}\,\mathrm{d}\,X_2 + \frac{\partial\, f_1}{\partial\, X_3}\,d\,X_3 \qquad (2.2.1.4)$$

Formulae (2.2.1.4) are more expressive than their counterparts (2.2.1.2), since the latter define a connection between a point before and after deformation, whereas the former represent a link between infinitesimal segments before and after distortion and, therefore, they are closer to the sought definition of strain.

To clear expression (2.2.1.3) from the rigid rotations, the Jacobian matrix is decomposed into the product of a "pure" deformation matrix by a rigid rotation matrix, R , which is characterized by the property that its inverse equal its transpose :

$$\mathrm{R}^{\mathrm{T}} = \mathrm{R}^{-1} \rightarrow \mathrm{R}^{\mathrm{T}}\mathrm{R} = \mathrm{I} \qquad (2.2.1.5)$$

where I denotes the identity matrix.

To reach the deformed configuration starting from the natural state, it would be possible to apply first a rigid rotation and, then, a "pure" deformation. Alternatively, the rigid rotation could follow the application of the deformation. If the Jacobian matrix F is known, the problem arises to determine the rigid rotation matrix, R , and the remaining matrix A , which expresses the actual deformation, since it is freed from the two rigid motion components. It is expected that A is symmetrical, since it represents a pure strain (Varga (1966), p. 19). The mathematical way to determine R and A is presented in detail in the case that the rigid rotation precedes the deformation. The properties exploited to perform the manipulations are reported between brackets :

$$
\begin{aligned}
&F = A\,R \\
&F = A^{T}\,R && (A = A^{T}) \\
&F^{T} = R^{-1}\,A && ((A^{T}R)^{T} = R^{T}A^{TT};\ R^{T} = R^{-1}) \\
&R\,F^{T} = A \\
&A\,R\,F^{T} = A\,A && (2.2.1.6) \\
&F\,F^{T} = A^{2} && (F = A\,R)
\end{aligned}
$$

so that A (the evaluation of A from A^2 is omitted) and R can be finally expressed as follows :

$$A^{2} = F\,F^{T}\ ;\quad R = A^{-1}F \qquad (2.2.1.7)$$

In practice, A^2 (as opposed to A) can be used as a measure of the strain (for small deformations, it is still adherent to the results of the linear theory of elasticity ; it is more easily computed than A ; it removes sign indeterminacy problems), and it is usually referred to as "left Cauchy-Green strain tensor", $G \equiv A^2$ (ABAQUS (1989)) (matrices are understood as representations of tensors). Its generic entry, g_{ij}, is, according to the definition of A^2 of eqn (2.2.1.7) :

$$g_{ij} = \frac{\partial f_i}{\partial X_k}\,\frac{\partial f_j}{\partial X_k} \qquad (k = 1, 2, 3 \text{ ; index summation convention}) \qquad (2.2.1.8)$$

By introducing the displacement components (2.2.1.1), expressions (2.2.1.8) can be reformulated as :

$$g_{ij} = \delta_{ij} + \frac{\partial u_i}{\partial X_j} + \frac{\partial u_j}{\partial X_i} + \frac{\partial u_i}{\partial X_k}\,\frac{\partial u_j}{\partial X_k} \qquad (k = 1, 2, 3) \qquad (2.2.1.9)$$

By indicating for clarity the three coordinates X_i with X, Y, and Z, and the three displacements u_i with u, v, and w, the expression for, say, g_{11} is :

$$g_{11} = \left[1 + \frac{\partial u}{\partial X}\right]^2 + \left[\frac{\partial u}{\partial Y}\right]^2 + \left[\frac{\partial u}{\partial Z}\right]^2 \qquad (2.2.1.10)$$

which, if u is X-oriented, becomes :

$$g_{11} = 1 + 2\frac{\partial u}{\partial X} + \left(\frac{\partial u}{\partial X}\right)^2 \qquad (2.2.1.11)$$

which shows the connection between g_{11} and the linear elasticity strain ϵ_{11} if $\partial u/\partial X$ is small. The expression for, say, g_{12} is :

$$g_{12} = \left(1 + \frac{\partial u}{\partial X}\right)\frac{\partial v}{\partial X} + \left(1 + \frac{\partial v}{\partial Y}\right)\frac{\partial u}{\partial Y} + \frac{\partial u}{\partial Z}\frac{\partial v}{\partial Z} \qquad (2.2.1.12)$$

which, if all differentials are small, becomes :

$$g_{12} \simeq \frac{\partial v}{\partial X} + \frac{\partial u}{\partial Y} \qquad (2.2.1.13)$$

showing the relationship between g_{12} and the linear elasticity strain ϵ_{12} .

2.2.2 On the definition of strain invariants in finite deformations

Since it is necessary to express a relationship between strains and stresses, it is convenient to formulate the stress field in terms of strain-related quantities which are independent of the relative position of the deformed body with respect to the reference frame. In fact, the indices of g_{ij} would change by substituting axis i with axis j . Such quantities are named Rivlin invariants, after the following definition of Rivlin (Varga (1966)) :

$$I_1 = \text{trace G}$$

$$I_2 = \frac{1}{2}\left\{ I_1^2 - \text{trace (G}\bullet\text{G)} \right\} \qquad (2.2.2.1)$$

$$I_3 = \det \text{G}$$

The physical meaning of I_1 is a global index of the variations in length of the sides of an infinitesimal cube. Similarly, I_2 represents an index of the variation in surface of the cube, and I_3 expresses its relative volume change to the cube (Williams (1973)). For an undeformed configuration, $I_1 = I_2 = 3$ and $I_3 = 1$. If the elastomer is incompressible, I_3 constantly equals unity in any deformed configuration, and it constitutes an internal constraint. If, in addition, the body is subject to a plane state of deformation, then $I_1 \equiv I_2$.

The (minor) limits of the Rivlin invariants (2.2.2.1) emerge if it is appreciated that elastomeric materials are nearly incompressible. A suitable stress-strain relationship must therefore rely upon hydrostatic tests, where a (small) volume variation is imposed to the specimen, and upon deviatoric measurements, in which a change of shape is applied in the experiments, while the volume is kept constant. As a consequence, the strain energy function (Section 2.2.3) is necessarily constituted by two main parts, one referring to the deviatoric strain part, and the other to the hydrostatic component. While I_3 is a suitable index of the hydrostatic deformation, invariants I_1 and I_2 , which represent variations in length and surface, are not purely deviatoric. In fact, the first two Rivlin invariants are influenced, even if

slightly, by a hydrostatic strain field. For instance, a purely hydrostatic deformation applied to the unit cube modifies it into a (slightly) altered cube with a varied surface. It is concluded that invariant I_2 , which expresses the surface change of a unit cube, is modified by a hydrostatic deformation and, therefore, it does not represent a purely deviatoric strain component.

Penn (1970) introduces a slightly modified definition for the strain invariants, which removes the above minor limitations. Eqn (2.2.1.3) defining the Jacobian matrix is altered as follows :

$$\bar{f}_{i,j} = I_3^{-1/3} \frac{\partial f_i}{\partial X_j} \tag{2.2.2.1}$$

so that the modified Jacobian matrix [$\bar{f}_{i,j}$] is now purged from the volume changes (ABAQUS (1989)). Based on this improved definition, G is redefined following (2.2.1.8) and, consequently, new invariants are introduced, named "Penn strain invariants". Now $\bar{I}_1$ and $\bar{I}_2$ describe the purely deviatoric strain component and, therefore, they are particularly suitable for expressing the strain energy function connecting strains to stresses, examined in the following Section.

2.2.3 On the strain energy function in finite elasticity

As mentioned in the previous Section, the experiments performed to define the stress-strain relationship in elastomers are of two types : a) deviatoric tests and b) hydrostatic readings. The second measurement is extensively treated in Section 3 . Only a perfunctory description of the deviatoric experiment is given in this Section. A thin, square sheet of elastomer is pulled along the two sides for prescribed amounts, and the resulting stresses are measured via electrical strain gauges. Since the square plate is not restrained in the direction of its thickness, this specimen undergoes a plane state of stress. The hydrostatic stress component is limited, so that the volume changes are negligible. As a consequence, this experiment is classified as a deviatoric test. It should furnish experimental readings useful for defining a relationship between the first two strain invariants and the stress state. Specific works addressing unidimensional or two-dimensional tests are those of Hencky (1933), Treloar (1948), Blatz and Ko (1962) (who propose strain invariants very close to those of Penn), Sharma (1966), Alexander (1968), Parks and Durelli (1969), Rigbi (1969), Levinson and Burgess (1971), Ogden (1972), Treloar (1975), p. 230 , Zapas (1981), Medri (1982b), Medri (1984b), Beatty (1987), Gadala (1991). Extensions to the viscoelastic field are given by Christensen (1980), Morman (1984), and Lubliner (1985).

A general polynomial form of the strain energy function U is (ABAQUS (1989)) :

$$U = \sum_{i+j=1}^{N} C_{ij} (I_1 - 3)^i (I_2 - 3)^j + \sum_{i=1}^{N} D_i (I_3 - 1)^{2i} \qquad (2.2.3.1)$$

which evidences the deviatoric and hydrostatic parts. In fact, coefficient D_1 is closely connected to the bulk modulus of the elastomer (Section 3). The invariants of expression (2.2.3.1) may be understood as Rivlin or Penn strain invariants, where their conceptual, more than practical, difference has been elucidated in the previous Section.

Studies comparing the effects of different strain energy functions on the mechanical response of rubber units are rarely encountered in the technical literature. Oden (1972) analyses numerically a plate with a hole, stretched along its plane, and compares the deformations of the plate contours for various strain energy functions. Prati and Strozzi (1984) compute numerically the contact pressure in an elastomeric, rectangular seal for two strain energy functions, and discuss the differences noted between the two pressure profiles. The simpler strain energy function tested by Prati and Strozzi (1984) is usually named "compressible neo-Hookean law" since it is perhaps the most elementary extension of Hooke's law to the nonlinear elasticity field. It is formed by a deviatoric part, where the Young's modulus acts as a multiplying factor of the variations in length expressed via the strain invariant I_1 , and by a hydrostatic component, controlled by the bulk modulus multiplied by the volume changes expressed via I_3 . From the forecasts of Prati and Strozzi (1984) it can be deduced that the compressible neo-Hookean law is sufficiently accurate in their application. The same conclusion is accepted by Gabelli, Ponson, and Poll (1992), who favour the use of a neo-Hookean law in the numerical simulation of elastomeric lip seals. Such applications refer to situations where the strain deviatoric components prevails, so that it can be surmised that the deviatoric part of the neo-Hookean strain energy function is sufficiently accurate for practical purposes. In addition, it can be speculated that a modification of the formulation for the strain energy function when applied to essentially deviatoric situations is analogous to an alteration of the Young's modulus of the material. It can, therefore, be surmised from the forecasts of Prati and Strozzi (1984) that a modification of the Young's modulus generally results in a comparable proportional alteration of the stress field.

Conversely, if the hydrostatic stress field prevails (as it occurs in hip joints with elastomeric coatings under high loads), it is known that the stress level highly depends on the Poisson's ratio adopted (Dragoni and Strozzi (1988)). In this case, a perturbation of the Poisson's ratio generally results in a magnified alteration of the stress distribution.

The previous observations indicate that, with regard to the elastic constants affecting the neo-Hookean strain energy function, an approximation in the definition

of the Young's modulus would result in comparable errors in the stress field, while an inaccuracy in the selection of the Poisson's ratio may promote magnified errors if the stress field is mainly hydrostatic. Since the stress distribution is not known in advance, it is generally advisable to pay more attention to the correctness of the Poisson's ratio or at least, when the measurements of the cubic compressibility of the elastomer are unreliable or not available, to assess the effects of perturbations of the Poisson's ratio on the stress levels.

The formulae expressing the stresses as functions of the strain invariants through the strain energy function (ABAQUS (1989)) are not reported here. In practical applications, it is convenient to formulate the stress state in terms of Cauchy stresses (Ogden (1984)) which, referring to the convected unit surface, are more meaningful for an engineering viewpoint.

2.3 CONCLUSIONS

The definitions of strain, strain invariants and strain energy function, pertaining to the finite elasticity realm, have been introduced, to permit an unequivocal interpretation of the terminology used in Chapters 3, 6 and 7, with respect to the employ of the nonlinear finite element package ABAQUS (1989) in the structural analysis of elastomeric parts.

CHAPTER 3. ON THE CUBIC COMPRESSIBILITY OF ELASTOMERIC MATERIALS

3.1 INTRODUCTION

3.2 LITERATURE REVIEW

3.3 THE EXPERIMENTAL MEASUREMENT OF THE BULK MODULUS

3.3.1 The apparent bulk modulus measurements

3.3.2 The radial deformability of a hollow cylinder

3.3.2.1 Literature review

3.3.2.2 Basic equations

3.3.2.3 Formulation of the boundary conditions

3.3.2.4 Equations relating the series coefficients to the boundary conditions

3.3.2.5 Expressions of some series coefficients

3.3.2.6 Solution method

3.3.2.7 Numerical validation

3.3.2.8 The piston device radial deformation

3.3.3 The extrusion of the elastomer in the piston device

3.3.3.1 General aspects

3.3.3.2 Finite element forecasts

3.3.3.3 A theoretical model of the elastomer extrusion

3.3.4 The corrected bulk modulus measurements

3.4 CONCLUSIONS

3.1 INTRODUCTION

The possible influence of the Poisson's ratio, ν , which is connected to the cubic compressibility of the material (an alternative parameter is the bulk modulus) on the structural behaviour of elastomeric components is not always fully realized by the researchers. For instance, in Tuomala, Owen, and Zienkiewicz (1981) it reads: "the volume change resulting from the deformation of rubberlike materials is small (typically of the order of 10^{-4}) and, therefore, the assumption of a complete incompressible material is acceptable". On the contrary, it is recognized by Levinson and Burgess (1971) that, boundary conditions being similar, the structural behaviour of units supposed compressible and incompressible can differ noticeably. Well documented cases in which this circumstance occurs are presented by Rightmire (1970), Holownia (1971, 1972), Al-Qureshi and Das (1976), Medri (1984), Dimnikov, Sniegs and Erdmanis (1984), and Dragoni and Strozzi (1988). For a geometry of engineering interest, Holownia (1985b) finds that a change of ν from 0.4990 to 0.4999 produces a doubling of the stress peak.

An exhaustive information about the correctness of the experimental measurements of the bulk modulus and the possible influence of a cubic compressibility perturbation on the stress-strain field is desirable, since a) the experimental measurement of the bulk modulus in elastomers is inevitably approximate; b) the numerical problems encountered in employing finite element programs for elastomers are exacerbated as Poisson's ratio approaches 0.5 ; c) in photoelastic studies it is difficult to mimic the actual Poisson's ratio; d) some theoretical problems become more easily solvable with particular values of the Poisson's ratio (*e.g.* 0) . This Chapter analyses problems connected with the experimental measurement of the bulk modulus in elastomeric materials, and it is organized as follows. Section 3.2 summarizes the state of the art. There follows a Section devoted to the apparent experimental readings, and to their correction to account for the deformability of the measuring device and rubber extrusion problems.

3.2 LITERATURE REVIEW

In this Section the state of the art on the experimental measurement of the cubic compressibility in rubber-like materials is presented with reference to recent literature and personal research.

In the case of elastomeric materials, which by definition exhibit a small cubic compressibility, it is advantageous to refer to the bulk modulus, K , as an alternative parameter to the Poisson's ratio, ν . The bulk modulus expresses the ratio of the hydrostatic pressure acting upon a unit cube to its relative volume change. In linear elasticity it is linked to the Young's Modulus, E, and to the Poisson's ratio, ν, in the following way (Timoshenko and Goodier (1970)) :

$$K = \frac{E}{3\,(1-2\nu)} \tag{3.2.1}$$

For incompressible materials, $\nu \rightarrow 0.5$, and $K \rightarrow \infty$.

As a norm, K is determined via tests in which an essentially hydrostatic stress field is imposed on an elastomeric specimen. It would be extremely interesting to undertake experimental tests in which K is measured in the presence of highly deviatoric stress fields, since they could clarify the interaction among the essentially deviatoric and mainly hydrostatic strain invariants in the expression of the strain energy function (Ogden (1976)). In other words, if the unit cube is first deformed to become a parallelepiped (deviatoric deformations) and, then, a hydrostatic pressure is applied, is the bulk modulus affected by the previously imposed deviatoric state of strain ? Anyway, the traceable experimental measurements of the specimen cubic compressibility carried out in the presence of a deviatoric stress field produced questionable results, in the sense that the experimental scattering was comparable, if not higher, than the parameters to be measured, or a Poisson's ratio higher than 0.5 was found (Forster (1955), Blatz and Ko (1962), Lindley (1967), Alexander (1968), Sekiguchi, Kakiuchi, Morimoto, Fujimoto, and Yoshimura (1969), Durelli and Chen (1973), Mrowczynski and Bezinski (1973), Coumans and Heikens (1980), Medri (1982)).

In the case of simple tension, credible measurements of the Poisson's ratio were performed by Posfalvi (1982) for highly compressible elastomers ($\nu \simeq 0.3$). The pioneering work of Röntgen (1876) (who also discovered X rays) should also be quoted with reference to simple tension tests to measure ν .

Finally, in Bathurst and Rothenburg (1988) theoretical aspect concerning a constitutive relation with a negative Poisson's ratio and possibly valid for granular materials are discussed.

The most common devices for the measurement of the bulk modulus are the dilatometer, the piston device, the belt apparatus and the diamond anvil (Warfield, (1980)). Their application field covers hydrostatic pressures up to 10^2 MPa , 1 GPa , 10 GPa , 10^2 GPa, respectively (Warfield (1980)). The most widely used rig is the piston device, since it is simple to construct and sufficiently accurate, and since the hydrostatic pressures in elastomeric units are usually lower than 1 GPa . Because of the above-mentioned reasons, this Section will deal exclusively with the piston device. This rig consists of a thick, hollow, mild-steel cylinder (1) (Fig. 3.2.1) into which a solid cylindrical rubber specimen (2) is placed. The specimen is axially compressed between a mobile, steel piston (3) and a steel bottom (4) . The usual dimensions of the elastomeric specimen are: diameter $\simeq$ 25 mm, height $\simeq$ 50 mm . The ratio of height to diameter of the specimen (slenderness ratio) reconciles two contradictory needs. The piston compression stroke for a given axial load increases with the slenderness ratio and, therefore, the experimental measurement of the specimen volume change becomes more accurate for longer specimens. On the other hand, the Young's Modulus of the elastomer can be evaluated from the initial compression of the specimen before the specimen cylindrical surface contacts the cavity surface of the hollow cylinder. Such a measurement is possible only if no lateral bending occurs in the specimen and, therefore, a low slenderness ratio is desirable if both the bulk modulus and the Young's modulus are to be evaluated with a unique test (Warfield, Cuevas and Barnet (1968), Holownia (1974), Polvara (1978), Holownia (1980)). In some cases, a specimen with a low slenderness ratio (0.2 - 0.6) (Heydemann and Howck (1972), Zagorskii, Balashow, Roginskaya and Surdutovich (1976), Johannesson (1980)) was employed, since it was cut from commercial sheets, but in this event the measurement of the piston stroke is inevitably less accurate.

The clearance between the piston and the cylinder cavity is of the order of 1 — 10 μm, in order to limit extrusion of rubber at high pressures (Holownia (1974), Polvara (1978), Holownia (1980)). Despite these precautions, the occurrence of some extrusions which blocked the piston was reported in the case of unfilled natural rubbers (Lindley (1980)).

The measured value of the bulk modulus for an elastomer tends to diminish slightly when the speed of the piston compression stroke is lowered, and this is seemingly attributable to frictional effects between the specimen and the internal walls of the hollow cylinder. For instance, in the case of a polyurethane elastomer (Hysol CP 4485) it was found by the writer that, when the speed was lowered from 90 mm/min to 0.3 mm/min, the bulk modulus diminished by 5 percent. For speeds between 0.3 and 0.1 mm/min, no perceivable variation of the bulk modulus was spotted and, therefore, such speeds should be adopted in the experiments (Holownia (1974, 1980)).

Inaccuracies in the evaluation of K can derive from four sources of error: 1) the flexibility of the press which loads the piston; 2) the axial deformability of both the piston and the bottom of the device; 3) the radial compliance of the metal hollow cylinder; 4) the extrusion of the elastomer through the narrow radial gap between piston and hollow cylinder. If neglected, such effects can produce values of K lower than the real ones by 30 percent (Holownia (1974, 1980)). While an exhaustive study has been devoted to the first two sources of errors, the third aspect has been investigated only qualitatively (O'Neill (1976), Holownia (1980)), although the proper analytical tools are available (Bariani (1977)). The fourth aspect has been quoted by Burchett and Bert (1972), but no estimates for the extruded volume are supplied.

The stress field within the specimen is nearly hydrostatic (Piragino (1945), Polvara (1978)), and the error due to the fact that the deformation imposed is uniaxial and not equitriaxial decreases as ν approaches 0.5 (Gilmour, Trainor, and Haward, (1974)). A study of the stress state within the sample is presented by Da Rios and Rinelli (1980).

In Figure 3.2.2 a typical load-deflection curve is presented for a compressed

nylon specimen, for which certain aspects of the loading curve - discussed in the following - can be appreciated more easily, since its Poisson's ratio (about 0.39) is not close to the incompressibility figure 0.5 . The diagram is essentially bilinear; the slope of the first part is related to the situation in which the specimen lateral walls are not in contact with the internal walls of the metal hollow cylinder and, therefore, it permits E to be measured; the slope of the second part is associated with the condition in which the specimen fills the cavity completely and, consequently, it allows K to be evaluated. Since for an elastomer K is often 10^3 times E, it is difficult to plot load against deflection on such a scale that both the E and K slopes are equally legible. For an elastomer the diagram is usually focused on the K slope and, therefore, the E part is not well represented.

In Fig. 3.2.3 typical loading and unloading curves are displayed on a scale addressing K. The two curves are not superimposed, and this is usually attributed to frictional effects. In Burchett and Bert (1972) an investigation about this and other sources of errors is performed. In Holownia (1979) the lack of coincidence between the loading and unloading curves is ascribed also to hysteresis effects. In Fig. 3.2.4, three possible configurations of the load-deflection curve (or, alternatively, hydrostatic pressure versus relative volume change) are displayed. Some elastomers exhibit a nearly linear load-deflection curve up to hydrostatic pressures of the order of 1 GPa (Tarasov and Tyutekin (1960), Holownia (1974)); in other cases, the p - $\Delta V/V$ diagram presents a concavity upwards (Wood and Martin (1964)); more rarely, a sigmoidal curve is found (Pampillo and Davis (1971), Gilmour, Trainor and Haward (1974), Key (1974), Polvara (1978)). This S-shaped trend becomes more apparent in the case of a porous elastomer, for which the curve of Fig. 3.2.5 was found (Key (1974)). In general, for a hydrostatic pressure of 10^2 MPa, the normalized volume change is in the region of a few percent (apparently, the maximum imposed relative volume change reported in the literature is about 16 percent, reached by Warfield (1980)). At least for the curves with concavity upwards (Fig. 3.2.4), the error on the normalized change of volume which would be made if a pressure of 10^2 MPa and a diagram linearized at the origin were considered instead of the real curve, is of the order of 20 percent in excess. In Jana, Renganathan and Venkateswara Rao (1987) the effects of the non-linearity of the

bulk modulus on the stress field in propellant grains is investigated numerically.

All the devices proposed produce a compressive hydrostatic stress field. In the practical cases (seals, rubber springs, shock absorbers, rubber pads, elastomeric layers in artificial hip joints) the hydrostatic stress is often compressive; nevertheless some data about a tensile hydrostatic stress would be desirable. Apparently, such an experimental problem has not been solved so far: efforts made in this direction are mentioned in Blatz and Ko (1962), while in Kuske (1968) (see also Johnson (1969)) it is shown that for an epoxy-resin the Poisson's ratio ranges from 0.487 in tension to 0.4944 in compression. If such a noticeable difference were found also for elastomeric materials, it would cause extra-difficulties in the characterization of the cubic compressibility of the elastomers.

A topic just touched upon in this bibliographic review is the dependence of the bulk modulus upon the specimen temperature. This aspect has been treated by Fritzsche (1974), Ol'khovik and Grigoryan (1974), George (1984), and Strozzi (1984), where a general increase of the cubic compressibility with temperature is quantified. Anyway, in some practical studies the bulk modulus it assumed as temperature independent (Batra (1977)). Finally, Holownia (1977) studies the temperature buildup in a compressed rubber block.

Another aspect here only mentioned is the measurement of the dynamic bulk modulus, treated by Billington (1971) and by Holownia (1985a, 1986).

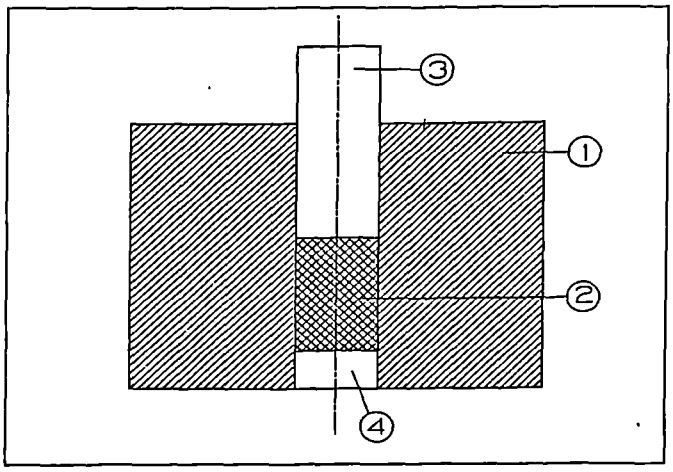

Fig. 3.2.1 : The piston device, where (1) is a thick, hollow, mild-steel cylinder, (2) is a solid cylindrical rubber specimen, (3) is a steel piston, and (4) is a steel bottom.

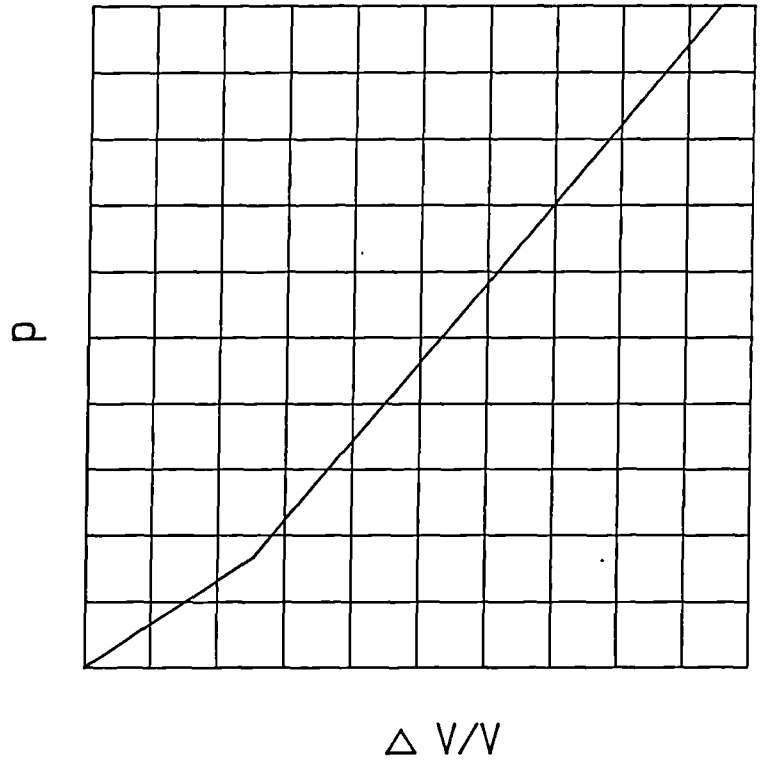

Fig. 3.2.2 : A typical load-deflection curve for a compressed nylon specimen.

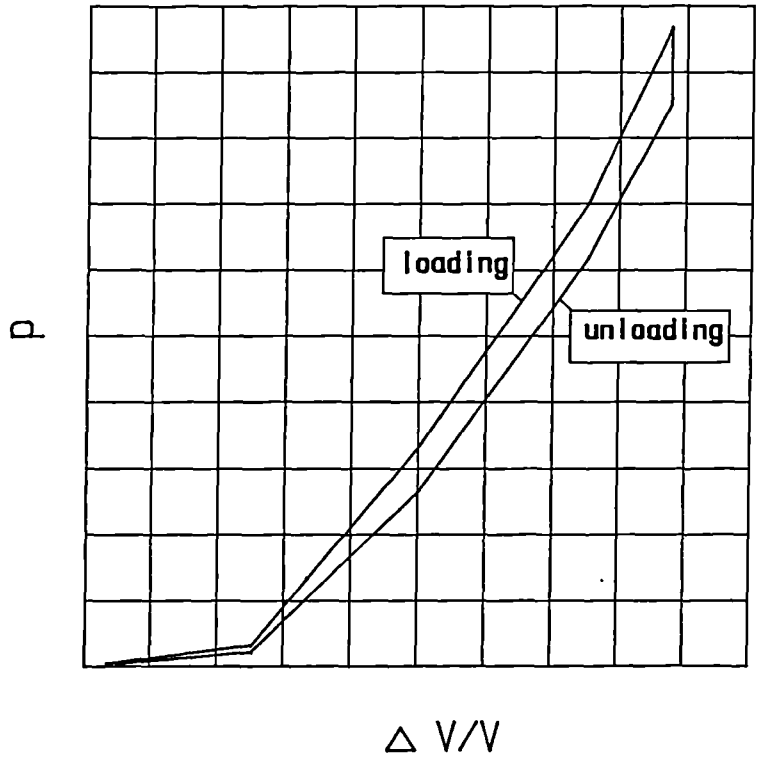

Fig. 3.2.3 : Typical loading and unloading curves.

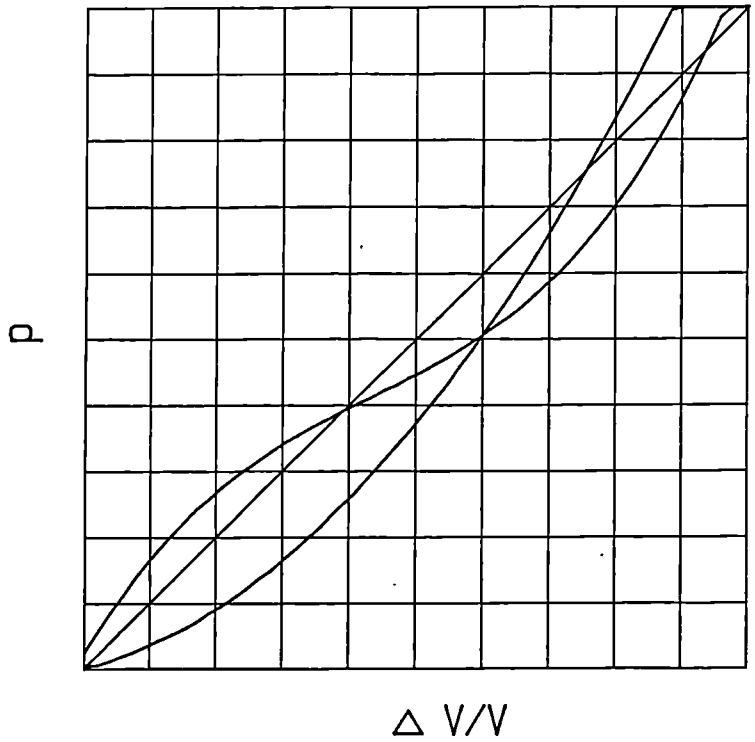

Fig. 3.2.4 : Three possible configurations for the hydrostatic pressure-volume change curve.

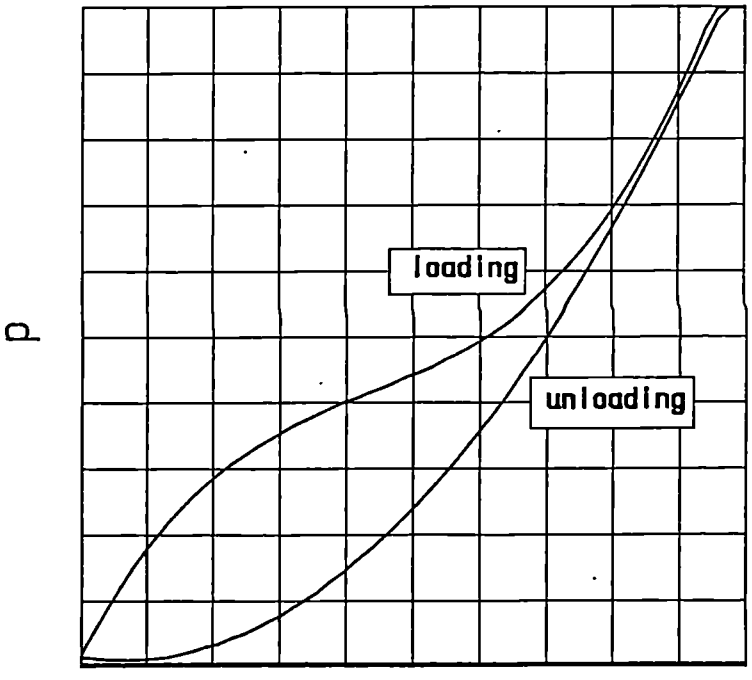

Fig. 3.2.5 : The sigmoidal hydrostatic pressure-volume change curve for a porous elastomer.

3.3 THE EXPERIMENTAL MEASUREMENT OF THE BULK MODULUS

This Section deals with the measurement of the cubic compressibility of two elastomers, namely Hysol CP 4485 (a polyurethane which is used in the experimental Section 5.4), and a second elastomer named "Estane" 5714F1 adopted for the elastomeric layer of the actual artificial hip joint. Section 3.3 is organised as follows. The results retrieved by employing a piston device are presented first in a specific Subsection 3.3.1 . As already mentioned in Section 3.2, these measurements are affected by four sources of error: 1) the flexibility of the press which loads the piston; 2) the axial deformability of both the piston and the bottom of the device; 3) the radial compliance of the metal hollow cylinder; 4) the extrusion of the elastomer through the narrow radial gap between piston and hollow cylinder. Error 1) can be avoided by measuring directly with a precision micrometer for depth measurements (gauge) the piston stroke. Error 2) can be corrected by applying simple concepts of the theory of elasticity and, therefore, it will not be treated in detail. Errors 3) and 4) can be corrected by resorting to complex theoretical models, treated in the individual Subsections 3.3.2 and 3.3.3 . A final Section 3.3.4 addresses the correction of the apparent bulk modulus measurements to derive the actual values.

3.3.1 The apparent bulk modulus measurements

A piston device was built in the laboratory of Dipartimento DIEM, Facolta' di Ingegneria, Universita' di Bologna, Italy. The nominal dimensions of the metal hollow cylinder are as follows: outer diameter: 150 mm ; inner diameter: 25 mm ; height : 123 mm . The surfaces of the cylinder cavity and of the metal piston are lapped. Fig. 3.3.1.1 shows the experimental set-up. In particular, the gauge which allows the piston stroke to be measured with respect to the cylinder is clearly visible.

As already mentioned, two different elastomers were studied. The first rubber is actually employed in artificial joints (only a specimen was available), named in the following as "Estane" 5714F1 , whereas the second elastomer is Hysol

CP 4485 , which was available in sheets and, therefore, was employed in the experimental study of Section 5.4 . The nominal height of the Hysol CP 4485 cylindrical specimen is 32 mm, whereas that of the elastomer employed in artificial joints is 23 mm. The nominal diameter of both specimens is 25 mm. The final load imposed by the Instron press is 50 kN, which implies a hydrostatic pressure of about 100 MPa (or 1000 atmospheres), a figure typical of many practical applications, *e.g.*, elastomeric seals. The selected force rate was 0.1 kN/s . Since the piston stroke is often of the order of 1 ÷ 3 mm, the compression rate is in the region of 0.1 ÷ 0.3 mm/min , an interval consistent with the recommendations of Section 3.2 .

Figs. 3.3.1.2 and 3.3.1.3 present the diagrams of piston stroke versus force for Hysol CP 4485 and for "Estane" 5714F1 , as released by the Instron press and, therefore, affected by the errors discussed in Section 3.2 . A moderate concavity upwards (Section 3.2) is perceivable. It also clearly emerges that the loading (upper) and unloading (lower) curves are not superimposed. As discussed in Section 3.2 , this lack of coincidence is presumably attributable to both frictional and hysteresis effects. It is believed that the frictional effects predominate. (The writer developed experimental devices to evaluate the viscoelastic behaviour of a rubber specimen subject to an essentially hydrostatic pressure field, whose results support this conclusion). Since the frictional forces act in opposite directions during loading and unloading, their effects can be compensated by referring to the average piston strokes during loading and unloading for a fixed applied force (or vice versa). This approach, together with the corrections related to the device deformability examined in the following, permits the actual bulk modulus to be estimated.

The Young's moduli for the two elastomers under study were measured via simple compression tests (the specimens were calibrated and, therefore, the Young's modulus could not be measured with the piston device, see Section 3.2), and the elastic constants were found to be 3.52 MPa (Hysol CP 4485) and 8.506 MPa ("Estane" 5714F1). These data are necessary to compute the bulk modulus according to expression (3.2.1) .

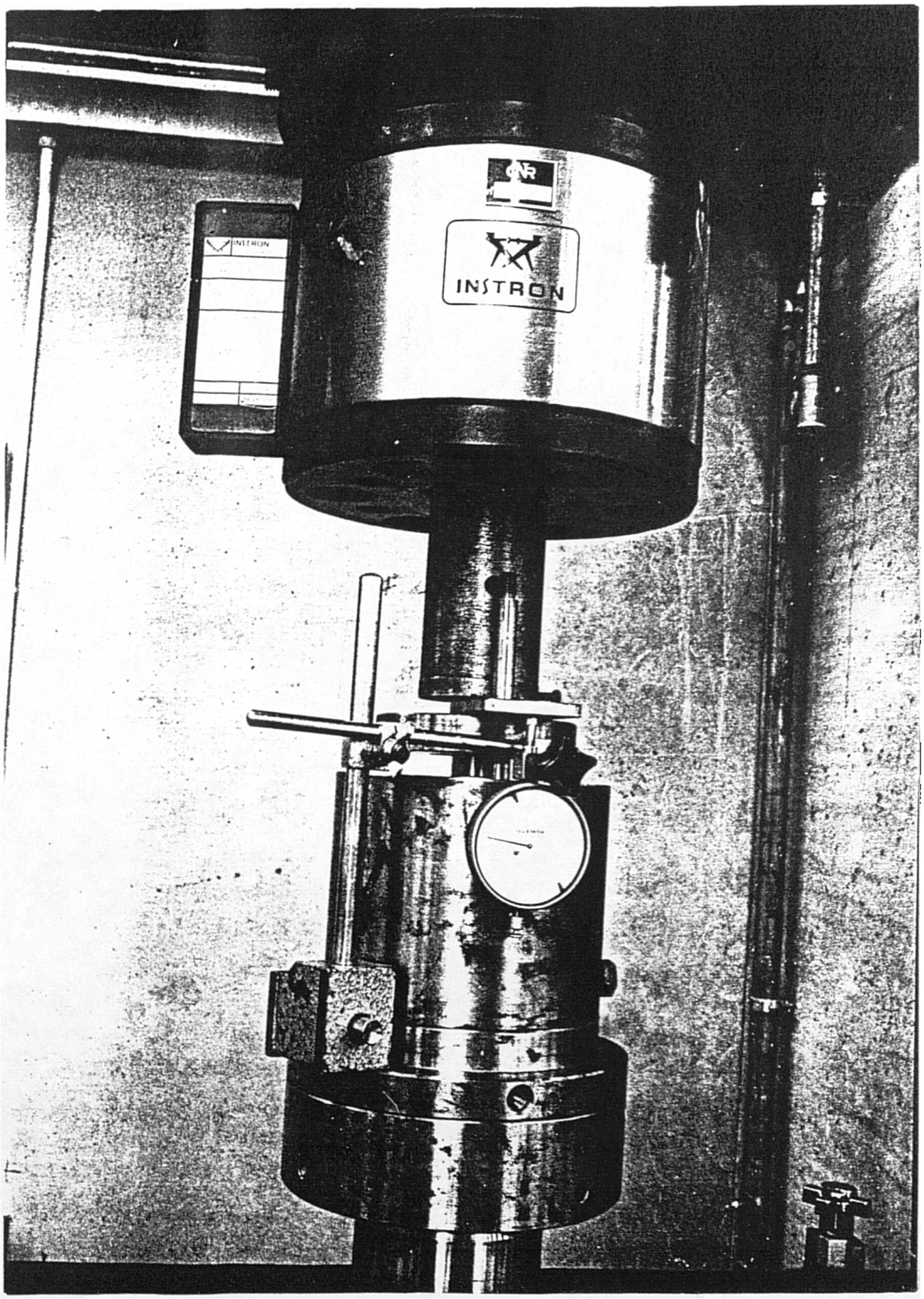

Fig. 3.3.1.1 : The experimental set-up, with the piston device loaded by an Instron press, and the micrometer (gauge) for the piston stroke measurement.

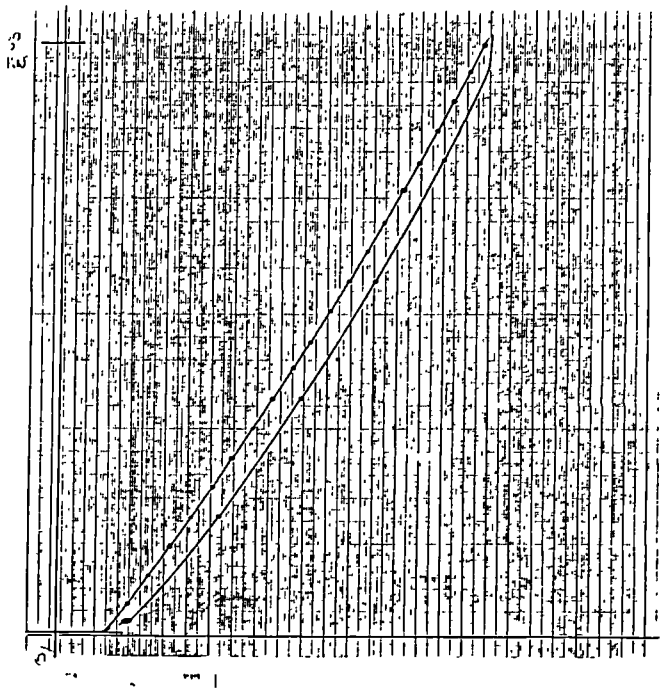

Fig. 3.3.1.2 : The diagrams of piston stroke versus force for Hysol CP 4485.

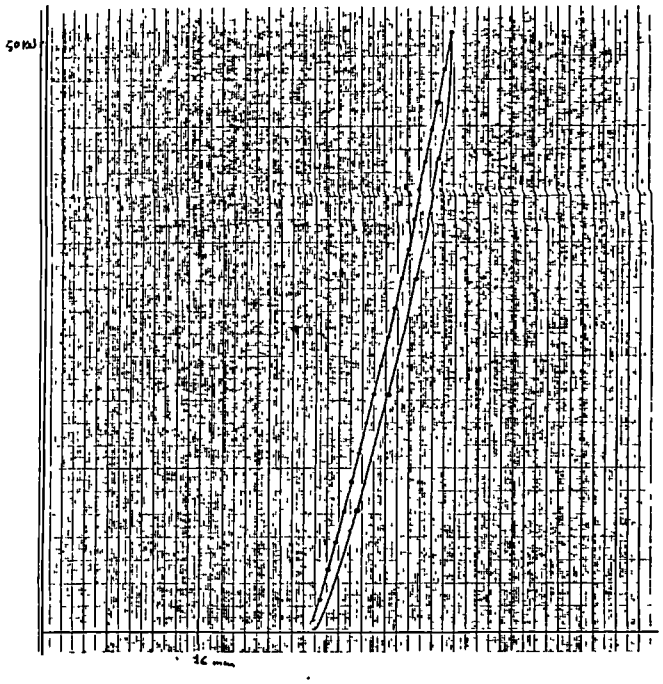

Fig. 3.3.1.3 : The diagrams of piston stroke versus force for "Estane" 5714F1 .

3.3.2 The radial deformability of a hollow cylinder

The aim of this Subsection is to evaluate the radial deformability of the metal hollow cylinder of the piston device, under the pressure effects of the compressed elastomeric specimen. As discussed in Section 3.2 , this piece of information permits the apparent bulk modulus measurements to be corrected. A brief literature review on this topic is presented first. Then, the formulation of the basic equations leading to a series solution (Section 3.3.2.2), of the boundary conditions (Section 3.3.2.3) and of their implications on the series solution coefficients (Section 3.3.2.4) are reported. There follow Subsections devoted to series expansion problems (Section 3.3.2.5), and to the solution method adopted (Section 3.3.2.6) . The final parts address the numerical validation of the solution obtained (Section 3.3.2.7) and the examination of the deformation of the actual hollow cylinder (Section 3.3.2.8) .

3.3.2.1 Literature review

The analytical solution methods for a structural analysis of a hollow cylinder are of two types, namely a displacement-based formulation (Papkovich-Neuber) or a stress-based approach (stress function).

Beginning from the papers based on a stress function modelling, Okubo (1952) examines a long shaft pressfitted with a collar, and proposes approximate solutions. Bazarenko and Vorovich (1965) analyze a hollow cylinder of finite length subject to an axisymmetric pressure profile, in the case of thin wall. An asymptotic solution is obtained. Dornig (1965) considers a press-fit problem, adopting the severe assumption that the hollow cylinder and the shaft possess the same axial length. The solution is expressed in terms of a series involving Bessel functions. Shibahara and Oda (1968) obtain for the stress distribution a series solution in terms of Bessel functions for the geometry of a hollow cylinder of finite length, loaded by an axisymmetric pressure distribution which is not necessarily constant, but must be symmetrical, with respect to the cylinder axis. The series coefficients are computed

via a method of successive approximations not described in detail. Oda, Shibahara, and Miyamoto, (1972) apply the Shibahara and Oda (1968) solution to study the contact pressure for a shrink-fit between an infinite solid cylinder and a finite hollow cylinder. Bernasconi (1971) studies the shrink-fit between two hollow cylinders, where the imposed interference is supposed to be variable along the axial direction. Bariani (1977) expands the work of Shibahara and Oda (1968) to include both symmetrical and skew-symmetrical stress distributions in the cylinder axis direction. Bariani (1983a) applies his solution to study the contact pressure in a shrink-fitted forming die assembly. Various practically significant results are collected in Bariani (1983b). Finally, Cappello and Nigrelli (1987,1989,1990) revisit the Bariani work, but they retain various misprints from the Bariani (1977) paper.

The studies based on a displacement approach include the paper by Sierakowski and Sun (1968), who present an elastic analysis for a hollow cylinder of finite length, subject to axisymmetric thermal and mechanical loads. The surface pressure acting along the tube end faces is assumed as uniform.

Moving to the analytical papers dealing with geometries still comparable with that of a tube of finite length, which employ solution techniques apparently applicable to the tube problem, Valov (1962) obtains a stress-based series solution in terms of Bessel functions for the geometry of a circular solid cylinder of finite length subject to axisymmetric, mixed boundary conditions. Spillers (1964) presents a solution for an infinite solid cylinder, the surface of which is traction-free except for a band which is subjected to a prescribed axisymmetric radial displacement. This problem, which is the axisymmetric analogue of a plane indentation situation, is formulated in terms of dual integral equations. A comparison between plane strain and axisymmetric contact stresses is presented. Yogananda (1967) examines an infinitely long, cylindrical shell enclosed in an elastic casing and sustaining a ring of radial load, based on a stress function formulation. Youngdahl (1969) discusses the completeness of the stress function for the elasticity problem in cylindrical coordinates. He compares Papkovich-Neuber and stress function approaches. Litovchenko and Nuller (1973) examine the case of an infinitely long shaft, acted upon by a force and a moment, and sustained by a rigid, frictionless bearing. Steven (1973) addresses the eigenvalue problem for a hollow circular cylinder, and

particularly examines the cases of thin and thick walls. Ramachandra Rao, Kandya, and Gopalacharyulu (1976) examine a similar problem for a solid cylinder loaded axisymmetrically, and with prescribed displacements or stresses along the end faces. Mukhopadhyah (1982) analyze the effects of non-homogeneity of yield stress in a thick-walled tube under pressure, subject to a plane state of strain. Tang and Erdogan (1984) study a thick-walled tube containing a radial crack and reinforced by an elastic membrane on its inner surface. The problem is formulated in terms of a singular integral equation, which is solved numerically.

The present study is based upon the paper due to Bariani (1977) as well as upon that of Shibahara and Oda (1968). As already noted, Shibahara and Oda (1968) develop the hollow cylinder solution for the case of a pressure symmetrically distributed with respect to the axial coordinate (that is, the pressure is axisymmetric and equal for points equally distant, along the axial direction, from the cylinder centre), whereas Bariani (1977) extends this solution to the equally common situations where the pressure profile is not symmetrical with regard to the axial coordinate. In the piston device the cylinder loading conditions consist of a band of essentially uniform pressure, corresponding to the zone where the bulky cylindrical elastomeric specimen touches the metal hollow cylinder under the compression exerted by the metal piston. The pressure band extent depends upon the rubber specimen height, and it is not generally centered with respect to the axial extent of the metal cylinder. Consequently, the problem of evaluating the radial expansion of the internal cavity of the hollow metal cylinder as a function of the high contact pressure exerted by the elastomeric specimen can be correctly analyzed by resorting to the theory of Bariani (1977).

The contributions given by the writer to this problem are: a) all mathematical passages of Bariani (1977) have been checked, and a certain number of misprints have been spotted and corrected (the less obvious mistakes will be underlined during the exposition of the theory); b) an original solution method has been developed, which is based upon an internal condensation of the degrees of freedom of the original problem, thus permitting a considerable reduction of the number of equations to be solved simultaneously; c) a stabilizing procedure for the series solution, known as "Lanczos σ method", is adapted to this problem.

3.3.2.2 Basic equations

This Subsection deals with the elastic analysis of a hollow cylinder of finite axial length and loaded by an axisymmetrical pressure band, and it closely follows the exposition of Bariani (1977). Fig. 3.3.2.2.1 describes the hollow cylinder, the reference frame, and it clarifies the meaning of the symbols employed.

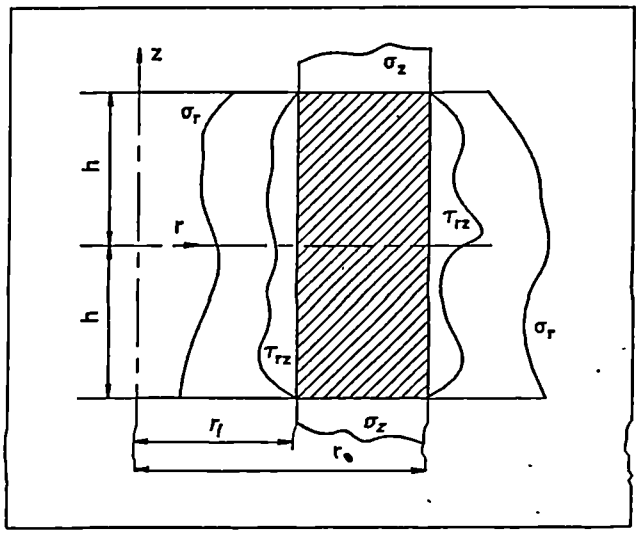

Fig. 3.3.2.2.1 : The hollow cylinder, the reference frame and the meaning of the symbols employed.

The equilibrium equations in cylindrical coordinates r, θ , z are (Timoshenko and Goodier (1970), p. 380) :

$$\frac{\partial \sigma_r}{\partial r} + \frac{\partial \tau_{rz}}{\partial z} + \frac{\sigma_r - \sigma_\theta}{r} = 0 \qquad (3.3.2.2.1)$$

$$\frac{\partial \tau_{rz}}{\partial r} + \frac{\partial \sigma_z}{\partial z} + \frac{\partial \tau_{rz}}{\partial r} = 0$$

The equations expressing the internal compatibility are (Shibahara and Oda (1968)) :

$$\nabla^2 \sigma_r - \frac{2}{r^2}(\sigma_r - \sigma_\theta) + \frac{1}{1+\nu}\frac{\partial^2}{\partial r^2}(\sigma_r + \sigma_\theta + \sigma_z) = 0$$

$$\nabla^2 \sigma_\theta + \frac{2}{r^2}(\sigma_r - \sigma_\theta) + \frac{1}{1+\nu}\frac{1}{r}\frac{\partial}{\partial r}(\sigma_r + \sigma_\theta + \sigma_z) = 0$$

$$\nabla^2 \sigma_z + \frac{1}{1+\nu}\frac{\partial^2}{\partial z^2}(\sigma_r + \sigma_\theta + \sigma_z) = 0$$

$$\nabla^2 \tau_{rz} - \frac{1}{r^2}\tau_{rz} + \frac{1}{1+\nu}\frac{\partial^2}{\partial r\,\partial z}(\sigma_r + \sigma_\theta + \sigma_z) = 0$$

(3.3.2.2.2)

where :

$$\nabla^2 = \frac{\partial^2}{\partial r^2} + \frac{1}{r}\frac{\partial}{\partial r} + \frac{\partial^2}{\partial z^2} \qquad (3.3.2.2.3)$$

A stress *function* Φ (r,z) is introduced. The radial, σ_r , circumferential, σ_θ , axial, σ_z , and tangential, τ_{rz} stresses, as well as the radial, u, and axial, w, displacements are defined as derivatives of the stress function Φ (r,z) (Timoshenko and Goodier (1970), p. 381) :

$$\sigma_r = \frac{\partial}{\partial z}\left(\nu \nabla^2 \Phi - \frac{\partial^2 \Phi}{\partial r^2}\right)$$

$$\sigma_\theta = \frac{\partial}{\partial z}\left(\nu \nabla^2 \Phi - \frac{1}{r}\frac{\partial \Phi}{\partial r}\right)$$

$$\sigma_z = \frac{\partial}{\partial z} \left((2 - \nu) \nabla^2 \Phi - \frac{\partial^2 \Phi}{\partial z^2} \right)$$

$$\tau_{rz} = \frac{\partial}{\partial r} \left((1 - 2\nu) \nabla^2 \Phi - \frac{\partial^2 \Phi}{\partial z^2} \right)$$

$$u = - \frac{1+\nu}{E} \frac{\partial^2 \Phi}{\partial r \, \partial z}$$

$$w = \frac{1+\nu}{E} \left[(1 - 2\nu) \nabla^2 \Phi + \frac{\partial^2 \Phi}{\partial r^2} + \frac{1}{r} \frac{\partial \Phi}{\partial r} \right] \qquad (3.3.2.2.4)$$

These stresses identically satisfy the equilibrium equations *regardless of the* expression of the stress function (Timoshenko and Goodier (1970), p. 380), provided that the stress function satisfies the following fourth order equation (Bariani (1977)), which expresses the equilibrium condition in the axial direction (Cicala (1985)) and a requirement for the satisfaction of the compatibility equations (3.3.2.2.2) :

$$\nabla^2 \nabla^2 \Phi = 0 \qquad (3.3.2.2.5)$$

It is convenient to express the stress function Φ (r,z) in terms of a series which identically satisfies the compatibility equation (3.3.2.2.5), and which contains a number of unknown coefficients sufficient to express all boundary conditions. A discussion on the completeness of the stress function is beyond the aim of this study. The interested reader is referred to Youngdahl (1969), who treats this specific aspect. The stress function proposed by Shibahara and Oda (1968), satisfying only stress boundary conditions symmetrical with respect to the axial coordinate,. has been completed by Bariani (1977) by adding the contribution dealing with the skew-symmetrical stresses. The resulting expression of the stress function is :

$$\Phi(r,z) = A_0 \frac{z^3}{6} + B_0\, z\, ln\, r + C_0\, z\, \frac{r^2}{2} +$$

$$\sum_{n=1}^{\infty} \frac{1}{\alpha_n^3} [\, A_n\, I_0(\alpha_n r) + B_n\, \alpha_n\, r\, I_1(\alpha_n r) + C_n\, K_0(\alpha_n r) + D_n\, \alpha_n\, r\, K_1(\alpha_n r)\,]\, sin\,(\alpha_n z) +$$

$$\frac{1}{\beta_n^3} [\, A'_n\, I_0(\beta_n r) + B'_n\, \beta_n\, r\, I_1(\beta_n r) + C'_n\, K_0(\beta_n r) + D'_n\, \beta_n\, r\, K_1(\beta_n r)\,]\, cos\,(\beta_n z) +$$

$$\sum_{m=1}^{\infty} \frac{1}{\gamma_n^3} (\, [\, A_m\, J_0(\gamma_m r) + B_m\, Y_0(\gamma_m r)\,]\, sinh\,(\gamma_m z) +$$

$$[\, E_m\, J_0(\gamma_m r) + F_m\, Y_o(\gamma_m r)\,]\, \gamma_m\, z\, cosh\,(\gamma_m z)\,) +$$

$$\sum_{m=1}^{\infty} \frac{1}{\gamma'^{\,3}_n} (\, [\, A'_m\, J_0(\gamma'_m r) + B'_m\, Y_0\,(\gamma'_m r)\,]\, cosh\,(\gamma'_m z) +$$

$$[\, E'_m J_0(\gamma'_m r) + F'_m\, Y_0(\gamma'_m r)\,]\, \gamma'_m\, z\, sinh\,(\gamma'_m z)\,)$$

(3.3.2.2.6)

where coefficients A_0 , B_0 , C_0 , A_n , B_n , C_n , D_n , A'_n , B'_n , C'_n , D'_n , A_m , B_m , E_m , F_m , A'_m , B'_m , E'_m , F'_m , as well as α_n , β_n , γ_m , γ'_m are constants to be determined via the boundary conditions. The constants with apex refer to the skew-symmetrical part of the solution. Moreover, I_0 , I_1 , J_0 , J_1 , K_0 , K_1 , Y_0 , Y_1 are (modified) Bessel functions of first and second kind, respectively.

The expressions of the stresses and displacements are obtained introducing in formulae (3.3.2.2.4) the form of Φ of (3.3.2.2.6), and they are reported in the follow-up. The expression of the stress radial component, $\sigma_r\,(r,z)$, is :

$$\sigma_r\,(r,z) = \nu\,A_0 + \frac{1}{r^2}\,B_0 - (1 - 2\nu)\,C_0 +$$

$$\sum_{n=1}^{\infty}\,[\,\sigma^{e}_{rn}\,cos\,(\alpha_n z) - \sigma^{o}_{rn}\,sin\,(\beta_n z)\,] +$$

$$\sum_{m=1}^{\infty}\,[\,\sigma^{e}_{rm}\,cosh\,(\gamma_m z) + \sigma^{e}_{rmz}\,\gamma_m\,z\,sinh\,(\gamma_m z) + \sigma^{o}_{rm}\,sinh\,(\gamma'_m z) + \sigma^{o}_{rmz}\,\gamma'_m z\,cosh\,(\gamma'_m z)\,]$$

(3.3.2.2.7)

where :

$$\sigma^{e}_{rn} = A_n\,[\,-I_0\,(\alpha_n r) + \frac{I_1\,(\alpha_n r)}{\alpha_n\,r}\,] - B_n\,[\,(1 - 2\,\nu)\,I_0\,(\alpha_n r) + \alpha_n\,r\,I_1\,(\alpha_n r)\,] -$$

$$C_n\,[\,K_0\,(\alpha_n r) + \frac{K_1\,(\alpha_n r)}{\alpha_n\,r}\,] + D_n\,[\,(1 - 2\,\nu)\,K_0\,(\alpha_n r) - \alpha_n\,r\,K_1\,(\alpha_n r)\,]$$

$$\sigma^{e}_{rm} = A_m\,[\,J_0\,(\gamma_m r) - \frac{J_1\,(\gamma_m r)}{\gamma_m r}\,] + B_m\,[\,Y_0\,(\gamma_m r) - \frac{Y_1\,(\gamma_m r)}{\gamma_m r}\,] +$$

$$E_m\,[\,(1 + 2\,\nu)\,J_0\,(\gamma_m r) - \frac{J_1\,(\gamma_m r)}{\gamma_m r}\,] + F_m\,[\,(1 + 2\,\nu)\,Y_0\,(\gamma_m r) - \frac{Y_1\,(\gamma_m r)}{\gamma_m r}\,]$$

$$\sigma^{e}_{rmz} = E_m\,[\,J_0\,(\gamma_m r) - \frac{J_1\,(\gamma_m r)}{\gamma_m r}\,] + F_m\,[\,Y_0\,(\gamma_m r) - \frac{Y_1\,(\gamma_m r)}{\gamma_m r}\,]$$

(3.3.2.2.8)

The expressions of the components referring to the odd contribution, marked with apex *o* (that is, odd) instead of apex *e* (that is, even) are obtained from the components dealing with the even contribution, by substituting the series constants with those endowed with apex, and by changing α_n with β_n . This rule is valid also for the following stress and displacement expressions.

The expression of the stress circumferential component, $\sigma_\theta\,(r,z)$, is :

$$\sigma_\theta\,(r,z) = \nu\,A_0 - \frac{1}{r^2}\,B_0 - (1 - 2\nu)\,C_0 +$$

$$\sum_{n=1}^{\infty}\,[\,\sigma^e_{\theta n}\,cos\,(\alpha_n z) - \sigma^o_{\theta n}\,sin\,(\beta_n z)\,] +$$

$$\sum_{m=1}^{\infty}\,[\,\sigma^e_{\theta m}\,cosh\,(\gamma_m z) + \sigma^e_{\theta mz}\,\gamma_m\,z\,sinh\,(\gamma_m z) + \sigma^o_{\theta m}\,sinh\,(\gamma'_m z) + \sigma^o_{\theta mz}\,\gamma'_m z\,cosh\,(\gamma'_m z)\,]$$

(3.3.2.2.9)

where :

$$\sigma^e_{\theta n} = -\,A_n\,\frac{I_1\,(\alpha_n r)}{\alpha_n\,r} - B_n\,(1 - 2\,\nu)\,I_0\,(\alpha_n r) + C_n\,\frac{K_1\,(\alpha_n r)}{\alpha_n\,r} + D_n\,(1 - 2\,\nu)\,K_0\,(\alpha_n r)$$

$$\sigma^e_{\theta m} = A_m\frac{J_1(\gamma_m r)}{\gamma_m r} + B_m\frac{Y_1(\gamma_m r)}{\gamma_m r} + E_m[2\,\nu\,J_0(\gamma_m r) + \frac{J_1(\gamma_m r)}{\gamma_m r}] + F_m[2\,\nu\,Y_0(\gamma_m r) + \frac{Y_1(\gamma_m r)}{\gamma_m r}]$$

$$\sigma^e_{\theta mz} = E_m\,\frac{J_1\,(\gamma_m r)}{\gamma_m r} + F_m\,\frac{Y_1\,(\gamma_m r)}{\gamma_m r} \qquad (3.3.2.2.10)$$

The expression of the stress axial component, $\sigma_z\,(r,z)$, is :

$$\sigma_z\,(r,z) = (1 - \nu)\,A_0 + 2\,(2 - \nu)\,C_0 +$$

$$\sum_{n=1}^{\infty}\,[\,\sigma^e_{zn}\,cos\,(\alpha_n z) - \sigma^o_{zn}\,sin\,(\beta_n z)\,] +$$

$$\sum_{m=1}^{\infty} [\ \sigma^{e}_{zm}\ cosh\ (\gamma_m z) + \sigma^{e}_{zmz}\ \gamma_m\ z\ sinh\ (\gamma_m z) + \sigma^{o}_{zm}\ sinh\ (\gamma'_m z) + \sigma^{o}_{zmz}\ \gamma'_m z\ cosh\ (\gamma'_m z)\ ]$$

(3.3.2.2.11)

where :

$$\sigma^{e}_{zn} = A_n\ I_0\ (\alpha_n r) + B_n\ [\ 2\ (2 - \nu)\ I_0\ (\alpha_n r) + \alpha_n\ r\ I_1\ (\alpha_n r)\ ] +$$

$$C_n\ K_0\ (\alpha_n r) - D_n\ [2\ (2 - \nu)\ K_0\ (\alpha_n r) - \alpha_n\ r\ K_1\ (\alpha_n r)\ ]$$

$$\sigma^{e}_{zm} = - A_m\ J_0\ (\gamma_m r) - B_m\ Y_0\ (\gamma_m r) + E_m\ (1 - 2\ \nu)\ J_0\ (\gamma_m r) + F_m\ (1 - 2\ \nu)\ Y_0\ (\gamma_m r)$$

$$\sigma^{e}_{zmz} = - E_m\ J_0\ (\gamma_m r) - F_m\ Y_0\ (\gamma_m r)$$

(3.3.2.2.12)

In the Bariani (1977) paper a minus sign in the expression of σ^{e}_{zm} is missing before the first right-hand side term.

The expression of the tangential stress component, $\tau_{rz}\ (r,z)$, is :

$$\tau_{rz}\ (r,z) = \sum_{n=1}^{\infty} [\ \tau^{e}_{rzn}\ sin\ (\alpha_n z) + \tau^{o}_{rzn}\ cos\ (\beta_n z)\ ] +$$

$$\sum_{m=1}^{\infty} [\ \tau^{e}_{rzm}\ sinh\ (\gamma_m z) + \tau^{e}_{rzmz}\ \gamma_m\ z\ cosh\ (\gamma_m z) + \tau^{o}_{rzm}\ cosh\ (\gamma'_m z) + \tau^{o}_{rzmz}\ \gamma'_m z\ sinh\ (\gamma'_m z)\ ]$$

(3.3.2.2.13)

where :

$$\tau^{e}_{rzn} = A_n\, I_1(\alpha_n r) + B_n\,[\,2(1-\nu)\, I_1(\alpha_n r) + \alpha_n\, r\, I_0(\alpha_n r)\,] -$$

$$C_n\, K_1(\alpha_n r) + D_n\,[2(1-\nu)\, K_1(\alpha_n r) - \alpha_n\, r\, K_0(\alpha_n r)\,]$$

$$\tau^{e}_{rzm} = A_m\, J_1(\gamma_m r) + B_m\, Y_1(\gamma_m r) + E_m\, 2\,\nu\, J_1(\gamma_m r) + F_m\, 2\,\nu\, Y_1(\gamma_m r)$$

$$\tau^{e}_{rzmz} = E_m\, J_1(\gamma_m r) + F_m\, Y_1(\gamma_m r)$$

(3.3.2.2.14)

The expression of the radial displacement, $u\,(r,z)$, is :

$$u\,(r,z) = -\frac{1+\nu}{E}\,\left(\frac{B_0}{r} + C_0\, r\right) +$$

$$\sum_{n=1}^{\infty} \frac{1+\nu}{E}\,[\,u^{e}_{n}\cos(\alpha_n z) - u^{o}_{n}\sin(\beta_n z)\,] +$$

$$\sum_{m=1}^{\infty} \frac{1+\nu}{E}\,[\,u^{e}_{m}\cosh(\gamma_m z) + u^{e}_{mz}\,\gamma_m\, z\sinh(\gamma_m z) + u^{o}_{m}\sinh(\gamma'_m z) + u^{o}_{mz}\,\gamma'_m z\cosh(\gamma'_m z)\,]$$

(3.3.2.2.15)

where :

$$u^{e}_{n} = -\frac{1}{\alpha_n}\,[\,A_n\, I_1(\alpha_n r) + B_n\,\alpha_n\, r\, I_0(\alpha_n r) - C_n\, K_1(\alpha_n r) - D_n\,\alpha_n\, r\, K_0(\alpha_n r)\,]$$

$$u^{e}_{m} = \frac{1}{\gamma_m}\,[\,A_m\, J_1(\gamma_m r) + B_m\, Y_1(\gamma_m r) + E_m\, J_1(\gamma_m r) + F_m\, Y_1(\gamma_m r)\,]$$

$$u^{e}_{mz} = \frac{1}{\gamma_m} [\, E_m J_1 (\gamma_m r) + F_m Y_1 (\gamma_m r) \,]$$

(3.3.2.2.16)

Finally, the expression of the axial displacement, $w\,(r,z)$, is :

$$w\,(r,z) = \frac{1+\nu}{E} [\, (1 - 2\,\nu)\, A_0\, z + 4\,(1-\nu)\, C_0\, z \,] +$$

$$\sum_{n=1}^{\infty} \frac{1+\nu}{E} [\, w^{e}_{n} \sin(\alpha_n z) + w^{o}_{n} \cos(\beta_n z) \,] +$$

$$\sum_{m=1}^{\infty} \frac{1+\nu}{E} [\, w^{e}_{m} \sinh(\gamma_m z) + w^{e}_{mz}\, \gamma_m\, z \cosh(\gamma_m z) + w^{o}_{m} \cosh(\gamma'_m z) + w^{o}_{mz}\, \gamma'_m z \sinh(\gamma'_m z) \,]$$

(3.3.2.2.17)

where :

$$w^{e}_{n} = \frac{1}{\alpha_n} (\, A_n I_0 (\alpha_n r) + B_n [4\,(1-\nu)\, I_0 (\alpha_n r) + \alpha_n\, r\, I_1 (\alpha_n r) \,] +$$

$$C_n K_0 (\alpha_n r) - D_n [4\,(1-\nu)\, K_0 (\alpha_n r) - \alpha_n\, r\, K_1 (\alpha_n r) \,] \,)$$

$$w^{e}_{m} = - \frac{1}{\gamma_m} [A_m J_0(\gamma_m r) + B_m Y_0(\gamma_m r) - 2\, E_m(1-2\,\nu)\, J_0(\gamma_m r) - 2\, F_m(1-2\,\nu) Y_0 (\gamma_m r) \,]$$

$$w^{e}_{mz} = - \frac{1}{\gamma_m} [\, E_m J_0 (\gamma_m r) + F_m Y_0 (\gamma_m r) \,]$$

(3.3.2.2.18)

3.3.2.3 Formulation of the boundary conditions

For $r = r_i$, and for a generic z position, the imposed radial and tangential stresses can be expressed in terms of a converging Fourier expansion, provided that they are sufficiently regular. Consequently, the following expressions hold true :

$$\sigma_r (r_i,z) = a_0 + \sum_{n=1}^{\infty} [\, a_n \cos(\alpha_n z) + a'_n \sin(\beta_n z) \,]$$
$$\tau_{rz} (r_i,z) = \sum_{n=1}^{\infty} [\, s_n \sin(\alpha_n z) + s'_n \cos(\beta_n z) \,] \qquad (3.3.2.3.1)$$

It can be noted that, in the series expansion of σ_r , term a_0 expresses the average value between $+ h$ and $- h$ of the radial stress at the inner radius of the cylinder (h represents the cylinder half height). In fact, the integrals between $+ h$ and $- h$ of both expressions $a_n \cos(\alpha_n z)$ and of $a'_n \sin(\beta_n z)$ vanish. (This is due to the expressions of α_n and of β_n , computed in the next section.) Conversely, in the series expansion of τ_{rz} an initial term (analogous to a_0) is not necessary, since the integral between $+ h$ and $- h$ of $s_n \sin(\alpha_n z)$ vanishes, but the analogous integral of $s'_n \cos(\beta_n z)$ does not, thus taking the place of a_0 . In our case, however, the imposed shear stress vanishes at both inner and outer radii and, therefore, both s_n and s'_n vanish.

Similarly, for $r = r_e$, and for a generic z position, the following boundary conditions hold true :

$$\sigma_r (r_e,z) = b_0 + \sum_{n=1}^{\infty} [\, b_n \cos(\alpha_n z) + b'_n \sin(\beta_n z) \,]$$
$$\tau_{rz} (r_e,z) = \sum_{n=1}^{\infty} [\, t_n \sin(\alpha_n z) + t'_n \cos(\beta_n z) \,] \qquad (3.3.2.3.2)$$

For $z = +h$, and for a generic r position, it is supposed that no boundary shear stress takes place, whereas the possible existence of an axial stress is taken into account. Consequently, the following conditions hold true:

$$\tau_{rz}(r, h) = 0$$

$$\sigma_z(r, h) = h_0 + \sum_{m=1}^{\infty} h_m T_{0m}(\gamma_m r)$$

(3.3.2.3.3)

where T_{0m} is expressed in terms of Bessel functions :

$$T_{0m}(\gamma_m r) = J_0(\gamma_m r) - \frac{J_1(\gamma_m r_t)}{Y_1(\gamma_m r_t)} Y_0(\gamma_m r)$$

(3.3.2.3.4)

It is observed that the boundary condition on the axial stress at the cylinder extremities is not expressed in terms of Fourier expansion, but in terms of Bessel functions. The relevance of this approach, as well as its advantages, will become clear in the next Sections.

Finally, for $z = -h$, and for a generic r position, the following conditions hold true:

$$\tau_{rz}(r, -h) = 0$$

$$\sigma_z(r, -h) = h'_0 + \sum_{m=1}^{\infty} h'_m T_{0m}(\gamma_m r)$$

(3.3.2.3.5)

The boundary conditions referring to σ_z (r, h) and to σ_z $(r, -h)$ are expressed in a different way in the Bariani (1977) paper. In particular, these two conditions (referring to $+h$ and to $-h$, respectively) are made to coincide, as if the axial stresses acting at the two cylinder extremities had to be necessarily equal. The formulation adopted here is, therefore, more general.

As a final observation, the global axial equilibrium of the hollow cylinder will be discussed in Subsection 3.3.2.4 , only with regard to the specific boundary conditions encountered in the piston device.

3.3.2.4 Equations relating the series coefficients to the boundary conditions

This Subsections treats the impositions exerted by the boundary conditions on the expressions of the series solution coefficients.

It is convenient to start from the boundary conditions (3.3.2.3.1,2) referring to the shear strain acting at the inner (r_i) and outer (r_e) radii :

$$\tau_{rz}\,(r_i,z) = \sum_{n=1}^{\infty} \left[\, s_n \sin(\alpha_n z) + s'_n \cos(\beta_n z) \,\right]$$

$$\tau_{rz}\,(r_e,z) = \sum_{n=1}^{\infty} \left[\, t_n \sin(\alpha_n z) + t'_n \cos(\beta_n z) \,\right] \qquad (3.3.2.4.1)$$

By remembering the generic expression of $\tau_{rz}\,(r,\,z)$ (see equation (3.3.2.2.13) and expressions (3.3.2.2.14)), by equalling it to the two above-mentioned boundary conditions, it is inferred that the coefficients multiplying the trigonometric and transcendental functions in expression (3.3.2.2.13) must satisfy the following conditions :

$$\tau^{e}_{rzn} \,|_{\,r=r_i} = s_n$$

$$\tau^{o}_{rzn} \,|_{\,r=r_i} = s'_n$$

$$\tau^{e}_{rzn} \,|_{\,r=r_e} = t_n$$

$$\tau^{o}_{rzn} \,|_{\,r=r_e} = t'_n$$

$$\tau^{e}_{rzm} \mid_{r=r_i} = 0$$

$$\tau^{o}_{rzm} \mid_{r=r_i} = 0$$

$$\tau^{e}_{rzm} \mid_{r=r_e} = 0$$

$$\tau^{o}_{rzm} \mid_{r=r_e} = 0$$

$$\tau^{e}_{rzmz} \mid_{r=r_i} = 0$$

$$\tau^{o}_{rzmz} \mid_{r=r_i} = 0$$

$$\tau^{e}_{rzmz} \mid_{r=r_e} = 0$$

$$\tau^{o}_{rzmz} \mid_{r=r_e} = 0 \qquad (3.3.2.4.2)$$

If the fifth and seventh equations of (3.3.2.4.2) are written in an extended form by introducing the second expression of (3.3.2.2.14), and if the last equation of (3.3.2.2.14) and the penultimate equation of (3.3.2.4.2) are taken into account (so that terms in E_m and in F_m are cancelled in the second expression of (3.3.2.2.14)) , it is obtained :

$$\tau^{e}_{rzm} \mid_{r=r_i} = A_m J_1(\gamma_m r_i) + B_m Y_1(\gamma_m r_i) = 0$$

$$\tau^{e}_{rzm} \mid_{r=r_e} = A_m J_1(\gamma_m r_e) + B_m Y_1(\gamma_m r_e) = 0 \qquad (3.3.2.4.3)$$

As a consequence, a non-trivial solution in terms of A_m and B_m exists only if the determinant vanishes, that is, if the following characteristic equation holds true :

$$J_1(\gamma_m r_i)\, Y_1(\gamma_m r_e) - Y_1(\gamma_m r_i)\, J_1(\gamma_m r_e) = 0 \qquad (3.3.2.4.4)$$

or, alternatively :

$$\frac{J_1(\gamma_m r_i)}{Y_1(\gamma_m r_i)} = \frac{J_1(\gamma_m r_e)}{Y_1(\gamma_m r_e)} \qquad (3.3.2.4.5)$$

This also clarifies that in expression (3.3.2.3.4) of T_{0m} it could have been equally possible to refer, with regard to the fraction at the right-hand side, either to inner (as done in expression (3.3.2.3.4)) or to outer radii.

In a similar way the following equation is obtained in treating the sixth and eight odd boundary conditions (3.3.2.4.2) :

$$J_1(\gamma'_m r_i)\, Y_1(\gamma'_m r_e) - Y_1(\gamma'_m r_i)\, J_1(\gamma'_m r_e) = 0 \qquad (3.3.2.4.6)$$

which coincides with the even characteristic equation (3.3.2.4.4). As a consequence, the "radial" (since they refer to boundary conditions on both inner and outer radii) even (γ_m) and odd (γ'_m) eigenvalues are in fact the same variable. Consistently, only symbol γ_m will be employed in the following, to express both even and odd radial eigenvalues. A discussion on the numerical evaluation of these radial eigenvalues is deferred to Subsection 3.3.2.6 .

The first expressions of boundary conditions (3.3.2.3.3) and (3.3.2.3.5) are now treated, which deal with the vanishing of the shear stress at the two cylinder extremities (that is, for $z = +/- h$). Expression (3.3.2.2.13) of τ_{rz} is composed by a first part (the sum with index n) containing trigonometric functions, and by a

second part (the sum with index m) exhibiting hyperbolic functions. For $z = +/-h$, the first part vanishes if the trigonometric functions vanish, that is :

$$sin\ (\alpha_n) = 0$$

$$cos\ (\beta_n) = 0 \qquad (3.3.2.4.7)$$

Consequently, the "axial" (that is, referring to conditions on the axial coordinate z) eigenvalues are:

$$\alpha_n = \frac{n\ \pi}{h} \qquad \beta_n = \frac{(2\ n - 1)\ \pi}{2\ h} \qquad (3.3.2.4.8)$$

It can be observed that, for very high values of index n, eigenvalue α_n approaches eigenvalue β_n . From eqn (3.3.2.2.13) it appears that eigenvalue β_n refers to an odd part. Consequently, symbol α'_n would have been more proper. Anyway, following Bariani (1977), symbol β_n is here retained.

The second part of expression (3.3.2.2.13), that containing hyperbolic functions, is now treated. The symmetrical components, that is, those with apex e are examined first. This part vanishes if :

$$\tau^{e}_{rzm}\ sinh\ (\gamma_m z) + \tau^{e}_{rzmz}\ \gamma_m\ z\ cosh\ (\gamma_m z) \quad z = +/-h \quad = 0 \qquad (3.3.2.4.9)$$

It can be verified that the same equation holds true for $z = +/- h$.

By substituting to τ^{e}_{rzm} and to τ^{e}_{rzmz} their expressions (3.3.2.2.14), this equation becomes :

$$[\ A_m\ J_1\ (\gamma_m r) + B_m\ Y_1\ (\gamma_m r) + E_m\ 2\ \nu\ J_1\ (\gamma_m r) + F_m\ 2\ \nu\ Y_1\ (\gamma_m r)\ ]\ sinh\ (\gamma_m h) +$$

$$[\ E_m\ J_1\ (\gamma_m r) + F_m\ Y_1\ (\gamma_m r)\ ]\ \gamma_m\ h\ cosh\ (\gamma_m h) = 0 \qquad (3.3.2.4.10)$$

By collecting separately the terms multiplying the Bessel functions J_1 and Y_1 , it is obtained :

$$J_1(\gamma_m r)\,[\,A_m\,sinh(\gamma_m h) + E_m\,(\,2\,\nu\,sinh(\gamma_m h) + \gamma_m\,h\,cosh(\gamma_m h))\,] = 0$$

$$Y_1(\gamma_m r)\,[\,B_m\,sinh(\gamma_m h) + F_m\,(\,2\,\nu\,sinh(\gamma_m h) + \gamma_m\,h\,cosh(\gamma_m h))\,] = 0 \qquad (3.3.2.4.11)$$

Alternatively, it is possible to write :

$$A_m = E_m\,(\,-\gamma_m\,h\,coth(\gamma_m h) - 2\,\nu\,)$$
$$B_m = F_m\,(\,-\gamma_m\,h\,coth(\gamma_m h) - 2\,\nu\,) \qquad (3.3.2.4.12)$$

By introducing symbol δ_m :

$$\delta_m = -\gamma_m\,h\,coth(\gamma_m h) - 2\,\nu \qquad (3.3.2.4.13)$$

the boundary conditions under scrutiny can be expressed in the following way :

$$A_m = E_m\,\delta_m$$
$$B_m = F_m\,\delta_m \qquad (3.3.2.4.14)$$

It is noted that the expression of δ_m given in the Bariani (1977) paper appears to be not exact.

The skew-symmetrical components are now treated, that is, those with apex o . The part of the expression of the shear stress (3.3.2.2.13) containing hyperbolic functions vanishes if :

$$\tau^0_{rzm}\,cosh(\gamma_m z) + \tau^0_{rzmz}\,\gamma_m\,z\,sinh(\gamma_m z)\,]_{\,z\,=\,+/-h} = 0 \qquad (3.3.2.4.15)$$

It can be verified that the same equation holds true for $z = +/- h$.

By substituting to τ^0_{rzm} and to τ^0_{rzmz} their expressions (3.3.2.2.14), this equation becomes :

$$[A'_m J_1(\gamma_m r) + B'_m Y_1(\gamma_m r) + E'_m 2\nu J_1(\gamma_m r) + F'_m 2\nu Y_1(\gamma_m r)] \cosh(\gamma_m h) +$$

$$[E'_m J_1(\gamma_m r) + F'_m Y_1(\gamma_m r)] \gamma_m h \sinh(\gamma_m h) = 0 \qquad (3.3.2.4.16)$$

By collecting separately terms multiplying the Bessel functions J_1 and Y_1 , it is obtained :

$$J_1(\gamma_m r) [A'_m \cosh(\gamma_m h) + E'_m (2\nu \cosh(\gamma_m h) + \gamma_m h \sinh(\gamma_m h)] = 0$$

$$Y_1(\gamma_m r) [B'_m \cosh(\gamma_m h) + F'_m (2\nu \cosh(\gamma_m h) + \gamma_m h \sinh(\gamma_m h)] = 0 \qquad (3.3.2.4.17)$$

Alternatively, it is possible to write :

$$A'_m = E'_m (- \gamma_m h \tanh(\gamma_m h) - 2\nu)$$
$$B'_m = F'_m (- \gamma_m h \tanh(\gamma_m h) - 2\nu) \qquad (3.3.2.4.18)$$

By introducing symbol δ'_m :

$$\delta'_m = - \gamma_m h \tanh(\gamma_m h) - 2\nu \qquad (3.3.2.4.19)$$

these boundary conditions can be expressed in the following way :

$$A'_m = E'_m \delta'_m$$

$$B'_m = F'_m \delta'_m \qquad (3.3.2.4.20)$$

It is noted that the expression of δ'_m furnished in the Bariani (1977) paper appears to be not correct. It is also observed that δ_m approaches δ'_m for relatively high values of index m, since $tanh\ (\gamma_m h)$ rapidly approaches unity.

As a final observation, if equations (3.3.2.4.14) are introduced into the expressions of τ^e_{rzm} (3.3.2.2.14), and if the boundary conditions (3.3.2.3.1) and (3.3.2.3.2) addressing the shear stress at the inner and outer radii are expressed according to the fifth and seventh conditions of (3.3.2.4.2), it is obtained :

$$\tau^e_{rzm} \mid_{r=r_i} = J_1(\gamma_m r_i)\, E_m (\delta_m + 2\nu) + Y_1(\gamma_m r_i)\, F_m (\delta_m + 2\nu) = 0$$

$$\tau^e_{rzm} \mid_{r=r_e} = J_1(\gamma_m r_e)\, E_m (\delta_m + 2\nu) + Y_1(\gamma_m r_e)\, F_m (\delta_m + 2\nu) = 0$$

$$\vdots \qquad (3.3.2.4.21)$$

and these equations produce a non-trivial solution in terms of constants E_m and F_m only when the determinant vanishes. In other words, the same conditions (3.3.2.4.4), which were found by imposing a vanishing shear strain for $z = +/- h$ and not necessarily $r = r_i$ or $r = r_e$ are found again. An analogous observation holds true for the odd τ^o_{rzm} components.

The boundary conditions are now treated which impose that the radial stress at the inner and outer radii equals the assigned distribution according to the first equations of (3.3.2.3.1) and of (3.3.2.3.2). In such equations the boundary radial stress distribution is expanded in terms of trigonometric functions, whereas in equation (3.3.2.2.7) z variable is the argument of both trigonometric and hyperbolic functions. The imposition of the boundary conditions requires that the coefficients of the trigonometric expansions of (3.3.2.3.1) and (3.3.2.3.2) are made to coincide with those of the expression of σ_r derived from (3.3.2.2.7) and computed at the

inner and outer radii. This in turn requires that the even hyperbolic functions *cosh* $(\gamma_m z)$ and z *sinh* $(\gamma_m z)$ as well as the odd hyperbolic functions *sinh* (γ_m) and z *cosh* (γ_m) are expanded in series of *cos* $(\alpha_n z)$ and of *sin* $(\beta_n z)$, respectively. The following series expansions are of use :

$$cosh\ (\gamma_m z) = H_{0,m} + \sum_{n=1}^{\infty} H_{n,m}\ cos\ (\alpha_n z)$$

$$z\ sinh\ (\gamma_m z) = L_{0,m} + \sum_{n=1}^{\infty} L_{n,m}\ cos\ (\alpha_n z)$$

$$sinh\ (\gamma_m z) = \sum_{n=1}^{\infty} H'_{n,m}\ sin\ (\beta_n z)$$

$$z\ cosh\ (\gamma_m z) = \sum_{n=1}^{\infty} L'_{n,m}\ sin\ (\beta_n z)$$

(3.3.2.4.22)

where the expressions of $H_{0,m}$, $L_{0,m}$, $H_{n,m}$, $H'_{n,m}$, $L_{n,m}$, $L'_{n,m}$ are reported in the following Subsection. By employing the aforementioned series expansions, the boundary conditions referring to the radial stress at the inner radius, r_i , and expressed by the first equations of (3.3.2.3.1) and (3.3.2.3.1), can be written as follows:

$$A_0\ \nu + \frac{B_0}{r_i^2} + C_0\ (2\nu - 1) + \sum_{m=1}^{\infty} \left(\sigma^e_{rm}\ |_{r=r_i}\ H_{0,m} + \sigma^e_{rmz}\ |_{r=r_i}\ \gamma_m\ L_{0,m} \right) = a_0$$

$$\sigma^e_{rn}\ |_{r=r_i} + \sum_{m=1}^{\infty} \left(\sigma^e_{rm}\ |_{r=r_i}\ H_{n,m} + \sigma^e_{rmz}\ |_{r=r_i}\ \gamma_m\ L_{n,m} \right) = a_n$$

$$-\ \sigma^o_{rn}\ |_{r=r_i} + \sum_{m=1}^{\infty} \left(\sigma^o_{rm}\ |_{r=r_i}\ H'_{n,m} + \sigma^o_{rmz}\ |_{r=r_i}\ \gamma_m\ L'_{n,m} \right) = a'_n$$

(3.3.2.4.23)

In Bariani (1977) a minus sign is missing at the beginning of this last equation. In addition, symbol γ_m appearing in the bracketed expressions of (3.3.2.4.23) is also missing.

The boundary conditions referring to the outer radius, r_e , can be treated in a similar fashion. It is obtained :

$$A_0\,\nu + \frac{B_0}{r_e^2} + C_0\,(2\nu - 1) + \sum_{m=1}^{\infty} \left(\sigma^e_{rm}\,|_{r=re}\;\; H_{0,m} + \sigma^e_{rmz}\,|_{r=re}\;\; \gamma_m\, L_{0,m} \right) = b_0$$

$$\sigma^e_{rn}\,|_{r=re} + \sum_{m=1}^{\infty} \left(\sigma^e_{rm}\,|_{r=re}\;\; H_{n,m} + \sigma^e_{rmz}\,|_{r=re}\;\; \gamma_m\, L_{n,m} \right) = b_n$$

$$- \sigma^o_{rn}\,|_{r=re} + \sum_{m=1}^{\infty} \left(\sigma^o_{rm}\,|_{r=re}\;\; H'_{n,m} + \sigma^o_{rmz}\,|_{r=re}\;\; \gamma_m\, L'_{n,m} \right) = b'_n$$

(3.3.2.4.24)

In Bariani (1977), expression (3.3.2.4.24) is affected by the same mistakes mentioned before with reference to formula (3.3.2.4.23).

The final boundary conditions regard the vanishing of the axial stress, σ_z , at the two end surfaces of the hollow cylinder. In equation (3.3.2.2.11), the argument of the sum in index m can be expressed in a compact way by remembering that, according to the ninth and tenth equations of (3.3.2.4.2), and by considering the last equation of (3.3.2.2.14) :

$$F_m = - E_m \frac{J_1(\gamma_m\, r_i)}{Y_1(\gamma_m\, r_i)}$$

$$F'_m = - E'_m \frac{J_1(\gamma_m\, r_e)}{Y_1(\gamma_m\, r_e)}$$

(3.3.2.4.25)

In addition, from equations (3.3.2.4.14), by accounting from the previous equations, it is obtained :

$$B_m = A_m \frac{F_m}{E_m} = - A_m \frac{J_1 (\gamma_m r_i)}{Y_1 (\gamma_m r_i)}$$

$$B'_m = A'_m \frac{F'_m}{E'_m} = - A'_m \frac{J_1 (\gamma_m r_e)}{Y_1 (\gamma_m r_e)} \qquad (3.3.2.4.26)$$

With these premises, and remembering definition (3.3.2.3.4), the argument of the sum in index m in equation (3.3.2.2.11) becomes, for $z = + h$:

$$T_{0m} (\gamma_m r) \{ - A_m \cosh (\gamma_m h) + E_m [(1-2\nu) \cosh (\gamma_m h) - \gamma_m h \sinh (\gamma_m h)] -$$

$$A'_m \sinh (\gamma_m h) + E'_m [(1-2\nu) \sinh (\gamma_m h) - \gamma_m h \cosh (\gamma_m h)] \} \qquad (3.3.2.4.27)$$

Similarly, for $z = - h$, it is obtained :

$$T_{0m} (\gamma_m r) \{ - A_m \cosh (\gamma_m h) + E_m [(1-2\nu) \cosh (\gamma_m h) - \gamma_m h \sinh (\gamma_m h)] +$$

$$A'_m \sinh (\gamma_m h) - E'_m [(1-2\nu) \sinh (\gamma_m h) - \gamma_m h \cosh (\gamma_m h)] \} \qquad (3.3.2.4.28)$$

In the Bariani (1977) paper, the two expressions (3.3.2.4.27) and (3.3.2.4.28) referring to $z = + h$ and to $z = - h$, respectively, are erroneously made to

coincide.

In equation (3.3.2.2.11), it is convenient to express the argument of the sum in index n in terms of the eigenfunction $T_{0m}\ (\gamma_m\ r)$ defined in (3.3.2.3.4). To this aim, the following series expansions are of use :

$$I_0\ (\alpha_n r) = P_{n,0} + \sum_{m=1}^{\infty} P_{n,m}\ T_{0m}\ (\gamma_m\ r)$$

$$I_0\ (\beta_n r) = P'_{n,\,0} + \sum_{m=1}^{\infty} P'_{n,\,m}\ T_{0m}\ (\gamma_m\ r)$$

$$K_0\ (\alpha_n r) = R_{n,0} + \sum_{m=1}^{\infty} R_{n,m}\ T_{0m}\ (\gamma_m\ r)$$

$$K_0\ (\beta_n r) = R'_{n,\,0} + \sum_{m=1}^{\infty} R'_{n,\,m}\ T_{0m}\ (\gamma_m\ r)$$

$$r\ I_1\ (\alpha_n r) = Q_{n,0} + \sum_{m=1}^{\infty} Q_{n,m}\ T_{0m}\ (\gamma_m\ r)$$

$$r\ I_1\ (\beta_n r) = Q'_{n,\,0} + \sum_{m=1}^{\infty} Q'_{n,\,m}\ T_{0m}\ (\gamma_m\ r)$$

$$r\ K_1\ (\alpha_n r) = S_{n,0} + \sum_{m=1}^{\infty} S_{n,m}\ T_{0m}\ (\gamma_m\ r)$$

$$r\ K_1\ (\beta_n r) = S'_{n,\,0} + \sum_{m=1}^{\infty} S'_{n,\,m}\ T_{0m}\ (\gamma_m\ r)$$

(3.3.2.4.29)

where, as already expressed in formula (3.3.2.3.4) :

$$T_{0m}(\gamma_m r) = J_0(\gamma_m r) - \frac{J_1(\gamma_m r_i)}{Y_1(\gamma_m r_i)} Y_0(\gamma_m r)$$

(3.3.2.4.30)

With regard to these expansions, the Bariani (1983a) paper is followed, in which more proper series expansions of Bessel functions (Spiegel (1968)) than those of Shibahara and Oda (1968) and of Bariani (1977) are proposed. The expressions of the series coefficients of (3.3.2.4.29) are reported in the following Subsection.

For $z = +h$, the boundary condition on σ_z of (3.3.2.3.3) must be confronted with equation (3.3.2.2.11) expressed, as previously discussed, via eigenfunction T_{om}. The new expression of (3.3.2.2.11) thus becomes :

$$\sigma_z(r,+h) = A_0(1-\nu) + 2(2-\nu)C_0 +$$

$$\sum_{n=1}^{\infty}(-1)^n \{ A_n P_{n,0} + B_n [2(2-\nu) P_{n,0} + \alpha_n Q_{n,0}] +$$

$$C_n R_{n,0} - D_n [2(2-\nu) R_{n,0} - \alpha_n S_{n,0}] +$$

$$A'_n P'_{n,0} + B'_n [2(2-\nu) P'_{n,0} + \beta_n Q'_{n,0}] +$$

$$C'_n R'_{n,0} - D'_n [2(2-\nu) R'_{n,0} - \beta_n S'_{n,0}] +$$

$$\sum_{m=1}^{\infty} T_{0m}(\gamma_m r) \left\{ \sum_{n=1}^{\infty} (-1)^n \{ A_n P_{n,m} + B_n [2(2-\nu) P_{n,m} + \alpha_n Q_{n,m}] + \right.$$

$$C_n R_{n,m} - D_n [2(2-\nu) R_{n,m} - \alpha_n S_{n,m}] +$$

$$A'_n P'_{n,m} + B'_n [2(2-\nu) P'_{n,m} + \beta_n Q'_{n,m}] +$$

$$\left. C'_n R'_{n,m} - D'_n [2(2-\nu) R'_{n,m} - \beta_n S'_{n,m}] \right\} -$$

$$A_m \cosh(\gamma_m h) + E_m [(1 - 2\nu)\cosh(\gamma_m h) - \gamma_m h \sinh(\gamma_m h)] -$$

$$A'_m \sinh(\gamma_m h) + E'_m [(1 - 2\nu)\sinh(\gamma_m h) - \gamma_m h \cosh(\gamma_m h)] \Big\}$$

(3.3.2.4.31)

Similarly, for $z = -h$ the new expression of (3.3.2.2.11) becomes :

$$\sigma_z(r,-h) = A_0(1-\nu) + 2(2-\nu)C_0 +$$

$$\sum_{n=1}^{\infty} (-1)^n \Big\{ A_n P_{n,0} + B_n [2(2-\nu) P_{n,0} + \alpha_n Q_{n,0}] +$$

$$C_n R_{n,0} - D_n [2(2-\nu) R_{n,0} - \alpha_n S_{n,0}] -$$

$$A'_n P'_{n,0} - B'_n [2(2-\nu) P'_{n,0} + \beta_n Q'_{n,0}] -$$

$$C'_n R'_{n,0} + D'_n [2(2-\nu) R'_{n,0} - \beta_n S'_{n,0}] +$$

$$\sum_{m=1}^{\infty} T_{0m}(\gamma_m r) \Big\{ \sum_{n=1}^{\infty} (-1)^n \Big\{ A_n P_{n,m} + B_n [2(2-\nu) P_{n,m} + \alpha_n Q_{n,m}] +$$

$$C_n R_{n,m} - D_n [2(2-\nu) R_{n,m} - \alpha_n S_{n,m}] -$$

$$A'_n P'_{n,m} - B'_n [2(2-\nu) P'_{n,m} + \beta_n Q'_{n,m}] -$$

$$C'_n R'_{n,m} + D'_n [2(2-\nu) R'_{n,m} - \beta_n S'_{n,m}] \Big\} -$$

$$A_m \cosh(\gamma_m h) + E_m [(1 - 2\nu)\cosh(\gamma_m h) - \gamma_m h \sinh(\gamma_m h)] +$$

$$A'_m \sinh(\gamma_m h) - E'_m [(1 - 2\nu)\sinh(\gamma_m h) - \gamma_m h \cosh(\gamma_m h)] \Big\}$$

(3.3.2.4.32)

By comparing expressions (3.3.2.4.31) and (3.3.2.4.32) with the boundary conditions on σ_z (3.3.2.3.3), the following equations regarding the series coefficients of (3.3.2.3.3) are obtained :

$$A_0 (1 - \nu) + 2 (2 - \nu) C_0 +$$

$$\sum_{n=1}^{\infty} (-1)^n \{ A_n P_{n,0} + B_n [2 (2 - \nu) P_{n,0} + \alpha_n Q_{n,0}] +$$

$$C_n R_{n,0} - D_n [2 (2 - \nu) R_{n,0} - \alpha_n S_{n,0}] +$$

$$A'_n P'_{n,0} + B'_n [2 (2 - \nu) P'_{n,0} + \beta_n Q'_{n,0}] +$$

$$C'_n R'_{n,0} - D'_n [2 (2 - \nu) R'_{n,0} - \beta_n S'_{n,0}] = h_0$$

(3.3.2.4.33)

$$\left\{ \sum_{n=1}^{\infty} (-1)^n \{ A_n P_{n,m} + B_n [2 (2 - \nu) P_{n,m} + \alpha_n Q_{n,m}] + \right.$$

$$C_n R_{n,m} - D_n [2 (2 - \nu) R_{n,m} - \alpha_n S_{n,m}] +$$

$$A'_n P'_{n,m} + B'_n [2 (2 - \nu) P'_{n,m} + \beta_n Q'_{n,m}] +$$

$$\left. C'_n R'_{n,m} - D'_n [2 (2 - \nu) R'_{n,m} - \beta_n S'_{n,m}] \right\} -$$

$$A_m \cosh (\gamma_m h) + E_m [(1 - 2 \nu) \cosh (\gamma_m h) - \gamma_m h \sinh (\gamma_m h)] -$$

$$\left. A'_m \sinh (\gamma_m h) + E'_m [(1 - 2 \nu) \sinh (\gamma_m h) - \gamma_m h \cosh (\gamma_m h)] \right\} = h_m$$

(3.3.2.4.34)

$$A_0 (1 - \nu) + 2 (2 - \nu) C_0 +$$

$$\sum_{n=1}^{\infty} (-1)^n \{ A_n P_{n,0} + B_n [2 (2 - \nu) P_{n,0} + \alpha_n Q_{n,0}] +$$

$$C_n R_{n,0} - D_n [2 (2 - \nu) R_{n,0} - \alpha_n S_{n,0}] -$$

$$A'_n P'_{n,0} - B'_n [2 (2 - \nu) P'_{n,0} + \beta_n Q'_{n,0}] -$$

$$C'_n R'_{n,0} + D'_n [2 (2 - \nu) R'_{n,0} - \beta_n S'_{n,0}] = h'_0$$

(3.3.2.4.35)

$$\left\{ \sum_{n=1}^{\infty} (-1)^n \{ A_n P_{n,m} + B_n [2 (2 - \nu) P_{n,m} + \alpha_n Q_{n,m}] + \right.$$

$$C_n R_{n,m} - D_n [2 (2 - \nu) R_{n,m} - \alpha_n S_{n,m}] -$$

$$A'_n P'_{n,m} - B'_n [2 (2 - \nu) P'_{n,m} + \beta_n Q'_{n,m}] -$$

$$\left. C'_n R'_{n,m} + D'_n [2 (2 - \nu) R'_{n,m} - \beta_n S'_{n,m}] \right\} -$$

$$A_m \cosh (\gamma_m h) + E_m [(1 - 2 \nu) \cosh (\gamma_m h) - \gamma_m h \cdot \sinh (\gamma_m h)] +$$

$$\left. A'_m \sinh (\gamma_m h) - E'_m [(1 - 2 \nu) \sinh (\gamma_m h) - \gamma_m h \cosh (\gamma_m h)] \right\} = h'_m$$

(3.3.2.4.36)

It is convenient to split the even and odd components in conditions (3.3.2.4.33,36). This is achieved by substituting conditions (3.3.2.4.33) and (3.3.2.4.35) with two new expressions, obtained summing and subtracting the previous conditions, respectively. It is obtained :

$$A_0 (1 - \nu) + 2 (2 - \nu) C_0 +$$

$$\sum_{n=1}^{\infty} (-1)^n \left\{ A_n P_{n,0} + B_n [2 (2 - \nu) P_{n,0} + \alpha_n Q_{n,0}] + \right.$$

$$\left. C_n R_{n,0} - D_n [2 (2 - \nu) R_{n,0} - \alpha_n S_{n,0}] \right\} = \frac{(h_0 + h_0')}{2}$$

(3.3.2.4.37)

$$\sum_{n=1}^{\infty} (-1)^n \left\{ A_n' P_{n,0}' + B_n' [2 (2 - \nu) P_{n,0}' + \beta_n Q_{n,0}'] + \right.$$

$$\left. C_n' R_{n,0}' - D_n' [2 (2 - \nu) R_{n,0}' - \beta_n S_{n,0}'] \right\} = \frac{(h_0 - h_0')}{2}$$

(3.3.2.4.38)

Operating similarly on eqns (3.3.2.4.34) and (3.3.2.4.36), the following expressions are obtained :

$$\left\{ \sum_{n=1}^{\infty} (-1)^n \left\{ A_n P_{n,m} + B_n [2 (2 - \nu) P_{n,m} + \alpha_n Q_{n,m}] + \right. \right.$$

$$\left. C_n R_{n,m} - D_n [2 (2 - \nu) R_{n,m} - \alpha_n S_{n,m}] \right\} -$$

$$\left. A_m \cosh (\gamma_m h) + E_m [(1 - 2 \nu) \cosh (\gamma_m h) - \gamma_m h \sinh (\gamma_m h)] \right\} = \frac{(h_m + h_m')}{2}$$

(3.3.2.4.39)

$$\left\{ \sum_{n=1}^{\infty} (-1)^n \left\{ A_n' P_{n,m}' + B_n' [2 (2 - \nu) P_{n,m}' + \beta_n Q_{n,m}'] + \right. \right.$$

$$C'_n\ R'_{n,m} - D'_n\ [\ 2\ (2 - \nu)\ R'_{n,m} - \beta_n\ S'_{n,m}]\ \Big\} -$$

$$A'_m \sinh(\gamma_m h) + E'_m[\ (1 - 2\nu)\ \sinh(\gamma_m h) - \gamma_m h \cosh(\gamma_m h)]\ \Big\} = \frac{(h_m - h'_m)}{2}$$

(3.3.2.4.40)

Now, conditions (3.3.2.4.37) and (3.3.2.4.39) contain only even coefficients, whereas conditions (3.3.2.4.38) and (3.3.2.4.40) include only odd (that is, with apex) coefficients. If no shear strain is imposed along the inner surface of the hollow cylinder, the axial stress applied to the two end surfaces must be self-equilibrated. This implies that h_0 and h'_0, which represent the mean axial stress applied to the top and bottom extremities, respectively, must coincide and, consequently, that the right member in (3.3.2.4.38) vanishes. With regard to the left-hand side member of eqn (3.3.2.4.38), the stresses expressed via the stress function (Section 3.3.2.2) identically satisfy the equilibrium equations. Consequently, they verify them in a global sense too, that is, if no shear stress is applied to the inner surface of the hollow cylinder, the mean of the axial stress along the two end surfaces must be the same. So, the vanishing of both members of eqn (3.3.2.4.38) is naturally satisfied (this becomes obvious in the case of symmetrical loading with respect to the axial direction, when all odd constants endowed with apex vanish) and, therefore, eqn (3.3.2.4.38) does not represent an additional condition. In summary, conditions (3.3.2.4.37), (3.3.2.4.39) and (3.3.2.4.40) describe the boundary conditions with regard to the axial stress component applied to the cylinder extremity faces.

As a final observation, in the Bariani (1977) paper such boundary conditions are expressed in a different way , which does not appear to be correct.

3.3.2.5 Expressions of some series coefficients

This Subsecion reports the expressions of the coefficients of three series expansions, employed in the previous Sections. The boundary condition referring to the radial stress acting at the inner surface of the hollow cylinder, expressed in (3.3.2.3.1) is examined first. The aim is to determine the expressions of coefficients a_0 , a_n and a'_n of (3.3.2.3.1) when a uniform radial stress is imposed along an axial region defined by h_{pl} and h_{pu} (p , l and u stand for "pressure" , "lower" and "upper") (see Fig. 3.3.2.2.1). By applying the usual procedures (Spiegel (1968)), it is obtained :

$$a_0 = \frac{h_{pu} - h_{pl}}{2\,h}$$

$$a_n = \frac{sin\,(\alpha_n\,h_{pu}) - sin\,(\alpha_n\,h_{pl})}{n\,\pi}$$

$$a'_n = \frac{2\,[-\,cos\,(\beta_n\,h_{pu}) + cos\,(\beta_n\,h_{pl})\,]}{\pi\,(2\,n - 1)} \qquad (3.3.2.5.1)$$

It is known that the convergence of the Fourier series in mimicking a step function is slow. In addition, spurious undulations affect the series expansion. A practically relevant improvement of the convergence rate as well as a reduction of the undesired oscillations can be achieved resorting to the so called "Lanczos σ factor" (Lanczos (1964),(1966), Scheid (1968)), which constitutes an original contribution given by the writer with respect to Bariani (1977). The original series is smoothed by substituting its local value with an average computed on a proper period. So doing, the so called "Gibbs" oscillations are attenuated (that is, the convergence rate is improved), at the cost of a somewhat less steep ascent at the extremities of a square wave. This is numerically proved in Subsection 3.3.2.7 . From an applied viewpoint, if index n in (3.3.2.3.1) related to the radial stress

component runs from 1 to, say, k, then coefficients a_n and a'_n must be multiplied by the following factor :

$$\frac{\sin\left(\frac{\pi\, n}{k+1}\right)}{\frac{\pi\, n}{k+1}} \qquad (3.3.2.5.2)$$

The series expansions (3.3.2.4.22), expressing hyperbolic functions in terms of trigonometric functions, are now considered. Coefficients $H_{0,m}$, $L_{0,m}$, $H_{n,m}$, $H'_{n,m}$, $L_{n,m}$, $L'_{n,m}$ are to be defined. By exploiting, as usual, the orthogonality conditions of the trigonometric functions, the following expressions for $H_{0,m}$, $L_{0,m}$, $H_{n,m}$, $H'_{n,m}$, $L_{n,m}$, $L'_{n,m}$ are obtained :

$$H_{0,m} = \frac{1}{2h}\int_{-h}^{h} \cosh(\gamma_m z)\, dz = \frac{\sinh(\gamma_m h)}{\gamma_m h}$$

$$L_{0,m} = \frac{1}{2h}\int_{-h}^{h} z\, \sinh(\gamma_m z)\, dz = \frac{\gamma_m h \cosh(\gamma_m h) - \sinh(\gamma_m h)}{\gamma_m^2 h}$$

$$H_{n,m} = \frac{1}{h}\int_{-h}^{h} \cosh(\gamma_m z)\cos\left(\frac{n\pi}{h} z\right) dz = (-1)^n \frac{2h}{\pi^2}\,\frac{\gamma_m \sinh(\gamma_m h)}{\left(\frac{\gamma_m h}{\pi}\right)^2 + n^2}$$

$$H'_{n,m} = \frac{1}{h}\int_{-h}^{h} \sinh(\gamma_m z)\sin\left(\frac{(2n-1)\pi}{2h} z\right) dz = -(-1)^n \frac{2h}{\pi^2}\,\frac{\gamma_m \cosh(\gamma_m h)}{\left(\frac{\gamma_m h}{\pi}\right)^2 + \left(\frac{2n-1}{2}\right)^2}$$

$$L_{n,m} = \frac{1}{h}\int_{-h}^{h} z\, \sinh(\gamma_m z)\cos\left(\frac{n\pi}{h} z\right) dz =$$

$$(-1)^n \frac{2h^2}{\pi^2}\,\frac{\gamma_m \cosh(\gamma_m h)}{\left(\frac{\gamma_m h}{\pi}\right)^2 + n^2} - (-1)^n \frac{2h}{\pi^2}\,\frac{\left[\left(\frac{\gamma_m h}{\pi}\right)^2 - n^2\right]\sinh(\gamma_m h)}{\left[\left(\frac{\gamma_m h}{\pi}\right)^2 + n^2\right]^2}$$

$$L'_{n,m} = \frac{1}{h} \int_{-h}^{h} z \cosh(\gamma_m z) \sin\left(\frac{(2n-1)\pi}{2h} z\right) dz =$$

$$-(-1)^n \frac{2h^2}{\pi^2} \frac{\gamma_m \sinh(\gamma_m h)}{\left(\frac{\gamma_m h}{\pi}\right)^2 + \left(\frac{2n-1}{2}\right)^2} +$$

$$(-1)^n \frac{2h}{\pi^2} \frac{\left[\left(\frac{\gamma_m h}{\pi}\right)^2 - \left(\frac{2n-1}{2}\right)^2\right] \cosh(\gamma_m h)}{\left[\left(\frac{\gamma_m h}{\pi}\right)^2 + \left(\frac{2n-1}{2}\right)^2\right]^2}$$

(3.3.2.5.3)

These coefficients too can be modified according to the Lanczos σ factor, by employing the same correction factor of (3.3.2.5.2).

The last coefficients to be examined are those of (3.3.2.4.30), in which the Bessel functions I_0 , K_0 , I_1 , K_1 are expanded in terms of the eigenfunction T_{0m} , defined in (3.3.2.3.4). The coefficients to be computed are $P_{n,0}$, $P'_{n,0}$, $R_{n,0}$, $R'_{n,0}$, $Q_{n,0}$, $Q'_{n,0}$, $S_{n,0}$, $S'_{n,0}$, $P_{n,m}$, $P'_{n,m}$, $R_{n,m}$, $R'_{n,m}$, $Q_{n,m}$, $Q'_{n,m}$, $S_{n,m}$, $S'_{n,m}$.

The computations which bring to the expressions of these coefficients are reported in the sequel. They follow the exposition of Bariani (1983a), with some corrections. The orthogonality properties exploited here are treated by Wylie (1975), p. 421 . The main point is that $\frac{d}{dr} T_{0m}(\gamma_m r)$ vanishes for both $r = r_i$ and $r = r_e$, according to (3.3.2.4.5). It is obtained :

$$P_{n,0} \frac{(r_e^2 - r_i^2)}{2} = \int_{r_i}^{r_e} r I_0(\alpha_n r) dr = \frac{1}{\alpha_n} [r_e I_1(\alpha_n r_e) - r_i I_1(\alpha_n r_i)]$$

$$R_{n,0} \frac{(r_e^2 - r_i^2)}{2} = \int_{r_i}^{r_e} r K_0(\alpha_n r) dr = \frac{1}{\alpha_n} [r_i K_1(\alpha_n r_i) - r_e K_1(\alpha_n r_e)]$$

$$Q_{n,0}\,\frac{(r_e^2 - r_i^2)}{2} = \int_{r_i}^{r_e} r^2\, I_1(\alpha_n\, r)\, dr = \frac{1}{\alpha_n}\left[\, r_e^2\, I_2(\alpha_n\, r_e) - r_i^2\, I_2(\alpha_n\, r_i)\,\right]$$

$$S_{n,0}\,\frac{(r_e^2 - r_i^2)}{2} = \int_{r_i}^{r_e} r^2\, K_1(\alpha_n\, r)\, dr = \frac{1}{\alpha_n}\left[r_i^2\, K_2(\alpha_n\, r_i) - r_e^2\, I_2(\alpha_n\, r_e)\,\right]$$

(3.3.2.5.4)

It is observed that the left-hand members in Bariani (1983a) paper are incorrect.

$$P_{n,m}\, N_m = \int_{r_i}^{r_e} r\, I_0(\alpha_n\, r)\, T_{0m}(\gamma_m\, r)\, dr =$$

$$\frac{\alpha_n}{\alpha_n^2 + \gamma_m^2}\left\{\, r_e\, I_1(\alpha_n\, r_e)\, T_{0m}(\gamma_m\, r_e) - r_i\, I_1(\alpha_n\, r_i)\, T_{0m}(\gamma_m\, r_i)\right\}$$

$$Q_{n,m}\, N_m = \int_{r_i}^{r_e} r^2\, I_1(\alpha_n\, r)\, T_{0m}(\gamma_m\, r)\, dr =$$

$$\frac{\alpha_n}{\alpha_n^2 + \gamma_m^2}\left\{\, r_e^2\, I_0(\alpha_n\, r_e)\, T_{0m}(\gamma_m\, r_e) - r_i^2\, I_0(\alpha_n\, r_i)\, T_{0m}(\gamma_m\, r_i) -\right.$$

$$\left.\frac{2\,\alpha_n}{\alpha_n^2 + \gamma_m^2}\left[\, r_e\, I_1(\alpha_n\, r_e)\, T_{0m}(\gamma_m\, r_e) - r_i\, I_1(\alpha_n\, r_i)\, T_{0m}(\gamma_m\, r_i)\,\right]\right\}$$

$$R_{n,m}\, N_m = \int_{r_i}^{r_e} r\, K_0(\alpha_n\, r)\, T_{0m}(\gamma_m\, r)\, dr =$$

$$\frac{-\,\alpha_n}{\alpha_n^2 + \gamma_m^2}\left\{\, r_e\, K_1(\alpha_n\, r_e)\, T_{0m}(\gamma_m\, r_e) - r_i\, K_1(\alpha_n\, r_i)\, T_{0m}(\gamma_m\, r_i)\right\}$$

$$S_{n,m}\, N_m = \int_{r_i}^{r_e} r^2\, K_1(\alpha_n\, r)\, T_{0m}(\gamma_m\, r)\, dr =$$

$$\frac{\alpha_n}{\alpha_n^2 + \gamma_m^2}\left\{ - r_e^2\, K_0(\alpha_n\, r_e)\, T_{0m}(\gamma_m\, r_e) + r_i^2\, I_0(\alpha_n\, r_i)\, T_{0m}(\gamma_m\, r_i) + \right.$$

$$\left. \frac{2\,\alpha_n}{\alpha_n^2 + \gamma_m^2}\left[- r_e\, K_1(\alpha_n\, r_e)\, T_{0m}(\gamma_m\, r_e) + r_i\, K_1(\alpha_n\, r_i)\, T_{0m}(\gamma_m\, r_i) \right]\right\}$$

(3.3.2.5.5)

where :

$$N_m = \int_{r_i}^{r_e} r\, T_{0m}^2(\gamma_m\, r)\, dr = \frac{r_e^2}{2}\, T_{0m}^2(\gamma_m\, r_e) - \frac{r_i^2}{2}\, T_{0m}^2(\gamma_m\, r_i)$$

(3.3.2.5.6)

In the Bariani (1983a) paper there are two errors in the exponents of α_n appearing in the expressions regarding $Q_{n,m}$ and $S_{n,m}$, and a sign error affects the expression of $S_{n,m}$. Various results useful for performing the previous integrations are contained in Wheelon (1968) and in Luke (1962). Anyway, integrals referring to $Q_{n,m}\, N_m$ and to $S_{n,m}\, N_m$, given by Bariani (1977), could not be traced in the above books, so that they seem an original contribution, even if similar integral are reported by Lur'e, McVean, and Radok (1964) .

It is now shown that the σ factor can be applied in an approximate, but still effective, way to the series expansion (3.3.2.4.30) . It is first noted that an estimate of eigenvalue γ_m of (3.3.2.4.4) can be obtained by resorting to the following asymptotic expansions (Spiegel (1968)) :

$$J_1(x) \simeq \frac{sin\,(x) - cos\,(x)}{\sqrt{\pi x}}$$

$$Y_1(x) \simeq - \frac{sin\,(x) + cos\,(x)}{\sqrt{\pi x}}$$

(3.3.2.5.7)

Once these approximate expressions are introduced in (3.3.2.4.4), the following estimate for eigenvalue γ_m is derived :

$$\gamma_m \simeq \frac{m\,\pi}{r_e - r_i} \tag{3.3.2.5.8}$$

The asymptotic expression for T_{0m} of (3.3.2.3.4) requires the following additional asymptotic formulae (Spiegel (1968)) :

$$J_0(x) \simeq \frac{sin\,(x) + cos\,(x)}{\sqrt{\pi x}}$$

$$Y_0(x) \simeq -\frac{sin\,(x) - cos\,(x)}{\sqrt{\pi x}} \tag{3.3.2.5.9}$$

By substituting expressions (3.3.2.5.7,9) in (3.3.2.3.4), the following asymptotic expression for T_{0m} is obtained :

$$T_{0m}(\gamma_m r) \simeq \frac{2}{\sqrt{\pi\,\gamma_m\,r}}\;\frac{cos\,(\gamma_m(r_i - r))}{sin\,(\gamma_m r_i) + cos\,(\gamma_m r_i)} \tag{3.3.2.5.10}$$

where expression (3.3.2.5.8) for γ_m should be used in (3.3.2.5.10) . Application of Lanczos σ method would require the integration of (3.3.2.5.10) in dr along a proper period. Such integration cannot be performed in closed form (the analytic expression of the integral of $cos\,(r)/\sqrt{r}$ does not exist), but it can be observed that, for sufficiently high indices m, this period becomes very small and, therefore, $\sqrt{r}$ can be treated as a constant. With these approximations, the series coefficients must be multiplied by the same factor previously determined in (3.3.2.4.29) .

3.3.2.6 Solution method

This Subsection treats the computation of the unknown series coefficients A_0 , B_0 , C_0 , A_n , B_n , C_n , D_n , A'_n , B'_n , C'_n , D'_n , A_m , B_m , E_m , F_m , A'_m , B'_m , E'_m , F'_m, and it constitutes an original contribution to the thick pipe problem. In the Bariani (1977) paper no particular strategy aimed at reducing the number of equations to be solved simultaneously is presented. It is observed that in Subsection 3.3.2.4 all boundary conditions contain only either even (without apex) or odd (with apex) coefficients. Consequently, the even and odd problems can be solved separately. Only the even part is here treated in detail. If indices n and m of (3.3.2.2.6) run from 1 to, say, k, the presence of coefficients A_n , B_n , C_n , D_n , A_m , B_m , E_m , F_m results in a set of eight times k linear equations to be solved. In this Subsection a methodology is developed based upon an internal condensation of the unknowns, which permits the set of equations to be noticeably reduced.

The salient points of the methodology proposed here are briefly summarized first, followed by a detailed description of the corresponding formal developments. By exploiting the boundary conditions, coefficients B_m , E_m and F_m can be expressed as simple functions of A_m . As a consequence, both σ^e_{rm} and σ^e_{rmz} of (3.3.2.2.8) evaluated at the inner and outer radii can be formulated in terms of A_m only and of known coefficients. Coefficients A_n , B_n , C_n , D_n are now examined. It is possible to express C_n and D_n as functions of A_n and B_n by applying proper boundary condition equations. As a consequence, both $\sigma^e_{rn}\,|_{r_i}$ and $\sigma^e_{rn}\,|_{r_e}$ can be arranged in terms of A_n and B_n only. From equations (3.3.2.4.23) and (3.3.2.4.24) the separate expressions of A_n and B_n can be computed in terms of σ^e_{rm} and of σ^e_{rmz} , that is, in terms of A_m . It is now clear that the boundary condition (3.3.2.4.39) can be formulated in terms of constant A_m only, although its extended expression is inevitably complex. The remaining constants are computed by back substitution. With this approach, the number of unknowns is lowered from eight times k down to only k .

The formal developments just touched upon are now re-examined in deeper detail. Constants B_m , E_m and F_m are first expressed as functions of A_m . From (3.3.2.4.14) it is derived :

$$E_m = \frac{A_m}{\delta_m} \tag{3.3.2.6.1}$$

From the ninth and eleventh conditions (3.3.2.4.2), by remembering (3.3.2.2.14) and (3.3.2.4.5), it is obtained :

$$F_m = -\frac{E_m\, J_1(\gamma_m\, r_i)}{Y_1(\gamma_m\, r_i)} = -\frac{E_m\, J_1(\gamma_m\, r_e)}{Y_1(\gamma_m\, r_e)} \tag{3.3.2.6.2}$$

and, therefore, the following result is derived from (3.3.2.6.1) :

$$F_m = -\frac{A_m\, J_1(\gamma_m\, r_i)}{\delta_m\, Y_1(\gamma_m\, r_i)} = -\frac{A_m\, J_1(\gamma_m\, r_e)}{\delta_m\, Y_1(\gamma_m\, r_e)} \tag{3.3.2.6.3}$$

From the second expression of (3.3.2.4.14) and from (3.3.2.6.3) it is attained :

$$B_m = F_m\, \delta_m = -\frac{A_m\, J_1(\gamma_m\, r_i)}{Y_1(\gamma_m\, r_i)} = -\frac{A_m\, J_1(\gamma_m\, r_e)}{Y_1(\gamma_m\, r_e)} \tag{3.3.2.6.4}$$

Formulae (3.3.2.6.1,3,4) collect the expressions of B_m , E_m , F_m as functions of A_m only.

Terms σ^e_{rm} and σ^e_{rmz} of (3.3.2.2.8) computed at the inner and outer radii are now considered, with the aim to express them in terms of A_m only. The following formulae are derived :

$$\sigma^e_{rm}\,|_{r_i} = A_m \left[J_0(\gamma_m r_i) - \frac{J_1(\gamma_m r_i)}{\gamma_m r_i} \right] + B_m \left[Y_0(\gamma_m r_i) - \frac{Y_1(\gamma_m r_i)}{\gamma_m r_i} \right] +$$

$$E_m \left[(1 + 2\nu) J_0(\gamma_m r_i) - \frac{J_1(\gamma_m r_i)}{\gamma_m r_i} \right] + F_m \left[(1 + 2\nu) Y_0(\gamma_m r_i) - \frac{Y_1(\gamma_m r_i)}{\gamma_m r_i} \right] =$$

$$A_m \left[J_0(\gamma_m r_i) - \frac{J_1(\gamma_m r_i)}{\gamma_m r_i} - \frac{J_1(\gamma_m r_i)\, Y_0(\gamma_m r_i)}{Y_1(\gamma_m r_i)} + \frac{J_1(\gamma_m r_i)}{\gamma_m r_i} + \right.$$

$$\left. (1 + 2\nu) \frac{J_0(\gamma_m r_i)}{\delta_m} - \frac{J_1(\gamma_m r_i)}{\delta_m \gamma_m r_i} - (1 + 2\nu) \frac{Y_0(\gamma_m r_i)\, J_1(\gamma_m r_i)}{\delta_m Y_1(\gamma_m r_i)} + \frac{J_1(\gamma_m r_i)}{\delta_m \gamma_m r_i} \right] =$$

$$A_m \left[1 + \frac{(1 + 2\nu)}{\delta_m} \right] \left[J_0(\gamma_m r_i) - \frac{J_1(\gamma_m r_i)\, Y_0(\gamma_m r_i)}{Y_1(\gamma_m r_i)} \right] \qquad (3.3.2.6.5)$$

$$\sigma^e_{rmz}\,|_{r_i} = E_m \left[J_0(\gamma_m r_i) - \frac{J_1(\gamma_m r_i)}{\gamma_m r_i} \right] + F_m \left[Y_0(\gamma_m r_i) - \frac{Y_1(\gamma_m r_i)}{\gamma_m r_i} \right] =$$

$$A_m \left[\frac{J_0(\gamma_m r_i)}{\delta_m} - \frac{J_1(\gamma_m r_i)}{\delta_m \gamma_m r_i} - \frac{J_1(\gamma_m r_i)\, Y_0(\gamma_m r_i)}{\delta_m Y_1(\gamma_m r_i)} + \frac{J_1(\gamma_m r_i)}{\delta_m \gamma_m r_i} \right] =$$

$$\frac{A_m}{\delta_m} \left[J_0(\gamma_m r_i) - \frac{J_1(\gamma_m r_i)\, Y_0(\gamma_m r_i)}{Y_1(\gamma_m r_i)} \right] \qquad (3.3.2.6.6)$$

Similarly, for the outer radius the following expressions are derived :

$$\sigma^e_{rm}\,|_{r_e} = A_m \left[1 + \frac{(1 + 2\nu)}{\delta_m} \right] \left[J_0(\gamma_m r_e) - \frac{J_1(\gamma_m r_e)\, Y_0(\gamma_m r_e)}{Y_1(\gamma_m r_e)} \right] \qquad (3.3.2.6.7)$$

$$\sigma^e_{rmz}\,|_{r_e} = \frac{A_m}{\delta_m} \left[J_0(\gamma_m r_e) - \frac{J_1(\gamma_m r_e)\, Y_0(\gamma_m r_e)}{Y_1(\gamma_m r_e)} \right] \qquad (3.3.2.6.8)$$

Formulae (3.3.2.6.5,8) collect the expressions of σ^e_{rm} and σ^e_{rmz} at the inner and outer radii in terms of A_m only. Compact expressions of these equations can be obtained by introducing constants $C_{A_{mr_i}}$, $C_{A_{mzr_i}}$, $C_{A_{mr_e}}$, $C_{A_{mzr_e}}$, whose meaning is easily identifiable :

$$\sigma^e_{rm}\,|_{r_i} = A_m\, C_{A_{mr_i}}$$

$$\sigma^e_{rmz}\,|_{r_i} = A_m\, C_{A_{mzr_i}}$$

$$\sigma^e_{rm}\,|_{r_e} = A_m\, C_{A_{mr_e}}$$

$$\sigma^e_{rmz}\,|_{r_e} = A_m\, C_{A_{mzr_e}} \qquad (3.3.2.6.9)$$

Coefficients A_n , B_n , C_n , D_n are now considered. From the first and third boundary conditions (3.3.2.4.2), with the help of (3.3.2.2.14), coefficients C_n and D_n can be expressed as functions of A_n and B_n . In fact, such boundary conditions imposed at the inner and outer radii, respectively, can be written, supposing $\tau\,|_{r_i,\,r_e} \equiv 0$ so that s_n of (3.3.2.4.2) are neglected (but the extension to cases where the shear stress does not vanish is simple), as :

$$C_n\, K_1(\alpha_n r_i) - D_n\,[2\,(1-\nu)\,K_1(\alpha_n r_i) - \alpha_n\, r_i\, K_0(\alpha_n r_i)\,]$$

$$= A_n\, I_1(\alpha_n r_i) + B_n\,[\,2\,(1-\nu)\,I_1(\alpha_n r_i) + \alpha_n\, r_i\, I_0(\alpha_n r_i)\,] \qquad (3.3.2.6.10)$$

$$C_n\, K_1(\alpha_n r_e) - D_n\,[2\,(1-\nu)\,K_1(\alpha_n r_e) - \alpha_n\, r_e\, K_0(\alpha_n r_e)\,]$$

$$= A_n\, I_1(\alpha_n r_e) + B_n\,[\,2\,(1-\nu)\,I_1(\alpha_n r_e) + \alpha_n\, r_e\, I_0(\alpha_n r_e)\,]$$

from which the sought for expressions for C_n , D_n can be derived. The determinant Δ of the system of equations (3.3.2.6.10) in the unknowns C_n , D_n is :

$$\Delta = \alpha_n [r_e K_1 (\alpha_n r_i) K_0 (\alpha_n r_e) - r_i K_1 (\alpha_n r_e) K_0 (\alpha_n r_i)] \qquad (3.3.2.6.11)$$

The expressions of C_n and D_n are :

$$C_n = \frac{A_n}{\Delta} \{ I_1 (\alpha_n r_i) [- 2 (1 - \nu) K_1 (\alpha_n r_e) + \alpha_n r_e K_0 (\alpha_n r_e)] -$$

$$I_1 (\alpha_n r_e) [- 2 (1 - \nu) K_1 (\alpha_n r_i) + \alpha_n r_i K_0 (\alpha_n r_i)] \} +$$

$$\frac{B_n}{\Delta} \{ [2 (1 - \nu) I_1 (\alpha_n r_i) + \alpha_n r_i I_0 (\alpha_n r_i)] [- 2 (1 - \nu) K_1 (\alpha_n r_e) + \alpha_n r_e K_0 (\alpha_n r_e)] -$$

$$[2 (1 - \nu) I_1 (\alpha_n r_e) + \alpha_n r_e I_0 (\alpha_n r_e)] [- 2 (1 - \nu) K_1 (\alpha_n r_i) + \alpha_n r_i K_0 (\alpha_n r_i)] \}$$

$$D_n = \frac{A_n}{\Delta} \{ K_1 (\alpha_n r_i) I_1 (\alpha_n r_e) - K_1 (\alpha_n r_e) I_1 (\alpha_n r_i) \} +$$

$$\frac{B_n}{\Delta} \{ K_1 (\alpha_n r_i) [2 (1 - \nu) I_1 (\alpha_n r_e) + \alpha_n r_e I_0 (\alpha_n r_e)] -$$

$$K_1 (\alpha_n r_e) [2 (1 - \nu) I_1 (\alpha_n r_i) + \alpha_n r_i I_0 (\alpha_n r_i)] \}$$

(3.3.2.6.12)

Expressions (3.3.2.6.12) are rewritten in compact form as :

$$C_n = A_n\, C_{AC_n} + B_n\, C_{BC_n}$$
$$D_n = A_n\, C_{AD_n} + B_n\, C_{BD_n} \qquad (3.3.2.6.13)$$

where the meaning of constants C_{AC_n} , C_{BC_n} , C_{AD_n} and C_{BD_n} is easily identifiable.

By employing (3.3.2.2.8), both $\sigma^e_{rn}\,|_{r_i}$ and $\sigma^e_{rn}\,|_{r_e}$ can be formulated in terms of a linear combination of A_n and B_n only. The following expressions are obtained :

$$\sigma^e_{rn}\,|_{r_i} = A_n \left\{ - I_0\,(\alpha_n r_i) + \frac{I_1(\alpha_n r_i)}{\alpha_n r_i} - \right.$$

$$\left\{K_0(\alpha_n r_i) + \frac{K_1(\alpha_n r_i)}{\alpha_n r_i}\right\} C_{AC_n} + \left\{(1 - 2\,\nu)\,K_0\,(\alpha_n r_i) - \alpha_n\, r_i\, K_1\,(\alpha_n r_i)\right\} C_{AD_n} \Bigg\} +$$

$$B_n \left\{ - (1 - 2\nu)\, I_0\,(\alpha_n r_i) - \alpha_n r_i\, I_1(\alpha_n r_i) - \left\{ K_0(\alpha_n r_i) + \frac{K_1(\alpha_n r_i)}{\alpha_n r_i} \right\} C_{BC_n} + \right.$$

$$\left\{(1 - 2\,\nu)\,K_0\,(\alpha_n r_i) - \alpha_n\, r_i\, K_1\,(\alpha_n r_i)\right\} C_{BD_n} \Bigg\}$$

(3.3.2.6.14)

$$\sigma^{e}_{rn}\,|_{r_e} = A_n \left\{ - I_0\,(\alpha_n r_e) + \frac{I_1(\alpha_n r_e)}{\alpha_n r_e} - \right.$$

$$\left\{K_0(\alpha_n r_e) + \frac{K_1(\alpha_n r_e)}{\alpha_n r_e}\right\} C_{AC_n} + \left\{(1 - 2\,\nu)\,K_0\,(\alpha_n r_e) - \alpha_n\, r_e\, K_1\,(\alpha_n r_e)\right\} C_{AD_n} \Bigg\} +$$

$$B_n \left\{ - (1 - 2\nu)\,I_0\,(\alpha_n r_e) - \alpha_n r_e\, I_1(\alpha_n r_e) - \left\{K_0(\alpha_n r_e) + \frac{K_1(\alpha_n r_e)}{\alpha_n r_e}\right\} C_{BC_n} \right. +$$

$$\left\{(1 - 2\,\nu)\,K_0\,(\alpha_n r_e) - \alpha_n\, r_e\, K_1\,(\alpha_n r_e)\right\} C_{BD_n} \Bigg\}$$

(3.3.2.6.15)

The previous expressions (3.3.2.6.14) and (3.3.2.6.15) are written in a more compact form as follows :

$$\sigma^{e}_{rn}\,|_{r_i} = A_n\, C_{Anr_i} + B_n\, C_{Bnr_i}$$

$$\sigma^{e}_{rn}\,|_{r_e} = A_n\, C_{Anr_e} + B_n\, C_{Bnr_e} \qquad \text{(3.3.2.6.16)}$$

where the meaning of constants C_{Anr_i} , C_{Bnr_i}, C_{Anr_e}, C_{Bnr_e} is easily identifiable from (3.3.2.6.14) and (3.3.2.6.15).

The next step is to obtain the separate expressions of A_n and B_n in terms of σ^{e}_{rm} and of σ^{e}_{rmz} , that is, of A_m . From equations (3.3.2.4.23), (3.3.2.4.24) and (3.3.2.6.16) it is derived :

$$\sigma^e_{rn}\,|_{r_i} = A_n\,C_{Anr_i} + B_n\,C_{Bnr_i} = a_n - \sum_{m=1}^{\infty}\,(\,\sigma^e_{rm}\,|_{r_i}\;H_{n,m} + \sigma^e_{rmz}\,|_{r_i}\;\gamma_m\,L_{n,m}\,)$$

(3.3.2.6.17)

$$\sigma^e_{rn}\,|_{r_e} = A_n\,C_{Anr_e} + B_n\,C_{Bnr_e} = b_n - \sum_{m=1}^{\infty}\,(\,\sigma^e_{rm}\,|_{r_e}\;H_{n,m} + \sigma^e_{rmz}\,|_{r_e}\;\gamma_m\,L_{n,m}\,)$$

where $\sigma^e_{rm}\,|_{r_i}$, $\sigma^e_{rmz}\,|_{r_i}$, $\sigma^e_{rm}\,|_{r_e}$ and $\sigma^e_{rmz}\,|_{r_e}$ can be expressed in terms of constant A_m only, according to equations (3.3.2.6.9). The set (3.3.2.6.17) of two equations in the unknowns A_n and B_n is solved to produce the following expressions for A_n and B_n :

$$A_n = \Big\{\,a_n - \sum_{m=1}^{\infty}\,A_m\,(\,C_{Amr_i}\;H_{n,m} + C_{Amzr_i}\;\gamma_m\,L_{n,m}\,)\,\Big\}\,\frac{C_{Bnr_e}}{\Lambda} -$$

$$\Big\{\,b_n - \sum_{m=1}^{\infty}\,A_m\,(\,C_{Amr_e}\,H_{n,m} + A_m\,C_{Amzr_e}\;\gamma_m\,L_{n,m}\,)\,\Big\}\,\frac{C_{Bnr_i}}{\Lambda}$$

$$B_n = \Big\{\,b_n - \sum_{m=1}^{\infty}\,A_m\,(\,C_{Amr_e}\,H_{n,m} + A_m\,C_{Amzr_e}\;\gamma_m\,L_{n,m}\,)\,\Big\}\,\frac{C_{Anr_i}}{\Lambda} -$$

$$\Big\{\,a_n - \sum_{m=1}^{\infty}\,(\,A_m\,C_{Amr_i}\;H_{n,m} + A_m\,C_{Amzr_i}\;\gamma_m\,L_{n,m}\,)\,\Big\}\,\frac{C_{Anr_e}}{\Lambda}$$

(3.3.2.6.18)

where determinant Λ of system (3.3.2.6.17) possesses the following expression :

$$\Lambda = C_{Anr_i}\,C_{Bnr_e} - C_{Anr_e}\,C_{Bnr_i} \qquad (3.3.2.6.19)$$

In conclusion, formulae (3.3.2.6.18) separately express coefficients A_n and B_n as functions of A_m only.

The boundary condition (3.3.2.4.39) are now treated, which expresses the vanishing of the axial stress component at the cylinder end faces. For the sake of clarity, this equation is rewritten here without modification.

$$\left\{ \sum_{n=1}^{\infty} (-1)^n \left\{ A_n P_{n,m} + B_n \left[2(2-\nu) P_{n,m} + \alpha_n Q_{n,m} \right] + C_n R_{n,m} - D_n \left[2(2-\nu) R_{n,m} - \alpha_n S_{n,m} \right] \right\} - A_m \cosh(\gamma_m h) + E_m \left[(1-2\nu)\cosh(\gamma_m h) - \gamma_m h \sinh(\gamma_m h) \right] \right\} = \frac{(h_m + h'_m)}{2}$$

(3.3.2.6.20)

This equation can be formulated in terms of A_m only. In fact, by employing formulae (3.3.2.6.12), coefficients C_n and D_n are expressed in terms of A_n and B_n . With the help of (3.3.2.6.18), coefficients A_n and B_n are then formulated in terms of A_m only. Finally, coefficient E_m is defined via A_m with the help of (3.3.2.6.1) . The boundary condition (3.3.2.6.20) thus becomes :

$$\sum_{n=1}^{\infty} (-1)^n \left\{ \left[\left\{ a_n - \sum_{m=1}^{\infty} A_m \left(C_{A_{mr_i}} H_{n,m} + C_{A_{mzr_i}} \gamma_m L_{n,m} \right) \right\} \frac{C_{B_{nre}}}{\Lambda} - \left\{ b_n - \sum_{m=1}^{\infty} A_m \left(C_{A_{mre}} H_{n,m} + C_{A_{mzre}} \gamma_m L_{n,m} \right) \right\} \frac{C_{B_{nr_i}}}{\Lambda} \right] \left[P_{n,j} + C_{AC_n} R_{n,j} - C_{AD_n} \left[2(2-\nu) R_{n,j} - \alpha_n S_{n,j} \right] \right] + \left[\left\{ b_n - \sum_{m=1}^{\infty} A_m \left(C_{A_{mre}} H_{n,m} + C_{A_{mzre}} \gamma_m L_{n,m} \right) \right\} \frac{C_{A_{nr_i}}}{\Lambda} - \right.$$

$$\left\{ a_n - \sum_{m=1}^{\infty} \left(A_m C_{Amr_i} H_{n,m} + C_{Amzr_i} \gamma_m L_{n,m} \right) \right\} \frac{C_{Anre}}{\Lambda} \Bigg]$$

$$\left\{ \left[2 (2 - \nu) P_{n,j} + \alpha_n Q_{n,j} \right] + C_{BC_n} R_{n,j} - C_{BD_n} \left[2 (2 - \nu) R_{n,j} - \alpha_n S_{n,j} \right] \right\} -$$

$$A_j \left\{ \cosh (\gamma_j h) + \frac{\left[(1 - 2\nu) \cosh (\gamma_j h) - \gamma_j h \sinh (\gamma_j h) \right]}{\delta_j} \right\} = \frac{(h_j + h'_j)}{2}$$

(3.3.2.6.21)

Three indices appear in expressions (3.3.2.6.21), namely j , m , n . If equations (3.3.2.6.21) are described via a matrix approach, j is the column index, m is the row index, while n is an internal loop index. When programming this equation, it is useful to distinguish among known terms, and matrix diagonal terms and off-diagonal terms to be assembled into a stiffness matrix. The known terms collect a_n and b_n multiplied by the proper coefficients according to (3.3.2.6.21), plus terms in h_j . The diagonal terms in the stiffness matrix are expressed in the last line of (3.3.2.6.21). The remaining terms, related to index m, contain essentially off-diagonal terms (more exactly, they include both diagonal and out-of-diagonal terms). Index n is responsible for a generic stiffness matrix coefficient being obtained as the sum in index n of various terms.

The remaining indexed constants can be computed by back substitution. In particular, coefficients B_m , E_m and F_m are evaluated via (3.3.2.6.1,3,4). Coefficients A_n and B_n can be calculated via (3.3.2.6.18), whereas C_n , D_n are determined via (3.3.2.6.13).

The evaluation of coefficients A_0 , B_0 , C_0 is now considered. The corresponding equations are the first expressions of (3.3.2.4.23) and of (3.3.2.4.24), plus (3.3.2.4.37), which constitute a system of three equations in the unknown coefficients A_0 , B_0 , C_0 .

The odd part of the solution can be treated similarly, and its corresponding equations are not reported here. It is only remembered (see Section 3.3.2.4 , where the case of vanishing shear stresses at the cylinder lateral walls was discussed) that equation (3.3.2.4.38) is identically verified and, therefore, it does not actually impose any restrictions on the coefficients involved. In other words, this equation is not employed in the solution of the odd part problem.

The fact that eqns (3.3.2.4.38) and (3.3.2.4.39) are not linearly independent is valid for any boundary conditions (that is, even for non vanishing shear stresses at the inner and outer surfaces of the hollow cylinder), and is due to the circumstances that a) the system of boundary stresses imposed as boundary conditions must be axially self equilibrated; b) the expressions of the internal stresses in terms of stress functions identically verify the equilibrium equations. In conclusion, between eqns (3.3.2.4.38) and (3.3.2.4.39), only one equation must be used in computing coefficients A_0 , B_0 , C_0 .

The close of this Subsection is dedicated to the numerical evaluation of eigenvalue γ_m . Expression (3.3.2.5.8) supplies a first estimate for γ_m , which is then refined via a standard Newton method. In all calculations, the Bessel functions involved were evaluated numerically via the interpolating formulae reported in Abramowitz and Stegun (1972) .

As an alternative solution method, a relaxation technique was also developed, following the suggestions of Shibahara and Oda (1968), who mention a successive approximation method, even if they do not explain it in detail. Coefficients with index m were put equal to zero, and coefficients with index n were computed. Then, the solution was iterated to compute n indexed coefficients. Alternatively, coefficients with index n were set to zero, to compute subsequently m indexed coefficients. Unfortunately, neither strategy was found to converge and, therefore, this solution approach was abandoned.

3.3.2.7 Numerical validation

Two geometries were studied, for which previous solutions are available. The first case is that of a hollow cylinder having $r_i = 0.4$, $r_e = 1.$, $h = 1.$ (abstract dimensions) , subject to a unit pressure band applied to the tube inner surface and acting between $h_{pu} = 0.5$ and $h_{pl} = 0.$, treated in Bariani (1977) and, therefore, referred to in the following as "Bariani" geometry. The second configuration is defined by $r_i = 0.25$, $r_e = 1.$, $h = 1.$, and is subject to a unit pressure band applied to the pipe inner surface and acting between $h_{pu} = 0.2$ and $h_{pl} = -0.2$, treated in Shibahara and Oda (1968) and hereinafter named "Shibahara" configuration. In both cases, the elastic constants were taken as $E = 1.$, $\nu = 0.3$.

Fig. 3.3.2.7.1 details a convergence study for the Bariani cylinder. The number of series terms adopted (more exactly, the maximum value of $n \equiv m$ index) is indicated along x-axis. When subject to the radial pressure band, its inner surface deforms radially, and the initial volume of the inner pressurized cavity (that is, the volume containing the rubber specimen) increases by an amount (referred to a unit p/E ratio) reported along y-axis. In addition, y-axis includes the axial integral of the radial pressure, to appraise its closeness to the nominally imposed value of 0.5 . This indication permits a tentative extrapolation of the volume change to be forecast, aimed at possibly improving the series convergence rate. If symbols ΔV , ΔV_{appr} , p_{int} , $p_{int,appr}$ indicate the volume change (per unit p/E), the approximate volume change for a certain $n \equiv m$ maximum series index, the axial integral of the radial pressure band and its approximate value for a certain $n \equiv m$ series index, respectively, it can be speculated that the relative error of the volume change approximately equals that of the pressure integral :

$$\frac{\Delta V - \Delta V_{appr}}{\Delta V} \simeq \frac{p_{int} - p_{int,appr}}{p_{int}} \qquad (3.3.2.7.1)$$

from which :

$$\Delta V \simeq \Delta V_{appr} \frac{p_{int}}{p_{int,appr}} \qquad (3.3.2.7.2)$$

This extrapolation too is reported in Fig. 3.3.2.7.1 , but it appears that the convergence towards the final volume change does not substantially improve when referring to the extrapolated volume change series instead of the original one. As a consequence, in the practical applications of Section 2.3.2.8 the volume change was not modified as indicated in (3.3.2.7.2) . Fig. 3.3.2.7.1 also indicates that a maximum index number in the region of 20 is suitable for most applications, since the volume change reaches a stagnation value. (The Bariani (1977) reports data referring to 15 and 17 series terms.) An unexpected, undesired and inexplicable event is the appearance of a spurious undulation in the volume change curve when the series index equals 15 . This wiggle affects the subsequent series terms, which are not well aligned to the series values referring to indices lower than 15 and, therefore, it is not simply a local phenomenon. This oscillation is possibly ascribable to the undulation of the solution, visible in Figs 14 and 15 of the Bariani (1977) paper, or to the errors inherent in the approximations for the Bessel functions as supplied by Abramowitz and Stegun (1972), but it is not clear why this phenomenon becomes dramatic only for a certain series index.

Fig. 3.3.2.7.2 treats the parallel Shibahara case, were the pressure integral equals this time 0.4 . This geometry is not affected by spurious undulations. Also for this case 20 series terms appear to be a felicitous choice.

In the interest of conciseness, no comparison in terms of stress field between the Bariani results and those of this study is presented. In general, the agreement is good but not excellent, where the mismatches are possibly ascribable to the inaccuracies signalled in the Bariani (1977) formulae, which may be interpreted either as misprints or as miscalculations.

A parallel stress analysis performed for the Shibahara case produced similar results. In particular, the agreement with the radial displacements reported in Table 4 of Shibahara and Oda (1968) and referring to 15 series terms is good, a circumstance which is in favour of the correctness of the analysis developed in this thesis. Various Figures are presented in the following which illustrate the smoothing effect of the Lanczos σ factor (see Section 2.3.2.5), by comparing traditional series expansions to their counterparts evaluated according to the Lanczos σ method.

Fig. 3.3.2.7.3 presents the Fourier expansion of a unit pressure band as in the Bariani study for 10, 15 and 20 series terms, and Fig. 3.3.2.7.4 displays its counterpart after the Lanczos smoothing. The Gibbs oscillations are attenuated, at the cost of a less steep ascent at the extremities of the square wave.

Figs 3.3.2.7.5 and 3.3.2.7.6 illustrate the parallel Shibahara case, obtaining similar results. Figs 3.3.2.7.7,8,9, 10,11,12,13,14,15,16,17,18 address four functions containing hyperbolic functions, appearing at the left hand-sides of expressions (3.3.2.4.22) and detailed in the insets, for the first three γ radial eigenvalues (see equation (3.3.2.4.6)) of both the Bariani and Shibahara geometries, and for ten series terms, as functions of the tube axial coordinate, z (see Fig. 3.3.2.2.1). Each Figure contains the exact curves for the four hyperbolic-type functions, together with their Fourier expansions according to expressions (3.3.2.4.22). Such Figures should be mentally grouped in pairs of diagrams, the first referring to a purely Fourier expansion, the second to a Lanczos smoothed version. It emerges that the Lanczos σ method actually reduces the oscillations, at the cost of a decrease of accuracy in the vicinity of $z = +/- 1$, that is, by the tube axial extremities. These border inaccuracies are visible in, *e.g.*, Figs 14 and 15 of the Bariani (1977) study, but they should not compromise the solution precision, since they act on tube portions far from the central part, which is of higher interest. The smoothing effect is more appreciable for higher order γ radial eigenvalues.

The following Figures refer only to the Bariani geometry. Figs 3.3.2.7.7,19,20,21,22,23,24,25,26,27,28,29,30 address four functions containing Bessel functions, figuring at the left hand-sides of expressions (3.3.2.4.29) and detailed in the insets, for the first three α axial eigenvalues (see formulae (3.3.2.4.8)) and for ten series terms, as functions of the tube radial coordinate, r (see Fig. 3.3.2.2.1). Each Figure includes the exact curve for the four Bessel-type functions, together with their expansions according to expressions (3.3.2.4.29). These Figures too should be ideally arranged in pairs of diagrams, the first addressing a non-smoothed expansion, the second its Lanczos smoothed counterpart. As for the hyperbolic functions, the Lanczos σ method placates the oscillations, again at the cost of a precision decline in the vicinity of r_i and r_e . Similar to the hyperbolic functions, the smoothing effect is more noticeable for higher order α axial eigenvalues.

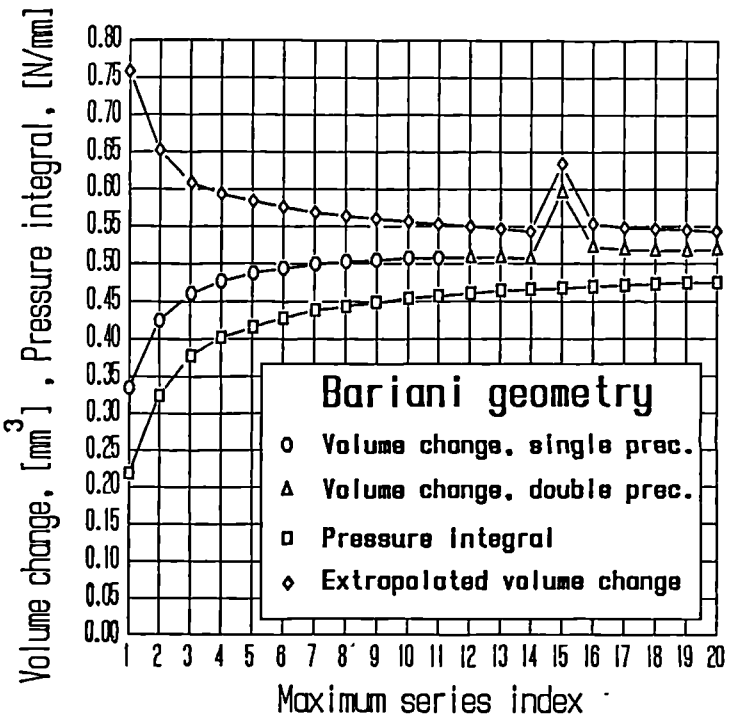

Fig. 3.3.2.7.1 : The volume change and the pressure integral as functions of the number of series terms, for the Bariani geometry.

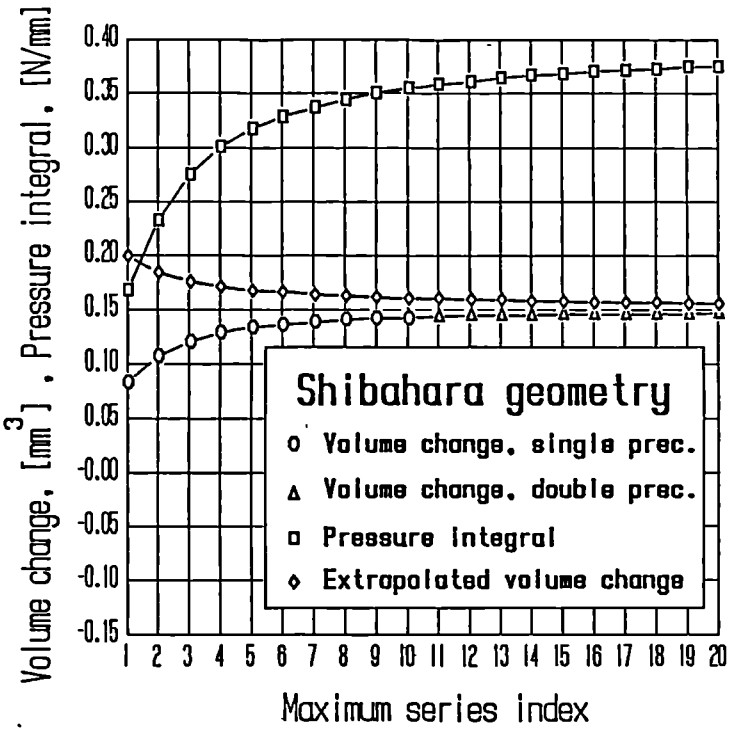

Fig. 3.3.2.7.2 : The volume change and the pressure integral as functions of the number of series terms, for the Shibahara geometry.

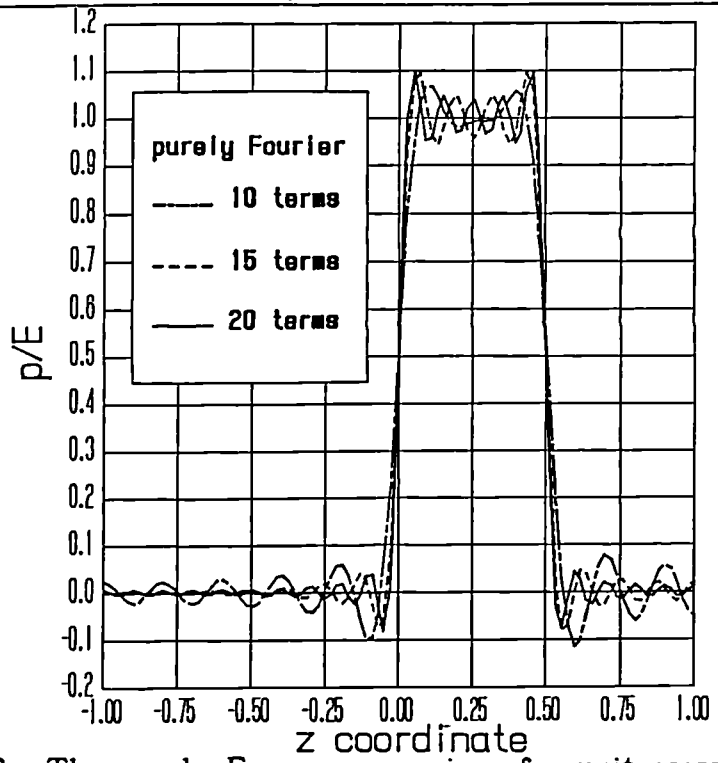

Fig. 3.3.2.7.3 : The purely Fourier expansion of a unit pressure band for 10, 15 and 20 series terms, for the Bariani case.

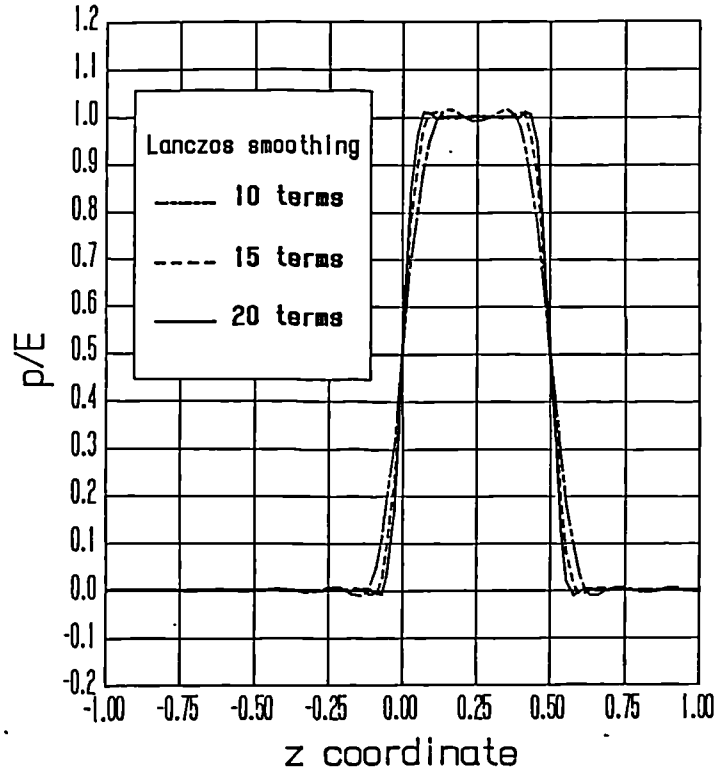

Fig. 3.3.2.7.4 : The Fourier expansion of a unit pressure band for 10, 15 and 20 series terms after the Lanczos smoothing, for the Bariani case.

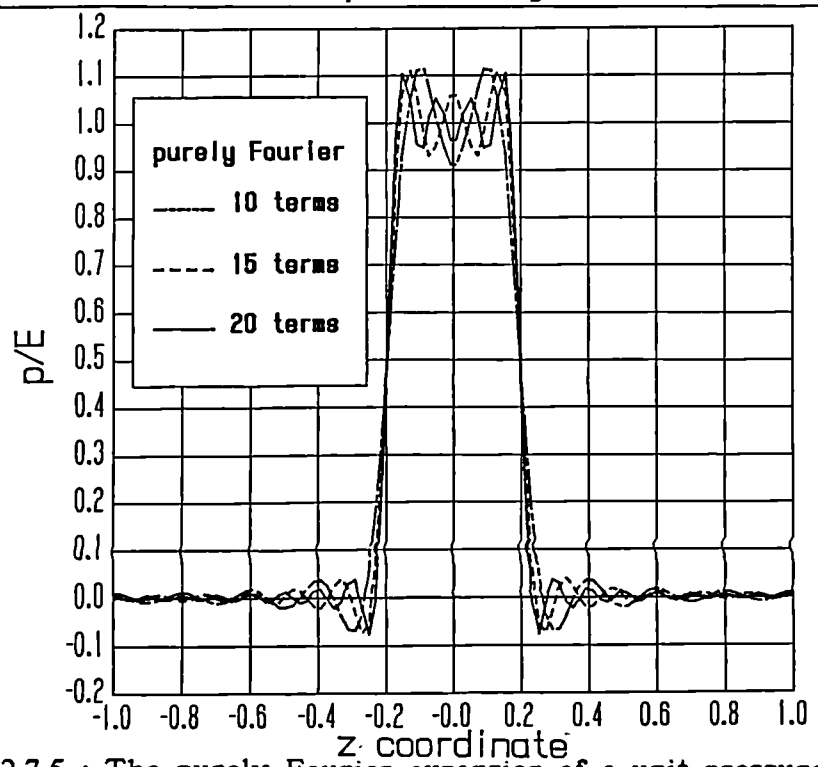

Fig. 3.3.2.7.5 : The purely Fourier expansion of a unit pressure band for 10, 15 and 20 series terms, for the Shibahara case.

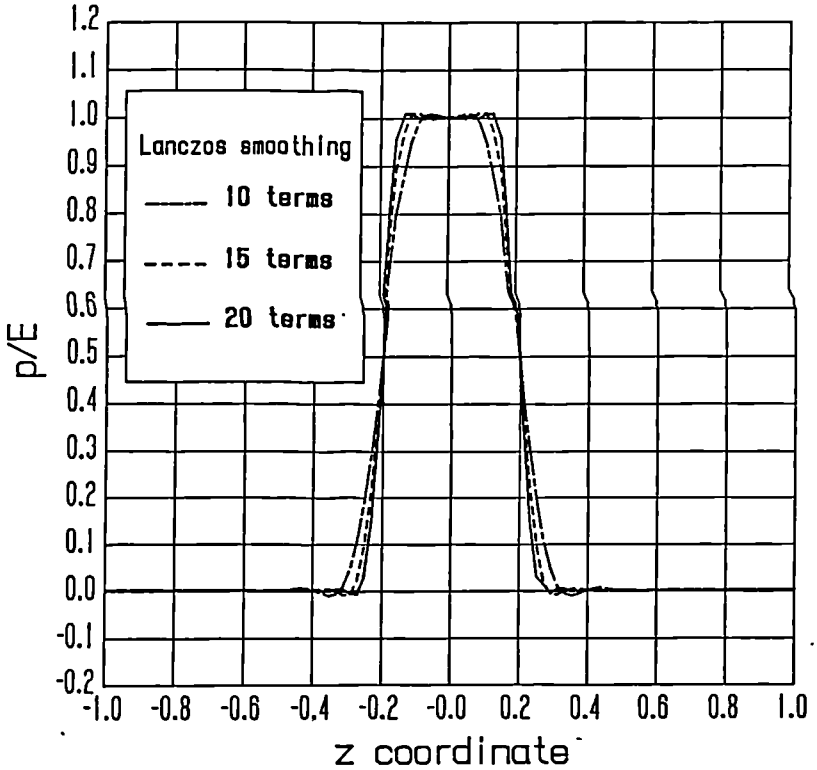

Fig. 3.3.2.7.6 : The Fourier expansion of a unit pressure band for 10, 15 and 20 series terms after the Lanczos smoothing, for the Shibahara case.

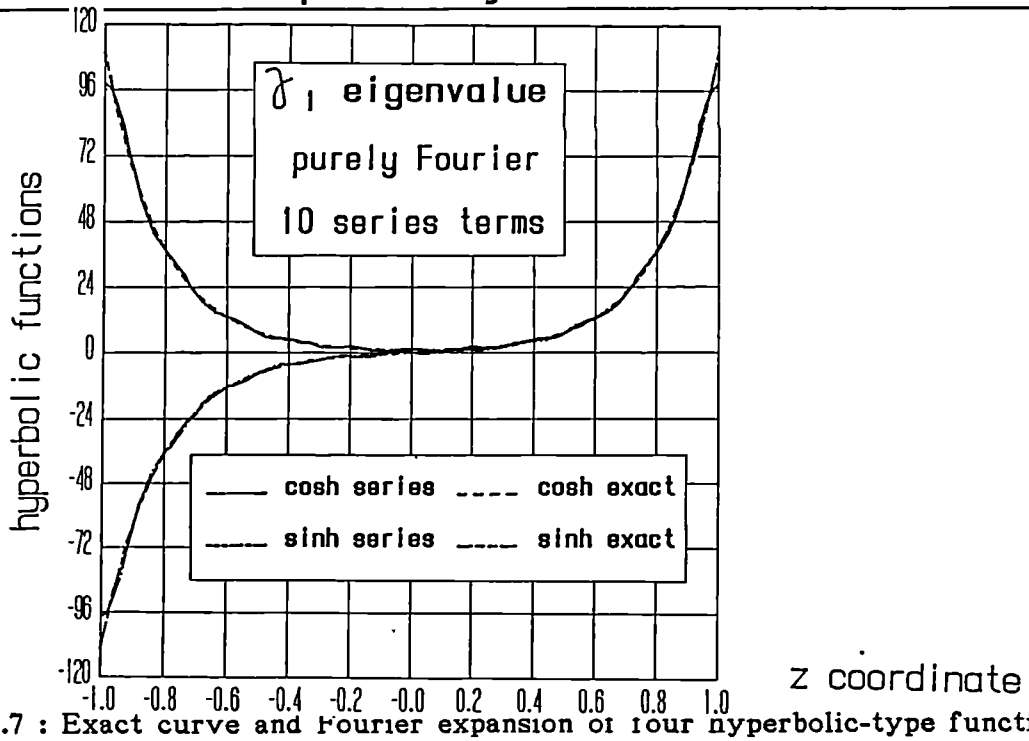

Fig. 3.3.2.7.7 : Exact curve and Fourier expansion of four hyperbolic-type functions detailed in the inset, for the first γ radial eigenvalue of the Bariani geometry and for ten series terms, as functions of the tube axial coordinate, z .

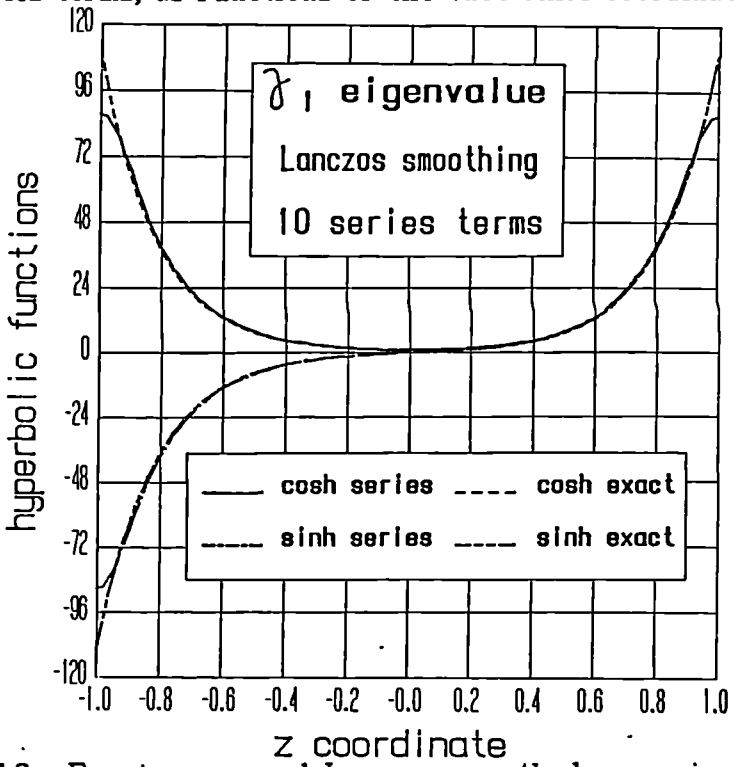

Fig. 3.3.2.7.8 : Exact curve and Lanczos smoothed expansion of four hyperbolic-type functions detailed in the inset, for the first γ radial eigenvalue of the Bariani geometry and for ten series terms, as functions of the tube axial coordinate, z .

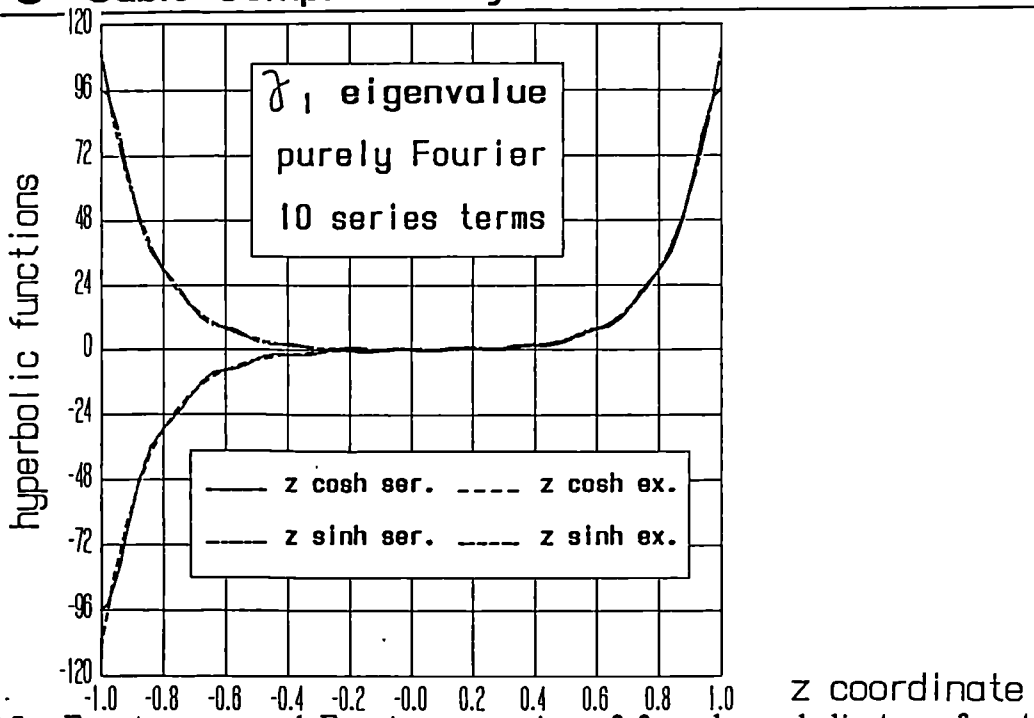

Fig. 3.3.2.7.9 : Exact curve and Fourier expansion of four hyperbolic-type functions detailed in the inset, for the first γ radial eigenvalue of the Shibahara geometry and for ten series terms, as functions of the tube axial coordinate, z .

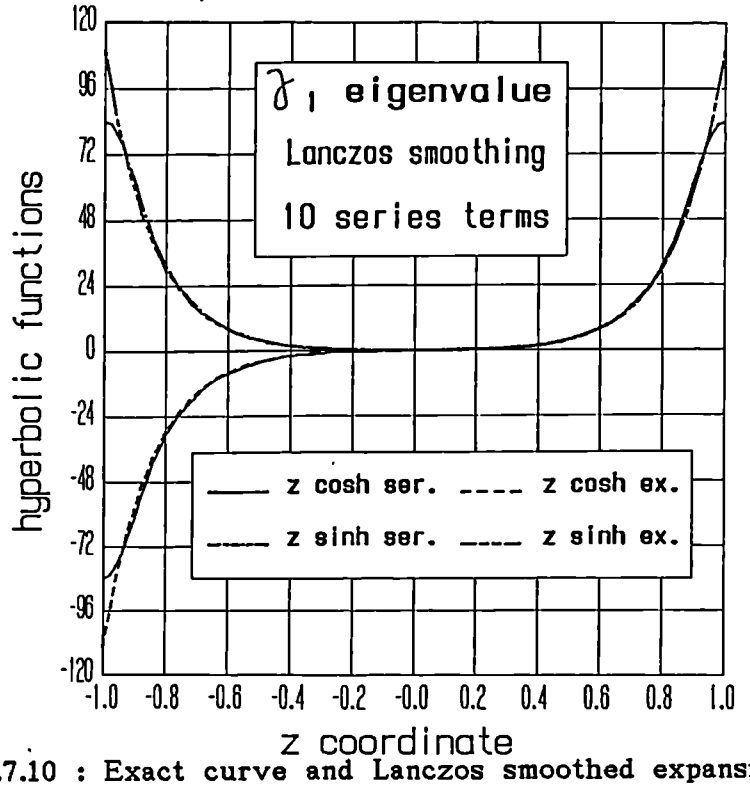

Fig. 3.3.2.7.10 : Exact curve and Lanczos smoothed expansion of four hyperbolic-type functions detailed in the inset, for the first γ radial eigenvalue of the Shibahara geometry and for ten series terms, as functions of the axial coordinate, z .

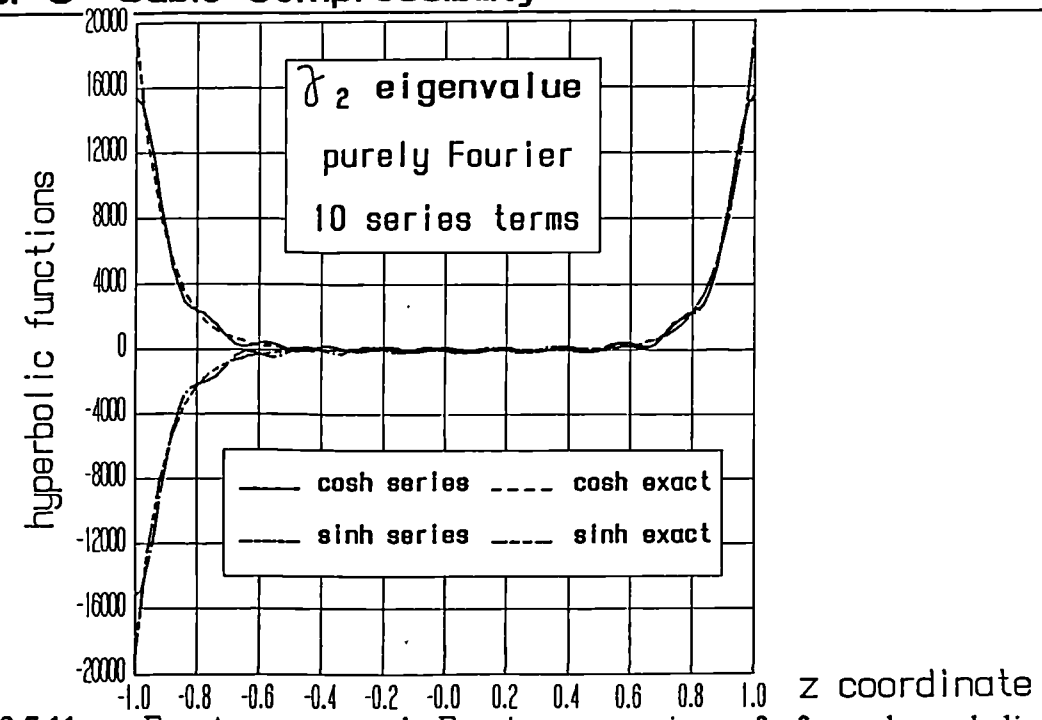

Fig. 3.3.2.7.11 : Exact curve and Fourier expansion of four hyperbolic-type functions detailed in the inset, for the second γ radial eigenvalue of the Bariani geometry and for ten series terms, as functions of the tube axial coordinate, z .

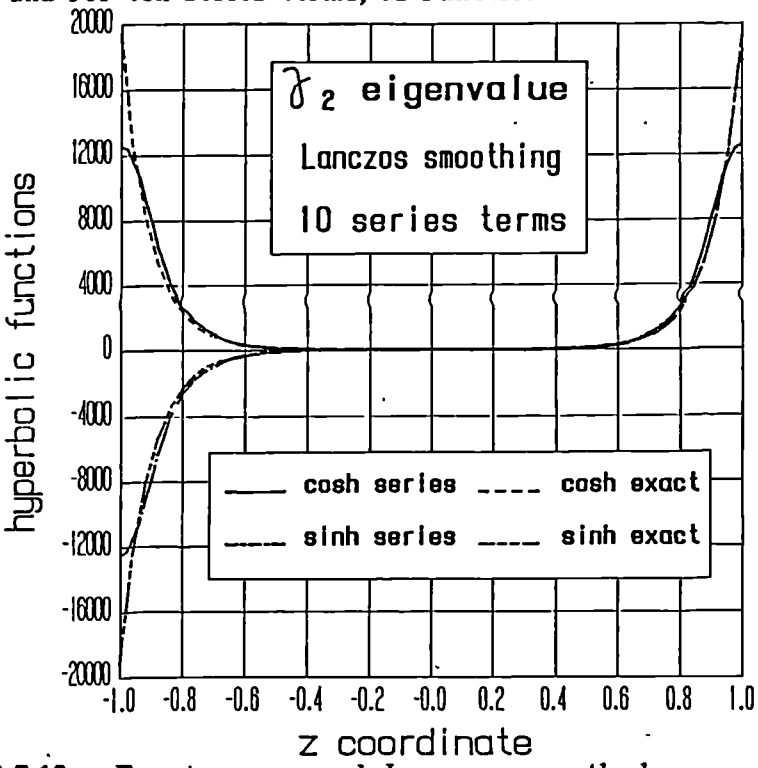

Fig. 3.3.2.7.12 : Exact curve and Lanczos smoothed expansion of four hyperbolic-type functions detailed in the inset, for the second γ radial eigenvalue of the Bariani geometry and for ten series terms, as functions of the axial coordinate, z .

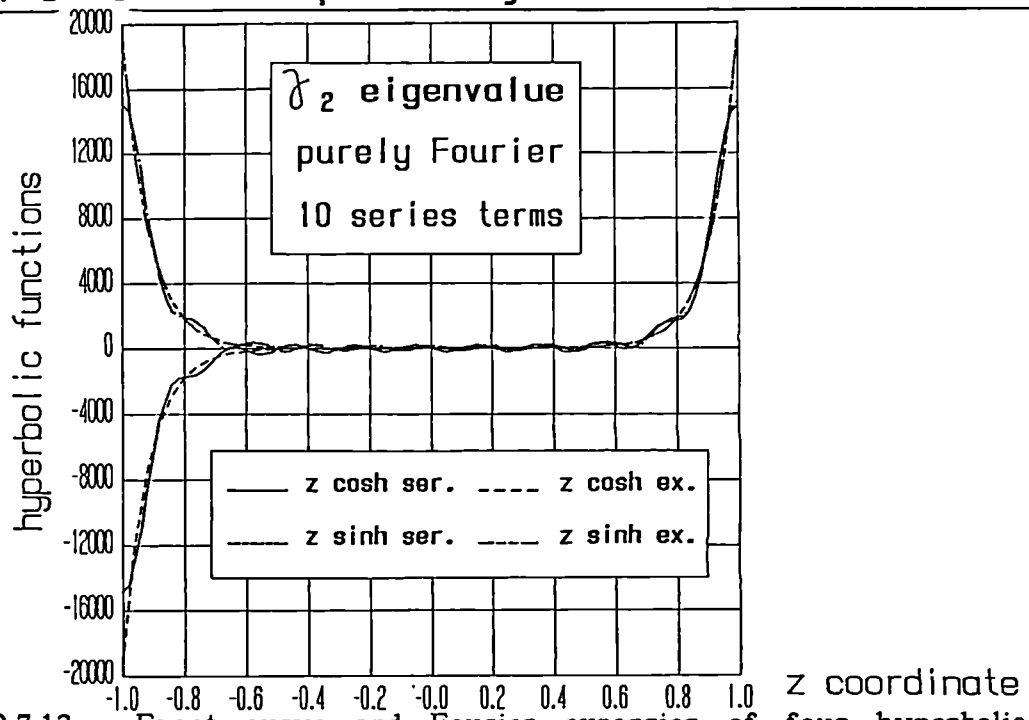

Fig. 3.3.2.7.13 : Exact curve and Fourier expansion of four hyperbolic-type functions detailed in the inset, for the second γ radial eigenvalue of the Shibahara geometry and for ten series terms, as functions of the tube axial coordinate, z .

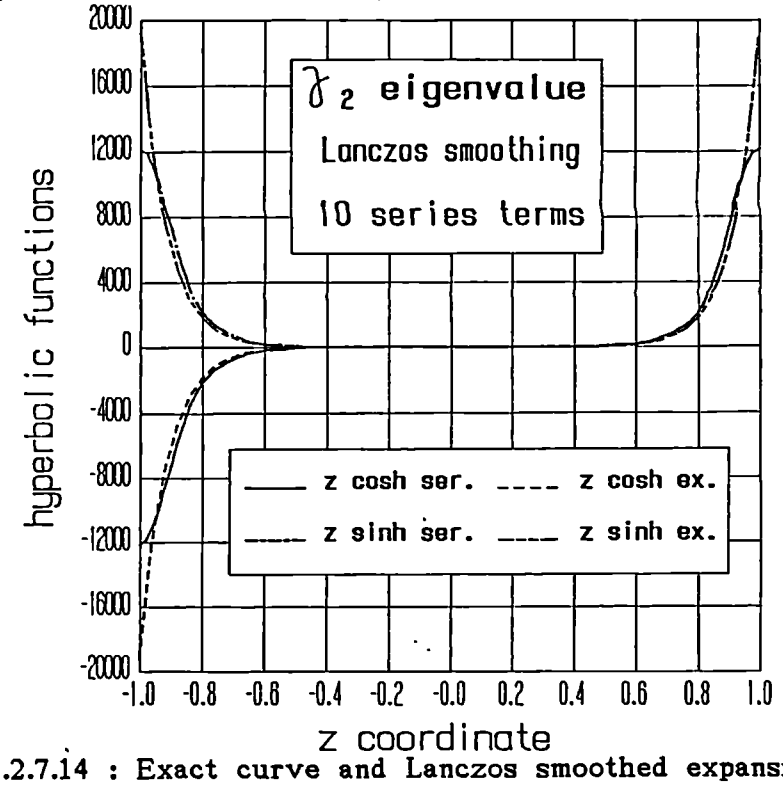

Fig. 3.3.2.7.14 : Exact curve and Lanczos smoothed expansion of four hyperbolic-type functions detailed in the inset, for the second γ radial eigenvalue of the Shibahara geometry and for ten series terms, as functions of the axial coordinate, z .

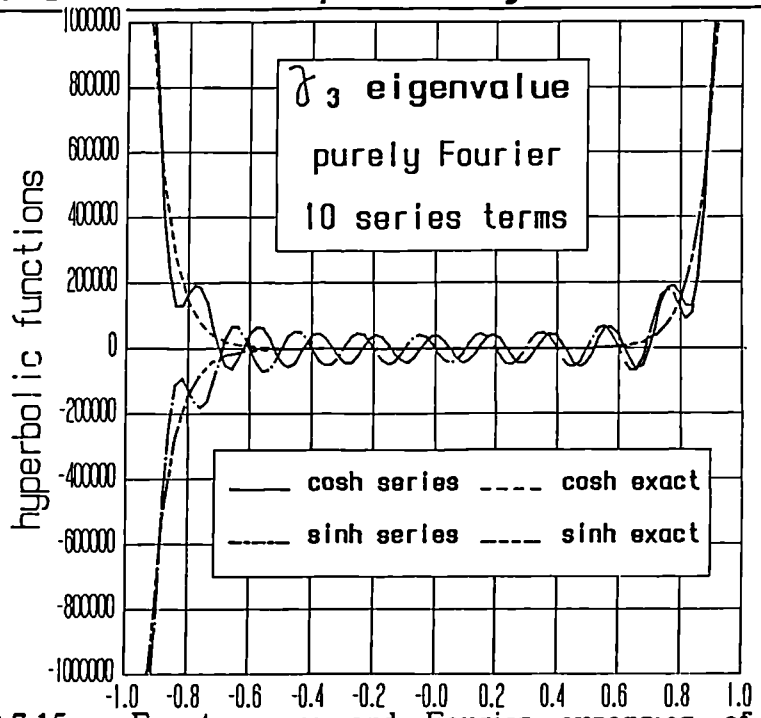

Fig. 3.3.2.7.15 : Exact curve and Fourier expansion of four hyperbolic-type functions detailed in the inset, for the third γ radial eigenvalue of the Bariani geometry and for ten series terms, as functions of the tube axial coordinate, z .

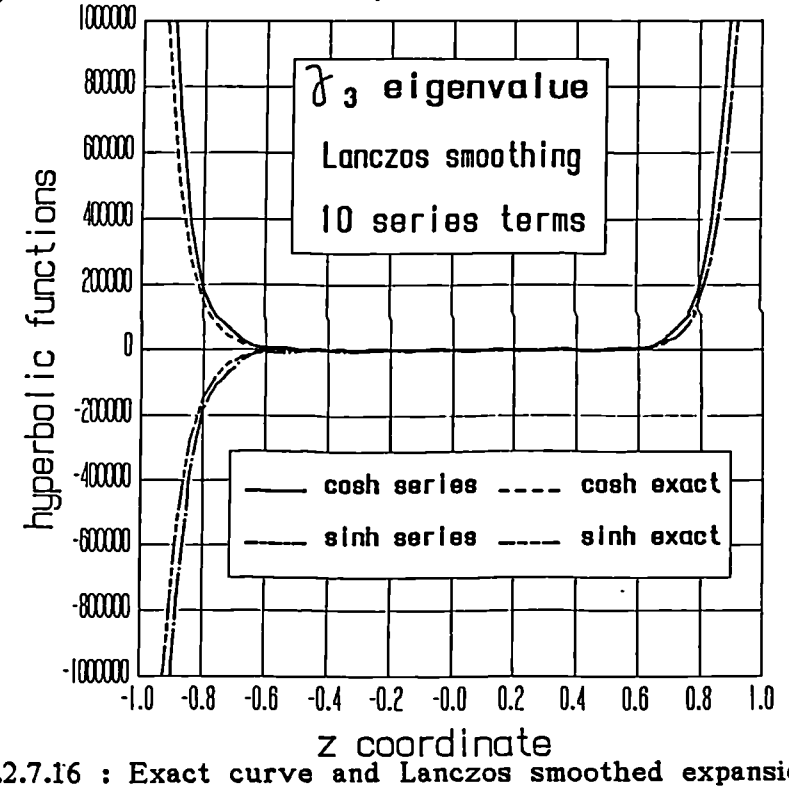

Fig. 3.3.2.7.16 : Exact curve and Lanczos smoothed expansion of four hyperbolic-type functions detailed in the inset, for the third γ radial eigenvalue of the Bariani geometry and for ten series terms, as functions of the tube axial coordinate, z .

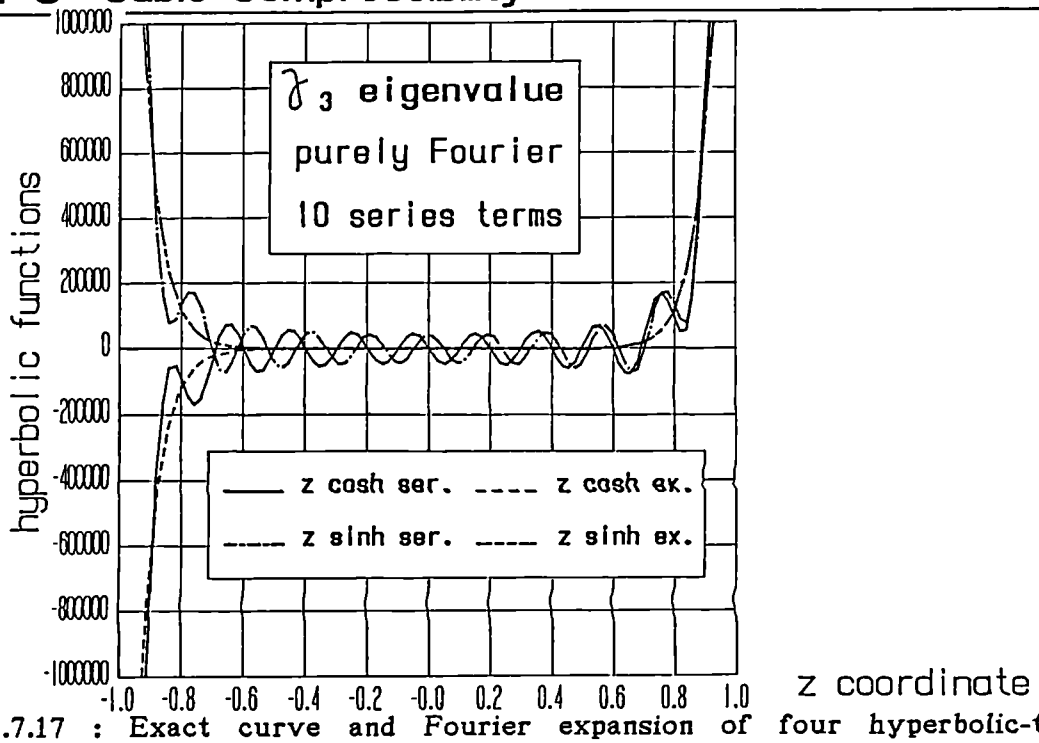

Fig. 3.3.2.7.17 : Exact curve and Fourier expansion of four hyperbolic-type functions detailed in the inset, for the third γ radial eigenvalue of the Shibahara geometry and for ten series terms, as functions of the tube axial coordinate, z .

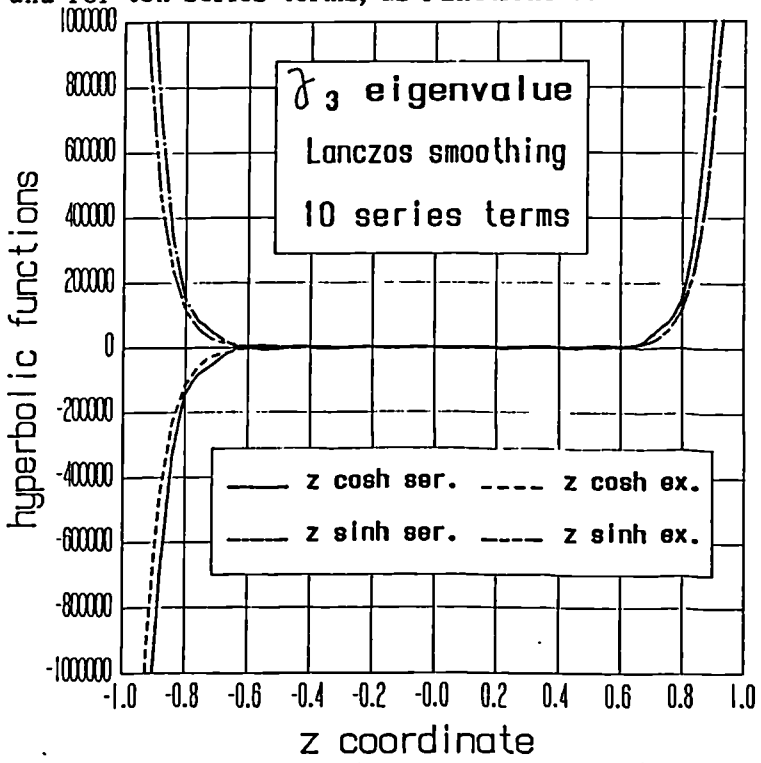

Fig. 3.3.2.7.18 : Exact curve and Lanczos smoothed expansion of four hyperbolic-type functions detailed in the inset, for the third γ radial eigenvalue of the Shibahara geometry and for ten series terms, as functions of the axial coordinate, z .

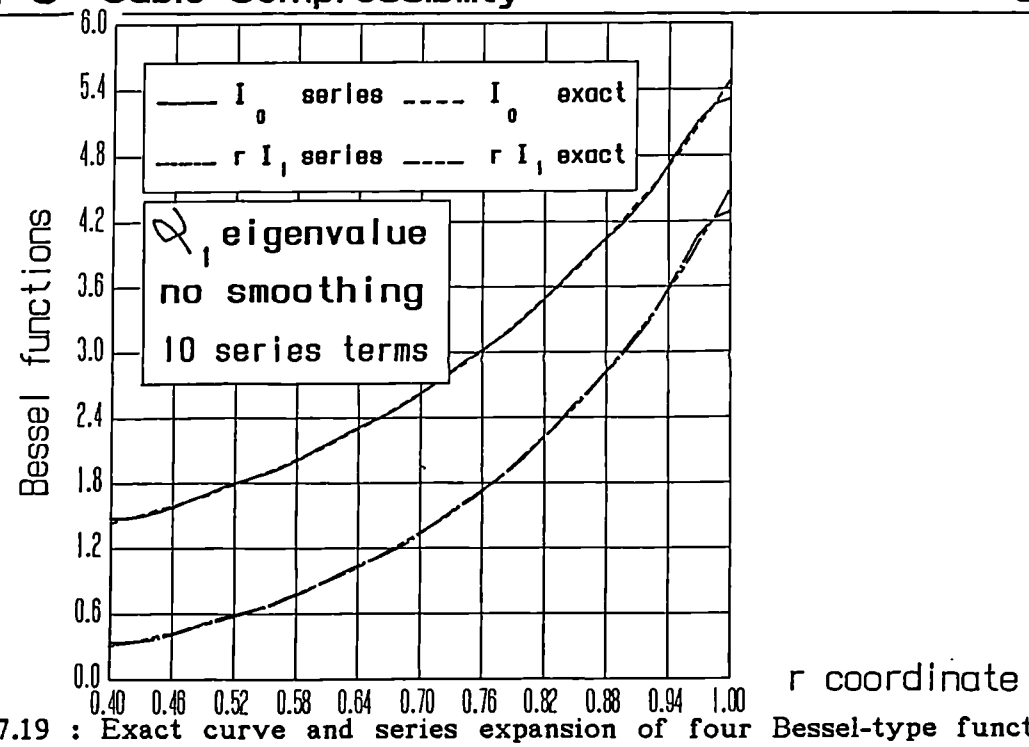

Fig. 3.3.2.7.19 : Exact curve and series expansion of four Bessel-type functions detailed in the inset, for the first α axial eigenvalue of the Bariani geometry and for ten series terms, as functions of the tube radial coordinate, r .

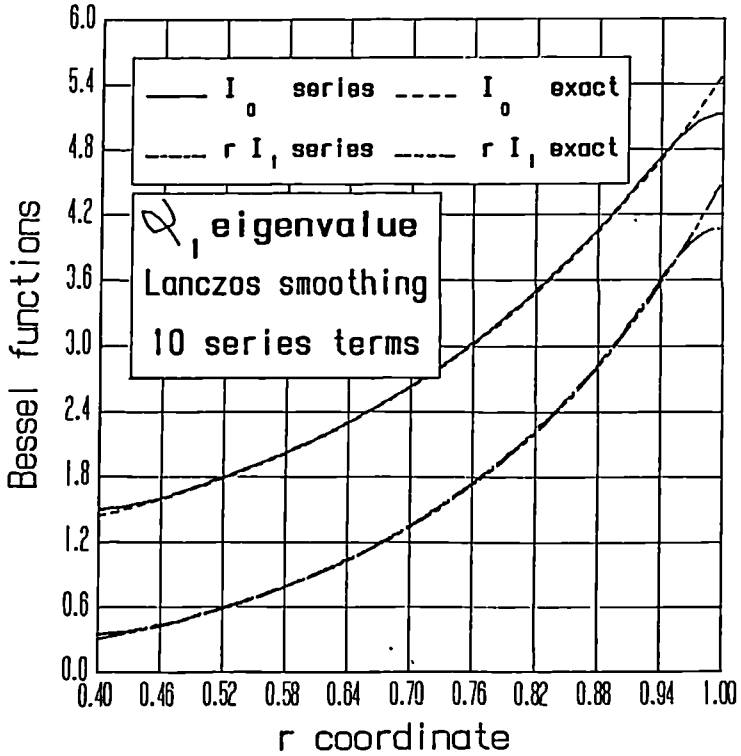

Fig. 3.3.2.7.20 : Exact curve and Lanczos smoothed expansion of four Bessel-type functions detailed in the inset, for the first α axial eigenvalue of the Bariani geometry and for ten series terms, as functions of the tube radial coordinate, r .

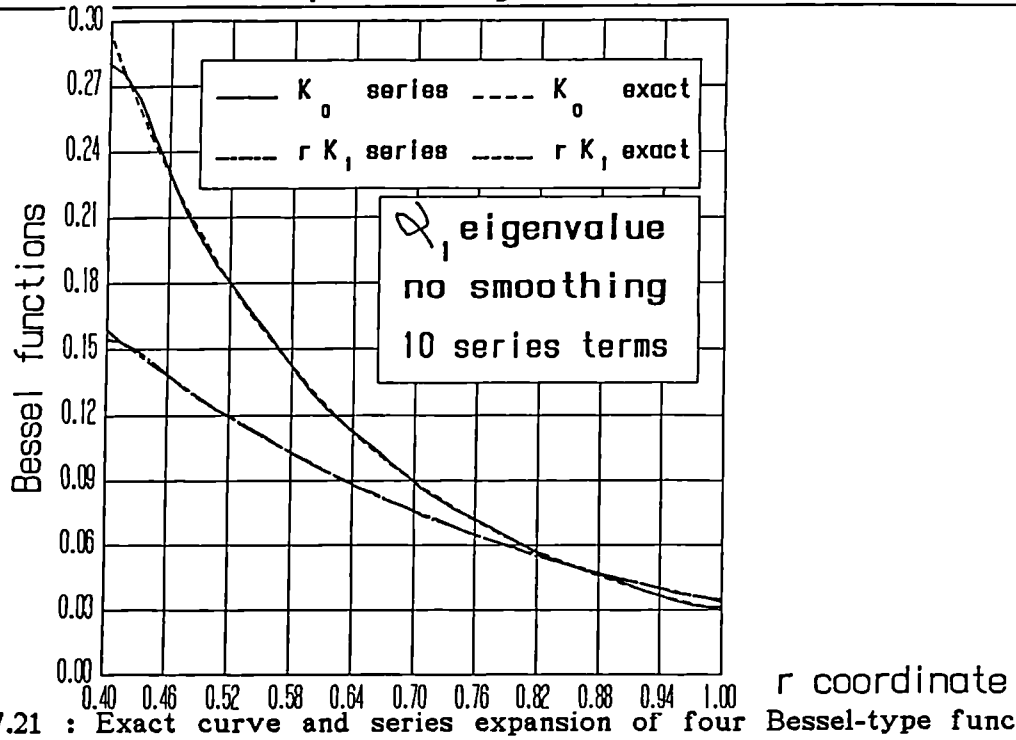

Fig. 3.3.2.7.21 : Exact curve and series expansion of four Bessel-type functions detailed in the inset, for the first α axial eigenvalue of the Bariani geometry and for ten series terms, as functions of the tube radial coordinate, r .

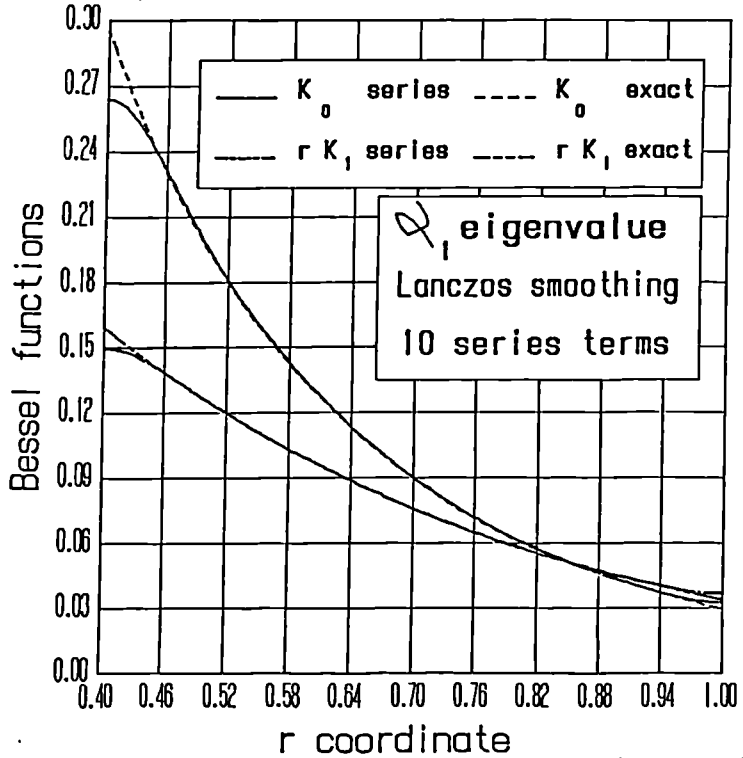

Fig. 3.3.2.7.22 : Exact curve and Lanczos smoothed expansion of four Bessel-type functions detailed in the inset, for the first α axial eigenvalue of the Bariani geometry and for ten series terms, as functions of the radial coordinate, r .

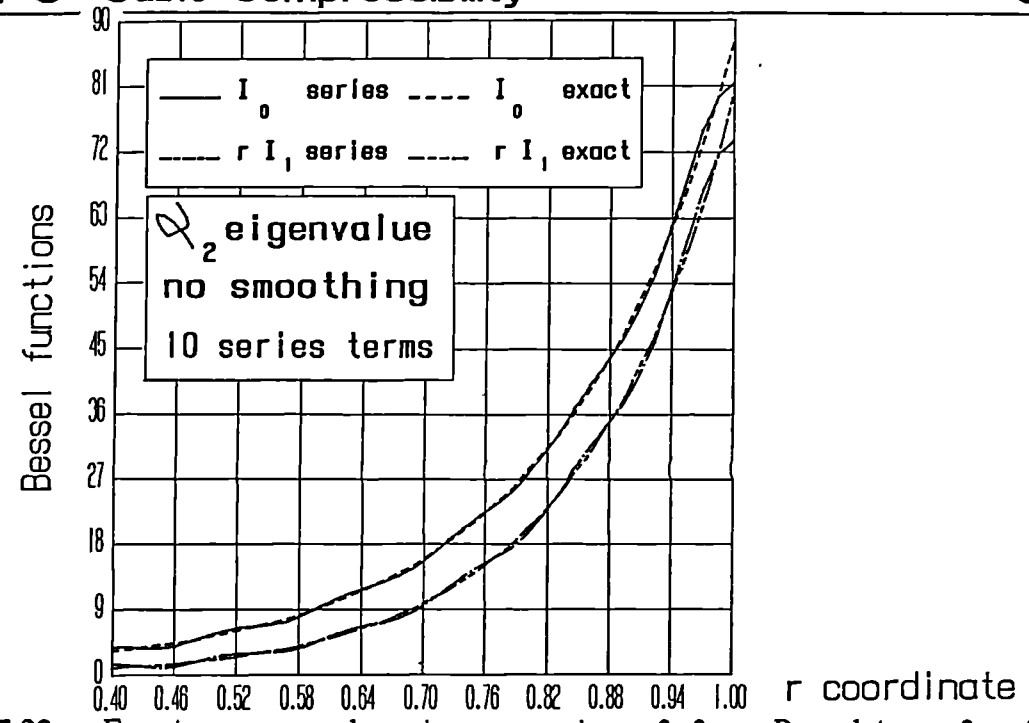

Fig. 3.3.2.7.23 : Exact curve and series expansion of four Bessel-type functions detailed in the inset, for the second α axial eigenvalue of the Bariani geometry and for ten series terms, as functions of the tube radial coordinate, r .

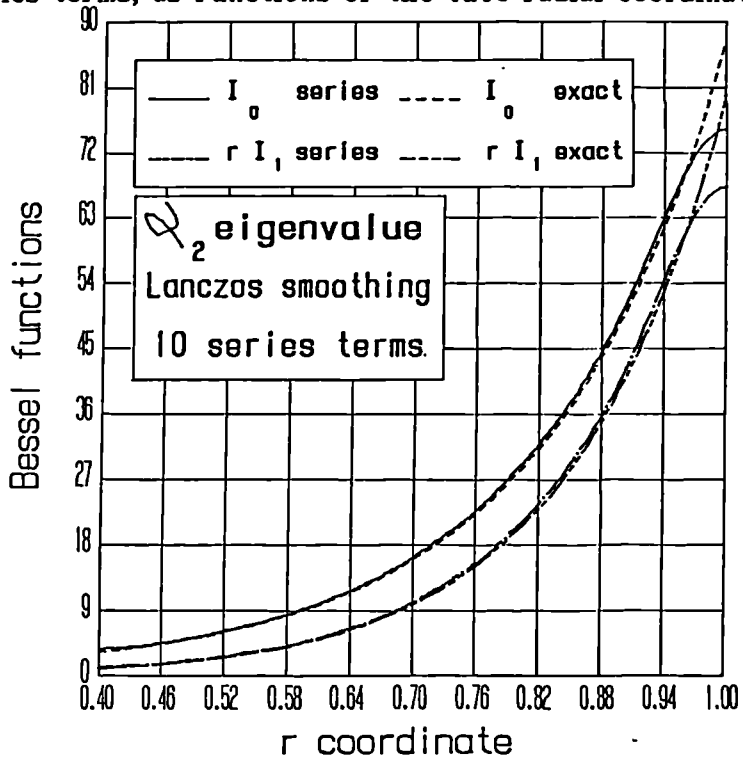

Fig. 3.3.2.7.24 : Exact curve and Lanczos smoothed expansion of four Bessel-type functions detailed in the inset, for the second α axial eigenvalue of the Bariani geometry and for ten series terms, as functions of the tube radial coordinate, r .

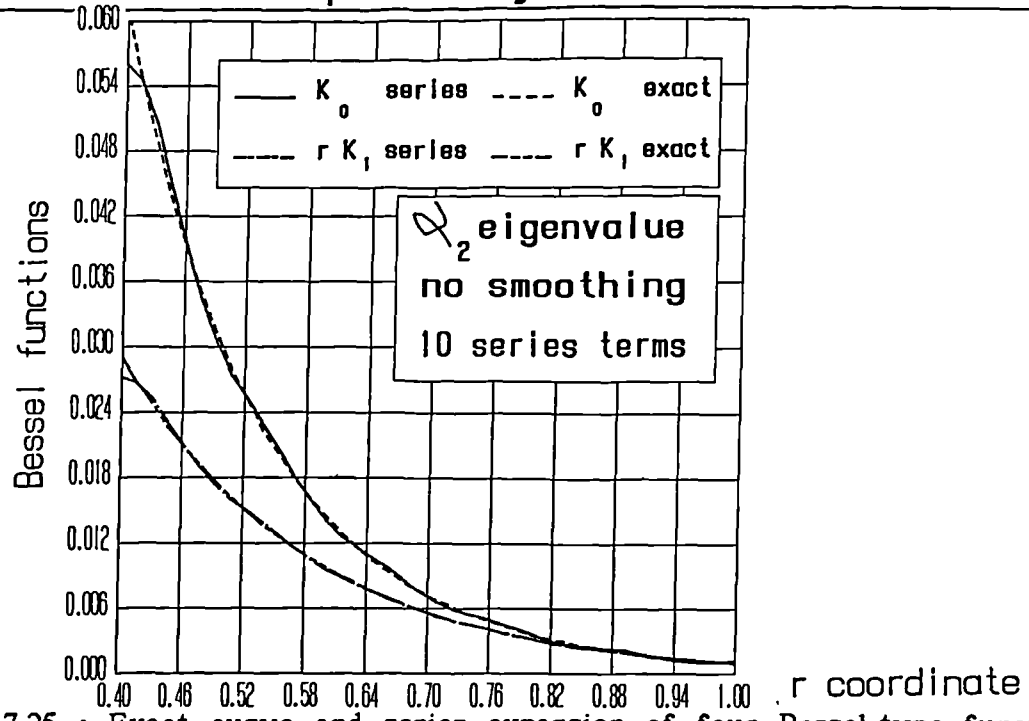

Fig. 3.3.2.7.25 : Exact curve and series expansion of four Bessel-type functions detailed in the inset, for the second α axial eigenvalue of the Bariani geometry and for ten series terms, as functions of the tube radial coordinate, r .

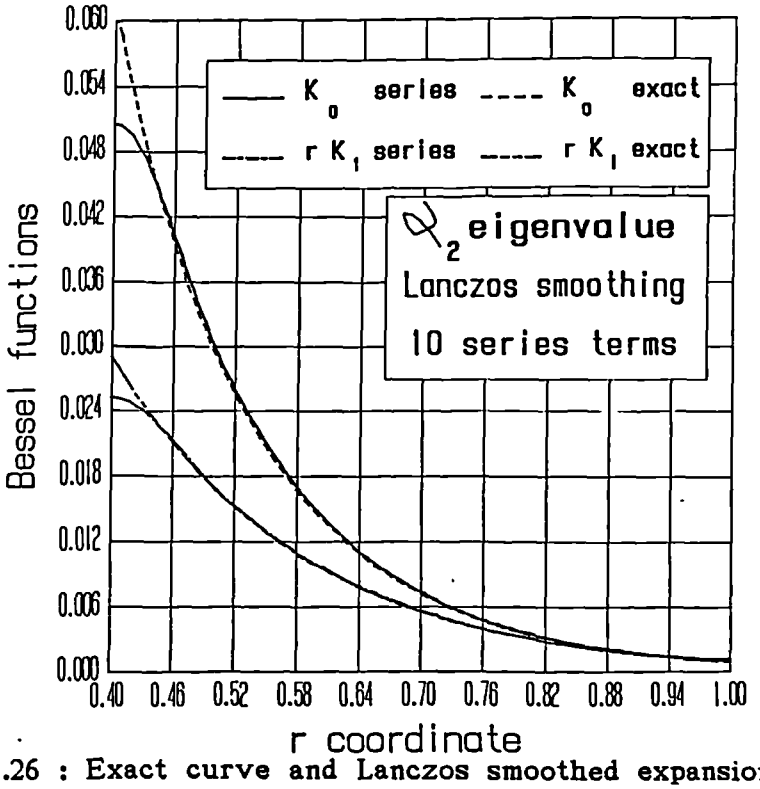

Fig. 3.3.2.7.26 : Exact curve and Lanczos smoothed expansion of four Bessel-type functions detailed in the inset, for the second α axial eigenvalue of the Bariani geometry and for ten series terms, as functions of the radial coordinate, r .

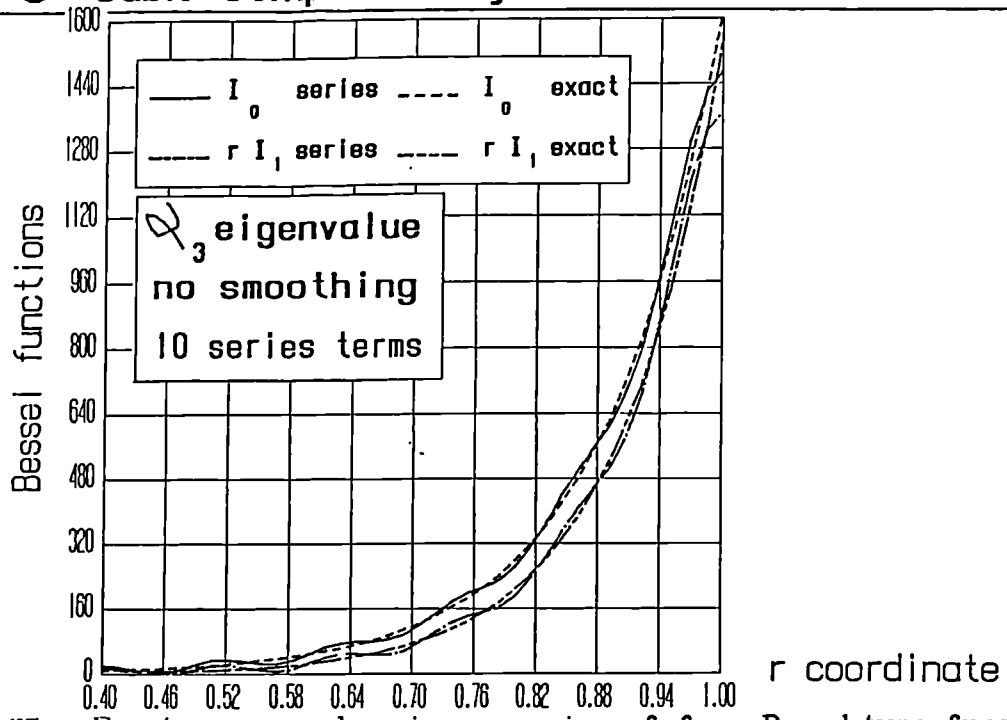

Fig. 3.3.2.7.27 : Exact curve and series expansion of four Bessel-type functions detailed in the inset, for the third α axial eigenvalue of the Bariani geometry and for ten series terms, as functions of the tube radial coordinate, r .

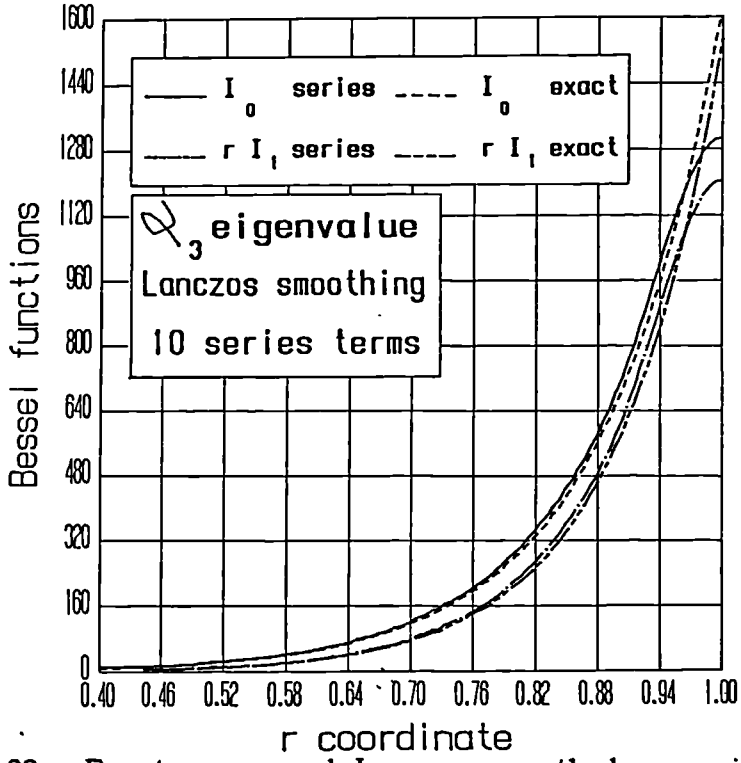

Fig. 3.3.2.7.28 : Exact curve and Lanczos smoothed expansion of four Bessel-type functions detailed in the inset, for the third α axial eigenvalue of the Bariani geometry and for ten series terms, as functions of the tube radial coordinate, r .

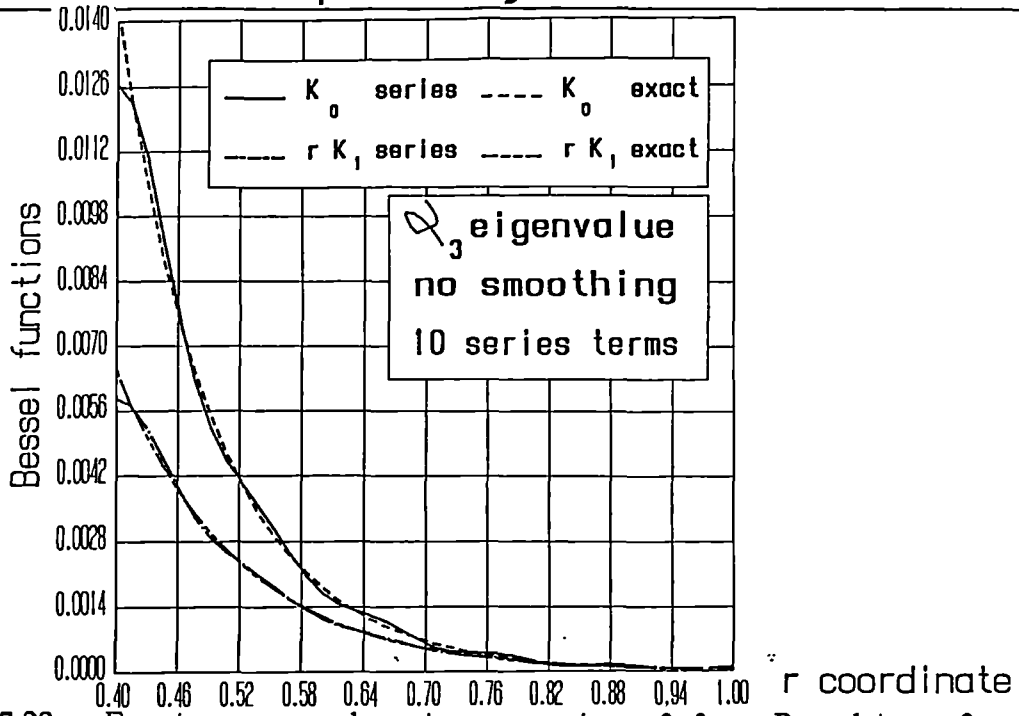

Fig. 3.3.2.7.29 : Exact curve and series expansion of four Bessel-type functions detailed in the inset, for the third α axial eigenvalue of the Bariani geometry and for ten series terms, as functions of the tube radial coordinate, r .

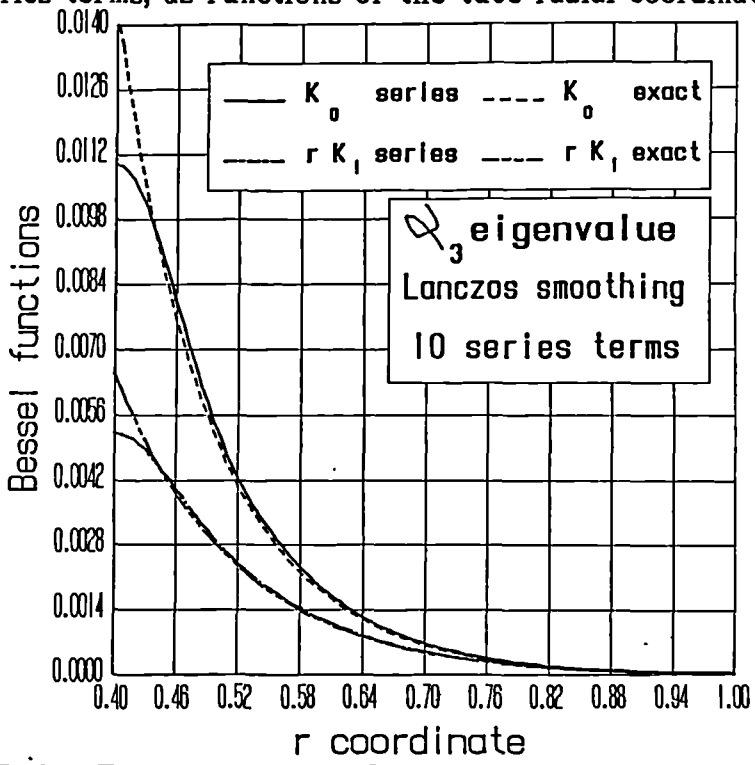

Fig. 3.3.2.7.30 : Exact curve and Lanczos smoothed expansion of four Bessel-type functions detailed in the inset, for the third α axial eigenvalue of the Bariani geometry and for ten series terms, as functions of the radial coordinate, r .

3.3.2.8 The piston device radial deformation

One of the advantages of the series solution of Section 3.3.2 with respect to a finite element approach is that it can mimic a pressure band of continuously varying height, as it occurs in the compression of the elastomeric specimen within the piston device, during the experimental measurement of the bulk modulus. With reference to the rubber specimen employed in real applications, made of "Estane" 5714F1 elastomer (see Section 3.3.1), Fig. 3.3.2.8.1 reports the metal hollow cylinder volume change (for unit p/E) due to its radial expansion, when subjected to an axisymmetric uniform pressure profile along part of a generatrix. More exactly, the radial displacement is computed for the tube inner surface subject to the pressure band. This displacement, once integrated with respect to z and θ coordinates, defines a volume change useful in correcting in Section 3.3.4 the cubic compressibility apparent experimental measurements of Section 3.3.1 . Three pressure band heights are considered, which mimic the piston stroke when compressing the "Estane" 5714F1 elastomer. In particular, the metal hollow cylinder undeformed dimensions (averaged with respect to three readings) are : r_i = 12.5582 mm , r_e = 74.775 mm , h = 61.525 mm , h_{pi} = -16.465 mm . In addition, the three upper pressure band limits describing the piston compression stroke are h_{pu} = 6.385 , 5.955 , 5.525 mm . A maximum index $n=m=20$ was chosen. It was numerically tested that spurious undulations for the volume change (like those affecting Fig. 3.3.2.7.1) did not occur for this configuration. Analogously, Fig. 3.3.2.8.2 displays the forecasts related to the Hysol CP 4485 specimen, used in the experimental study of plane models for the hip replacement of Section 5.4 . In this case the same metal tube dimensions are valid, apart from h_{pu} = 15.305 , 14.682 , 14.059 mm , related to different specimen dimensions and, therefore, to changed piston strokes.

In both Figures the volume variation appears to be essentially linear with the pressure band height. These two Figures include the approximate theoretical forecasts based upon the thick pipe theory applied as explained in the following. The axial length of the hollow cylinder is ideally assumed to coincide with the pressure band width. Then, the volume change is computed according to a plane stress version of the thick pipe theory, only with reference to the loaded axial

portion. Since in this modelling the restraining effects exerted by the hollow cylinder extremities free from the radial pressure on its central part are neglected, the approximate predictions overrate the actual volume change. The results obtained demonstrate that the hollow cylinder volume change cannot be accurately estimated via a simplified thick pipe theory.

Figs 3.3.2.8.3 and 3.3.2.8.4 describe the radial displacement at the upper and lower axial pressure band extremities, for three piston strokes, as functions of the upper extremity, and for the "Estane" 5714F1 and Hysol CP 4485 elastomers, respectively. As in Figs 3.3.8.1,2 , an essentially linear radial displacement with the pressure band height is found again. This information is useful in evaluating the extrusion of the elastomer through the radial gaps between piston and hollow cylinder, examined in the next Section.

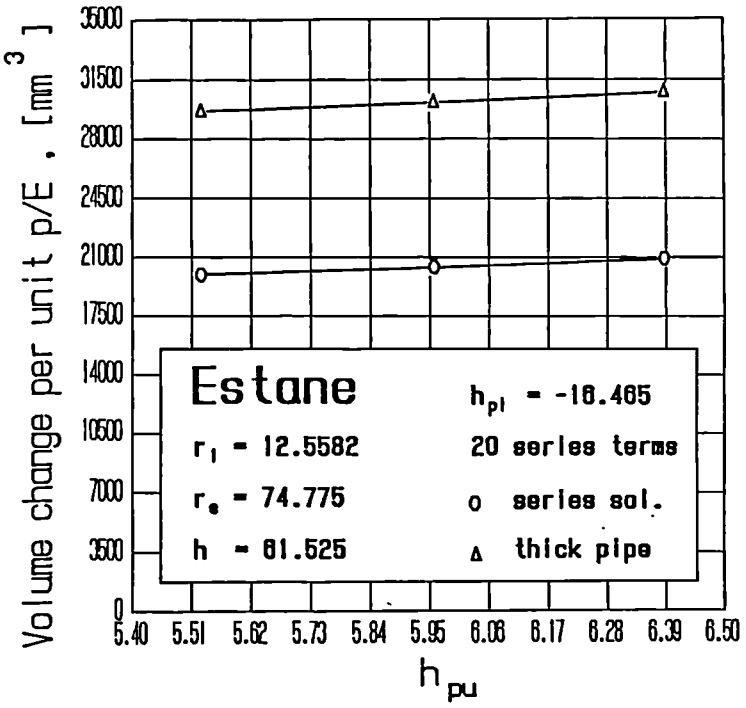

Fig. 3.3.2.8.1 : The metal tube volume change for the "Estane" 5714F1 elastomer.

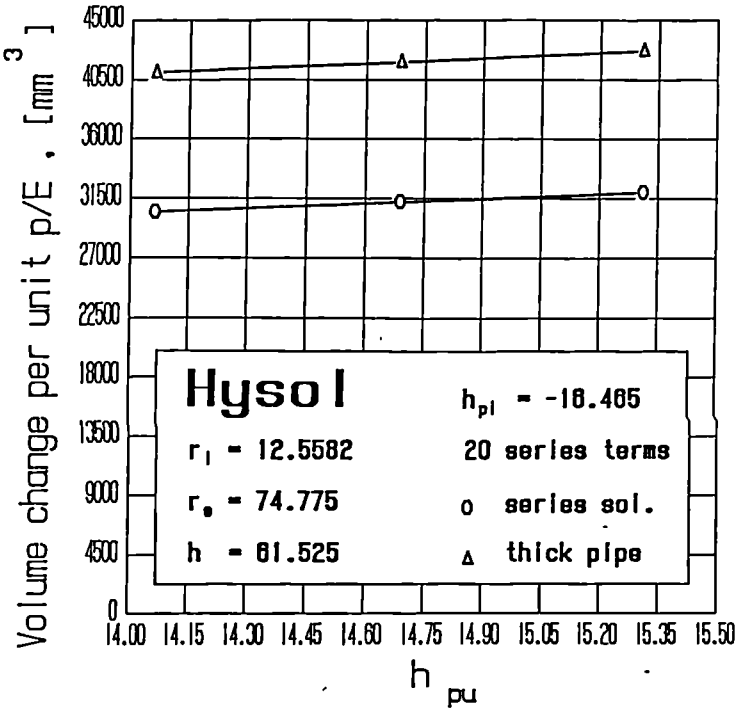

Fig. 3.3.2.8.2 : The metal tube volume change for the Hysol CP 4485 elastomer.

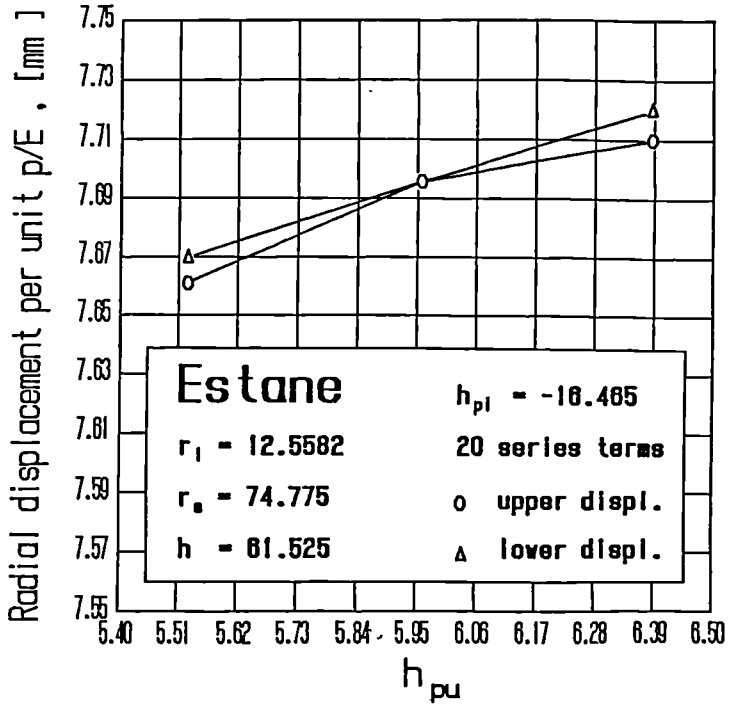

Fig. 3.3.2.8.3 : The metal tube radial displacement for the "Estane" 5714F1 elastomer.

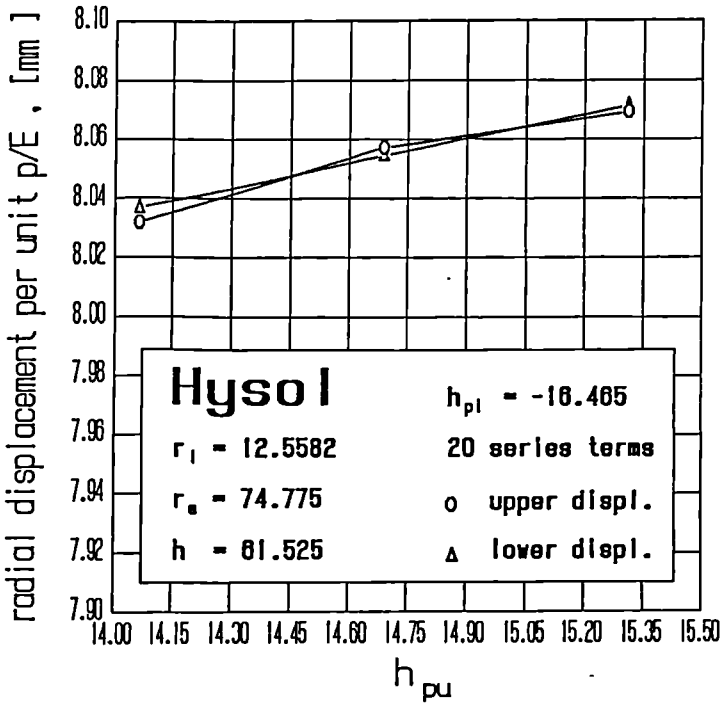

Fig. 3.3.2.8.4 : The metal tube radial displacement for the Hysol CP 4485 elastomer.

3.3.3 The extrusion of the elastomer in the piston device

This Section examines the possible extrusion of the elastomer through the narrow gap between piston and hollow cylinder, and its repercussions on the apparent experimental readings of Section 3.3.1 .

3.3.3.1 General aspects

When the cylindrical elastomeric specimen is compressed by the piston, it tends to extrude through the narrow radial gap inevitably present between piston and hollow cylinder. It is the aim of this Section to identify models suitable to quantify the amount of extruded volume of the elastomeric specimen during the experimental measurement of the cubic compressibility of the elastomer. This information allows the apparent experimental measurements to be corrected by accounting for an effective volume change of the elastomeric specimen *slightly* lower than the apparently imposed one. In the case of finely toleranced piston devices, this correction is presumably negligible, whereas it may become appreciable when the radial tolerances of the piston and hollow cylinder cavities are relatively great. Unfortunately, no pertinent literature could be traced on this topic, apart from a mention of this problem in Burchett and Bert (1972). In particular, since extrusion phenomena often interest severely pressurized elastomeric seals, the proceedings of BHRA Fluid Sealing were scanned, but unsuccessfully. In the lack of the proper information, it becomes difficult to appraise the clearance fits beyond which the extruded volume perceivably alters the experimental measurements. It should be also appreciated that an accurate model of the elastomer extruded volume would permit less stringent tolerances to be adopted for the piston-hollow cylinder gap, which in turn would result in a cheaper piston device construction.

The following Subsection deals with a numerical finite element analysis of the extrusion problem, whose results suggest the formulation of a theoretical model, developed in the subsequent Subsection.

3.3.3.2 Finite element forecasts

The configuration sketched in Fig. 3.3.3.2.1 was numerically studied. In the following the expression "extruded volume" denotes the area (per unit thickness, according to a plane strain model) of elastomer protruding through the gap of Fig. 3.3.3.2.1 beyond the line defined by the piston bottom face. Due to the narrowness of the radial gap in the piston device and to the essentially axial flow of the elastomeric portion extruded (so that the hoop strains in the elastomer insist on a small radial interval and are limited), a plane strain model (as opposed to axisymmetric) was adopted in the numerical study. This simplification aims at avoiding the introduction of the additional variables describing the radii of the gap inner and outer extremities, which are believed to be scarcely influential. Owing to mesh difficulties, the gap examined in the numerical study cannot be so small as in the actual configuration. Consequently, gaps in the region of 1\10 the side of a 10 x 10 (abstract units) plane strain specimen were considered. The automatically generated, undeformed mesh (Medri and Strozzi (1984)) is displayed in Fig. 3.3.3.2.2. It exhibits a concentration of elements in the region affected by extrusion. The finite element computations were performed via ABAQUS program, which possesses a release addressed to the mechanical analysis of elastomeric units, incorporating geometrical and material non-linearities (Chapter 2). The possibility for the elastomer extruded to move apart from the left vertical wall was introduced via a unilateral contact simulation. Frictionless contacts were always adopted between specimen and walls. A total amount of 13 cases differing in compressions (the vertical displacement of the top wall ranges between 0.02 and 0.5 in abstract units) and Poisson's ratios (ranging from 0.49 to 0.5) were examined. In the lack of proper data, a neo-Hookean constitutive relation connecting stress to strain with unit Young's modulus was adopted (Section 2.2.3). As an example of the numerical predictions, Fig. 3.3.3.2.3 displays a deformed mesh for an incompressible elastomer and for a vertical displacement of the top side of 0.02 . It clearly appears that the extruded portion does not appreciably move apart from the left wall (with the exception of a very localized upper zone, perceivable in Fig. 3.3.3.2.3). Fig. 3.3.3.2.4 represents the Von Mises equivalent stress, which shows that the specimen region

for which the stress state appreciably deviates from being hydrostatic is relatively small. Fig. 3.3.3.2.5 collects the above mentioned 13 numerical previsions, where the extruded volume (more exactly, it is an extruded area, since the problem is modelled via a plane approach) has been normalized with respect to the gap squared, where a unit normalized contact pressure, p/E, is imposed by the indenter centre. More precisely, since it is not easy to achieve in the finite element study a unit pressure by the punch centre, the indenter penetration depth was actually assigned and, then, the extruded volume was simply normalized versus the central pressure computed via a constitutive relationship possessing a unit Young's modulus. It is appreciated that this normalization is only approximate, since it presupposes a linear structural behaviour, while in fact finite deformations affect especially the extruded part of the elastomeric specimen. On the other side, the ABAQUS forecasts were compared to previsions obtained with a linear finite element program (Bandera and Strozzi (1991)), obtaining a satisfactory agreement. This favourable correlation is seemingly ascribable to the circumstance that even a linear finite element program mimics the limited cubic compressibility of the elastomeric medium, thus practically preserving the volume constancy before and after loading and, consequently, imposing constraints on the extruded volume entity, which compensate for the lack of modelling of finite strains. It is therefore concluded that the normalization adopted with respect to the central pressure is acceptable, since the non-linearity of the relationship between extruded volume and central pressure is modest.

Some scattering of the results affects Fig. 3.3.3.2.5 , possibly ascribable to the above simplified normalization, that is, to finite strain effects at the highest compressions. It is however noted that the Poisson's ratio is not a dominant parameter, provided that it is close to the incompressibility figure 0.5 . Finally, Fig. 3.3.3.2.6 illustrates the finite element contact pressure (normalized with respect to its value by the symmetry axis according to Fig. 3.3.3.2.1) for an incompressible elastomer, for a displacement of the vertical side of 0.02 , and for a gap of 1.086 . It clearly emerges that the contact pressure is uniform, apart from a concentrated spike in the vicinity of the gap. The flatness of the central part of the pressure profile implies that a correct numerical study of the rubber extrusion does not necessarily need to simulate the whole radial extent of the rubber specimen. The

finite element mesh of fig. 3.3.3.2.2 can thus be interpreted as a description of the elastomeric specimen portion closer to the device gap, see Fig. 3.3.3.2.1 , so that the numerical study furnishes results applicable also to gaps considerably smaller than 1\10 the discretized square side. For the same reason, in Fig. 3.3.3.2.5 the indenter width does not appear as a parameter, since it is scarcely influential, provided that the gap extent is much smaller. The spurious numerical undulations affecting the pressure profile in the peak regions frequently appear when dealing with nearly incompressible materials (Dragoni and Strozzi (1988)).

The circumstance that the extruded portion does not essentially lose contact with the left wall of Fig. 3.3.3.2.1 suggests that the projecting rubber can be mimicked in terms of a symmetric bump whose symmetry axis coincides with the left wall of Fig. 3.3.3.2.1 , and projecting between two contiguous, equally compressed indenters simulating the piston penetration effect. In the next Section it is shown that a proper theoretical model for this problem can be based upon a deformable half space compressed by a rigid punch, and that it is not necessary to resort to a more complex quarter of plane description of the indented specimen (Hetenyi (1960), Hanson and Keer (1989)).

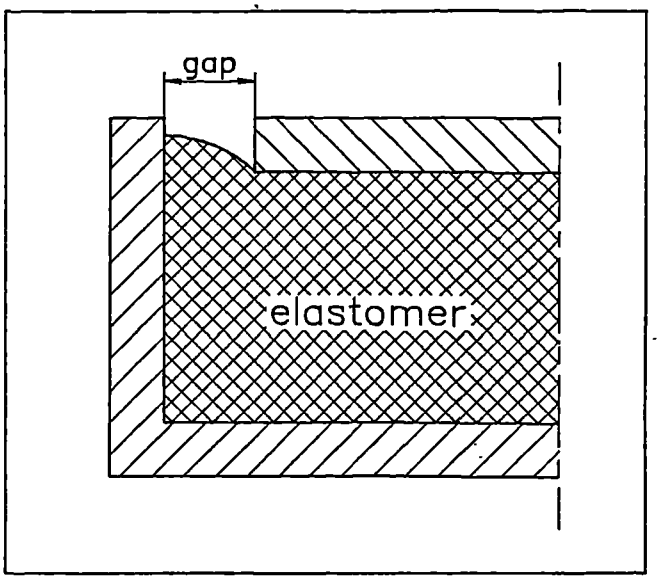

Fig. 3.3.3.2.1 : The configuration mimicking the extrusion of the elastomeric specimen.

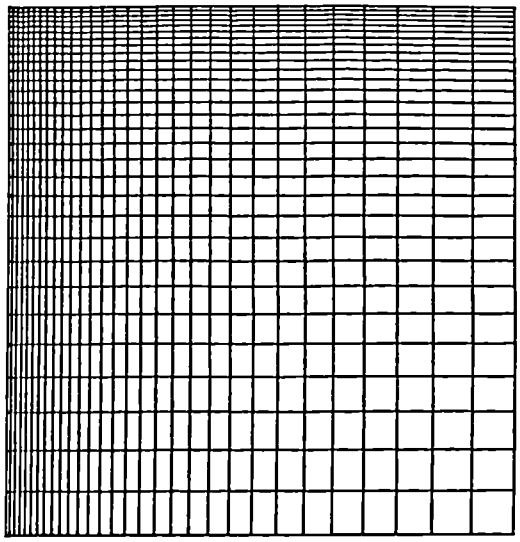

EXTRUSION OF ELASTOMERS IN PISTON DEVICE

Fig. 3.3.3.2.2 : The automatically generated, undeformed finite element mesh.

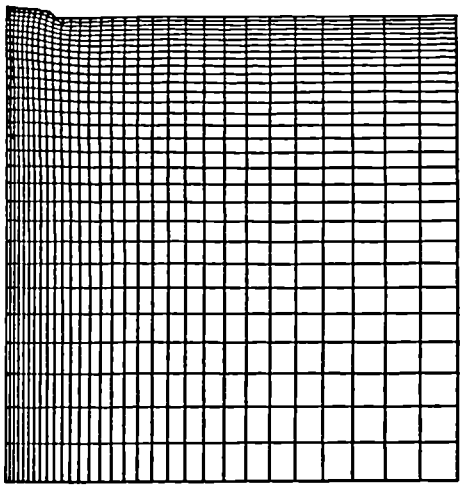

EXTRUSION OF ELASTOMERS IN PISTON DEVICE

Fig. 3.3.3.2.3 : The deformed mesh for a top side vertical displacement of 0.02 .

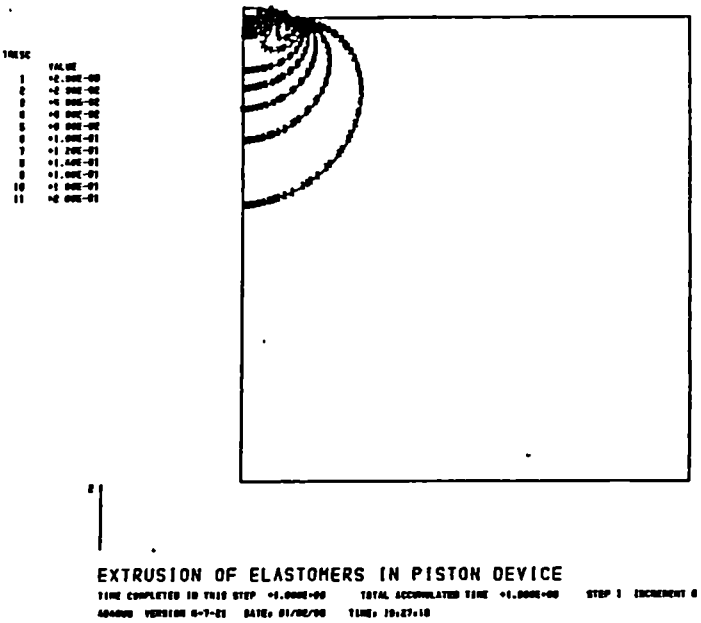

Fig. 3.3.3.2.4 : The Von Mises equivalent stress pattern.

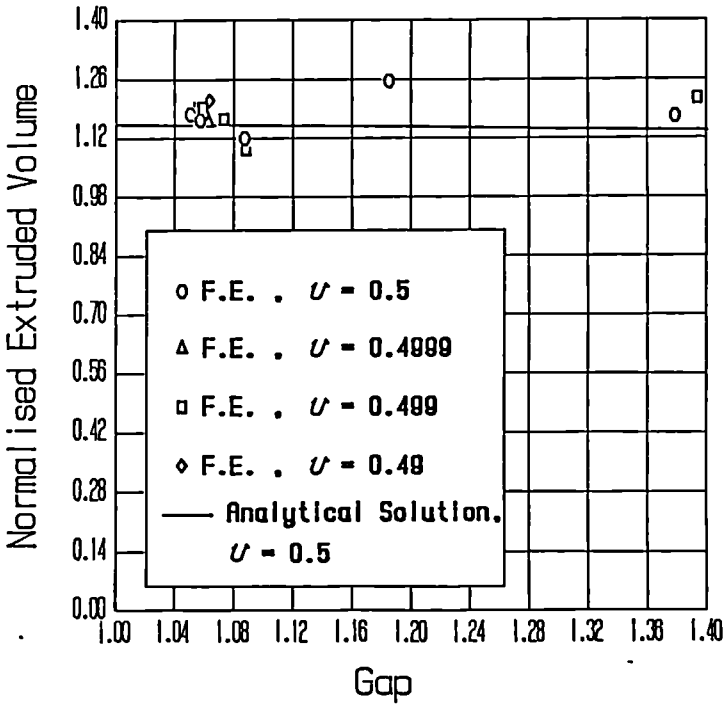

Fig. 3.3.3.2.5 : Analytical and numerical forecasts for the normalized extruded volume.

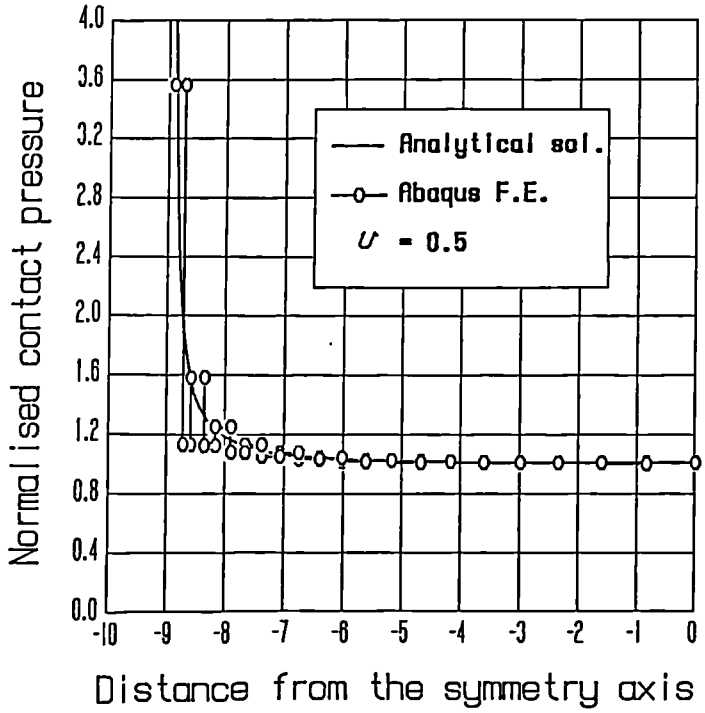

Fig. 3.3.3.2.6 : The analytical and finite element normalized contact pressures.

3.3.3.3 A theoretical model of the elastomer extrusion

Among the cases in which the contact pressure between a rigid punch and a deformable half plane is theoretically known, those potentially suitable to describe the title problem are the single rigid flat punch frictionlessly compressing a deformable half space (Johnson (1985), p. 35) and the infinite series of equidistant flat punches (Gladwell (1980), p. 181). Comparison with the numerical findings will eventually suggest which model better mimics the extrusion of the elastomeric specimen. As already noted, the essential lack of gap (see Fig. 3.3.3.2.3) between elastomer and left wall as ideally sketched in Fig. 3.3.3.2.1 suggests that the latter can be assumed as a symmetry axis in the theoretical modelling.

The first description here analyzed relies upon two flat punches equidistant from the left wall (interpreted as a symmetry axis), whose width equals twice that of the top wall in Fig. 3.3.3.2.1. The gap between these two punches is thus twice that indicated in Fig. 3.3.3.2.1 . The expression of the pressure profile under a single punch is known in closed form, but in the case under scrutiny the presence of the second punch considerably alters this pressure distribution (Galin (1961), p. 72 , and p. 75 , where the case of two frictionless punches simultaneously indenting a half space is mentioned). Anyway, although the pressure profile equation is known, the corresponding displacement field and, consequently, the extruded volume seem difficult to evaluate, due to the complexity of the pressure equation. If the mutual alteration of the pressure profile is neglected and the single punch pressure profile is retained also for the case of two punches acting simultaneously, the analytical expression of the free edge of the deformed half plane between the two punches can be derived from Johnson (1985), p. 38 , and the extruded volume can be computed numerically. Anyway, this modelling disagrees with the numerical forecasts of Fig. 3.3.3.2.6 referring to the case of Fig. 3.3.3.2.1 , since they indicate that the pressure profile is nearly uniform, apart from a localized peak, whereas the above-mentioned two punch model would produce a much less uniform contact curve (see Johnson (1985), p. 41, Fig. 2. 14).

The second possible model, that of an infinite series of punches, seems physically more sound, and the pressure equation appears less complex, although

only moderately, than that of two contiguous punches. The theory this time accounts for the mutual influence of the punches in terms of contact pressure, and all gaps between two subsequent punches are in the same condition. Consequently, the punch contact pressure is symmetrical, as in the actual device, whereas an exact expression of the contact pressure for the model consisting of two adjacent indenters would not possess this symmetry. The contact pressure of this second approach agrees with the numerical calculations, as shown in Fig. 3.3.3.2.6 . In addition, Fig. 3.3.3.3.1 presents the contact pressure profile (normalized to produce a unity value at the symmetry axis) by the punch extremity, according to the single and multiple punch pressure distribution (plane strain models), and for a geometrical configuration close to the actual piston device. It appears that in the case of small radial gaps, the single punch pressure deviates from unity starting from relatively low piston radii, whereas the multiple punch pressure exhibits a very localized peak, which is physically more sound.

The determination of the deformed free border of the half plane compressed by an infinite series of rigid punches requires the following (singular) integral (containing the product of the pressure distribution (Gladwell (1980), p. 181) by a logarithmic "influence" function, typical of a half plane) to be computed, where d is the pitch between two adjacent punches, and a is their half width :

$$\int \frac{\cos\frac{\pi t}{d}\ \ln|t-x|}{\sqrt{\sin^2\frac{\pi a}{d}-\sin^2\frac{\pi t}{d}}}\,dt \qquad (3.3.3.3.1)$$

More exactly, this integral should be evaluated to determine (apart from a constant) the vertical displacement of the, say, left edge of a punch, due to its pressure (singular integral), the displacement of the same point due to the pressure of the punch at its left and, then, the effects of the remaining infinite punches on the same point. This latter contribution can be ignored especially if the gap is small in comparison to the punch width. In fact, the contributions due to punches far away from the zone of interest should be small from a physical viewpoint (but mathematically it tends logarithmic ally to infinity) and, in addition, their effects on

the deflection of the free border of the half plane should consist in a nearly uniform horizontal displacement, which can be likened to a constant and, therefore, it is scarcely influential in the computation of the extruded volume.

Once the displacement of the punch left edge has been computed (apart from a constant), the half plane free border can be calculated with respect to this reference point, and this curve can be integrated to express the extruded volume, that is, the volume of elastomer higher than the piston bottom face. Unfortunately, it was not possible to integrate exactly the above mentioned deformed profile, nor did various algebraic manipulators produce any analytical results. It was, therefore, decided to resort to numerical integration. Fig. 3.3.3.3.2 displays a convergence study in the case of histogram-type integration, for one of the configurations numerically examined in Fig. 3.3.3.2.5 . The nodes describing the contact area between punch and half plane range from 100 to 1000, whereas 30 nodes are always used to discretize the free boundary and to compute the extruded volume. It emerges that the convergence towards a stable value of the extruded volume (normalized with respect of the gap squared) is too slow. As an alternative, the pressure profile multiplied by the logarithmic "influence" function was expanded into a Taylor series in the vicinity of the pressure singularity (the algebraic manipulator MAPLE (Harper (1989)) was employed) and, then, the first three terms of this expansion were integrated exactly. (It was numerically tested that the third term contribution was very small and, therefore, higher order terms were disregarded.) In particular, only the first term of this Taylor expansion possesses a square-root singularity in the denominator, whereas the second and third terms simply exhibit in the numerator a square root and a square root to the cube, respectively. These exact integrals of approximate functions were used only for the element closest to the punch edge, whereas for the other elements a usual histogram-type approximate integration was employed. Fig. 3.3.3.3.2 demonstrates the advantages of this approach over a histogram-type integration, since the normalized extruded volume remains fairly constant when the number of nodes ranges between 500 and 1000. This also is an indirect check for the exactness of the numerical program. In fact, as the number of nodes is, say, doubled, the width of the element for which the integral is computed via a Taylor expansion technique is (nearly

exactly) halved. With reference to the indenter left corner, the right half of the element defined by the coarser mesh, describing the punch-half plane contact zone and adjacent to the left pressure singularity is, with the finer mesh, treated with a histogram approach. Since this zone is close but not adjacent to the pressure singularity, the Taylor and histogram approaches are expected to supply similar values for the integrals. In other words, the extruded volume furnished by a correct numerical program is expected to be essentially independent of the number of nodes for a wide range, a fact confirmed by Fig. 3.3.3.3.2 .

The normalized extruded volume computed analytically according to the infinite series of equispaced punches and for an incompressible elastomer is reported in Fig. 3.3.3.2.5 (the details of the normalization adopted are commented in Section 3.3.3.2 with reference to this Figure), and it is nearly independent of the gap extent, as commented in Section 3.3.3.2 . The analytical forecasts are in reasonable agreement with the finite element previsions, so that they constitute a model suitable for amending the apparent measurements of the bulk modulus (Section 3.3.4) .

Finally, Fig. 3.3.3.3.3 presents the results useful in correcting the experimental measurement of the elastomer cubic compressibility via the piston device. It essentially links the elastomer extruded volume to the gap extent and to the central contact pressure between punch and elastomeric medium. More precisely, Fig. 3.3.3.3.3 reports the extruded volume in μm^2 for a thickness of 1 mm (it is treated as a plane strain problem, see Section 3.3.3.2, so that it should be more exact to refer to "extruded area", more consistent with the dimensions adopted (μm^2), but the real problem to be amended is axisymmetric) as a function of the radial gap between piston and cylinder, for the undeformed value of the hollow cylinder inner diameter, $r_i = 12.5582$ mm , for $E = 1$ MPa , $\nu = 0.5$ (as suggested by Fig. 3.3.3.2.5 , the Poisson's ratio adopted is not a critical factor) and for a unit pressure by the piston centre. Critical remarks on the normalization adopted are contained in Section 3.3.3.2 . In addition, it is observed that, during operating conditions, the cylinder diameter slightly increases, but it was numerically verified that this increase does not significantly affect the results of Fig. 3.3.3.3.3 , and this agrees with the indenter-elastomer contact pressure becoming rapidly uniform at a relatively small distance from the punch edge (Fig. 3.3.3.3.1), as commented in

Section 3.3.3.2 .

The same Figure also includes the extruded volume according to the two punch approach, which supplies results very different from a multiple punch theory. In particular, for exiguous gaps the multiple punch description furnishes higher extruded volumes than the two punch modelling. The rationale beyond the latter point is as follows. In the multiple punch case, the only free boundary of the compressed half plane occurs between any pair of punches. As the punches indent the half plane, the elastic material must extrude through these narrow openings. In the case of two adjacent punches, instead, the free boundary which is external to the pair of indenters can easily protrude, thus lowering the amount of extrusion in the narrow gap between the two punches.

From Fig. 3.3.3.3.3 it also appears that for relatively large gaps the double punch solution furnishes higher extruded volumes than the multiple punch modelling. This result may be rationalized as follows. Since the comparison between the two approaches is made for a unit contact pressure by the indenter centre, the total load applied to any punch is much higher for the double punch approach than for the multiple punch description, as a consequence of the rather different contact pressure profiles characterizing the two above modellings (see Fig. 3.3.3.3.1) . The higher total load is expected to produce a greater indentation depth and, consequently, a more relevant extrusion of the elastomer. The results of Fig. 3.3.3.3.3 indicate that this effect prevails only for relatively high gaps. In any case, it should be remembered that the double punch modelling here developed is only approximate, so that conclusions based upon physical considerations are inevitably questionable.

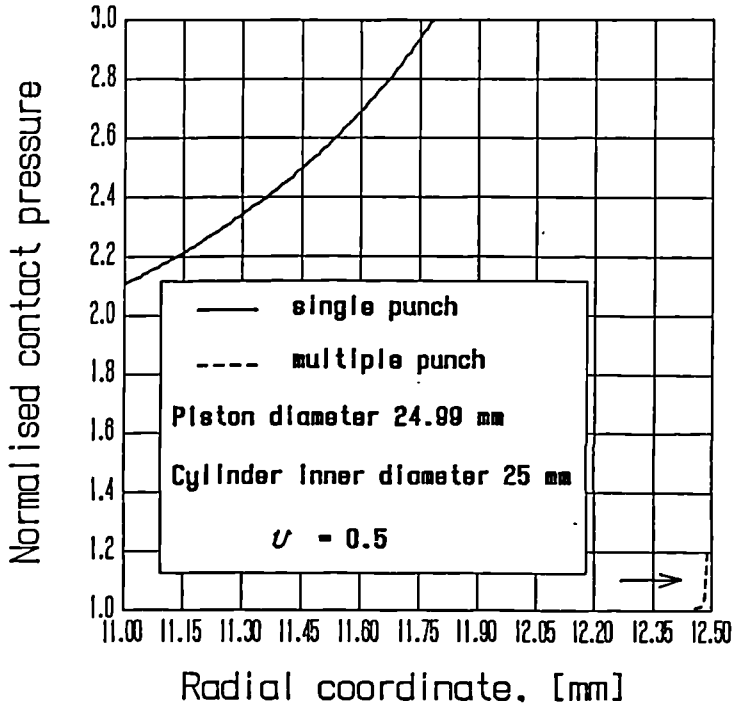

Fig. 3.3.3.3.1 : The normalized contact pressure profile by the punch extremity, according to the single and multiple punch models.

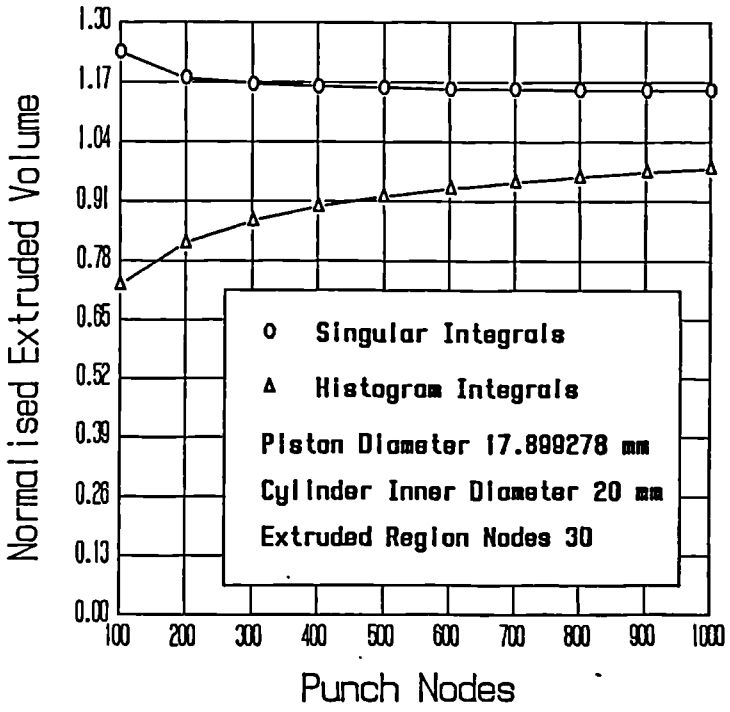

Fig. 3.3.3.3.2 : A convergence study on singular integrals computed numerically and by series expansion.

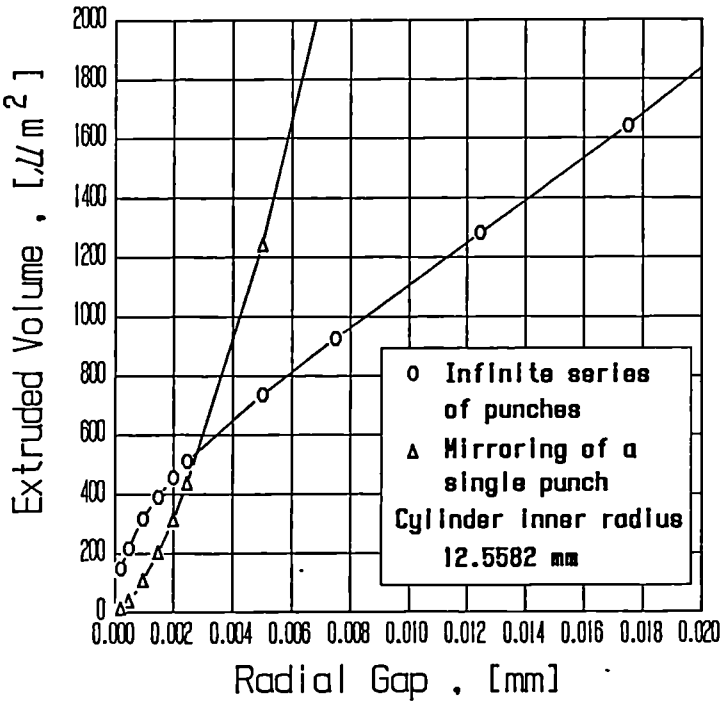

Fig. 3.3.3.3.3 : The extruded volume versus radial gap diagram for two modellings.

3.3.4 The corrected bulk modulus measurements

This Section deals with the correction of the apparent bulk modulus by accounting for the four sources of experimental errors mentioned in Section 3.2 : 1) the flexibility of the press loading the piston; 2) the axial deformability of both the piston and the bottom of the device; 3) the radial deformability of the metal hollow cylinder; 4) the extrusion of the elastomer through the narrow radial gap between piston and hollow cylinder.

Four values of increasing accuracy for the bulk modulus were elaborated via a purposely developed computer program for the "Estane" 5714F1 and Hysol CP 4485 elastomers. The first figure is the apparent bulk modulus, as directly derived from the experimental measurements. Only the first source of error is eliminated, since the piston stroke is measured via a precision micrometer (gauge) acting between piston and metal cylinder. Then, the second inaccuracy is simply compensated by estimating theoretically the piston reduction in length due to the axial load. The consequences of the hollow cylinder radial deformability are subsequently corrected via the theory of Section 3.3.2 . The shear stress effects describing the frictional force exerted by the rubber specimen against the inner surface of the metal hollow cylinder are ignored. This is consistent with the averaging between loading and unloading discussed in Section 3.3.1 , which essentially frees the experimental values from the frictional effects. The hydrostatic pressure affecting the elastomeric specimen is computed by accounting for the (slight) increase in the elastomeric specimen end face diameters, as a result of the metal cylinder expansion. Finally, the elastomer extrusion component is compensated according to Section 3.3.3 .

Tables 3.3.4.1 and 3.3.4.2 present these four figures for four strokes and for the two elastomers considered, namely the "Estane" 5714F1 and Hysol CP 4485 specimens, whose Young's moduli are 8.506 MPa ("Estane" 5714F1) and 3.52 MPa (Hysol CP 4485), see Section 3.3.1 . The nominal value of the stroke is also included. The corrected hydrostatic pressure (it accounts for the cylinder radial expansion) is also indicated. These four corrections are generally of decreasing importance.

TABLE 3.3.4.1 : bulk modulus of the "Estane" 5714F1 elastomer

stroke = 0.292 mm		
force = 10000 N	bulk modulus MPa	Poisson's ratio
pressure = 20.184 MPa		
Apparent	1578.5125	0.49910191
Piston deformation	1650.5909	0.49914113
Cylinder expansion	1674.4107	0.49915335
Specimen extrusion	1674.4125	0.49915335
stroke = 0.489 mm		
force = 20000 N	bulk modulus MPa	Poisson's ratio
pressure = 40.362 MPa		
Apparent	1885.8963	0.49924827
Piston deformation	1989.7025	0.49928749
Cylinder expansion	2023.7164	0.49929947
Specimen extrusion	2023.7193	0.49929947
stroke = 0.662 mm		
force = 30000 N	bulk modulus MPa	Poisson's ratio
pressure = 60.536 MPa		
Apparent	2088.3168	0.49932113
Piston deformation	2216.3593	0.49936035
Cylinder expansion	2258.0063	0.49937215
Specimen extrusion	2258.0122	0.49937215
stroke = 0.818 mm		
force = 40000 N	bulk modulus MPa	Poisson's ratio
pressure = 80.743 MPa		
Apparent	2255.2890	0.49937141
Piston deformation	2405.3610	0.49941063
Cylinder expansion	2453.8315	0.49942225
Specimen extrusion	2453.8371	0.49942225

TABLE 3.3.4.2 : bulk modulus for the Hysol CP 4485 elastomer

stroke = 0.347 mm		
force = 10000 N	bulk modulus MPa	Poisson's ratio
pressure = 20.182 MPa		
Apparent	1853.3203	0.49968344
Piston deformation	1923.9855	0.49969506
Cylinder expansion	1959.7581	0.49970064
Specimen extrusion	1959.7640	0.49970064
stroke = 0.616 mm		
force = 20000 N	bulk modulus MPa	Poisson's ratio
pressure = 40.363 MPa		
Apparent	2089.3066	0.49971920
Piston deformation	2179.5517	0.49973083
Cylinder expansion	2225.0554	0.49973634
Specimen extrusion	2225.0612	0.49973634
stroke = 0.859 mm		
force = 30000 N	bulk modulus MPa	Poisson's ratio
pressure = 60.536 MPa		
Apparent	2247.9189	0.49973902
Piston deformation	2352.7299	0.49975064
Cylinder expansion	2405.0336	0.49975607
Specimen extrusion	2405.0385	0.49975607
stroke = 1.085 mm		
force = 40000 N	bulk modulus MPa	Poisson's ratio
pressure = 80.702 MPa		
Apparent	2373.2060	0.49975279
Piston deformation	2490.3303	0.49976441
Cylinder expansion	2548.1071	0.49976978
Specimen extrusion	2548.1169	0.49976978

The assumptions adopted in the evaluation of the bulk modulus are discussed in the following. The bulk modulus is evaluated as the ratio of the hydrostatic pressure to the relative volume change (Section 3.2.1). The pressure is supposed to be uniform within the specimen; the final volume of the compressed rubber specimen incorporates the extruded volume by the specimen top and bottom extremities.

The last assumption is discussed hereinafter. The fact that the specimen deformed volume includes the extruded portions in the evaluation of the corrected bulk modulus implies that, as a consequence of the correction accounting for extrusion phenomena, the volume variation of the compressed specimen slightly diminishes and its bulk modulus increases, as physically expected. The justification for incorporating the extruded portions into the specimen compressed volume stems from the assumption of uniform hydrostatic stress field within the specimen. In fact, the contact pressure between piston bottom surface and elastomeric specimen is mainly uniform, but it exhibits two localized pressure peaks by the piston border (Fig. 3.3.3.2.6), so that the stress level in these portions is higher than that in the adjacent regions. Conversely, the extruded volume is less stressed than the average specimen level (Fig. 3.3.3.2.4), so that the presence of over and under-stresses specimen portions should produce compensatory effects, and the corrected readings should correspond to an ideal, uniformly stressed specimen.

In all cases, an axisymmetric gap between piston and metal cylinder cavity is postulated (the undeformed hollow cylinder inner radius is 12.5582 mm (see Section 3.3.2.8) and the undeformed piston radius is 12.550 mm so that the initial radial gap is 0.0082 mm), even if eccentricities between hollow cylinder and piston axes are inevitably likely to occur during the piston stroke. In any case, the assumption adopted still gives an indication about the sensitivity of the bulk modulus to this correction.

Tables 3.3.4.1,2 also include the Poisson's ratios, based upon the Young's moduli of Section 3.3.1 . The last correction does not appreciably alter the Poisson's ratio value.

Figs 3.3.4.3 and 3.3.4.4 diagrammatically present the bulk moduli (extracted from the previous Tables; only the apparent and fully corrected values are

reported) for the two elastomers, as functions of the applied pressure. As expected from Figs 3.3.1.2,3 , the bulk modulus slightly increases (non-linearly) with pressure.

It is here observed that both the corrections connected to the cylinder expansion and to the specimen extrusion influence only marginally the Poisson's ratio ((Tables 3.3.4.1 and 3.3.4.2), so that the complex modellings presented in this thesis for for these two corrections appear perhaps unjustified for the elastomers under scrutiny. On the other side, it can be observed that these amendments would permit less thick cylinders and less stringent tolerances to be used. In addition, the above corrections are more important for an elastomer closely approaching incompressibility, so that there might well be joint rubbers for which such refinings become more significant.

It is finally observed that an error analysis was not effected on the reliability of the reported readings. It is usually admitted that the measurements of the Poisson's ratio are reliable up to at least four decimal digits, so that for the readings here presented, which are fully corrected, five or more decimal digits are deemed to be valid. In the case of the "Estane" 5714F1 elastomer (E = 8.506 MPa), the bulk moduli for, say, ν = 0.499422 and ν = 0.499423 are 2452.7107 MPa and 2456.9613 MPa , respectively, thus providing an indication about the relative influence of an inaccuracy of ν on K .

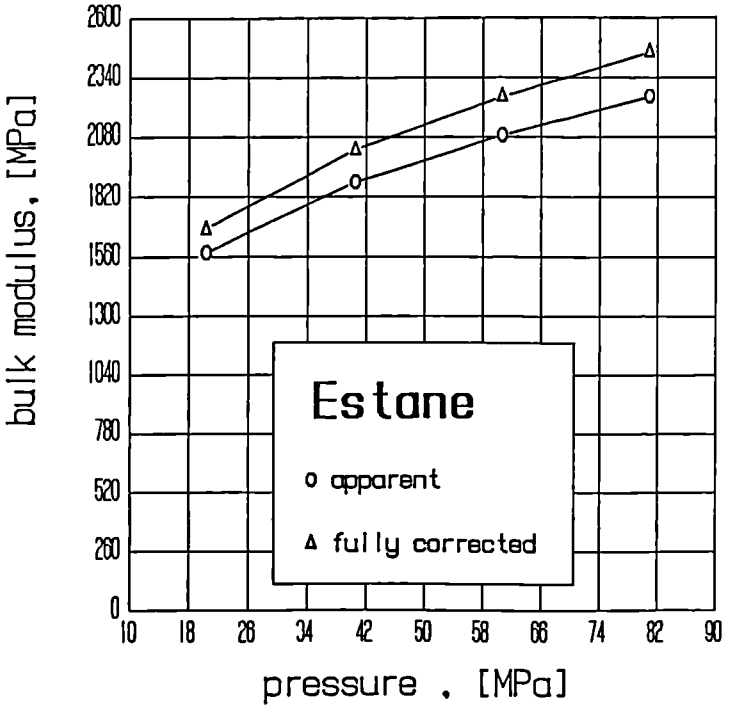

Fig 3.3.4.3 : The apparent and fully corrected bulk modulus as function of the applied hydrostatic pressure, for the "Estane" 5714F1 elastomer.

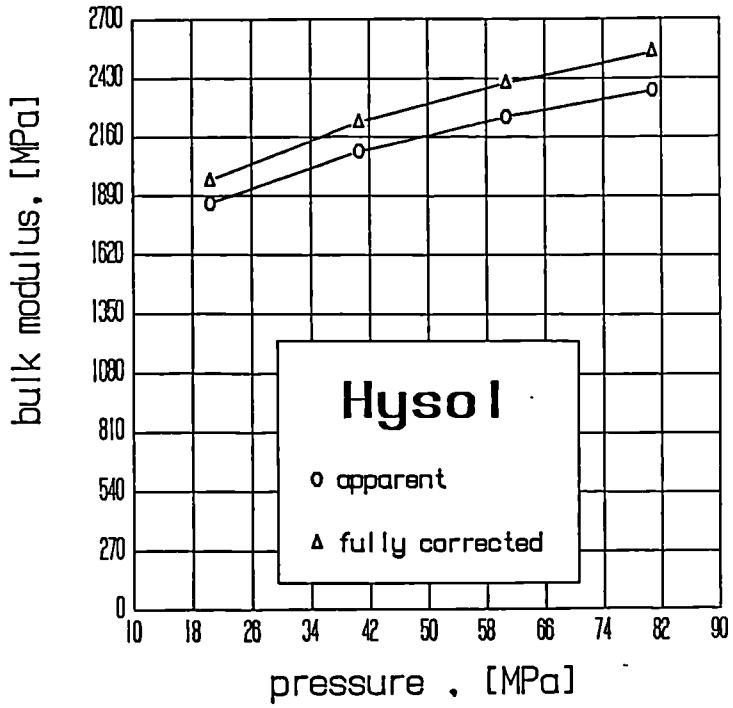

Fig 3.3.4.4 : The apparent and fully corrected bulk modulus as function of the applied hydrostatic pressure, for the Hysol CP 4485 elastomer.

3.4 CONCLUSIONS

A piston device has been built to measure the cubic compressibility of elastomeric materials. Theories have been developed to correct the experimental measurements by accounting for elastic distortions of the device and possible extrusions of the elastomeric specimen. Apparent and compensated values of the bulk moduli have been obtained for two elastomers of practical relevance, which indicate the relative importance of such corrections.

CHAPTER 4. THE PLANE STRAIN, FLAT ELASTOMERIC LAYER : THEORY

4.1 INTRODUCTION

This Chapter deals with the deflections of a deformable layer firmly bonded to a rigid substrate and frictionlessly compressed by a rigid indenter. Several engineering applications can be described in terms of the title problem. For instance, Parish (1958) mentions applications in the textile industry and, more generally (Parish (1961)), in the processing of materials in sheet forms. Miller (1964) refers to rotary letterpress and lithographic printing. Hooke (1986) employs the layer theory to analyze bearings with rubber linings. Matthewson (1981) mentions the use of elastic coatings to protect aircraft components from rain erosion. A leading ball bearing company is experimenting with cases coated with elastomer to reduce friction (Gabelli and Jacobson (1990)). Finally, applications of the layer theory are recorded in the field of Biomechanics. For instance, Armstrong (1986) studies the contact pressure in the articular cartilage in a synovial joint, described as a biphasic material. Unsworth, Pearcy, White and White (1987) examine experimentally an artificial hip joint covered with an elastic layer. Jin (1988) deals with micro-elastohydrodynamic aspects in synovial joints described via the title model.

This Chapter addresses the mechanical behaviour of an elastic layer having in mind rubber covered artificial hip joints (for which the plane model of this Chapter is a first order approximation), or, alternatively, aiming at applications in the field of knee joints, and its outline is as follows. The second Section presents a literature review, and underlines the fact that two main analytical approaches are available. The third Section presents a solution method developed by the writer and based upon an approximate analytical integral approach. The fourth Section further develops an already existing approximate differential theory. A comparison between theoretical predictions and experimental readings is deferred to Chapter 5 .

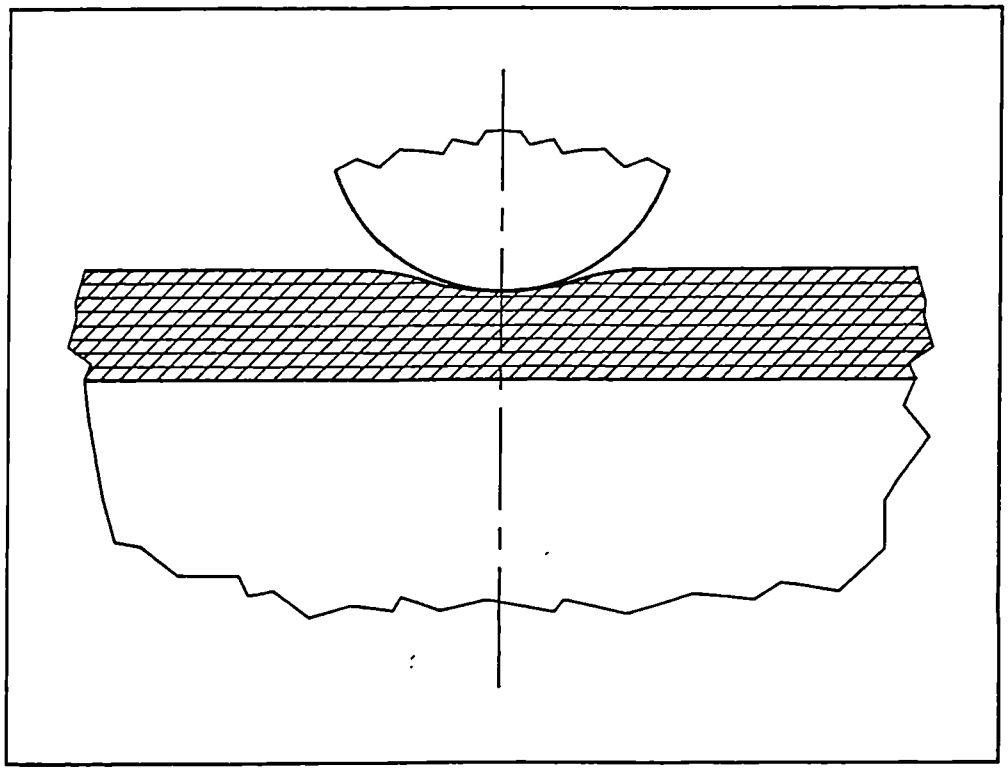

Fig. 4.1.1 : A cylindrical indenter compressing a layer anchored to a substrate.

4.2 LITERATURE REVIEW

As already mentioned, two main approaches to the layer problem can be traced in the literature. The first description, here named "the integral approach" because it leads to an integral equation, is reviewed first. The second method examined is called "the differential approach" because it reduces to a differential equation.

A fundamental paper describing the mechanical behaviour of an elastic layer in terms of a Fredholm integral equation of the first kind was produced by Hannah (1951). By extending a method based upon Fourier integrals developed by Coker and Filon (1957) for a similar case (see p. 436), she obtained the expression for the transverse displacement of the free boundary of the layer bonded to a rigid substrate and loaded by a unit transverse concentrated force. In other words, she developed the Green function for this elasticity problem, on whose grounds the practically more relevant problem of a layer loaded by a distributed pressure can also be described. More exactly, Hannah (1951) treated the generalized plane stress situation. The plane strain configuration, more common in practical applications, requires a simple modification of the elastic constants, and it was developed by Parish (1957), to produce an integral representation of the Green function. An extension of the Green function for the configuration of an elastic layer supported by a Winkler foundation is given by Dempsey, Zhao, Minnetyan, and Li (1990).

It can be shown that, similar to the Boussinesq case (Timoshenko and Goodier (1970)), the vertical displacement becomes infinite under the load (Hannah (1951)) but, contrary to the Boussinesq results, the vertical displacement of the layer free boundary dies away in the regions sufficiently far from the point of application of the load.

Concerning the reliability of a Boussinesq-type approach in modelling the distortions of a deformable layer, De Mul, Kalker and Fredriksson (1986) report an observation due to Reusner, taken from a thesis quoted in their reference list but not accessible to the writer, dealing with the description of the deflections of a deformable body of finite depth according to the theory of elasticity. They write :

"Modeling a body of finite depth by a half space is often questionable. Reusner observed when playing with a rubber eraser on a table top, that under a load the rubber gave way at the pressurized area, but at some distance from this area the surface of the rubber hardly moved. This was not as predicted by the half space theory . . " . Another word of caution on the physical correctness of a Boussinesq-type solution is expressed by Parish (1958), who noted that "Most of the [experimental] *pressure distributions were noticeably* different in shape from the theoretical distributions." He attributed such discrepancies to "non-linearity in the elastic properties of rubber." In a following paper, Parish (1961) proposed a design formula based upon a Hertzian expression corrected via empirical coefficients, thus abandoning Hannah (1951) formulation, which he must have believed as theoretically more sound but weaker from a reliability viewpoint. Anyway, other researchers (*e.g.* Miller (1964)) found a good correlation between experimental measurements and theoretical forecasts.

As noted by Bentall and Johnson (1968), the integral in expression (4.2.1) is analytically "intractable" and, therefore, no relatively simple results as those describing the parallel case of a half plane loaded by a concentrated force (Hertz solution, see Johnson (1985)) are available. Even when the integral of the expression for the displacement due to a concentrated load has been estimated, other formidable difficulties are encountered when the case of a rigid indenter pressing a deformable layer is treated. In this case, the contact pressure can be described in terms of a series of adjacent infinitesimal forces acting simultaneously. In other words, this problem can be formulated in terms of an integral over the contact length, where the pressure profile multiplies a kernel expressing the displacement due to a concentrated load (eqn 4.3.2.1)), which represents the Green function (influence function) (Tuncel (1964)). The indenter profile and the indentation depth are known, whereas the pressure distribution is the unknown. The deflection of the pressed layer border must conform to the indenter profile. In other words, the problem at hand can be formulated in terms of a Fredholm integral equation of the first kind (Gladwell (1980)). In summary, two difficult integrals have to be dealt with, the first connected to the Green function, and the second encountered in the integral equation.

The approximate methods which have been developed to solve the Fredholm integral equation can be classified into two main categories, namely an essentially numerical approach, referred to in the following as "finite element", and a "series" solution.

The finite element formulation is analyzed first. This method has been employed in several papers (Conway and Farnham (1968a), Loss (1964), Bentall and Johnson (1968)). Essentially, the (estimated) contact length is divided into a series of elements defined by nodes, and the contact pressure is approximated by a piecewise constant (*e.g.* Conway and Farnham (1968a)) or piecewise linear (*e.g.* Bentall and Johnson (1968)) curve, which is related to the position of the element nodes. By substituting the simplified pressure profile in equation (4.3.2.2.), it is possible to express the displacements at the centres of each element (piecewise constant pressure profile) or, alternatively, at the nodal points (piecewise linear pressure profile) as functions of the pressure values at the centres or at the nodes of the elements, respectively. These values must coincide with the imposed displacements referring to the previously mentioned points (collocation approach), to form a set of linear algebraic equations whose solution supplies the approximate pressure profile curve. Since the contact length is generally not known a priori (unilateral contact problem, (Cannarozzi (1980)), some iteration may be necessary to define it. This aspect will be examined in Section 4.3.3. .

Some papers dealing with the numerical treatment of contact problems explicitly report the possible outcome of numerical instabilities, especially when Gauss-type solvers are employed in the solution of the discretized problem. In other words, the pressure profile was sometimes found to be affected by spurious numerical undulations or unrealistic concentrated pressure peaks. Such papers include Poulos (1968), Hooper (1974), Sing and Paul (1974), Hartnett (1979), Hartnett (1980), Ahmadi, Keer and Mura (1983) (who actually refer to numerical instabilities encountered by other researchers), Solecki and Ohgushi (1984) (who mention the possible outcome of ill-conditioned matrices), and Dragoni and Strozzi (1989). In other papers, however, it is clearly stated that numerical instability problems were not encountered at all, even if direct solution procedures were used. These works include Brothers and Sinclair (1977), and Bentall and Johnson (1968). It is not easy to

clarify which physical parameters render either stable or unstable numerical schemes that look similar. However, it appears from the above-mentioned papers that, contrary to the pessimistic remarks of Rice (1983), p. 145, a relaxation-type solver (Hartnett (1979)) effectively smoothes out the spurious pressure undulations often delivered by Gauss-type solvers.

The solution of the Fredholm integral equation via a "series" approach is now considered. Hannah (1951) expands the pressure profile in terms of a Fourier series (plus a singular term), and computes the series coefficients. Meijers (1968) expands the regular part of the contact pressure in the form of a power series, and finds the coefficients via a perturbation approach. Mozarovsky, Shylkc, and Starzynsky (1986) develop a similar solution. Additional perturbed terms are computed by Jaffar and Savage (1988). Series expansions are employed by Wu and Chiu (1967) in an abstract paper. Finally, eigenfunction expansions are adopted by Smith (1964), who reports a load formula as function of the normalized contact width.

The series technique supplies analytical, although approximate, solutions, but it is practically applicable only to relatively simple indenter profiles, where flat and circular (approximated by a parabolic curve) shapes are the most frequently studied. As a consequence, the series solution does not practically lend itself to the treatment of soft lubricated conjunctions, where the deformed profile can exhibit complex features (Prati and Strozzi (1984)). In addition, it must be remarked that, in biomechanical applications, the contact width between cylindrical indenter and cup can be high and, therefore, a parabolic approximation may lead to questionable results (Mattewson (1981)).

Always with regard to the integral approach, an alternative solution method to the perturbation scheme is now considered. In the perturbation solution the original problem is decomposed into a series of hopefully simpler sub-problems, for which exact solutions are often derived. On the contrary, according to the alternative approach here discussed, the kernel is substituted by a properly simplified version, and this single, approximate integral equation is amenable to closed form solutions. In this respect the works of Latta (1956) and of Shinbrot (1959) are pertinent, who develop a method for solving exactly a class of Fredholm first kind integral equations. Ling (1959) and (1973) report various examples of

integral equations solved exactly. This method has been extended by Pearson (1957), who in fact quotes the strip problem. Margetson (1970) follows a similar trend, obtaining a closed form solution for a simplified integral equation, where the kernel is expanded in terms of Chebyshev series. An open point concerning this solution technique is that the examples of Latta (1956) clearly show that a (the) solution exists provided that certain links hold among the coefficients of the kernel expansion. This may imply that the solution obtained is valid only for certain elastic constants or geometrical proportions, a difficulty which is not encountered with perturbed solution methods. It is believed that this aspect should deserve more attention with regard to the layer problem.

The second solution method for the title problem, that named "the differential approach" is now reviewed. The basic paper is that of Armstrong (1986), where the author reformulates the plane equilibrium differential equations in Cartesian coordinates in terms of normalized displacements and of an ϵ perturbation parameter, which expresses the ratio of the layer thickness to the (yet unknown) semicontact length. He solves the case of compressible materials for the ϵ^0 (Armstrong (1986)) and ϵ^2 (Armstrong (1988)) terms, and treats the situation of incompressible layers for the ϵ^2 order (Armstrong (1986)). Following a perturbation scheme (Bender and Orszag (1978)), he faces difficulties in properly expressing the boundary conditions. When higher-order terms are considered, the order of the differential equation increases too, thus requiring additional boundary conditions. In Armstrong (1988) the author imposes a vanishing pressure gradient by the contact extremities for compressible materials, which is a questionable condition. In addition, the coefficients of the highest order differential term rapidly vanish as the perturbation order is increased, thus giving rise to a singular perturbation problem (Bender and Orszag (1978)), which is affected by numerical problems in treating the boundary conditions. Okubo (1951) studies the case of an elastic half plane loaded by a deformable, rectangular punch, via a stress function-type solution, which does not involve the treatment of an integral equation.

The differential approach supplies an analytical, although approximate, pressure profile but, similar to the integral approach solved via a series technique, its practical applicability field is limited to simple indenter profiles.

Some papers dealing with the compressed layer employ traditional finite element packages (*e.g.* Hooper (1974), Komvopoulos (1988), Björkman (1991)), but these studies are believed to be more relevant from a technical viewpoint than from a scientific standpoint.

The pertinent literature is now examined with regard to the applicability of a purely Hertzian approach to layers of finite depth. In other words, which is the ratio of the layer thickness to the contact semiwidth, beyond which the Hertzian formulae, referring to an infinitely deep half plane, produce a contact pressure hardly distinguishable from the theory which accounts for the narrowness of the layer thickness ? Nowell and Hills (1988) claim that this ratio is 10. Hui Li and Dempsey (1988) favour a ratio of about 6 for the case of a beam resting on elastic foundations. Matthewson (1981) favours a ratio as low as 1 for an axisymmetric situation. Finally, Miller and Poulter (1962) and Miller (1966) claim that Hannah theory is appropriate when the contact width is less than four times the strip thickness. In addition, Björkman (1991) examines numerically the influence of geometrical non-linearities for the situation of a rigid cylinder indenting a very thick layer mimicking an elastic half space, for $\nu = 0.42$. Two indentation depths are imposed. The first case treated exhibits a ratio of contact semiwidth to cylinder radius of 0.581 ($\delta\ R/h^2 \simeq 0.0033$), and the second situation shows a ratio of 0.774 ($\delta\ R/h^2 \simeq 0.0084$). The Hertzian peak pressure overestimates the numerical forecasts by 3.7 percent for the first case, while it underestimates the finite element predictions by 12 percent for the second circumstance. While the first mismatch may be partially imputable to errors in measuring the relevant data from Figs 9 and 10 of Björkman (1991) , the second, more substantial disagreement can be confidently attributed to nonlinear effects. In fact, the geometrical distortions imposed to the layer in Figs 9 and 10 of Björkman (1991) look appreciable. The trend of the second error is also consistent with Fig 6.5.2.1 , indicating that for a prescribed indentation depth the non linear effects stiffen the layer, thus producing a higher peak contact pressure. (The useful part of the curves of Fig. 6.5.2.1 is in fact visible only for much higher $\delta\ R/h^2$ values). For the same load, lower displacements are expected (at least for nearly incompressible materials) as the cylinder radius is increased and, consequently, the contact width becomes wider,

since the stress field under the indenter is essentially hydrostatic, and scarcely incompressible materials behave in a very stiff fashion when compressed. It can be concluded that the effects of the large deformations as derived from Björkman (1991) paper look modest, and they are expected to become smaller in biomechanical applications, characterized by higher contact widths.

As a final point, the pertinent literature is now analyzed with reference to the Poisson's ratio effects. It is known that, as ν approaches the incompressibility figure 0.5, the actual situation can be mimicked by adopting a perfectly incompressible model whereas, as ν is far from 0.5 (say, 0.46, which is a low figure for an elastomer, see Section 3), a Winkler-type model (Johnson (1985)) is applicable. Some authors indicate the transitional value of Poisson's ratio, under which a Winkler model is preferable, and beyond which an incompressible approach is applicable. Bentall and Johnson (1968) suggest that the Winkler results be applied for $\nu < 0.45$ and the incompressible results be valid for $\nu > 0.48$. Armstrong (1988) correctly proposes that the ν transition figure depend upon the contact semiwidth, a , and the layer thickness, h , according to the following formula : $(h/a)^2 \simeq (1 - 2\nu)(1 - \nu)/(4\nu - 1)$. This expression suffers from the limit that the contact width is not generally known. Finally, Jaffar (1988),(1989) examines the effect of a perturbation of ν for an axisymmetric case, but he does not clearly indicate a transition value for ν.

4.3 INTEGRAL APPROACH

4.3.1 Introduction

In this Section an approximate analytical expression for the Green function is obtained (Chapter 4.3.2) and, then, a finite element solution is developed for the case of a rigid cylindrical indenter pressed against a deformable layer firmly anchored to a rigid foundation (Chapter 4.3.3). The numerical results are presented in Section 4.3.4. Finally, part 4.3.5 is devoted to an appraisal of Meijers (1968) theory.

4.3.2 The approximate evaluation of the infinite integral

The transverse displacement of the free surface of a layer firmly bonded to a rigid substrate and acted upon by a unit transverse concentrated force applied at $x = 0$ (where x is the distance from the contact centre along the undeformed layer loaded border) is (Jaffar and Savage (1988)) :

$$v(x) = \frac{2\lambda}{\pi} \int_0^\infty \frac{2(k \sinh(2\omega) - 2\omega)}{\omega (2k \cosh(2\omega) + 4\omega^2 + k^2 + 1)} \cos\left[\frac{x\omega}{t}\right] d\omega \qquad (4.3.2.1)$$

where $\lambda = \frac{(1 - \nu^2)}{E}$, $k = 3 - 4\nu$, E is the Young's Modulus, ν the Poisson's ratio, and ω is an integration device. Since for elastomeric materials ν approaches the incompressibility value 0.5 , $k \simeq 1$. Fig. 4.3.2.1 presents the deformable layer of thickness t , firmly bonded to a rigid substrate and indented by a rigid cylinder of radius R, a case for which the Green function is expressed by eqn 4.3.2.1 . In addition, a indicates the semicontact width and δ the indentation depth.

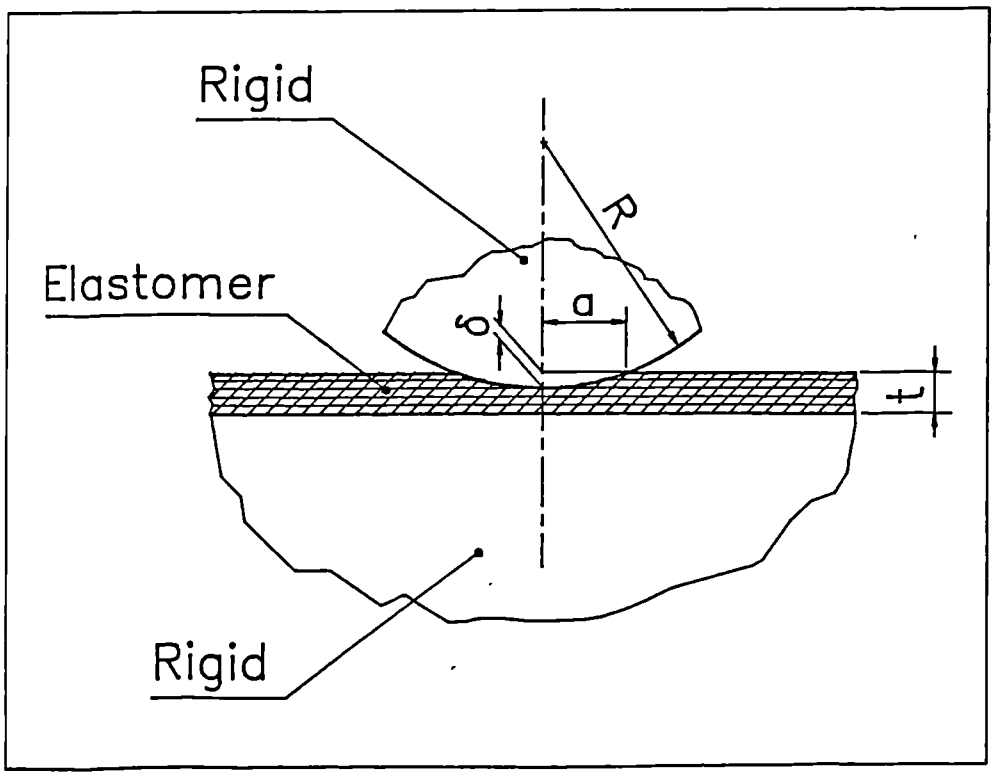

Fig. 4.3.2.1 : The meaning of symbols a, R, t and δ.

It is derived from equation (4.3.2.1) that, when a distributed pressure, p, acts upon an elastomeric layer bonded to a rigid substrate, the transverse displacement, v, of the upper boundary of the layer can be expressed via the following integral equation :

$$v(x) = \frac{2\lambda}{\pi} \int_a^b p(s)\, K(x - s)\, ds \qquad (4.3.2.2)$$

where a and b describe the extremes along x-axis of the layer boundary segment subject to a distributed pressure p , and K represents the following influence function :

$$K(x-s) = \int_0^\infty \frac{2(k\ sinh\ (2\omega) - 2\omega)}{\omega\ (2k\ cosh\ (2\omega) + 4\omega^2 + k^2 + 1)}\ cos\left[\frac{(x - s)\omega}{t}\right] d\omega \qquad (4.3.2.3)$$

It is the aim of this Section to determine an analytical approximation of the integrand of expression (4.3.2.1), which can be integrated in closed form according to (4.3.2.3) . Moreover, such an integral (4.3.2.3) , once multiplied by a simple pressure profile discretization (*e.g.* uniform or linear approximations, see Section 4.3.3), should be analytically integrable according to equation (4.3.2.2) . (For a somewhat similar approximate integration, based upon simplified integrands, see Sneddon (1946).) To this end, the behaviour of the following part of the integrand of (4.3.2.1) is examined :

$$\frac{2(k\ sinh\ (2\omega) - 2\omega)}{\omega\ (2k\ cosh\ (2\omega) + 4\omega^2 + k^2 + 1)} \tag{4.3.2.4}$$

This function dies away for $\omega \rightarrow \infty$ as $1/\omega$. Fig. 4.3.2.2 shows function (4.3.2.4) together with its approximation $1/\omega$, for $\nu = 0.5$ and $\nu = 0.46$. The exact kernels for both $\nu = 0.5$ and 0.46 become hardly distinguishable from function $1/\omega$ for $\omega \geq 5$. The influence of a change of Poisson's ratio becomes appreciable for small ω values. For ν different from the incompressiblity values 0.5, the Meijers kernel does not vanish for $\omega = 0$. For very small ω , expression (4.3.2.4) is detailed in Fig. 4.3.2.3 , only for $\nu = 0.5$. The following results hold true for any Poisson's ratios (the approximate values given for the following formulae refer to $\nu = 0.5$, that is, $k \simeq 1$) :

$$lim\ |_{\omega \rightarrow 0}\ \frac{2(k\ sinh\ (2\omega) - 2\omega)}{\omega\ (2k\ cosh\ (2\omega) + 4\omega^2 + k^2 + 1)} = 4\ \frac{k-1}{(1+\kappa)^2} \simeq 0$$

$$lim\ |_{\omega \rightarrow 0}\ \frac{d}{d\ \omega}\ \frac{2(k\ sinh\ (2\omega) - 2\omega)}{\omega\ (2k\ cosh\ (2\omega) + 4\omega^2 + k^2 + 1)} = 0$$

$$lim\ |_{\omega \rightarrow 0}\ \frac{d^2}{d\ \omega^2}\ \frac{2(k\ sinh\ (2\omega) - 2\omega)}{\omega\ (2k\ cosh\ (2\omega) + 4\omega^2 + k^2 + 1)} = \frac{16}{3}\ \frac{(3-k)\ (2-k)}{(1+k^2)^3} \simeq 1.33$$

$$lim\ |_{\omega \rightarrow 0}\ \frac{d^3}{d\ \omega^3}\ \frac{2(k\ sinh\ (2\omega) - 2\omega)}{\omega\ (2k\ cosh\ (2\omega) + 4\omega^2 + k^2 + 1)} = 0 \tag{4.3.2.5}$$

These analytical results correlate well with Fig. 4.3.2.3 , where function (4.3.2.4) vanishes together with its derivative (at least for $\nu = 0.5$, see (4.3.2.5)) for $\omega = 0$. For Poisson's ratios other than 0.5 , the derivative still vanishes, but the function no more vanishes for $\omega = 0$ (see Fig. 4.3.2.2) . The curvature, instead, is always positive.

The properties of (4.3.2.4) freed from term $1/\omega$ are now analyzed. In other words, the following function is studied :

$$\frac{2(k\ sinh\ (2\omega) - 2\omega)}{(2k\ cosh\ (2\omega) + 4\omega^2 + k^2 + 1)} \tag{4.3.2.6}$$

Fig. 4.3.2.4 displays function (4.3.2.6) for two different ν values. As expected, this function approaches unity for $\omega \simeq 5$. For small ω, the effect of a change in ν becomes noticeable. Fig. 4.3.2.5 reports expression (4.3.2.6) for small ω and for a selection of Poisson's ratios, and evidences the effects of ν. It is instructive to study analytically the behaviour of (4.3.2.6) as $\omega \to 0$. The following results hold true (the approximate values refer to $\nu = 0.5$, that is, $k \simeq 1$) :

$$lim\ |_{\omega \to 0}\ \frac{2(k\ sinh\ (2\omega) - 2\omega)}{(2k\ cosh\ (2\omega) + 4\omega^2 + k^2 + 1)} = 0$$

$$lim\ |_{\omega \to 0}\ \frac{d}{d\ \omega}\ \frac{2(k\ sinh\ (2\omega) - 2\omega)}{(2k\ cosh\ (2\omega) + 4\omega^2 + k^2 + 1)} = 4\ \frac{k - 1}{(1 + \kappa)^2} \simeq 0$$

$$lim\ |_{\omega \to 0}\ \frac{d^2}{d\ \omega^2}\ \frac{2(k\ sinh\ (2\omega) - 2\omega)}{(2k\ cosh\ (2\omega) + 4\omega^2 + k^2 + 1)} = 0$$

$$lim\ |_{\omega \to 0}\ \frac{d^3}{d\ \omega^3}\ \frac{2(k\ sinh\ (2\omega) - 2\omega)}{(2k\ cosh\ (2\omega) + 4\omega^2 + k^2 + 1)} = \frac{16}{3}\ \frac{(3 - k)\ (2 - k)}{(1 + k^2)^3} \simeq 1.33$$

(4.3.2.7)

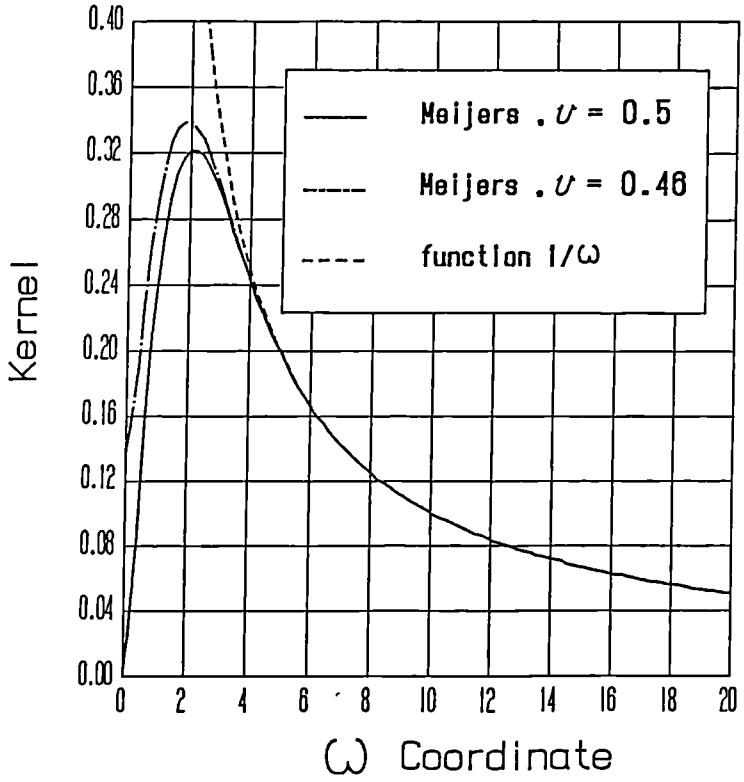

Fig. 4.3.2.2 : Function (4.3.2.4) and its $1/\omega$ approximation, for ν = 0.46 and 0.5.

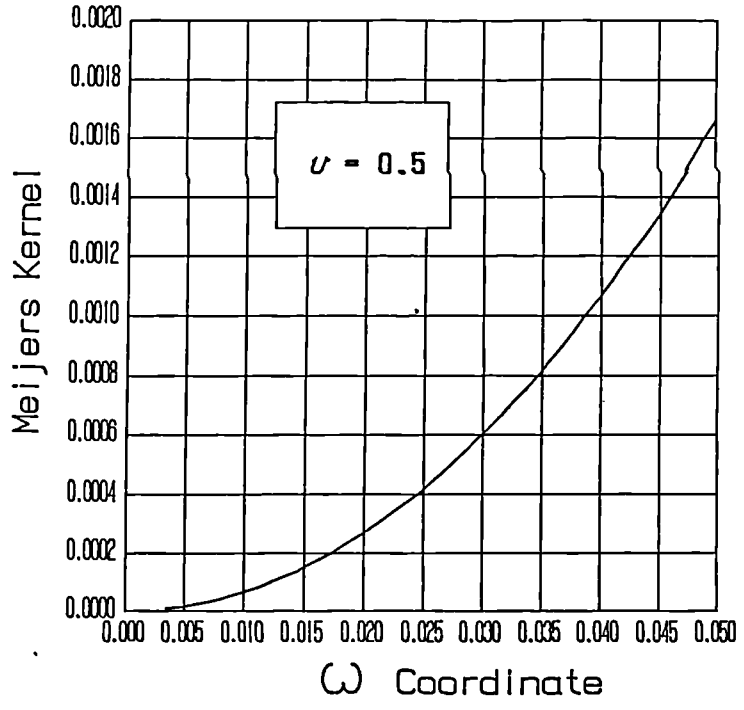

Fig. 4.3.2.3 : Function (4.3.2.4) , for ν = 0.5 and for small ω.

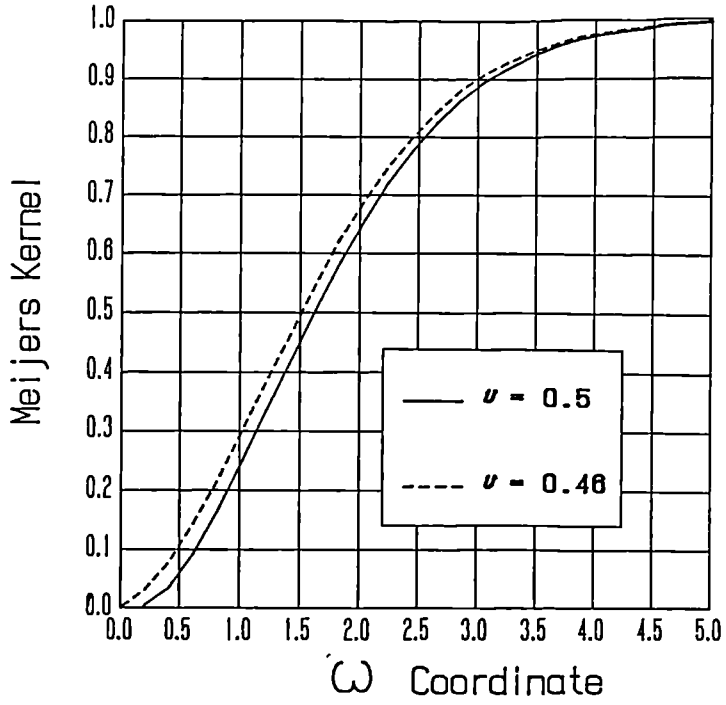

Fig. 4.3.2.4 : Function (4.3.2.6) for ν = 0.5 and 0.46 .

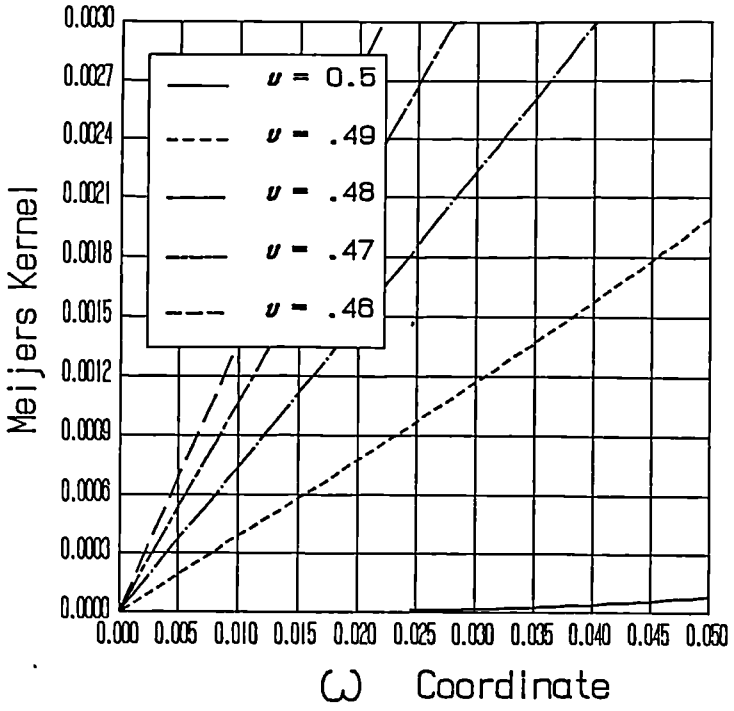

Fig. 4.3.2.5 : Function (4.3.2.6) for ν = 0.5, 0.49, 0.48, 0.47, 0.46 and for small ω .

From Fig. 4.3.2.5 it clearly appears that the first derivative is zero only for $\nu = 0.5$. Independent of the value of ν, all curves are nearly linear in the vicinity of $\omega = 0$, since the second derivative vanishes for any ν value, see (4.3.2.7) .

Having explored the main aspects of functions (4.3.2.4) and (4.3.2.6), expression (4.3.2.4) is approximated via an integrable (in the sense of (4.3.2.3)) function. An approximation for high ω is first sought for, by analyzing the asymptotic behaviour of (4.3.2.4) for $\omega \to \infty$ and, subsequently, an approximation for small ω is explored. As already mentioned, function (4.3.2.4) behaves asymptotically as $1/\omega$ for large values of ω . If one subtracts from the original function (4.3.2.4) its asymptotic approximation, $1/\omega$, the resulting function vanishes more rapidly as $\omega \to \infty$. This technique — known as Kummer method (Knopp (1928), p. 260) — is usually employed to improve the convergence of the sum of numerical series (*e.g.* Barton (1941), Strozzi (1989)). If this technique is repeated, that is, if one subtracts from this resulting function its new asymptotic approximation (Strozzi (1989)), one expectedly further enhances the trend of the newly modified function to vanish starting from increasingly lower values of ω . So doing, a kind of series expansion of the original function is generated, whose terms are suggested by the behaviour of the function for $\omega \to \infty$. Unfortunately, the iterated application of this technique will not necessarily be increasingly beneficial, since a function becoming vanishingly small for increasingly lower values of ω is desired, by exploiting data related to $\omega = \infty$. In other words, when the degree of extrapolation of the function — evaluated from data referring to $\omega = \infty$ — to represent its value for a relatively low ω becomes exceedingly large, the iteration scheme here proposed may fail to be advantageous. Anyway, the optimal number of iterations can be evaluated by numerical tests. Eventually, a vanishingly small function for values of ω relatively low up to infinity is obtained. This function is in fact the difference between the original expression (4.3.2.4) and its subsequent asymptotic approximations. In conclusion, a good approximation of (4.3.2.4) valid for a wide interval of ω values — from a finite figure up to infinity — is the sum of its subsequent asymptotic approximations.

Another point deserves some comments. Since an exact integral of an approximation of (4.3.2.4) is desired, it is important that the following asymptotic

expansion terms, once multiplied by *cos* function (see (4.3.2.3)), be analytically integrable. Since there is generally more than one asymptotic approximation for a given function, it is necessary to select the one whose product by *cos* function is exactly integrable. These inevitably abstract comments will hopefully become clearer in the following text, where the strategy just summarized is applied to expression (4.3.2.4) .

As already mentioned, function (4.3.2.4) behaves asymptotically as $1/\omega$. Anyway, this asymptotic approximation, once multiplied by *cos* function, is not integrable in closed form. In other words (Gröbner and Hofreiter (1958), second volume, p. 121, n. 333.22b) :

$$\int_a^\infty \frac{1}{\omega} \cos\left[\frac{(x-s)\omega}{t}\right] d\omega = \text{integralcos}\left[\frac{(x-s)a}{t}\right] \qquad (4.3.2.8)$$

which is not expressible analytically and, when $a \to 0$:

$$\int_0^\infty \frac{1}{\omega} \cos\left[\frac{(x-s)\omega}{t}\right] d\omega = \infty \qquad (4.3.2.9)$$

Jin (1988) , p. 297, follows this path, by computing the cosine integral via a NAG library routine.

The mechanical interpretation of result (4.3.2.9) is as follows. When the vertical displacement of the layer upper boundary loaded by a concentrated force applied at $x = 0$ is studied, this displacement at a generic coordinate y from the same origin of x-axis becomes infinite as $y \to 0$. In other words, the displacement under the applied concentrated force is unbounded. Unfortunately, this singularity is not analytically expressed by (4.3.2.8,9) . This singular behaviour occurs also in the case of a half plane loaded by a concentrated force (Johnson (1985)) . In addition, a comparison with the half plane case suggests that the displacement singularity in the vicinity of the applied force be logarithmic. With these premises

in mind, an analytically integrable asymptotic expression equivalent to $1/\omega$ is now sought for, and it is conjectured that, if this equivalent approximation is correct, its integral according to (4.3.2.3) contains a logarithmic singularity. Gladwell (1976) proposes the following equivalent asymptotic expression :

$$\frac{2(k\ sinh\ (2\omega) - 2\omega)}{\omega\ (2k\ cosh\ (2\omega) + 4\omega^2 + k^2 + 1)} \rightarrow \frac{1 - e^{-q\omega}}{\omega} \qquad (4.3.2.10)$$

for which the following integral exists in closed form (Gröbner and Hofreiter (1958), second volume, p.140, n. 336.13c), exhibiting, as expected, a logarithmic singularity as $x \rightarrow s$:

$$\int_0^\infty \frac{1 - e^{-q\omega}}{\omega} cos\left[\frac{(x - s)\omega}{t}\right] d\omega = - log\left[\frac{(x - s)}{t}\right] + \frac{1}{2} log\left[q^2 + \frac{(x - s)^2}{t^2}\right]$$

(4.3.2.11)

It is clear that the above (4.3.2.10) asymptotic function behaves as $1/\omega$ for high values of ω, since the exponential function vanishes quickly. The selection of coefficient q to be given to the exponent of the exponential function is problematic. Gladwell (1976) chooses $q = 2$. It is shown in the following that the "spurious" function introduced, $e^{-2\omega}/\omega$, vanishes more rapidly than the term obtained by subtracting from the previous function the asymptotic expression (4.3.2.10) . This point will be further examined later, but an optimization of such an exponent is beyond the scope of this study.

Once term (4.3.2.10) has been subtracted, the remaining function behaves asymptotically for $\omega \rightarrow \infty$ as :

$$\frac{2(k\ sinh\ (2\omega) - 2\omega)}{\omega\ (2k\ cosh\ (2\omega) + 4\omega^2 + k^2 + 1)} - \frac{1 - e^{-2\omega}}{\omega} \rightarrow - \frac{4}{k}\ \omega\ e^{-2\omega} \qquad (4.3.2.12)$$

which is analytically integrable in the sense of (4.3.2.3) (Gröbner and Hofreiter (1958), second volume, p. 139, n. 336.4c) :

$$-\frac{4}{k}\int_0^\infty \omega\, e^{-2\omega}\cos\left[\frac{(x-s)\omega}{t}\right]d\omega = -\frac{4}{k}\,\frac{4-\frac{(x-s)^2}{t^2}}{\left[4+\frac{(x-s)^2}{t^2}\right]^2}$$

(4.3.2.13)

By proceeding similarly, the new function obtained by subtracting to the previous expression the asymptotic term (4.3.2.12) behaves asymptotically as :

$$\frac{2(k\,\sinh(2\omega)-2\omega)}{\omega\,(2k\,\cosh(2\omega)+4\omega^2+k^2+1)} - \frac{1-e^{-2\omega}}{\omega} + \frac{4}{k}\,\omega\,e^{-2\omega} \to -\frac{4}{k}\,e^{-2\omega}$$

(4.3.2.14)

and this asymptotic approximation too is analytically integrable in the sense of (4.3.2.3) (Gröbner and Hofreiter (1958), second volume, p. 135, n. 335.2) :

$$-\frac{4}{k}\int_0^\infty e^{-2\omega}\cos\left[\frac{(x-s)\omega}{t}\right]d\omega = -\frac{4}{k}\,\frac{2}{4+\frac{(x-s)^2}{t^2}}$$

(4.3.2.15)

By insisting with this procedure, one subtracts the approximation of (4.3.2.14) and obtain the subsequent asymptotic approximation :

$$\frac{2(k\,\sinh(2\omega)-2\omega)}{\omega\,(2k\,\cosh(2\omega)+4\omega^2+k^2+1)} - \frac{1-e^{-2\omega}}{\omega} + \frac{4}{k}\,\omega\,e^{-2\omega} + \frac{4}{k}\,e^{-2\omega} \to$$

$$\frac{k - (1 + k^2)}{k} \frac{e^{-2\omega}}{\omega} \tag{4.3.2.16}$$

Anyway, this approximation (4.3.2.16) is not analytically integrable (Gradshteyn and Ryzhik (1980), p. 489, n. 3.941.2) since :

$$\frac{k - (1 + k^2)}{k} \int_0^\infty \frac{e^{-2\omega}}{\omega} \cos\left[\frac{(x - s)\omega}{t}\right] d\omega = \infty \tag{4.3.2.17}$$

The fact that this integral is unbounded is not due to the behaviour of the integrand for $\omega \to \infty$, but to its singularity when $\omega \to 0$. In fact, the integral parallel to (4.3.2.17) in which function *cos* is substituted by *sin* — which behaves similarly when $\omega \to \infty$ but not when $\omega \to 0$ — is finite (Gradshteyn and Ryzhik (1980), p. 489, n. 3.941.1). As previously seen, in this case an equivalent asymptotic expression must be resorted to, which is analytically integrable. The following function possesses this property :

$$\frac{k - (1 + k^2)}{k} \frac{e^{-2\omega} - e^{-4\omega}}{\omega} \tag{4.3.2.18}$$

and (4.3.2.16) must be rewritten in the following way :

$$\frac{2(k \sinh(2\omega) - 2\omega)}{\omega (2k \cosh(2\omega) + 4\omega^2 + k^2 + 1)} - \frac{1 - e^{-2\omega}}{\omega} + \frac{4}{k} \omega e^{-2\omega} + \frac{4}{k} e^{-2\omega} \to$$

$$\frac{k - (1 + k^2)}{k} \frac{e^{-2\omega} - e^{-4\omega}}{\omega} \tag{4.3.2.19}$$

The integral of this equivalent asymptotic expression is (Gröbner and ofreiter (1958), second volume, p. 140, n. 336.12b) :

$$\frac{k - (1 + k^2)}{k} \int_0^{\infty} \frac{e^{-2\omega} - e^{-4\omega}}{\omega} \cos\left[\frac{(x - s)\omega}{t}\right] d\omega =$$

$$\frac{k - (1 + k^2)}{2\,k} \left\{ ln\left[16 + \frac{(x - s)^2}{t^2}\right] - ln\left[4 + \frac{(x - s)^2}{t^2}\right] \right\} \qquad (4.3.2.20)$$

By proceeding forward, the approximation (4.3.2.19) is subtracted to obtain the subsequent asymptotic approximation :

$$\frac{2(k\ sinh\ (2\omega) - 2\omega)}{\omega\ (2k\ cosh\ (2\omega) + 4\omega^2 + k^2 + 1)} - \frac{1 - e^{-2\omega}}{\omega} + \frac{4}{k}\,\omega\, e^{-2\omega} +$$

$$\frac{4}{k}\ e^{-2\omega} - \frac{k - (1 + k^2)}{k}\ \frac{e^{-2\omega} - e^{-4\omega}}{\omega} \rightarrow \frac{16}{k^2}\,\omega^3 e^{-4\omega}$$

(4.3.2.21)

The integral of this equivalent asymptotic expression is (Gröbner and Hofreiter (1958), second volume, p. 139, n. 336.4a) :

$$\frac{16}{k^2} \int_0^{\infty} \omega^3 e^{-4\omega} \cos\left[\frac{(x - s)\omega}{t}\right] d\omega = \frac{16}{k^2} \frac{8}{\left[16 + \frac{(x - s)^2}{t^2}\right]^3} \left[16 - 3\,\frac{(x - s)^2}{t^2}\right]$$

(4.3.2.22)

The last approximation considered in this study is that of (4.3.2.21) . The approximation (4.3.2.21) is subtracted from the left-hand member of (4.3.2.21) to

obtain the subsequent asymptotic approximation :

$$\frac{2(k\ sinh\ (2\omega) - 2\omega)}{\omega\ (2k\ cosh\ (2\omega) + 4\omega^2 + k^2 + 1)} - \frac{1 - e^{-2\omega}}{\omega} + \frac{4}{k}\,\omega\, e^{-2\omega} +$$

$$\frac{4}{k}\ e^{-2\omega} - \frac{k - (1 + k^2)}{k}\ \frac{e^{-2\omega} - e^{-4\omega}}{\omega} - \frac{16}{k^2}\,\omega^3 e^{-4\omega} \rightarrow \frac{16}{k^2}\,\omega^2 e^{-4\omega}$$

(4.3.2.23)

The integral of this equivalent asymptotic expression is (Gröbner and Hofreiter (1958), second volume, p. 139, n. 336.4a) :

$$\frac{16}{k^2}\int_0^\infty \omega^2 e^{-4\omega}\ cos\left[\frac{(x - s)\omega}{t}\right] d\omega =$$

$$\frac{16}{k^2}\ \frac{6}{\left[16 + \frac{(x - s)^2}{t^2}\right]^4}\left[256 - 96\,\frac{(x - s)^2}{t^2} + \frac{(x - s)^4}{t^4}\right] \quad (4.3.2.24)$$

It was decided not to compute extra asymptotic terms, since the numerical tests indicated that no appreciable advantage could be achieved.

The sequence of asymptotic terms is now re-obtained in a slightly different way, which is perhaps clearer, and which permits the numerical value to be attributed to coefficient q of the exponent of formula (4.3.2.11) to be discussed in deeper detail. The following truncated series expansion is employed :

$$\frac{1}{1 + x} \simeq 1 - x + x^2 - \ldots \quad (4.3.2.25)$$

Now, kernel (4.3.2.4) can be rewritten as :

$$\frac{2(k\ sinh\ (2\omega) - 2\omega)}{\omega\ (2k\ cosh\ (2\omega) + 4\omega^2 + k^2 + 1)} = \frac{k\ e^{2\omega} - 4\omega - k\ e^{-2\omega}}{\omega\ (k\ e^{2\omega} + 4\omega^2 + k^2 + 1 + k\ e^{-2\omega})} =$$

$$\frac{k\ e^{2\omega} - 4\omega - k\ e^{-2\omega}}{\omega\ k\ e^{2\omega}\ (1 + \frac{4\omega^2 + k^2 + 1 + k\ e^{-2\omega}}{k\ e^{2\omega}})} =$$

$$(\frac{1}{\omega} - \frac{4}{k}\ e^{-2\omega} - \frac{e^{-4\omega}}{\omega})\ \frac{1}{(1 + \frac{4\omega^2 + k^2 + 1 + k\ e^{-2\omega}}{k\ e^{2\omega}})}$$

(4.3.2.26)

By applying (4.3.2.25), it is obtained :

$$(\frac{1}{\omega} - \frac{4}{k}\ e^{-2\omega} - \frac{e^{-4\omega}}{\omega})\ \frac{1}{(1 + \frac{4\omega^2 + k^2 + 1 + k\ e^{-2\omega}}{k\ e^{2\omega}})} \simeq$$

$$(\frac{1}{\omega} - \frac{4}{k}\ e^{-2\omega} - \frac{e^{-4\omega}}{\omega})\ (1 - \frac{4}{k}\ \omega^2\ e^{-2\omega} - \frac{1 + k^2}{k}\ e^{-2\omega} - e^{-4\omega} + \frac{16}{k^2}\ \omega^4\ e^{-4\omega} + \ldots) \simeq$$

$$\frac{1}{\omega} - \frac{4}{k}\ \omega\ e^{-2\omega} - \frac{4}{k}\ e^{-2\omega} - \frac{1 + k^2}{k}\ \frac{e^{-2\omega}}{\omega} + \frac{16}{k^2}\ \omega^3\ e^{-4\omega} + \frac{16}{k^2}\ \omega^2\ e^{-4\omega} + \ldots$$

(4.3.2.27)

The final expression of (4.3.2.27) represents an asymptotic approximation of kernel (4.3.2.4). Anyway, it contains two asymptotic terms, namely $1/\omega$ and $(1 + k^2)\, e^{-2\omega}/(k\,\omega)$, which cannot be integrated in closed form in the sense of (4.3.2.1) . To overcome this problem, in (4.3.2.27) one sums and subtracts terms $e^{-2\omega}/\omega$ and $(k - (1 + k^2))\, e^{-4\omega}/(k\,\omega)$, to obtain :

$$\frac{1}{\omega} - \frac{4}{k}\,\omega\, e^{-2\omega} - \frac{4}{k}\, e^{-2\omega} - \frac{1 + k^2}{k}\,\frac{e^{-2\omega}}{\omega} + \frac{16}{k^2}\,\omega^3\, e^{-4\omega} + \frac{16}{k^2}\,\omega^2\, e^{-4\omega} + \ldots \simeq$$

$$\frac{1 - e^{-2\omega}}{\omega} - \frac{4}{k}\,\omega\, e^{-2\omega} - \frac{4}{k}\, e^{-2\omega} + \frac{k - (1 + k^2)}{k}\,\frac{e^{-2\omega} - e^{-4\omega}}{\omega} +$$

$$\frac{16}{k^2}\,\omega^3\, e^{-4\omega} + \frac{16}{k^2}\,\omega^2\, e^{-4\omega} + \ldots \qquad (4.3.2.28)$$

This latter expression is integrable according to (4.3.2.3) . The selection of coefficient q of exponent of (4.3.2.11) is now briefly discussed. By selecting $q = 2$, a "spurious" term , $e^{-2\omega} / \omega$, is introduced, whose form already exists in the asymptotic expansion (4.3.2.27) , and it appears as the fourth term in the final expression of (4.3.2.27) . In other words, the exponent selection $q = 2$ produces a spurious term which vanishes faster than the two terms following the altered component (that is, $1/\omega$) . It can be concluded that the introduction of this "spurious" term does not appreciably alter the behaviour of the "natural" asymptotic expansion, at least for sufficiently high values of ω .

A rough estimate of parameter ω starting from which the asymptotic expression approaches the actual kernel is now made. Relation (4.3.2.25) requires $x < 1$. From the last expression of (4.3.2.26), and by remembering that, in the case of elastomeric materials, $k \simeq 1$, the following result is derived :

$$\frac{4\omega^2 + k^2 + 1 + k\, e^{-2\omega}}{k\, e^{2\omega}} < 1 \quad \rightarrow \quad \sinh(2\omega) - 2\,\omega^2 - 1 > 0 \quad \rightarrow \quad \omega > 0.75$$

(4.3.2.29)

In other words, it cannot be expected that the asymptotic expression (4.3.2.28) accurately represents kernel (4.3.2.4) even for low values of variable ω. To retrieve indications about the proper number of asymptotic terms according to (4.3.2.28) to be actually employed, the behaviour of the original function (4.3.2.4) and of its modifications is numerically explored. In particular, the following nomenclature is adopted : expression "initial kernel" refers to (4.3.2.4) ; "first modified kernel" denotes the initial kernel minus its asymptotic approximation, see (4.3.2.12); "second modified kernel" means the modified kernel of (4.3.2.14); "third modified kernel" addresses the altered kernel of (4.3.2.16); "fourth modified kernel" is that of (4.3.2.19) and, finally, the "fifth modified kernel" is that of (4.3.2.21) . All computations have been limited to the case $\nu = 0.5$, since a perturbation of the Poisson's ratio does not appreciably alter the character of the curves to be approximated. Fig. 4.3.2.6 displays the numerical findings. It appears that to modify the original kernel (4.3.2.4) beyond the second alteration is not beneficial. We, therefore, employ the following approximation :

$$\frac{2(k\ sinh\ (2\omega) - 2\omega)}{\omega\ (2k\ cosh\ (2\omega) + 4\omega^2 + k^2 + 1)} \simeq \frac{1 - e^{-2\omega}}{\omega} - \frac{4}{k}\,\omega\, e^{-2\omega} \quad ;\ \omega > 2 \tag{4.3.2.30}$$

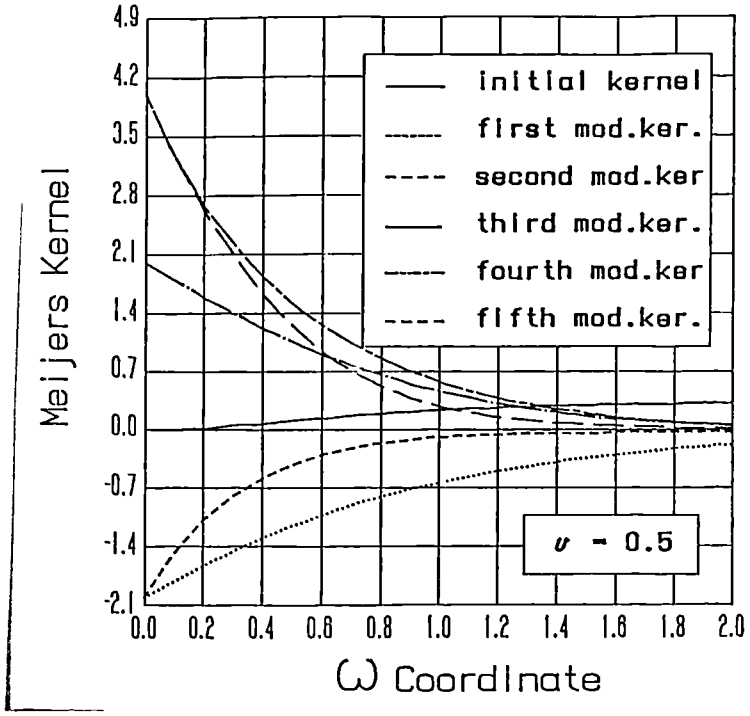

Fig. 4.3.2.6 : The original kernel (4.3.2.6) and its modifications for $\nu = 0.5$.

The approximation problem for small ω is now treated. To do so, the following function is studied :

$$\frac{2(k\ sinh\ (2\omega) - 2\omega)}{\omega\ (2k\ cosh\ (2\omega) + 4\omega^2 + k^2 + 1)} - \frac{1 - e^{-2\omega}}{\omega} + \frac{4}{k}\ \omega\ e^{-2\omega} \quad ;\ 0 \leq \omega \leq 2$$

(4.3.2.31)

and such a function is approximated with a simpler expression, which is integrable according to (4.3.2.3) . First of all, the behaviour of (4.3.2.31) for $\omega \rightarrow 0$ is studied. The following result holds true :

$$\lim |_{\omega \rightarrow 0} \left\{ \frac{2(k\ sinh\ (2\omega) - 2\omega)}{\omega\ (2k\ cosh\ (2\omega) + 4\omega^2 + k^2 + 1)} - \frac{1 - e^{-2\omega}}{\omega} + \frac{4}{k}\ \omega\ e^{-2\omega} \right\} =$$

$$- 2\ \frac{(3 + k^2)}{(1 + k)^2} \simeq - 2$$

$$\lim |_{\omega \rightarrow 0} \frac{d}{d\ \omega} \left\{ \frac{2(k\ sinh\ (2\omega) - 2\omega)}{\omega\ (2k\ cosh\ (2\omega) + 4\omega^2 + k^2 + 1)} - \frac{1 - e^{-2\omega}}{\omega} + \frac{4}{k}\ \omega\ e^{-2\omega} \right\} =$$

$$\left(2 + \frac{4}{k} \right) \simeq 6$$

$$\lim |_{\omega \rightarrow 0} \frac{d^2}{d\ \omega^2} \left\{ \frac{2(k\ sinh\ (2\omega) - 2\omega)}{\omega\ (2k\ cosh\ (2\omega) + 4\omega^2 + k^2 + 1)} - \frac{1 - e^{-2\omega}}{\omega} + \frac{4}{k}\ \omega\ e^{-2\omega} \right\} =$$

$$- \frac{8}{3}\ \frac{k^4 + 7\ k^3 + 31\ k^2 + 7\ k + 6}{k\ (\ 1 + k\ )^3} \simeq - \frac{52}{3}$$

$$\lim |_{\omega \to 0} \quad \frac{d^3}{d\,\omega^3} \left\{ \frac{2(k\ sinh\ (2\omega) - 2\omega)}{\omega\ (2k\ cosh\ (2\omega) + 4\omega^2 + k^2 + 1)} - \frac{1 - e^{-2\omega}}{\omega} + \frac{4}{k}\,\omega\, e^{-2\omega} \right\} =$$

$$4\ \frac{12 + k}{k} \simeq 52$$

$$\lim |_{\omega \to 0} \quad \frac{d^4}{d\,\omega^4} \left\{ \frac{2(k\ sinh\ (2\omega) - 2\omega)}{\omega\ (2k\ cosh\ (2\omega) + 4\omega^2 + k^2 + 1)} - \frac{1 - e^{-2\omega}}{\omega} + \frac{4}{k}\,\omega\, e^{-2\omega} \right\} =$$

$$-\frac{32}{5}\ \frac{k^5 + 22\ k^4 + 142\ k^3 - 98\ k^2 + 321\ k + 20}{k\ (\ 1 + k\ )^4} \simeq -\frac{816}{5}$$

(4.3.2.32)

In (4.3.2.32) the approximate results refer to the incompressibility condition, that is, to $k = 1$. Various approximating expressions to (4.3.2.31) were tested, and the best results were obtained with the following expression :

$$C_1\ e^{-a\omega}\ cos\ (b\ \omega) \qquad (4.3.2.33)$$

which is integrable in the sense of (4.3.2.3), since (Gröbner and Hofreiter (1958), second volume, p. 136, n. 335.6c) :

$$\int_0^\infty e^{-a\omega}\ cos\ (b\ \omega)\quad cos\left[\ \frac{(x - s)\omega}{t}\ \right] d\omega =$$

$$\frac{a\left[\ a^2 + b^2 + \frac{(x - s)^2}{t^2}\ \right]}{\left[a^2 + \left[b - \frac{(x - s)}{t}\ \right]^2\right]\left[\ a^2 + \left[b + \frac{(x - s)}{t}\ \right]^2\right]}$$

(4.3.2.34)

The selection of constants C_1 , a and b of (4.3.2.33) is now discussed. The following results for expression (4.3.2.33) hold true :

$$\lim |_{\omega \to 0} \quad C_1 \, e^{-a\omega} \cos (b\,\omega) \; = C_1$$

$$\lim |_{\omega \to 0} \quad \frac{d}{d\,\omega} \left[\, C_1 \, e^{-a\omega} \cos (b\,\omega) \, \right] = - \, a \, C_1$$

$$\lim |_{\omega \to 0} \quad \frac{d^2}{d\,\omega^2} \left[\, C_1 \, e^{-a\omega} \cos (b\,\omega) \, \right] = C_1 \left[\, a^2 - b^2 \, \right]$$

$$\lim |_{\omega \to 0} \quad \frac{d^3}{d\,\omega^3} \left[\, C_1 \, e^{-a\omega} \cos (b\,\omega) \, \right] = a \, C_1 \left[\, 3\,b^2 - a^2 \, \right]$$

$$\lim |_{\omega \to 0} \quad \frac{d^4}{d\,\omega^4} \left[\, C_1 \, e^{-a\omega} \cos (b\,\omega) \, \right] = \; C_1 \left[\, a^4 - 6\,a^2\,b^2 + b^4 \, \right]$$

(4.3.2.35)

To compute constants C_1 , a , and b of (4.3.2.33), it is imposed that the value assumed by (4.3.2.33) together with its first and second derivative for $\omega \to 0$ coincide with the corresponding expressions (4.3.2.32). Higher order derivatives are not employed here. By comparing the first equations of (4.3.2.32) and of (4.3.2.35), the expression for C_1 is obtained :

$$C_1 = - \, 2 \, \frac{(3 + k^2)}{(1 + k)^2} \; \simeq \; - \, 2 \qquad (4.3.2.36)$$

By comparing the second equations of (4.3.2.32) and of (4.3.2.35), it is obtained :

$$- \, a \, C_1 = \left(\, 2 + \frac{4}{k} \, \right) \; \rightarrow \; a \; = \frac{(2 + k)\,(1 + k)^2}{k\,(3 + k^2)} \; \simeq \; 3 \qquad (4.3.2.37)$$

Finally, by comparing the third equations of (4.3.2.32) and of (4.3.2.35), it is obtained :

$$C_1 \left[a^2 - b^2 \right] = -\frac{8}{3} \frac{k^4 + 7\,k^3 + 31\,k^2 + 7\,k + 6}{k\,(1+k)^3} \rightarrow$$

$$b = \sqrt{\frac{(2+k)^2\,(1+k)^4}{k^2\,(3+k^2)^2} - \frac{4}{3}\frac{(k^4 + 7\,k^3 + 31\,k^2 + 7\,k + 6)}{k\,(1+k)\,(3+k^2)}} \simeq \frac{1}{\sqrt{3}} \simeq 0.57$$

(4.3.2.38)

Various approximating functions other than (4.3.2.33) were also tested. These functions were :

$$C_1\,e^{-a\omega} \;;\; C_1\,\omega\,e^{-a\omega} \;;\; C_1\,(c + d\,\omega)\,e^{-a\omega} \;;\; C_1\,\omega^2\,e^{-a\omega} \;;\; C_1\,\omega^2 e^{-a\omega^2};$$

$$C_1\,e^{-a\omega}\,sin\,(b\,\omega) \;;\; C_1\,e^{-a\omega}\,sin^2\,(b\,\omega) \;;\; C_1\,e^{-a\omega}\,cos^2\,(b\,\omega)$$

(4.3.2.39)

These functions are all integrable in the sense of (4.3.2.3), that is, the integral between 0 and ∞ of these functions multiplied by *cos* function can be analytically determined. Anyway, the results obtained with these expressions were either poorer than those retrieved with (4.3.2.33) or, when of similar accuracy, the expressions involved were more complex. A Taylor expansion in the vicinity of $\omega = 0$ of (4.3.2.31) was also tried, but some numerical test showed a poor degree of approximation.

It appears from the previous comments that a good approximation of (4.3.2.4), valid for $0 \leq \omega < \infty$ is the following :

$$\frac{2(k\,sinh\,(2\omega) - 2\omega)}{\omega\,(2k\,cosh\,(2\omega) + 4\omega^2 + k^2 + 1)} \simeq \frac{1 - e^{-2\omega}}{\omega} - \frac{4}{k}\,\omega\,e^{-2\omega} + C_1\,e^{-a\omega}\,cos\,(b\,\omega)$$

(4.3.2.40)

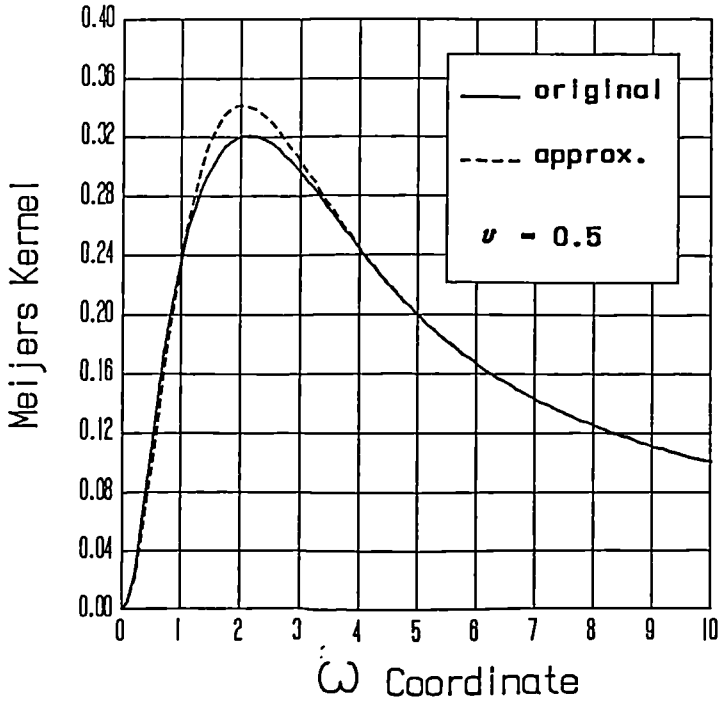

Fig. 4.3.2.7 : The original kernel (4.3.2.6) and its approximation (4.3.2.40) for ν = 0.5 .

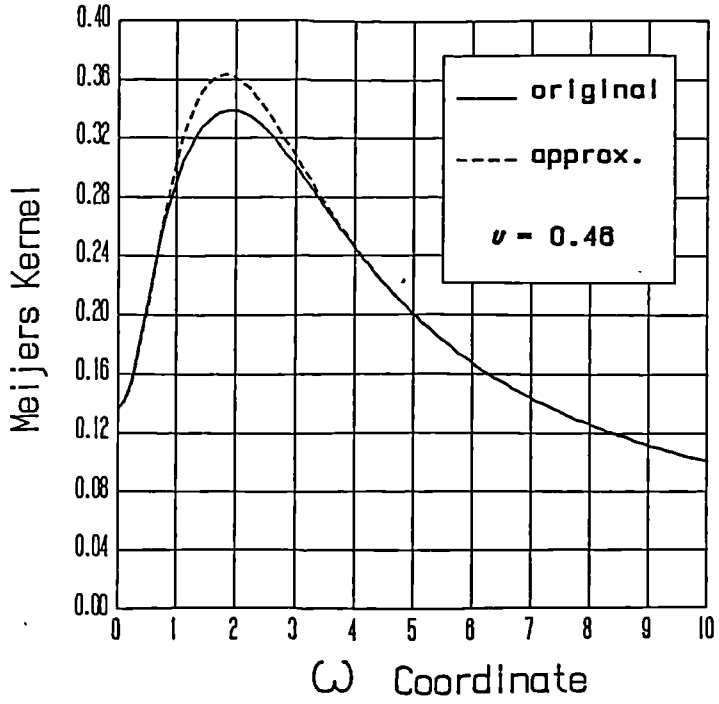

Fig.4.3.2.8: The original kernel (4.3.2.6) and its approximation (4.3.2.40) for ν =0.46.

where the values of constants C_1 , a and b in terms of k (that is, of ν) are given by formulae (4.3.2.36) (4.3.2.37) and (4.3.2.38), respectively. Figs 4.3.2.7,8 display the function expressed by equation (4.3.2.40) together with the original (4.3.2.4) kernel for $\nu = 0.5$ and 0.46 , respectively, as functions of ω . The degree of approximation is very good, apart from a reduced portion, $1 \leq \omega \leq 4$, where the approximate expression (4.3.2.40) supplies values at most 6 percent higher than the right ones. It was, therefore, decided to apply a local correction to (4.3.2.40), aimed at improving its accuracy in this ω region. A correction function $F(\omega)$ of the following polynomial form (which is integrable in the sense of (4.3.2.3)) was used :

$$F(\omega) = C (1 + a \omega + b \omega^2 + c \omega^3) \qquad (4.3.2.41)$$

Constants a , b and c were found by imposing that, as suggested by Figs 4.3.2.7,8 , expression (4.3.2.41) vanishes for $\omega = 1$ and $\omega = 4$, and that $dF/d\omega$ vanishes for $\omega = 2$. Finally, constant C was chosen to minimize the error when $\nu = 0.5$. The final expression of (4.3.2.41) is as follows :

$$F(\omega) = \frac{-0.0216}{4} (- 16 + 24 \omega - 9 \omega^2 + \omega^3) \qquad (4.3.2.42)$$

Expression (4.3.2.42) is integrable in the sense of (4.3.2.23), since (Gröbner and Hofreiter (1958), first volume, p. 128, n. 333.3b) :

$$\frac{-0.0216}{4} \int_1^4 (- 16 + 24 \omega - 9 \omega^2 + \omega^3) \cos \left[\frac{(x - s)\omega}{t} \right] d\omega =$$

$$+ 3 \frac{0.0216\, t^4}{4 (x - s)^4} \left[2 \frac{(x - s)}{t} \sin \left[\frac{4 (x - s)}{t} \right] + 2 \cos \left[\frac{4 (x - s)}{t} \right] + \right.$$

$$\left. 4 \frac{(x - s)}{t} \sin \left[\frac{(x - s)}{t} \right] - 2 \cos \left[\frac{(x - s)}{t} \right] + 3 \frac{(x - s)^2}{t^2} \cos \left[\frac{(x - s)}{t} \right] \right]$$

(4.3.2.43)

In particular, when $x = s$, expression (4.3.2.43) assumes the following value :

$$- \frac{27}{16} 0.0216 \qquad (4.3.2.44)$$

In conclusion, the final form of the approximation of (4.3.2.4) is as follows :

$$\frac{2(k\ sinh\ (2\omega) - 2\omega)}{\omega\ (2k\ cosh\ (2\omega) + 4\omega^2 + k^2 + 1)} \simeq \frac{1 - e^{-2\omega}}{\omega} - \frac{4}{k}\ \omega\ e^{-2\omega} + C_1\ e^{-a\omega}\ cos\ (b\ \omega) -$$

$$\frac{0.0216}{4}\ (\ -\ 16 + 24\ \omega - 9\ \omega^2 + \omega^3\ ) \qquad (4.3.2.45)$$

where the last term in (4.3.2.45) must be applied only when $1 \leq \omega \leq 4$.

Figs 4.3.2.9.10 show the corrected (4.3.2.45) approximation, together with the original (4.3.2.4) kernel, for $\nu = 0.5$ and 0.46 . Since the correction (4.3.2.42) is calibrated againts the incompressible results, the approximation referring to $\nu = 0.5$ is better (Fig. 4.3.2.9). Anyway, the degree of accuracy remains good even for a Poisson's ratio as low as 0.46 . Since the actual figures are very close to 0.5 , where values in the region of 0.4997 are plausible (Section 3), the accuracy of (4.3.2.45) is good for practical applications. To quantify the error induced by (4.3.2.45), this expression is applied to cases where other solutions are already known. This analysis will be performed in the following Section 4.3.3 .

It is now possible to get an analytical expression for kernel (4.3.2.3) . By introducing (4.3.2.45) into (4.3.2.3) it is obtained :

$$K(x-s) = \int_0^\infty \frac{2(k\ sinh\ (2\omega) - 2\omega)}{\omega\ (2k\ cosh\ (2\omega) + 4\omega^2 + k^2 + 1)} cos\left[\frac{(x - s)\omega}{t}\right] d\omega \simeq$$

$$\int_0^\infty \left[\ \frac{1 - e^{-2\omega}}{\omega} - \frac{4}{k}\omega e^{-2\omega} + C_1\ e^{-a\omega} cos\ (b\ \omega)\right] cos\left[\frac{(x - s)\omega}{t}\right] d\omega -$$

$$\int_1^4 \left[\frac{0.0216}{4} \left(-16 + 24\,\omega - 9\,\omega^2 + \omega^3 \right) \right] \cos\left[\frac{(x-s)\omega}{t} \right] d\omega \simeq$$

$$-\log\left[\frac{(x-s)}{t} \right] + \frac{1}{2}\log\left[4 + \frac{(x-s)^2}{t^2} \right] - \frac{4}{k} \frac{4 - \frac{(x-s)^2}{t^2}}{\left[4 + \frac{(x-s)^2}{t^2} \right]^2} -$$

$$\frac{2\,(2+k)}{k} \frac{\left[a^2 + b^2 + \frac{(x-s)^2}{t^2} \right]}{\left[a^2 + \left[b - \frac{(x-s)}{t} \right]^2 \right] \left[a^2 + \left[b + \frac{(x-s)}{t} \right]^2 \right]} +$$

$$3\,\frac{0.0216\,t^4}{4\,(x-s)^4} \left[2\,\frac{(x-s)}{t} \sin\left[\frac{4\,(x-s)}{t} \right] + 2\cos\left[\frac{4\,(x-s)}{t} \right] + \right.$$

$$\left. 4\,\frac{(x-s)}{t} \sin\left[\frac{(x-s)}{t} \right] - 2\cos\left[\frac{(x-s)}{t} \right] + 3\,\frac{(x-s)^2}{t^2} \cos\left[\frac{(x-s)}{t} \right] \right]$$

(4.3.2.46)

Formula (4.3.2.1) shows that expression (4.3.2.46) can be interpreted — apart from coefficient $2\lambda/\pi$ — as the vertical displacement of the layer free boundary when loaded by a concentrated force. Figs 4.3.2.11,12 display the exact displacement (according to (4.3.2.1), and employing a numerical integration scheme based on a high number of nodes) and the approximate (following (4.3.2.46)) displacements for two Poisson's ratios, namely 0.5 and 0.46 . The vertical displacement becomes unbounded under the singular load ($x/t = 0$, where t represents the layer thickness). At x/t

$\simeq$ 0.5 the layer begins to project beyond its undeformed profile. For $x/t \simeq 5$ the layer deformation dies away. For $\nu = 0.5$ (Fig. 4.3.2.11) the reentrant layer portion compressed by the force must exactly compensate the volume projecting beyond the undeformed free boundary. For both Figures 4.3.2.11,12 the agreement between exact and approximate numerical forecasts is good. Anyway, an assessment of the error incurred by employing expression (4.3.2.46) is more significant when referred to the practically more relevant situation of a layer indented by a rigid cylinder. This problem is examined in Section 4.3.3 .

The distribution of the shear stress at the interface between layer and rigid foundation, upon application of a unit concentrated load, is now addressed. This information is useful in forecasting debonding phenomena between elastomeric layer and substrate. Following the complex analysis approach of Jaffar and Savage (1988), the shear stress, τ_{xy} , has the following integral expression :

$$\tau_{xy}(x) = \frac{1+k}{\pi t} \int_0^\infty \frac{2\omega \cosh\omega + (1-k)\sinh\omega}{2k\cosh(2\omega) + 4\omega^2 + k^2 + 1)} \sin\left[\frac{x\omega}{t}\right] d\omega \qquad (4.3.2.47)$$

which depends on ν but not on E . When a penetration depth by a punch is imposed, since the displacement of (4.3.2.1) for a unit load is inversely proportional to E , the whole stress field is proportional to E , as expected. Expression (4.3.2.47) was not used in practical applications, since its counterpart for curved layers (see Section 5.4.2) can cover both appreciably curved and essentially straight layers. Comparable studies have been developed by Burmister (1944) for the axisymmetric case of a layer either adherent or frictionlessly supported by a half space, and loaded by a uniform pressure insisting ona circular region. Shelest (1975) examines the axisymmetric case of a rigid circular plate compressing a deformable layer frictionlessly supported by a rigid foundation.

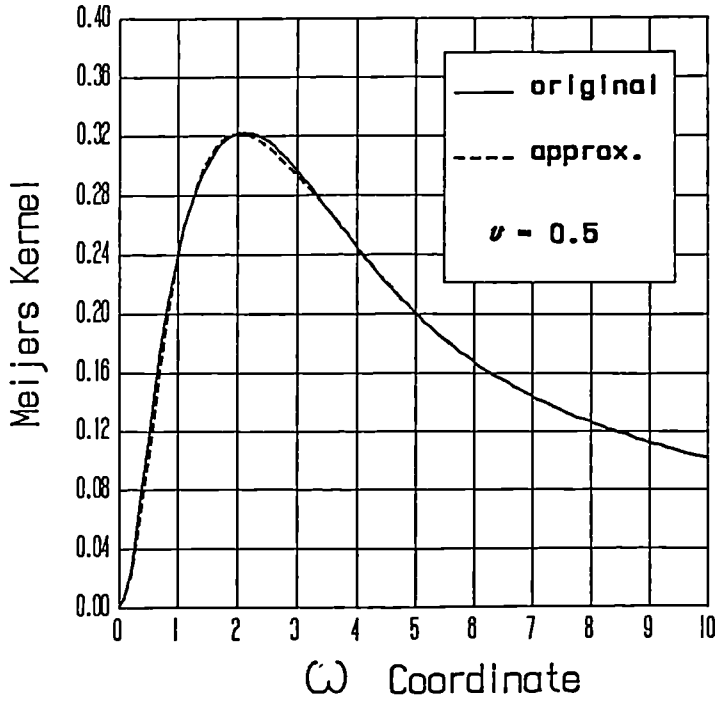

Fig.4.3.2.9: The original kernel (4.3.2.6) and its approximation (4.3.2.45) for $\nu = 0.5$.

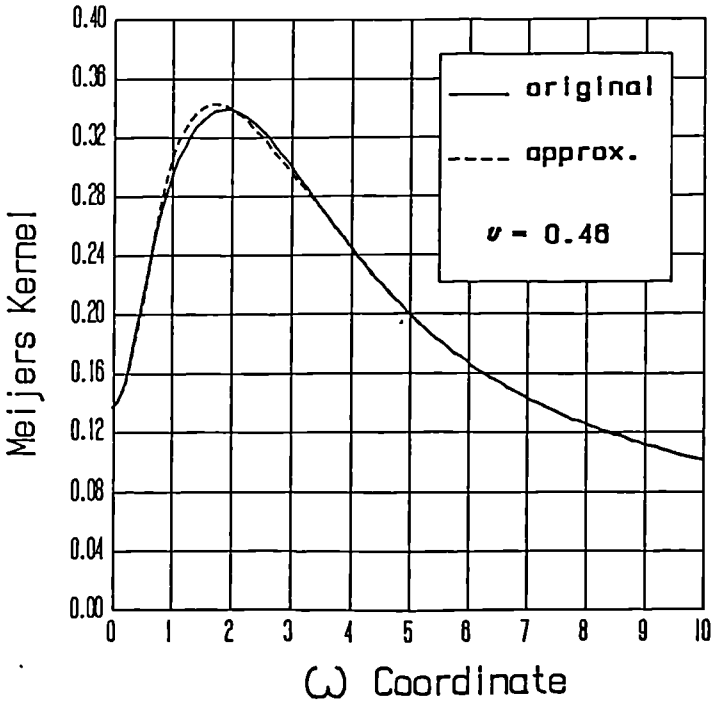

Fig.4.3.2.10: The original kernel (4.3.2.6) and its approximation (4.3.2.45) for $\nu = 0.46$.

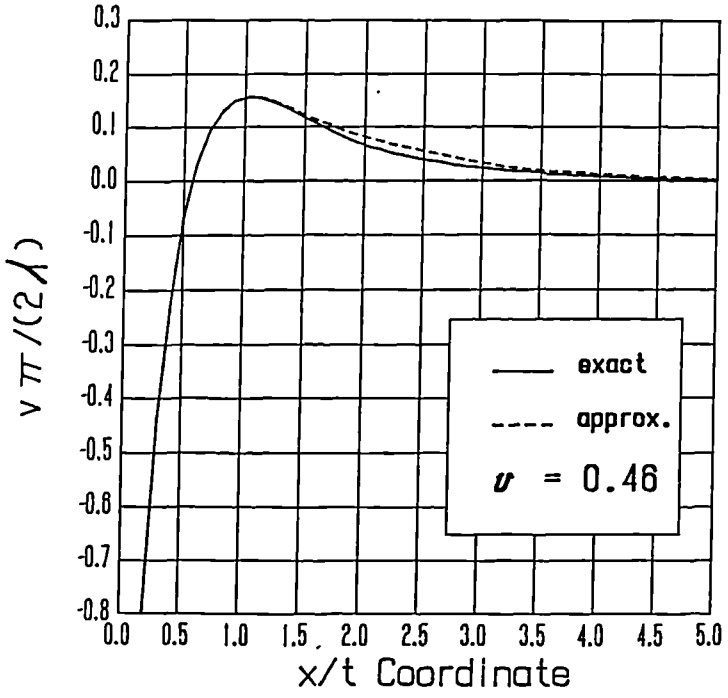

Fig.4.3.2.11 : The exact (4.3.2.1) and approximate (4.3.2.46) displacements for $\nu = 0.5$.

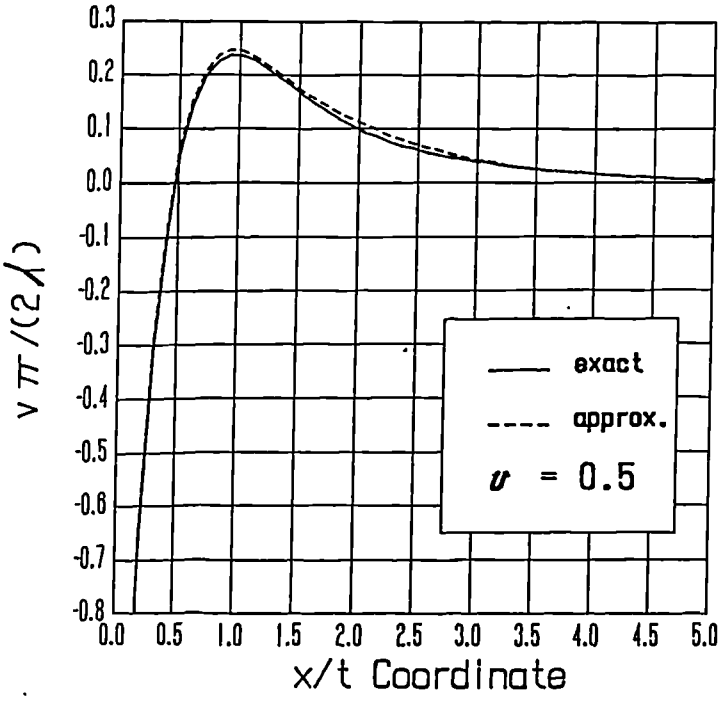

Fig.4.3.2.12 : The exact (4.3.2.1) and approximate (4.3.2.46) displacements for $\nu = 0.46$.

4.3.3 The pressure profile for a cylindrical indenter

The approximate analytical expression (4.3.2.46) of kernel (4.3.2.1) lends itself to be conveniently employed in numerical programs treating deformable layers compressed by rigid indenters of any profile. The main advantages with respect to more traditional approaches are twofold : a) the numerical evaluation of (4.3.2.46) is considerably faster than that of the exact expression (4.3.2.1), which requires a refined mesh; b) a numerical program can treat indenters of any profile, *e.g.* , completely different from a cylindrical approximation. These two advantages appear to be particularly relevant in the modelling of elastohydrodynamic regimes where, due to the nonlinear features of this problem, a considerable computational effort is required, and where the layer deformed profile exhibits a peculiar shape with a "nip" at the outlet (Prati and Strozzi (1984)) and, therefore, is not cylindrical.

In this Chapter a numerical scheme is developed which adopts the approximate analytical kernel (4.3.2.46) and treats an indenter of a generic profile described by an (approximately) piecewise linear curve. More exactly, the pressure profile is assumed as piecewise linear, and the layer deformed boundary shape results as a consequence of this assumption. Numerical findings will be retrieved for a layer compressed by a rigid cylindrical indenter, in order to obtain quantitative indications about the accuracy of (4.3.2.46) .

The pressure profile can be chosen as piecewise constant (*e.g.* Dragoni and Strozzi (1989)) or piecewise linear (*e.g.* Bentall and Johnson (1968)). A linear interpolation is here adopted because it is estimated to be more accurate. From a practical viewpoint, it is necessary to evaluate the vertical displacement field of a deformable layer loaded by a linearly varying pressure profile applied at any distance from the origin (Johnson (1985), p. 144). In other words, according to (4.3.2.2), the following integral must be computed :

$$v(x) = \frac{2\,\lambda}{\pi} \int_a^b p(s)\, K(x - s)\, ds \qquad (4.3.3.1)$$

where kernel K is expressed by (4.3.2.46) and p is a linear function acting between coordinates s_l and s_r (indices l and r stand for left and right) :

$$p(s) = p_l + \frac{(p_r - p_l)(s - s_l)}{(s_r - s_l)} \qquad (4.3.3.2)$$

As already mentioned, the integrals stemming from (4.3.3.1) can be mainly computed in analytical form. The exception is the last term of (4.3.2.46), that deriving from the local polynomial correction in (4.3.2.45), whose integral according to (4.3.3.1) would involve integralsinus and integralcosinus functions. Only for this part, a numerical integration was resorted to. In particular, a simple histogram technique was adopted, together with a limited number of nodal points ($\simeq$ 5) .

The problems connected with the numerical solution procedure and with the definition of the contact extent are treated hereinafter. Once a certain penetration depth, δ, is given (Jaffar and Savage (1988), p.68), which represents the imposed rigid body penetration of the indenter into the deformable layer (see Fig. 4.3.2.1), an approximate pressure profile is estimated from the asymptotic (infinite contact width), incompressible solution (Johnson (1985), formula 5.75), from which a piecewise linear pressure curve having the same nodal values as the analytical incompressible asymptotic solution is derived. From this starting point in terms of piecewise linear pressure profile, a relaxation procedure is activated, which permits a refinement to be achieved accounting for the actual Poisson's ratio and for the narrowness of the contact width. In particular, the vertical displacement at the first node of the mesh is computed from the pressure starting point. Then, this displacement is compared with that imposed at that point by the penetration depth, δ, and by the indenter shape. The pressure of the first node is subsequently altered in such a way that its vertical displacement equals the imposed one, whereas the remaining nodal pressures are kept unaltered. The same procedure is performed for the second node, and all nodal points are sequentially examined. Then, the whole cycle is repeated again and again, until the solution converges. Particular attention must be devoted to the definition of the contact width, which is an extra unknown. During the above explained relaxation procedure, the sign of the nodal pressure must always be examined. If this nodal value becomes negative, the corresponding pressure must be set equal to zero. In other words, this node is released, and it is no longer obliged to stay in contact with the indenter.

An alternative approach to unilateral contact problems is the complementarity

formulation (Cannarozzi (1980), Dragoni and Strozzi (1989)). Although mathematically more sound, this modelling requires the resolution of a system of equations equal to the number of nodes, which often exceeds the memory resources of personal computers. In addition, such direct solvers can produce spurious peaks in terms of contact pressure profile, which in turn derive from the ill-conditioned character of many contact problems (Hartnett (1980)).

4.3.4 Numerical results

In order to compare the results here retrieved with other solutions, a quadratic, parabolic description of the indenter profile (Jaffar and Savage (1988)) is adopted. It is shown in the following Section 4.4 that both the normalized peak contact pressure, $p\,R/(Ea)$, and the normalized semicontact width, a/h , can be linked to parameter $\delta\,R/h^2$, where E is the Young's modulus of the layer, δ is the rigid body approach between cylinder and layer, R is the cylinder radius, p is the peak contact pressure, a is the semicontact width between cylinder and layer and, finally, h is the layer thickness. Figs 4.3.4.1,2,3,4,5,6 display the normalized peak pressure as function of the aforementioned parameter, for ν = 0.5 , 0.4999 , 0.4997, 0.499 , 0.49 , 0.48, respectively, and for $\delta\,R/h^2$ parameter (along x-axis) ranging from 0 to 300 . In typical biomechanical applications, $h \simeq 0.5 \div 3.$ mm , $R \simeq 1000.$ mm and $E \simeq 3 \div 7$ MPa (see Section 7.3.2). In addition, δ can be estimated by considering that the load practically applied to a hip joint can reach values of twice the body weight during walking (Kilvington and Goodman (1981)) and as much as ten times during running (Paul (1976)). The axisymmetric, asymptotic, incompressible solution of Jaffar (1989) furnishes $P = 2\,\pi\,E\,\delta^3\,R^2\,/(3\,h^3)$ (constant E is missing in formula (25) of Jaffar (1989)), where P *is the total load*, δ *the indentation depth*, h the layer thickness, and R the equivalent radius. If P = 2000 N , R = 1000 mm , h = 1 mm , E = 3 MPa , then $\delta \simeq 0.07$ mm and $\delta\,R/h^2 \simeq 70$. Consistently, most Figures of this Section refer to an x-axis parameter, $\delta\,R/h^2$, ranging from 0 up to 300 . The above estimates rely on a presumed similarity between plane and axisymmetric solutions. This aspect is commented at the end of Section 6.5.2 , where the differences between plane and axisymmetric solutions are critically examined, even if the orders of magnitudes of the two solutions appear to be substantially the same.

The Winkler previsions (eqns 4.4.2.2.3-4) and the asymptotic incompressible forecasts (eqns 4.4.2.2.8-11) are included, whenever possible. Figs 4.3.4.7,8,9,10,11,12 deal with the normalized semicontact width for the same Poisson's ratios. The results presented refer to 30 equispaced nodes, 100 relaxation iterations, and to 5 numerical integration points for the part of the Green function which cannot be

integrated in closed form (Section 4.3.3). Higher values of parameter $\delta\ R/h^2$, ranging from 300 to 10000 , are examined in Figs 4.3.4.13,14 with respect to normalized pressure and in Figs 4.3.4.15,16 with regard to normalized semicontact width. The variations in terms of pressure and contact width when adopting the parabolic profile (eqn (4.4.2.2.1)) or the exact cylindrical indenter were also tested numerically. Matthewson (1980) reports that for ratios of semicontact width to radius less than 0.2 , the error in the profile (between exactly cylindrical and parabolic curves) is less than 1 percent, thus implying that the errors in pressure and contact width must be small. Although not immediately evident from Figs 4.3.4.1,14 , this condition is practically respected in our applications (see the Table in Section 7.3.7). The numerical results retrieved showed in fact no appreciable pressure and contact width changes and, therefore, they are not reported here. It must be, however, noted that for high loads the differences between the two pressures referring to parabolic or cylindrical indenters may become more significant. This aspect is examined in other Chapters of this thesis. In particular, the plane strain, curved layer numerical solution of Section 5.3.4 was used to assess the influence of the layer profile on the contact pressure, where the predictions obtained reveal an increasing influence for high indentation depths. Similarly, the axisymmetric forecasts of Section 7.3.6 show a perceivable, although moderate, difference between the two solutions referring to the above indenter profiles.

On the whole, the results obtained indicate that, as the Poisson's ratio approaches the incompressibility figure 0.5, the corresponding data get nearer to the incompressible model, whereas for low ν values the Winkler assumption is more accurate. Anyway, there is a ν range for which neither the Winkler modelling nor the incompressible predictions are in acceptable agreement with the numerical forecasts.

An examination was also made of the influence of the number of nodes on the quality of the solution in terms of contact pressure and contact width, and the corresponding results are displayed in the following TABLE :

TABLE

reporting the normalized peak contact pressure, $pR/(Ea)$, and contact width, a/h ,

as function of three numbers of nodal points (30, 50, 100),
for $\delta = 0.3$ mm, $R = 4000$ mm , $\nu = 0.4997$, $h = 3$ mm ,
100 relaxation iterations and 5 integration points.

Number of nodes	$\delta R/h^2$	$pR/(Ea)$	a/h
30	133.333	749.198	25.748
50	133.333	767.074	25.398
100	133.333	769.944	25.142

It appears that the relative error between the pressure parameters referring to 30 an 100 nodes is about 2.6 percent, whereas that representing the normalized semicontact width is of about 2.3 percent. Both inaccuracies appear to be negligible, thus supporting the choice of 30 nodes for all diagrams presented in this Section.

The above comparison would have been possibly more informative if non-normalized variables, as p and a, had been referred to. Anyway, the smallness of the above deviations suggests that a more exhaustive error analysis is not relevant.

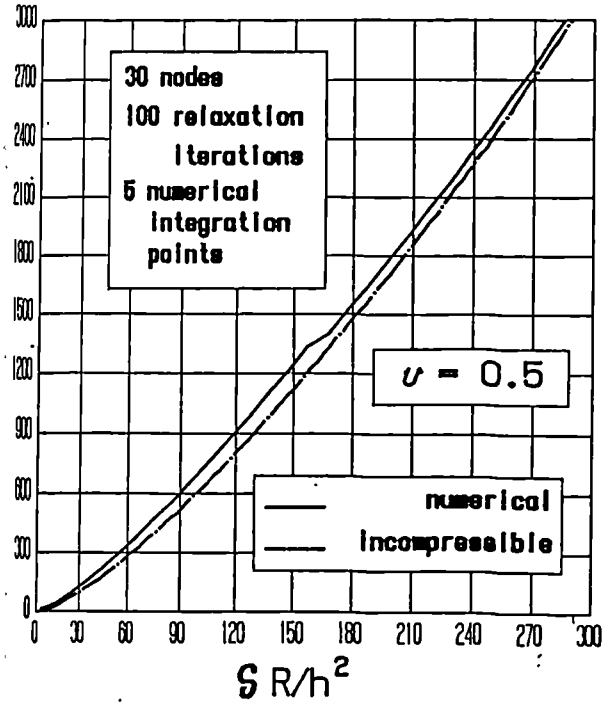

Fig. 4.3.4.1

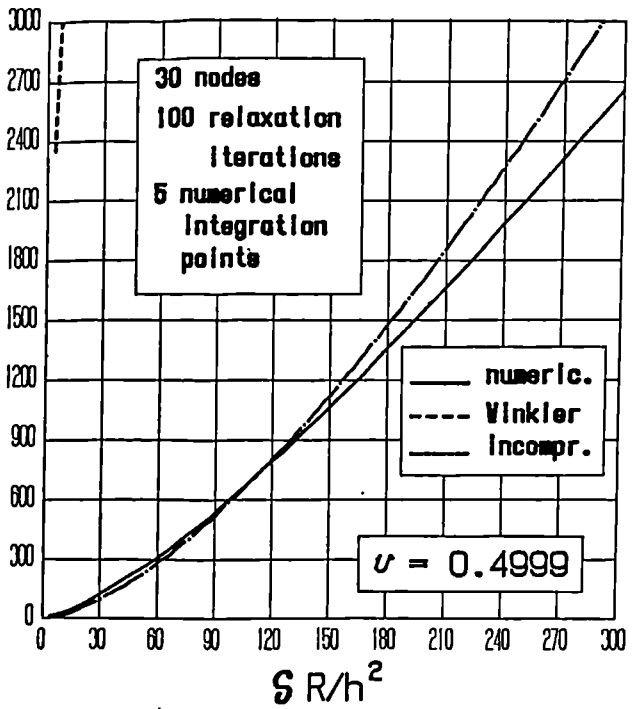

Fig. 4.3.4.2

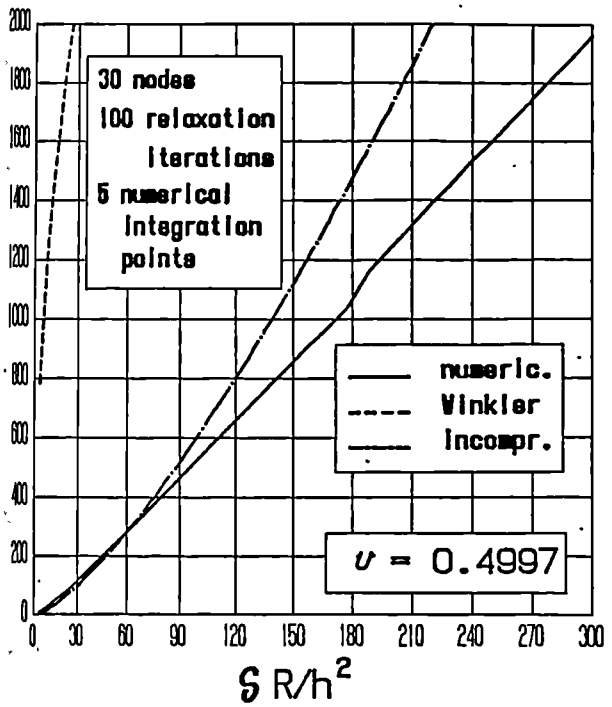

Fig. 4.3.4.3

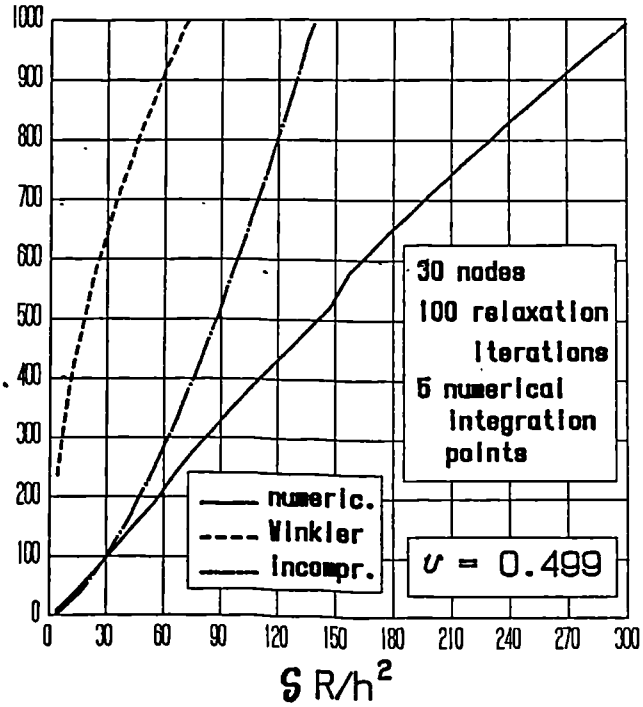

Fig. 4.3.4.4

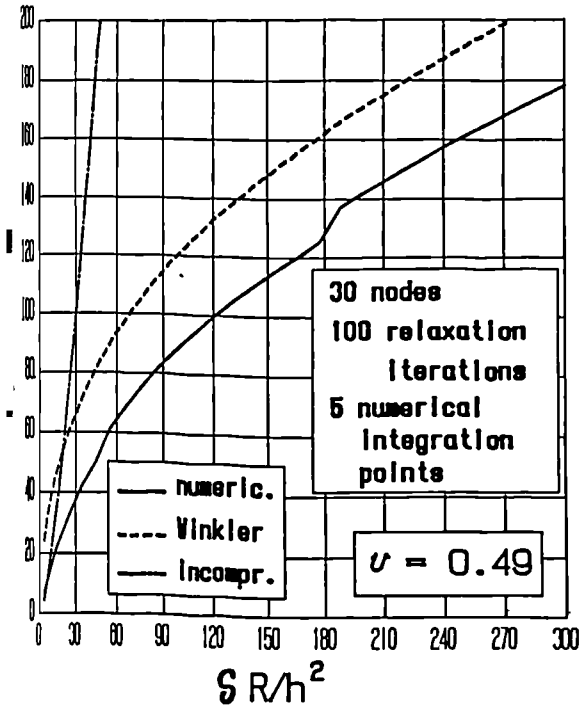

Fig. 4.3.4.5

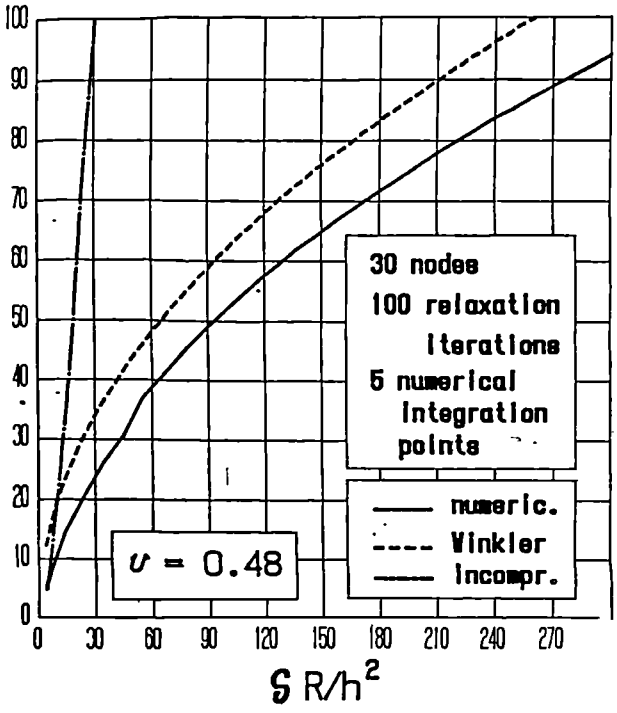

Fig. 4.3.4.6

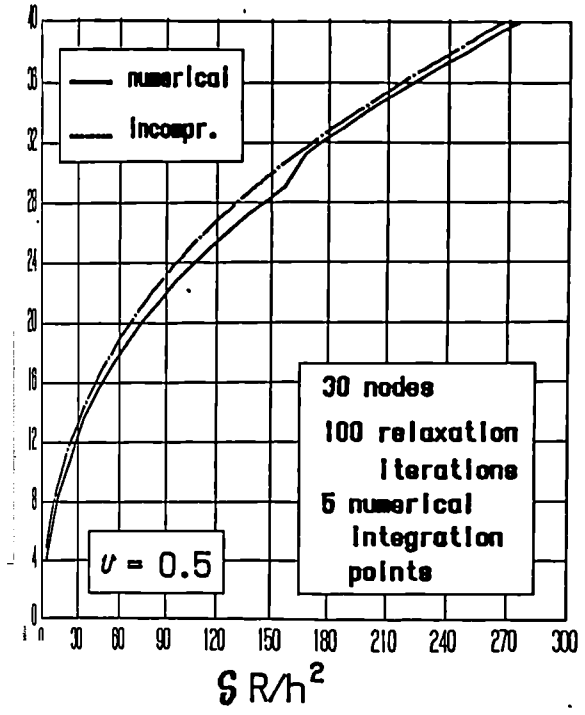

Fig. 4.3.4.7

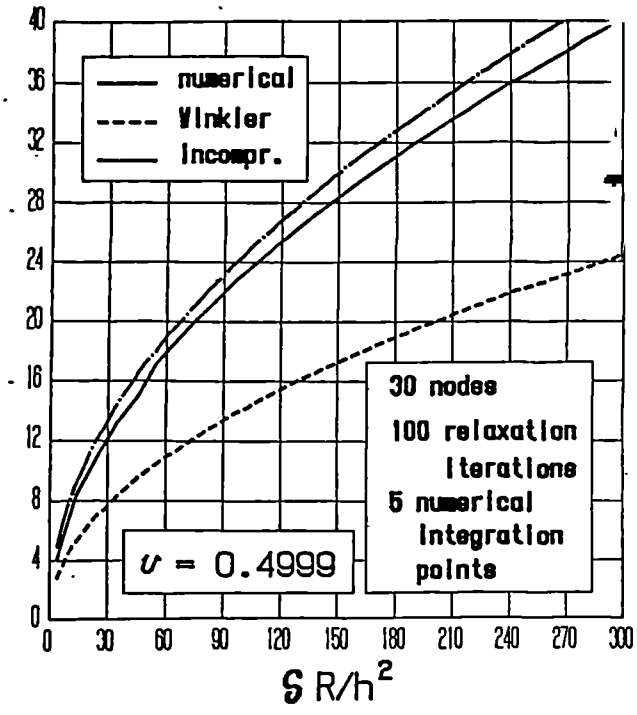

Fig. 4.3.4.8

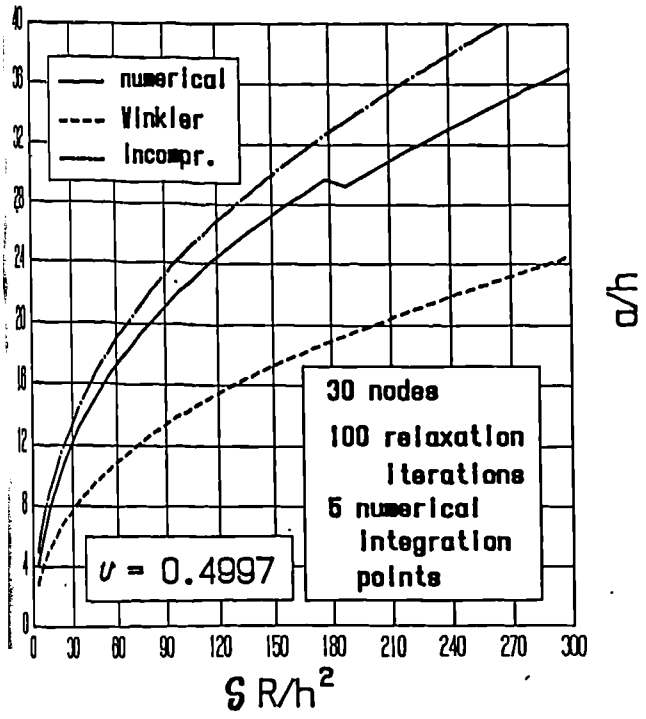

Fig. 4.3.4.9

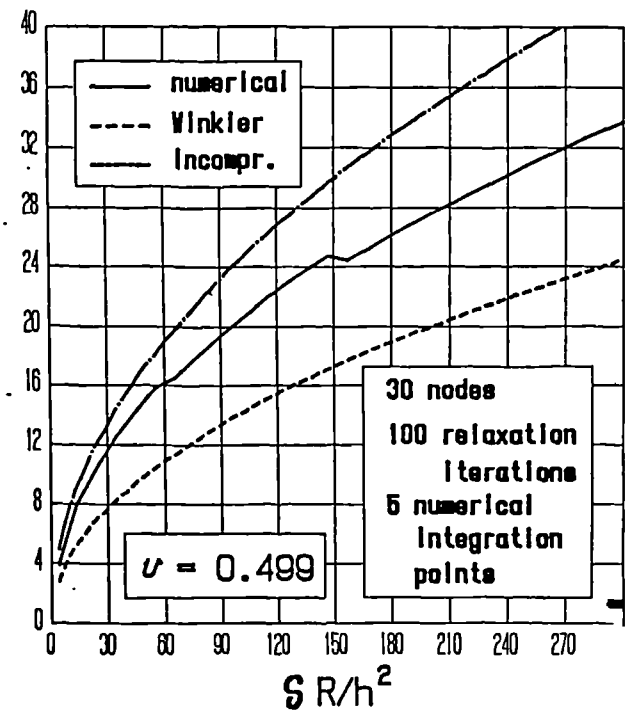

Fig. 4.3.4.10

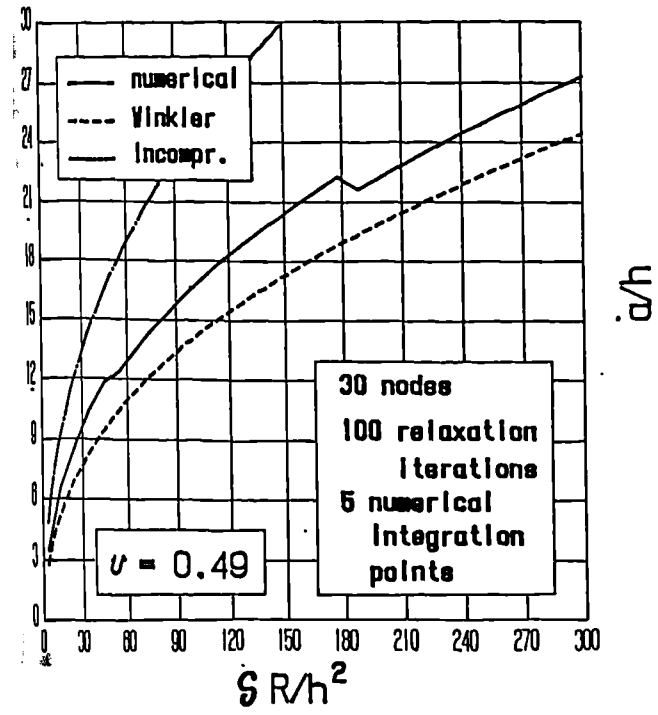

Fig. 4.3.4.11

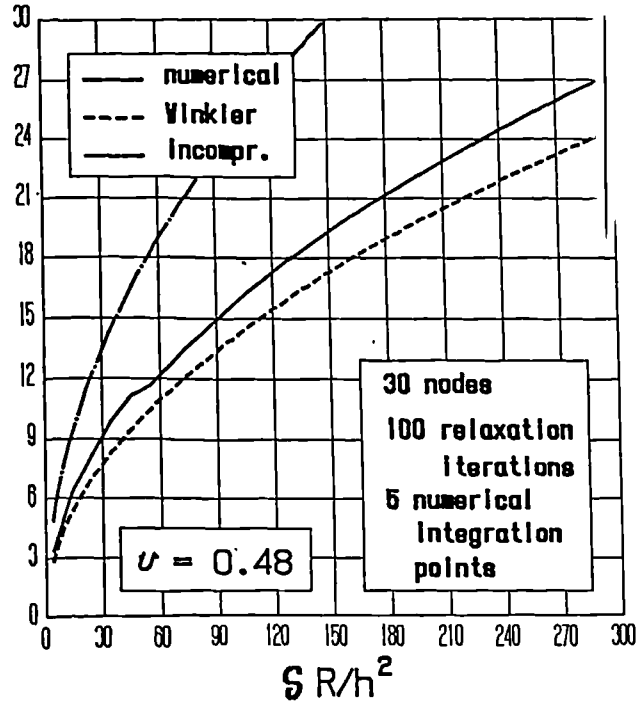

Fig. 4.3.4.12

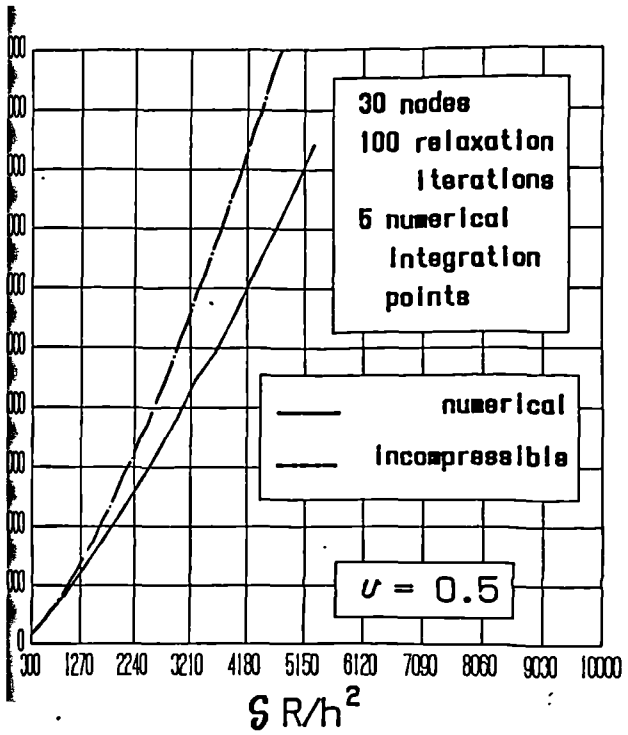

Fig. 4.3.4.13

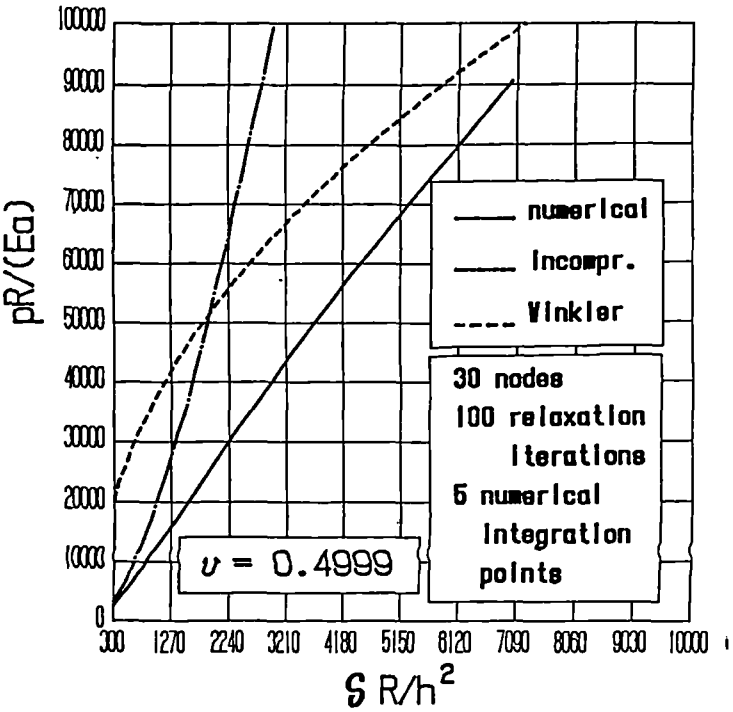

Fig. 4.3.4.14

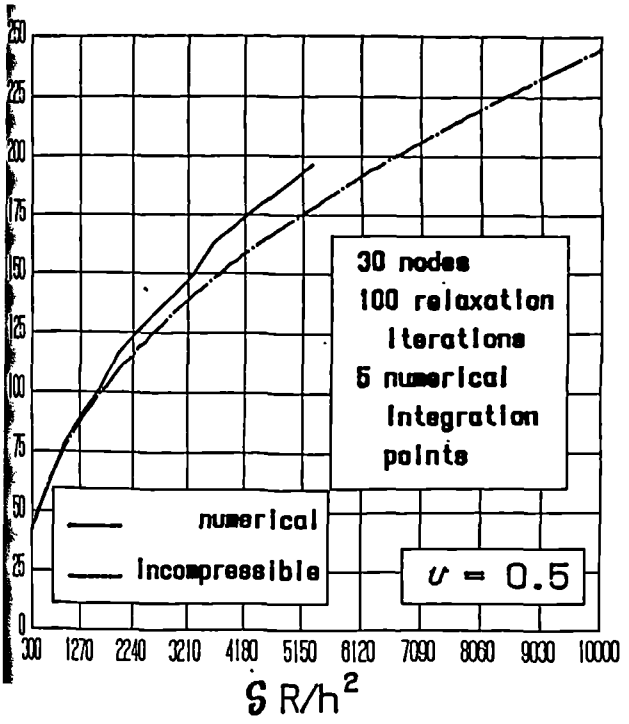

Fig. 4.3.4.15

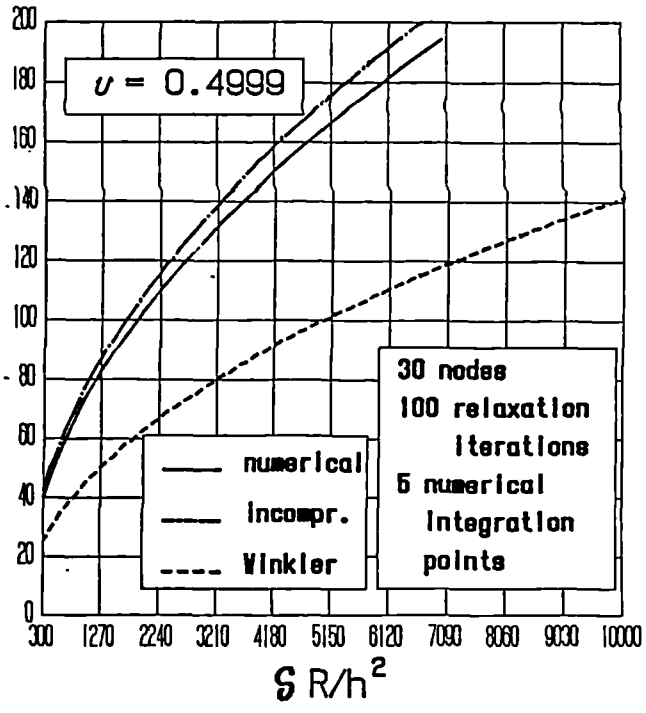

Fig. 4.3.4.16

4.3.5 A contribution to Meijers theory

In this Section the Meijers analytical solution valid for small values of the ratio between contact semiwidth and layer thickness, a/t , is revisited. (Consistent with the Meijers (1968) paper, the layer thickness is here denoted by t , but symbol h is also used in this thesis.) The aim is fourfold : a) to verify the coefficients of the series solution as functions of ν ; b) to examine the dependence of the solution accuracy in terms of contact pressure on the number of series terms considered ; c) to complete the expression for the indentation depth up to the eighth perturbation order; d) to check the precision of the numerical solution developed in Section 4.3.4 . The Meijers (1968) solution for high values of contact width-layer thickness ratios is not examined, since its complexity would require a specifically addressed study. It is first noted that the Meijers solution is of perturbation kind, where the perturbed series solution requires the definition of α_k coefficients (Meijers (1968), p. 355, formula (2.3)). Secondly, *n-th perturbed terms for pressure profile and* cylinder indentation are to be evaluated (Meijers (1968), p. 357, formulae (2.10-2.12) and p. 359, formula (2.14)). The contributions given to these two points consist in a) showing how to compute α_k more quickly, b) correcting the expressions of the perturbed pressure profile, and c) computing a more complete expression for the cylinder indentation depth.

According to (4.3.2.3) and to formula (2.2) of Meijers (1968) paper, p. 355, kernel K possesses the following expression (according to Meijers (1968) a factor of two is incorporated into (4.3.5.1) with respect to (4.3.2.3)) :

$$K(x) = \int_0^\infty \frac{4(k\ sinh\ (2\omega) - 2\omega)}{\omega\ (2k\ cosh\ (2\omega) + 4\omega^2 + k^2 + 1)} cos\left[\frac{x\ \omega}{t}\right] d\omega \qquad (4.3.5.1)$$

In equation (3.2) of Meijers (1968) the following relation is reported :

$$K(x) = -2\ ln\ \left|\frac{x}{2\ t}\right| + \sum_{k=0}^{\infty} \alpha_k \left[\frac{x}{2\ t}\right]^{2k} \quad \left(\frac{x}{2\ t} < 1\right) \qquad (4.3.5.2)$$

where the first term of (4.3.5.2) expresses the logarithmic singularity inherent in (4.3.5.1) in the vicinity of $x = 0$, and the summation represents the regular part of (4.3.5.1). It is the aim of this study to identify the corresponding singular and regular parts in the integrand of (4.3.5.1). In other words, a function is looked for which, once integrated between 0 and ∞ , produces the logarithmic expression contained in (4.3.5.2). This result is of relevance in computing coefficients α_k of (4.3.5.2). (It is not evident how Meijers (1968) computes coefficients α_k .) From the results of (4.3.2.10) it is derived that the part of the integrand of (4.3.5.1) which multiplies *cos* function vanishes as $2/\omega$ when $\omega \rightarrow \infty$ (a factor of two is still present between this result and (4.3.2.10)). Following again (4.3.2.10), an equivalent asymptotic expression is resorted to which does not exhibit a singularity for $x = 0$ and which is integrable in closed form (Gröβner and Hofreiter (1958), second volume, formula 13 b).

$$\int_0^\infty 2 \frac{1 - e^{-a\omega}}{\omega} \cos\left(\frac{x\,\omega}{t} \right) d\omega = ln\left(1 + \frac{t^2\,a^2}{x^2} \right) \qquad (4.3.5.3)$$

Constant a can be evaluated by equalling the right-hand expression of (4.3.5.3) to the logarithmic singularity of (4.3.5.2) :

$$ln\left(1 + \frac{t^2\,a^2}{x^2} \right) = -\,2\,ln\,\left| \frac{x}{2\,t} \right| \qquad (4.3.5.4)$$

from which the following expression for a is derived :

$$a = \sqrt{4 - \left(\frac{x}{t} \right)^2} \qquad (4.3.5.5)$$

Going back to expression (4.3.5.1), it is convenient to subtract and sum to the original integrand that of equation (4.3.5.3), which is exactly integrable, where the

value for a follows from equation (4.3.5.5) :

$$K(x) = \int_0^\infty \frac{4(k\ sinh\ (2\omega) - 2\omega)}{\omega\ (2k\ cosh\ (2\omega) + 4\omega^2 + k^2 + 1)} cos\left[\frac{x\ \omega}{t}\right] d\omega =$$

$$\int_0^\infty \left[\frac{4(k\ sinh\ (2\omega) - 2\omega)}{\omega\ (2k\ cosh\ (2\omega) + 4\omega^2 + k^2 + 1)} - 2\ \frac{1 - e^{-\omega\sqrt{4 - (\frac{x}{t})^2}}}{\omega}\right] cos\left[\frac{x\ \omega}{t}\right] d\omega +$$

$$\int_0^\infty 2\ \frac{1 - e^{-\omega\sqrt{4 - (\frac{x}{t})^2}}}{\omega}\ cos\left[\frac{x\ \omega}{t}\right] d\omega =$$

$$- 2\ ln\ |\frac{x}{2\ t}\ | +$$

$$\int_0^\infty \left[\frac{4(k\ sinh\ (2\omega) - 2\omega)}{\omega\ (2k\ cosh\ (2\omega) + 4\omega^2 + k^2 + 1)} - 2\ \frac{1 - e^{-\omega\sqrt{4 - (\frac{x}{t})^2}}}{\omega}\right] cos\left[\frac{x\ \omega}{t}\right] d\omega$$

(4.3.5.6)

The integrand is now a regular function, and its integral is finite for any x value. In fact, the part of the integrand multiplying cos function vanishes for $\omega \rightarrow \infty$ as $- 8\ \omega\ e^{-2\omega}/\ k$. Since this integral must be computed numerically, it is convenient to sum and subtract its asymptotic expression, so that the modified integrand essentially vanishes for relatively small values of the variable of integration, ω . It is obtained :

$$- 2 \ln \left| \frac{x}{2t} \right| +$$

$$\int_0^\infty \left\{ \frac{4(k \sinh(2\omega) - 2\omega)}{\omega (2k \cosh(2\omega) + 4\omega^2 + k^2 + 1)} - 2 \frac{1 - e^{-\omega \sqrt{4 - (\frac{x}{t})^2}}}{\omega} \right\} \cos\left[\frac{x\,\omega}{t} \right] d\omega =$$

$$- 2 \ln \left| \frac{x}{2t} \right| +$$

$$\int_0^\infty \left\{ \frac{4(k \sinh(2\omega) - 2\omega)}{\omega (2k \cosh(2\omega) + 4\omega^2 + k^2 + 1)} - 2 \frac{1 - e^{-\omega \sqrt{4 - (\frac{x}{t})^2}}}{\omega} + \frac{8}{k} \omega e^{-2\omega} \right\} \bullet$$

$$\cos\left[\frac{x\,\omega}{t} \right] d\omega - \int_0^\infty \frac{8}{k} \omega e^{-2\omega} \cos\left[\frac{x\,\omega}{t} \right] d\omega =$$

$$- 2 \ln \left| \frac{x}{2t} \right| - \frac{8}{k} \frac{4 - (\frac{x}{t})^2}{\left[4 + (\frac{x}{t})^2\right]^2} +$$

$$\int_0^\infty \left\{ \frac{4(k \sinh(2\omega) - 2\omega)}{\omega (2k \cosh(2\omega) + 4\omega^2 + k^2 + 1)} - 2 \frac{1 - e^{-\omega \sqrt{4 - (\frac{x}{t})^2}}}{\omega} + \frac{8}{k} \omega e^{-2\omega} \right\} \bullet$$

$$\cos\left[\frac{x\,\omega}{t} \right] d\omega \qquad (4.3.5.7)$$

The integrand of (4.3.5.7) rapidly vanishes for low values of ω parameter. For the numerical evaluation of this integral, an upper integration limit in the region of 30 can be adopted.

Expression (4.3.5.2) is now revisited to determine coefficients α_k . To do this, the following part of (4.3.5.7) is expanded in a convergent power series :

$$- \frac{8}{k} \frac{4 - (\frac{x}{t})^2}{\left[4 + (\frac{x}{t})^2\right]^2} +$$

$$\int_0^\infty \left\{ \frac{4\,(k\,\sinh(2\omega) - 2\omega)}{\omega\,(2k\,\cosh(2\omega) + 4\omega^2 + k^2 + 1)} - 2\,\frac{1 - e^{-\omega\sqrt{4 - (\frac{x}{t})^2}}}{\omega} + \frac{8}{k}\,\omega\,e^{-2\omega} \right\} \bullet$$

$$\cos\left[\frac{x\,\omega}{t}\right] d\omega \qquad (4.3.5.8)$$

The following power series in x/t was obtained with the aid of the algebraic manipulator MACSYMA (1983) :

$$- \frac{8}{k} \frac{4 - (\frac{x}{t})^2}{\left[4 + (\frac{x}{t})^2\right]^2} +$$

$$\int_0^\infty \left\{ \frac{4\,(k\,\sinh(2\omega) - 2\omega)}{\omega\,(2k\,\cosh(2\omega) + 4\omega^2 + k^2 + 1)} - 2\,\frac{1 - e^{-\omega\sqrt{4 - (\frac{x}{t})^2}}}{\omega} + \frac{8}{k}\,\omega\,e^{-2\omega} \right\} \bullet$$

$$\cos\left(\frac{x\,\omega}{t}\right) d\omega \simeq -\frac{2}{k} +$$

$$\int_0^\infty \left[\frac{4\,(k\,\sinh(2\omega) - 2\omega)}{\omega(2k\cosh(2\omega) + 4\omega^2 + k^2 + 1)} - 2\,\frac{1 - e^{-\omega\sqrt{4 - (\frac{x}{t})^2}}}{\omega} + \frac{8}{k}\,\omega\, e^{-2\omega} \right] d\omega +$$

$$\left\{ \frac{3}{2\,k} + \right.$$

$$\left. \int_0^\infty \left[-4\,\frac{\omega^3\, e^{-2\omega}}{k} + \omega(1 - e^{-2\omega}) + \frac{e^{-2\omega}}{2} - \frac{2\omega\,(k\,\sinh(2\omega) - 2\omega)}{(2k\cosh(2\omega) + 4\omega^2 + k^2 + 1)} \right] d\omega \right\} \frac{x^2}{t^2} +$$

$$\left\{ -\frac{5}{8k} + \right.$$

$$\int_0^\infty \left[-\frac{2\omega^5\, e^{-2\omega}}{3\,k} - \frac{\omega^3\,(1 - e^{-2\omega})}{12\,k} - \frac{\omega^2\, e^{-2\omega}}{4} + \frac{(1 + 2\omega)\, e^{-2\omega}}{32} - \right.$$

$$\left. \left. \frac{2\omega^3\,(k\,\sinh(2\omega) - 2\omega)}{3\,(2k\cosh(2\omega) + 4\omega^2 + k^2 + 1)} \right] d\omega \right\} \frac{x^4}{t^4} +$$

$$\left\{ \frac{7}{32\,k} + \right.$$

$$\int_0^\infty \left[-\frac{\omega^7\, e^{-2\omega}}{90\,k} + \frac{\omega^5\,(1 - e^{-2\omega})}{360} + \frac{\omega^4\, e^{-2\omega}}{48} - \frac{(1 + 2\omega)\,\omega^2 e^{-2\omega}}{64} + \right.$$

$$\left. \left. \frac{(3 + 6\omega + 4\omega^2)\, e^{-2\omega}}{768} - \frac{\omega^5\,(k\,\sinh(2\omega) - 2\omega)}{1800\,(2k\cosh(2\omega) + 4\omega^2 + k^2 + 1)} \right] d\omega \right\} \frac{x^6}{t^6} +$$

$$\left\{ -\frac{9}{128\,k} + \right.$$

$$\int_0^\infty \left\{ \frac{\omega^9 e^{-2\omega}}{5040\,k} - \frac{\omega^7(1 - e^{-2\omega})}{20160} - \frac{\omega^5 e^{-2\omega}}{1440} + \frac{(1 + 2\omega)\,\omega^4 e^{-2\omega}}{768} - \frac{(3 + 6\omega + 4\omega^2)\omega^2 e^{-2\omega}}{1536} + \right.$$

$$\left. \left. \frac{(15 + 30\omega + 24\omega^2 + 8\,\omega^3)e^{-2\omega}}{24576} + \frac{\omega^7\,(k\,sinh\,(2\omega) - 2\omega)}{10080\,(2k\,cosh\,(2\omega) + 4\omega^2 + k^2 + 1)} \right] d\omega \right\} \frac{x^8}{t^8} + \ldots$$

(4.3.5.9)

Following (4.3.5.2), coefficients α_k can be computed from the part of (4.3.5.9) which is independent of x/t (coefficient α_0) , from the part which is multiplied by x^2/t^2 (coefficient α_1) , from the coefficient of x^4/t^4 (coefficient α_2), and so on.

The integral from 0 to infinity in equation (4.3.5.9) was computed from 0 to 30 , since the integrand becomes vanishingly small beyond this upper limit. The following two Tables compare the α_k coefficients according to Meijers (1968), p. 355 , with those due to Jaffar and Savage (1988), p. 69 and with those computed by the author, for $\nu = 0.48$ and 0.5 :

TABLE of α_k for $\nu = 0.48$

	α_0	α_1	α_2	α_3	α_4	α_5
Meijers	-3.1889	7.7938	-11.7696			
Jaffar	-3.188898	7.793725	-11.76717	16.12477	-20.19970	
Strozzi	-3.1888	7.7937	-11.7679	16.1370	-20.3000	24.1993

TABLE of α_k for $\nu = 0.5$

	α_0	α_1	α_2	α_3	α_4	α_5
Meijers	-3.3392	8.1888	-12.5334			
Jaffar	-3.339168	8.188796	-12.53088	17.29113	-21.73677	
Strozzi	-3.3391	8.1887	-12.5317	17.3043	-21.8446	26.0831

It clearly emerges that the various α_k values are in good agreement. It is not clear how Jaffar and Savage (1988) can rely on the exactness of such a high number of figures. (The figures reported in the previous Tables and referring to Strozzi are those which are stable as the number of nodal integration points and the integration interval are augmented, so that these figures should be exact.) It is also noted that the α_k coefficients do not critically depend upon the Poisson's ratio, ν. This result confirms the finding that, in the case of small contact lengths, ν does not noticeably affect the contact pressure for a given indentation depth. The author has also checked all the results at p. 373 of Meijers (1968) referring to small contact lengths, which were found to be all correct.

The expression of the perturbed pressure profile is now considered, and the various terms up to the fifth order are revisited (the 0 , first and second terms are presented by Meijers (1968), while the third and the fourth are reported by Jaffar and Savage (1988)). In particular, it is shown that the fourth pressure term of Jaffar and Savage (1988), p. 68 , is wrong. It is first noted that the expressions for p_0 , p_1 and p_2 at p. 357 of Meijers (1968) are correct, apart from symbol π, which should be removed.

The exact expression for p_4 (the symbols of Jaffar and Savage (1988) are employed; a indicates the semicontact length , t denotes the layer thickness and x

represents the X coordinate normalized with respect to the semicontact width a) is :

$$p_4 = \frac{\sqrt{1-x^2}}{32768}\,\frac{a}{2R\lambda}\left\{\left(8\,\alpha_1^4 + 136\,\alpha_1^2\,\alpha_2 + 516\,\alpha_1\,\alpha_3 + 264\,\alpha_2^2 + 1284\,\alpha_4\right) + x^2\left(32\,\alpha_1^2\,\alpha_2 + 192\,\alpha_2^2 + 288\,\alpha_1\,\alpha_3 + 1888\,\alpha_4\right) + x^4\left(96\,\alpha_1\,\alpha_3 + 1472\,\alpha_4\right) + x^6\,256\,\alpha_4\right\} \qquad (4.3.5.10)$$

Finally, the third contribution of this Section is addressed, that is, the expression of the cylinder indentation depth. It is first noted that expression v_0 at p. 359 of Meijers (1968) including c/b terms (Meijers (1968) symbolism; c indicates the semicontact length and b denotes the layer thickness) up to the fourth order is correct. The formula for the central indentation up to the eighth order of c/b ratio, not included by Jaffar and Savage (1988), is reported hereinafter :

$$v_0 = \frac{c^2}{R}\left\{ln\left[\frac{4b}{c}\right]\left[\frac{1}{2} + \frac{\alpha_1}{16}\left(\frac{c}{b}\right)^2 + \frac{1}{128}\left(\alpha_1^2 + 6\,\alpha_2\right)\left(\frac{c}{b}\right)^4 + \frac{1}{2048}\left(2\,\alpha_1^3 + 24\,\alpha_1\,\alpha_2 + 75\,\alpha_3\right)\left(\frac{c}{b}\right)^6 + \frac{1}{8192}\left(\alpha_1^4 + 39\,\alpha_2^2 + 18\,\alpha_1^2\,\alpha_2 + 75\,\alpha_1\,\alpha_3 + 245\,\alpha_4\right)\left(\frac{c}{b}\right)^8\right] + \frac{1}{4} + \frac{\alpha_0}{4} + \frac{1}{64}\left[3\,\alpha_1 + 2\,\alpha_0\,\alpha_1\right]\left(\frac{c}{b}\right)^2 + \frac{1}{512}\left(2\,\alpha_0\,\alpha_1^2 + 12\,\alpha_0\,\alpha_2 + 3\,\alpha_1^2 + 10\,\alpha_2\right)\left(\frac{c}{b}\right)^4 + \frac{1}{16384}\left(96\,\alpha_0\,\alpha_1\,\alpha_2 + 8\,\alpha_0\,\alpha_1^3 + 300\,\alpha_0\,\alpha_3 + 12\,\alpha_1^3 + 116\,\alpha_1\,\alpha_2 + 175\,\alpha_3\right)\left(\frac{c}{b}\right)^6 + \frac{1}{65536}\left(4\,\alpha_0\,\alpha_1^4 + 156\,\alpha_0\,\alpha_2^2 + 72\,\alpha_0\,\alpha_1^2\,\alpha_2 + 300\,\alpha_0\,\alpha_1\,\alpha_3 + 980\,\alpha_0\,\alpha_4 + 6\,\alpha_1^4 + 94\,\alpha_1^2\,\alpha_2 + 335\,\alpha_1\,\alpha_3 + 135\,\alpha_2^2 + 441\,\alpha_4\right)\left(\frac{c}{b}\right)^8\right\} \qquad (4.3.5.11)$$

Graphical representations of the analytical results just presented are now considered, to get indications about the actual need to consider higher order terms in the perturbed pressure and indentation depth expressions. Fig. 4.3.5.1 reports the analogue of Fig. 3 of Meijers (1968), p. 358 , where now five different normalized contact pressure profiles are presented, up to the eighth perturbation order (a/h = 0.8). Although the curves are similar for orders from the second up to the eighth, their difference is perceivable. In particular, the fourth order pressure curve is less accurate than the second order counterpart (the eighth order being assumed as a benchmark). The sixth and eighth order pressure profiles are very close, a result which suggests that there is no need to proceed beyond order six.

Figs 4.3.5.2. and 4.3.5.3 deal with a Poisson's ratio of 0.48 and with pressure profile and contact width, respectively, as functions of the normalized indentation depth, for a/h ratios ≤ 0.9 . Figs 4.3.5.4 and 4.3.5.5 treat a Poisson's ratio of 0.5 . The perturbed fourth and eighth order curves are displayed together with the numerical results (Section 4.3.4). Some differences between the fourth and eighth order curves are perceivable only when a/h approaches unity. The numerical predictions are in reasonable agreement with the analytical forecasts. The oscillations affecting the numerical curves are due to the contact width being defined in a discontinuous way, the benchmarks being the nodes of the discretization adopted for the deformable layer. In other words, the contact length increases with the indentation depth only when a new node defining the layer profile comes into contact with the cylindrical rigid indenter. As a consequence, the contact pressure too is affected by some undulations.

In addition, Fig. 4.3.5.5 includes the asymptotic, normalized contact width (see (4.4.2.2.8)) which, being accurate only for high contacts, is unreliable for this x-coordinate range, since it noticeably overestimates the actual contact width, a result consistent with Fig. 4.3.4.7 . The asymptotic, normalized peak pressure is not reported in Fig. 4.3.5.4 , since it falls below the y-axis origin. In particular, when $\delta R/h^2 = 0.5$, then $p R/(Ea) = \sqrt{3}/8 \simeq 0.217$ (see (4.4.2.2.11)), which considerably underestimates the actual normalized pressure, a finding in line with Fig. 4.3.4.1 (even if it regards a part of the diagram close to the origin and difficult to read). In conclusion, the asymptotic solution is not applicable for normalized indentation

depths as shallow as those of x-axes of Figs 4.3.5.2,3 .

The $\delta R/h^2$ value beyond which the asymptotic solution becomes applicable is difficult to estimate accurately. It must be certainly higher than 0.5 , as demonstrated by Figs 4.3.5.4,5 . With regard to higher x-coordinate values, Figs 4.3.4.1 and 4.3.4.7 report numerical and asymptotic forecasts for an incompressible elastomer. The numerical predictions exhibit some oscillations related to the discretization process, so that an error estimate of the asymptotic solution becomes problematic. It appears, however, that for $\delta R/h^2$ values greater than, say, 30 , the agreement between numerical and asymptotic forecasts is good both in terms of contact width and pressure. As commented in Section 6.6 (which refers to the analogue axisymmetric situation), this parameter corresponds to a/h ratios beyond approximately 10 in practical circumstances. In any case, the asymptotic incompressible solution is only applicable to ideally incompressible elastomers, since the stress field highly depends on the Poisson's ratio adopted (Section 4.3.4). As a consequence, the asymptotic incompressible solution does not appear to be particularly useful in biomechanical applications.

As a final remark, the contact width is less sensitive to perturbations of the Poisson's ratio than the pressure profile. In fact, Figs 4.3.5.3 and 4.3.5.5 are very similar, whereas the differences between Figs 4.3.5.2 and 4.3.5.4 are appreciable. This result is in line with the findings of Dragoni and Strozzi (1988) referring to an elastomeric O Ring.

The main results obtained in this Section are now summarized : a) a method was developed for computing the coefficients of the Meijers (1968) series solution, the already existing values were checked and found correct, and new higher order coefficients were computed as functions of ν (TABLES at p. 4.57,58) ; a mistake was detected in the expression of the fourth perturbation order pressure given by Jaffar and Savage (1988), and the exact expression (4.3.5.10) was computed ; b) it was found that the solution accuracy is not appreciably improved by terms beyond the sixth perturbation order (Figs 4.3.5.1,2,3) ; c) the expression for the indentation depth was completed up to the eighth perturbation order (eqn (4.3.5.11)) ; d) the Meijers (1968) analytical results were found to agree with the numerical solution developed in Section 4.3.4 and referring to small values of ratio a/h (Figs 4.3.5.3,5) .

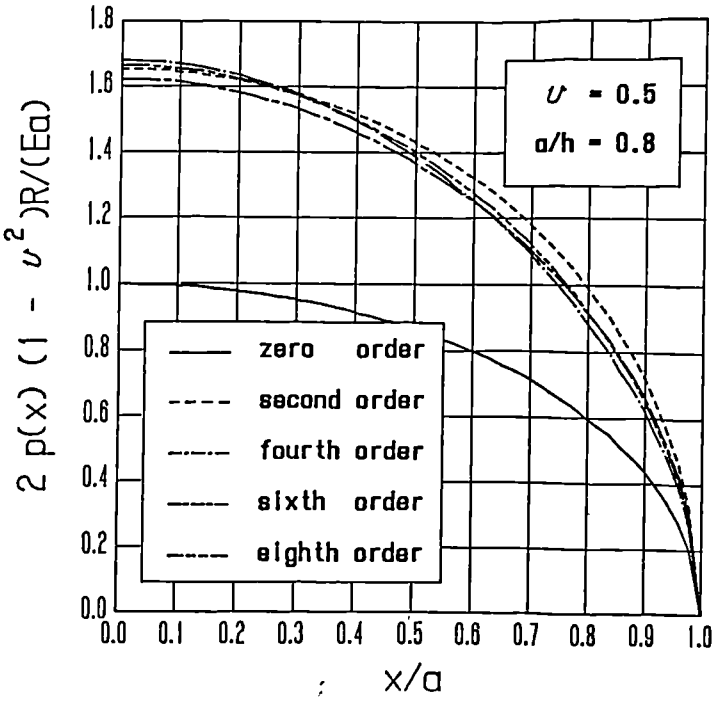

Fig. 4.3.5.1 : Analogue of Fig. 3 of Meijers (1968) up to the eighth order.

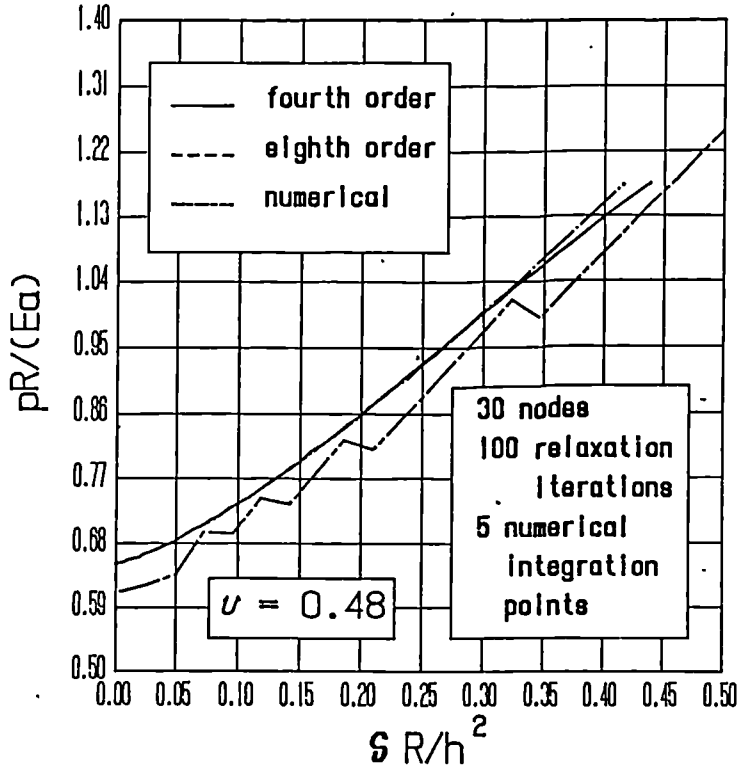

Fig. 4.3.5.2 : Analytical pressure profile and numerical results for $\nu = 0.48$.

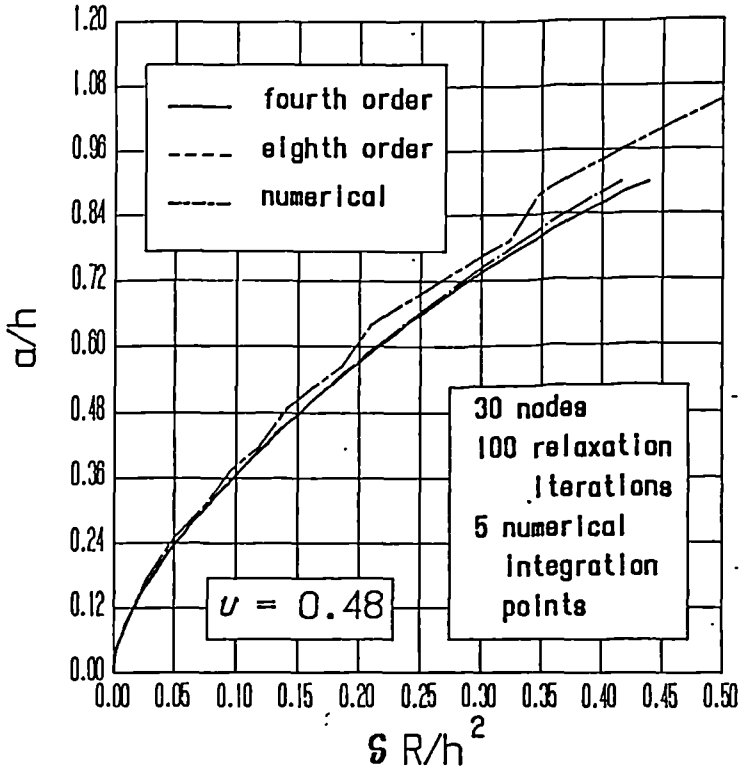

Fig. 4.3.5.3 : Analytical semicontact width and numerical results for $\nu = 0.48$.

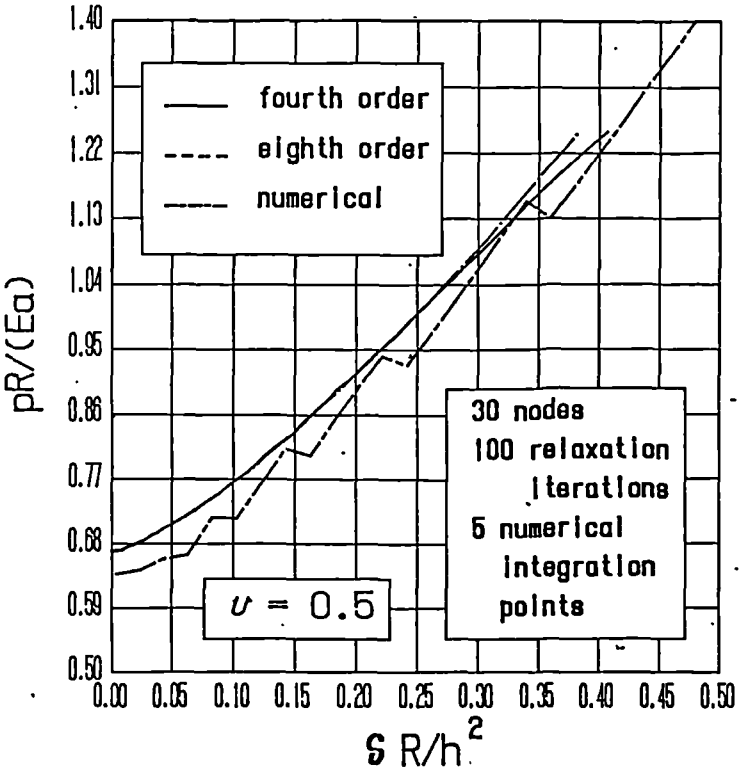

Fig. 4.3.5.4 : Analytical pressure profile and numerical results for $\nu = 0.5$.

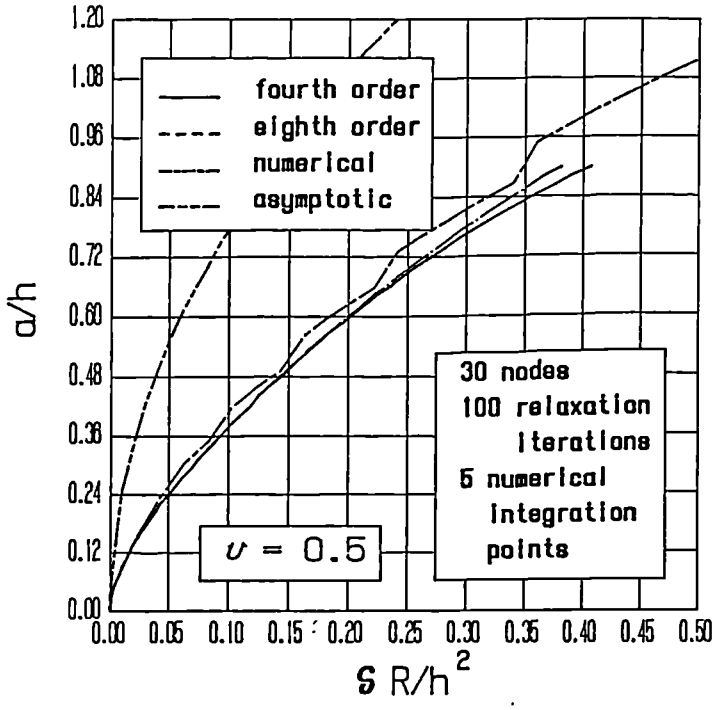

Fig. 4.3.5.5 : Analytical semicontact width and numerical results for $\nu = 0.5$.

4.4 DIFFERENTIAL APPROACH

4.4.1 Introduction

In Subsection 4.4.2 the theory developed Armstrong (1986) is closely followed and the results he obtained by applying perturbation techniques to the layer problem are reported. The study of Armstrong (1986) limits itself to a few perturbed terms. In order to analyze the effects of higher-order terms on the accuracy of the solution, the Armstrong (1986) methodology is further developed in Section 4.4.3 . It is also noted that, while the perturbed solution of the integral approach 4.3 is valid for small contact widths, the perturbed solution of the differential formulation holds for high contact widths.

4.4.2 The existing solution

The paper of Armstrong (1986) develops the following steps: a) the two-dimensional equilibrium equations are expressed in terms of the displacement field; b) the equilibrium equations are normalized with respect to proper variables, and a small parameter ϵ is identified, which renders this problem amenable to perturbation solution techniques; c) an approximate solution is achieved for parameter ϵ up to the second order, which connects the pressure (as well as its derivatives) acting upon an elastomeric layer to its local deflection; d) the pressure profile and contact width are determined for the case of a rigid cylinder indenting a deformable layer only for solutions for ϵ up to the second order. The above-mentioned steps are now treated in greater detail, to serve as an introduction to the extension of this procedure given in Section 4.4.3 . In particular, steps a) , b) and c) are treated in Section 4.4.2.1 , whereas step d) is analized in Section 4.4.2.2 .

In this Section the Armstrong (1986) nomenclature is adopted. In particular, a indicates the semicontact width, and h denotes the layer thickness.

4.4.2.1 The perturbed pressure-deflection solution

The two-dimensional equilibrium equations expressed in terms of stresses are (Timoshenko and Goodier (1970)) :

$$\frac{\partial \sigma_x}{\partial x} + \frac{\partial \tau_{xy}}{\partial y} = 0$$

$$\frac{\partial \tau_{yx}}{\partial x} + \frac{\partial \sigma_y}{\partial y} = 0 \qquad (4.4.2.1.1)$$

In plane strain situations, the Hooke law linking stresses to strains is (Timoshenko and Goodier (1970)):

$$\sigma_x = \lambda \left(\frac{\partial u}{\partial x} + \frac{\partial v}{\partial y} \right) + 2\mu \frac{\partial u}{\partial x}$$

$$\sigma_y = \lambda \left(\frac{\partial u}{\partial x} + \frac{\partial v}{\partial y} \right) + 2\mu \frac{\partial v}{\partial y} \qquad (4.4.2.1.2)$$

$$\tau_{xy} = \mu \left(\frac{\partial u}{\partial y} + \frac{\partial v}{\partial x} \right)$$

where u and v are the x—oriented and y—oriented displacements, and λ and μ are the so called Lame' constants, which are expressible in terms of Young's Modulus, E, and Poisson's ratio, ν (Timoshenko and Goodier (1970)) :

$$\lambda = \frac{\nu E}{(1 + \nu)(1 - 2\nu)} \qquad \mu = \frac{E}{2(1 + \nu)} \qquad (4.4.2.1.3)$$

(Constant μ coincides with the so called shear Modulus, G .) In elastomeric materials ν approaches the incompressibility value 0.5 (Section 3). In this case, $\lambda = \infty$ and $\mu = E/3$. For a realistic figure of $\nu = 0.499$ (Section 3), $\lambda = 166.444\ E$, $\mu = 0.333\ E$, that is, $\lambda \simeq 500\ \mu$.

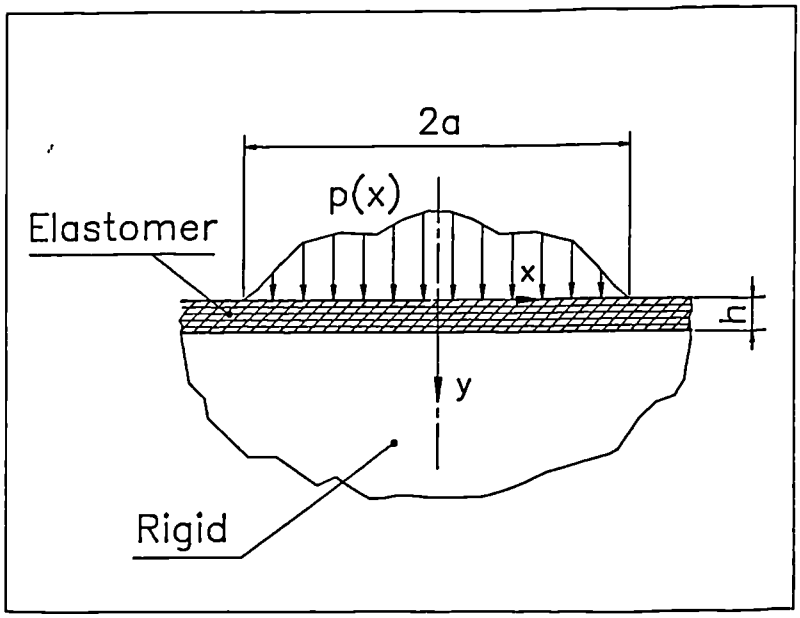

Fig. 4.4.2.1.1 : Coordinates x and y, *and* the meaning of symbols h, a, $p(x)$.

By introducing formulae (4.4.2.1.2) into (4.4.2.1.1), the equilibrium equations are expressed in terms of the displacement field :

$$\mu \frac{\partial^2 u}{\partial y^2} + (\lambda + \mu) \frac{\partial^2 v}{\partial x \partial y} + (\lambda + 2\mu) \frac{\partial^2 u}{\partial x^2} = 0$$

(4.4.2.1.4)

$$(\lambda + 2\mu) \frac{\partial^2 v}{\partial y^2} + (\lambda + \mu) \frac{\partial^2 u}{\partial x \partial y} + \mu \frac{\partial^2 v}{\partial x^2} = 0$$

The boundary conditions must represent the following aspects : a) the layer is firmly bonded to a rigid substrate; b) due to the small frictional coefficient, only a normal pressure affects the upper boundary of the layer. According to Fig. 4.4.2.1.1 , such boundary conditions are :

$$\text{for } y = 0 , \qquad \sigma_y = -p(x) \quad ; \quad \tau_{xy} = 0$$

(4.4.2.1.5)

$$\text{for } y = h , \qquad u = 0 \quad ; \quad v = 0$$

where $p\ (x)$ is the applied pressure and h is the (supposed constant) layer thickness. Armstrong (1986) normalizes equations (4.4.2.1.4) by introducing the following non–dimensionalized variables :

$$U = \frac{u}{h} \ ; \ V = \frac{v}{h} \ ; \ X = \frac{x}{a} \ ; \ Y = \frac{y}{h} \qquad (4.4.2.1.6)$$

where a is the contact half width (Fig. 4.4.2.1.1). Equations (4.4.2.1.4) thus become :

$$\frac{\partial^2 U}{\partial Y^2} + \epsilon \frac{\lambda + \mu}{\mu} \frac{\partial^2 V}{\partial X \, \partial Y} + \epsilon^2 \frac{\lambda + 2\mu}{\mu} \frac{\partial^2 U}{\partial X^2} = 0$$

$$\frac{\partial^2 V}{\partial Y^2} + \epsilon \frac{\lambda + \mu}{\lambda + 2\mu} \frac{\partial^2 U}{\partial X \, \partial Y} + \epsilon^2 \frac{\mu}{\lambda + 2\mu} \frac{\partial^2 V}{\partial X^2} = 0 \qquad (4.4.2.1.7)$$

where $\epsilon = h/a$ is a small parameter. It should be noted that in many practically relevant problems the contact width is not known *a priori* and, therefore, ϵ too is not initially known. Nevertheless, it can be conjectured that ϵ is often sufficiently small. The boundary conditions (4.4.2.1.5), once normalized according to variables (4.4.2.1.6), become :

$$\text{for } Y = 0 \ , \ \frac{\partial V}{\partial Y} + \epsilon \frac{\lambda}{\lambda + 2\mu} \frac{\partial U}{\partial X} = - P\,(X) \ ; \ \frac{\partial U}{\partial Y} + \epsilon \frac{\partial V}{\partial X} = 0$$

$$\text{for } Y = 1 \ , \qquad U = 0 \ ; \qquad V = 0 \qquad (4.4.2.1.8)$$

where $P = p/(\lambda + 2\mu)$.

Armstrong (1986) develops an approximate solution to this problem by a perturbation method (Bender and Orszag (1978)). The dimensionless horizontal, U, and vertical, V, displacements are expressed via a series of functions in powers of ϵ :

$$U = U_0 + \epsilon U_1 + \epsilon^2 U_2 + \ldots$$

$$V = V_0 + \epsilon V_1 + \epsilon^2 V_2 + \ldots \qquad (4.4.2.1.9)$$

Expressions (4.4.2.1.9) are then substituted into (4.4.2.1.7), and terms in the same power of ϵ are collected. The terms of order 0 (obtained by putting $\epsilon = 0$) supply the following equations (indices 0 indicate the zero order components) :

$$\frac{\partial^2 U_0}{\partial Y^2} = 0$$

$$\frac{\partial^2 V_0}{\partial Y^2} = 0 \qquad (4.4.2.1.10)$$

The boundary conditions (4.4.2.1.8), when limited to the zero term, become :

$$\text{for } Y = 0 , \quad \frac{\partial V_0}{\partial Y} = - P(X) ; \quad \frac{\partial U_0}{\partial Y} = 0$$

$$\text{for } Y = 1 , \quad U_0 = 0 \quad ; \quad V_0 = 0 \qquad (4.4.2.1.11)$$

The expressions of U_0 and V_0 satisfying equations (4.4.2.1.10) and the boundary conditions (4.4.2.1.11) are :

$$U_0 = 0$$

$$V_0 = P (1 - Y) \qquad (4.4.2.1.12)$$

The zero order approximate solution (4.4.2.1.12) exhibits no lateral displacements of the layer. From expressions (4.4.2.1.12) the dimensional horizontal, u, and vertical, v, displacements are :

$$u\,(x,y) = 0$$

$$v\,(x,y) = \frac{p\,(x)\,h}{\lambda + 2\mu}\,(1 - \frac{y}{h}) \qquad (4.4.2.1.13)$$

This result coincides with a Winkler—type model of the layer (Kerr (1964), Strozzi (1984)), where each column is laterally constrained (that is, the column is subject to a plane—strain condition along both its lateral sides). If the elastomer is ideally incompressible, then $\lambda = \infty$, μ is finite, and $v = 0$. This is an unrealistic result, since an incompressible layer, when indented by a rigid cylinder, would still flow laterally and, therefore, it would not fully prevent any vertical movements of the rigid indenter. Since this behaviour is not simulated by the zero order solution, higher ϵ orders must be accounted for in the case of incompressible materials. In particular, the first order ϵ solution is now treated, as done by Armstrong (1986). According to (4.4.2.1.9), the first order solution comprises functions U_1 and V_1 (index 1 refers to the first order perturbed components), which are the unknowns, as well as functions U_0 and V_0 , which have already been determined, see (4.4.2.1.12) . Indeed, it is typical of perturbation approaches to exploit the solutions referring to lower order terms, when dealing with higher order components. Collecting in (4.4.2.1.7) terms of the first order in ϵ , it is obtained :

$$\frac{\partial^2 U_1}{\partial Y^2} + \frac{\lambda + \mu}{\mu}\,\frac{\partial^2 V_0}{\partial X\,\partial Y} = 0$$

$$\frac{\partial^2 V_1}{\partial Y^2} + \frac{\lambda + \mu}{\lambda + 2\mu}\,\frac{\partial^2 U_0}{\partial X\,\partial Y} = 0 \qquad (4.4.2.1.14)$$

By introducing expressions (4.4.2.1.12) of U_0 and V_0 into (4.4.2.1.14), the following equations are obtained :

$$\frac{\partial^2 U_1}{\partial Y^2} = \frac{\lambda + \mu}{\mu}\,\frac{dP}{dX}$$

$$\frac{\partial^2 V_1}{\partial Y^2} = 0 \qquad (4.4.2.1.15)$$

The boundary conditions (4.4.2.1.8), when referring to ϵ terms of the first order, become (the boundary conditions related to ϵ zero order terms have already been imposed in (4.4.2.1.11), and they affect the expressions of U_0 and V_0) :

$$\text{for } Y = 0 , \quad \frac{\partial V_1}{\partial Y} + \frac{\lambda}{\lambda + 2\mu} \frac{\partial U_0}{\partial X} = 0 \; ; \quad \frac{\partial U_1}{\partial Y} + \frac{\partial V_0}{\partial X} = 0$$

$$\text{for } Y = 1 , \quad U_1 = 0 \; ; \quad V_1 = 0 \qquad (4.4.2.1.16)$$

By substituting formulae (4.4.2.1.12) into the boundary conditions (4.4.2.1.16) , it is obtained :

$$\text{for } Y = 0 , \quad \frac{\partial V_1}{\partial Y} = 0 \; ; \quad \frac{\partial U_1}{\partial Y} = - \frac{dP}{dX}$$

$$\text{for } Y = 1 , \quad U_1 = 0 \; ; \quad V_1 = 0 \qquad (4.4.2.1.17)$$

The expressions of the solutions U_1 and V_1 are :

$$U_1 = - \frac{dP}{dX} \left(\frac{\lambda - \mu}{2 \mu} + Y - \frac{\lambda + \mu}{2 \mu} Y^2 \right)$$

$$V_1 = 0 \qquad (4.4.2.1.18)$$

The formulae for u and v in dimensional form are obtained by summing the U and V contributions referring to zero and first order ϵ terms according to (4.4.2.1.9) and, then, by substituting relations (4.4.2.1.6) . It is obtained :

$$u(x,y) = - \frac{h^2}{2\mu} \frac{dp(x)}{dx} \left(\frac{\lambda - \mu}{\lambda + 2\mu} + \frac{2\mu}{\lambda + 2\mu} \frac{y}{h} - \frac{\lambda + \mu}{\lambda + 2\mu} \frac{y^2}{h^2} \right)$$

$$v(x,y) = \frac{p(x)\, h}{\lambda + 2\mu} \left(1 - \frac{y}{h}\right) \qquad (4.4.2.1.19)$$

With respect to the zero order solution (4.4.2.1.13), the up to the first order expressions (4.4.2.1.19) exhibit the same vertical displacement function (it still vanishes for incompressible elastomers), whereas a non vanishing horizontal displacement formula is achieved.

Following Armstrong (1986), the ϵ second order solution is now treated. According to (4.4.2.1.9), the second order solution comprises functions U_2 and V_2, which are the unknowns, as well as functions U_1, V_1, U_0 and V_0, which have already been determined, see (4.4.2.1.12) and (4.4.2.1.18) . Collecting in (4.4.2.1.7) terms of the second order in ϵ, it is obtained :

$$\frac{\partial^2 U_2}{\partial Y^2} + \frac{\lambda + \mu}{\mu} \frac{\partial^2 V_1}{\partial X \partial Y} + \frac{\lambda + 2\mu}{\mu} \frac{\partial^2 U_0}{\partial X^2} = 0$$

$$\frac{\partial^2 V_2}{\partial Y^2} + \frac{\lambda + \mu}{\lambda + 2\mu} \frac{\partial^2 U_1}{\partial X \partial Y} + \frac{\mu}{\lambda + 2\mu} \frac{\partial^2 V_0}{\partial X^2} = 0 \qquad (4.4.2.1.20)$$

By introducing expressions (4.4.2.1.12) of U_0 and V_0 and formulae (4.4.2.1.18) of U_1 and V_1 into (4.4.2.1.20), the following equations are obtained :

$$\frac{\partial^2 U_2}{\partial Y^2} = 0$$

$$\frac{\partial^2 V_2}{\partial Y^2} = \frac{d^2 P}{dX^2} \left[\frac{\lambda}{\lambda + 2\mu} - \frac{\lambda}{\mu} Y \right] \qquad (4.4.2.1.21)$$

The boundary conditions (4.4.2.1.8) addressing ϵ terms of the second order become (the boundary conditions referring to ϵ zero and first orders have already been imposed in (4.4.2.1.11) and (4.4.2.1.17)) :

$$\text{for } Y = 0\,, \quad \frac{\partial V_2}{\partial Y} + \frac{\lambda}{\lambda + 2\mu}\frac{\partial U_1}{\partial X} = 0 \;; \quad \frac{\partial U_2}{\partial Y} + \frac{\partial V_1}{\partial X} = 0$$

$$\text{for } Y = 1\,, \quad U_2 = 0 \;; \quad V_2 = 0 \tag{4.4.2.1.22}$$

By substituting formulae (4.4.2.1.18) into the boundary conditions (4.4.2.1.22), it is obtained :

$$\text{for } Y = 0\,, \quad \frac{\partial V_2}{\partial Y} = \frac{d^2P}{dX^2}\left[\frac{\lambda - \mu}{2(\lambda + 2\mu)}\frac{\lambda}{\mu}\right] \;; \quad \frac{\partial U_2}{\partial Y} = 0$$

$$\text{for } Y = 1\,, \quad U_2 = 0 \;; \quad V_2 = 0 \tag{4.4.2.1.23}$$

The expressions of the solutions U_2 and V_2 are :

$$U_2 = 0 \tag{4.4.2.1.24}$$

$$V_2 = \frac{d^2P}{dX^2}\left[-\frac{\lambda - \mu}{\lambda + 2\mu}\frac{\lambda}{3\mu} + \frac{\lambda - \mu}{\lambda + 2\mu}\frac{\lambda}{2\mu}Y + \frac{\lambda}{2(\lambda + 2\mu)}Y^2 - \frac{\lambda}{6\mu}Y^3\right]$$

The formulae for u and v in dimensional form are obtained by summing the U and V contributions referring to zero, first and second ϵ terms according to (4.4.2.1.9) and, then, by substituting relations (4.4.2.1.6) . Thus :

$$u(x,y) = -\frac{h^2}{2\mu}\frac{dp(x)}{dx}\left[\frac{\lambda - \mu}{\lambda + 2\mu} + \frac{2\mu}{\lambda + 2\mu}\frac{y}{h} - \frac{\lambda + \mu}{\lambda + 2\mu}\frac{y^2}{h^2}\right]$$

$$v(x,y) = \frac{p(x)\,h}{\lambda + 2\mu}\left(1 - \frac{y}{h}\right) -$$

$$\frac{h^3}{6\mu}\frac{\lambda}{\lambda + 2\mu}\frac{d^2p(x)}{dx^2}\left[\frac{2(\lambda - \mu)}{\lambda + 2\mu} - \frac{3(\lambda - \mu)}{\lambda + 2\mu}\frac{y}{h} - \frac{3\mu}{\lambda + 2\mu}\frac{y^2}{h^2} + \frac{y^3}{h^3}\right] \tag{4.4.2.1.25}$$

For an incompressible material, $\lambda = \infty$, and function $v(x,y)$ of (4.4.2.1.25) simplifies to :

$$v\,(x,y) = -\frac{h^3}{6\mu}\,\frac{d^2p\,(x)}{dx^2}\left[\,2 - 3\,\frac{y}{h} + \frac{y^3}{h^3}\,\right] \qquad (4.4.2.1.26)$$

which, contrary to the vertical displacement of (4.4.2.1.13), does not necessarily vanish for incompressible materials.

4.4.2.2 The pressure profile for a cylindrical indenter

Once the pressure distribution, $p(x)$, is known, equations (4.4.2.1.13), (4.4.2.1.25) and (4.4.2.1.26) permit the vertical displacement of the layer upper boundary ($y=0$) to be computed. More exactly, expression (4.4.2.1.13) refers to the zero order vertical compression, relation (4.4.2.1.25) describes the second order results (the first order findings coincide with the zero order forecasts) and, finally, formula (4.4.2.1.26) covers the second order incompressible case. Armstrong (1986) treats the practically more relevant situation of a known displacement function, where the pressure profile is the unknown which has to be determined. In particular, Armstrong (1986) studies two cases : a) a compressible layer indented by a rigid cylinder, studied via the zero order equation (4.4.2.1.13) ; b) an incompressible layer pressed by a rigid cylindrical indenter, analyzed through the second order expression (4.4.2.1.26). These two cases are examined in detail in the follow-up, since they constitute an introduction to the more complex situations analyzed in Section 4.4.3 .

As usual (Jaffar and Savage (1988)), the imposed displacement is approximated by a second degree (parabolic) expression :

$$v(x,0) = \delta - \frac{x^2}{2R} \qquad (4.4.2.2.1)$$

where δ is the rigid body vertical displacement, and R is the (relative) radius of curvature of the two contacting surfaces. A note of caution is here introduced on the accuracy of (4.4.2.2.1) in describing very high contact widths. Anyway, the influence of the indenter profile (parabolic or circular) does not seem to be generally relevant, as the numerical forecasts of Section 7.3.6 indicate. The zero order solution is treated first. By introducing (4.4.2.2.1) into the vertical displacement expression of (4.4.2.1.13) referring to the layer upper boundary ($y=0$), it is obtained :

$$\frac{p(x)\,h}{\lambda + 2\mu} = \delta - \frac{x^2}{2R} \qquad (4.4.2.2.2)$$

from which the contact half width, a, is computed by expressing the condition that for $x=a$ the pressure, p, vanishes :

$$\delta - \frac{a^2}{2R} = 0 \quad \rightarrow \quad a = \sqrt{2R\delta} \tag{4.4.2.2.3}$$

The expression of the pressure profile as a function of the peak pressure, p_0 , and of the normalized X coordinate (see (4.4.2.1.6)) is :

$$p\,(x) = p_0\,(1 - X^2) \tag{4.4.2.2.4}$$

where :

$$p_0 = \frac{(\lambda + 2\mu)\delta}{h} \tag{4.4.2.2.5}$$

This solution coincides with formula (5.73) of Johnson (1985) .

The incompressible case according to (4.4.2.1.26) is now treated. By introducing expression (4.4.2.2.1) into (4.4.2.1.26) and by putting $y=0$, there follows :

$$-\frac{h^3}{3\mu}\frac{d^2p\,(x)}{dx^2} = \delta - \frac{x^2}{2R} \tag{4.4.2.2.6}$$

The integration of the second order differential equation (4.4.2.2.6) requires the imposition of two boundary conditions. The first requirement has already been used in the first order solution, and it expresses the fact that the pressure must vanish at the contact ends ($x = +/-a$, see (4.4.2.2.3)). The second imposition requires that the first derivative of the pressure also vanishes at the contact extremities. This boundary condition is suggested by a result obtained by Meijers (1968), p. 378, who showed that the pressure derivative vanishes for incompressible materials and for a contact width infinitely larger than the layer thickness. Anyway, Meijers (1968) shows that for incompressible elastomers and finite contact

widths the pressure derivative is infinite at the contact extremities. As a consequence, the imposition in (4.4.2.2.6) of a vanishing pressure slope at the contact ends is inevitably questionable. Integrating (4.4.2.2.6) once with respect to x coordinate gives :

$$\frac{d\ p\ (x)}{d\ x} = \frac{3\mu}{h^3}\left[\frac{x^3}{6R} - \delta\ x\right] + A \qquad (4.4.2.2.7)$$

The integration constant A is zero, since the pressure gradient is expected to vanish for $x = 0$, owing to the symmetrical profile of the indenter.

As previously discussed, the condition is imposed that the pressure derivative vanishes for $x = a$. This allows the contact half width, a, to be computed. From (4.4.2.2.7) it is derived :

$$\frac{a^3}{6R} - \delta\ a = 0 \rightarrow a = \sqrt{6R\delta} \qquad (4.4.2.2.8)$$

a result coinciding with formula (5.77) of Johnson (1985) .

By integrating (4.4.2.2.7) with respect to x, the expression of $p\ (x)$ is obtained, apart from the integration constant B :

$$p\ (x) = \frac{3\mu}{2\ h^3}\left[\frac{x^4}{12\ R} - \delta\ x^2 + B\right] \qquad (4.4.2.2.9)$$

Constant B can be found by imposing the condition that the pressure profile vanishes for $x = a = \sqrt{6R\delta}$ (see 4.4.2.2.8) . Therefore :

$$\frac{36\ R^2\delta^2}{12\ R} - 6\ R\ \delta^2 + B = 0 \rightarrow B = 3\ R\ \delta^2 = \frac{a^2\delta}{2} \qquad (4.4.2.2.10)$$

By substituting the value of B into (4.4.2.2.9), the final expression for $p(x)$ becomes :

$$p(x) = \frac{3\,\mu\,a^2\delta}{4\,h^3}\left(\frac{x^4}{a^4} - 2\frac{x^2}{a^2} + 1\right) = p_0\,(1 - X^2)^2 \quad (4.4.2.2.11)$$

where $p_0 = 3\,\mu\,a^2\delta\,/(4\,h^3)$. Formula (4.4.2.2.11) coincides with (5.75) of Johnson (1985) .

An important point concerns the employ of solutions (4.4.2.2.4) and (4.4.2.2.11). In particular, it should be clarified for which Poisson's ratio intervals solution (4.4.2.2.4) can be employed, and when formula (4.4.2.2.11) is more appropriate (that is, for which Poisson's ratios the elastomer can be assumed as fully incompressible). Armstrong (1988) observes that the normalized vertical displacement of the layer upper boundary, complete up to the second order (see (4.4.2.1.9), (4.4.2.1.12), (4.4.2.1.18) and (4.4.2.1.24)), is :

$$V_0 + \epsilon\,V_1 + \epsilon^2\,V_2 \mid_{Y=0} = P - \frac{\lambda - \mu}{\lambda + 2\mu}\,\frac{\lambda}{3\mu}\,\frac{h^2}{a^2}\,\frac{d^2P}{dX^2} \quad (4.4.2.2.12)$$

At the right-hand side of (4.4.2.2.12), the unity coefficient multiplying P is characteristic of the zero order solution (see (4.4.2.1.12)), whereas the coefficient multiplying the second derivative of the pressure identifies the incompressible, second order solution (see (4.4.2.1.18)). The first order solution, V_1 , identically vanishes (see (4.4.2.1.12)) and, therefore, it does not appear in (4.4.2.2.12) . Following Armstrong (1988), it can be speculated that the transitional value of the Poisson's ratio is the one which renders equal the absolute values of the two above-mentioned coefficients :

$$\frac{\lambda - \mu}{\lambda + 2\mu}\,\frac{\lambda}{3\mu}\,\frac{h^2}{a^2} \simeq 1 \rightarrow \frac{\nu\,(4\nu - 1)}{3\,(1 - \nu)\,(1 - 2\nu)} = \frac{a^2}{h^2} \quad (4.4.2.2.13)$$

where coefficient 3 at the denominator of the fraction expressed in terms of Poisson's ratio is missing in Armstrong (1988). From (4.4.2.2.13) the transitional value ν_{trans} is obtained as a function of the ratio between contact half width and layer thickness :

$$\nu_{trans} = \frac{1 - 9\frac{a}{h} + \sqrt{1 + 30\frac{a}{h} + 9\frac{a^2}{h^2}}}{4\left(2 - 3\frac{a}{h}\right)} \qquad (4.4.2.2.14)$$

According to Armstrong (1988), the zero order compressible model (4.4.2.1.13) should be employed for lower figures than the transitional Poisson's ratio, whereas for higher values than ν_{trans} the fully incompressible modelling (4.4.2.1.26) is recommended. Unfortunately, the contact half width, a, is not known (the Winkler and incompressible models supply appreciably different results) and, therefore, it is not easy to determine the transitional Poisson's ratio.

The second order complete solution is now treated for the case of a cylindrical indenter, based upon (4.4.2.2.12). This case is analyzed in Armstrong (1988), but not in Armstrong (1986). By equalling (4.4.2.2.12) to the cylindrical displacement (4.4.2.2.1) normalized with respect to h, it is obtained :

$$P - \frac{\lambda - \mu}{\lambda + 2\mu}\frac{\lambda}{3\mu}\frac{h^2}{a^2}\frac{d^2P}{dX^2} = V_0 + \epsilon V_1 + \epsilon^2 V_2 \mid_{Y=0} = \frac{\delta}{h} - \frac{x^2}{2hR} \qquad (4.4.2.2.15)$$

Equation (4.4.2.2.15) can be rewritten in terms of p and x , by employing (4.4.2.1.6) and the definition of P given in (4.4.2.1.8) :

$$\frac{d^2p}{dx^2} - \frac{3\mu(\lambda + 2\mu)}{h^2\lambda(\lambda - \mu)}p = \frac{3\mu(\lambda + 2\mu)^2}{h^2\lambda(\lambda - \mu)}\left(\frac{x^2}{2hR} - \frac{\delta}{h}\right) \qquad (4.4.2.2.16)$$

The homogeneous solution is :

$$p(x) = A\cosh\left(\sqrt{\frac{3\mu(\lambda + 2\mu)}{\lambda(\lambda - \mu)}}\frac{x}{h}\right) + B\sin\left(\sqrt{\frac{3\mu(\lambda + 2\mu)}{\lambda(\lambda - \mu)}}\frac{x}{h}\right) \qquad (4.4.2.2.17)$$

A particular solution to (4.4.2.2.16) is :

$$p(x) = \frac{\lambda + 2\mu}{h} \left[\delta - \frac{h^2 \lambda (\lambda - \mu)}{3 R \mu (\lambda + 2\mu)} \right] - \frac{(\lambda + 2\mu) x^2}{2 h R} \quad (4.4.2.2.18)$$

The complete solution to (4.4.2.2.16) is the sum of (4.4.2.2.17) and (4.4.2.2.18), where coefficient B of (4.4.2.2.17) is set equal to zero since the pressure profile must be symmetrical with respect to x-coordinate, as a consequence of the indenter symmetry :

$$p(x) = A \cosh \left[\sqrt{\frac{3 \mu (\lambda + 2\mu)}{\lambda (\lambda - \mu)}} \frac{x}{h} \right] + \frac{\lambda + 2\mu}{h} \left[\delta - \frac{h^2 \lambda (\lambda - \mu)}{3 R \mu (\lambda + 2\mu)} \right] - \frac{(\lambda + 2\mu) x^2}{2 h R}$$

(4.4.2.2.19)

The unknowns in (4.4.2.2.19) are constant A and contact half width, a (which does not explicitly appear in (4.4.2.2.19), but it affects the imposition of the boundary conditions). According to Armstrong (1988), the boundary conditions which permit constants A and a to be determined are the vanishing of both p and of dp/dx at the contact extremities ($x = +/- a$). The condition on the vanishing of the pressure derivative is suggested by the fact that, for infinite contact widths and both compressible and incompressible elastomers, dp/dx actually vanishes at the contacts ends (Meijers (1968), pp. 377-378). Anyway, in the case of finite contact widths, the pressure slope is vertical at the contact extremities. Consequently, the boundary conditions assumed by Armstrong (1988) are inevitably questionable. The vanishing of the pressure by the contact ends requires that :

$$A \cosh \left[\sqrt{\frac{3 \mu (\lambda + 2\mu)}{\lambda (\lambda - \mu)}} \frac{a}{h} \right] + \frac{\lambda + 2\mu}{h} \left[\delta - \frac{h^2 \lambda (\lambda - \mu)}{3 R \mu (\lambda + 2\mu)} \right] - \frac{(\lambda + 2\mu) a^2}{2 h R} = 0$$

(4.4.2.2.20)

Similarly, the extinction of the pressure gradient at the contact extremities imposes that :

$$A \sqrt{\frac{3\,\mu\,(\lambda + 2\mu)}{\lambda\,(\lambda - \mu)}} \; sinh\left[\sqrt{\frac{3\,\mu\,(\lambda + 2\mu)}{\lambda\,(\lambda - \mu)}}\;\frac{a}{h}\right] - \frac{(\lambda + 2\mu)\,a}{R} = 0$$

(4.4.2.2.21)

Equations (4.4.2.2.20,21) permit constants A and a to be determined. To define the equation referring to the computation of the contact half width, a, equations (4.4.2.2.20,21) are rewritten by keeping at the left-hand sides only the hyperbolic functions. Then, such modified equations are mutually divided to produce the following relation :

$$\left[\frac{a}{h} + \frac{2h\lambda(\lambda-\mu)}{3a\mu(\lambda+2\mu)} - \frac{2\delta\,R}{a\,h}\right]\sqrt{\frac{3\mu(\lambda+2\mu)}{\lambda(\lambda-\mu)}}\; tanh\left[\sqrt{\frac{3\mu\,(\lambda+2\mu)}{\lambda\,(\lambda-\mu)}}\;\frac{a}{h}\right] - 2 = 0$$

(4.4.2.2.22)

Equation (4.4.2.2.22) in unknown a may be solved only numerically. A standard Newton method was employed in this study. The starting point may be chosen in two ways. First, expression (4.4.2.2.8) for a in the case of incompressible materials can be adopted (the Poisson's ratios for actual elastomers are very close to the incompressibility value 0.5 , see Section 3). Alternatively, it can be observed that, for sufficiently high a values, the *tanh* function at the left-hand member in expression (4.4.2.2.22) approaches unity. More precisely, this presupposition requires that the radical appearing as the argument of *tanh* function is not too small. This in turn demands that λ does not prevail too much with respect to μ . With this assumption, formula (4.4.2.2.22) can be solved in closed form to supply an approximate expression for a , which can serve as a starting point :

$$a \simeq h\sqrt{\frac{\lambda\,(\lambda - \mu)}{3\,\mu\,(\lambda + 2\mu)}} + \sqrt{2\,\delta\,R - \frac{h^2\,\lambda\,(\lambda - \mu)}{3\,\mu\,(\lambda + 2\mu)}} \qquad (4.4.2.2.23)$$

Since λ is, in the case of elastomeric materials, higher than μ , the argument of the first radical in (4.4.2.2.23) is always positive. Instead, the argument of the second radical may become negative. Consequently, expression (4.4.2.2.23) can be used as a starting point for a only when the argument of the second radical is positive, that is, when :

$$\delta \geq \frac{h^2 \lambda (\lambda - \mu)}{6 R \mu (\lambda + 2\mu)} \qquad (4.4.2.2.24)$$

As already mentioned, formula (4.4.2.2.23) presupposes that λ does not prevail too much with respect to μ. By bringing this assumption to the extremes (*e.g.*, $\lambda = 0$), it can be shown from (4.4.2.2.23) that the contact semiwidth, a , tends to the value $\sqrt{2\delta R}$, which is in fact typical of very compressible materials (see (4.4.2.2.3)). The same expression for a can be derived by admitting that the argument of *tanh* is small and, consequently, $tanh\ (x) \simeq x$. These two findings are not contradictory. In fact, the result $a = \sqrt{2\delta R}$ is accurate both when the elastomer is compressible or when the contact half width a is very small.

It was numerically found that, when condition (4.4.2.2.24) is satisfied, the starting point (4.4.2.2.23) is preferable to that referring to incompressible elastomers. Problems of double numerical solutions for a were never encountered. Once the contact half width, a, is known, constant A can be computed from equation (4.4.2.2.20) or, alternatively, from (4.4.2.2.21). From (4.4.2.2.20) it is obtained :

$$A = \frac{(\lambda + 2\mu)\left[a^2 - 2\,\delta\,R + \frac{2\,h^2\lambda\,(\lambda - \mu)}{3\,\mu\,(\lambda + 2\mu)}\right]}{2\,h\,R\ \cosh\left[\sqrt{\frac{3\,\mu\,(\lambda + 2\mu)}{\lambda\,(\lambda - \mu)}}\ \frac{a}{h}\right]} \qquad (4.4.2.2.25)$$

Alternatively, the following expression for A is derived from (4.4.2.2.21) :

$$A = \frac{(\lambda + 2\mu)\ a}{R\sqrt{\frac{3\,\mu\,(\lambda + 2\mu)}{\lambda\,(\lambda - \mu)}}\ \sinh\left[\sqrt{\frac{3\,\mu\,(\lambda + 2\mu)}{\lambda\,(\lambda - \mu)}}\ \frac{a}{h}\right]} \qquad (4.4.2.2.26)$$

When inserting the expression for A in equation (4.4.2.2.19), formula (4.4.2.2.25) is perhaps preferable, since it is defined in terms of *cosh* , a function already present in (4.4.2.2.19) . Upon introduction of (4.4.2.2.25), the final form of (4.4.2.2.19) is :

$$\frac{p(x)}{(\lambda+2\mu)} = \frac{\cosh\left[\sqrt{\frac{3\mu(\lambda+2\mu)}{\lambda\,(\lambda-\mu)}}\,\frac{x}{h}\right]}{\cosh\left[\sqrt{\frac{3\mu(\lambda+2\mu)}{\lambda\,(\lambda-\mu)}}\,\frac{a}{h}\right]}\left[\frac{a^2}{2\,hR} - \frac{\delta}{h} + \frac{\lambda\,(\lambda-\mu)\,h}{3\,\mu(\lambda+2\mu)R}\right] +$$

$$\frac{\delta}{h} - \frac{\lambda\,(\lambda-\mu)\,h}{3\,\mu\,(\lambda+2\mu)\,R} - \frac{x^2}{2\,R\,h} \qquad (4.4.2.2.27)$$

where constant a must be computed from (4.4.2.2.22) . The maximum contact pressure is obtained from (4.4.2.2.27) by putting $x = 0$. Extensive numerical results are deferred to Section 4.4.4 . For the time being, expressions (4.4.2.2.4) (Winkler solution), (4.4.2.2.11) (incompressible solution) are compared to (4.4.2.2.27) (complete second order solution) for various Poisson's ratios, in order to assess the concept of transitional Poisson's ratio of (4.4.2.2.14) . The following values were chosen : $E = 3.52$ MPa , $h = 3$ mm , $R = 4000$ mm , $\delta = 0.3$ mm . These figures are analogous to those adopted in the experimental study of Section 5. Figure 4.4.2.2.1 shows that the maximum normalized contact pressure according to a Winkler model approaches the second order complete solution (here assumed as the "exact" solution or, better, as a solution one order of magnitude more accurate that the Winkler and the incompressible approaches) for Poisson's ratios lower than 0.47 . The incompressible idealization holds true when $\nu \geq 0.4999$. This latest value is more perceivable from Fig. 4.4.2.2.2 , which displays an enlarged representation of the right part of Fig. 4.4.2.2.1 . There is a huge ν interval ($0.47 \leq \nu \leq 0.4999$) including most of the physical values of ν for elastomers (see Section 3), for which neither the Winkler modelling nor the incompressible idealization supply results sufficiently close to the second order complete solution. It can be concluded that the concept of transitional ν of (4.4.2.2.14) is not particularly useful from a practical viewpoint, since Fig. 4.4.2.2.1 shows the existence of a sizeable transitional ν interval. There is also a need to assess the complete second order solution by accounting for higher order perturbation terms, an aspect covered in Section 4.4.3 .

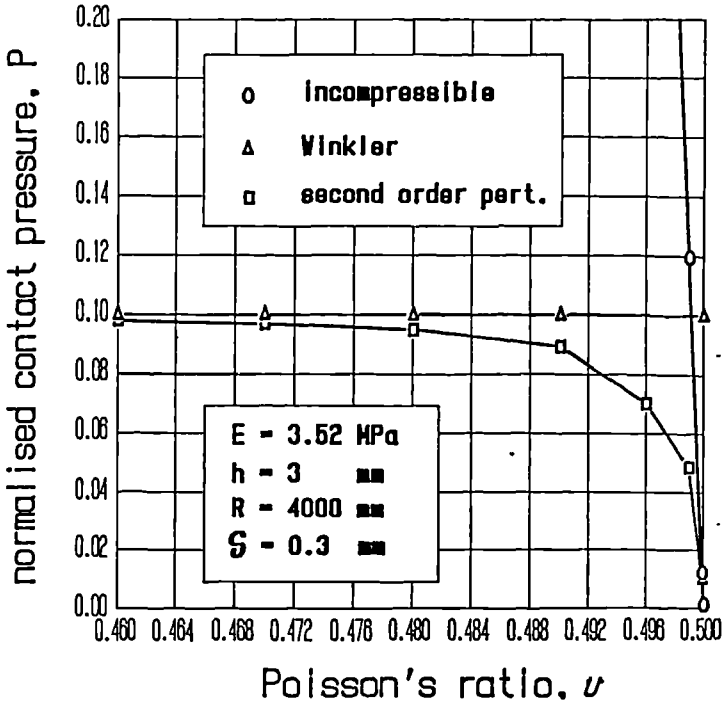

Fig. 4.4.2.2.1 : The incompressible, Winkler and second order models, as functions of ν.

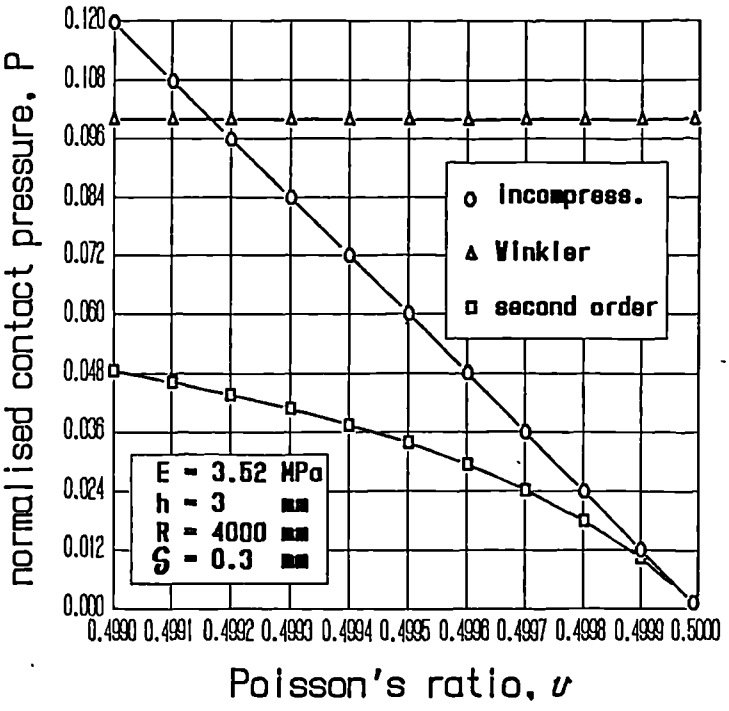

Fig. 4.4.2.2.2 : Enlarged view of Fig. 4.4.2.2.1 .

4.4.3 The new results

In this Section the approach due to Armstrong (1986) is extended to produce ϵ perturbed terms higher than the second order. Section 4.4.3.1 presents the analytical expressions of the coefficients of the differential equation correlating pressure profile and its derivatives to the layer deflection. In Section 4.4.3.2 these results are employed to evaluate the pressure profile when the layer is indented by a rigid cylinder.

4.4.3.1 The Perturbed Pressure-Deflection Solution

In this Section the perturbed solutions to equations (4.4.2.1.7) subject to the boundary conditions (4.4.2.1.8) are determined up to a high ϵ-order. First, equations (4.4.2.1.7) are rewritten up to a generic n order :

$$\epsilon^0 \left[\frac{\partial^2 U_0}{\partial Y^2} \right] + \epsilon^1 \left[\frac{\partial^2 U_1}{\partial Y^2} + \frac{\lambda + \mu}{\mu} \frac{\partial^2 V_0}{\partial X \, \partial Y} \right] +$$

$$\epsilon^2 \left[\frac{\partial^2 U_2}{\partial Y^2} + \frac{\lambda + \mu}{\mu} \frac{\partial^2 V_1}{\partial X \, \partial Y} + \frac{\lambda + 2\mu}{\mu} \frac{\partial^2 U_0}{\partial X^2} \right] +$$

$$\epsilon^3 \left[\frac{\partial^2 U_3}{\partial Y^2} + \frac{\lambda + \mu}{\mu} \frac{\partial^2 V_2}{\partial X \, \partial Y} + \frac{\lambda + 2\mu}{\mu} \frac{\partial^2 U_1}{\partial X^2} \right] + \quad \ldots$$

$$\epsilon^n \left[\frac{\partial^2 U_n}{\partial Y^2} + \frac{\lambda + \mu}{\mu} \frac{\partial^2 V_{n-1}}{\partial X \, \partial Y} + \frac{\lambda + 2\mu}{\mu} \frac{\partial^2 U_{n-2}}{\partial X^2} \right] + \quad \ldots = 0 \, ;$$

$$\epsilon^0 \left[\frac{\partial^2 V_0}{\partial Y^2} \right] + \epsilon^1 \left[\frac{\partial^2 V_1}{\partial Y^2} + \frac{\lambda + \mu}{\lambda + 2\mu} \frac{\partial^2 U_0}{\partial X \partial Y} \right] +$$

$$\epsilon^2 \left[\frac{\partial^2 V_2}{\partial Y^2} + \frac{\lambda + \mu}{\lambda + 2\mu} \frac{\partial^2 U_1}{\partial X \partial Y} + \frac{\mu}{\lambda + 2\mu} \frac{\partial^2 V_0}{\partial X^2} \right] +$$

$$\epsilon^3 \left[\frac{\partial^2 V_3}{\partial Y^2} + \frac{\lambda + \mu}{\lambda + 2\mu} \frac{\partial^2 U_2}{\partial X \partial Y} + \frac{\mu}{\lambda + 2\mu} \frac{\partial^2 V_1}{\partial X^2} \right] + \quad \ldots$$

$$\epsilon^n \left[\frac{\partial^2 V_n}{\partial Y^2} + \frac{\lambda + \mu}{\lambda + 2\mu} \frac{\partial^2 U_{n-1}}{\partial X \partial Y} + \frac{\mu}{\lambda + 2\mu} \frac{\partial^2 V_{n-2}}{\partial X^2} \right] + \ldots = 0$$

(4.4.3.1.1)

Equations (4.4.3.1.1) are subject to the following boundary conditions, which are here formulated for a generic order (see (4.4.2.1.8)) :

for $Y = 0$

$$\epsilon^0 \left[\frac{\partial V_0}{\partial Y} \right] + \epsilon^1 \left[\frac{\partial V_1}{\partial Y} + \frac{\lambda}{\lambda + 2\mu} \frac{\partial U_0}{\partial X} \right] + \epsilon^2 \left[\frac{\partial V_2}{\partial Y} + \frac{\lambda}{\lambda + 2\mu} \frac{\partial U_1}{\partial X} \right] +$$

$$\epsilon^3 \left[\frac{\partial V_3}{\partial Y} + \frac{\lambda}{\lambda + 2\mu} \frac{\partial U_2}{\partial X} \right] + \epsilon^n \left[\frac{\partial V_n}{\partial Y} + \frac{\lambda}{\lambda + 2\mu} \frac{\partial U_{n-1}}{\partial X} \right] + \ldots = - P(X) ;$$

$$\epsilon^0 \left[\frac{\partial U_0}{\partial Y} \right] + \epsilon^1 \left[\frac{\partial U_1}{\partial Y} + \frac{\partial V_0}{\partial X} \right] + \epsilon^2 \left[\frac{\partial U_2}{\partial Y} + \frac{\partial V_1}{\partial X} \right] +$$

$$\epsilon^3 \left[\frac{\partial U_3}{\partial Y} + \frac{\partial V_2}{\partial X} \right] + \epsilon^n \left[\frac{\partial U_n}{\partial Y} + \frac{\partial V_{n-1}}{\partial X} \right] + \ldots = 0$$

for $Y = 1$

$$\epsilon^0 U_0 + \epsilon^1 U_1 + \epsilon^2 U_2 + \epsilon^3 U_3 + \ldots = 0 \ ;$$

$$\epsilon^0 V_0 + \epsilon^1 V_1 + \epsilon^2 V_2 + \epsilon^3 V_3 + \ldots = 0 \qquad (4.4.3.1.2)$$

where, as already seen in (4.4.2.1.8), $P = p/(\lambda + 2\mu)$.

It has already been shown that $U_0 = U_2 = 0$ (see (4.4.2.1.12) and (4.4.2.1.24)). Similarly, it has been found that $V_1 = 0$ (see (4.4.2.1.18)). It is now demonstrated that $V_3 = 0$. Equation (4.4.3.1.1) requires that :

$$\frac{\partial^2 V_3}{\partial Y^2} = - \frac{\lambda + \mu}{\lambda + 2\mu} \frac{\partial^2 U_2}{\partial X \, \partial Y} - \frac{\mu}{\lambda + 2\mu} \frac{\partial^2 V_1}{\partial X^2} \qquad (4.4.3.1.3)$$

subject to the boundary conditions (see (4.4.3.1.2)) :

$$\text{for } Y = 0 \qquad \frac{\partial V_3}{\partial Y} = - \frac{\lambda}{\lambda + 2\mu} \frac{\partial U_2}{\partial X}$$

$$\text{for } Y = 1 \qquad V_3 = 0 \ . \qquad (4.4.3.1.4)$$

Since $U_2 = V_1 = 0$, equation (4.4.3.1.3) requires that the second derivative of V_3 with respect to Y vanishes. The boundary conditions (4.4.3.1.4) impose also that the first V_3 derivative with respect to Y vanishes for $Y = 0$, and that $V_3 = 0$ for $Y = 1$. It is concluded that $V_3 = 0$ is the solution to this problem. Proceeding similarly, it can be shown that $U_{2n} = 0$ and $V_{2n-1} = 0$ for a generic perturbation order n . Consequently, only terms U_{2n-1} and V_{2n} are examined. The corresponding computations are straightforward, but particularly lengthy and tedious. In the following, it is shown that such expressions lend themselves to be

computed with the aid of an algebraic manipulator. The expressions for U and V up to the second order are already known. To compute U_3 , expression (4.4.3.1.1) is resorted to :

$$\frac{\partial^2 U_3}{\partial Y^2} = - \frac{\lambda + \mu}{\mu} \frac{\partial^2 V_2}{\partial X \, \partial Y} - \frac{\lambda + 2\mu}{\mu} \frac{\partial^2 U_1}{\partial X^2} \qquad (4.4.3.1.5)$$

By introducing in (4.4.3.1.5) the formulae for V_2 and U_1 , the second derivative of U_3 with respect to Y is expressed in terms of a known function, say $F(X,Y)$:

$$\frac{\partial^2 U_3}{\partial Y^2} = F(X,Y) \qquad (4.4.3.1.6)$$

An algebraic manipulator can easily integrate twice $F(X,Y)$, to supply the expression for U_3 . Anyway, this integral is a particular integral since the results retrieved via an algebraic manipulator do not include the integration constants necessary to impose the boundary conditions (Harper (1989)). It is convenient to add to the particular integral, PI , the proper integration constants C_1 and C_2 to obtain the indefinite integral :

$$U_3(X,Y) = PI(X,Y) + C_1(X)\, Y + C_2(X) \qquad (4.4.3.1.7)$$

The two integration constants can be evaluated from the following boundary conditions :

$$\text{for } Y = 0 \quad \frac{\partial U_3}{\partial Y} = - \frac{\partial V_2}{\partial X} \rightarrow C_1(X) = - \frac{\partial V_2(X,0)}{\partial X} - \frac{\partial\, PI(X,Y)}{\partial Y}\Big|_{Y=0} \qquad (4.4.3.1.8)$$

$$\text{for } Y = 1 \quad U_3 = 0 \rightarrow C_2(X) = - C_1(X) - PI(X,1)$$

The way in which an algebraic manipulator can be exploited is now summarized. First, $PI(X,Y)$ is computed by integrating twice $F(X,Y)$ according to (4.4.3.1.6) . Then, $C_1(X,Y)$ and $C_2(X,Y)$ are calculated from (4.4.3.1.8). Knowing

already PI , C_1 and C_2 , the final formula for U_3 is derived from (4.4.3.1.7) . It has already been observed that $V_3 = 0$.

The evaluation of V_4 is now treated. From (4.4.3.1.1) it follows :

$$\frac{\partial^2 V_4}{\partial Y^2} = - \frac{\lambda + \mu}{\mu} \frac{\partial^2 U_3}{\partial X \, \partial Y} - \frac{\lambda + 2\mu}{\mu} \frac{\partial^2 V_2}{\partial X^2} \qquad (4.4.3.1.9)$$

Terms U_3 and V_2 have already been computed. So, the second derivative of V_4 with respect to Y is a known function. This expression is integrated twice, to obtain a particular integral, $PI\ (X,Y)$, which becomes general by adding $C_1\ (X)\ Y + C_2$:

$$V_4\ (X,Y) = PI\ (X,Y) + C_1\ (X)\ Y + C_2 \qquad (4.4.3.1.10)$$

Constants C_1 and C_2 are computed from the boundary conditions :

for $Y = 0$ $\qquad \frac{\partial V_4}{\partial Y} = - \frac{\lambda}{\lambda + 2\mu} \frac{\partial U_3}{\partial X} \quad \rightarrow$

$$C_1\ (X) = - \frac{\lambda}{\lambda + 2\mu} \frac{\partial U_3(X,0)}{\partial X} - \frac{\partial\ PI(X,Y)}{\partial Y} \Big|_{Y=0}$$

for $Y = 1$ $\qquad U_3 = 0 \quad \rightarrow \quad C_2\ (X) = - C_1\ (X) - PI\ (X,1) \qquad (4.4.3.1.11)$

Having computed $PI\ (X,Y)$, $C_1\ (X)$ and $C_2\ (X)$, the final expression for V_4 is obtained from (4.4.3.1.10) . It has already been shown that $U_4 = 0$.

It is now clear that such computations can be extended to any ϵ perturbation order . In particular, the expressions for U_3 and V_4 are reported — computed via the algebraic manipulator *REDUCE* (1987) — in normalized form :

$$U_3 = \frac{d^3 P}{d X^3}\left[-\frac{\lambda + \mu}{12\,\mu} Y^4 + \frac{3\lambda + 4\mu}{6\,(\lambda + 2\mu)} Y^3 + \frac{(\lambda - \mu)\,(3\lambda + 4\mu)}{4\,\mu\,(\lambda + 2\mu)} Y^2 + \right.$$

$$\left. \frac{\lambda\,(\lambda - \mu)}{3\mu\,(\lambda + 2\mu)} Y - \frac{6\lambda^2 + \lambda\mu - 3\mu^2}{6\,\mu\,(\lambda + 2\mu)} \right] \qquad (4.4.3.1.12)$$

$$V_4 = \frac{d^4 P}{d X^4}\left[\frac{2\lambda + \mu}{120\,\mu} Y^5 - \frac{3\lambda + 2\mu}{24\,(\lambda + 2\mu)} Y^4 - \frac{(\lambda - \mu)\,(3\lambda + 2\mu)}{12\,\mu\,(\lambda + 2\mu)} Y^3 - \right.$$

$$\left. \frac{\lambda^2\,(\lambda - \mu)}{6\mu(\lambda + 2\mu)^2} Y^2 + \frac{\lambda(6\lambda^2 + \lambda\mu - 3\mu^2)}{6\mu\,(\lambda + 2\mu)^2} Y + \frac{-9\lambda^3 + 2\lambda^2\mu + 6\lambda\mu^2 - 3\mu^3}{15\,\mu\,(\lambda + 2\mu)^2} \right]$$

(4.4.3.1.13)

The expressions of V_6 , V_8 , V_{10} are also reported, with reference to the condition $Y = 0$, since in practical circumstances only the deflection the layer upper surface is usually requested :

$$V_6 |_{Y=0} = -\frac{(\lambda + 3\mu)\,(345\,\lambda^3 + 313\,\lambda^2\mu - 123\,\lambda\mu^2 - 103\,\mu^3)}{315\,\mu\,(\lambda + 2\mu)^3}$$

$$V_8 |_{Y=0} = -\frac{(\lambda + 3\mu)\,(2219\,\lambda^4 + 9766\,\lambda^3\mu + 6537\,\lambda^2\mu^2 - 3341\,\lambda\mu^3 - 2491\,\mu^4)}{2835\,\mu\,(\lambda + 2\mu)^4}$$

$$V_{10} |_{Y=0} = -\frac{(\lambda + 3\mu)}{155925\,\mu\,(\lambda + 2\mu)^5}$$

$$(71040\,\lambda^5 + 593701\,\lambda^4\mu + 1424393\,\lambda^3\mu^2 + 703764\,\lambda^2\mu^3 - 494653\,\lambda\mu^4 - 310829\,\mu^5)$$

(4.4.3.1.14)

Indications about the behaviour of these high order perturbation terms are now sought for by referring, in the interest of greater simplicity, only to the incompressibility condition $\lambda = \infty$ (that is, $\nu = 0.5$) . It is noted that P expressed in terms of p exhibits λ at the denominator (see (4.4.2.1.8)). If one refers to p (instead of P) derivatives and to $Y = 0$, the limits for $\lambda \to \infty$ of the coefficients multiplying the p derivative in the expressions of V_n are finite. Such coefficients are :

$$\frac{V_0\,\mu}{\lambda}\Big|_{Y=0\,,\,\lambda\to\infty} = 0$$

$$\frac{V_2\,\mu}{\lambda}\Big|_{Y=0\,,\,\lambda\to\infty} = -\frac{1}{3} \simeq -0.333$$

$$\frac{V_4\,\mu}{\lambda}\Big|_{Y=0\,,\,\lambda\to\infty} = -\frac{9}{15} \simeq -0.600$$

$$\frac{V_6\,\mu}{\lambda}\Big|_{Y=0\,,\,\lambda\to\infty} = -\frac{345}{315} \simeq -1.095$$

$$\frac{V_8\,\mu}{\lambda}\Big|_{Y=0\,,\,\lambda\to\infty} = -\frac{2219}{2835} \simeq -0.782$$

$$\frac{V_{10}\,\mu}{\lambda}\Big|_{Y=0\,,\,\lambda\to\infty} = -\frac{71040}{155925} \simeq -0.455 \qquad (4.4.3.1.15)$$

These expressions show that V_n does not diverge as n is increased. Since the total V is the sum of V_n each multiplied by ϵ^n (which rapidly decreases with n), the high order coefficients of the differential equation in p originated by the perturbation approach become vanishingly small. So, a perturbation problem is faced which is represented by a n-order differential equation in which the maximum order derivative of the unknown function is multiplied by the smallest coefficient. In other words, the perturbation approach leads to a "singular perturbation problem" (Smith (1985), Nayfeh (1973)) , which is inevitably difficult to treat, since the maximum order of the derivative of the differential equation, which characterizes the problem mathematically, becomes insignificant. The obstacles connected to the boundary conditions are examined in the following Section.

4.4.3.2 The pressure profile for a cylindrical indenter

The case in which the terms up to the fourth perturbed order are considered is treated first. The aim is to find the (normalized) pressure distribution when the layer is pressed by a cylindrical indenter. From (4.4.2.1.9), (4.4.2.1.12), (4.4.2.1.24) and (4.4.3.1.13) the link is obtained between normalized deflection of the upper surface of the layer and dimensionless pressure distribution together with its derivatives up to the fourth order, which is equalled to the displacement imposed by the cylindrical indenter according to a parabolic, second degree approximation (Jaffar and Savage (1988)) :

$$V_0 + \epsilon V_1 + \epsilon^2 V_2 + \epsilon^4 V_4 \mid_{Y=0} = \frac{\delta}{h} - \frac{x^2}{2 h R} \rightarrow$$

$$p - \frac{\lambda - \mu}{\lambda + 2\mu} \frac{\lambda}{3\mu} \frac{h^2}{a^2} \frac{d^2 P}{dX^2} + \frac{-9\lambda^3 + 2\lambda^2\mu + 6\lambda\mu^2 - 3\mu^3}{15\mu(\lambda + 2\mu)^2} \frac{h^4}{a^4} \frac{d^4 P}{dX^4} = \frac{\delta}{h} - \frac{X^2 a^2}{2 h R} \qquad (4.4.3.2.1)$$

The homogeneous solution requires the treatment of the following characteristic equation in ω :

$$\frac{-9\lambda^3 + 2\lambda^2\mu + 6\lambda\mu^2 - 3\mu^3}{15\mu(\lambda + 2\mu)^2} \frac{h^4}{a^4} \omega^4 - \frac{\lambda - \mu}{\lambda + 2\mu} \frac{\lambda}{3\mu} \frac{h^2}{a^2} \omega^2 + 1 = 0 \qquad (4.4.3.2.2)$$

By putting $\omega^2 \frac{h^2}{a^2} = \alpha$, it follows :

$$\frac{-9\lambda^3 + 2\lambda^2\mu + 6\lambda\mu^2 - 3\mu^3}{15\mu(\lambda + 2\mu)^2} \alpha^2 - \frac{\lambda - \mu}{\lambda + 2\mu} \frac{\lambda}{3\mu} \alpha + 1 = 0 \qquad (4.4.3.2.3)$$

and its roots are :

$$\alpha_1 = \frac{5\,(\lambda + 2\mu)}{2\,(-9\lambda^3 + 2\lambda^2\mu + 6\lambda\mu^2 - 3\mu^3)}$$

$$\left[\lambda(\lambda-\mu) - \sqrt{\lambda^2(\lambda-\mu)^2 - \frac{12\mu}{5}(-9\lambda^3 + 2\lambda^2\mu + 6\lambda\mu^2 - 3\mu^3)}\right];$$

$$\alpha_2 = \frac{5\,(\lambda + 2\mu)}{2\,(-9\lambda^3 + 2\lambda^2\mu + 6\lambda\mu^2 - 3\mu^3)}$$

$$\left[\lambda(\lambda-\mu) + \sqrt{\lambda^2(\lambda-\mu)^2 - \frac{12\mu}{5}(-9\lambda^3 + 2\lambda^2\mu + 6\lambda\mu^2 - 3\mu^3)}\right]$$

(4.4.3.2.4)

Roots (4.4.3.2.4) depend only on Poisson's ratio, ν, and not on Young's modulus, E . Fig. 4.4.3.2.1 presents roots (4.4.3.2.4) as Poisson's ratio varies from 0 to 0.5 . It emerges that root α_1 is always positive and root α_2 is negative. In particular, for $\nu \to 0.5$, that is, $\lambda \to \infty$, the positive root vanishes behaving as $3\mu(\lambda + 2\mu)/(\lambda(\lambda - \mu))$, whereas the negative root approaches $-5/9$. Consequently, the four roots ω of (4.4.3.2.2) are two real and two purely complex conjugate ones for finite λ values . They are :

$$\omega_1 = +\frac{a}{h}\sqrt{\alpha_1} \;;\; \omega_2 = -\frac{a}{h}\sqrt{\alpha_1} \;;\; \omega_3 = +i\frac{a}{h}\sqrt{-\alpha_2} \;;\; \omega_4 = -i\frac{a}{h}\sqrt{-\alpha_2}$$

(4.4.3.2.5)

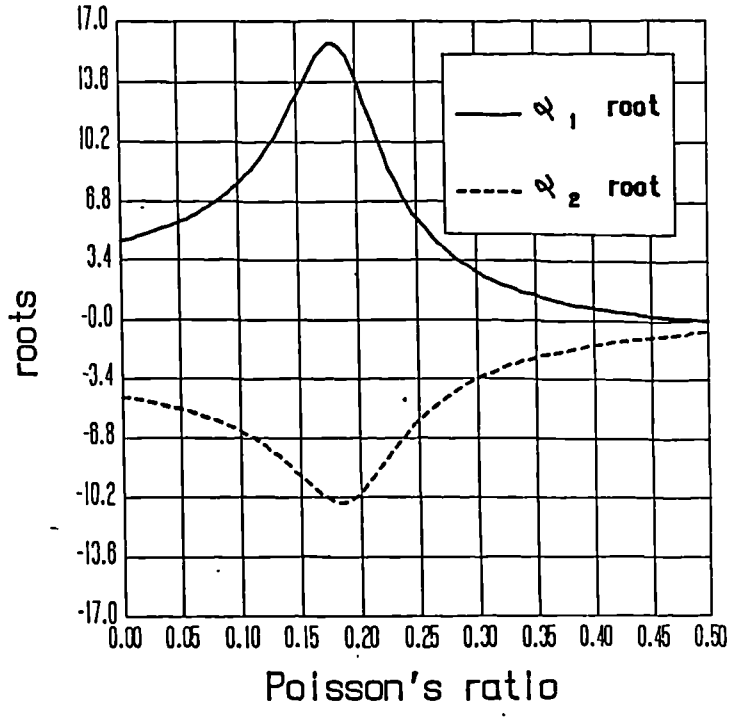

Fig. 4.4.3.2.1 : The roots of the second degree equation (4.4.3.2.3), as functions of ν .

The homogeneous solution of (4.4.3.2.1) is :

$$P(X) = A\cosh\left(\sqrt{\alpha_1}\,\frac{a}{h}\,X\right) + B\sinh\left(\sqrt{\alpha_1}\,\frac{a}{h}\,X\right) + C\cos\left(\sqrt{-\alpha_2}\,\frac{a}{h}\,X\right) + D\sin\left(\sqrt{-\alpha_2}\,\frac{a}{h}\,X\right)$$

(4.4.3.2.6)

As already observed (see comments on (4.4.2.2.17)), the homogeneous solution must be symmetrical with respect to X , as is the indenter profile. Consequently, constants B and D in (4.4.3.2.6) vanish. A particular solution to (4.4.3.2.6) is :

$$P(X) = \frac{\delta}{h} - \frac{\lambda\,(\lambda - \mu)\,h}{3\mu\,(\lambda + 2\mu)\,R} - \frac{a^2\,X^2}{2\,Rh} \qquad (4.4.3.2.7)$$

The complete solution to (4.4.3.2.1) is therefore :

$$P(X) = A\cosh\left(\sqrt{\alpha_1}\,\frac{a}{h}\,X\right) + B\cos\left(\sqrt{-\alpha_2}\,\frac{a}{h}\,X\right) + \frac{\delta}{h} - \frac{\lambda\,(\lambda-\mu)\,h}{3\mu\,(\lambda+2\mu)\,R} - \frac{a^2\,X^2}{2\,Rh}$$

(4.4.3.2.8)

The unknowns in (4.4.3.2.8) are A, B and a. As already observed (see comments to (4.4.2.2.19)), constant a (which represents the contact half width) does not directly appear in (4.4.3.2.8), but it affects the imposition of the three boundary conditions. The vanishing of P and of its first derivative by the contact extremities has already been imposed in the second order perturbed solution (see (4.4.2.20,21)), and these two boundary conditions are again adopted in the following. Concerning the third boundary condition, two different impositions are proposed. The first approach is treated hereinafter, whereas the second description is deferred to eqn (4.4.3.2.16).

First, the just mentioned boundary conditions are extended to admit that the pressure profile must smoothly vanish at the contact ends, by imposing that the second pressure derivative vanishes as well. In fact, the pressure profile obtained from the perturbation method is the solution of a fourth order differential equation in P and, therefore, a high degree of smoothness of the solution is required. This observation justifies the boundary conditions employed here. Despite these encouraging comments, the conditions on the pressure derivatives by the contact extremities are inevitably doubtful. The corresponding equations are :

$$A\cosh\left(\sqrt{\alpha_1}\,\frac{a}{h}\right) + B\cos\left(\sqrt{-\alpha_2}\,\frac{a}{h}\right) + \frac{\delta}{h} - \frac{\lambda\,(\lambda-\mu)\,h}{3\mu(\lambda+2\mu)R} - \frac{a^2}{2\,Rh} = 0$$

$$A\,\sqrt{\alpha_1}\,\sinh\left(\sqrt{\alpha_1}\,\frac{a}{h}\right) - B\,\sqrt{-\alpha_2}\,\sin\left(\sqrt{-\alpha_2}\,\frac{a}{h}\right) - \frac{a}{R} = 0$$

$$A\,\alpha_1\cosh\left(\sqrt{\alpha_1}\,\frac{a}{h}\right) + B\,\alpha_2\cos\left(\sqrt{-\alpha_2}\,\frac{a}{h}\right) - \frac{h}{R} = 0$$

(4.4.3.2.9)

To determine constant A as a function of a , one multiplies the first equation of (4.4.3.2.9) by α_2 and subtracts from it the third equation :

$$A = \frac{\frac{h}{R} + \alpha_2 \left(\frac{\delta}{h} - \frac{a^2}{2\,Rh} - \frac{\lambda\,(\lambda - \mu)\,h}{3\mu\,(\lambda + 2\mu)\,R} \right)}{(\alpha_1 - \alpha_2)\,\cosh\left(\sqrt{\alpha_1}\,\frac{a}{h} \right)} \qquad (4.4.3.2.10)$$

Similarly, to compute constant B as a function of a , one multiplies the first equation of (4.4.3.2.9) by α_1 and subtract from it the third equation :

$$B = \frac{\frac{h}{R} + \alpha_1 \left(\frac{\delta}{h} - \frac{a^2}{2\,Rh} - \frac{\lambda\,(\lambda - \mu)\,h}{3\mu\,(\lambda + 2\mu)\,R} \right)}{(\alpha_2 - \alpha_1)\,\cos\left(\sqrt{-\alpha_2}\,\frac{a}{h} \right)} \qquad (4.4.3.2.11)$$

Finally, to evaluate the contact half width, a , expressions (4.4.3.2.10,11) are introduced into the second equation (4.4.3.2.9) to obtain a single equation in a :

$$\sqrt{\alpha_1}\,\tanh\left(\sqrt{\alpha_1}\,\frac{a}{h} \right) \left\{ \frac{h}{R} + \alpha_2 \left(\frac{\delta}{h} - \frac{a^2}{2\,Rh} - \frac{\lambda\,(\lambda - \mu)\,h}{3\mu\,(\lambda + 2\mu)\,R} \right) \right\} +$$

$$\sqrt{-\alpha_2}\,\tan\left(\sqrt{-\alpha_2}\,\frac{a}{h} \right) \left\{ \frac{h}{R} + \alpha_1 \left(\frac{\delta}{h} - \frac{a^2}{2\,Rh} - \frac{\lambda\,(\lambda - \mu)\,h}{3\mu\,(\lambda + 2\mu)\,R} \right) \right\} = \frac{a\,(\alpha_1 - \alpha_2)}{R}$$

(4.4.3.2.12)

Equation (4.4.3.2.12) is not suitable from a numerical viewpoint, since function *tan* assumes high values due to the greatness of a/h ($\alpha_2 \simeq -5\,a^2 / (9\,h^2)$, see comments to (4.4.3.2.4)). It is, therefore, convenient to multiply both members of (4.4.3.2.12) by $\cos\left(\sqrt{-\alpha_2}\; a/h \right)$. Once a has been evaluated from (4.4.3.2.12), constants A and B are computed via (4.4.3.2.10) and (4.4.3.2.11), respectively. A

starting point for a can be obtained by assuming in (4.4.3.2.12) that $tanh \rightarrow 1$ (see comments to (4.4.2.2.22)) and that, since a/h is great, $tan \rightarrow \infty$. As a consequence, coefficient multiplying function tan in (4.4.2.2.22) must vanish :

$$\frac{h}{R} + \alpha_1 \left(\frac{\delta}{h} - \frac{a^2}{2\,Rh} - \frac{\lambda\,(\lambda - \mu)\,h}{3\mu\,(\lambda + 2\mu)\,R} \right) = 0 \qquad (4.4.3.2.13)$$

from which an estimate for a is derived :

$$a \simeq \sqrt{2} \sqrt{\frac{h^2}{\alpha_1} + R\delta - \frac{\lambda\,(\lambda - \mu)\,h^2}{3\mu\,(\lambda + 2\mu)}} \qquad (4.4.3.2.14)$$

Similar to (4.4.2.2.24), equation (4.4.23.2.14) is applicable provided that the radical is positive, that is :

$$\delta \geq \frac{\lambda\,(\lambda - \mu)\,h^2}{3\mu\,(\lambda + 2\mu)\,R} - \frac{h^2}{\alpha_1 R} \qquad (4.4.3.2.15)$$

An alternative starting point is that referring to the perfectly incompressible elastomer (see (4.4.2.2.8)).

A FORTRAN code was developed following the above theory, and results were obtained concerning the contact pressure profile. It was found that the solution of (4.4.3.2.12) is not unique. This problem can be circumvented by adopting for the contact length the value closer to the figure obtained from the second order complete solution of (4.4.2.2.27) . Moreover, the presence of the *cos* function in (4.4.3.2.8) produces unphysical undulations in the contact pressure profile. Numerical results showing such oscillations are deferred to the treatment of the alternative boundary condition, see (4.4.3.2.16).

Expression (4.4.3.2.8) is now reconsidered, but now constant B is set equal to 0 , to remove the non physical pressure undulations. So doing, the general solution becomes (in fact, it is no longer strictly general) :

$$P(X) = A \cosh\left(\sqrt{\alpha_1}\,\frac{a}{h}\,X\right) + \frac{\delta}{h} - \frac{\lambda(\lambda-\mu)\,h}{3\mu(\lambda+2\mu)\,R} - \frac{a^2\,X^2}{2\,Rh} \qquad (4.4.3.2.16)$$

Constants A and a are found by expressing the conditions that both pressure and pressure derivative vanish by the contact extremities :

$$P(1) = A \cosh\left(\sqrt{\alpha_1}\,\frac{a}{h}\right) + \frac{\delta}{h} - \frac{\lambda(\lambda-\mu)\,h}{3\mu(\lambda+2\mu)\,R} - \frac{a^2}{2\,Rh} = 0$$

$$\frac{\partial P(X)}{\partial X}\Big|_{X=1} = A\sqrt{\alpha_1}\sinh\left(\sqrt{\alpha_1}\,\frac{a}{h}\right) - \frac{a}{R} = 0 \qquad (4.4.3.2.17)$$

To evaluate constant A as a function of a , the first equation in (4.4.3.2.17) is employed. This equation is preferable to the second one, since it involves function $\cosh$, which is already present in (4.4.3.2.16) . Thus :

$$A = \frac{\dfrac{a^2}{2\,Rh} - \dfrac{\delta}{h} + \dfrac{\lambda(\lambda-\mu)\,h}{3\mu(\lambda+2\mu)\,R}}{\cosh\left(\sqrt{\alpha_1}\,\dfrac{a}{h}\right)} \qquad (4.4.3.2.18)$$

By introducing expression (4.4.3.2.18) for A in the second equation of (4.4.3.2.17), a single equation in the contact half width, a , is obtained :

$$\left[\frac{a}{h} + \frac{2\,h\,\lambda(\lambda-\mu)}{3\,a\,\mu(\lambda+2\mu)} - \frac{2\delta\,R}{a\,h}\right]\sqrt{\alpha_1}\tanh\left(\sqrt{\alpha_1}\,\frac{a}{h}\right) - 2 = 0 \qquad (4.4.3.2.19)$$

This equation can be compared with formula (4.4.2.2.22) expressing the contact half width for the complete second order solution. It appears that the two formulae are very similar, apart from the presence of α_1 in (44.3.2.19) and of $3\mu\ (\lambda + 2\mu)/(\lambda(\lambda - \mu))$ in (4.4.2.2.22) . It has already been commented with respect to expressions (4.4.3.2.4) that root α_1 does in fact approach $3\mu\ (\lambda + 2\mu)/(\lambda(\lambda - \mu))$ as $\lambda \rightarrow \infty$. Consequently, the contact width referring to the complete second order solution is very similar to that describing the fourth order solution without oscillatory functions in its general solution. The numerical solution to (4.4.3.2.19) was obtained via a Newton method, by assuming as starting point the contact half width referring to the complete second order solution (4.4.2.2.22) .

By introducing (4.4.3.2.18) into (4.4.3.2.16), it follows :

$$P(X) = \frac{\cosh\left(\sqrt{\alpha_1}\,\frac{a}{h}\,X\right)}{\cosh\left(\sqrt{\alpha_1}\,\frac{a}{h}\right)}\left[\frac{a^2}{2\,Rh} - \frac{\delta}{h} + \frac{\lambda\,(\lambda-\mu)\,h}{3\mu\,(\lambda+2\mu)\,R}\right] +$$

$$\frac{\delta}{h} - \frac{\lambda\,(\lambda-\mu)\,h}{3\mu\,(\lambda+2\mu)\,R} - \frac{a^2\,X^2}{2\,Rh} \qquad (4.4.3.2.20)$$

Expression (4.4.3.2.20) is very similar to formula (4.4.2.2.27) referring to the complete second order solution, due to the already commented similarity between root α_1 of (4.4.3.2.4) and factor $3\mu.(\lambda + 2\mu)/(\lambda(\lambda - \mu))$ as $\lambda \rightarrow \infty$. Fig. 4.4.3.2.2 presents some numerical results comparing the incompressible modelling and the complete second order solution (4.4.2.2.27) to the two expressions (4.4.3.2.8) and (4.4.3.2.20) of the fourth order solution, referring to different boundary conditions.

The numerical forecasts are presented for $\nu = 0.4997$ (a figure close to the experimental readings of Section 3, and for which the incompressible and Winkler solutions are both inaccurate, see Figs 4.4.2.2.1,2) . The same values as in Figs 4.4.2.2.1,2 were adopted for the following additional variables : $E = 3.52$ MPa , $h = 3$ mm , $R = 4000$ mm , $\delta = 0.3$ mm . It emerges that, while the incompressible forecasts are inaccurate, the previsions retrieved from the complete second order

solution are hardly distinguishable from those referring to the fourth order solution. Figure 4.4.3.2.2 also displays the predictions achieved with sixth, eighth and tenth order models. They do not appear to improve appreciably the precision of the solution. In the interest of completeness, the corresponding theory is briefly treated hereinafter.

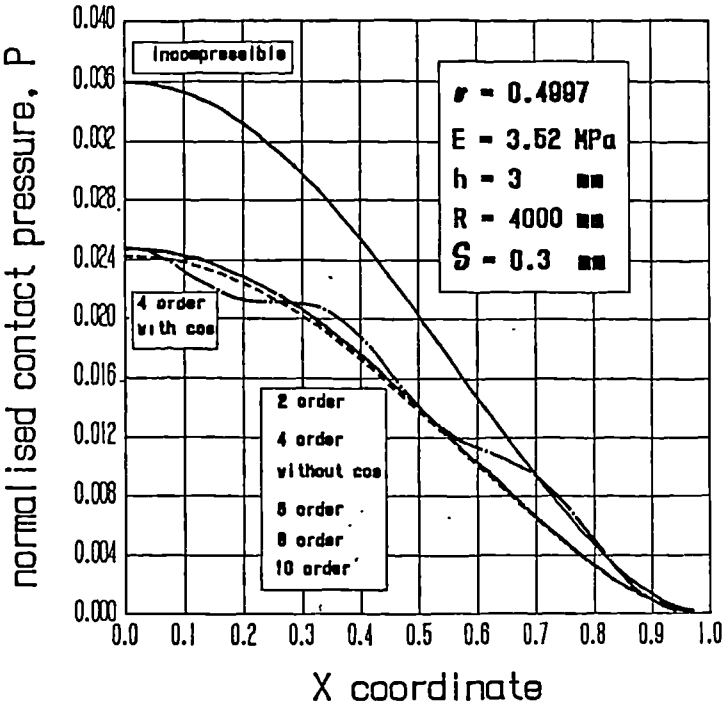

Fig. 4.4.3.2.2 : The incompressible, second, fourth, sixth, eighth, tenth order solutions.

When the perturbation terms up to ϵ^6 are considered, the corresponding differential equation in normalized pressure, P, becomes :

$$V_0 + \epsilon V_1 + \epsilon^2 V_2 + \epsilon^4 V_4 + \epsilon^6 V_6 \mid_{Y=0} = \frac{\delta}{h} - \frac{x^2}{2hR} \rightarrow$$

$$P - \frac{\lambda - \mu}{\lambda + 2\mu} \frac{\lambda}{3\mu} \frac{h^2}{a^2} \frac{d^2P}{dX^2} + \frac{-9\lambda^3 + 2\lambda^2\mu + 6\lambda\mu^2 - 3\mu^3}{15\mu(\lambda + 2\mu)^2} \frac{h^4}{a^4} \frac{d^4P}{dX^4} -$$

$$\frac{(\lambda + 3\mu)\,(345\,\lambda^3 + 313\,\lambda^2\mu - 123\,\lambda\mu^2 - 103\,\mu^3)}{315\,\mu\,(\lambda + 2\mu)^3}\,\frac{h^6}{a^6}\,\frac{d^6P}{dX^6} = \frac{\delta}{h} - \frac{X^2\,a^2}{2\,h\,R}$$

(4.4.3.2.21)

The homogeneous solution requires the treatment of the following characteristic equation in ω :

$$-\frac{(\lambda + 3\mu)\,(345\,\lambda^3 + 313\,\lambda^2\mu - 123\,\lambda\mu^2 - 103\,\mu^3)}{315\,\mu\,(\lambda + 2\mu)^3}\,\frac{h^6}{a^6}\,\omega^6 +$$

$$\frac{-9\lambda^3 + 2\,\lambda^2\mu + 6\,\lambda\mu^2 - 3\mu^3}{15\,\mu\,(\lambda + 2\mu)^2}\,\frac{h^4}{a^4}\,\omega^4 - \frac{\lambda - \mu}{\lambda + 2\mu}\,\frac{\lambda}{3\mu}\,\frac{h^2}{a^2}\,\omega^2 + 1 = 0$$

(4.4.3.2.22)

By putting $\omega^2\,\frac{h^2}{a^2} = \alpha$ (see (4.4.3.2.2,3)), it follows :

$$-\frac{(\lambda + 3\mu)\,(345\,\lambda^3 + 313\,\lambda^2\mu - 123\,\lambda\mu^2 - 103\,\mu^3)}{315\,\mu\,(\lambda + 2\mu)^3}\,\alpha^3 +$$

$$\frac{-9\lambda^3 + 2\,\lambda^2\mu + 6\,\lambda\mu^2 - 3\mu^3}{15\,\mu\,(\lambda + 2\mu)^2}\,\alpha^2 - \frac{\lambda - \mu}{\lambda + 2\mu}\,\frac{\lambda}{3\mu}\,\alpha + 1 = 0$$

(4.4.3.2.23)

The roots of the third degree algebraic equation in α (4.4.3.2.23) can be computed by evaluating parameters Q and R (Spiegel (1974)) :

$$Q = \frac{35\,\lambda\,(\lambda - \mu)\,(\lambda + 2\mu)^2}{(\lambda + 3\mu)\,(345\,\lambda^3 + 313\,\lambda^2\mu - 123\,\lambda\mu^2 - 103\,\mu^3)} -$$

$$\frac{49\,(\lambda + 2\mu)^2\,(-9\lambda^3 + 2\lambda^2\mu + 6\lambda\mu^2 - 3\mu^3)^2}{(\lambda + 3\mu)^2\,(345\lambda^3 + 313\lambda^2\mu - 123\lambda\mu^2 - 103\mu^3)^2}$$

$$R = -\frac{735\lambda(\lambda - \mu)(\lambda + 2\mu)^3(-9\lambda^3 + 2\lambda^2\mu + 6\lambda\mu^2 - 3\mu^3)}{2(\lambda + 3\mu)^2(345\lambda^3 + 313\lambda^2\mu - 123\lambda\mu^2 - 103\mu^3)^2} +$$

$$\frac{315\mu(\lambda + 2\mu)^3}{2(\lambda + 3\mu)(345\lambda^3 + 313\lambda^2\mu - 123\lambda\mu^2 - 103\mu^3)} +$$

$$\frac{343\,(\lambda + 2\mu)^3(-9\lambda^3 + 2\lambda^2\mu + 6\lambda\mu^2 - 3\mu^3)^3}{(\lambda + 3\mu)^3(345\lambda^3 + 313\lambda^2\mu - 123\lambda\mu^2 - 103\mu^3)^3}$$

(4.4.3.2.24)

The discriminant D is :

$$D = Q^3 + R^2 \qquad (4.4.3.2.25)$$

The roots of (4.4.3.2.23) and discriminant D depend only on Poisson's ratio, ν, and not on Young's modulus, E . Figure 4.4.3.2.3 presents discriminant D when the Poisson's ratio ranges from 0 to the incompressibility value 0.5 . It appears that discriminant D is always positive and, therefore, there is always a single real α solution to the cubic equation (4.4.3.2.23) , displayed in Fig. 4.4.3.2.3 . This solution is negative for $\nu \leq 0.18$, which implies that no real solution ω exists for the original sixth degree algebraic equation (4.4.3.2.22) in this ν range. Conversely, for $0.18 \leq \nu < 0.5$ — the field in which elastomeric materials (porous elastomers being excluded) fall — the α solution to the third degree equation (4.4.3.2.23) is positive and, consequently, one real solution ω exists to the sixth degree equation (4.4.3.2.22) for these ν values. When $\nu = 0.5$, $\lambda = \infty$ and the real root $\alpha = 0$. The behaviour of the solution for $\nu \simeq 0.18$ has been examined only numerically. It

appears that the real root rapidly changes its sign, but no singularity could be spotted via numerical tests. Anyway, this $\nu \simeq 0.18$ value is not relevant in practical applications of elastomeric (non porous) layers. Similar to (4.4.3.2.16), the form of the solution is :

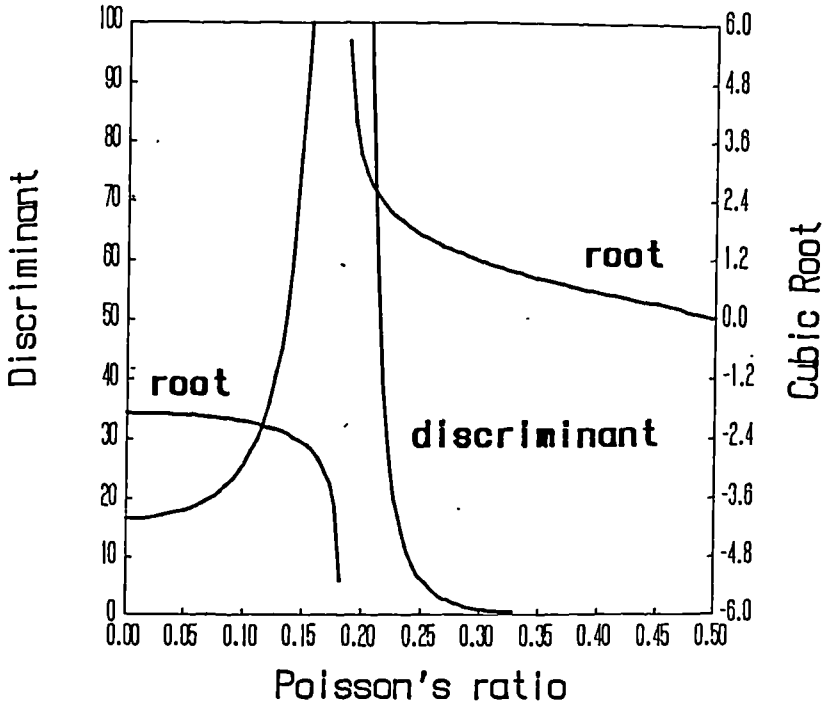

Fig. 4.4.3.2.3 : The roots and the discriminant of equation (4.4.3.2.23).

$$P(X) = A \cosh\left(\sqrt{\alpha}\,\frac{a}{h}\,X\right) + \frac{\delta}{h} - \frac{\lambda(\lambda-\mu)h}{3\mu(\lambda+2\mu)R} - \frac{a^2X^2}{2Rh} \qquad (4.4.3.2.26)$$

where α is the solution to (4.4.3.2.23) . The integration constants A and a are found similar to (4.4.3.2.17,18) . So, a formula for P analogous to (4.4.3.2.20) holds for this case too, provided that root α_1 of (4.4.3.2.20) is here interpreted as root α of (4.4.3.2.23) .

Moving to the eighth order solution, the paths followed are much the same.

The ϵ^8 differential equation becomes :

$$V_0 + \epsilon V_1 + \epsilon^2 V_2 + \epsilon^4 V_4 + \epsilon^6 V_6 + \epsilon^8 V_8 \mid_{Y=0} = \frac{\delta}{h} - \frac{x^2}{2 h R} \rightarrow$$

$$P - \frac{\lambda - \mu}{\lambda + 2\mu} \frac{\lambda}{3\mu} \frac{h^2}{a^2} \frac{d^2P}{dX^2} + \frac{-9\lambda^3 + 2\lambda^2\mu + 6\lambda\mu^2 - 3\mu^3}{15\mu(\lambda + 2\mu)^2} \frac{h^4}{a^4} \frac{d^4P}{dX^4} -$$

$$\frac{(\lambda + 3\mu)(345\lambda^3 + 313\lambda^2\mu - 123\lambda\mu^2 - 103\mu^3)}{315\mu(\lambda + 2\mu)^3} \frac{h^6}{a^6} \frac{d^6P}{dX^6} -$$

$$\frac{(\lambda + 3\mu)(2219\lambda^4 + 9766\lambda^3\mu + 6537\lambda^2\mu^2 - 3341\lambda\mu^3 - 2491\mu^4)}{2835\mu(\lambda + 2\mu)^4} \frac{h^8}{a^8} \frac{d^8P}{dX^8}$$

$$= \frac{\delta}{h} - \frac{X^2 a^2}{2 h R} \qquad (4.4.3.2.27)$$

which requires the solution of an eight degree (reducible to the fourth degree) characteristic equation. This equation was treated numerically, assuming as starting point for the root that referring to the sixth degree characteristic equation. The pressure P function is assumed to possess the form (4.4.3.2.26) .

Finally, the treatment of the tenth order perturbed problem is considered. This time, the ϵ^{10} differential equation linking pressure P to layer top boundary deflection is :

$$V_0 + \epsilon V_1 + \epsilon^2 V_2 + \epsilon^4 V_4 + \epsilon^6 V_6 + \epsilon^8 V_8 + \epsilon^{10} V_{10} \mid_{Y=0} = \frac{\delta}{h} - \frac{x^2}{2 h R} \rightarrow$$

$$P - \frac{\lambda - \mu}{\lambda + 2\mu} \frac{\lambda}{3\mu} \frac{h^2}{a^2} \frac{d^2P}{dX^2} + \frac{-9\lambda^3 + 2\lambda^2\mu + 6\lambda\mu^2 - 3\mu^3}{15\mu(\lambda + 2\mu)^2} \frac{h^4}{a^4} \frac{d^4P}{dX^4} -$$

$$\frac{(\lambda + 3\mu)\,(345\,\lambda^3 + 313\,\lambda^2\mu - 123\,\lambda\mu^2 - 103\,\mu^3)}{315\,\mu\,(\lambda + 2\mu)^3}\,\frac{h^6}{a^6}\,\frac{d^6P}{dX^6} -$$

$$\frac{(\lambda + 3\mu)(2219\,\lambda^4 + 9766\,\lambda^3\mu + 6537\,\lambda^2\mu^2 - 3341\,\lambda\mu^3 - 2491\,\mu^4)}{2835\,\mu\,(\lambda + 2\mu)^4}\,\frac{h^8}{a^8}\,\frac{d^8P}{dX^8} -$$

$$(71040\,\lambda^5 + 593701\,\lambda^4\mu + 1424393\,\lambda^3\mu^2 + 703764\,\lambda^2\mu^3 - 494653\,\lambda\mu^4 - 310829\,\mu^5)$$

$$\frac{(\lambda + 3\mu)}{155925\,\mu\,(\lambda + 2\mu)^5}\,\frac{h^{10}}{a^{10}}\,\frac{d^{10}P}{dX^{10}} = \frac{\delta}{h} - \frac{X^2\,a^2}{2\,h\,R} \qquad (4.4.3.2.28)$$

which leads to the (numerical) treatment of a tenth degree (reducible to the fifth degree) characteristic equation. The pressure P function adopted has still the form (4.4.3.2.26) .

4.4.4 Numerical Results

This Section is devoted to numerical tests of the perturbed solutions, for a selection of ν values. In particular, the peak contact pressure and contact width as functions of the cylinder indentation are examined. The Winkler and incompressibility approaches are compared to high order perturbed solutions, to retrieve indications about the validity fields of these simplified solutions. It may be conjectured that for low indentations and, consequently, for small contact widths, the perturbed approach is less accurate, since h/a is not negligible and, therefore, higher order perturbed solutions may be needed. These previsions are numerically tested in Figures 4.4.4.1,2,3,4,5 and 4.4.4.6,7,8,9,10 , with reference to peak contact pressure and contact width, respectively. More precisely, the parameter indicated along the x-axis is always $\delta R/h^2$, whereas the variable reported along the y-axis is, in the case of Figs 4.4.4.1,2,3,4,5, , the peak normalized pressure, $pR/(Ea)$, whereas in Figs 4.4.4.6,7,8,9,10 the normalized semicontact width, a/h is indicated. The asymptotic incompressible and Winkler modellings are also included for comparison. The choice of x and y-axis parameters stems from examination of equations 4.4.2.2.22 and 4.4.2.2.27 with regard to the second order perturbed solution, and of similar expressions for different perturbation orders. A dimensional analysis approach (Langhaar (1951)) was also useful. The following selection of Poisson's ratio figures ν = 0.4999 , 0.4997 , 0.499 , 0.49 , 0.48 is studied. It clearly emerges that the second order perturbed solution is not appreciably improved by considering higher order perturbations. In particular, the perturbed solution of fourth order produces peak contact pressures only slightly higher than its second order counterpart. It is observed that, contrary to the expectations expressed at the beginning of this Section, the second order perturbed solution is equally accurate for relatively small and large contact widths. For very small contacts, however, the precision of the second order perturbed solution declines, even if diagrams explicitly addressing this point have not been included. Anyway, this aspect is discussed in Section 4.3.5 with regard to the asymptotic incompressible solution, which may be interpreted as a particular version of the perturbed solution for incompressible materials. The conclusion reached there was that the asymptotic incompressible

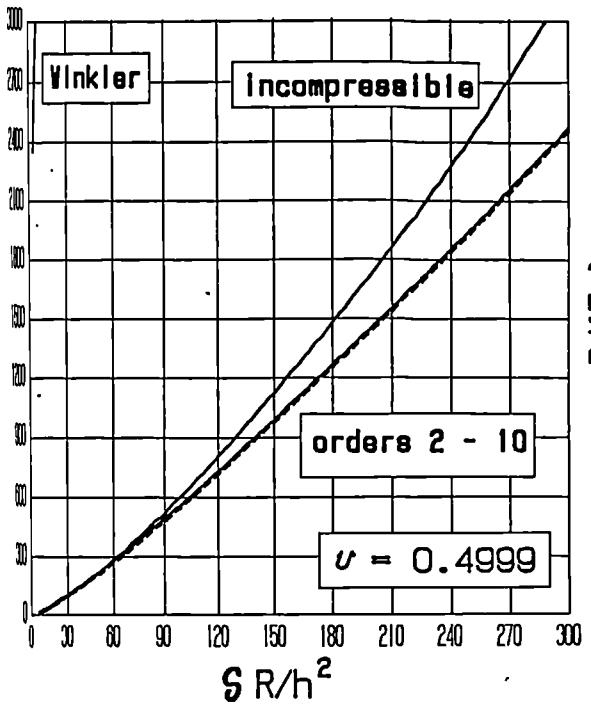

Fig. 4.4.4.1

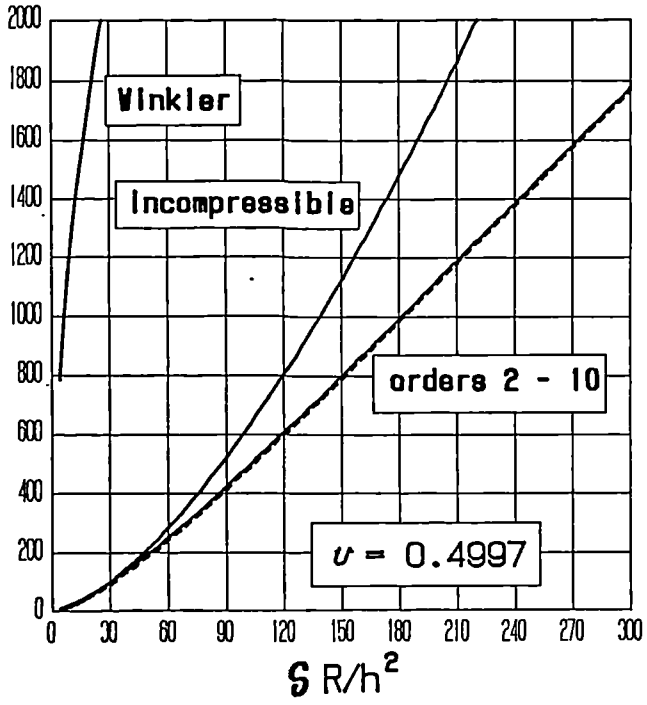

Fig. 4.4.4.2

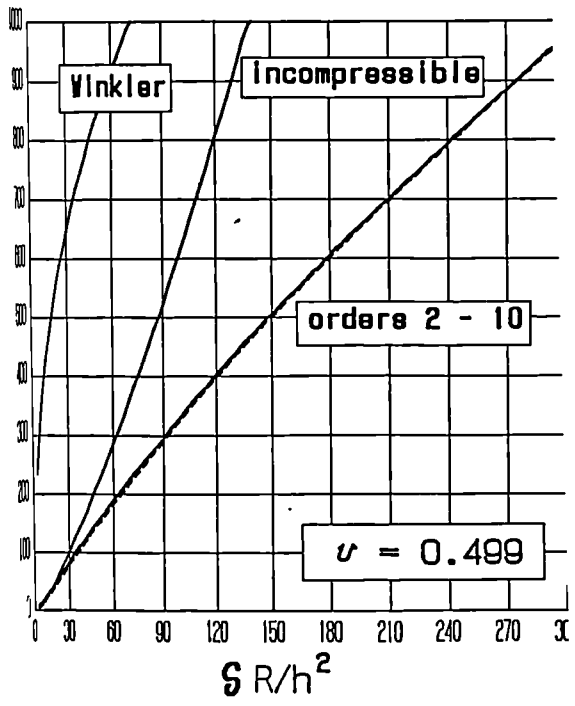

Fig. 4.4.4.3

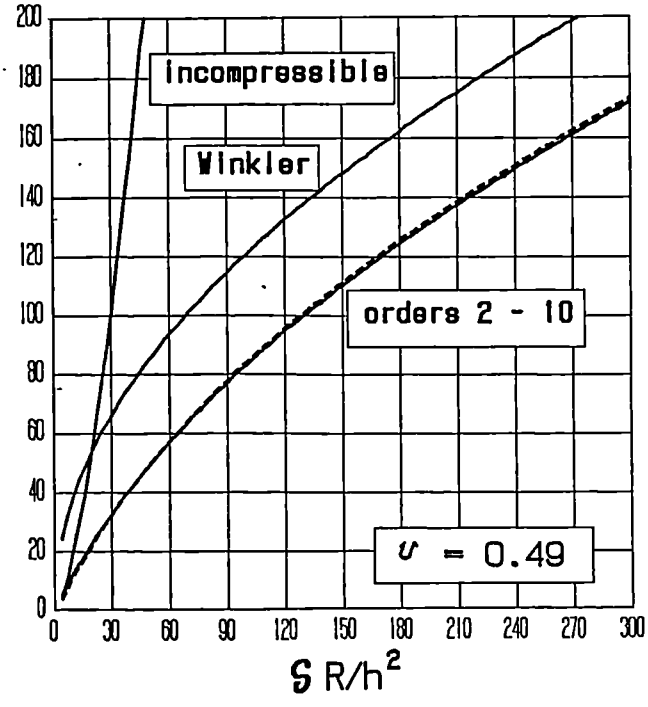

Fig. 4.4.4.4

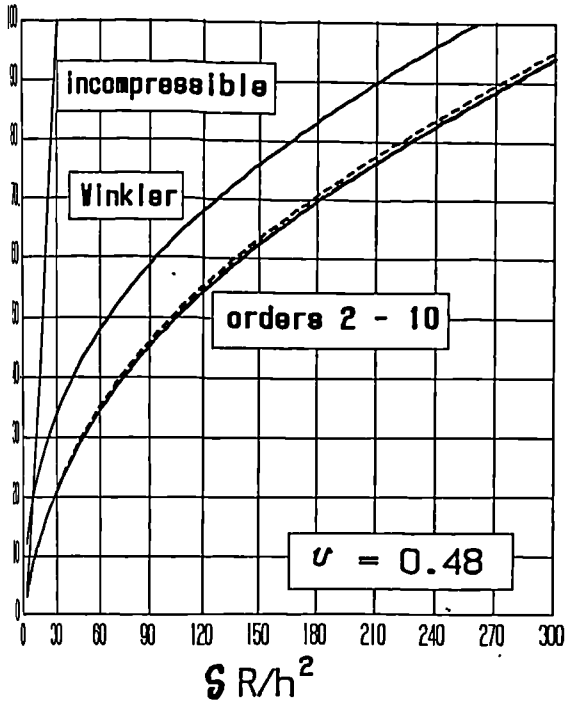

Fig. 4.4.4.5

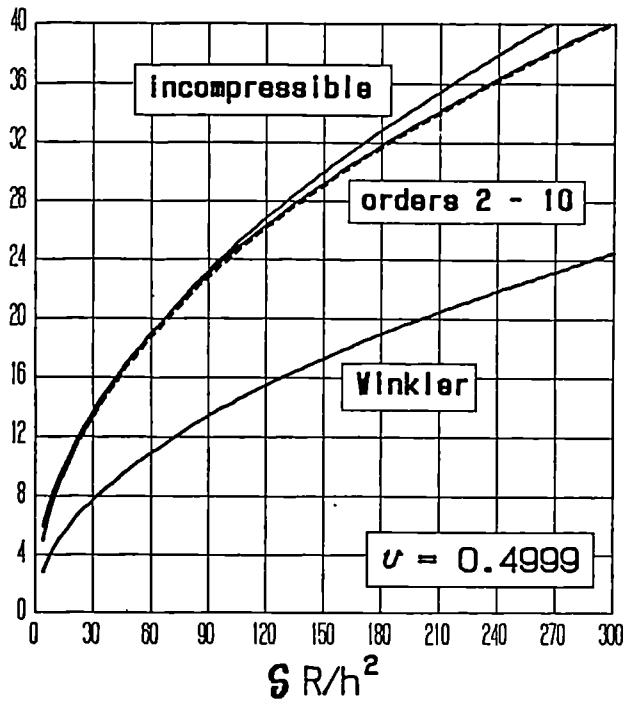

Fig. 4.4.4.6

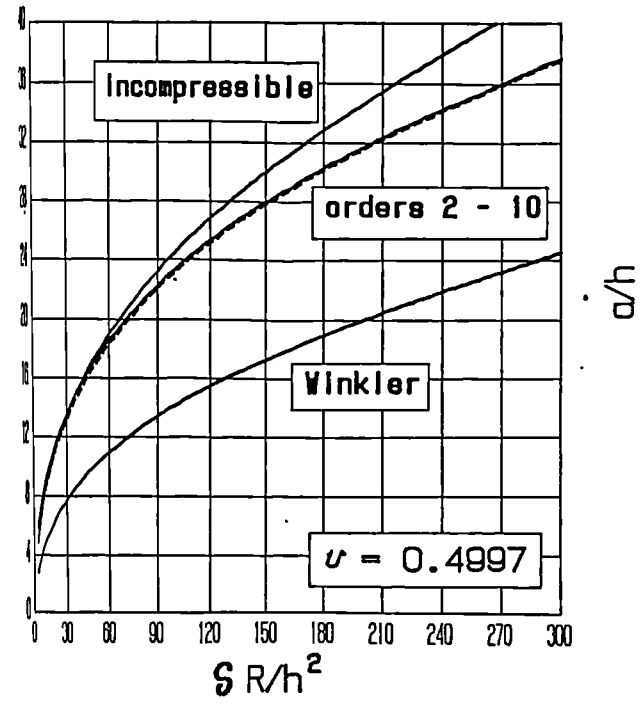

Fig. 4.4.4.7

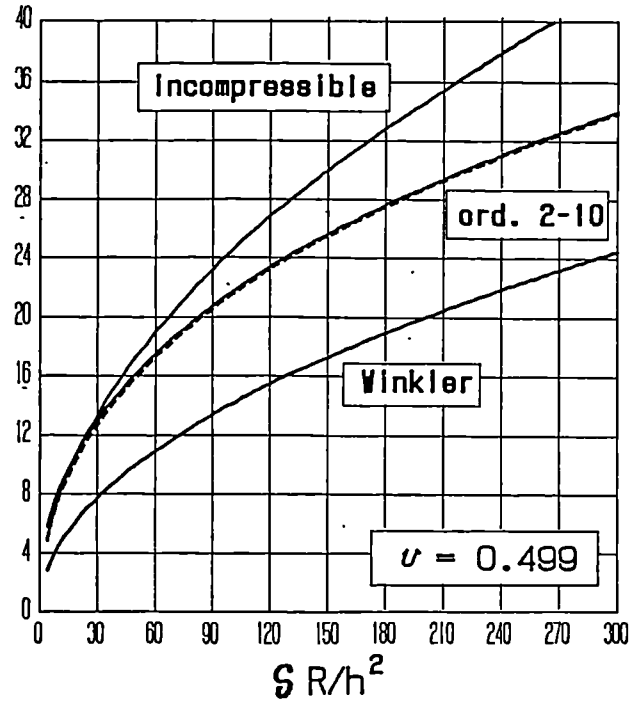

Fig. 4.4.4.8

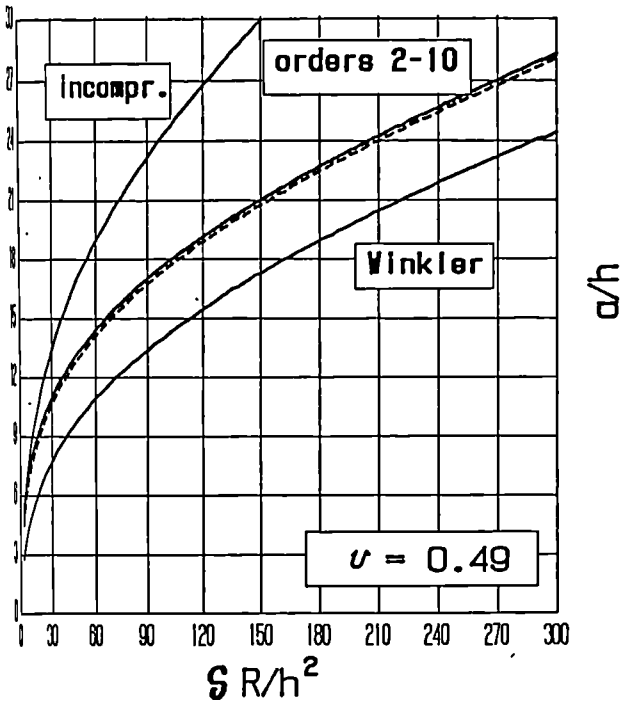

Fig. 4.4.4.9

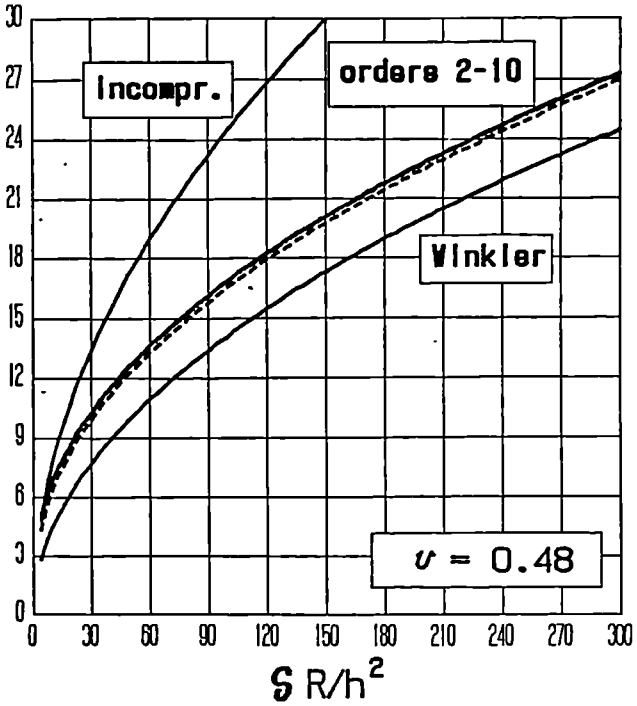

Fig. 4.4.4.10

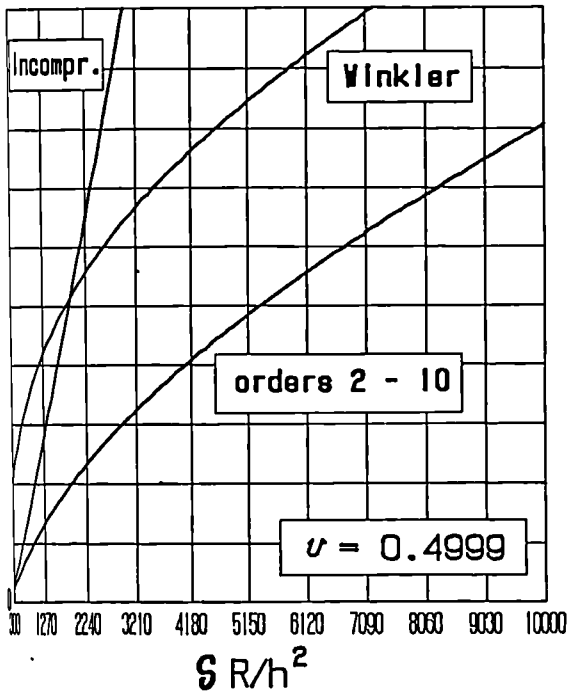

Fig. 4.4.4.11

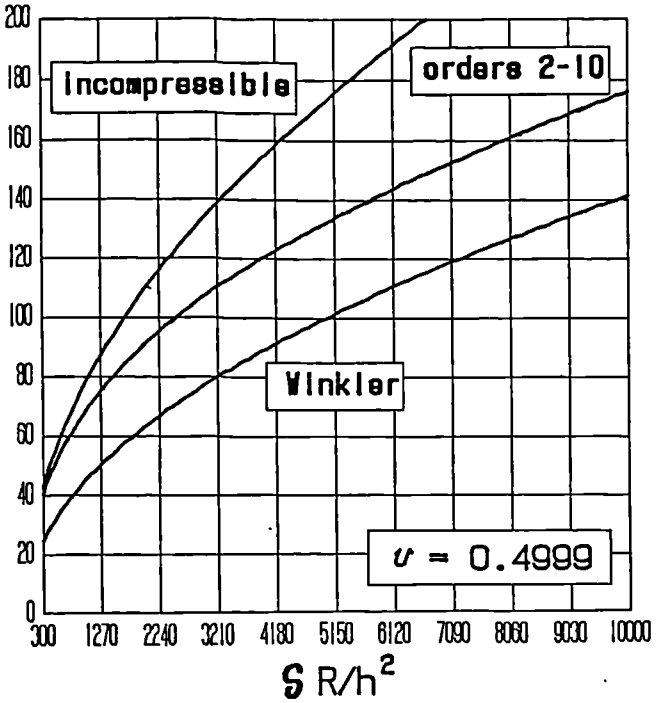

Fig. 4.4.4.12

solution was applicable for a/h ratios beyond 10 .

By comparing Fig. 4.4.4.1 to Fig. 4.4.4.5 , it appears that, when ν = 0.48 , the Winkler approach produces acceptable results in terms of peak contact pressure, whereas for ν = 0.4999 the incompressible solution is more accurate. To examine thoroughly intermediate Poisson's ratios, the second order perturbed solution is sufficient. Similar conclusions hold true when the determination of the contact semiwidth is concerned, as it appears from Figs 4.4.4.6,10 . In this case too, the fourth order solution results in a contact semiwidth moderately higher than its second order analogue.

Figs 4.4.4.1 and 4.4.4.6 show that, even when ν = 0.4999 (that is, the Poisson's ratio approaches the incompressibility figure 0.5) the second order solution deviates from the incompressible curve for high values of x-parameter. It was, therefore, decided to analyze the behaviour of both peak contact pressure and contact semiwidth for even higher values of parameter $\delta R/h^2$. Figs 4.4.4.11 and 4.4.4.12 reproduce pressure and contact width for high values of x-variable and only for ν = 0.4999 . Both peak contact pressure and contact semiwidth deviate substantially from the incompressible results. Such disagreement appears unjustified on physical grounds, and it is seemingly attributable to the imposition of approximate boundary conditions, as discussed in Sections 4.4.2.2 and 4.4.3.2 .

An alternative explanation for the above disagreement is reported hereinafter. Eqns (4.4.3.1.1) contain coefficients $(\lambda + \mu)/\mu$ and $(\lambda + 2\mu)/\mu$ multiplying ϵ , ϵ^2 . . . ϵ^n terms in the first equation, and coefficients $(\lambda + \mu)/(\lambda + 2\mu)$ and $\mu/(\lambda + \mu)$ multiplying ϵ , ϵ^2 . . . ϵ^n terms in the second equation. Now, the first pair of coefficients degenerates as the material becomes incompressible, whereas the second pair does not. As a consequence, for scarcely compressible elastomers the terms of the first equation of (4.4.3.1.1) which contain ϵ^n (for n sufficiently high) may not become smaller than the previous terms, so implying that the perturbed solution may not be applicable for nearly incompressible elastomers. In other words, this interpretation of the above disagreement refers more to the incompressibility difficulty than to the boundary condition problems. Anyway, it is observed that Figs 4.4.4.11-12 do not exhibit any differentiation among the solutions referring to orders 2 - 10 , while the explanation based upon incompressibility

problems should be consistent with a stabilization of the solution as the order of the perturbed solution is increased, that is, a dissimilarity among the perturbed solutions referring to highly different orders should occur. In conclusion, the explanation based upon boundary condition difficulties seems more convincing to the present author.

In the following, the asymptotic behaviour of the second order perturbed solution for $\nu \rightarrow 0.5$ and for a fixed $\delta R/h^2$ parameter is examined in an approximate way. It should be remembered that equation (4.4.2.2.22) defines the contact semiwidth. When $\nu \rightarrow 0.5$, then $\lambda \rightarrow \infty$ and $\mu \rightarrow E/3$. In addition, it can be speculated on physical grounds that when $\nu \rightarrow 0.5$ the contact width remains finite. Consequently, in equation (4.4.2.2.22) the radical appearing as the argument of *tanh* becomes vanishingly small. Since the contact width is admitted to stay finite, it is concluded that for any a value there exists a ν (that is, a λ) figure beyond which the argument of *tanh* is very small. In this case $tanh\,(x) \simeq x$, and with this assumption equation (4.4.2.2.22) can be solved in closed form to supply $a = \sqrt{2\delta R}$, as already commented in Section 4.4.2.2 . In other words, for a fixed $\delta R/h^2$ parameter, when $\nu \rightarrow 0.5$ the contact semiwidth is expected to approach the Winkler value and to deviate from the incompressible expression $a = \sqrt{6\delta R}$. These forecasts are at least partially confirmed by Fig. 4.4.4.12 , which shows that for very high values of x-parameter the second order solution becomes closer to the Winkler than to the incompressible previsions. As already noted, this behaviour is physically unsound. The normalized pressure is now analyzed from equation (4.4.2.2.27). By letting $\lambda \rightarrow \infty$ in the argument of *cosh* (if a stays finite) , $cosh \rightarrow 1$. By inserting the expression $a = \sqrt{2\delta R}$ and putting $x = 0$, it is obtained :

$$p(0) = (\lambda + 2\mu)\,\frac{\delta}{h} \qquad (4.4.4.1)$$

which is again a result typical of a Winkler idealization. Fig. 4.4.4.11 shows that for very high x-coordinate values, the second order perturbation solution is closer to the Winkler forecasts than to the incompressible predictions. In conclusions, it is believed that, especially for very high x-coordinate values, the perturbed solution supplies results which deviate substantially from the incompressible forecasts and,

therefore, the validity of such modelling is questionable on physical grounds. As already said, this non physical behaviour is attributable to the imposition of approximate boundary conditions.

The perturbed solution to the differential approach should be particularly valid for very small $\epsilon = h/a$ values, that is, for high contact widths. Conversely, the results of Figs 4.4.4.11,12 indicate that the perturbation solution degenerates for very large contacts. Although the x-axis range of Figs 4.4.4.11,12 hardly interests practically relevant cases (it would correspond to closely conforming profiles, possessing a high equivalent radius), this unphysical asymptotic behaviour betrays a weakness in the theoretical development.

In Fig. 4.4.4.11 , the Winkler and incompressible curves cross each other for a certain value of $\delta R/h^2$ parameter. Its analytical expression can be obtained as follows. The y-variable $pR/(Ea)$ becomes the same for Winkler (eqn 4.4.2.1.19) and incompressible (eqn 4.4.2.2.11) models when :

$$\frac{\delta E(1-\nu)}{h\,(1+\nu)(1-2\nu)\,\sqrt{2\delta R}} = \frac{3\,E\,R\,\delta^2}{h^2\,\sqrt{6\delta R}} \rightarrow \frac{\delta\,R}{h^2} = \frac{2\,(1-\nu)}{\sqrt{3}\,(1+\nu)(1-2\nu)} \qquad (4.4.4.2)$$

When $\nu = 0.4999$, $\delta R/h^2 = 1925.0141$, which agrees with the results of Fig. 4.4.4.11 .

4.5 CONCLUSIONS

It has been shown that the analytical solutions (the integral approach and the differential modelling, both solved via perturbations) lend themselves only to the treatment of simple indenter profiles. The differential approach produces questionable results for very large contact widths, and this fact has been attributed to the circumstance that the imposed boundary conditions are inevitably questionable.

An analytical approximate Green function has been developed which forms the basis of an integral formulation solved via a finite element approach, capable of treating a generic indenter profile. Comparisons with other methods have shown that this approach is accurate. The results retrieved indicate that the contact pressure for an imposed contact penetration depth is very sensitive to perturbations of the Poisson's ratio especially when the following situations occur simultaneously: a) the Poisson's ratio is close to its incompressibility figure 0.5 ; b) the contact width is considerably larger than the layer thickness. The changes in the contact pressure when passing from a cylindrical indenter to a parabolic approximation have been explored numerically and found to be negligible in biomechanical applications.

The Meijers (1968) theory has been revisited and some contributions have been given by computing higher order perturbation terms. Similarly, the Armstrong (1986) approach has been examined in detail, and its limits have been underlined.

It has also been clarified that, the classical asymptotic incompressible solution becomes acceptable for $\delta R/h^2$ values beyond about 30 .

CHAPTER 5. THE PLANE STRAIN, CURVED ELASTOMERIC LAYER: THEORY AND EXPERIMENTS

Chapter 5 The Plane Strain, Curved Elastomeric Layer 5.2

5.1 INTRODUCTION

A few analyses have concerned themselves with the problem of the indentation of a curved elastic layer by a rigid cylinder, as shown in Fig. 5.1.1 for two different situations. In fact, most of the studies devoted to deformable strips deal with flat layers, where the effects of curvature are often neglected in view of the smallness of the layer thickness (Hannah (1951)) and of the contact width (Miller (1964)).

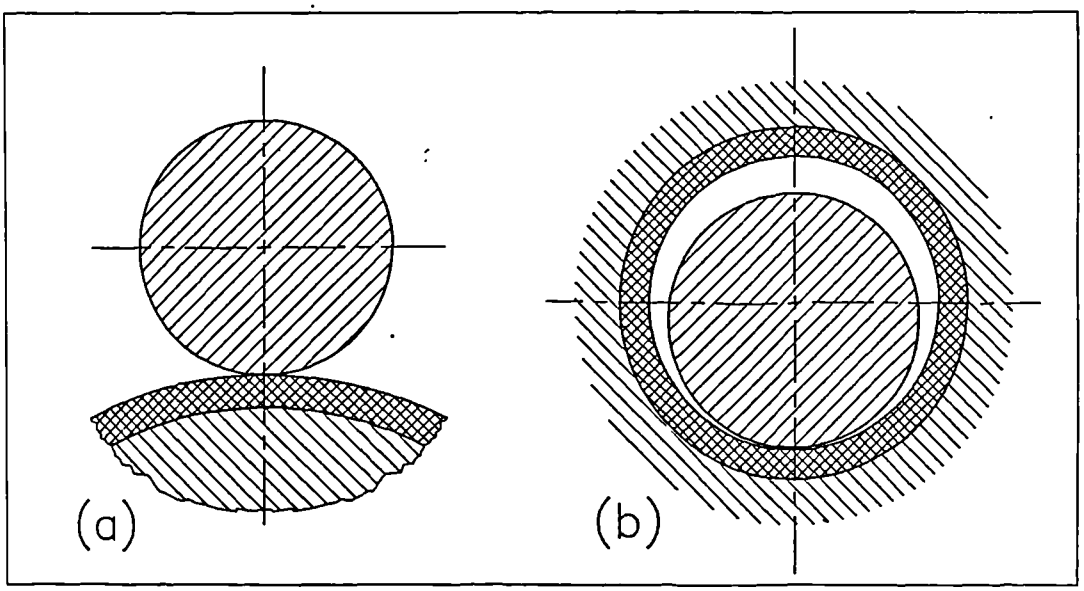

Fig. 5.1.1 : Two configurations of curved layers indented by a cylinder.

In biomechanical applications the ratio between external and internal radii defining a curved deformable layer anchored to a rigid foundation and indented by a cylinder is often as small as 1.03 . Consequently, it can be argued on physical grounds that a flat elastomeric layer is a proper model, and with such proportions there is no need for a curved layer approach. On the other side, values of the above-mentioned ratio up to about 1.2 are recorded in technical practice, a figure

for which the curvature effects may become significant. In addition, it is convenient to develop a model which can equally treat thin and thick curved layers, especially when optimization studies (on the influence of the layer thickness and elastic coefficients, Unsworth, Pearcy and White, (1987)) are needed. In addition, ceramic cups (Fessler and Fricker (1989), Andrisano, Dragoni and Strozzi (1990)) can be interpreted as thick axisymmetric layers, for which the plane strain model of this Chapter can be interpreted either as a simplified idealization (Barton (1941)), or as an analytical starting point for the axisymmetric situation (Gladwell (1980), p. 509). This Chapter deals with an analytical series solution of a rigidly backed, plane-strain, curved elastic lining indented by a rigid cylinder, where most of the tedious and lengthy analytical passages have been relegated to the algebraic manipulator MACSYMA (1983). Experimental research has also been performed and the results obtained are compared with the analytical forecasts.

5.2 LITERATURE REVIEW

The analytical papers devoted to this problem can be classified into two main categories. A first group comprises contributions based upon a series solution of real (as opposed to "complex analysis") expressions in terms of displacements or stresses, whereas the second class embraces complex analysis approaches. The first kind of contributions includes the work of O'Donoghue, Brighton and Hooke (1967), who study the elastic distortions in journal bearings and shafts under plane conditions. They start from a series solution in terms of displacements, and obtain closed form expressions for the series coefficients in the cases of shafts (vanishing inner radius) and of bearings of infinite outer radius, subject to concentrated (or, more exactly, line) loads. Hahn and Levinson (1974a) and (1974b) adopt a classical stress function (Timoshenko and Goodier (1970), p. 132) expressed in the form of a series, and they assume a Fourier expansion for the boundary stresses. The coefficients of such expansions are found by exploiting orthogonal properties of the functions involved. A worrying slowness of convergence is signalled, which is partially overcome with the aid of a Kummer-type (Chapter 4) acceleration technique. Some indications about the curvature effects in comparison to a flat layer are also presented. Finally, the relevance of the shear stresses by the layer-foundation interface is properly underlined. Soong and Li (1980) and (1981) follow a similar path, but they adopt a simpler collocation method for the computation of the series coefficients. Even with these approximations, the evaluation of the series coefficients requires numerical inversions of various matrices, thus possibly compromising the precision of the calculations. Solecki and Ohgushi (1984) start from a displacement formulation analogous to that of O'Donoghue, Brighton and Hooke (1967), still in the form of a series, and they compute analytically the series coefficients in the case of a curved layer of finite inner and outer radii and sustaining a concentrated load. This solution constitutes the Green function which allows the indentation by a rigid cylinder to be described in terms of a Fredholm integral equation of the first kind, whose kernel is in fact the above-mentioned Green function. However, Solecki and Ohgushi (1984) do not try to solve this integral equation analytically in terms of the unknown contact pressure profile, but

they follow a slightly different, essentially numerical path. They expand the boundary pressure in terms of a Fourier series, introduce this expression into the integral equation, and compute the series coefficients numerically. The authors face ill-conditioning problems, which they overcome by evaluating more precisely the influence coefficients, that is, the series sums expressing the layer deflections under an imposed reference loading. Their Fig. 3 presents a comparison between the curved layer solution and forecasts referring to a flat strip, thus providing further information on the curvature effects. Zhang (1987) employs the annulus theory to study the deformations of a journal bearing, but he introduces drastically simplifying assumptions, which in the writer's opinion undermine the validity of the theoretical results obtained. In particular, he supposes that the shear stresses vanish at the layer-bearing interface, whereas the results of Hahn and Levinson (1974a) and those of this Chapter indicate that such stresses play an important role.

Moving to the complex function approach, Tiffen and Semple (1965) examine the annulus problem, for which they express the complex stresses via a series description. They also mention the possibility of applying these procedures to the solution of problems involving segments of an annulus. In Hooke and O'Donoghue (1972) the complex analysis approach is applied to the examination of the dry contact pressure distribution in a journal bearing with soft, elastic lining. Mathematically oriented contributions are due to Milne-Thompson (1960), p. 131 , and to England (1971), p. 90 .

Various numerical papers based upon a finite element formulation, dealing with curved elastomeric layers anchored to metal cores and addressing applications in the field of paper printing are reviewed in the following. Batra, Levinson and Betz (1976), Batra (1977), (1978), (1980a), (1980b), (1980c) and (1982), Batap and Batra (1982) and (1984) obtain various numerical solutions incorporating the non-linearities due to the constitutive law (stress-strain link, material non-linearity) and to the large deformations (geometric non-linearities), and they emphasize that "the compressibility of rubber has more effect on the pressure at the contact surface than the material and geometric nonlinearities." (Batra (1981)).

With reference to the experimental field, the technical literature is even more devoid of pertinent contributions. Parish (1955), (1958) and (1961) measures

various contact forces and pressure profiles with the aid of a radial pressure pin. He finds that the experimental readings deviate significantly from the analytical predictions based upon a straight layer assumption. He attributes such errors to "non-linearities in the elastic properties of the rubber" (Parish (1958)), which, in fact, are found by Batra (1981) not to be relevant. He studies situations defined by ratios of cover thickness to core radius ranging from 0.03 to 0.22 , and ratios of contact width to cover thickness from 1.6 to 4 . The indenting cylinder radius is of the same order of magnitude as the indented, rubber covered cylinder (Parish (1955)). The author does not explicitly report the indentation depths prescribed, but with the help of the analytical incompressible contact width-indentation penetration relationship (Johnson (1985), p. 139, eqn (5.71)) it can be estimated that the ratio between indentation depth and layer thickness ranges from 0.02 to 0.27 . Miller and Poulter (1962) present various diagrams connecting the cylindrical indenter impression to the load, and they too report some discrepancies between their experiments dealing with curved strips and the theoretical forecasts referring to a flat layer, especially at high indentation depths. In the experimental study the layer thickness is 0.43 times the roller radius, and the penetrations prescribed are from 0.008 to 0.054 times the layer thickness. A Poisson's ratio of 0.5 , denoting incompressibility, is constantly employed in the analytical computations. The need for "the general solution to the problem of a circular ring under given edge tractions and displacements in cylindrical polar co-ordinates . ." is also emphasized. In contrast to the previous papers, Miller (1964) experiences a good agreement between experimental readings referring to a curved cover and straight layer predictions, apart from one case and only for the highest indentation depths. He analyses layers whose thickness ranges from 0.02 to 0.1 times the roller radius, and indentation depths lower than 0.08 times the layer thickness. Since both such ratios are particularly low, it can be speculated that the curvature effects are in this case negligible, thus rationalizing the good agreement experienced between experiments and theory. In any case, Miller (1964) observes that "a more satisfactory result might be possible through further development of the general solution in cylindrical polar coordinates . . ". Spengos (1965) presents experimental pressure profiles via a crystal pickup embedded in the shell of the indenting cylinder, a device comparable to that developed by Parish (1955) and by Gent, Henry

and Roxbury (1974). He analyses situations in which a significant tangential force is transmitted, and measures the shear stress distribution along the contact width. More recently, Auger, Medley and Dowson (1990) examine experimentally the frictional coefficient in a 'cushion bearing' with the aim to investigate the generation of a fully lubricated contact.

A contribution specifically addressing the curvature effects is now examined. Yao (1990), p. 231 , quantifies the error induced by neglecting the curvature effects by resorting to the thick pipe theory (Timoshenko and Goodier (1970), pp. 69-71). In other words, he adopts a Winkler-type foundation model, in the sense that he treats only a uniformly loaded strip. For the configuration of natural hip joints (ν = 0.4 , ratio of layer thickness to core radius $\simeq$ 0.05 , Yao (1990)) the error incurred by neglecting curvature, evaluated in terms of indentation resulting from an imposed uniform pressure, is estimated to be as low as 3.3 percent. Anyway, in the case of artificial joints with scarcely compressible elastomeric layers, ν approaches 0.5 and, consequently, the Winkler foundation model is no longer valid. In fact, the Winkler description presupposes that, during indentation, the elastomeric strip moves radially without flowing laterally, a mechanism which is realistic for Poisson's ratios as low as 0.4 , but which becomes no longer dominant in the case of moderately compressible rubbers (see Chapter 4). In addition, the layer thicknesses adopted in artificial joints are often higher than their natural counterparts, thus suggesting that the curvature effects may become more relevant. In conclusion, the error estimate produced by Yao (1990) may not be realistic in the case of artificial hip joints with elastomeric, nearly incompressible layers.

5.3 THEORETICAL SERIES SOLUTION

This Section presents the basic theory leading to the series solution of the plane strain, curved elastomeric layer, and reports the analytical expressions of the series coefficients.

5.3.1 Series coefficients

The generalized equilibrium equations in cylindrical coordinates in terms of radial and circumferential displacements (under plane-strain conditions) can be obtained from the equilibrium equations in terms of stresses (Timoshenko and Goodier (1970), p. 66), by expressing the stresses in terms of displacements (Timoshenko and Goodier (1970), p. 76) :

$$\frac{\partial^2 u}{\partial r^2} + \frac{\nu}{1-\nu}\left[\frac{1}{r}\frac{\partial u}{\partial r} - \frac{u}{r^2} + \frac{1}{r}\frac{\partial^2 v}{\partial r\,\partial\theta} - \frac{1}{r^2}\frac{\partial v}{\partial\theta}\right] +$$

$$\frac{1-2\nu}{1-\nu}\left[\frac{1}{r}\frac{\partial u}{\partial r} - \frac{u}{r^2} - \frac{1}{r^2}\frac{\partial v}{\partial\theta}\right] +$$

$$\frac{1-2\nu}{2(1-\nu)}\left[\frac{1}{r^2}\frac{\partial^2 u}{\partial\theta^2} + \frac{1}{r}\frac{\partial^2 v}{\partial r\,\partial\theta} - \frac{1}{r^2}\frac{\partial v}{\partial\theta}\right] = 0 \;;$$

$$\frac{(1-\nu)}{(1-2\nu)}\left[\frac{1}{r^2}\frac{\partial u}{\partial\theta} + \frac{1}{r^2}\frac{\partial^2 v}{\partial\theta^2} + \frac{\nu}{(1-\nu)}\frac{1}{r}\frac{\partial^2 u}{\partial r\,\partial\theta}\right] +$$

$$\frac{1}{2}\left[\frac{1}{r}\frac{\partial^2 u}{\partial r\,\partial\theta} - \frac{1}{r^2}\frac{\partial u}{\partial\theta} + \frac{\partial^2 v}{\partial r^2} - \frac{1}{r}\frac{\partial v}{\partial r} + \frac{v}{r^2}\right] +$$

$$\left[\frac{1}{r^2}\frac{\partial u}{\partial\theta} + \frac{1}{r}\frac{\partial v}{\partial r} - \frac{v}{r^2}\right] = 0 \qquad (5.3.1)$$

where u and v are the radial and circumferential displacements, respectively, and r and θ are the cylindrical coordinates. The single-valued series solution to (5.3.1) is (Solecki and Ohgushi, (1984), where some misprints have been corrected) :

$$\frac{2\pi E u(\rho,\theta)}{P} = a_0 \rho + \frac{b_0}{\rho} + \left(a_1 + b_1 \rho^2 + \frac{c_1}{\rho^2} + d_1 ln \rho \right) cos \theta +$$

$$\sum_{n=2}^{\infty} \left(a_n \rho^{n-1} + b_n \rho^{n+1} + c_n \rho^{-n-1} + d_n \rho^{-n+1} \right) cos (n \theta) ;$$

$$\frac{2\pi E v(\rho,\theta)}{P} = c_0 \rho + \frac{d_0}{\rho} + \left(- a_1 - \frac{1}{3-4\nu} d_1 + \frac{5-4\nu}{1-4\nu} b_1 \rho^2 + \frac{c_1}{\rho^2} - d_1 ln \rho \right) sin \theta +$$

$$\sum_{n=2}^{\infty} \left(- a_n \rho^{n-1} + \frac{4(1-\nu)+n}{2(1-2\nu)-n} b_n \rho^{n+1} + \right.$$

$$\left. c_n \rho^{-n-1} + \frac{n-4(1-\nu)}{n+2(1-2\nu)} d_n \rho^{-n+1} \right) sin (n \theta) \qquad (5.3.2)$$

Here the normalized radius, $\rho = r/r_t$ is employed, where r_t denotes the loaded radius (that is, the radius defining the layer contour sustaining the load). In addition, the displacements are multiplied by the Young's modulus, E, and divided by the total applied load, P , having in mind the solution for the case of a concentrated load.

In this Section the layer is assumed to be firmly bonded to a rigid substrate, and the layer is supposed to be loaded by a concentrated force applied at $\rho = 1$, $\theta = 0$. As mentioned in the Literature Review, the solution of this problem supplies the Green function, which can be employed to mimic more complex loadings. As it will appear from the following Section, a solution in terms of Green function allows the series convergence to be improved independently of the profile of the applied pressure, thus achieving an appreciable reduction in the computer time of general

validity.

The boundary conditions impose the disappearance of both radial and circumferential displacements at the radius, r_b , along which the layer is bonded to the rigid substrate, the vanishing of the shear stress along the loaded radius, r_i , and the outcome of the radial stress singularity occurring at $r = r_i$, $\theta = 0$, where the radial force P is applied, Fig. 5.3.1 .

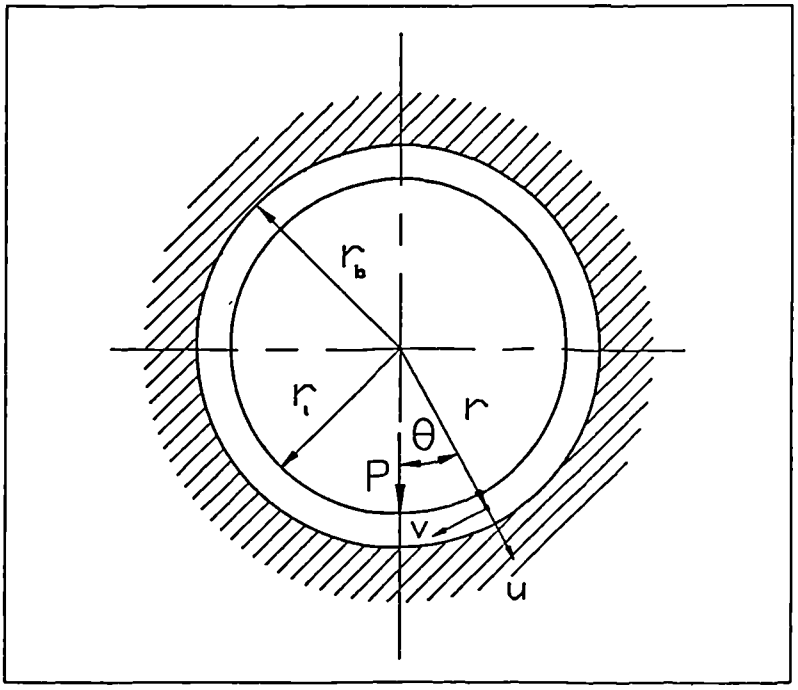

Fig. 5.3.1 : The meaning of symbols r , r_b , r_i , θ , u , v and P .

Following Timoshenko and Woinowsky-Krieger (1959), p. 291 , the equation expressing the radial stress singularity resulting from the application of the concentrated load, P , is more easily formulated by expanding force P in terms of a Fourier (locally non converging, Reißner (1929)) series :

$$P = \frac{P(\rho,\theta)}{2\pi r_i}\left[1 + \sum_{n=2}^{\infty} 2\cos(n\theta)\right] \qquad (5.3.3)$$

The four boundary conditions mentioned above must be verified for each index, n, of the series solution (5.3.2). In particular, the singularity of the radial stress demands that, for each series index, the radial stress profile evaluated by properly differentiating eqns (5.3.2) must coincide with the n-th term of the series expansion (5.3.3) of load P. Proceeding in this way, a linear system of four algebraic equations whose four unknowns are the series coefficients must be solved for indices 0 , 1 and $n \geq 2$, respectively (Strozzi (1989)). Since the computations are tedious and prone to errors, they were relegated to the algebraic manipulator MACSYMA (1983). The resulting coefficients are (symbol ρ_b stays for r_b/r_t , where index b stands for "bonded") :

$$a_0 = - \frac{(1 + \nu)(1 - 2\nu)}{1 + (1 - 2\nu)\rho_b^2}$$

$$b_0 = + \rho_b^2 \frac{(1 + \nu)(1 - 2\nu)}{1 + (1 - 2\nu)\rho_b^2}$$

$$c_0 = 0$$

$$d_0 = 0$$

$$a_1 = + \frac{(1 + \nu)\left[2(3 - 4\nu)\left[(3 - 4\nu)\rho_b^4 + 1\right] ln\, \rho_b + (1 - 4\nu)\rho_b^4 - 2(1 - 2\nu)\rho_b^2 + 1\right]}{4(1 - \nu)\left[(3 - 4\nu)\rho_b^4 + 1\right]}$$

$$b_1 = - \frac{(1 + \nu)(1 - 4\nu)\left[\rho_b^2 + (1 - 2\nu)\right]}{4(1 - \nu)\left[(3 - 4\nu)\rho_b^4 + 1\right]}$$

$$c_1 = + \rho_b^2 \frac{(1 + \nu)\left[(1 - 2\nu)(3 - 4\nu)\rho_b^2 - 1\right]}{4(1 - \nu)\left[(3 - 4\nu)\rho_b^4 + 1\right]}$$

$$d_1 = -\frac{(1+\nu)(3-4\nu)}{2(1-\nu)}$$

$$a_n = \frac{(1+\nu)\left\{\left[(n^2+8)-8\nu(3-2\nu)\right]\rho_b^{2n+2} - n(n-1)\rho_b^{2n} + n(3-4\nu)\right\}}{(n-1)\mathfrak{D}_n}$$

$$b_n = -\frac{(1+\nu)(4\nu+n-2)\left\{(n+1)\rho_b^{2n} - n\rho_b^{2n-2} + (3-4\nu)\right\}}{(n+1)\mathfrak{D}_n}$$

$$c_n = \frac{(1+\nu)\rho_b^{2n}\left\{n(3-4\nu)\rho_b^{2n} + 8\nu(3-2\nu)\rho_b^2 - (8+n^2)\rho_b^2 + n(n+1)\right\}}{(n+1)\mathfrak{D}_n}$$

$$d_n = +\frac{(1+\nu)(4\nu-n-2)\rho_b^{2n}\left\{(3-4\nu)\rho_b^{2n} - (n-1) + n\rho_b^{-2}\right\}}{(n-1)\mathfrak{D}_n}$$

where :

$$\mathfrak{D}_n = -(3-4\nu)(\rho_b^{4n}+1) + \left[8\nu(3-2\nu) - (n^2+8)\right]\rho_b^{2n+2} + 2(n^2-1)\rho_b^{2n} - n^2\rho_b^{2n-2}$$

(5.3.3)

The series coefficients depend on the geometric ratio ρ_b . So, the properly normalized radial displacements of the layer border sustaining a point load are functions of this shape factor only. Anyway, when the more complex situation is examined of a curved layer indented by a rigid cylinder, the geometric ratios influencing the solution become more complex.

It is important to underline that the expressions of the series coefficients do not degenerate for $\nu = 0.5$. In other words, the series solution can be equally employed for studying compressible and incompressible curved layers. Although Solecki and Ohgushi (1984) compute the series coefficients exactly, they still retain expression $k = 1/(1 - 2\nu)$ (*e.g.* their eqns (A8) and (A9)), which becomes unbounded for $\nu = 0.5$. As a consequence, the solution of Solecki and Ohgushi (1984) degenerates for $\nu = 0.5$.

As a final observation, the relevant stresses can be computed by properly differentiating eqn (5.3.2) after introduction of the series coefficients (5.3.3). Similar to the displacements, the stresses too are expressed in terms of an infinite series. For conciseness, the corresponding expressions are not reported here, where the interested reader is addressed to Soong and Li (1981), formula (2) .

An integral formulation is now developed for the layer border loaded by the concentrated load, whose possible usefulness is discussed at the end of this Section. This formulation is mathematically based upon an important integral relation (Gröβner and Hofreiter (1958), second volume, p. 119 , formula 14 a)) :

$$\int_0^\infty \frac{\sin n\theta}{\theta}\, d\theta = \begin{cases} 0 & n = 0 \\ \\ \frac{\pi}{2} & n > 0 \end{cases} \tag{5.3.4}$$

It is further noted that the *n-th* radial displacement is proportional to cos $(n\theta)$ (eqn (5.3.2)). The resultant force, F_n , referring to the *n-th* harmonic and computed between $\theta = \alpha$ and $\theta = \beta$ is proportional to :

$$F_n \simeq \int_{\alpha}^{\beta} \cos(n\,\theta)\, d\theta \;=\; \frac{\sin(n\beta) - \sin(n\alpha)}{n} \tag{5.3.5}$$

In addition, the resultant force between $\theta = \alpha$ and β , deriving from the application of infinite harmonics and referring to a continuous variation of index n is :

$$F = \int_{0}^{\infty} \frac{\sin(n\beta) - \sin(n\alpha)}{n}\, dn = \begin{cases} \frac{\pi}{2} - \frac{\pi}{2} = 0 & \alpha\,,\ \beta > 0 \\ \\ \frac{\pi}{2} & \alpha = 0\,,\ \beta > 0 \end{cases} \tag{5.3.6}$$

These notes indicate that F is in fact a concentrated load of intensity π (and not $\pi/2$, due to symmetry reasons about $\theta = 0$ axis) applied at $\theta = 0$. Having these premises in mind, the integral formulation of the radial displacement of the layer border sustaining a singular load is derived from (5.3.2) as :

$$\frac{2\,\pi^2\, E\, u\,(1,\theta)}{P} = \int_{0}^{\infty} \left[\, a_n + b_n + c_n + d_n \,\right] \cos(n\,\theta)\, dn \tag{5.3.7}$$

It is underlined that eqn (5.3.7) solves the case of an infinitely long, curved layer (Fig. 5.3.2), and not the situation of an annulus. It can be conjectured on physical grounds that, if the angular contact width is less than, say, π , the two above-mentioned solutions would give very similar results. In a hip joint, the cup covered with an elastomeric layer possesses an angular width slightly lower than π, thus limiting the angular contact width to smaller figures. In addition, it should be noted that neither of the two models can mimic the finiteness of the layer angular width, an aspect whose importance is shown in the remainder of this Chapter. Papers dealing with layers of finite length are those of Keer and Miller (1983) and of Solecki (1986).

The integral formulation for the radial displacement (5.3.7) is not directly exploited in this study. Anyway, it is still relevant because it may be employed as a starting point to treat the corresponding axisymmetric case (Gladwell (1980), p. 509).

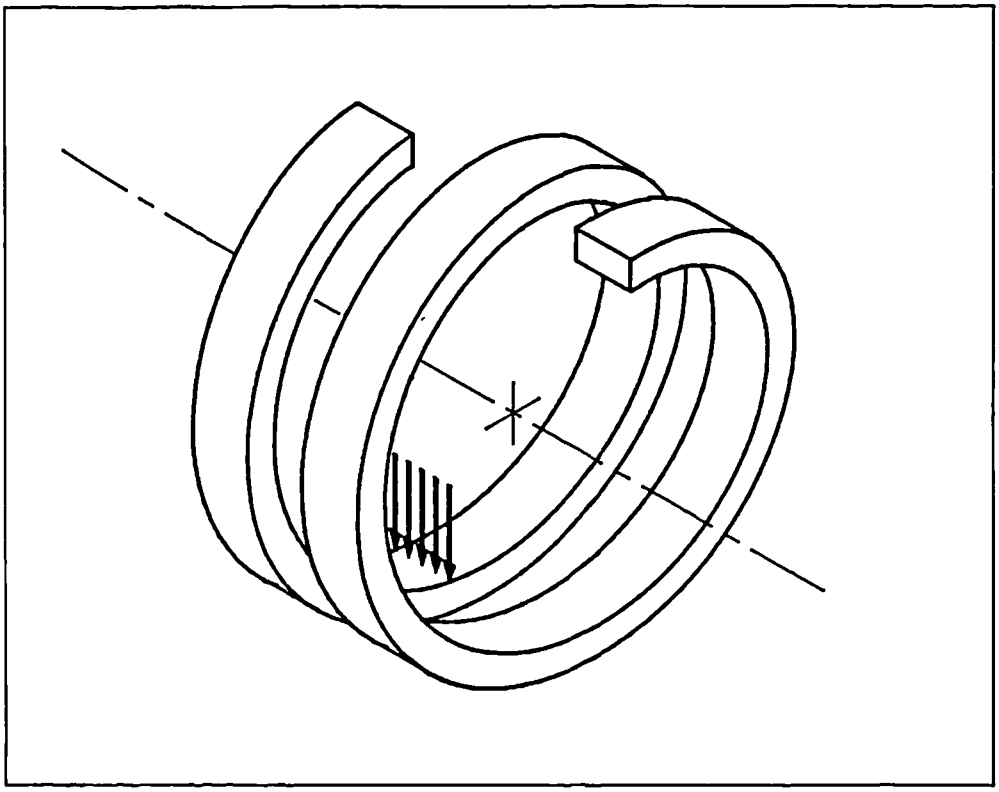

Fig. 5.3.2 : The mathematical model of an infinitely long curved layer .

5.3.2 Acceleration of the series convergence

This Section shows how to accelerate the series convergence via the Kummer technique (Knopp (1928), p. 260). Kummer method is applicable provided that a series is found which can be summed exactly, and which has terms as similar in construction as possible to those of the original series. In particular, this new series must behave asymptotically as the original one and, therefore, it is henceforth referred to as "the asymptotic series". By subtracting from the terms of the original series those of the asymptotic one, a series of faster convergence is usually obtained, named in the following as "the accelerated series". The sum of the initial series can thus be computed by adding to the exact sum of the asymptotic series an approximate value of the accelerated series, for which only a limited number of terms need to be computed (Strozzi (1989)). In the present case it is noted that the n-th term of the normalized radial displacement u (Fig. 5.3.1), computed for $r = r_i$, that is, for $\rho = 1$, is (see eqn (5.3.2)) :

$$\frac{2\,\pi\,E\,u_n(1,\theta)}{P} = \left[\, a_n + b_n + c_n + d_n \,\right] cos\,(n\,\theta) \qquad (5.3.2.1)$$

It is, therefore, relevant for the application of the Kummer technique to examine the asymptotic behaviour of $a_n + b_n + c_n + d_n$. With the aid of MACSYMA (1983), it was found that, for high values of the series index n, the following asymptotic expression holds true :

$$a_n + b_n + c_n + d_n \simeq \frac{4\,(\,1 - \nu^2)}{n} + \frac{2\,(1 + \nu)\,(1 - 2\nu)}{n^2} + \frac{4\,(1 - \nu^2)}{n^3} \qquad (5.3.2.2)$$

Similar to Strozzi (1989), this asymptotic expression is independent of the radii along which the constraints and the loads are imposed. The following Figs 5.3.2.1 and 5.3.2.2 show the original $a_n + b_n + c_n + d_n$ term as a function of the series index, n, and three asymptotic expressions. In particular, the first asymptote is the first term on the right hand-side of (5.3.2.2), the second asymptote is the sum

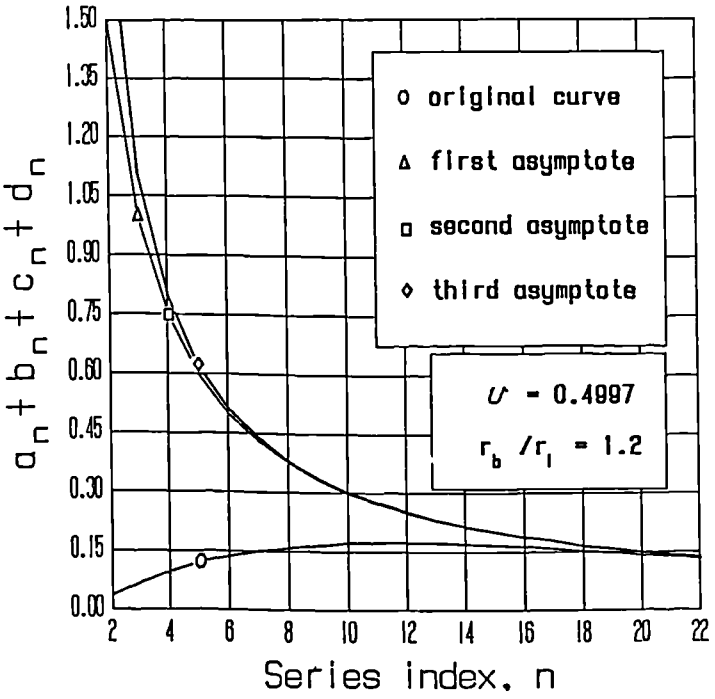

Fig. 5.3.2.1 : Convergence of series terms for r_b / r_i = 1.2 .

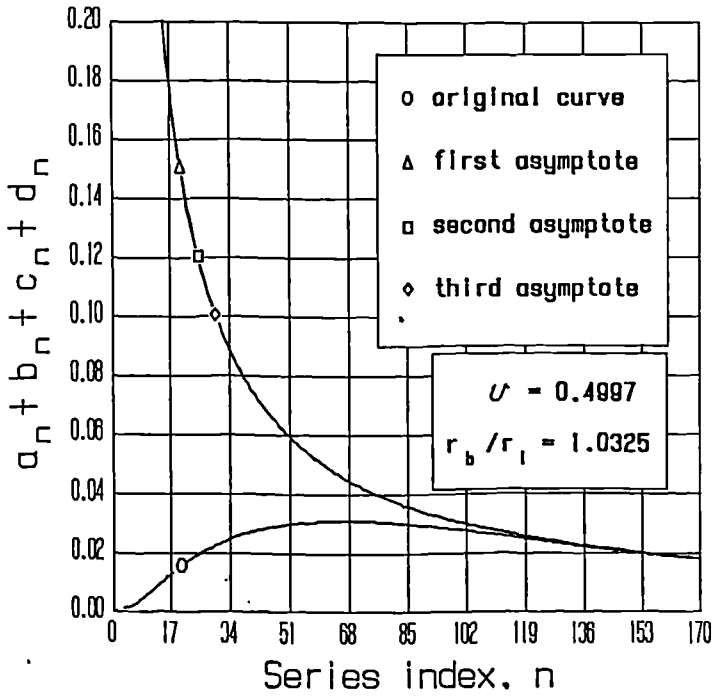

Fig. 5.3.2.2 : Convergence of series terms for r_b / r_i = 1.0325 .

of the first two terms on the right hand-side of (5.3.2.2) and, finally, the third asymptote is the total right hand-side expression of (5.3.2.2). Both Figures refer to $\nu = 0.4997$, a realistic value (Chapter 3). In addition, Fig. 5.3.2.1 refers to $r_b/r_t = \rho_b = 1.2$, whereas Fig. 5.3.2.2 examines $\rho_b = 1.0325$, which are plausible shape ratios.

It appears that, when ρ_b is appreciably higher than unity (*e.g.* 1.2), its asymptotic approximation approaches the exact curve for series indices as low as 20. Conversely, for ρ_b ratios close to unity (*e.g.* 1.0325), more than 120 series terms are necessary to get the same accuracy. In addition, the three asymptotic expressions behave essentially equivalently in mimicking the exact curve for both small and relatively high ρ_b ratios and, therefore, it seems advisable to use the simplest expression for the asymptotic term.

Since ratio ρ_b highly influences the accuracy of the asymptotic expression, a slightly different approach to the determination of the asymptotic expression is developed in the following which, contrary to the previous results (5.3.2.2), produces asymptotic terms depending on the above-mentioned ratio and, therefore, hopefully permits a good precision to be attained independently of ρ_b . It is anticipated that the results retrieved do not completely fulfil this expectation. Nevertheless, this analytical approach is here presented, since it is still beneficial in certain conditions. According to (5.3.3), the denominators of all series coefficients behave as $n\,\mathfrak{D}_n$, which in turn can be rewritten in the following way:

$$n\mathfrak{D}_n=(4\nu-3)n\rho_b^{4n}\left[1+\frac{\left[8\nu(3-2\nu)-(n^2+8)\right]\rho_b^{2n+2}+2(n^2-1)\rho_b^{2n}-n^2\rho_b^{2n-2}+(4\nu-3)}{(4\nu-3)\,\rho_b^{4n}}\right] \qquad (5.3.2.3)$$

where the fraction between brackets becomes vanishingly small for high values of index n. Consequently, by remembering that $1/(1+x) \simeq 1 - x$, $1/(n\mathfrak{D}_n)$ can be reformulated as :

$$\frac{1}{n\mathfrak{D}_n} \simeq (4\nu-3)n\rho_b^{4n}\left[1-\frac{\left[8\nu(3-2\nu)-(n^2+8)\right]\rho_b^{2n+2}+2(n^2-1)\rho_b^{2n}-n^2\rho_b^{2n-2}+(4\nu-3)}{(4\nu-3)\,\rho_b^{4n}}\right]$$

(5.3.2.4)

As a result of (5.3.2.4), $a_n + b_n + c_n + d_n$ can be expressed as the product of two parts, the first referring to the numerator of the sum of the series coefficients, and the second dealing with (the reciprocal of) its denominator. Such parts can be studied separately with regard to their asymptotic behaviours. In other words, their "asymptotic series" can be evaluated, and this procedure can be repeated (see Chapter 4, Section 4.3.2) to obtain the following equivalent asymptotic expression :

$$a_n + b_n + c_n + d_n \simeq \left[\frac{4\,(1-\nu^2)}{n} + \frac{2\,(1+\nu)\,(1-2\nu)}{n^2} + \frac{4\,(1-\nu^2)}{n^3}\right]$$

$$\left[1 - \frac{(\rho_b^2-1)^2\,n^2}{(3-4\nu)\,\rho_b^{2n+2}} - \frac{8\,(1-\nu)\,(1-2\nu)\,\rho_b^2+2}{(3-4\nu)\,\rho_b^{2n}} - \frac{1}{\rho_b^{4n}}\right] \simeq$$

$$\frac{4\,(1-\nu^2)}{n}\left[1 - \frac{(\rho_b^2-1)^2\,n^2}{(3-4\nu)\,\rho_b^{2n+2}}\right] \qquad (5.3.2.5)$$

The series having as generic terms those of the last expression of (5.3.2.5), once multiplied by $\cos(n\,\theta)$ (see (5.3.2.1)), are summable, a condition necessary for the application of Kummer method (Gradshteyn and Ryzhik (1979), p. 38 , and Guarnieri (1965), p. XI.1 , formula (11.1) via differentiation) :

$$\sum_{n=1}^{\infty} \frac{\cos(n\,\theta)}{n} = -\frac{1}{2}\log(2-2\cos\theta)$$

$$\sum_{n=1}^{\infty} n\,a^n \cos(n\,\theta) = \frac{a\cos\theta\,(1+a^2)-2\,a^2}{(1-2\,a\cos\theta+a^2)^2} \qquad (5.3.2.6)$$

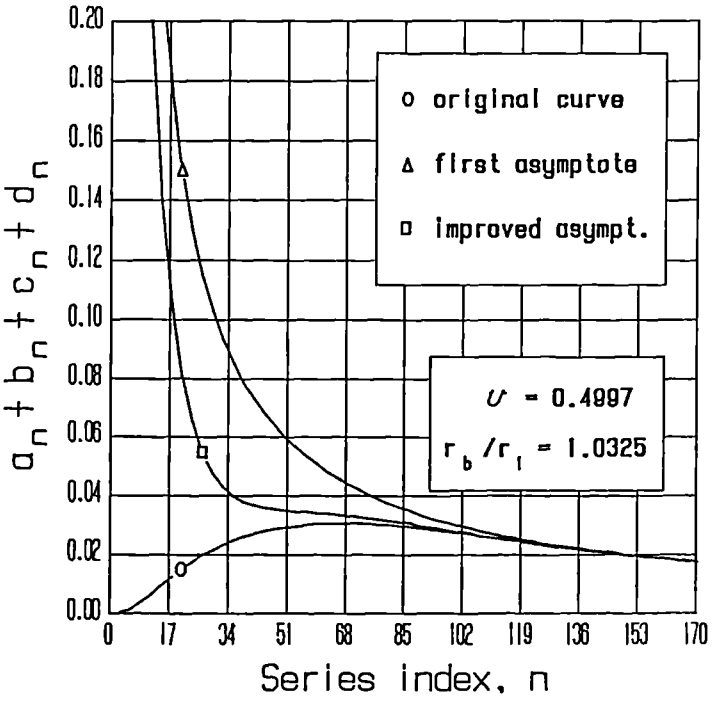

Fig. 5.3.2.3 : Convergence of series terms for r_b / r_i = 1.0325 .

Contrary to (5.3.2.2), the asymptotic expression (5.3.2.5) now accounts for ρ_b . Fig. 5.3.2.3 displays $a_n + b_n + c_n + d_n$ together with the first asymptotic term according to (5.3.2.2) and the final asymptotic expression of (5.3.2.5). It appears that, even if the improved asymptote is more accurate, it does not noticeably lower the number of series terms to get good accuracy (n passes from about 120 to about 100). The following TABLE summarizes the relative errors as functions of the series index, n, the geometric factor, ρ_b, and the Poisson's ratio, ν . It can be concluded that, if high accuracies are needed, the more complex acceleration technique based on (5.3.2.5) is no longer advantageous, whereas the simplest formula of (5.3.2.2) is preferable. Now, the literature review of Section 5.2 indicates that ill conditioning problems are often encountered, a problem which can be overcome by computing the series sums more exactly (Solecki and Ohgushi (1984)). As a consequence, the simplest acceleration method was mainly adopted in practice, even if it was experimented that, for the cases not affected by ill conditioning, the acceleration technique based upon (5.3.2.5) achieved considerable computer time

savings.

TABLE

reporting the relative error between exact and asymptotic terms

	first asymptote of (5.3.2.2)	last asymptote of (5.3.2.5)
$\rho_b = 1.0325$, $\nu = 0.4997$		
error after 100 terms	6 percent	1.5 percent
error after 130 terms	1.6 percent	0.4 percent
error after 160 terms	0.1 percent	0.1 percent
$\rho_b = 1.0325$, $\nu = 0.3$		
error after 100 terms	6 percent	1.2 percent
$\rho_b = 1.2$, $\nu = 0.4997$		
error after 30 terms	0.1 percent	0.1 percent

A further observation is developed hereinafter. Since the problem of a deformable layer indented by a rigid cylinder is addressed, the unknown pressure profile will be approximated with a piecewise constant pressure profile. The layer displacement due to a uniform pressure profile straddling θ origin and acting along an arc of angular width 2α is expressed by integrating (5.3.2) term by term with respect to θ . So doing, series terms including $sin\ (n\theta)/n$ are obtained, thus introducing a further n element at the denominator and, consequently, strengthening the series convergence. The behaviour of the asymptotic expressions according to (5.3.2.2) (expressions (5.3.2.5) are not employed according to the above critical

remarks) is examined for this case of uniform pressure applied to an arc of amplitude 2α in Figs 5.3.2.4 and 5.3.2.5 , referring to the same ρ_b of Figs 5.3.2.2,3 . It appears that, despite the improved series convergence, a considerable number of terms are needed to achieve a good precision of the asymptotic terms, that is, to get a sufficient accuracy in the evaluation of the series sum, even in the case of distributed loads. The exact number of series terms needed to avoid ill-conditioning will be clarified by numerical tests referring to the cylindrical indenter problem.

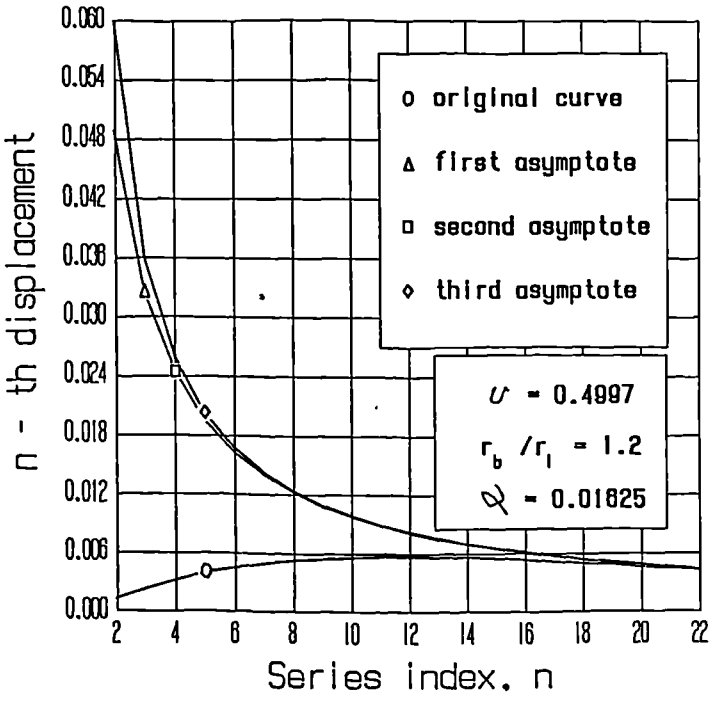

Fig. 5.3.2.4 : Convergence of series terms for a distributed load and for r_b / r_i = 1.2 .

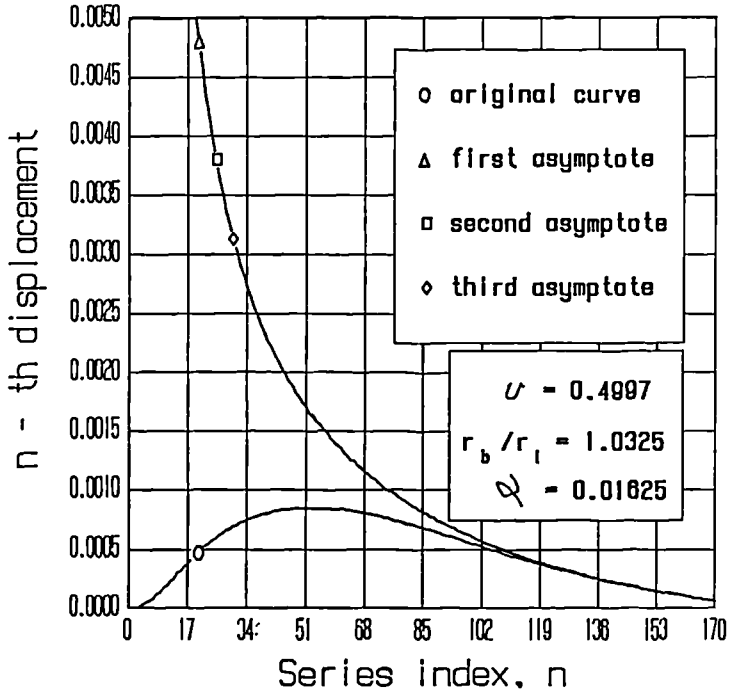

Fig. 5.3.2.5 : Convergence of series terms for a distributed load and for $r_b / r_i = 1.0325$.

5.3.3 Numerical program

The numerical program developed for the mechanical analysis of a curved deformable layer firmly bonded to a rigid foundation and indented by a rigid cylinder is similar to that developed in Chapter 4. There the contact pressure was approximated by a piecewise linear distribution, whereas now a simpler piecewise constant profile is adopted (Conway and Farnham (1968a)), to counterbalance the more complex equations encountered for curved linings. A relaxation procedure (Chapter 4) is employed to define the contact width and to solve the discretized problem. The indentation depth distribution, $\delta(\theta)$, is computed from the knowledge of the maximum indentation depth, δ_o , of the layer loaded radius, r_l , and of the indenting cylinder radius, r_c . Fig. 5.3.3.1 hopefully clarifies these symbols, and shows that $\delta(\theta)$ has been measured perpendicularly from the circumference of radius r_l , consistent with Section 4.3.3 of Chapter 4, where the distance between the compressed border of the elastomeric layer and the rigid indenter has been taken normal to the layer contour.

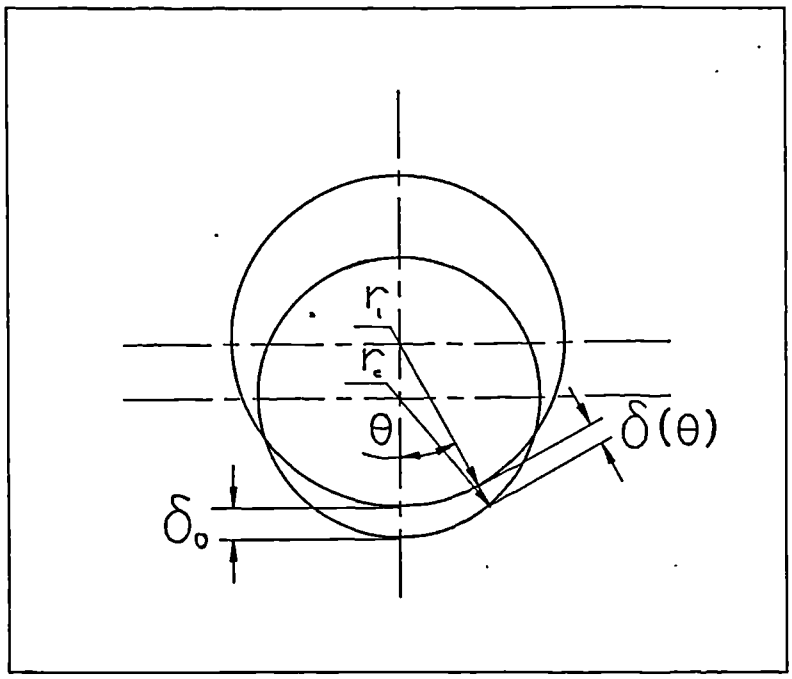

Fig. 5.3.3.1 : The meaning of symbols r_c , r_l , θ , δ_o and δ (θ).

(An alternative measure of $\delta(\theta)$ could have been assumed as perpendicular to the indenting cylinder radius, but the resulting pressure differences would have been in common circumstances a second order effect.)

The calculations to express $\delta(\theta)$ are similar to those of Dragoni and Strozzi (1986), and the following result is obtained in the case of a rigid cylinder indenting a curved layer bonded to a cavity :

$$\delta(\theta) = -r_i(1-\cos\theta) - (r_c - \delta_o)\cos\theta + \sqrt{r_c^2 - (r_i + \delta_o - r_c)^2 \sin^2\theta} \qquad (5.3.3.1)$$

Minor variations are needed to treat the situation of a rigid cylindrical indenter pressing a rigid cylinder covered with an elastomeric layer.

5.3.4 Selected numerical results

Curves for the indentation problem as general as those of Chapter 4 are not possible in the case of curved layers, because three radii, namely r_t , r_b , r_c and, therefore, two normalized ratios now define the geometry. As a consequence, the numerical results developed in this thesis refer to the numerical solution of the indentation by a cylindrical punch, and they mainly address the corresponding experimental configurations examined. The numerical forecasts are presented in Section 5.4.2 together with the experimental measurements. For the time being, selected numerical predictions obtained with the program of Section 5.3.3 are reported, aimed at a) validating the numerical program; b) retrieving information about the number of series terms sufficient to avoid ill-conditioning; c) assessing the influence of the layer curvature on the stress profile versus the available technical information.

First, reference is made to Fig. 3 of Solecki and Ohgushi (1984), and the contact is examined between a rigid cylinder of radius r_b = 176.35 mm , covered with an elastomeric layer 3.302 mm thick (so that r_t = 79.652 mm) , having a Young's modulus E = 3.004 MPa and a Poisson's ratio ν = 0.5 (the figure adopted for ν is not reported by Solecki and Ohgushi (1984), but is indicated by Miller and Poulter (1962), p. 44, from which the experimental results reported by Solecki and Ohgushi (1984) are extracted) and indented by a rigid cylinder of radius r_c = 76.35 mm . Penetrations up to 0.2 mm are imposed in this thesis, and the resulting repulsive load is computed. The forecasts in terms of contact force versus indentation depth are summarized in Fig. 5.3.4.1 . The curved layer predictions of the present author (referred to in the inset as "theor. Strozzi") are compared to the experimental (curved layer) and theoretical (flat layer) results of Miller and Poulter (1962), to the theoretical predictions of Solecki and Ohgushi (1984) (curved layer) and, finally, to the analytical forecasts referring to a flat layer indented by a cylinder of equivalent radius of 38.983 mm (the equivalent radius is computed via the classical formula referring to a parabolic approximation for the cylindrical profile, see Johnson (1985), p. 427 ; Miller and Poulter (1962), quote the same formula at their p. 41 , so that they should have used the same equivalent radius in their calculations),

examined with the theory of Chapter 4 and referred to in the inset as "theor. flat layer".

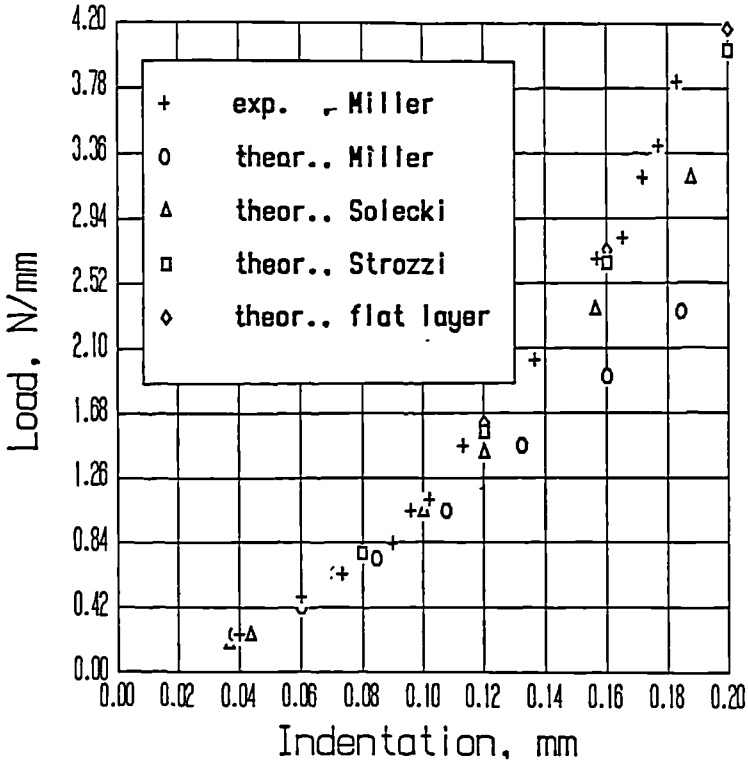

Fig. 5.3.4.1 : Compression force versus indentation depth .

It immediately appears from Fig. 5.3.4.1 that the theoretical forecasts of Miller and Poulter (1962) considerably deviate from all the other results reported. In particular, they show a relative error of about 30 percent with respect to the analytical forecasts according to Chapter 4 (flat layer), for an indentation depth of 0.16 mm. Since both these data refer to a straight layer geometry, these differences cannot be attributed to curved layer effects. In addition, since the straight layer solution of this author has been validated in Chapter 4 for comparable situations, it must be concluded that the exactness of the analytical forecasts of Miller and Poulter is questionable.

There is also a perceivable difference between the theoretical forecasts of Solecki and Ohgushi (1984) (referred to in the inset as 'theor. Solecki') and those of this Chapter (referred to in the inset as "theor. Strozzi"), both referring to curved layers. For an indentation depth of about 0.16 mm , the relative error is about 11

percent. Instead, the agreement is good among the experimental readings by Miller and Poulter (1962), and the analytical forecasts referring to flat or curved layers, due to the present author.

The small deviation between Solecki and Ohgushi (1984) predictions and Strozzi forecasts, both referring to curved layers, is tentatively attributed to discretization effects. The present author uses 50 finite elements, whereas Solecki and Ohgushi (1984) employ 20 Fourier terms. Finally, the good degree of agreement among the experimental reading by Miller and Poulter (1962) and the straight and curved layer analytical solutions by the present author indicates that the curvature effects are small for the geometry explored.

For the same geometry and elastic constants of Fig. 5.3.4.1 , the peak contact pressure is reported in Fig. 5.3.4.2 again as a function of the indentation depth, with reference to the curved layer theory developed in this Chapter, and to the flat layer modelling (indented by a cylinder of equivalent radius) according to Chapter 4 . In addition, the curved layer theory of this Chapter was used to mimic a straight layer of the same thickness, by adopting a high figure for the bonded radius, r_b = 1000 mm , from which the loaded radius is derived by adding the layer thickness, r_t = 1003.302 mm , whereas the radius of the indenting cylinder is computed from the request that the equivalent radius (see previous remarks) is again 38.983 mm , thus implying r_c = 40.5589 mm . This idealization is referred to in Fig. 5.3.4.2 as "equivalent flat layer". Finally, the incompressible layer asymptotic solution (Armstrong (1986)) is also included in Fig. 5.3.4.2 , shortly named in the inset "incompressible layer".

Not surprisingly, the asymptotic incompressible solution is totally inaccurate at the low indentations imposed, consistent with the lucid observations of Meijers (1968), p. 354 : "the asymptotic solution holds for very large values of c/b only", where c denotes the semicontact length and b indicates the layer thickness in Meijers (1968) paper. The small deviation between equivalent flat layer and flat layer solution (about 4 percent for δ = 0.2 mm) is possibly ascribable to the approximations inherent in the analytical Green function developed in Chapter 4 and to discretization effects (see the TABLE of Section 4.3.4). In any case, the approximations of the curved layer and equivalent flat layer solutions are exactly

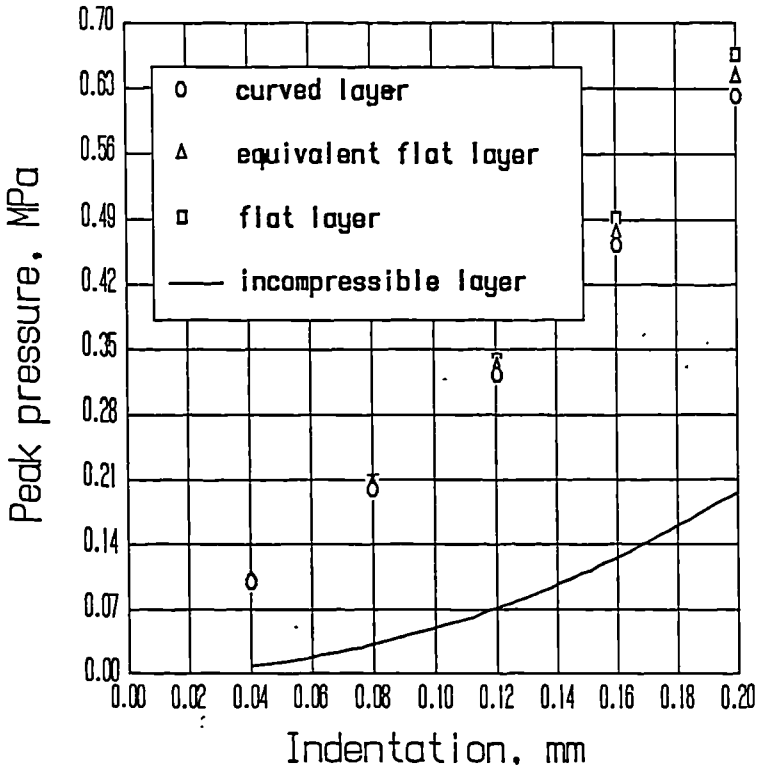

Fig. 5.3.4.2 : Peak contact pressure versus indentation depth .

the same and, consequently, it can be confidently speculated that the small differences between these two solutions are attributable to curvature effects. The equivalent flat layer model produces peak pressures slightly higher (about 3 percent for δ = 0.2 mm) than its curved layer counterpart.

It was also decided to examine the curvature effects for higher layer thicknesses and penetration depths. The same figure as before was taken for the bonded radius : r_b = 76.35 mm . The layer thickness was assumed of 15 mm - about 20 percent the bonded radius, consistent with the highest layer thicknesses employed in biomechanical applications, Section 5.1 - and, consequently, the loaded radius becomes r_l = 91.35 mm , whereas the radius of the indenting cylinder was kept as before, r_c = 76.35 mm . The indentations prescribed reached 10 mm . The elastic constants were left unchanged, E = 3.004 MPa , ν = 0.5 . Four peak pressure forecasts referring to this geometry and to different models are displayed in Fig. 5.3.4.3 . The peak pressure according to the curved layer model of this Chapter is reported together with the flat layer modelling of Chapter 4 with an equivalent radius of 41.5896 mm (as in Figs 5.3.4.1,2 , the parabolic approximation has been

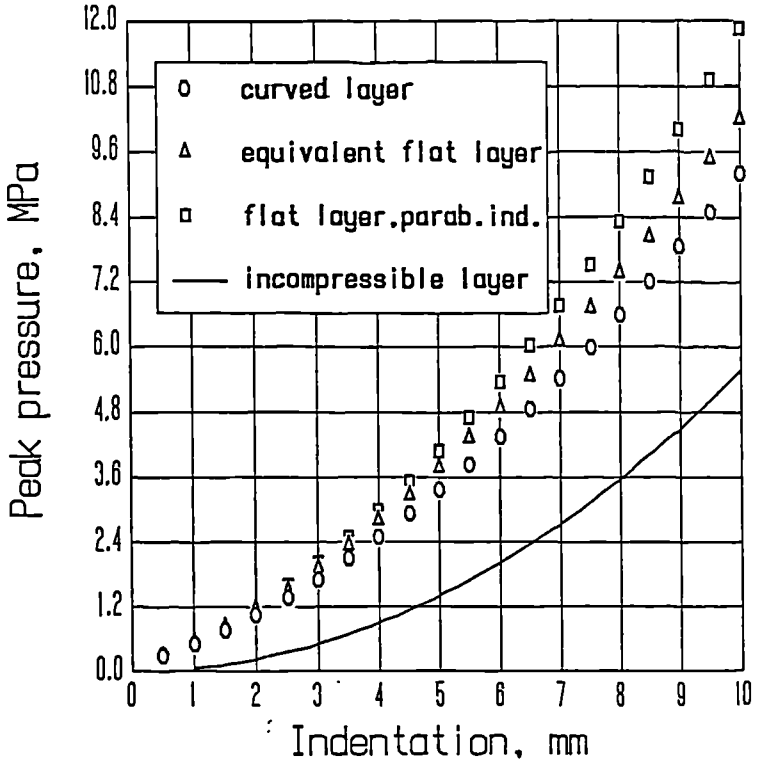

Fig. 5.3.4.3 : Peak contact pressure versus indentation depth .

assumed for the indenter profile pressing the straight layer), together with the equivalent flat layer previsions for r_b = 1000 mm , r_t = 1015 mm , r_c = 43.3665 mm (computed from Johnson (1985), p. 427 formula, so that the equivalent radius equals 41.5896 mm), and with the asymptotic incompressible layer (Armstrong (1986)) predictions, here referred to as "incompressible layer" for short.

As in Fig. 5.3.4.2 , the asymptotic solution in Fig. 5.3.4.3 is totally inaccurate. The curved layer pressure is lower than its equivalent flat layer analogue, consistent with Fig. 5.3.4.2 (for an indentation of 10 mm , there is a difference of 11 percent). The flat layer and the equivalent flat layer models should provide equal results, whereas their difference in Fig. 5.3.4.2 is limited for penetrations up to 5 mm - the error is 7.6 percent - but the mismatch becomes a disturbing 16 percent for δ = 10 mm. It was, therefore, decided to analyze in some detail the reasons of this unexpected discrepancy. First, the flat layer approach of Chapter 4 refers to a parabolic approximation for the indenting cylinder. In many circumstances this approximation does not produce appreciable errors, but for the geometry under scrutiny, characterized by high layer thicknesses and penetration

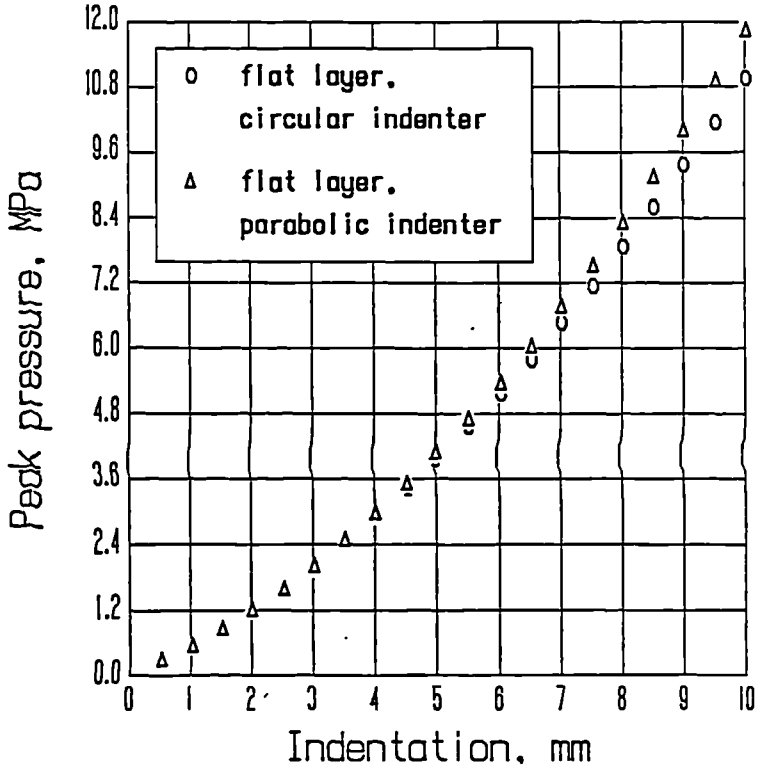

Fig. 5.3.4.4 : The differences in peak pressures between parabolic and circular indenter profiles .

depths, the consequences of this indenting profile error are appreciable. Fig. 5.3.4.4 reproduces the two peak contact pressures referring to the flat layer model of Chapter 5 and to an indenting radius of 41.5896 mm , both for a circular indenting profile and for its parabolic approximation. The error at the maximum penetration depth, δ = 10 mm , is about 8 percent, whereas it is negligible (about 3 percent) for δ lower than 5 mm.

Since the equivalent flat layer is still based upon a circular description of the indenting cylinder (Fig. 5.3.3.1), Fig. 5.3.4.3 was replotted by referring this time to a circular indenter in the flat layer modelling, thus obtaining Fig. 5.3.4.5 . This time the error between flat layer and equivalent flat layer - both now referring to a circular profile for the indenter - is 5 percent for δ = 5 mm , and for δ = 10 mm it becomes an acceptable 7.3 percent, whereas the (physically meaningful) difference between curved and equivalent flat layer is 13 percent for δ = 5 mm , and 11 percent for δ = 10 mm .

It should also been underlined that the application of the formula for the equivalent radius (Johnson (1985), p. 427) is questionable, especially because the

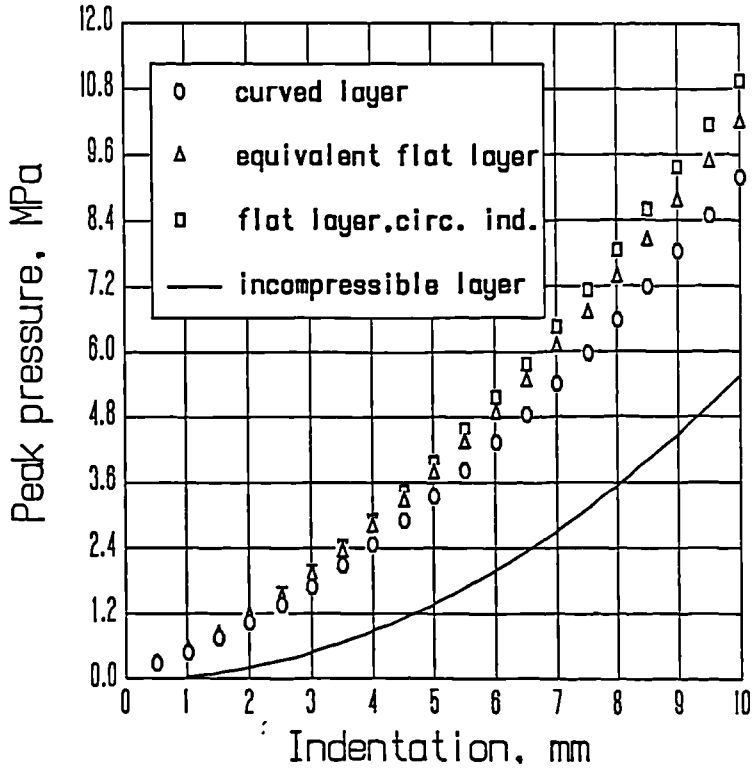

Fig. 5.3.4.5 : Fig. 5.3.4.3 replotted by considering a circular indenter .

equivalent radius is computed according to a parabolic approximation, and the cylindrical radius of the indenter (that adopted for the flat layer pressed by a circular indenter in Fig. 5.3.4.5) is again based upon this inevitably inaccurate idealization, just when the effects of the indenter profile on the contact pressure are to be examined. In other words, the aforementioned inaccuracies might, at least partially, account for the differences between flat and equivalent flat layer solutions of Fig. 5.3.4.5 . In addition, the equivalent flat layer is still slightly curved, thus involving some inevitable, although supposedly small, degree of approximation.

It was also decided to assess the curvature effects for the geometry of a rigid cylinder indenting a rigid cylindrical cavity covered with a curved elastomeric layer. This configuration is analogous to those encountered in biomechanical applications and, therefore, it is particularly relevant.

The radius for the indenting cylinder was r_c = 61 mm , that for the cylindrical cavity was r_b = 76.35 mm , and the layer thickness was 15 mm , as in Figs 5.3.4.3,4,5 , so that r_i = 61.35 mm . The elastic constants were kept as before,

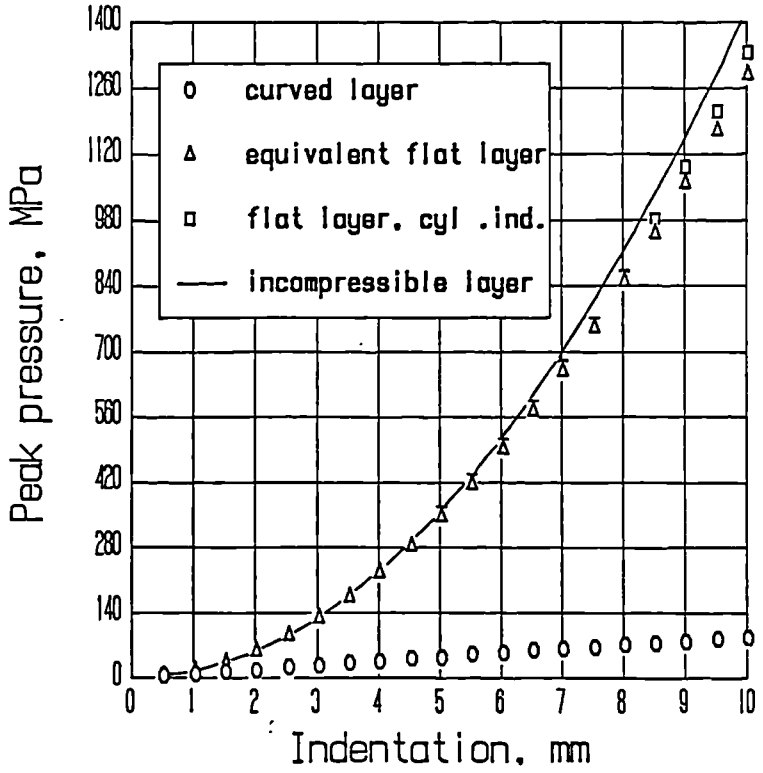

Fig. 5.3.4.6 : Peak contact pressure for curved and flat layers .

E = 3.004 MPa , ν = 0.5 . Fig. 5.3.4.6 presents the curved layer solution of this Chapter together with the flat layer forecasts according to Chapter 4 (the equivalent radius is 10692.4286 mm) and referring to a cylindrical (as opposed to parabolic) indenting profile, together with the equivalent flat layer (that is, the curved layer solution of this Chapter is employed to mimic a flat layer, by selecting r_b = 1000 mm , r_t = 985 mm and r_c = 901.9145 mm , so that the equivalent radius is still 10692.4286 mm), and together with the asymptotic solution for the incompressible layer, denoted in the inset "incompressible layer" for short.

Fig. 5.3.4.6 reveals that the flat layer, the equivalent flat layer and the asymptotic solution produce comparable peak contact pressures, whereas the curved layer predictions are unexpectedly much lower, of the order of one tenth the other figures. The first impression is that the curved layer solution of this Chapter is wrong, but a deeper investigation, whose results are illustrated in the follow-up, sheds light into the causes of the above-signalled discrepancy, and it further supports the correctness of the curved layer solution of this Chapter.

First, it was clarified that the disagreement between flat and curved layer

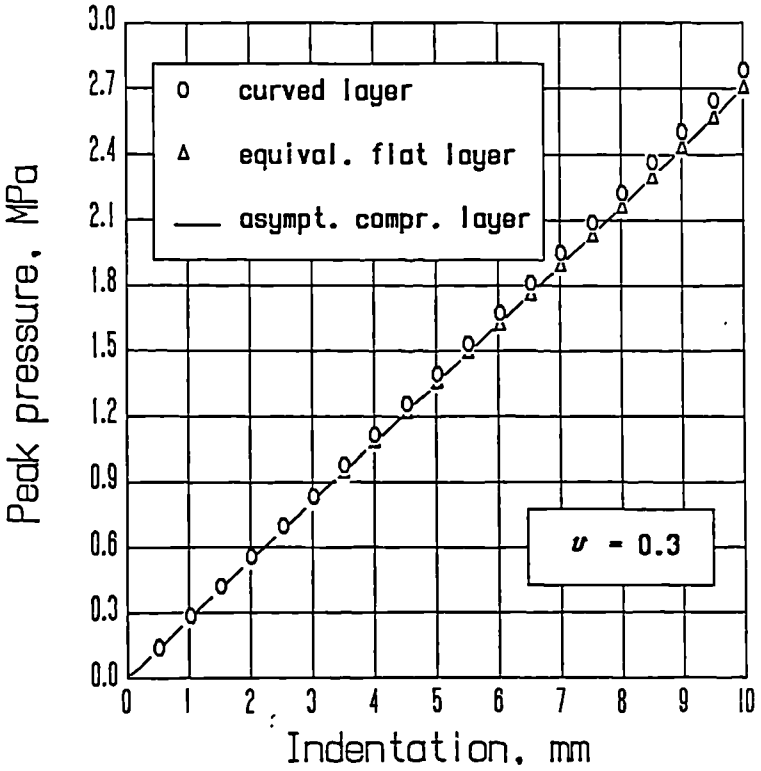

Fig. 5.3.4.7 : Peak contact pressure for curved and flat layers, for low Poisson's ratios.

forecasts immediately vanishes when lower Poisson's ratios are adopted for the layer elastomer. Fig. 5.3.4.7 reports the peak contact pressure for ν = 0.3 and for the curved layer, the equivalent flat layer and the asymptotic solution (the flat layer model of Chapter 4 could not be employed this time because it does not cover Poisson's ratios lower than 0.46 , see Section 4.3.2). The curved and flat layer forecasts are essentially superimposed to the asymptotic (this time compressible) analytical solution. It also appears that the peak pressure varies linearly with the prescribed indentation. In fact, when the compressibility of the layer is sufficiently high, the layer material moves radially more than laterally as a result of the indenter compression, a mechanism typical of Winkler models (Kerr (1964)) which are consistent with a linear pressure-indentation relationship (Armstrong (1986)). In conclusion, in the case of compressible materials the curved layer theory of this Chapter supplies correct results.

Secondly, in the interest of clarity, the region of Fig. 5.3.4.6 referring to low indentation depths was enlarged in Fig. 5.3.4.8 , which covers δ figures up to 1 mm . It clearly emerges that the curved layer peak pressure deviates from the other forecasts for indentations higher than 0.3 mm , thus supporting the suspicion

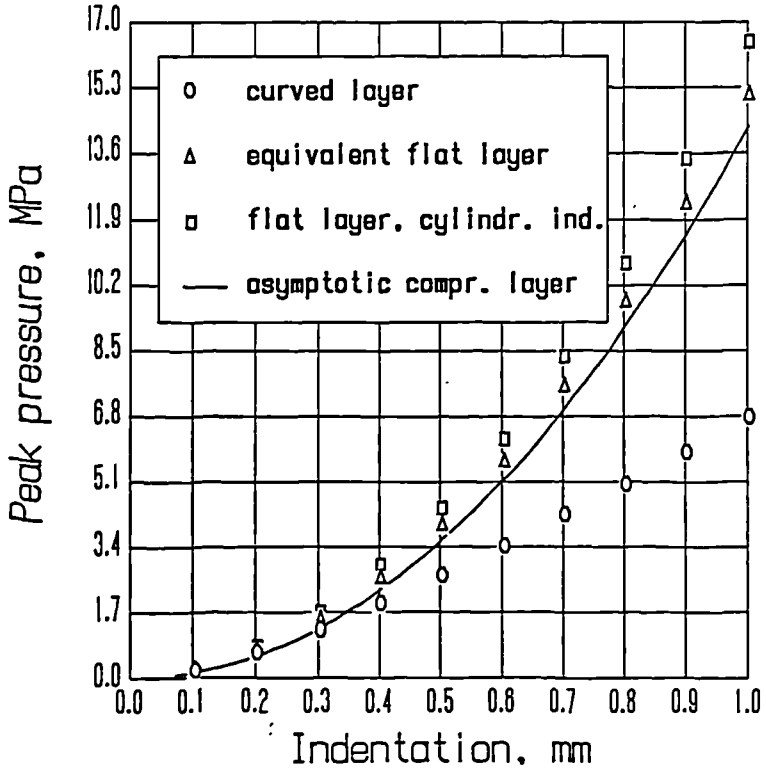

Fig. 5.3.4.8 : Peak contact pressure for curved and flat layers, for low indentations .

that some underestimated effects become dominant for high penetrations. It was, therefore, decided to examine the angular semicontact width as a function of the compression depth for the same conditions of Figs 5.3.4.6 and 5.3.4.8 (incompressible elastomer). The corresponding results are displayed in Figs 5.3.4.9 (δ up to 10 mm) and 5.3.4.10 (enlargement of the previous Figure for δ up to 1 mm), respectively. These two Figures reveal that a) the angular semicontact width (with respect to the centre of the indenting cylinder, see Fig. 5.3.1) becomes higher than $\pi/2$ for δ as low as 0.3 mm , which constitutes a limit figure beyond which the circular layer (annulus) solution is unrealistic, since in biomechanical applications only a half annulus exists (*e.g.* cups in hip joints) and, therefore, the angular semicontact width is inevitably lower than $\pi/2$; b) the angular semicontact width reaches a plateau of about 2.7 radians for indentations higher than 3 mm , in contrast with the flat layer forecasts, characterized by a contact width progressively increasing with compression (see asymptotic solutions, Armstrong (1986)). This second observation clarifies that the curved layer solution cannot behave as the flat layer modelling for high penetrations, since the two contact widths become completely different. In the case of scarcely compressible elastomers, the peak pressure highly depends upon

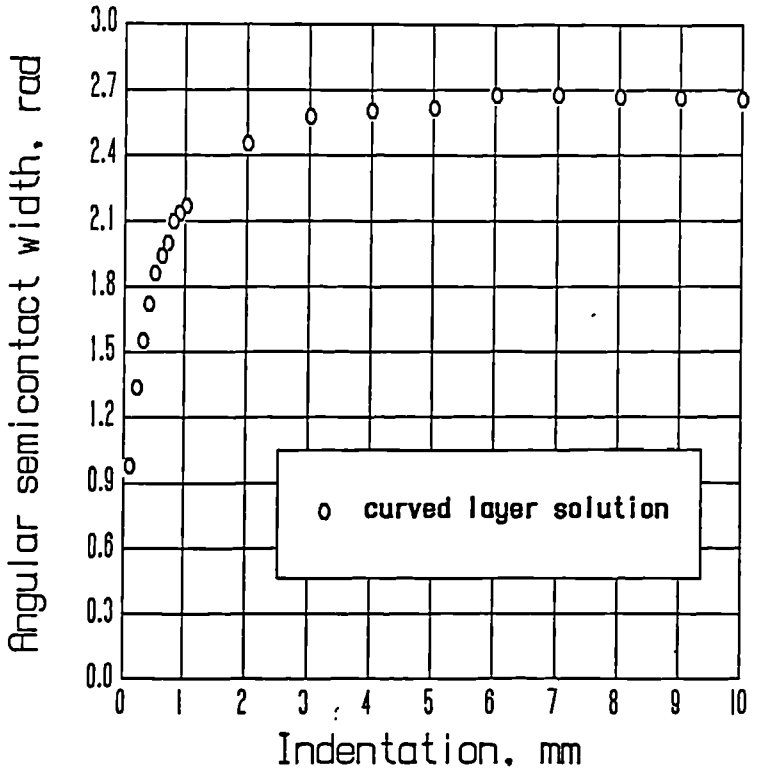

Fig. 5.3.4.9 : Angular semicontact width versus indentation for a curved layer .

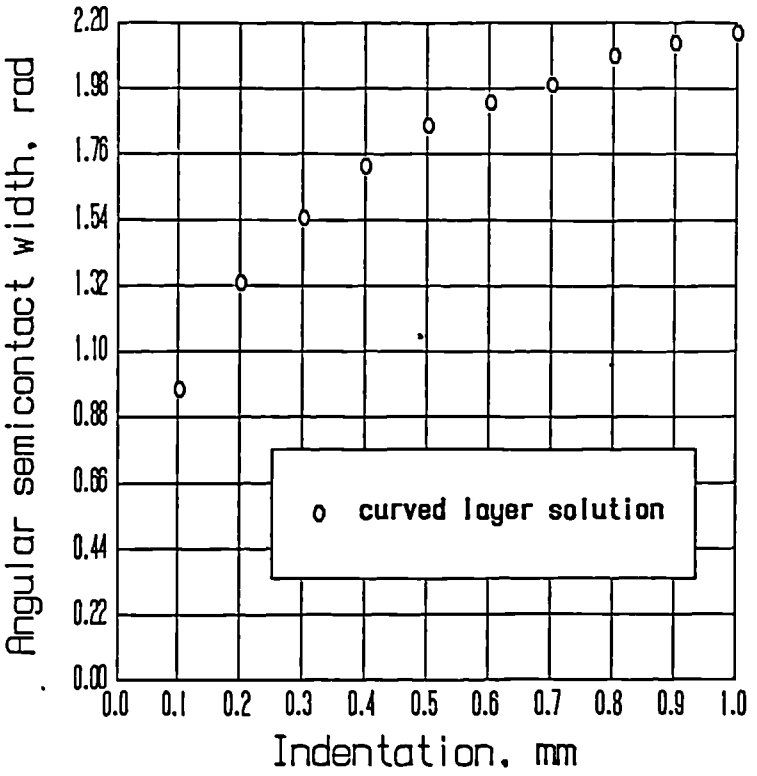

Fig. 5.3.4.10 : Angular semicontact width for a curved layer and low indentations .

the whole indentation distribution (see the results of Meijers (1968), p. 375, after his formula (5.4)). In other words, a modification of the contact width may well result in considerable alterations for the peak pressure, as it occurs in the situation under examination. Conversely, the error on the contact width is not relevant for low values of the Poisson's ratio, when a Winkler foundation model is applicable and, therefore, the peak pressure depends mainly upon the peak compression and not upon the contact width (see the asymptotic formulae for the compressible layer in Armstrong (1986)). The numerical results of fig. 5.3.4.8 clarify the transitional figure of the indentation depth beyond which the flat layer solution is no longer applicable.

It is finally observed that a parabolic description of the indenter profile should be more acceptable in the case of two contacting cylinders than in the situation of a cylinder compressing a cylindrical cavity, since in the first geometry the contact width is smaller for a prescribed penetration depth. This aspect has not been addressed in detail in this thesis.

Before leaving this Section, a concise answer is given to the three questions posed at its beginning: a) the selected results here presented support the correctness of the curved layer solution ; b) the number of series terms sufficient to avoid ill-conditioning ranges between 50 and 100 for most applications ; c) the curvature effects are identifiable in the case of a cylinder indenting a cylinder covered with an elastomeric layer, whereas for the situation of a cylinder indenting a circular cavity covered by a curved layer the curvature effects are masked by those connected to contact width aspects, previously discussed.

With regard to point b) , it is further underlined that a series acceleration technique is employed in this study, which reduces the number of series terms to be actually computed, with the help of an asymptotic series (Section 5.3.2). It was numerically found that the series index capable of preventing ill-conditioning is that for which the series term approaches its asymptotic counterpart by less than 10^{-10} , and this index is often in the region between 50 and 100 .

5.4 EXPERIMENTAL RESULTS

This Section deals with the description of the experimental apparatus developed to measure the pressure profile and contact width for plane cases mimicking geometries of practical relevance in biomechanical applications. The experimental readings obtained are then compared to the numerical predictions according to Section 5.3.3 of this Chapter.

5.4.1 The experimental device

The experimental device developed by the present author is an adaptation of a device which was previously employed to estimate the stress state in plane strain models of elastomeric seals (Strozzi (1986)). The reading technique is based upon the "compensation method" or "Muller method" (May (1957), Kawahara, Ohtake and Hirabayashi (1964), Wendt (1971)), commented *in the following.*

The device is sketched in Fig. 5.4.1.1 . It consists of a metal plane model of a head of an artificial hip joint (scale 3:1), Fig. 5.4.1.2 , through which eleven adjacent, 4 mm diameter holes are drilled. The pitch between the axes of the contiguous holes is 6.5 mm. The final part of the holes has a reduced diameter of 1.5 mm , and it is inclined with respect to the hole axis, so that its angular pitch is constant, and equal to 10° . The top part of the head plane model is connected to a metal, horizontal, sliding, loading bar, to which the desired head penetrations are imposed by turning two screws. The resulting indentations are read with a micrometer (gauge) having a precision of 1/100 mm . The model head compresses an elastomeric strip (polyurethane elastomer, Hysol CP 4485, Young's modulus = 3.52 MPa and Poisson's ratio in the region of 0.4997, an elastomer exhibiting material constants close to the actually employed material, see Chapter 3) glued to a metal plane model of the cup, whose angular extent is nearly π . (More precisely, the angular width is slightly less than π , so that the distance between the centre of the cup and the line connecting the two extremities of the layer is 3 mm.) The whole plane model of the hip joint is placed between two 20 mm thick, parallel Perspex

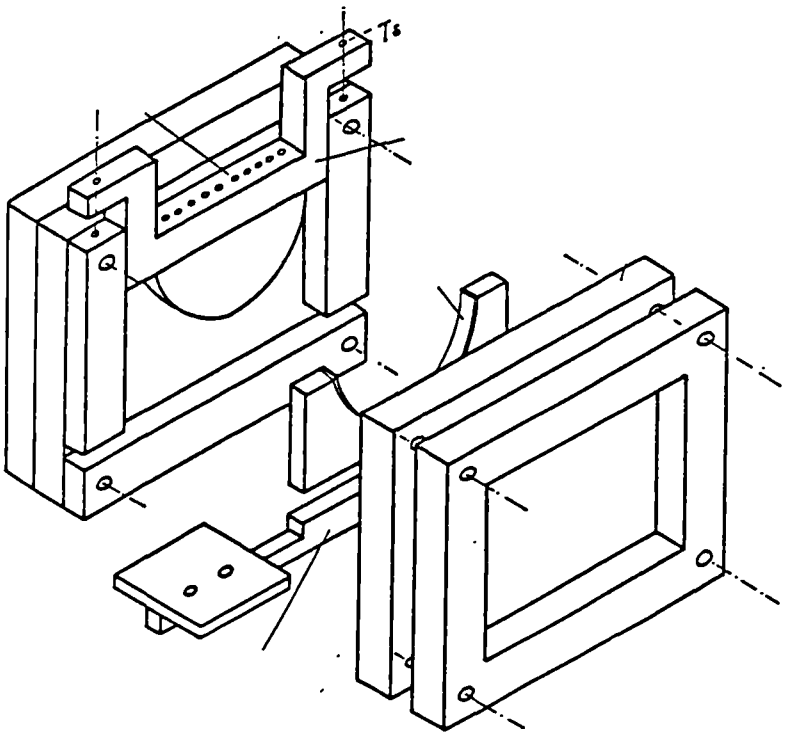

Fig. 5.4.1.1 : The experimental device .

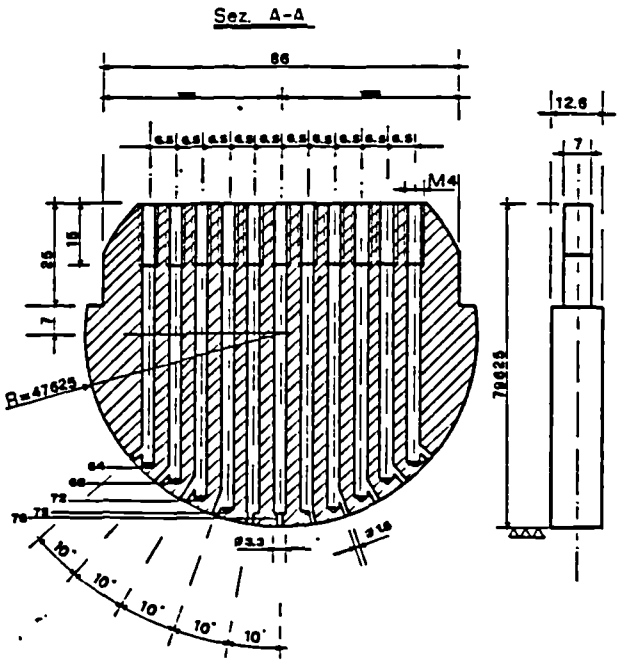

Fig. 5.4.1.2 : The flat model of the head with the pressurised holes .

plates to preclude any lateral displacements of the elastomeric layer, thus achieving a plane state of strain which approximately mimics an axisymmetric situation (Barton (1941)). In Dragoni and Strozzi (1988) it was verified that the lateral deformations of the Perspex plates are limited, and that they do not significantly undermine the correctness of the measurements. The contact zone between head model and elastomeric strip is lubricated to limit the frictional effects, essentially absent in operating conditions, due to the presence of the synovial fluid.

In order to measure the contact pressure profile, the holes are progressively and sequentially pressurized with air until the fluid begins to leak. The corresponding contact pressure is approximately equal to the pressure for which the air begins to leak. The resolution of the pressure gauge is in the region of 0.2 atmospheres (0.02 MPa), but the precision of the device is obviously lower, due to the difficulty in detecting the very first moment in which the pressurized air begins to leak. This precision is estimated to be in the region of 0.3 MPa , as suggested by the scattering of the experimental data. The pneumatic circuit tolerates a maximum pressure of about 50 atmospheres (5 MPa) . Fig. 5.4.1.3 shows the experimental device in operating conditions.

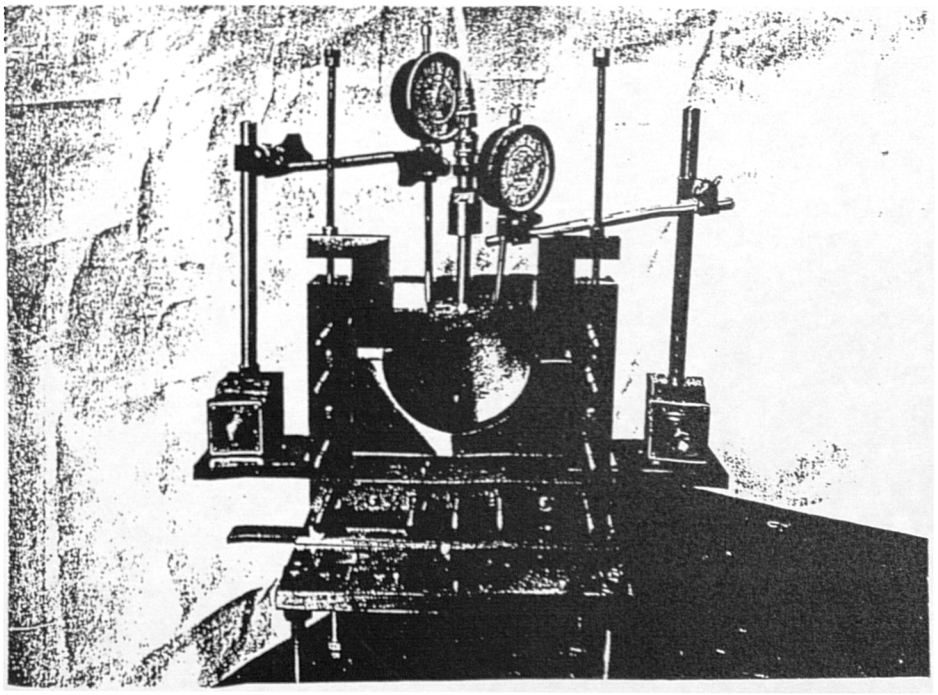

Fig. 5.4.1.3 : The experimental device in operating conditions .

The radius of the head model is of 47.625 mm, whereas four different elastomeric layers are considered, 1.55 mm, 3.15 mm, 6.44 mm and 9.49 mm thick, respectively. They are glued to four plane models of the cup cavity having a radius of 49.875 mm, 51.375 mm, 54.375 mm and 57.375 mm, respectively. These figures approximately exhibit a scale ratio 3:1 versus the actual hip joints, which are defined by a head diameter of 31.75 mm, and by three layer thicknesses of 0.5 mm, 1 mm, 2 mm and 3 mm, where the initial diameter clearance between head and loaded surface of the layer is always 0.5 mm (see Section 7.3.2). The main approximation is inherent in the elastomeric layer thickness, which is not exactly to scale; as a consequence, the initial radial gap between head model and layer loaded surface is out of scale (it should be 0.75 mm). With regard to this point, it should be underlined that the aforementioned gap significantly influences the pressure profile, so that the experimental results retrieved do not exactly correspond to the stress state they want to mimic. Indeed, a high surface finish of the elastomeric layer was favoured to the detriment of its thickness precision. Despite these approximations, the experimental readings still constitute a significant benchmark for the analytical previsions.

The notes which follow examine if the maximum tolerated pressure (5 MPa) is consistent with a load applied to the actual joint of about 2000 N (see Sections 4.3.4 and 7.3.2). The hip joint is to scale 3:1 , but the stresses in the elastomeric layer of the model must be the same as those in the real joint, since the material and geometrical non-linearities preclude a scaling of the stress field. Additional difficulties derive from the fact that the model is plane, while the actual geometry is axisymmetric. The total force, P , in an ideal axisymmetric version of the hip model exhibiting a peak pressure of 5 MPa can be roughly estimated as half the peak pressure (understood as a gross mean for the contact pressure) by the projected area of the head (since the angular contact width approaches π) :

$$P \simeq \frac{5}{2} \pi \, 47.625^2 \simeq 18000 \text{ N}$$

This force corresponds to 2000 N in a three times smaller joint, as is the actual joint. In performing this estimate, it has implicitly been assumed that the

plane and axisymmetric contact pressure profiles are similar. This point has already been discussed in Section 4.3.4 , on the basis of the results of Section 6.5.2 , which suggest a certain similarity between plane and axisymmetric modellings (for a given indentation depth, the two peak pressures possess the same order of magnitude). In conclusion, the limit value for the maximum applicable pressure (5 MPa) still imposes realistic loads in the region of twice the body weight, which are encountered during walking (Kilvington and Goodman (1981)). It should be however underlined that the loads sustained by the joint during running can reach ten times the body weight (Paul (1976)), a figure which cannot be mimicked with this device.

Critical remarks on the applicability of the reading technique here employed are reported by Strozzi (1986a,b), by George, Strozzi and Rich (1987), and by Dragoni and Strozzi (1987,1988). The good degree of agreement between experimental measurements and theoretical predictions emerging from the previously quoted papers supports the reliability of the measurements also for the configuration under scrutiny. In any case, the agreement between theory and experiments when treating elastomeric units is generally worse than that achieved when dealing with metal components, with regard to displacements (Lau and Jeans (1989)), loads (Matthewson (1981)) and stresses (Dragoni and Strozzi (1988)). This becomes particularly true when a nearly hydrostatic stress state takes place in the elastomer, since small compressions produce high pressures, as a result of the small cubic compressibility of the material. Unfortunately, the elastomeric layer of the hip joint is subject to a nearly hydrostatic stress state (Matthewson (1981)). It can be concluded that the pressure measurements are more problematical in the case of conforming contacts (Paul and Hashemi (1981) ("conforming" describes two contacting profiles which are very similar, so that a high contact width is expected even for small indentation depths, thus originating a nearly hydrostatic state of stress in the elastomeric layer and a noticeable sensitivity of the stress field to perturbations of ν ; this situation is encountered in hip joints) than in the case of non conformal contacts, characterized by small contact widths, when the Poisson's ratio plays a less dramatic role (Chapter 4, Figs 4.3.5.1,5 , a situation encountered in rotary letterpress).

A point for concern is the determination of the head position which does not

cause any indentation, that is, the determination of the reference point for the penetration depth. In fact, the contact pressure is very sensitive to indentation depth variations, so that an inaccurate reference point may result in unreliable pressure readings. Three independent pressure measurements were made by taking as reference position that assumed by the head model under its own load. It was found that the repeatability of the measurements was acceptable and, therefore, no more complicated methods were devised to position correctly the ball model. Matthewson (1981) notes for a comparable problem that "the point at which the indenter first contacts the coating is extremely difficult to observe" and that "any error in this datum will be extremely significant". For a comparable case, Goodman and Keer (1965) find deviations between theory and experiments with regard to relative approach versus load at the lowest loads, "where the measurement of relative approach is at a minimum accuracy".

5.4.2 Experimental results and comparisons with the analytical predictions

As anticipated in Section 5.4.1 , three configurations were examined. Their relevant dimensions are collected in the following TABLE 5.4.2.1 .

TABLE 5.4.2.1

reporting the dimensions of head and curved layer for the four configurations

	first case	second case	third case	fourth case
head radius, mm	47.625	47.625	47.625	47.625
layer bonded radius, mm	49.875	51.375	54.375	57.375
layer loaded radius, mm	48.325	48.225	47.935	47.885
layer thickness, mm	1.55	3.15	6.44	9.49
initial radial gap between head and layer, mm	0.35	0.3	0.155	0.13

Four diagrams are presented for each case, reporting a) the peak contact pressure versus the indentation depth; b) the maximum shear stress at the interface between layer and foundation, and the angle at which the maximum shear occurs, versus the indentation depth; c) two pressure profiles for intermediate indentations. Figs 5.4.2.1,4 refer to the first configuration, Figs 5.4.2.5,8 to the second case, Figs

5.4.2.9,12 to the third geometry and Figs 5.4.2.13,16 to the fourth setting. The experimental readings (points) are reported together with the analytical predictions (solid lines), referring to E = 3.52 MPa and to ν = 0.49970 (see Chapter 3 , Section 2.3.4 ; the value for ν corresponds to the minimum hydrostatic pressure imposed, of 20.182 MPa). The agreement between theory and experiments is always reasonable (the maximum errors of the peak contact pressure are in the region of 30 percent for the interval explored, apart from the low compressions, where the sensitivity of the device may be responsible for higher mismatches), but it worsens in the first and third cases, where a) the layer thickness is very small and, therefore, the contact pressure is extremely sensitive to the indentation depth and to its errors; b) the initial gap between head and layer profiles is small, so that exiguous compressions produce high contact widths, producing sizeable nearly hydrostatic regions which are very sensitive to any inaccuracies. Moreover, the contact width becomes comparable with the angular extent of the curved layer, so that the layer end effects may become significant, while they are not reproduced by the theory. (The minimum initial gap actually occurs for the fourth configuration, but the high layer thickness compensates for the smallness of the gap, in the sense that the stress field should be less hydrostatic.) This second observation may partially rationalize the fact that the theoretical results often overestimate the experimental readings, and especially for the highest compressions. In fact, the ability of the elastomer to flow laterally as a result of the head compression is enhanced by the finiteness of the angular extent of the elastomeric layer. The figures devoted to the pressure profile reproduce the analytical contact width, which appears to reach values in the region of π , and (slightly) more. Other sources of error are ascribable to frictional effects which, while limited by the presence of a lubricant, are still present.

The peak shear stress at the interface between layer and foundation is of the order of one tenth the peak pressure for the configurations explored. This result is relevant in predicting debonding phenomena between layer and substrate. The shear maximum is not located at the symmetry axis - where in fact the shear stress vanishes due to symmetry - but it occurs at an angle (referred to in the axes as "shear angle") which, measured in radians, is of the same order of magnitude of

the peak shear stress expressed in MPa , for the configurations examined.

As already mentioned, the maximum value of the interface shear stress is a fraction of the peak contact pressure. It is important to clarify whether for a given load the maximum shear stress is heavily dependent upon the layer thickness, or not. For a given indentation depth the contact width does not dramatically depend on the layer thickness (compare Figs 5.4.2.4 and 5.4.2.7 , Figs 5.4.2.8 and 5.4.2.11 , and Figs 5.4.2.12 and 5.4.2.15 ; these pairs of Figures refer to different layer thicknesses, but to the same penetration stroke), whereas the peak contact stress appreciably diminishes as the layer thickness augments. As a consequence, for a given indentation depth the reaction force diminishes (proportionally to the peak contact stress) as the layer thickness is increased, and so does the maximum shear stress, whereas the contact width is not dramatically altered. For a given load, the corresponding indentation depth augments with the layer thickness, and so does the contact width. The peak contact stress therefore diminishes with thickness, and so does the maximum shear stress. It is concluded that, for an imposed load, the maximum interface shear stress decreases as the layer thickness is increased.

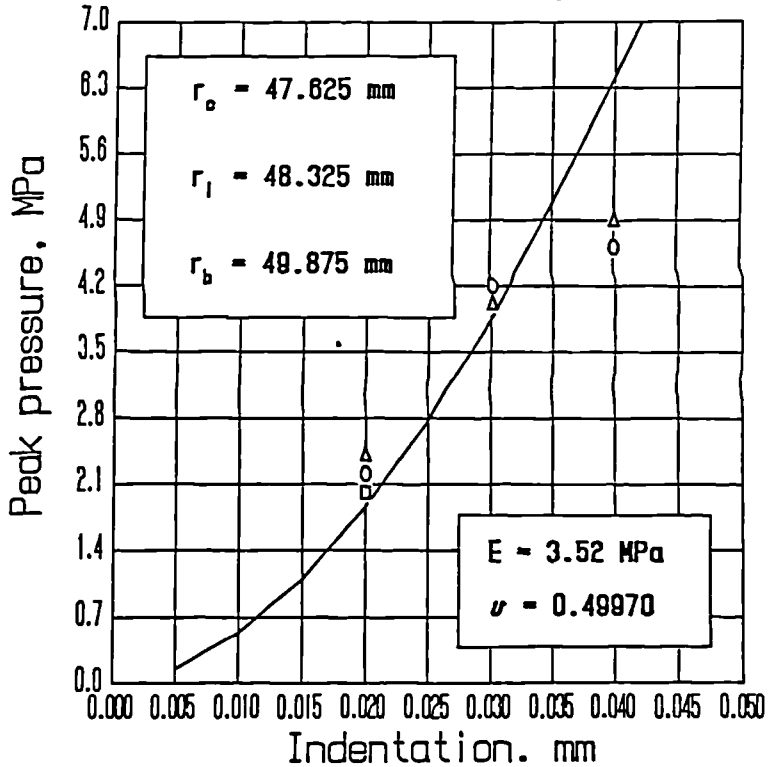

Fig. 5.4.2.1 : The peak pressure versus indentation for the first configuration .

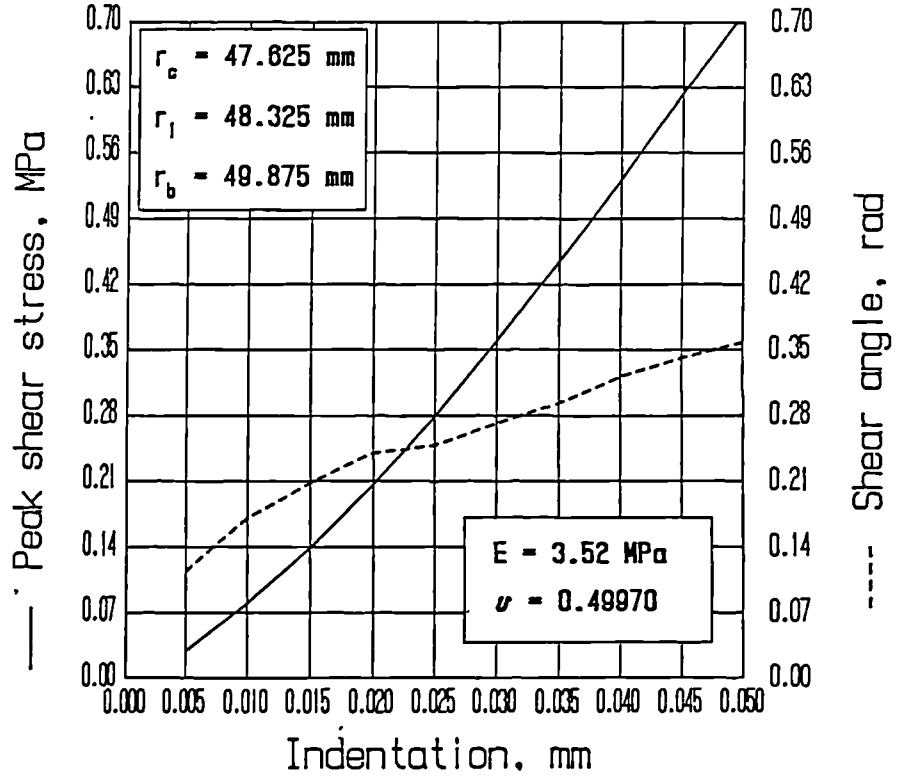

Fig. 5.4.2.2 : The peak shear stress and its angular position for the first configuration .

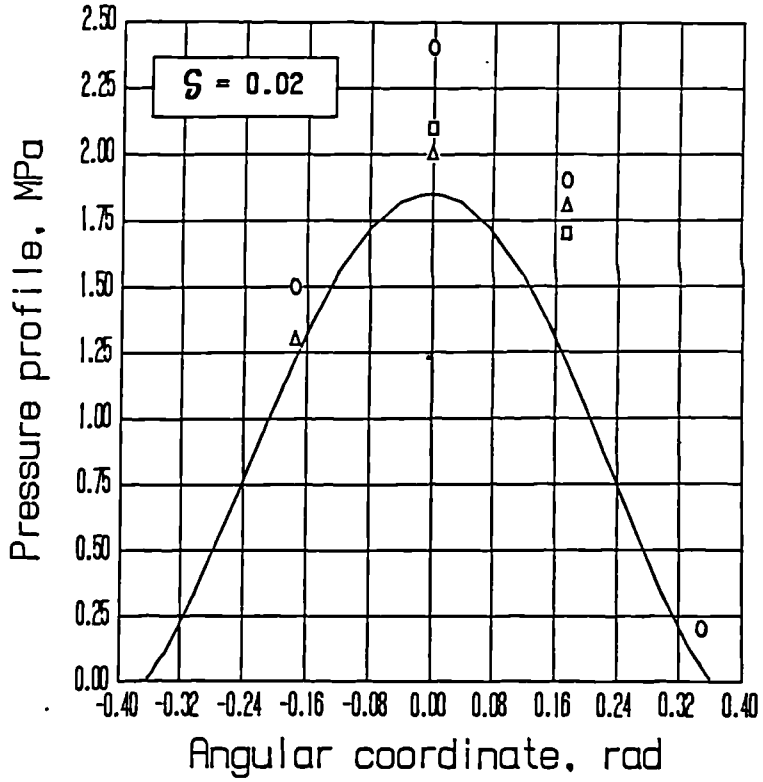

Fig. 5.4.2.3 : The pressure profile for δ = 0.02 mm for the first configuration .

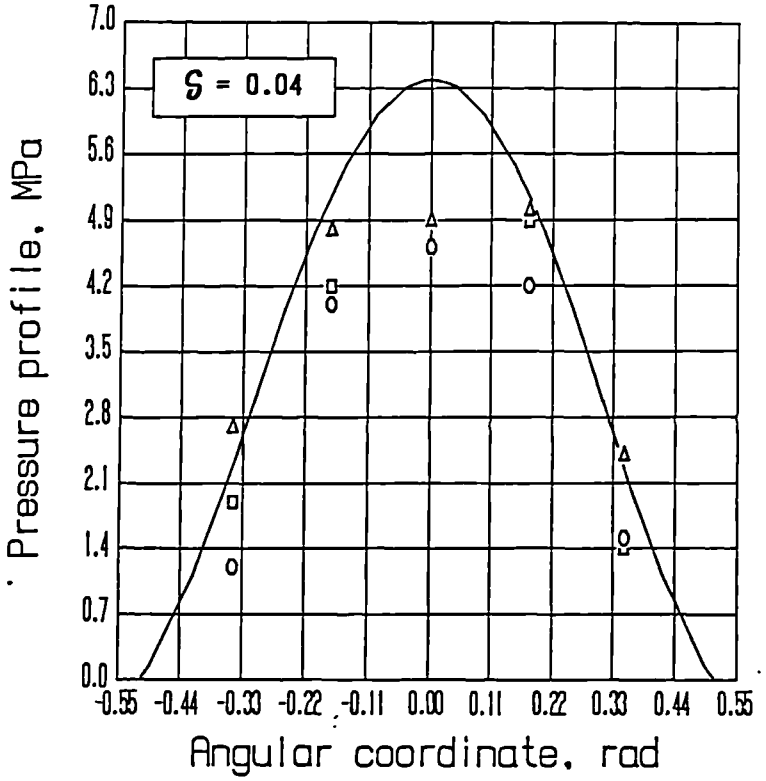

Fig. 5.4.2.4 : The pressure profile for δ = 0.04 mm for the first configuration .

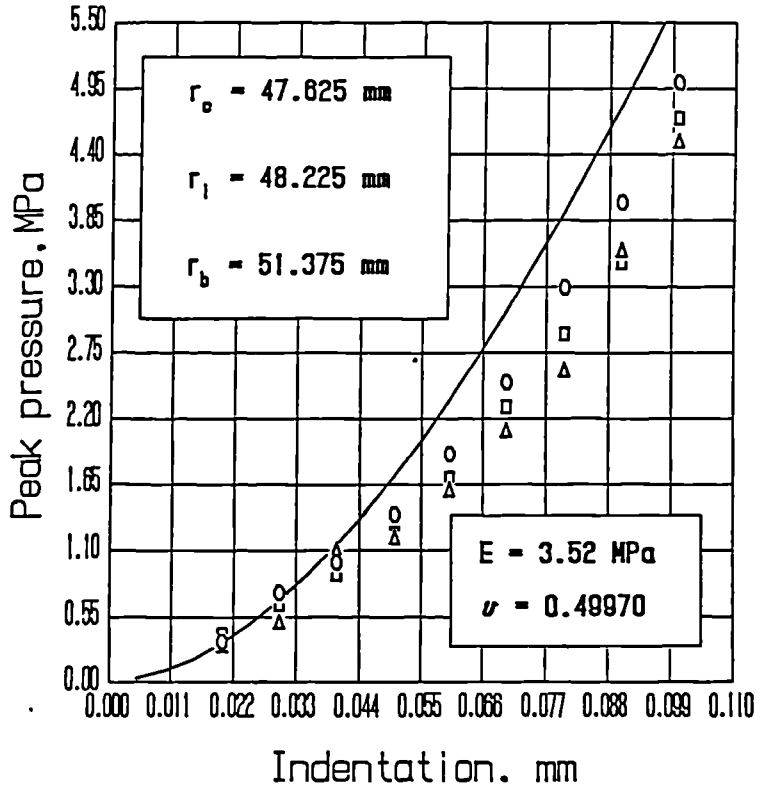

Fig. 5.4.2.5 : The peak pressure versus indentation for the second configuration .

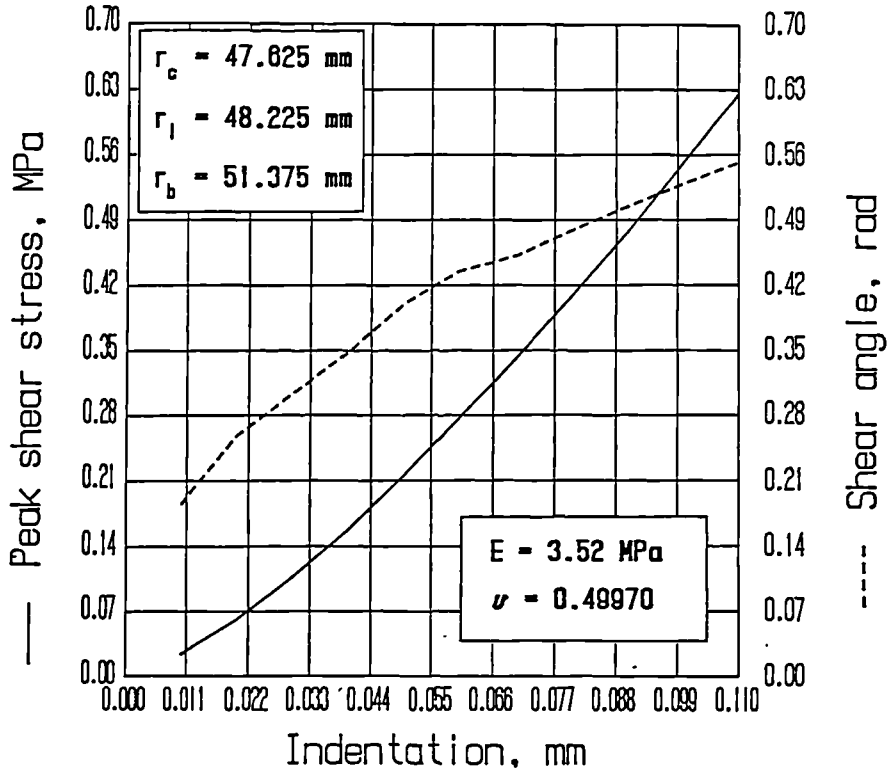

Fig. 5.4.2.6 : The peak shear stress and its angular position for the second configuration .

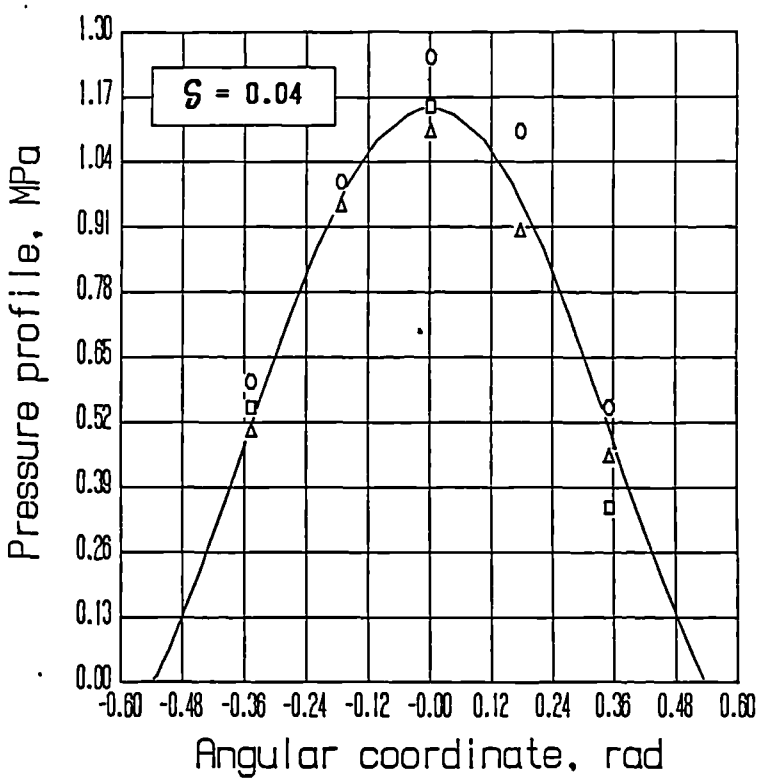

Fig. 5.4.2.7 : The pressure profile for δ = 0.04 mm for the second configuration .

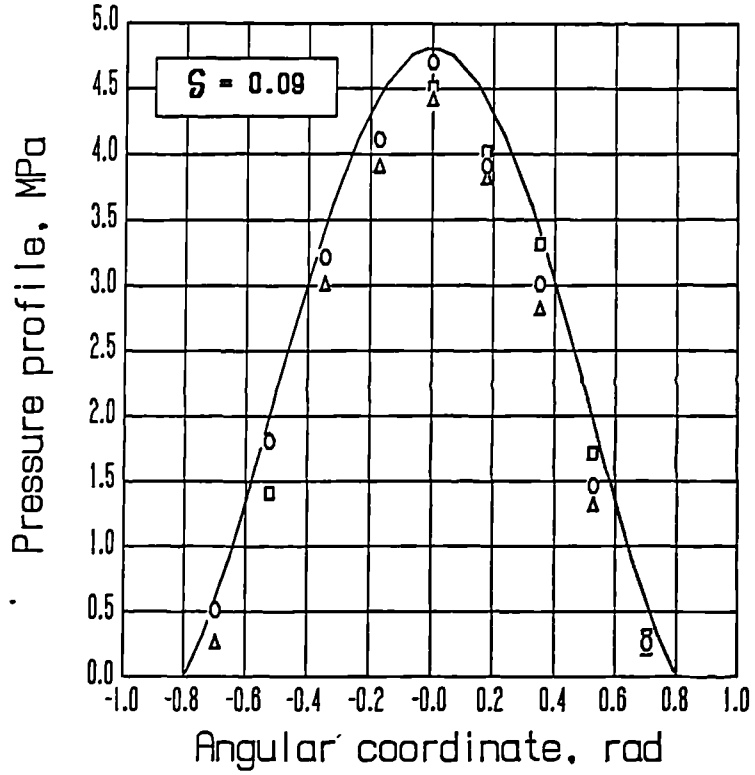

Fig. 5.4.2.8 : The pressure profile for δ = 0.09 mm for the second configuration .

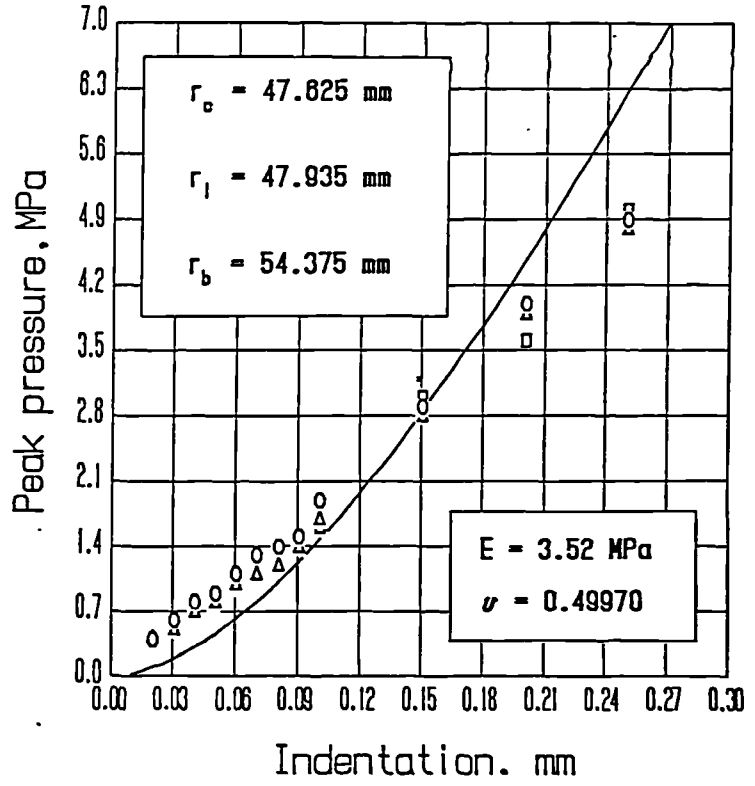

Fig. 5.4.2.9 : The peak pressure versus indentation for the third configuration .

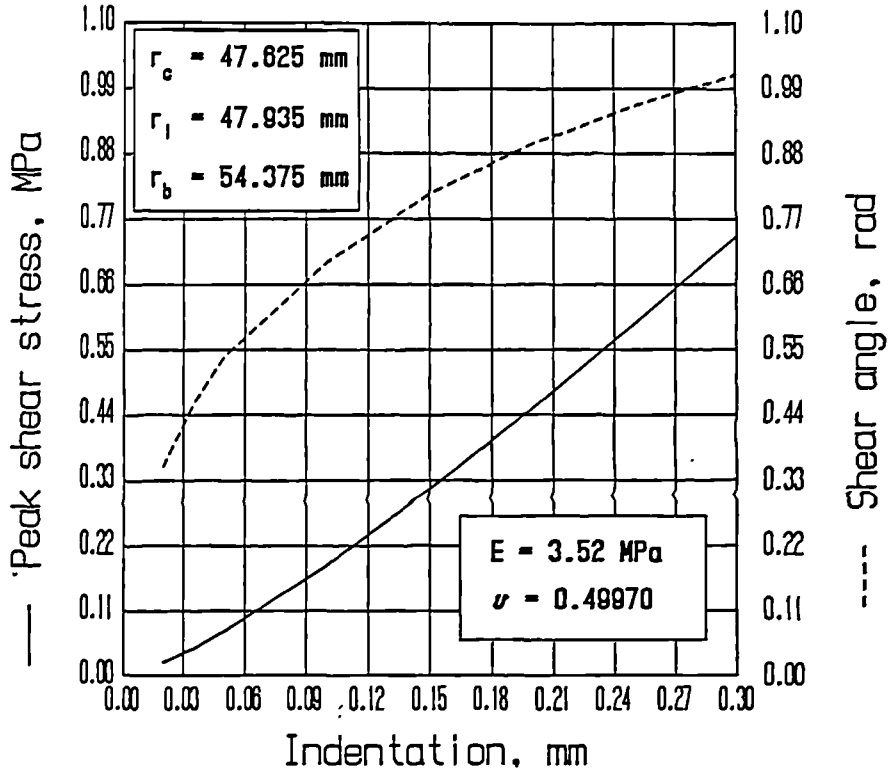

Fig. 5.4.2.10 : The peak shear stress and its angular position for the third configuration .

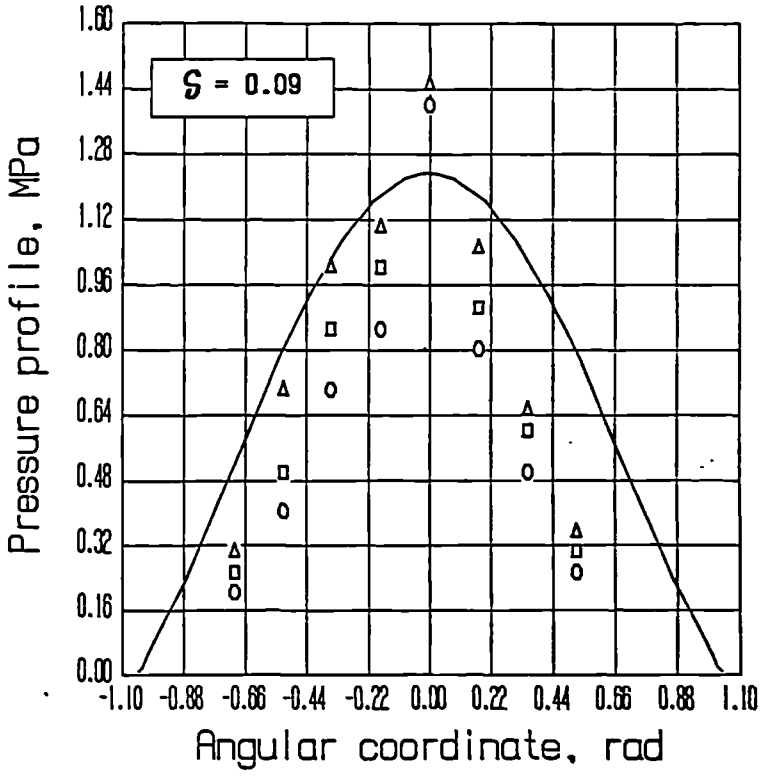

Fig. 5.4.2.11 : The pressure profile for δ = 0.09 mm for the third configuration .

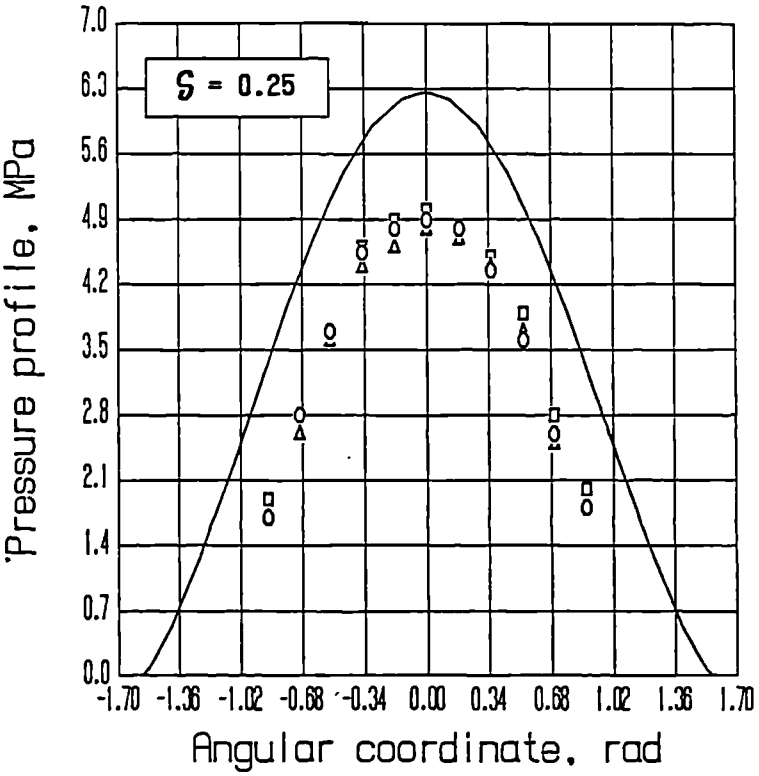

Fig. 5.4.2.12 : The pressure profile for δ = 0.25 mm for the third configuration .

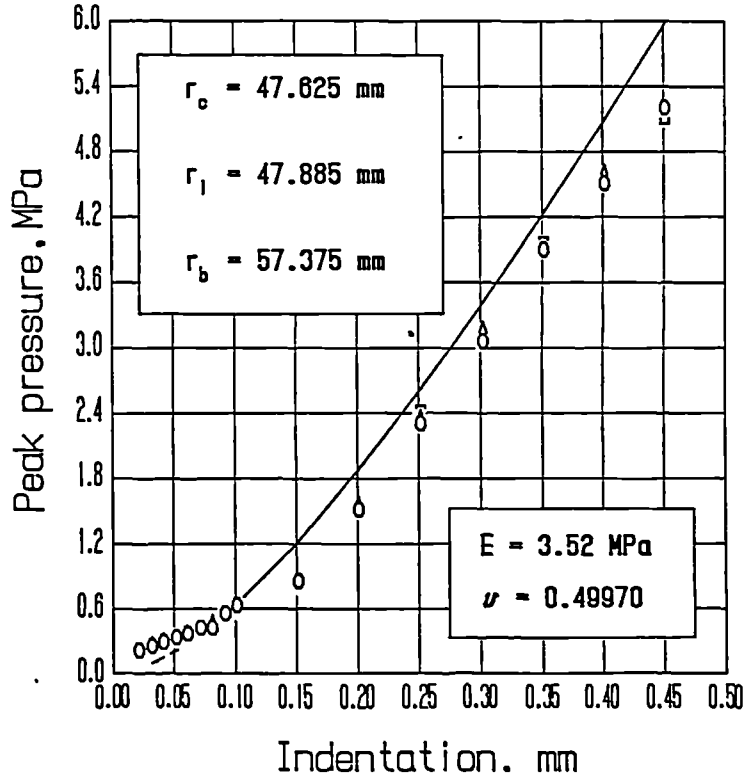

Fig. 5.4.2.13 : The peak pressure versus indentation for the fourth configuration .

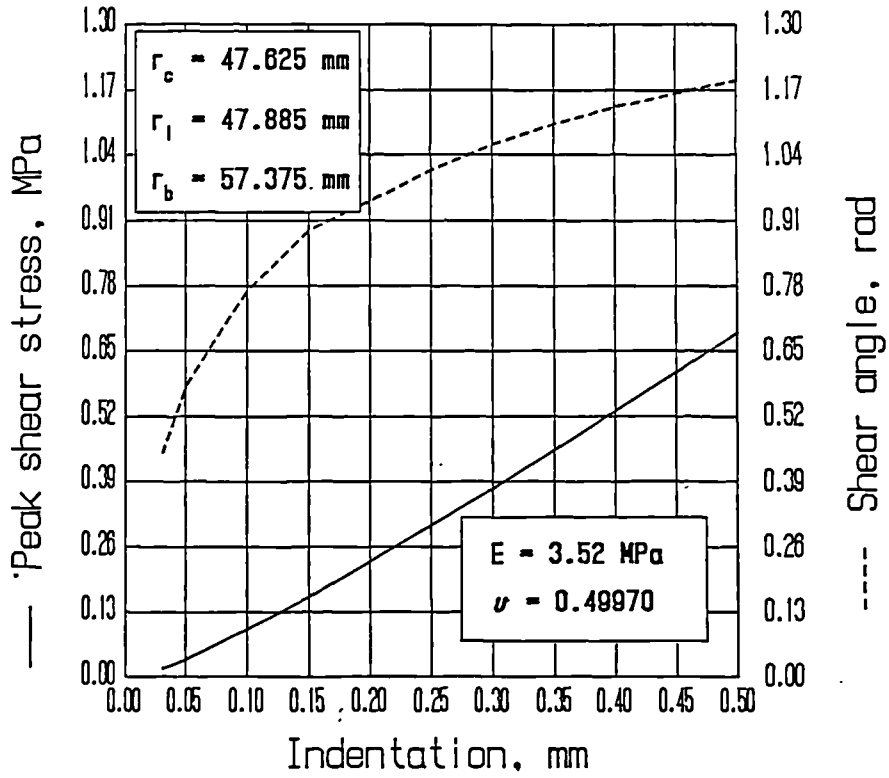

Fig. 5.4.2.14 : The peak shear stress and its angular position for the fourth configuration .

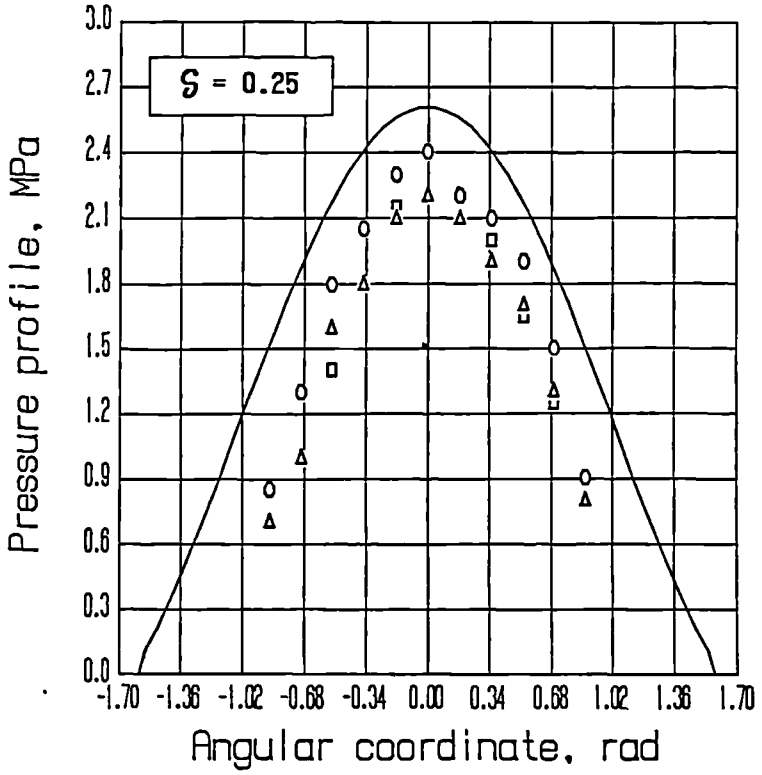

Fig. 5.4.2.15 : The pressure profile for δ = 0.25 mm for the fourth configuration .

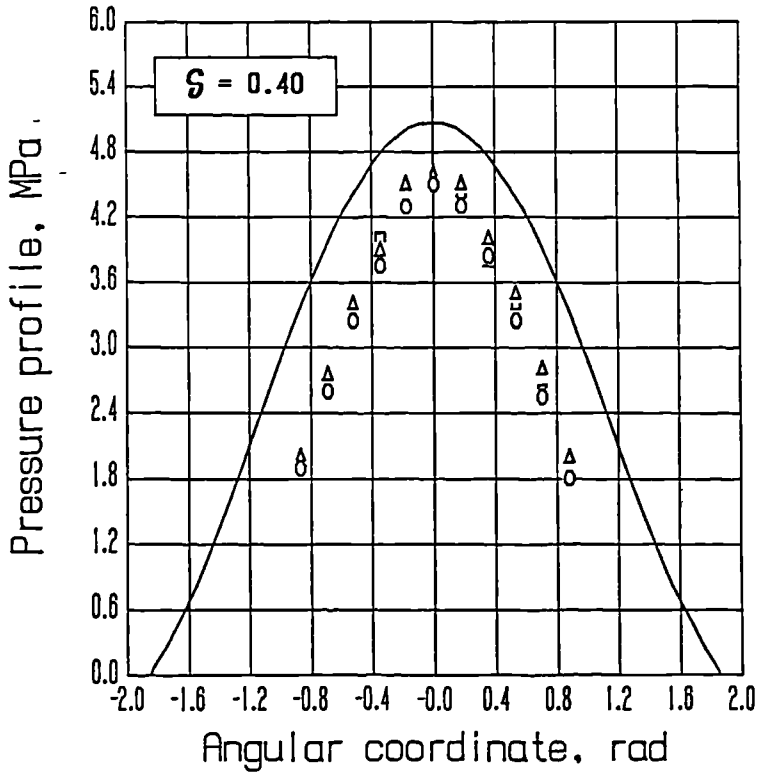

Fig. 5.4.2.16 : The pressure profile for δ = 0.40 mm for the fourth configuration .

Two additional Figures are presented, which explore analytically the consequences of a perturbation of the Poisson's ratio and the effects of curvature, respectively, with reference to the fourth configuration of TABLE 5.4.2.1 . Fig. 5.4.2.17 displays the peak contact pressure and the angular semicontact width versus the indentation depth, for the measured figure ν = 0.49970 and for the idealized incompressible value ν = 0.5 . The variation in the pressure curve is appreciable (the relative mismatch is about 10 percent) even for these two apparently very similar Poisson's ratios. The sensitivity of stresses and strains to ν is properly underlined by Matthewson (1981) for a comparable situation. Conversely, the angular contact width is essentially independent of ν. This result agrees with numerical (Dragoni and Strozzi (1988)) and experimental (Gorelik, Bukhina and Ratner (1961)) findings related to elastomeric seals.

Finally, Fig. 5.4.2.18 explores the curvature effects on the peak contact pressure and on the angular contact width, versus the indentation depth, with reference to the fourth configuration. The curved layer forecasts are compared to an "equivalent flat" layer geometry, defined by r_c = 1000 mm , r_b = 1138.1695 mm ,

and by r_i = 1128.6795 mm , so that the radius of curvature of the layer is much higher than its thickness, and the equivalent radius is the same as in the curved layer problem, that is, 8771.2428 mm . Finally, the portion of contacting head periphery is evaluated for the equivalent flat problem, and the same length has been ideally transferred along the actual head contour, to define a meaningful angular contact width also for the equivalent flat layer solution, which can be significantly confronted to that of the curved layer model.

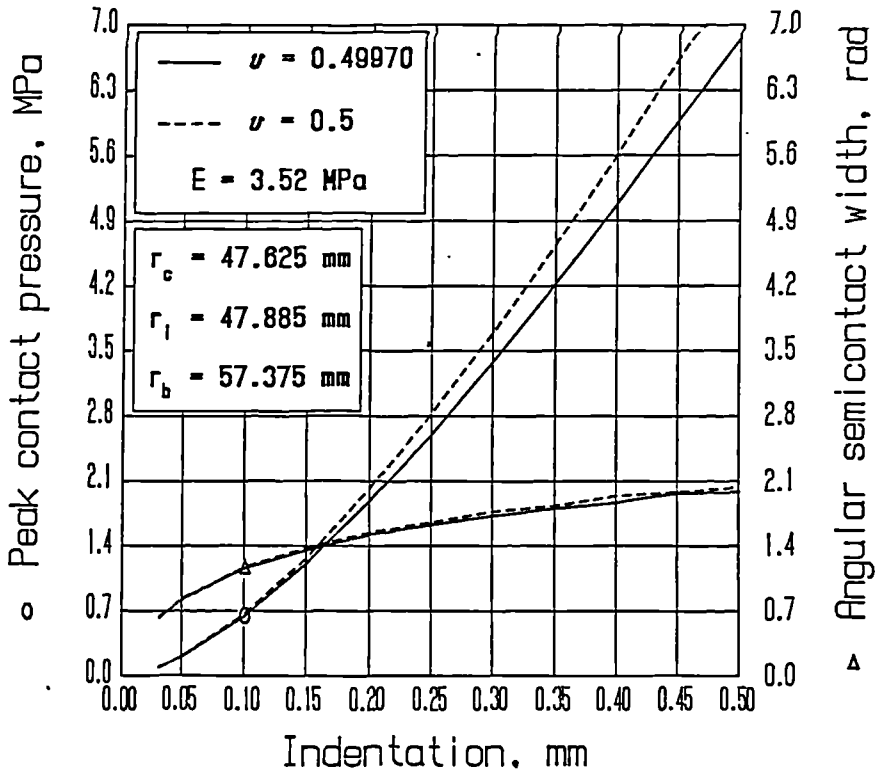

Fig. 5.4.2.17 : The dependence of the peak pressure on ν for the fourth configuration .

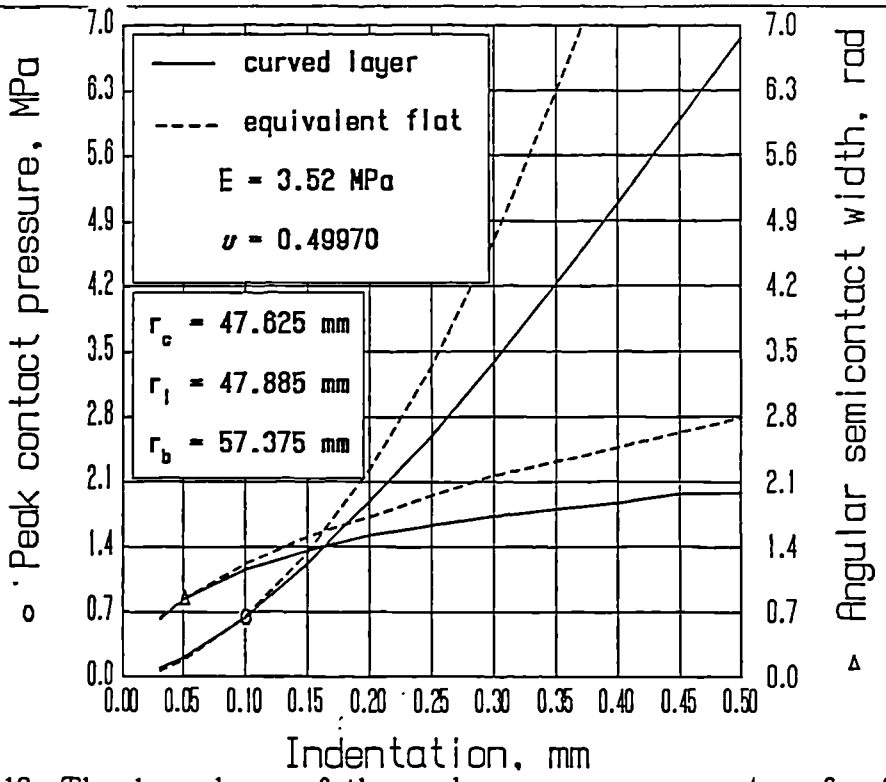

Fig. 5.4.2.18 : The dependence of the peak pressure on curvature for the fourth case .

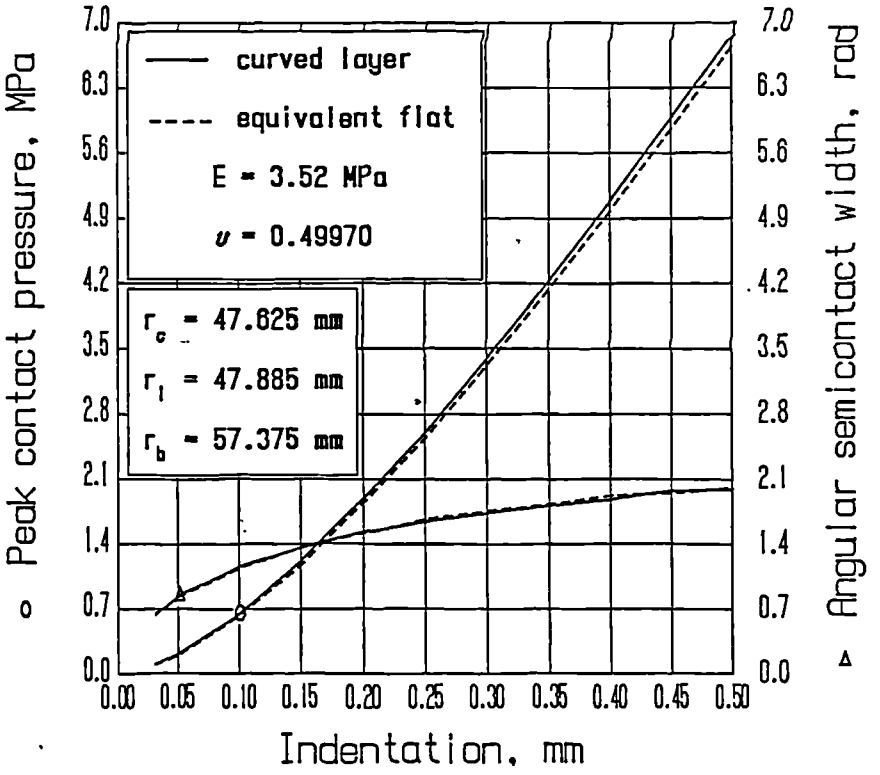

Fig. 5.4.2.19: The dependence of the peak pressure exclusively on curvature for the fourth case .

The results retrieved in terms of peak contact pressure and contact width show that the curvature effects are very important, the relative mismatch being about 30 percent. Following Yao (1990) in evaluating the curvature effects, reference is made to his expressions for δ and for δ_{asymp} at page 234 , valid for concave surfaces, and to his suggestions at page 239 , thus obtaining an estimated error of about 8.26 percent, much smaller than the analytical previsions of Fig. 5.4.2.18 . As already suspected in Section 5.2 , the Yao (1990) curvature error estimate, being based upon a Winkler foundation modelling, is not sound in the case of nearly incompressible layers. In fact Yao (1990) applies his estimate to layers possessing a Poisson's ratio as low as 0.4 , a figure for which his formulae are believed to be accurate, a conjecture supported by the results of Fig. 5.3.4.7 .

The differences in the two pairs of curves in fig. 5.4.2.18 are partially attributable to pure curvature effects, and partially to discrepancies in the head profile and, consequently, in the indentations imposed along the contact zone. It was decided to try to discriminate between the two contributions, by loading a nearly straight layer - defined, as in Fig. 5.4.2.18 , by r_b = 1138.1695 *mm* , r_t = 1128.6795 mm - by adopting an indenter capable of imposing penetration depths equal to those of the initial, curved problem. In other words, a flat layer is pressed by a rigid indenter, shaped so that the imposed indentation profile obeys formula (5.3.3.1), where r_c = 47.625 mm , r_t = 47.885 mm , as in the actual situation of the fourth configuration of Table 5.4.2.1 . The resulting forecasts are presented in Fig. 5.4.2.19 . It appears that the differences between peak contact pressures referring to the curved problem and to its flat counterpart with actual penetration profile is negligible, namely of the order of 2 percent. In addition, the two corresponding angular semicontact widths are hardly distinguishable.

It should also been underlined that the equivalent flat layer of Fig. 5.4.2.19 is still slightly curved and, therefore, it is expected to be slightly stiffer that its perfectly flat counterpart (Fig. 5.3.4.2 shows an opposite trend, since it refers to a contact between two cylinders; Figs 5.3.4.6,8 refer to the present geometry, that is, a cylinder indenting a cavity, but the effects of the approximations in the indenter profile mask the aspects to be clarified), thus producing slightly higher peak pressures with respect to a perfectly flat layer. Since the layer thickness is about

1/100 the loaded radius, this increase in pressure may be of the order of 1 percent. As a consequence, the mismatch between peak pressures, as appearing from Fig. 5.4.2.19 , might slightly underrate the actual error. Due to the above considerations, it is felt that the real deviation may be in the region of a few percent. In any case, the effects exclusively due to curvature are very small. As a consequence, a reliable mechanical model of a curved layer can be based upon a flat layer approximation and upon an indentation curve consistent with the actual curved profiles of the layer loaded border and of the indenting cylinder.

On the other side, this proposal partially contradicts the mathematical discussion of Goodman and Keer (1965), which refers to a deformable sphere indenting a deformable cavity. These authors observe that "higher approximations to the spherical surface that" "replace the spherical surfaces by their osculating paraboloids of revolution" "are mathematically inconsistent with retention of" "methods appropriate to the problem of the plane". In other words, according to Goodman and Keer (1965) it is not licit to refer to a flat model and to an accurate description of the indenter profile, a model which is favoured by the present author. A significant difference between the configuration here examined and that of Goodman and Keer (1965) is that they refer to a cavity in an infinite space, whereas here a layer of finite thickness is examined. This difference might at least partially account for these dramatically opposite opinions about the applicability of a flat model to describe a curved geometry.

As a final remark, the whole of the results presented in this Chapter confirms the importance of Poisson's ratio and underlines the need to consider the actual indentation curve. It also suggests that it should be desirable to incorporate in the theory of curved layers the end effects of the strip.

5.5 CONCLUSIONS

A series solution has been developed for a deformable annulus firmly bonded to a rigid substrate along one periphery and subject to a concentrated radial force acting at the other contour, with the aid of an algebraic manipulator. Series acceleration techniques have been developed. Contrary to the previous treatments, this solution does not degenerate for Poisson's ratios equal to half. This Green function has been exploited to treat numerically the biomechanically relevant case of a deformable annulus indented by a rigid cylinder. The effects of curvature and of Poisson's ratio perturbations have been explored numerically, and they have been found to become significant in geometries of interest in biomechanical problems. More exactly, the effects of layer curvature have been examined separately from those referring to the circumstance that the actual indentation curve of the cylinder is not precisely described by a cylindrical or parabolic profile. It has been found that the pure curvature effects are modest, whereas those deriving from the approximations in the description of the indenter profile may be relevant. As a consequence, a reliable mechanical model of a curved layer can be achieved by considering a flat layer approximation compressed by an indentation curve consistent with the actual curved profiles of the layer loaded border and of the indenting cylinder.

Four configurations have been examined experimentally in terms of pressure profile and contact width versus indentation, and they have been found to agree reasonably with the theoretical forecasts. The possible causes of errors have been discussed, and it has been underlined that the layer end effects may become significant in biomechanical applications and, therefore, they may be responsible for the disagreements between theory and experiments noted especially at the highest penetration depths. In other words, it should be of interest to incorporate the finiteness of the angular width of the curved layer into the theory.

The shear stress at the interface between layer and foundation has been examined analytically, and it has been clarified that, for an imposed load, the maximum interface shear stress decreases as the layer thickness is increased.

CHAPTER 6 . THE FLAT, AXISYMMETRICALLY LOADED, ELASTOMERIC LAYER: THEORY

Chapter 6 The Flat, Axisymmetric, Elastomeric Layer 6.2

6.1 INTRODUCTION

The two previous Chapters 4 and 5 address plane strain problems involving a layer indented by a cylindrical punch. This Chapter, instead, deals with axisymmetric situations. More precisely, the case is treated of an infinite flat layer firmly bonded to a rigid backing and frictionlessly indented by a rigid sphere, as shown in Fig. 6.1.1 . This model can mimic biomechanically significant geometries, such as hip prostheses possessing an elastomeric layer (Unsworth, Pearcy and White, (1987)). In particular, in this Chapter an analytical, perturbation-type solution is developed for small penetrations of the sphere, where most of the tedious and lengthy analytical passages have been relegated to the algebraic manipulator MACSYMA (1983). This analytical solution constitutes a benchmark against which to assess the finite element method, which is also employed to retrieve information for high penetration depths.

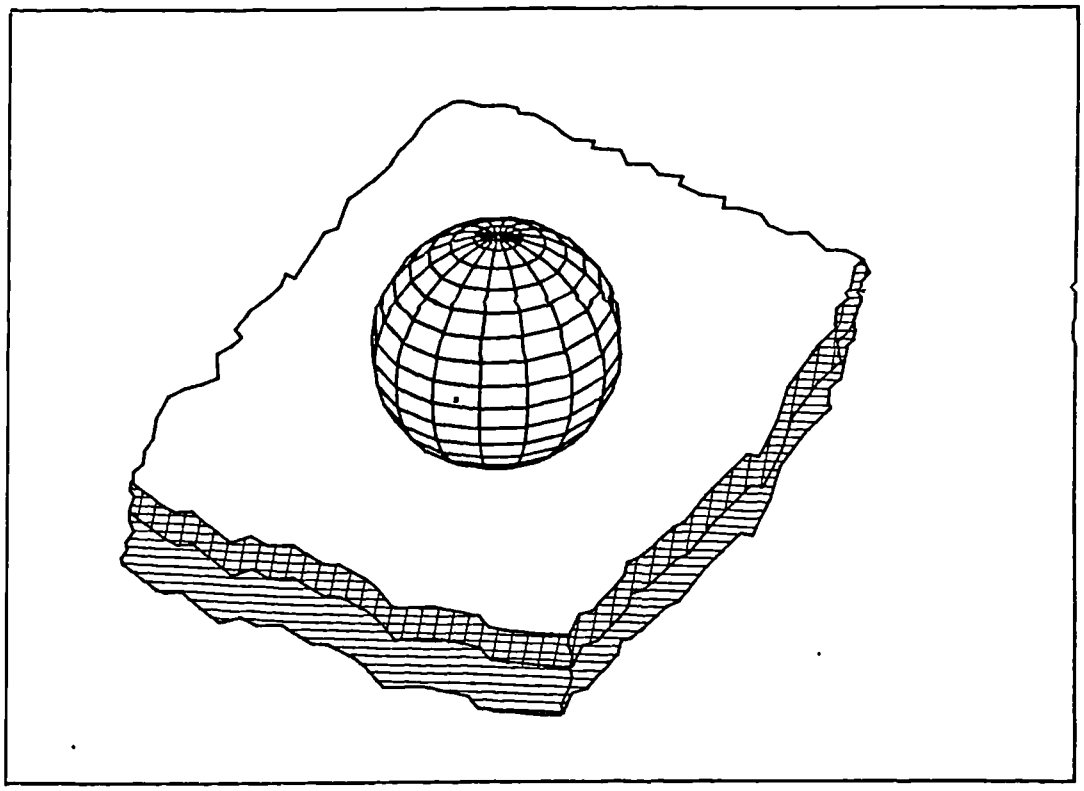

Fig. 6.1.1 : A flat layer indented by a sphere.

6.2 LITERATURE REVIEW

The papers referring to a deformable, infinite layer, firmly bonded to a rigid foundation and indented by a sphere are reviewed in this Section. In addition, contributions treating similar problems, as generally axisymmetric indenters, or three-dimensional contact problems, are also briefly mentioned because the solution techniques are generally applicable to the spherical indenter. The solution methods adopted are either mainly analytical or essentially numerical.

The analytical contributions fall into two main categories. The first field covers asymptotic contributions, which analyze either very thin or very thick layers. More exactly, low layer thickness to contact radius ratios or high aspect ratios are considered.

In the case of infinitely thick layers, the foundation becomes a half space. The pertinent papers are reviewed below. The related classical geometries are those of a rigid die in the form of a circular cylinder pressed against the plane boundary of a semi-infinite elastic solid (Timoshenko and Goodier (1970), p. 408), and the contact between two spherical bodies in contact (Timoshenko and Goodier (1970), p. 409), for which closed-form solutions have been obtained. Segedin (1957) notes that for an ellipsoidal indenter on a half space, the load-displacement ratio is the same as that for a flat-ended indenter for equal contact radii. Mossakovskii (1958) solves analytically the case of a circular die indenting an elastic half space, whose modulus of elasticity is an exponential function of depth. He corrects previous results quoted in his bibliography. Rvachev (1959) examines a rigid die of flat, polygonal planform indenting a half space, by solving the corresponding integral equation via the (numerical) Galerkin method. Sneddon (1965) considers variously shaped indenters acting upon a half-space. Aleksandrov and Babeshko (1972) study analytically a wedge-shaped stamp pressing an elastic half space. Mellin transformations and a series expansion are employed to solve the problem. Gladwell (1974) explores in a mathematically oriented paper the contact between a circular plate and an elastic half-space. An auxiliary function is expanded in terms of a polynomial expression. Fabrikant, Selvadurai, and Xistris (1985) consider a rigid circular punch indenting a half space, Fabrikant (1986) examines variously shaped,

flat punches, and Fabrikant (1990) considers a circular plate penetrating a half space and loaded also by a tangential force.

The existence in bibliography of asymptotic solutions for thick and thin layers is underlined by Johnson (1985) , p. 141 . The papers quoted are those by Aleksandrov (1968) (thick layers) and (1969) (thin layers), respectively. (To help the reader to trace the papers quoted, it is observed that the page numbers reported by Johnson (1985) correspond to the English translation, and not to the numbers reported under the title of the papers, that is, to those referring to the original paper.) Aleksandrov (1968) ranks a variety of solution techniques for extreme values of layer thickness to contact radius ratios, which include a perturbation approach and an exponential series expansion for the kernel of the integral equation. In Aleksandrov (1969) an asymptotic solution is achieved in the case of an axisymmetric, parabolic punch, for small layer thickness to contact radius ratios. Solutions, although too complex for everyday use, are obtained for the parabolic punch via a series expansion of the kernel and via a boundary layer approach, for both contact pressure and total load (see his formulae (5.26) and (5.29)). Additional asymptotic solutions are contained in the contribution by Aleksandrov (1963a), where it is shown that, when the layer thickness becomes very high, the mathematical model tends to that of a stamp acting upon an infinite half space. In addition, a formula is achieved "for very small values of h" which coincides with the typical Winkler solution, that is, the solution which ignores the lateral flow of the layer, but considers only its deformability in the direction of the layer thickness. This solution is identical to that of Armstrong (1986) (zero perturbed order) for plane strain conditions. The same solution of Aleksandrov (1963) is reprised without quotation by Jaffar (1989) in his formula (15), while developing asymptotic solutions valid for thin layers (that is, large contact widths) and for spherical indenters, by extending to axisymmetric geometries the plane strain results of Johnson (1985), p. 140 . Intriguingly, the contribution by Aleksandrov (1963) was properly quoted in a previous paper by Jaffar and Savage (1988), where the authors underline the existence in bibliography of "an asymptotic solution for both small and large a/t ". The paper by Jaffar (1989) contains, in addition, an original asymptotic solution for an incompressible, thin layer for which the Winkler model is no longer applicable

(Armstrong (1986)). (In his formula (25), variable E is missing). In fact, in a similar way to Johnson (1985), Jaffar (1989) has to treat compressible and incompressible layers separately. While performing a comparison between asymptotic and exact pressure profiles, Jaffar (1989) finds - consistent with Meijers (1968) - that the contact pressure is no longer Hertzian as the Poisson's ratio approaches the incompressibility value 0.5 , especially in the vicinity of the contact ends. Barber (1990) extends Jaffar (1989) asymptotic solutions to cover the general three-dimensional case. Finally, Li and Dempsey (1990) produce, among other interesting results, asymptotic expressions (see their formula (34)) which coincide with those of Jaffar (1990), formula (16).

Lebedev and Ufliand (1958) solve the case of an elastic layer indented by an axisymmetric punch. Asymptotic behaviours are explored for a stamp with a flat base and small radius to layer thickness ratios, but cases of stamps with a non plane base under incomplete penetration (as are those of a sphere indenting a layer) are also mentioned. Aleksandrov and Vorovich (1964) obtain an asymptotic solution for a thin plane layer indented by a flat punch, by exploiting a previous solution to which the new problem tends as a consequence of a change of variables. They observe that the same procedure could be applied to axisymmetric situations, but it is here noted that the limit of indenter flatness, to be converted to a parabolic profile, may be difficult to remove. Aleksandrov, Babeshko and Kucherov (1966) examine three-dimensional contact problems involving a thin layer, and in particular obtain asymptotic solutions for an axisymmetric stamp of any profile. Fourier-Bessel expansions are employed to describe the punch profile.

Moving to less idealized geometries, Goodman and Keer (1965) confront the difficult problem of a deformable sphere indenting a deformable cavity in an infinite space, where their treatment is based upon a paper by Sternberg, Eubanks and Sadowsky (1951), which presents a solution for the case of a hollow sphere subject to axisymmetric loading. A series solution (in which the kernel is evaluated numerically) is obtained for the resulting Fredholm integral equation of the first kind. Some experimental measurements in terms of relative approach versus load are also reported in their Fig. 2 . In addition, Goodman and Keer (1965) reach the mathematical conclusion that higher than parabolic approximations to the spherical

surface are inconsistent with a plane model of the deformed media. Finally they observe that, for an extension of the Hertz theory to be significant, the difference between the radii of sphere and cavity must be small.

The analytical contributions devoted to non asymptotic situations, that is, to layer thicknesses comparable to the contact widths, are examined hereinafter. Burmister (1945) examines the case of a deformable layer of finite thickness uniformly loaded over a circular region and underlain by a second flexible stratum, with shearing resistance fully active between them. Tabulated results are presented for incompressible materials. Vorovich and Ustinov (1959) treat the problem of a layer indented by an axisymmetric die. The case of a parabolic profile is considered in detail. A formidable mathematical development permits the axisymmetric indentation problem to be described in terms of a Fredholm integral equation of the second type (or closely associated to it), and amenable to recursive, Picard-type iterated solutions, which mathematically converge for ratios of layer thickness to contact radius higher than 1.27 , and in particular converge very fast for ratios higher than 1.7 . The zero order formula of the contact radius expressed as a function of the total load (last page of Vorovich and Ustinov (1959)) coincides with the purely Hertzian solution (Johnson (1985), p. 93), provided that their c of formula (1.16) is understood as indicated by Keer (1964), formula (1), that is, $c = E/(2(1 - \nu^2))$. This is also consistent with the Vorovich and Ustinov (1959) formulae as quoted by Ihara, Shaw and Bhushan (1986a). The validity field of the results of Vorovich and Ustinov (1959) is examined by Ihara, Shaw and Bhushan (1986a), and found to be consistent with the Vorovich and Ustinov (1959) suggestions, that is, $a/h < 0.67$. Pupyrev and Ufliand (1960) study again the case of an axisymmetric, flat punch indenting a layer of finite thickness. A mathematical manipulation permits the problem to be described in terms of a Fredholm integral equation of the second type (see their equation (2.8)), which is solved numerically. Aleksandrov and Vorovich (1960) solve the three dimensional indentation problem of a rigid die pressing a layer of finite thickness, by employing a perturbation-type solution. A flat, elliptic die is considered in detail. Keer (1964) further develops the study of Vorovich and Ustinov (1959) with reference to a sphere indenting a layer, by incorporating the ball compliance. Since his method is the same as that of

Vorovich and Ustinov (1959), his results too may suffer from the limits noted by Ihara, Shaw and Bhushan (1986a) with regard to the Vorovich and Ustinov (1959) contribution. This point is investigated by Li and Dempsey (1990) in their Fig. 6 . In addition, Keer (1964), following Galin (1961), notes that, if this problem is idealized to two half-spaces in contact, the equations are analogous to those of a half space compressed by a rigid punch, whereas if equations are employed which account for the finiteness of the layer width, the two solutions referring to rigid and elastic punches differ substantially. Tu and Gazis (1964) examine a plate compressed between two spheres, and obtain a solution by expanding the kernel of the integral equation in terms of Legendre polynomials. Due to numerical difficulties, the computations are performed only for thick plates, for which the contact radius does not exceed half the thickness of the plate. Aleksandrov (1967) examines axisymmetric problems, and shows the advantages of Legendre and Chebyshev polynomials in solving analytically the integral equations involved. The axisymmetric case of a flat die pressing on a layer is treated as an example. Noble and Hussain (1969) develop a different solution procedure, based upon a variational formulation, which lends itself to the analytical approximate solution of indentations by axisymmetric punches of any profile. Their examples include cases in which the exact solution is recovered, *e.g.* , for paraboloidal profiles and circular cones. Dhaliwal (1970) solves the problem of a cylindrical, flat punch indenting a layer bonded to a deformable half-space, by modelling the contact via a Fredholm equation of the second kind (by adopting the formulation due to Vorovich and Ustinov (1959)), treated via a perturbation technique. The method employed breaks down for relatively thin layers. It is found that a very slight change in the elastic modulus of the foundation to which the layer is bonded, from the rigid situation to a moderately deformable value, affects the results considerably, especially when the layer is thin. The extension to conical, paraboloidal, ellipsoidal and spherical punches is presented in Dhaliwal and Rau (1970), where the same perturbation-type technique is employed. Hayes, Keer, Herrmann and Mockros (1972) study indentation problems with regard to indentation tests of articular cartilage, defined by $\nu = 0.45$. The model adopted is that of an infinite elastic layer bonded to an immovable rigid foundation, and pressed by an axisymmetric, rigid punch. The problem is expressed in terms of a Fredholm integral equation of the second type, obtained following

Vorovich and Ustinov (1959), which is solved numerically via a finite element type approach. Both plane-ended cylindrical and spherical indenters are considered. The interface stresses are particularly addressed, for $\nu = 0.45$. Shelest (1975) examines a layer of finite thickness frictionlessly resting on a rigid base and frictionlessly indented by a circular rigid plate. Interesting approximations of integrands are presented, which permit improper integrals to be evaluated analytically. Gladwell (1980), p. 551 - 558 , reviews the major contributions referring to axisymmetric layer problems. Aleksandrov and Karpenko (1980) study a spherical layer, subject to a torsion caused by rotation imposed by a non-axisymmetrical punch. Matthewson (1981) employs an averaging technique to solve analytically layers indented by a sphere (parabolic approximation) and by a cone, and compares his solutions to a purely Hertzian approach. He also presents experimental measurements referring to a circular indenter. Matthewson (1981) also compares his results with those of McCormick (1978), a paper not available to this author. Chiu and Hartnett (1983) develop a theoretical-numerical solution for a layer loaded by a uniform pressure over a rectangular planform, having in mind applications to bearings. The authors approximate the kernel in terms of an exponential polynomial, and compute exactly the corresponding integral. However, a second integration is computed numerically. Johnson (1985), p. 140 , also reviews more applied contributions referring to axisymmetrical stresses in a layer. King (1987) examines flat-ended cylindrical, quadrilateral and triangular punches indenting a layered half-space (that is, a layer adherent to a half space). Jaffar (1988) produces solutions for flat-ended cylindrical, and for spherical indenters, for relatively small (lower than 20) contact radius to layer thickness ratios. (An extension to values up to 30 is reported in Jaffar (1989).) The integral equation describing the layered contact is solved analytically by employing Legendre polynomials, following Popov (1962). Dowson and Yao (1990) examine the lubrication regime in natural joints, by adopting a Winkler-type foundation model for the articular cartilage. Li and Dempsey (1990) solve analytically the case of an axisymmetric contact between an elastic layer anchored to a rigid base and a) a flat, cylindrical indenter, b) a rigid sphere, and c) an elastic sphere. They expand the kernel in a finite exponential series, a strategy comparable to that suggested by Sneddon (1946) and used by Aleksandrov (1968), Chiu and Hartnett (1983) and by Yao (1990), p. 86 . They make the interesting observation

that "the smooth base solutions are very close to those for a rough base with $\nu_1 = 0$." Dempsey, Zhao and Li (1991) extend the previous study to the situation of an elastic layer supported by a Winkler foundation, a case of particular relevance to civil engineering. Dowson, Fisher, Jin, Auger, and Jobbins (1991) study the compression of a sphere against an elastomeric layer as a geometry mimicking hip replacements with soft layers. The examine the importance of head diameter, radial clearance, layer thickness, and Young's modulus. Instead, the Poisson's ratio effects are not explored. An interesting comparison between the merits of hard and soft hip replacements is also presented. Finally, Fisher and Dowson (1991) discuss the potentials of cushion form bearings.

The analytical studies generally rely upon integral formulations of the contact problem. As a consequence, the fundamental solution of a layer loaded by a concentrated force (Green function) is relevant in formulating the integral equation. Sneddon (1951), p. 453 , solves this problem with the aid of Hankel Transforms. Chen (1971) examines the case of one or two layers bonded to another homogeneous half space. Yao (1990), p. 77, develops the solution for a two-layered system.

As a final observation concerning analytical papers, the differential approach of Armstrong (1986) does not appear to have been extended to axisymmetric situations.

Passing to the essentially numerical papers, Favretti (1966) treats the indentation of an axisymmetric, rigid punch compressing a plastic material, by resorting to numerical quadratures. Tu (1967) employs a numerical discretization technique to analyze a plate pressed between two identical spheres. He finds that, when the ratio of plate thickness to sphere radius is higher than 5 , a purely Hertzian solution is valid. Conway and Farnham (1967) and (1968) employ numerical solutions to evaluate penetrations by variously shaped indenters. In particular, Conway and Engel (1969) examine layers indented by spheres. Poulos (1968) develops a finite element type solution for the case of a circular plate resting on a layer of finite thickness and underlain by a rigid base. The effects of a variation of the Poisson's ratio are studied, and found to be appreciable. Chen and Engel (1972) analyze axisymmetric punches indenting multilayered media. In particular, they treat a parabolic punch pressed into a layered half-space. They use a series expansion

with five or six terms for the pressure, and find the series coefficients via a least square approach. The errors are found to be very small for a variety of significant tests, even when the layer becomes very thin. For contact radii as small as 0.2 times the layer thickness, the dimensional error (concerning the precision by which the boundary condition on the imposed displacement is respected) is of the order of 10^{-4} . It is also found that, when the layer thickness becomes four times the contact radius, the pressure profile tends to that of the half space solution, whereas the two penetrations are still perceivably *different. The problem of* curved, axisymmetric layers is mentioned as a particularly difficult aspect and, consequently, it is not treated. Hooper (1974) examines with the finite element method à circular raft of finite flexibility in adhesive contact with a thick isotropic elastic layer underlain by a rigid base. Singh and Paul (1974) develop numerical tools to cover non Hertzian, three dimensional contact problems. Brothers and Sinclair (1977) numerically study the indentation of an elastic half-space by a rigid rectangular punch, by resorting to a singularity-incorporating finite-element method. Their approach relies upon a technique developed by Emery and Segedin (1973). Ahmadi, Keer and Mura (1983) numerically study various contacts between cylinders and half planes, and assess the numerical forecasts with respect to the Hertzian theory for an elliptical contact. Ihara, Shaw and Bhushan (1986 a,b) treat the case of a sphere indenting a layer by the finite element method. Their sentence commenting Fig. 6 on p. 530 , which reads : "To a very good approximation, σ_z , σ_r , and σ_θ are principal stresses for $\theta = 0$.", where $\theta = 0$ represents the vertical axis (see their Fig. 1), is difficult to understand, since a symmetry axis must coincide with a principal direction. Perhaps this 'observation is related to the approximation mentioned while commenting Fig. 5, according to which "the stresses . . . are along a line displaced 0.1 mm from the z axis." These authors compare their results with those of Vorovich and Ustinov in their Fig. 9 , and they find that the latter solution deviates from the finite element forecasts for contact radius to layer thickness ratios higher than 0.5 . In addition, these authors explore numerically the relevance of a change in Poisson's ratio, by adopting the two values $\nu = 0.20$ and 0.49 . The captions of their Figures 12 (a) and (b) report that the confrontation has been made for the same geometry and for a fixed total load (0.346 N) and normalised penetration depth (0.2) . What is important is that from a physical point of view

the load is kept constant, while the absolute indentation depth as well as the layer thickness are varied until a) their ratio is 0.2 and b) the compression produces the desired load. (From a numerical viewpoint, simpler procedures are actually followed.) The authors come to the general conclusion that "ν has a small influence on the stresses in the thin elastic layer", an opinion which the present writer accepts provided that either the imposed force is kept constant (as suggested by the caption of their Fig. 12), or the penetration depth is small in comparison to the contact width. In fact, Hannah (1951) notes that "a change in Poisson's ratio makes an appreciable difference to the loading necessary for a given contact length, but has very little effect otherwise". She also notes that " Poisson's ratio can be seen to have little effect" on the pressure profile. In addition, from Figures 4.3.5.2,5 of Chapter 4 it appears that the Poisson's ratio is not the dominant parameter for low indentation depths. On the other side, as soon as the contact width increases, a perturbation of ν dramatically changes the stress field and, consequently, the reaction force, the indentation depth being kept fixed. This viewpoint is supported by the many results of Section 4.3.4 . In conclusion, the observations of Ihara, Shaw and Bhushan (1986a) regarding the Poisson's ratio effects do not seem to the writer to have been sufficiently discussed in their paper. More recently, Gueury, Bagur, Rezakhanlou and von Stebut (1990) numerically study the indentation of a rigid sphere into an elastic-plastic layer by considering the geometrical non-linearities. Some comparisons with experimental readings are also provided.

Moving to the mainly experimental contributions, Drutowski (1968) examines the indentation of a transparent spherical indenter into an elastomeric lining, to measure the Young's modulus. Similarly, Finkin (1972) experimentally verifies an analytical relationship derived from Vorovich and Ustinov (1959) paper, connecting Young's modulus to rubber hardness, with reference to a spherical indenter. Matthewson (1981) compares in Fig. 10 the total load to the theoretical predictions for the geometry of a sphere compressing an elastomeric layer, and he finds that the experimental measurements overestimate the analytical forecasts. Anyway, an offset in the penetration depth of less than 0.1 mm produces an appreciable modification of the total load, which renders the experimental readings consistent with the analytical forecasts. In other words, in this paper the disagreement between

experimental load and theoretical forecasts is essentially attributed to "the error in estimating the height at which the indenter just makes contact with the coating." Finally, O'Carrol, Jin, Dowson, Fisher and Jobbins (1990) measure total load and contact radius, and they too find that the experimental force is higher than the theoretical predictions based on linear elasticity. They attribute the mismatch mainly to non-linear elastic aspects and to frictional effects. Preliminary results of this study are presented by Dowson, Fisher, Jobbins, O'Carrol and Jin (1990).

6.3 GENERAL EQUATIONS

Following Aleksandrov (1967) and Jaffar (1988), the indentation of a deformable layer firmly anchored to a rigid backing and frictionlessly compressed by a rigid punch can be described in terms of the following Fredholm equation of the first kind :

$$w(\bar{r}) = \frac{2\alpha}{t} \int_0^a K_{axi}(\bar{r},\bar{s})\, p(\bar{s})\, \bar{s} d\bar{s} \qquad 0 \leq \bar{r} \leq a \tag{6.3.1}$$

where :

$$K_{axi}(\bar{r},\bar{s}) = \int_0^\infty L(\omega)\, J_o\left(\frac{\bar{r}\,\omega}{t}\right) J_o\left(\frac{\bar{s}\,\omega}{t}\right) d\omega \tag{6.3.2}$$

and :

$$L(\omega) = \frac{2\,\gamma\, sinh\, 2\omega - 4\omega}{2\,\gamma\, cosh\, 2\omega + 4\omega^2 + \gamma^2 + 1} \tag{6.3.3}$$

and $\alpha = (1 - \nu^2)/E$, t is the layer thickness, a denotes the contact radius, $\gamma = 3 - 4\nu$, and J_o indicates the Bessel function of the first kind of order 0 . In addition, $w(\bar{r})$ describes the imposed indentation depth profile. Finally, $K_{axi}(\bar{r},\bar{s})$ represents the axisymmetric kernel of the integral equation (6.3.1) .

It appears that function $L(\omega)$ of (6.3.3) coincides with a part of the kernel of the corresponding plane case (see Chapter 4, eqn (4.3.2.6)). This occurs because of the existing link between plane and axisymmetric cases, see Gladwell (1980), p. 509 . Actually, there is a general similarity between the integral equation (6.3.1) for axisymmetric situations and its counterpart (4.3.2.2) for plane configurations. The main difference is that in the plane case the kernel simply depends upon the absolute value of the difference between the coordinate denoting a specific point of

the punch (variable x in eqn (4.3.3.2)) and the integration variable (symbol s in eqn (4.3.3.2)), whereas in axisymmetric problems the corresponding kernel (6.3.2) exhibits a more complex dependence upon variables $\bar{r}$ and $\bar{s}$, which correspond to x and s , respectively, in the plane situation.

It can be shown that, when the layer thickness, t, tends to infinity, the integral equation (6.3.1) approaches the mathematical description of a rigid punch indenting a half-space, see Chiu and Hartnett (1983).

Following Jaffar (1988), the integral equation (6.3.1) is rewritten in terms of non-dimensionalized variables :

$$w(r) = 2\,\alpha\beta a \int_0^1 K_{axi}(r,s)\, p(s)\, s\, ds \qquad 0 \leq r \leq 1 \tag{6.3.4}$$

where :

$$K_{axi}(r,s) = \int_0^\infty L(\omega)\, J_o(\beta r\omega)\, J_o(\beta s\omega)\, d\omega \tag{6.3.5}$$

and where $r = \bar{r}/a$, $s = \bar{s}/a$, and $\beta = a/t$.

In the following the physical meaning is elucidated of the fact that the axisymmetric kernel (6.3.5) is symmetric with respect to variables r and s . Referring to Fig. 6.3.1 , $K_{axi}(r,s)$ represents the deflection in any point of the circumference of radius r , due to a unit linear load applied along a circumference of radius s . Since the axisymmetric kernel is symmetric with respect to r and s , this implies that the same deflection as before occurs for any point of the circumference of radius s due to the effect of a unit linear load applied to the circumference of radius r. This is indeed the axisymmetric version of Betti's theorem.

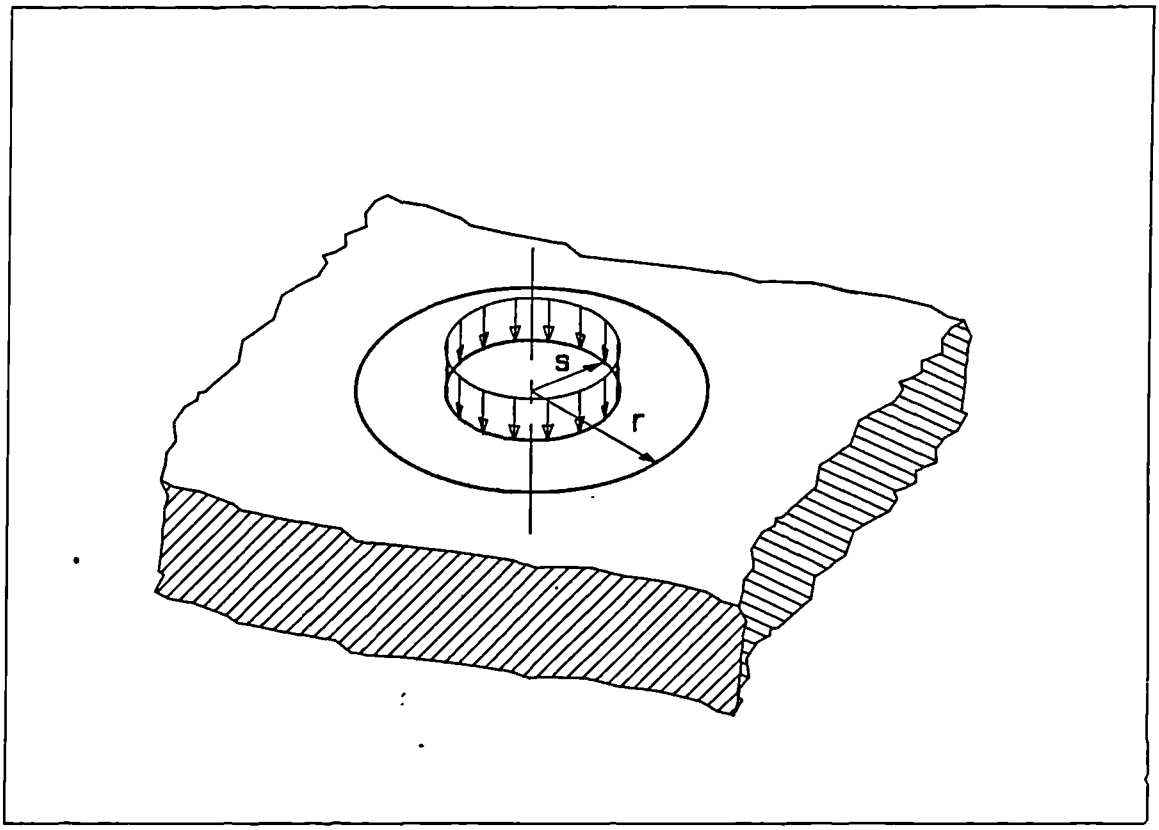

Fig. 6.3.1 : Deflection at radius r due to a unit linear load along a circumference of radius s.

6.4 PERTURBATION SOLUTION

Various authors have examined or exploited the possibility of solving axisymmetric contact problems via perturbation methods. Aleksandrov (1968) ranks a variety of solution techniques for extreme values of layer thickness to contact radius ratios, which include a perturbation approach, but he does not present applicable results. Aleksandrov and Vorovich (1960) solve the three dimensional indentation problem of a rigid die pressing a layer of finite thickness, by employing a perturbation-type solution. A flat, elliptic die pressing a layer of relatively high thickness is considered in detail. The perturbation method is employed by Dhaliwal (1970) to solve axisymmetric problems. In particular, the case of a cylindrical, flat punch indenting a layer bonded to a deformable half-space is treated, and various curves are presented. The extension to conical, paraboloidal, ellipsoidal and spherical punches is presented in Dhaliwal and Rau (1970), where the same perturbation-type technique is employed. In this paper, however, only the analytical aspects are addressed, and no practically significant results are presented.

The main idea of the perturbation solution is to express the unknown contact pressure profile in terms of a power series expansion with respect to the small parameter a/t , where a denotes the contact radius and t indicates the layer thickness, whose powers multiplies yet unknown functions p_j . Similarly, the kernel of the integral equation is expanded into a power series, where the small parameter a/t affects its coefficients. By collecting like powers of a/t , the initial integral equation is split into a series of simpler problems, whose solutions are the functions p_j (Bender and Orszag (1978)). Such functions constitute the terms of a series expansion for the unknown contact pressure. In comparison to solutions in which the shape of the pressure profile is defined *a priori* (Jaffar (1988)), the perturbation technique produces an analytical pressure profile for every perturbation order and, consequently, it hopefully reduces the number of series terms capable of expressing the contact pressure with a given accuracy.

The main limit of the perturbation approach is that it is valid only for a restricted a/h field, say $a/h < 1$. In biomechanical applications, the above ratio is generally very high, so that the applicability of the perturbed results is limited. On

the other side, during walking conditions situations are met when the load and, consequently, the contact radius, becomes small, so that the corresponding situation can be mimicked by the perturbed model. In any case, the perturbation solution constitutes a benchmark for numerical (finite element) results, whose accuracy is often questionable when treating nearly incompressible components.

The problem of the series expansion for the axisymmetric kernel (6.3.5) is treated below.

6.4.1 Kernel series expansion

Following Meijers (1968) and Jaffar (1988), the singularity of the form $1/r$ (as suggested by the purely Hertzian solution) will be extracted from the axisymmetric kernel (6.4.1.1), so that the regular remainder can be expanded in power series :

$$K_{axi}(r,s) = \int_0^\infty L(\omega)\, J_o(\beta r\omega)\, J_o(\beta s\omega)\, d\omega \qquad (6.4.1.1)$$

Function $L(\omega)$ approaches unity for $\omega \simeq 5$ (see Fig. 4.3.2.4), so that it seems natural to write, following Popov (1962), Aleksandrov (1967), and Jaffar (1988) :

$$L(\omega) = 1 - (1 - L(\omega)) \qquad (6.4.1.2)$$

By substituting (6.4.1.2) into (6.4.1.1), and by using the following result (Byrd and Friedman (1954), p. 249, formula 560.01 with p=0 , Luke (1962), p. 316, formula (16), Aleksandrov (1967), Jaffar (1988), Li and Dempsey (1990), formula (7) with a=0) :

$$\int_0^\infty J_o(\beta r\omega)\, J_o(\beta s\omega)\, d\omega = \frac{2}{\pi\beta\,(r+s)}\, K\left(\frac{2\sqrt{rs}}{r+s}\right) \qquad (6.4.1.3)$$

where K is the complete elliptic integral function of the first kind, one can write :

$$K_{axi}(r,s) = \frac{2}{\pi\beta\,(r+s)}\, K\left(\frac{2\sqrt{rs}}{r+s}\right) + \int_0^\infty (L(\omega) - 1)\, J_o(\beta r\omega)\, J_o(\beta s\omega)\, d\omega \qquad (6.4.1.4)$$

where the integral part of (6.4.1.4) constitutes the regular part of the axisymmetric kernel (6.4.1.1), and the remaining component corresponds to the purely Hertzian solution (Jaffar (1988)).

It was observed in Section 6.3 that the axisymmetric formulation is analogous to the plane case, where a main difference is that in plane problems the kernel depends upon the absolute value of the difference between variables x and s (see (4.3.2.6)), whereas in axisymmetric circumstances the dependence on the corresponding variables r and s is more complex. Anyway, it can be observed that a behaviour similar to an absolute value filtering is comprised in integral (6.4.1.3), as it appears from its equivalent formulation of Li and Dempsey (1990), formula (6) (see also Luke (1962), p. 326 , formula (11)).

From a practical viewpoint, the parenthetical term (L(ω) - 1) in (6.4.1.4) essentially vanishes for $\omega > 5$, see Fig. 4.3.2.4 , so that the numerical evaluation of the integral part of (6.4.1.4) can be limited to the interval $0 \leq \omega \leq 5$. Anyway, to ease the numerical evaluation of the derivatives of (6.4.1.4) with respect to r and s , which intervene in the power expansion of the kernel, and which vanish considerably more slowly, thus requiring a more generous integration interval, it is convenient to extract other terms from the integral part of (6.4.1.4), similarly to what was done in Section 4.3.5, formula (4.3.5.7). By applying the results of formula (4.3.2.27), the following approximation is obtained :

$$L(\omega) - 1 \simeq - \frac{4}{\gamma} \omega^2 e^{-2\omega} - \frac{4}{\gamma} \omega e^{-2\omega} + \ . \ . \ . \qquad (6.4.1.5)$$

where, as it appears from Fig. 4.3.2.6, it is not beneficial to account for additional asymptotic terms in (6.4.1.5).

The next step is to examine which integrals exist in analytical form, whose integrand is formed by the product of two Bessel functions - as in (6.4.1.1) - by the approximate expansion of function $L(\omega)$ according to (6.4.1.5). Luke (1962) reports the following integral at p. 316, formula (19) :

$$\int_0^\infty \omega e^{-p\omega} J_o(\beta r \omega) J_o(\beta s \omega) d\omega = \frac{p k^3 E(k)}{4 \pi \beta^3 (r s)^{3/2} (1 - k^2)} \qquad (6.4.1.6)$$

where :

$$k^2 = \frac{4\,\beta^2\,r\,s}{p^2 + \beta^2\,(r+s)^2} \tag{6.4.1.7}$$

and E denotes the complete elliptic integral of the second kind. The result of interest is obtained for $p = 2$.

According to (6.4.1.5), the next task is to evaluate the following integral :

$$\int_0^\infty \omega^2\, e^{-p\omega} J_o\,(\beta r\omega)\, J_o\,(\beta s\omega)\, d\omega \tag{6.4.1.8}$$

which could not be traced in the various specialized manuals quoted above. Anyway, this integral can be determined by differentiating both members of (6.4.1.6) with respect to p , and by remembering that (Byrd and Friedman (1954), p. 283 , formula 710.02) :

$$\frac{d\,E}{d\,k} = \frac{E - K}{k} \tag{6.4.1.9}$$

Therefore :

$$\int_0^\infty \omega^2\, e^{-p\omega} J_o\,(\beta r\omega)\, J_o\,(\beta s\omega)\, d\omega =$$

$$-\frac{k^3}{4\,\pi\,\beta^3\,(r\,s)^{3/2}\,(1-k^2)}\left[E\,(k)\left[1 - \frac{p^2k^2}{\beta^2\,r\,s} - \frac{p^2\,k^4}{2\,\beta^2\,r\,s\,(1-k^2)}\right] + K\,(k)\,\frac{p^2\,k^2}{4\,\beta^2\,r\,s}\right] \tag{6.4.1.10}$$

where the result of importance is achieved for $p = 2$. In formula (6.4.1.10), k is again defined by (6.4.1.7). Both integrals (6.4.1.6) and (6.4.1.10) were checked

numerically, by employing the polynomial approximations for the elliptic integrals of Abramowitz and Stegun (1972), pp. 591-592 , formulae (17.3.34) and (17.3.36) , and the polynomial approximations for the Bessel functions of Abramowitz and Stegun (1972), pp. 378-379 , formulae (9.8) .

By taking into account formulae (6.4.1.2), (6.4.1.3), (6.4.1.5), (6.4.1.6) and (6.4.1.10), and by setting $p = 2$ in (6.4.1.6) and in (6.4.1.10), formula (6.4.1.1) can be written as :

$$K_{axi}(r,s) = \frac{2}{\pi\beta\,(r+s)}\,K\left(\frac{2\sqrt{rs}}{r+s}\right) +$$

$$\frac{k^3}{\pi\,\beta^3\,\gamma\,(r\,s)^{3/2}\,(1-k^2)}\left[K(k)\,\frac{k^2}{\beta^2 r\,s} - E(k)\left(1+\frac{4\,k^2}{\beta^2 r\,s}+\frac{2\,k^4}{\beta^2\,r\,s\,(1-k^2)}\right)\right] +$$

$$\int_0^\infty \left[L(\omega) - 1 + \frac{4}{\gamma}\,\omega^2\,e^{-2\omega} + \frac{4}{\gamma}\,\omega\,e^{-2\omega}\right] J_o(\beta r\omega)\,J_o(\beta s\omega)\,d\omega \qquad (6.4.1.11)$$

where k is defined in (6.4.1.7), by setting $p = 2$.

The following equivalent formulation of (6.4.1.11), obtained by employing (6.4.1.7), lends itself to be more easily expanded in a power series :

$$K_{axi}(r,s) = \frac{2}{\pi\beta\,(r+s)}\,K\left(\frac{2\sqrt{rs}}{r+s}\right) +$$

$$\frac{8}{\pi\,\gamma}\,\frac{\left[4\,K(k) - E(k)\left[20+\beta^2(r+s)^2+\frac{32\,\beta^2\,r\,s}{4+\beta^2(r-s)^2}\right]\right]}{\left[4+\beta^2(r+s)^2\right]^{3/2}\left[4+\beta^2(r-s)^2\right]} +$$

$$\int_0^\infty \left[L(\omega) - 1 + \frac{4}{\gamma}\,\omega^2\,e^{-2\omega} + \frac{4}{\gamma}\,\omega\,e^{-2\omega}\right] J_o(\beta r\omega)\,J_o(\beta s\omega)\,d\omega \qquad (6.4.1.12)$$

The parenthetical part in the integral appearing in formula (6.4.1.12) vanishes very quickly, say for $\omega > 2$ (see Fig. 4.3.2.6), so that a numerical integration becomes feasible, where the integration field can be limited to the $0 \leq \omega \leq 2$ interval. Indeed, formulation (6.4.1.12) lends itself to a power expansion of the axisymmetric kernel, since the integral part to be computed numerically is now restricted to a limited ω interval.

The expression for the series expansion of a two-dimensional function is reported below, having in mind the regular part of the axisymmetric kernel (6.4.1.1). The Mac Laurin expansion of a generic function $f\ (x,y)$ is (Greenberg (1978), p. 126) :

$$f\ (x,y) = \sum_{m=0}^{\infty} \sum_{n=0}^{\infty} \frac{1}{m!\ n!} \frac{\partial^{m+n} f\ (0,0)}{\partial\ x^m\ \partial\ y^n}\ x^m\ y^n \qquad (6.4.1.13)$$

It should be observed that the centre of this expansion is taken at x , $y = 0$, whereas in the plane analogue (Chapter 4, Section 4.3.5) the centre was assumed at $x \equiv y$. A series expansion referring to $x \equiv y$ as its centre would exhibit coefficients depending on $x \equiv y$, since when $x \rightarrow 0$ the problem mimicked would be that of a concentrated force applied at the origin, whereas when $x \rightarrow \infty$ the situation described would approach that of a linear load applied along a straight line. Due to these prospected difficulties, it was decided to adopt a series expansion in the vicinity of the axis origin.

In the case under scrutiny the kernel is a symmetric function of its two variables. This implies that :

$$\frac{\partial^{m+n} f\ (0,0)}{\partial\ x^m\ \partial\ y^n} = \frac{\partial^{m+n} f\ (0,0)}{\partial\ x^n\ \partial\ y^m} \qquad (6.4.1.14)$$

so that our series expansion (6.4.1.13) simplifies to :

$$f(x,y) = f(0,0) + \frac{\partial f(0,0)}{\partial x}(x+y) +$$

$$\frac{1}{2}\left[\frac{\partial^2 f(0,0)}{\partial x^2}(x^2+y^2) + 2\,\frac{\partial^2 f(0,0)}{\partial x\,\partial y}\,x\,y\right] +$$

$$\frac{1}{6}\left[\frac{\partial^3 f(0,0)}{\partial x^3}(x^3+y^3) + 3\,\frac{\partial^3 f(0,0)}{\partial x^2\,\partial y}\,x\,y\,(x+y)\right] +$$

$$\frac{1}{24}\left[\frac{\partial^4 f(0,0)}{\partial x^4}(x^4+y^4) + 4\,\frac{\partial^4 f(0,0)}{\partial x^3\,\partial y}\,x\,y\,(x^2+y^2) + 6\,\frac{\partial^4 f(0,0)}{\partial x^2\,\partial y^2}\,x^2\,y^2\right] +$$

$$\frac{1}{120}\left[\frac{\partial^5 f(0,0)}{\partial x^5}(x^5+y^5) + 5\,\frac{\partial^5 f(0,0)}{\partial x^4\,\partial y}\,x\,y\,(x^3+y^3) +\right.$$

$$\left. 10\,\frac{\partial^5 f(0,0)}{\partial x^3\,\partial y^2}\,x^2\,y^2\,(x+y)\right] +$$

$$\frac{1}{720}\left[\frac{\partial f^6(0,0)}{\partial x^6}(x^6+y^6) + 6\,\frac{\partial^6 f(0,0)}{\partial x^5\,\partial y}\,x\,y\,(x^4+y^4) +\right.$$

$$\left. 15\,\frac{\partial^6 f(0,0)}{\partial x^4\,\partial y^2}\,x^2\,y^2\,(x^2+y^2) + 20\,\frac{\partial^6 f(0,0)}{\partial x^3\,\partial y^3}\,x^3\,y^3\right] + \ldots . \qquad (6.4.1.15)$$

In the following it is intended to show that, due to the specific character of the problem under study, many other parts of the series expansion (6.4.1.15) actually vanish. In fact, referring to Fig. 6.3.1 , the displacement by the axis origin

due to a unit linear load acting along the circumference of radius s must posses vanishing odd-order derivatives with respect to r and computed for $r = 0$. This it a physical consequence of the symmetry of the loading. More generally, all derivatives of the kind :

$$\frac{\partial^{n+m} f(0,0)}{\partial r^n \partial s^m} \Big|_{n \text{ odd}, m = 0,1,2,3..} \qquad (6.4.1.16)$$

must vanish. The analogous derivatives obtained by interchanging r and s must vanish too. This is mathematically confirmed by a close examination of (6.4.1.4), whose integral part contains the product of two Bessel functions of the first kind and order zero depending upon r and s , respectively. Now, the odd order derivatives of this Bessel function vanish for vanishing argument (Abramowitz and Stegun (1972), pp. 360 , formula (9.1.12)) .

An example is now treated which supports the above speculations regarding the vanishing parts of (6.4.1.15). It is first observed that the regular part of the axisymmetric kernel can be interpreted in physical terms, with the help of the following modelling. A half space is loaded by a unit linear load along a circumference of radius s. In the actual situation, however, the loading is sustained by a layer of thickness t , bonded to a rigid substrate. The axisymmetric loading acting upon the half space will produce a non vanishing displacement field at the depth t, where in the actual circumstances any deflection should be precluded. A half-space model can still be adopted to mimic a deformable layer anchored to a rigid foundation, provided that a corrective stress distribution is applied at a depth t , which makes the total displacement field (that due to the surface linear loading plus that deriving from this correction applied at a depth t) vanish. The regular part of the axisymmetric kernel represents such a correction. To support the above conclusions regarding the vanishing of several series terms as effected in (6.4.1.15), a situation representative of this correction term is examined, and the derivatives (6.4.1.16) are explicitly computed. Although the comparison here proposed is not completely rigorous, the correction factor is conjectured to behave - in terms of

displacements - similarly to the situation of a half space loaded along a surface circular portion by a unit, uniform pressure, the main source of dispute being the fact that this correction circular loading is applied to the surface of the half space, and not at a depth t. The above case is treated by Johnson (1985), p. 56 . For a point inside the loaded circumference of radius a , the surface vertical displacement is :

$$u = \frac{4\,(1 - \nu^2)\,a}{\pi\,E}\,E\left(\frac{r}{a}\right) \tag{6.4.1.17}$$

For a point outside the loaded circle, the surface vertical displacement is :

$$u = \frac{4\,(1 - \nu^2)\,r}{\pi\,E}\left[E\left(\frac{a}{r}\right) - \left(1 - \frac{a^2}{r^2}\right)K\left(\frac{a}{r}\right)\right] \tag{6.4.1.18}$$

From (6.4.1.17), by accounting for (6.4.1.9) and for the series expansions (17.3.11) of Abramowitz and Stegun (1972), p. 591 , it appears that :

$$\frac{\partial u}{\partial r}\Big|_{r=0} = \frac{4\,(1 - \nu^2)\,a}{\pi\,E}\,\frac{E\left(\frac{r}{a}\right) - K\left(\frac{r}{a}\right)}{r}\Big|_{r=0} \simeq$$

$$\frac{4\,(1 - \nu^2)\,a}{\pi\,E}\,\frac{\pi\left(1 - \frac{r^2}{4\,a^2} - 1 - \frac{r^2}{4\,a^2}\right)}{2\,r}\Big|_{r=0} = 0 \tag{6.4.1.19}$$

and any derivative of (6.4.1.19) with respect to a (which takes the part of variable s in the regular portion of the axisymmetric kernel (6.4.1.1)) would equally vanish.

It is derived from the above observations that the series expansion of the regular part (here denoted by f (x,y)) of the axisymmetric kernel simplifies to :

$$f(x,y) = f(0,0) + \frac{1}{2}\left[\frac{\partial^2 f(0,0)}{\partial x^2}(x^2 + y^2)\right] +$$

$$\frac{1}{24}\left[\frac{\partial^4 f(0,0)}{\partial x^4}(x^4 + y^4) + 6\,\frac{\partial^4 f(0,0)}{\partial x^2\,\partial y^2}\,x^2 y^2\right] +$$

$$\frac{1}{720}\left[\frac{\partial f^6(0,0)}{\partial x^6}(x^6 + y^6) + 15\,\frac{\partial^6 f(0,0)}{\partial x^4\,\partial y^2}\,x^2 y^2 (x^2 + y^2)\right] + \ldots$$

(6.4.1.20)

Going back to (6.4.1.12), it is possible to write:

$$K_{axi}(r,s) = \frac{2}{\pi\beta(r+s)}\,K\left(\frac{2\sqrt{rs}}{r+s}\right) + K_{axi,\,reg}(r,s) \qquad (6.4.1.21)$$

where $K_{axi,\,reg}(r,s)$ denotes the regular part of the axisymmetric kernel, and it is easily identifiable through a comparison with formula (6.4.1.12) :

$$K_{axi,\,reg}(r,s) =$$

$$\frac{8}{\pi\gamma}\,\frac{4K(k) - E(k)\left[20 + \beta^2(r+s)^2 + \dfrac{32\,\beta^2 r\,s}{4 + \beta^2(r-s)^2}\right]}{\left[4 + \beta^2(r+s)^2\right]^{3/2}\left[4 + \beta^2(r-s)^2\right]} +$$

$$\int_0^\infty \left[L(\omega) - 1 + \frac{4}{\gamma}\,\omega^2 e^{-2\omega} + \frac{4}{\gamma}\,\omega\, e^{-2\omega}\right] J_o(\beta r\omega)\, J_o(\beta s\omega)\, d\omega \qquad (6.4.1.22)$$

By employing a Taylor expansion according to (6.4.1.20) for the kernel regular part of (6.4.1.22) , expression (6.4.1.21) can be reformulated as :

$$K_{axi}(r,s) \simeq \frac{2}{\pi\beta\,(r+s)}\,K\left(\frac{2\sqrt{rs}}{r+s}\right) + K_{axi,\,reg}(0,0) +$$

$$\frac{1}{2}\left[\frac{\partial^2 K_{axi,\,reg}(0,0)}{\partial r^2}\,(r^2+s^2)\right] +$$

$$\frac{1}{24}\left[\frac{\partial^4 K_{axi,\,reg}(0,0)}{\partial r^4}\,(r^4+s^4) + 6\,\frac{\partial^4 K_{axi,\,reg}(0,0)}{\partial r^2\,\partial s^2}\,r^2 s^2\right] +$$

$$\frac{1}{720}\left[\frac{\partial^6 K_{axi,\,reg}(0,0)}{\partial r^6}\,(r^6+s^6) + 15\,\frac{\partial^6 K_{axi,\,reg}(0,0)}{\partial r^4\,\partial s^2}\,r^2 s^2\,(r^2+s^2)\right] + \ldots$$

(6.4.1.23)

In the following the series expansion is evaluated up to the sixth order included. It was decided not to examine higher order terms for two reasons : a) the results of Section 4.3.5 dealing with the corresponding plane problem indicate that the sixth order is a good trade-off between simplicity and accuracy; b) the computations become prohibitively complicated for higher derivatives.

Following Meijers (1968), formula (2.3), eqn (6.4.1.23) is rewritten by evidencing ratio a/t and by employing $r/2$ and $s/2$ variables :

$$K_{axi}(r,s) = \frac{2}{\pi\beta\,(r+s)}\,K\left(\frac{2\sqrt{rs}}{r+s}\right) + K_{axi,\,reg}(0,0) +$$

$$\left[\frac{a}{t}\right]^2 \left[2 \frac{\partial^2 K_{axi,\,reg}(0,0)}{\partial r^2} \left[\frac{t}{a}\right]^2 \right] \left[\left(\frac{r}{2}\right)^2 + \left(\frac{s}{2}\right)^2 \right] +$$

$$\left[\frac{a}{t}\right]^4 \left\{ \left[\frac{2}{3} \frac{\partial^4 K_{axi,\,reg}(0,0)}{\partial r^4} \left[\frac{t}{a}\right]^4 \right] \left[\left(\frac{r}{2}\right)^4 + \left(\frac{s}{2}\right)^4 \right] \right.$$

$$\left. + \left[4 \frac{\partial^4 K_{axi,\,reg}(0,0)}{\partial r^2 \partial s^2} \left[\frac{t}{a}\right]^4 \right] \left[\left(\frac{r}{2}\right)^2 \left(\frac{s}{2}\right)^2 \right] \right\} +$$

$$\left[\frac{a}{t}\right]^6 \left\{ \left[\frac{4}{45} \frac{\partial^6 K_{axi,\,reg}(0,0)}{\partial r^6} \left[\frac{t}{a}\right]^6 \right] \left[\left(\frac{r}{2}\right)^6 + \left(\frac{s}{2}\right)^6 \right] + \right.$$

$$\left. \left[\frac{4}{3} \frac{\partial^6 K_{axi,\,reg}(0,0)}{\partial r^4 \partial s^2} \left[\frac{t}{a}\right]^6 \right] \left(\frac{r}{2}\right)^2 \left(\frac{s}{2}\right)^2 \left[\left(\frac{r}{2}\right)^2 + \left(\frac{s}{2}\right)^2 \right] \right\} + \cdots$$

(6.4.1.24)

Finally, following again Meijers (1968) , formula (2.6), the equation (6.4.1.24) of this thesis can be rewritten, by introducing α_{ij} coefficients, as :

$$K_{axi}(r,s) = \frac{2}{\pi\beta (r+s)} K\left(\frac{2\sqrt{rs}}{r+s} \right) + \alpha_0 +$$

$$\left[\frac{a}{t}\right]^2 \alpha_{20} \left[\left(\frac{r}{2}\right)^2 + \left(\frac{s}{2}\right)^2 \right] +$$

$$\left[\frac{a}{t}\right]^4 \left[\alpha_{40} \left[\left(\frac{r}{2}\right)^4 + \left(\frac{s}{2}\right)^4 \right] + \alpha_{22} \left[\left(\frac{r}{2}\right)^2 \left(\frac{s}{2}\right)^2 \right] \right] +$$

$$\left(\frac{a}{t}\right)^6 \left[\alpha_{60}\left[\left(\frac{r}{2}\right)^6+\left(\frac{s}{2}\right)^6\right]+\alpha_{42}\left(\frac{r}{2}\right)^2\left(\frac{s}{2}\right)^2\left[\left(\frac{r}{2}\right)^2+\left(\frac{s}{2}\right)^2\right]\right]+$$

$$\ldots \qquad (6.4.1.25)$$

where :

$$\alpha_0 = K_{axt.\ reg}(0,0)$$

$$\alpha_{20} = 2\,\frac{\partial^2 K_{axt.\ reg}(0,0)}{\partial r^2}\left(\frac{t}{a}\right)^2$$

$$\alpha_{40} = \frac{2}{3}\,\frac{\partial^4 K_{axt.\ reg}(0,0)}{\partial r^4}\left(\frac{t}{a}\right)^4$$

$$\alpha_{60} = \frac{4}{45}\,\frac{\partial^6 K_{axt.\ reg}(0,0)}{\partial r^6}\left(\frac{t}{a}\right)^6$$

$$\alpha_{22} = 4\,\frac{\partial^4 K_{axt.\ reg}(0,0)}{\partial r^2\,\partial s^2}\left(\frac{t}{a}\right)^4$$

$$\alpha_{42} = \frac{4}{3}\,\frac{\partial^6 K_{axt.\ reg}(0,0)}{\partial r^4\,\partial s^2}\left(\frac{t}{a}\right)^6 \qquad (6.4.1.26)$$

The Taylor series convergence aspects are not examined here. It is only noted that for the plane case Meijers (1968) reports that the regular remainder possesses a uniformly convergent power series for $|x/2t| < 1$ and, similarly, Dhaliwal (1970) observes that by the ratio test it can be shown that for his axisymmetric case the corresponding series is absolutely convergent for $x < 2\,t$.

The next step is the computation of coefficients α_{ij} . High order derivatives of (6.4.1.22) with respect to variables r and s are needed. To do so, the derivatives of the complete elliptic integrals K (k) and E (k) with respect to their modulus k are of considerable help. Byrd and Friedman (1954) report at p. 282 these derivatives - expressed in terms of elliptic functions - up to the second order included, but they

express higher derivatives only in terms of the hypergeometric function. It was therefore decided to compute such derivatives - in terms of elliptic functions - up to the sixth order, where the algebraic manipulator MACSYMA (1983) was of considerable help in performing the very lengthy calculations. The results are as follows :

$$\frac{d\,K(k)}{d\,k} = \frac{E(k) - (1 - k^2)\,K(k)}{k\,(1 - k^2)}$$

$$\frac{d^2\,K(k)}{d\,k^2} = \frac{(1 - k^2)\,(1 - 2\,k^2)\;K(k) + (3\,k^2 - 1)\,E(k)}{k^2\,(1 - k^2)^2}$$

$$\frac{d^3\,K(k)}{d\,k^3} = \frac{-2\,(1 - k^2)\,(1 - 2\,k^2 + 3\,k^4)\;K(k) + (11\,k^4 - 5\,k^2 + 2)\,E(k)}{k^3\,(1 - k^2)^3}$$

$$\frac{d^4K(k)}{d\,k^4} = \frac{-(1 - k^2)(24\,k^6 - 13\,k^4 + 19\,k^2 - 6)\,K(k) + 2\,(25\,k^6 - 9\,k^4 + 11\,k^2 - 3)\,E(k)}{k^4\,(1 - k^2)^4}$$

$$\frac{d^5K(k)}{d\,k^5} = \frac{-(1 - k^2)\,(120\,k^8 - 17\,k^6 + 166\,k^4 - 101\,k^2 + 24)\,K(k)}{k^5\,(1 - k^2)^5} +$$

$$\frac{(274\,k^8 - 13\,k^6 + 212\,k^4 - 113\,k^2 + 24)\,E(k)}{k^5\,(1 - k^2)^5}$$

$$\frac{d^6K(k)}{d\,k^6} = \frac{-3\,(1 - k^2)\,(240\,k^{10} + 126\,k^8 + 549\,k^6 - 444\,k^4 + 209\,k^2 - 40)\,K(k)}{k^6\,(1 - k^2)^5} +$$

$$\frac{3\,(588\,k^{10} + 285\,k^8 + 759\,k^6 - 541\,k^4 + 229\,k^2 - 40)\,E(k)}{k^6\,(1 - k^2)^6} \qquad (6.4.1.27)$$

$$\frac{d\,E\,(k)}{d\,k} = \frac{E\,(k) - K\,(k)}{k}$$

$$\frac{d^2\,E\,(k)}{d\,k^2} = \frac{(1 - k^2)\,K\,(k) - E\,(k)}{k^2\,(1 - k^2)}$$

$$\frac{d^3\,E\,(k)}{d\,k^3} = \frac{(1 - k^2)\,(3\,k^2 - 2)\,K\,(k) - 2\,(2\,k^2 - 1)\,E\,(k)}{k^3\,(1 - k^2)^2}$$

$$\frac{d^4E\,(k)}{d\,k^4} = \frac{2\,(1 - k^2)(6\,k^4 - 7\,k^2 + 3)\,K\,(k) - (19\,k^4 - 17\,k^2 + 6)\,E\,(k)}{k^4\,(1 - k^2)^3}$$

$$\frac{d^5E\,(k)}{d\,k^5} = \frac{(1 - k^2)\,(60\,k^6 - 91\,k^4 + 79\,k^2 - 24)\,K\,(k)}{k^5\,(1 - k^2)^4} -$$

$$\frac{(107\,k^6 - 126\,k^4 + 91\,k^2 - 24)\,E\,(k)}{k^5\,(1 - k^2)^4}$$

$$\frac{d^6E\,(k)}{d\,k^6} = \frac{3\,(1 - k^2)\,(120\,k^8 - 207\,k^6 + 282\,k^4 - 171\,k^2 + 40)\,K\,(k)}{k^6\,(1 - k^2)^5} -$$

$$\frac{3\,(234\,k^8 - 315\,k^6 + 360\,k^4 - 191\,k^2 + 40)\,E\,(k)}{k^6\,(1 - k^2)^5} \qquad (6.4.1.28)$$

The following function is now introduced, which constitutes the non integral component of the regular part of the axisymmetric kernel (see (6.4.1.22)) :

$$K_{axi,\ reg,\ non\ int}\ (r,s) =$$

$$\frac{8}{\pi\,\gamma}\ \frac{4\,K\,(k) - E\,(k)\left[\,20 + \beta^2\,(r+s)^2 + \dfrac{32\,\beta^2\,r\,s}{4+\beta^2\,(r-s)^2}\,\right]}{\left[4+\beta^2\,(r+s)^2\,\right]^{3/2}\left[4+\beta^2\,(r-s)^2\,\right]} \qquad (6.4.1.29)$$

The following useful limits and derivatives of the non integral component of the regular part of the axisymmetric kernel were obtained after lengthy calculations partially performed with the aid of the algebraic manipulator MACSYMA (1983), by exploiting (6.4.1.28) :

$$K_{axi,\ reg,\ non\ int}\ (r,s)\ |_{\,r\,=\,0\,,\ s\,=\,0} = -\frac{2}{\gamma}$$

$$\frac{\partial^2 K_{axi,\ reg,\ non\ int}\ (r,s)}{\partial\, r^2}\ |_{\,r\,=\,0\,,\ s\,=\,0} = \frac{9}{4}\,\frac{\beta^2}{\gamma}$$

$$\frac{\partial^4 K_{axi,\ reg,\ non\ int}\ (r,s)}{\partial\, r^4}\ |_{\,r\,=\,0\,,\ s\,=\,0} = -\frac{45}{4}\,\frac{\beta^4}{\gamma}$$

$$\frac{\partial^6 K_{axi,\ reg,\ non\ int}\ (r,s)}{\partial\, r^6}\ |_{\,r\,=\,0\,,\ s\,=\,0} = \frac{7875}{64}\,\frac{\beta^6}{\gamma}$$

$$\frac{\partial^4 K_{axi,\ reg,\ non\ int}\ (r,s)}{\partial\, r^2\,\partial\, s^2}\ |_{\,r\,=\,0\,,\ s\,=\,0} = -\frac{15}{2}\,\frac{\beta^4}{\gamma}$$

$$\frac{\partial^6 K_{axi,\ reg,\ non\ int}\ (r,s)}{\partial\, r^4\,\partial\, s^2}\ |_{\,r\,=\,0\,,\ s\,=\,0} = \frac{4725}{64}\,\frac{\beta^6}{\gamma} \qquad (6.4.1.30)$$

The following limit values of the Bessel functions are also of use :

$$J_0(\beta r\omega)\,|_{r=o} = 1$$

$$J_0(\beta s\omega)\,|_{s=o} = 1$$

$$\frac{\partial^2 J_0(\beta r\omega)}{\partial r^2}\,|_{r=o} = -\frac{\beta^2\omega^2}{2}$$

$$\frac{\partial^4 J_0(\beta r\omega)}{\partial r^4}\,|_{r=o} = \frac{3\beta^4\omega^4}{8}$$

$$\frac{\partial^6 J_0(\beta r\omega)}{\partial r^6}\,|_{r=o} = -\frac{5\beta^6\omega^6}{16}$$

$$\frac{\partial^4 J_0(\beta r\omega)\,J_0(\beta s\omega)}{\partial r^2\,\partial s^2}\,|_{r=o,\,s=o} = \frac{\beta^4\omega^4}{4}$$

$$\frac{\partial^6 J_0(\beta r\omega)\,J_0(\beta s\omega)}{\partial r^4\,\partial s^2}\,|_{r=o,\,s=o} = -\frac{3\beta^6\omega^6}{16} \qquad (6.4.1.31)$$

By employing (6.4.1.26), (6.4.1.30) and (6.4.1.31), the following final expressions for coefficients α_{ij} are obtained :

$$\alpha_0 = -\frac{2}{\bar{\gamma}} + \int_0^\infty \left[L(\omega) - 1 + \frac{4}{\bar{\gamma}}\omega^2 e^{-2\omega} + \frac{4}{\bar{\gamma}}\omega e^{-2\omega} \right] d\omega$$

$$\alpha_{20} = \frac{9}{2\bar{\gamma}} - \int_0^\infty \left[L(\omega) - 1 + \frac{4}{\bar{\gamma}}\omega^2 e^{-2\omega} + \frac{4}{\bar{\gamma}}\omega e^{-2\omega} \right] \omega^2\, d\omega$$

$$\alpha_{40} = -\frac{15}{2\bar{\gamma}} + \frac{1}{4}\int_0^\infty \left[L(\omega) - 1 + \frac{4}{\bar{\gamma}}\omega^2 e^{-2\omega} + \frac{4}{\bar{\gamma}}\omega e^{-2\omega} \right] \omega^4\, d\omega$$

$$\alpha_{60} = \frac{175}{16\,\gamma} - \frac{1}{36}\int_0^\infty \left[L(\omega) - 1 + \frac{4}{\gamma}\,\omega^2\, e^{-2\omega} + \frac{4}{\gamma}\,\omega\, e^{-2\omega} \right] \omega^6\, d\omega$$

$$\alpha_{22} = -\frac{30}{\gamma} + \int_0^\infty \left[L(\omega) - 1 + \frac{4}{\gamma}\,\omega^2\, e^{-2\omega} + \frac{4}{\gamma}\,\omega\, e^{-2\omega} \right] \omega^4\, d\omega$$

$$\alpha_{42} = \frac{1575}{16\,\gamma} - \frac{1}{4}\int_0^\infty \left[L(\omega) - 1 + \frac{4}{\gamma}\,\omega^2\, e^{-2\omega} + \frac{4}{\gamma}\,\omega\, e^{-2\omega} \right] \omega^6\, d\omega \qquad (6.4.1.32)$$

When $\omega \to \infty$, the integrand of the integral part of (6.4.1.11) is asymptotically equivalent to $e^{-2\omega}$ (see formula (4.3.2.27), which should be multiplied by ω to change the plane case into the axisymmetric one), so that all integrands in (6.4.1.32) vanish rapidly and the corresponding integrals are finite, essentially regardless of the level of the differentiation order .

From a practical viewpoint, the integral from 0 to infinity in equations (6.4.1.32) can be computed from 0 to, say, 30 , since for any derivative considered (up to the sixth order) the integrand becomes vanishingly small beyond this upper limit. Similar to Chapter 4, Section 4.3.5 , the following TABLE reports the α_{ij} coefficients computed for ν = 0.48 and 0.5 :

TABLE of α_{ij}

	α_0	α_{20}	α_{40}	α_{60}	α_{22}	α_{42}
ν = 0.48	− 1.7067	3.6176	− 6.544	9.983	− 26.178	89.85
ν = 0.50	− 1.7702	3.8310	− 6.997	10.728	− 27.990	96.55

The decimal figures reported in this TABLE are believed to be exact, since they are stable with respect to changes in the integration upper limit and in the number of numerical integration points.

Similar to their plane counterparts of Chapter 4, in the axisymmetric geometry too the α_{ij} coefficients do not dramatically depend upon the value of the Poisson's ratio. This implies that the solution does not vary too much as a consequence of a perturbation of the Poisson's ratio, provided that the contact width is small. However, an opposite trend is expected for high contact width to layer thickness ratios.

The next step is the decomposition of the original integral problem (6.3.4), particularized to the case of a paraboloidal indenter, into a series of simpler subproblems, according to a typical perturbation scheme (Bender and Orszag (1978)).

6.4.2 Decomposition into subproblems

The normalized integral equation expressing the penetration δ of a paraboloidal indenter of radius R into a flat layer of thickness t firmly bonded to a rigid substrate is (see eqn (6.3.4)) :

$$2\,\alpha\beta a \int_0^1 K_{axi}(r,s)\, p(s)\, s\, ds = \delta - \frac{a^2 r^2}{2R} \qquad 0 \le r \le 1 \quad (6.4.2.1)$$

where a is the contact radius, $\alpha = (1 - \nu^2)/E$, $\beta = a/t$, $r = \bar{r}/a$, $s = \bar{s}/a$, where $\bar{r}$ and $\bar{s}$ denote the actual radial coordinates. Following (6.4.1.25), the axisymmetric kernel $K_{axi}(r,s)$ is approximated as follows :

$$K_{axi}(r,s) \simeq \frac{2t}{\pi a (r+s)} K\left(\frac{2\sqrt{rs}}{r+s}\right) + \alpha_0 +$$

$$\beta^2 \alpha_{20} \left[\left(\frac{r}{2}\right)^2 + \left(\frac{s}{2}\right)^2 \right] +$$

$$\beta^4 \left[\alpha_{40} \left[\left(\frac{r}{2}\right)^4 + \left(\frac{s}{2}\right)^4 \right] + \alpha_{22} \left[\left(\frac{r}{2}\right)^2 \left(\frac{s}{2}\right)^2 \right] \right] +$$

$$\beta^6 \left[\alpha_{60} \left[\left(\frac{r}{2}\right)^6 + \left(\frac{s}{2}\right)^6 \right] + \alpha_{42} \left(\frac{r}{2}\right)^2 \left(\frac{s}{2}\right)^2 \left[\left(\frac{r}{2}\right)^2 + \left(\frac{s}{2}\right)^2 \right] \right] +$$

. . . (6.4.2.2)

where term t/a has not been substituted by $1/\beta$ in the singular part of the approximate kernel, for reasons which will become clearer in the following Section. It is here anticipated that the presence of this term produces some problems in the perturbation technique, since the perturbed pressure terms will depend on β too. Anyway, if these aspects affect the mathematical clarity and perhaps they make a rigorous error estimate impossible, to the writer's opinion they do not undermine the usefulness of the solution achieved.

Following Meijers (1968), both members of (6.4.2.1) are differentiated with respect to r, where the approximate kernel (6.4.2.2) is employed, to eliminate both the rigid penetration, δ , and coefficient α_0 :

$$\int_0^1 \left[-\frac{t}{\pi a r} \left(\frac{K\left(\frac{2\sqrt{rs}}{r+s}\right)}{(r+s)} + \frac{E\left(\frac{2\sqrt{rs}}{r+s}\right)}{(r-s)} \right) + \right.$$

$$\beta^2 \left(\tfrac{1}{2} \alpha_{20} r \right) + \beta^4 \left(\tfrac{1}{4} \alpha_{40} r^3 + \tfrac{1}{8} \alpha_{22} r s^2 \right) +$$

$$\left. \beta^6 \left(\tfrac{3}{32} \alpha_{60} r^5 + \tfrac{1}{32} \alpha_{42} r s^2 (2 r^2 + s^2) \right) \right] p(s)\, s\, ds = -\frac{r t}{2 \alpha R} \qquad 0 \le r \le 1$$

(6.4.2.3)

In formula (6.4.3.2) the following derivative has been used, which has been computed with the help of the first result of (6.4.1.27) :

$$\frac{\partial}{\partial r} \frac{K\left(\frac{2\sqrt{rs}}{r+s}\right)}{(r+s)} = -\frac{1}{2r}\left[\frac{K\left(\frac{2\sqrt{rs}}{r+s}\right)}{(r+s)} + \frac{E\left(\frac{2\sqrt{rs}}{r+s}\right)}{(r-s)} \right] \qquad (6.4.2.4)$$

In addition, following Meijers (1968), his formula (2.7), the yet unknown contact pressure is expressed in the form of a power series with respect to the small parameter $\beta = a/t$, whose even powers multiply unknown p_i functions :

$$p(s) = p_0(s) + \beta^2 p_2(s) + \beta^4 p_4(s) + \beta^6 p_6(s) + \ldots \qquad (6.4.2.5)$$

By substituting (6.4.2.5) into (6.4.2.3) and by collecting like powers of β , the following four subproblems referring to β^0 , β^2 , β^4 , β^6 orders, respectively, are obtained :

$$\int_0^1 \left(\frac{K\left(\frac{2\sqrt{rs}}{r+s}\right)}{(r+s)} + \frac{E\left(\frac{2\sqrt{rs}}{r+s}\right)}{(r-s)} \right) s\, p_0(s)\, ds = \frac{\pi a r^2}{2 \alpha R} \quad ;$$

$$\int_0^1 \left(\frac{K\left(\frac{2\sqrt{rs}}{r+s}\right)}{(r+s)} + \frac{E\left(\frac{2\sqrt{rs}}{r+s}\right)}{(r-s)} \right) s\, p_2(s)\, s\, ds = \frac{\pi \alpha_{20} a r^2}{2 t} \int_0^1 p_0(s)\, s\, ds \quad ;$$

$$\int_0^1 \left(\frac{K\left(\frac{2\sqrt{rs}}{r+s}\right)}{(r+s)} + \frac{E\left(\frac{2\sqrt{rs}}{r+s}\right)}{(r-s)} \right) s\, p_4(s)\, s\, ds =$$

$$\frac{\pi a r^2}{8 t} \left(2 \alpha_{40} r^2 \int_0^1 p_0(s)\, s\, ds + \alpha_{22} \int_0^1 p_0(s)\, s^3\, ds + 4 \alpha_{20} \int_0^1 p_2(s)\, s\, ds \right) \quad ;$$

$$\int_0^1 \left[\frac{K\left(\frac{2\sqrt{rs}}{r+s}\right)}{(r+s)} + \frac{E\left(\frac{2\sqrt{rs}}{r+s}\right)}{(r-s)} \right] s\, p_6(s)\, s\, ds =$$

$$\frac{\pi a r^2}{32 t}\left(16\,\alpha_{20} \int_0^1 p_4(s)\, s\, ds + 8\, r^2\, \alpha_{40} \int_0^1 p_2(s)\, s\, ds + 4\,\alpha_{22} \int_0^1 p_2(s)\, s^3\, ds + \right.$$

$$\left. 3\, r^4\, \alpha_{60} \int_0^1 p_0(s)\, s\, ds + 2\, r^2\, \alpha_{42} \int_0^1 p_0(s)\, s^3\, ds + \alpha_{42} \int_0^1 p_0(s)\, s^5\, ds \right) \qquad (6.4.2.6)$$

6.4.3 Solution of the first and second subproblems

As already noted in Section 6.4.1, the first subproblem :

$$\int_0^1 \left[\frac{K\left(\frac{2\sqrt{rs}}{r+s}\right)}{(r+s)} + \frac{E\left(\frac{2\sqrt{rs}}{r+s}\right)}{(r-s)} \right] s\, p_0(s)\, ds = \frac{\pi\, a\, r^2}{2\,\alpha\, R} \qquad (6.4.3.1)$$

corresponds to the Hertzian problem of a paraboloidal indented compressed against a half space (Jaffar (1988)). It is, therefore, expected that the p_0 solution coincides with the Hertzian pressure profile. The following observations confirm this supposition.

The integral equation corresponding to the Hertzian problem is now formulated, whose solution is in fact the Hertzian pressure profile. The surface transverse deflection, w , of a half space loaded by a concentrated force, P , is (Johnson (1985), p. 52 , formula (3.22b)) :

$$w(\bar{r}) = \frac{1-\nu^2}{\pi E}\frac{P}{\bar{r}} \qquad (6.4.3.2)$$

where $\bar{r}$ is the distance from the applied load. Based on (6.4.3.2), the axisymmetric problem of a half-space loaded by an uniform linear load of intensity p (s) , applied along the circumference of radius s is now treated. Following Gladwell (1980), p. 81 , the corresponding surface transverse displacement at a distance $\bar{r}$ from the centre (Fig. 6.4.3.1 , where polar coordinates are used) is :

$$w(\bar{r}, \theta = 0) = \frac{1-\nu^2}{\pi E} 2 \int_0^{\pi} \frac{p(\bar{s})\,\bar{s}}{\sqrt{\bar{r}^2 + \bar{s}^2 - 2\,\bar{r}\,\bar{s}\cos\theta}}\, d\theta \qquad (6.4.3.3)$$

If the pressure is distributed along the radius $\bar{s}$ up to $\bar{s} = a$, the displacement, w , at point $(\bar{r}, \theta = 0)$ is :

$$w(\bar{r}, \theta = 0) = \frac{2(1 - \nu^2)}{\pi E} \int_0^{\pi} \int_0^{a} \frac{p(\bar{s})\, \bar{s}}{\sqrt{\bar{r}^2 + \bar{s}^2 - 2\bar{r}\bar{s}\cos\theta}}\, d\bar{s}\, d\theta =$$

$$\frac{2(1 - \nu^2)}{\pi E} \int_0^{a} p(\bar{s})\, \bar{s}\, d\bar{s} \int_0^{\pi} \frac{d\theta}{\sqrt{\bar{r}^2 + \bar{s}^2 - 2\bar{r}\,\bar{s}\cos\theta}} \qquad (6.4.3.4)$$

Following again Gladwell (1980), pp. 81-82 , the second integral is expressible in terms of the complete elliptic integral of the first kind :

$$\int_0^{\pi} \frac{d\theta}{\sqrt{\bar{r}^2 + \bar{s}^2 - 2\bar{r}\,\bar{s}\cos\theta}} = \int_0^{\pi} \frac{d\theta}{\sqrt{\bar{r}^2 + \bar{s}^2 - 2\bar{r}\,\bar{s}\,(2\cos^2\frac{\theta}{2} - 1)}} =$$

$$\int_0^{\pi} \frac{d\theta}{\sqrt{(\bar{r} + \bar{s})^2 - 4\bar{r}\,\bar{s}\cos^2\frac{\theta}{2}}} = \frac{2}{(\bar{r} + \bar{s})} \int_0^{\pi/2} \frac{d\alpha}{\sqrt{1 - 4\frac{\bar{r}\,\bar{s}}{(\bar{r} + \bar{s})^2}\cos^2\alpha}} =$$

$$\frac{2}{(\bar{r} + \bar{s})} K\left(\frac{2\sqrt{\bar{r}\,\bar{s}}}{\bar{r} + \bar{s}}\right) \qquad (6.4.3.5)$$

In conclusion, the axisymmetric Hertzian problem of a paraboloidal indenter of radius R is expressible in terms of the following Fredholm integral equation of the first kind, where the contact pressure , p , is the unknown :

$$\frac{4\alpha}{\pi} \int_0^{a} \frac{\bar{s}}{(\bar{r} + \bar{s})} K\left(\frac{2\sqrt{\bar{r}\,\bar{s}}}{\bar{r} + \bar{s}}\right) p(\bar{s})\, d\bar{s} = \delta - \frac{\bar{r}^2}{2R} \qquad (6.4.3.6)$$

By rewriting (6.4.3.6) with respect to normalized coordinates $r = \bar{r}/a$, $s = \bar{s}/a$, the following expression is finally obtained :

$$\frac{4\,\alpha\,a}{\pi}\int_0^1 \frac{s}{(r+s)}\,K\left(\frac{2\sqrt{r\,s}}{r+s}\right)p\,(s)\,ds \;=\; \delta - \frac{a^2\,r^2}{2\,R} \qquad (6.4.3.7)$$

The solution of this integral equation is the Hertzian pressure profile $p\,(r)$ (Johnson (1985), p. 92) :

$$p\,(r) = \frac{2\,a}{\pi\,\alpha\,R}\sqrt{1-r^2} \qquad (6.4.3.8)$$

This pressure profile is also the solution to the integral equation obtained by differentiating both members of (6.4.3.7) with respect to variable r :

$$\int_0^1 \left\{\frac{K\left(\frac{2\sqrt{rs}}{r+s}\right)}{(r+s)} + \frac{E\left(\frac{2\sqrt{rs}}{r+s}\right)}{(r-s)}\right\} s\,p\,(s)\,ds = \frac{\pi\,a\,r^2}{2\,\alpha\,R} \qquad (6.4.3.9)$$

which coincides with (6.4.3.1), apart from the use of symbols p and p_0 . As a consequence , the expression for p_0 which solves (6.4.3.1) is :

$$p_0\,(r) = \frac{2\,a}{\pi\,\alpha\,R}\sqrt{1-r^2} \qquad (6.4.3.10)$$

The second subproblem is now treated, defined by the second equation in (6.4.2.6) :

$$\int_0^1 \left(\frac{K\left(\frac{2\sqrt{rs}}{r+s}\right)}{(r+s)} + \frac{E\left(\frac{2\sqrt{rs}}{r+s}\right)}{(r-s)} \right) s\, p_2(s)\, s\, ds = \frac{\pi\, \alpha_{20}\, a\, r^2}{2\, t} \int_0^1 p_0(s)\, s\, ds \tag{6.4.3.11}$$

The following integrals hold :

$$\int_0^1 \sqrt{1-s^2}\; s\, ds = \frac{1}{3}\;;\quad \int_0^1 \sqrt{1-s^2}\; s^3\, ds = \frac{2}{15} \tag{6.4.3.12}$$

so that (6.4.3.11) becomes :

$$\int_0^1 \left(\frac{K\left(\frac{2\sqrt{rs}}{r+s}\right)}{(r+s)} + \frac{E\left(\frac{2\sqrt{rs}}{r+s}\right)}{(r-s)} \right) s\, p_2(s)\, s\, ds = \frac{\alpha_{20}\, \beta\, a\, r^2}{3\, \alpha\, R} \tag{6.4.3.13}$$

and, therefore, $p_2(r)$ is :

$$p_2(r) = \frac{4\, \alpha_{20}\, \beta\, a}{3\, \pi^2\, \alpha\, R} \sqrt{1-r^2} \tag{6.4.3.14}$$

It is observed that $p_2(r)$ depends on β , whereas its plane counterpart does not (Chapter 4, Section 4.3.5). This is due to the different form of eqn (6.3.4). Despite this limit, the traditional terminology referring to β^0 , β^2 , β^4 , β^6 perturbed terms is still employed.

The pressure terms p_4 and p_6 are solutions of integral equations whose known terms are more complex than those of (6.4.3.1) and (6.4.3.13). The general solution of the last two integral equations of (6.4.2.6) must be used to define p_4 and p_6 functions , a task which is left to the next Section.

6.4.4 Solution of the third and fourth subproblems

Alexsandrov (1967) treats the integral equation :

$$\int_0^1 \frac{s}{(r+s)} K\left(\frac{2\sqrt{r\,s}}{r+s}\right) p(s)\,ds = \frac{\pi}{2} g(r) \qquad (6.4.4.1)$$

where $g(r)$ is a generic known term, and reports its solution for $p(r)$:

$$p(r) = -\frac{2}{\pi}\frac{d}{d\,r} r \int_r^1 \frac{\frac{d}{d\,t}\int_0^t \frac{g(r)\,r}{\sqrt{t^2-r^2}}\,d\,r}{t\,\sqrt{t^2-r^2}}\,dt \qquad (6.4.4.2)$$

To reach the same form of the integral equations in (6.4.2.6), both members of (6.4.4.1) are differentiated with the aid of (6.4.2.4), thus obtaining :

$$\int_0^1 \left[\frac{K\left(\frac{2\sqrt{rs}}{r+s}\right)}{(r+s)} + \frac{E\left(\frac{2\sqrt{rs}}{r+s}\right)}{(r-s)}\right] s\,p(s)\,ds = -\pi\,r\,\frac{d\,g(r)}{d\,r} \qquad (6.4.4.3)$$

In the sequel the chain of calculations contained in (6.4.4.2) is followed, and the second member in the β^4 equation in (6.4.2.6) is computed by evaluating the corresponding integrals with the help of (6.4.3.10), (6.4.3.12) and (6.4.3.14), thus obtaining :

$$\left[\frac{\alpha_{22}\,a\,\beta}{30\,\alpha\,R} + \frac{2\,\alpha_{20}^2\,a\,\beta^2}{9\,\pi\,\alpha\,R}\right] r^2 + \frac{\alpha_{40}\,a\,\beta}{6\,\alpha\,R}\,r^4 \qquad (6.4.4.4)$$

Expression (6.4.4.4) can be written in the compact form :

$$A\,r^2 + B\,r^4 \tag{6.4.4.5}$$

where constants A and B are easily identifiable. Following (6.4.4.2), eqn (6.4.4.3) implies :

$$-\pi\,r\,\frac{d\,g\,(r)}{d\,r} = A\,r^2 + B\,r^4 \tag{6.4.4.6}$$

so that :

$$g\,(r) = -\frac{A}{2\,\pi}\,r^2 - \frac{B}{4\,\pi}\,r^4 + C \tag{6.4.4.7}$$

where constant C will eventually be computed so that the contact pressure stays finite by the contact periphery. Always conforming to (6.4.4.2), the following integral is evaluated :

$$\int_0^t \frac{g\,(r)\,r}{\sqrt{t^2 - r^2}}\,d\,r = -\frac{A}{2\,\pi}\int_0^t \frac{r^3}{\sqrt{t^2 - r^2}}\,d\,r -$$

$$\frac{B}{4\,\pi}\int_0^t \frac{r^5}{\sqrt{t^2 - r^2}}\,d\,r + C\int_0^t \frac{r}{\sqrt{t^2 - r^2}}\,d\,r \tag{6.4.4.8}$$

where the following integrals are of use :

$$\int_0^t \frac{r^5}{\sqrt{t^2 - r^2}}\,d\,r = \frac{8\,t^5}{15}$$

$$\int_0^t \frac{r^3}{\sqrt{t^2 - r^2}}\, dr = \frac{2\, t^3}{3}$$

$$\int_0^t \frac{r}{\sqrt{t^2 - r^2}}\, dr = t \qquad (6.4.4.9)$$

so that (6.4.4.8) becomes :

$$\int_0^t \frac{g\,(r)\, r}{\sqrt{t^2 - r^2}}\, dr = - \frac{A}{3\,\pi}\, t^3 - \frac{2\, B}{15\,\pi}\, t^5 + C\, t \qquad (6.4.4.10)$$

According to (6.4.4.2), the following expression is computed :

$$\frac{d}{d\, t} \int_0^t \frac{g\,(r)\, r}{\sqrt{t^2 - r^2}}\, dr = - \frac{A}{\pi}\, t^2 - \frac{2\, B}{3\,\pi}\, t^4 + C \qquad (6.4.4.11)$$

and, then :

$$\int_r^1 \frac{\dfrac{d}{d\, t} \displaystyle\int_0^t \frac{g\,(r)\, r}{\sqrt{t^2 - r^2}}\, dr}{t\, \sqrt{t^2 - r^2}}\, dt = - \frac{A}{\pi} \int_r^1 \frac{t}{\sqrt{t^2 - r^2}}\, dt -$$

$$\frac{2\, B}{3\,\pi} \int_r^1 \frac{t^3}{\sqrt{t^2 - r^2}}\, dt + C \int_r^1 \frac{dt}{t\, \sqrt{t^2 - r^2}} \qquad (6.4.4.12)$$

where the following integrals have been employed :

$$\int_r^1 \frac{t^3}{\sqrt{t^2 - r^2}}\, dt = \frac{1}{3}(1 + 2\,r^2)\sqrt{1 - r^2}$$

$$\int_r^1 \frac{t}{\sqrt{t^2 - r^2}}\, dt = \sqrt{1 - r^2}$$

$$\int_r^1 \frac{dt}{t\sqrt{t^2 - r^2}} = \frac{\pi}{2\,r} - \frac{asin\,(r)}{r} \qquad (6.4.4.13)$$

so that (6.4.4.12) becomes :

$$\int_r^1 \frac{\frac{d}{dt}\int_0^t \frac{g\,(r)\,r}{\sqrt{t^2 - r^2}}\, dr}{t\sqrt{t^2 - r^2}}\, dt = -\frac{A}{\pi}\sqrt{1 - r^2} -$$

$$\frac{2\,B}{9\,\pi}(1 + 2\,r^2)\sqrt{1 - r^2} + C\left(\frac{\pi}{2\,r} - \frac{asin\,(r)}{r}\right) \qquad (6.4.4.14)$$

Finally, the expression for $p_4\,(r)$ is :

$$p_4\,(r) = -\frac{2}{\pi}\frac{d}{dr}\,r\left[-\frac{A}{\pi}\sqrt{1 - r^2}\right.$$

$$- \frac{2\,B}{9\,\pi}\,(1 + 2\,r^2)\,\sqrt{1 - r^2} + C\left[\frac{\pi}{2\,r} - \frac{asin\,(r)}{r}\right]\Bigg] =$$

$$\frac{2}{\pi^2}\left[A\,(1 - 2\,r^2) + \frac{2\,B}{9}\,(1 + 4\,r^2 - 8\,r^4) + C\,\pi\right]\frac{1}{\sqrt{1 - r^2}}$$

(6.4.4.15)

As already anticipated, constant C must be computed so that the contact pressure stays finite by the contact contour $r = 1$ (in fact, it vanishes there). This implies :

$$C = \frac{3\,A + 2\,B}{3\,\pi} \qquad (6.4.4.16)$$

so that the final expression of p_4 is :

$$p_4\,(r) = \frac{2\,\alpha\,\beta}{9\,\pi^2\,\alpha\,R}\left[\frac{4}{3}\,\alpha_{40}\,(1 + 2\,r^2) + \frac{3}{5}\,\alpha_{22} + \frac{4}{\pi}\,\alpha_{20}^2\,\beta\right]\sqrt{1 - r^2}$$

(6.4.4.17)

It appears that p_4 depends on β , whereas in the plane case (Chapter 4, Section 4.3.5) the various pressure terms are independent of this ratio. This shortcoming is due to the different form of eqn (6.3.4) with respect to its plane analogue.

In the following the β^6 perturbed problem of (6.4.2.6) is treated, and the second member in the β^6 equation is computed by evaluating the corresponding integrals with the help of (6.4.3.10), (6.4.3.12), (6.4.3.14) and (6.4.4.17), thus obtaining the following expression :

$$\frac{a\,\beta}{\alpha\,R}\left[\left(\frac{4}{45\,\pi}\,\alpha_{20}\,\alpha_{40}\,\beta+\frac{2}{45\,\pi}\,\alpha_{20}\,\alpha_{22}\,\beta+\frac{4}{27\,\pi^2}\,\alpha_{20}^3\,\beta^2+\frac{1}{210}\,\alpha_{42}\right)r^2+\right.$$

$$\left.\left(\frac{1}{9\,\pi}\,\alpha_{20}\,\alpha_{40}\,\beta+\frac{1}{60}\,\alpha_{42}\right)r^4+\frac{1}{16}\,\alpha_{60}\,r^6\right] \qquad (6.4.4.18)$$

Expression (6.4.4.18) can be written in the compact form :

$$\cdot\ A\,r^2+B\,r^4+C\,r^6 \qquad (6.4.4.19)$$

where constants A , B and C are easily identifiable. It follows from (6.4.4.3) that :

$$-\pi\,r\,\frac{d\,g\,(r)}{d\,r}=A\,r^2+B\,r^4+C\,r^6 \qquad (6.4.4.20)$$

so that :

$$g\,(r)=-\frac{A}{2\,\pi}\,r^2-\frac{B}{4\,\pi}\,r^4-\frac{C}{6\,\pi}\,r^6+D \qquad (6.4.4.21)$$

where constant D will be computed so that the contact pressure vanishes by the contact periphery. According to (6.4.4.2), the following integral is evaluated :

$$\int_0^t\frac{g\,(r)\,r}{\sqrt{t^2-r^2}}\,d\,r=-\frac{A}{2\,\pi}\int_0^t\frac{r^3}{\sqrt{t^2-r^2}}\,d\,r-\frac{B}{4\,\pi}\int_0^t\frac{r^5}{\sqrt{t^2-r^2}}\,d\,r-$$

$$\frac{C}{6\,\pi}\int_0^t\frac{r^7}{\sqrt{t^2-r^2}}\,d\,r+D\int_0^t\frac{r}{\sqrt{t^2-r^2}}\,d\,r \qquad (6.4.4.22)$$

where, in addition to (6.4.4.9), the following integral is helpful :

$$\int_0^t \frac{r^7}{\sqrt{t^2 - r^2}}\, dr = \frac{16\, t^7}{35} \qquad (6.4.4.23)$$

so that (6.4.4.22) becomes :

$$\int_0^t \frac{g(r)\, r}{\sqrt{t^2 - r^2}}\, dr = -\frac{A}{3\pi} t^3 - \frac{2B}{15\pi} t^5 - \frac{8C}{105\pi} t^7 + D\, t \qquad (6.4.4.24)$$

According to (6.4.4.2), the following expression is computed :

$$\frac{d}{dt} \int_0^1 \frac{g(r)\, r}{\sqrt{t^2 - r^2}}\, dr = -\frac{A}{\pi} t^2 - \frac{2B}{3\pi} t^4 - \frac{8C}{15\pi} t^6 + D \qquad (6.4.4.25)$$

and, then :

$$\int_r^1 \frac{\frac{d}{dt} \int_0^t \frac{g(r)\, r}{\sqrt{t^2 - r^2}}\, dr}{t\, \sqrt{t^2 - r^2}} \cdot dt = -\frac{A}{\pi} \int_r^1 \frac{t}{\sqrt{t^2 - r^2}}\, dt -$$

$$\frac{2B}{3\pi} \int_r^1 \frac{t^3}{\sqrt{t^2 - r^2}}\, dt - \frac{8C}{15\pi} \int_r^1 \frac{t^5}{\sqrt{t^2 - r^2}}\, dt + D \int_r^1 \frac{dt}{t\, \sqrt{t^2 - r^2}} \qquad (6.4.4.26)$$

where the integrals of (6.4.4.13) and the following result are of service :

$$\int_r^1 \frac{t^5}{\sqrt{t^2 - r^2}}\, dt = \frac{1}{15}\,(3 + 4\,r^2 + 8\,r^4)\,\sqrt{1 - r^2} \qquad (6.4.4.27)$$

so that (6.4.4.26) becomes :

$$\int_r^1 \frac{\frac{d}{dt}\int_0^t \frac{g(r)\,r}{\sqrt{t^2 - r^2}}\, dr}{t\,\sqrt{t^2 - r^2}}\, dt = -\frac{A}{\pi}\sqrt{1 - r^2}$$

$$-\frac{2B}{9\pi}\,(1 + 2\,r^2)\,\sqrt{1 - r^2}$$

$$-\frac{8C}{225\,\pi}\,(3 + 4\,r^2 + 8\,r^4)\,\sqrt{1 - r^2}$$

$$+ D\left[\frac{\pi}{2\,r} - \frac{asin(r)}{r}\right] \qquad (6.4.4.28)$$

Finally, $p_6(r)$ becomes :

$$p_6(r) = -\frac{2}{\pi}\frac{d}{dr}\,r\left[-\frac{A}{\pi}\sqrt{1 - r^2}\right.$$

$$-\frac{2B}{9\pi}\,(1 + 2\,r^2)\,\sqrt{1 - r^2}$$

$$-\frac{8C}{225\,\pi}\,(3 + 4\,r^2 + 8\,r^4)\,\sqrt{1 - r^2}$$

$$\left. + D\left[\frac{\pi}{2\,r} - \frac{asin(r)}{r}\right]\right] =$$

$$\frac{2}{\pi^2}\left[A\,(1-2r^2) + \frac{2B}{9}\,(1+4r^2-8r^4) + \right.$$

$$\left. \frac{8C}{75}\,(1+2r^2+8r^4-16r^6) + D\,\pi \right] \frac{1}{\sqrt{1-r^2}} \qquad (6.4.4.29)$$

Constant D must be computed so that the contact pressure stays finite by the contact contour. This implies :

$$D = \frac{15A + 10B + 8C}{15\,\pi} \qquad (6.4.4.30)$$

so that the final expression of p_6 is :

$$p_6(r) = \frac{2\,\alpha\,\beta}{3\,\pi^2\,\alpha\,R}\left[\frac{8}{25}\,\alpha_{60}\,r^4 + \left(\frac{16}{27\,\pi^2}\,\alpha_{20}\,\alpha_{40}\,\beta + \frac{4}{25}\,\alpha_{60} + \frac{4}{45}\,\alpha_{42} \right) r^2 + \right.$$

$$\left. \left(\frac{3}{25}\alpha_{60} + \frac{23}{315}\,\alpha_{42} + \frac{112}{135\,\pi}\,\alpha_{20}\,\alpha_{40}\,\beta + \frac{4}{15\,\pi}\,\alpha_{20}\,\alpha_{22}\,\beta + \frac{8}{9\,\pi^2}\,\alpha_{20}^3\,\beta^2 \right) \right] \sqrt{1-r^2}$$

(6.4.4.31)

Similar to $p_4\,(r)$ expression, $p_6\,(r)$ too partially depends on β , so that its contribution is not entirely of the order of β^6 , but it becomes more complex. However, this shortcoming does not undermine the usefulness of the results obtained.

6.4.5 Expression for the indentation depth

The indentation depth, δ, can be computed from eqn (6.4.2.1) as a function of the pressure profile :

$$\delta = lim\ |_{r=0}\ \ 2\ \alpha\beta a \int_0^1 K_{axi}\ (r,s)\ p(s)\ s\ ds \qquad (6.4.5.1)$$

where $K_{axi}\ (r,s)$ is expressed in eqn (6.4.2.2), and $p\ (s)$ is that of eqn (6.4.2.5), where $p_o\ (s)$, $p_2\ (s)$, $p_4\ (s)$ and $p_6\ (s)$ contributions are reported in eqns (6.4.3.10), (6.4.3.14), (6.4.4.17) and (6.4.4.31), respectively.

It is observed that $p\ (s)$ up to β^6 is composed by the following functions :

$$\sqrt{1 - s^2} \quad ; \quad s^2 \sqrt{1 - s^2} \quad ; \quad s^4 \sqrt{1 - s^2} \qquad (6.4.5.2)$$

so that the following integrals are useful for the computation of (6.4.5.1) with respect to the regular part of the axisymmetric kernel (see (6.4.2.2)) :

$$\int_0^1 s\ \sqrt{1 - s^2}\ \ ds \doteq \frac{1}{3}$$

$$\int_0^1 s^3\ \sqrt{1 - s^2}\ \ ds = \frac{2}{15}$$

$$\int_0^1 s^5\ \sqrt{1 - s^2}\ \ ds = \frac{8}{105}$$

$$\int_0^1 s^7 \sqrt{1-s^2}\, ds = \frac{16}{315}$$

$$\int_0^1 s^9 \sqrt{1-s^2}\, ds = \frac{128}{3465}$$

$$\int_0^1 s^{11} \sqrt{1-s^2}\, ds = \frac{256}{9009} \qquad (6.4.5.3)$$

Similarly, the following integrals (obtained with the help of formulae (2.6.12) and (2.6.13) on p. 83 of Gladwell (1980), see also Jaffar (1988)) are helpful with regard to the singular component of the axisymmetric kernel :

$$lim\ |_{r=o} \int_0^1 K\left(\frac{2\sqrt{r\,s}}{r+s}\right) \frac{s}{(r+s)} \sqrt{1-s^2}\, ds = \frac{\pi^2}{8}$$

$$lim\ |_{r=o} \int_0^1 K\left(\frac{2\sqrt{r\,s}}{r+s}\right) \frac{s^3}{(r+s)} \sqrt{1-s^2}\, ds = \frac{\pi^2}{32}$$

$$lim\ |_{r=o} \int_0^1 K\left(\frac{2\sqrt{r\,s}}{r+s}\right) \frac{s^5}{(r+s)} \sqrt{1-s^2}\, ds = \frac{\pi^2}{64} \qquad (6.4.5.4)$$

With regard to results (6.4.5.4), it is interesting to observe that, when r is set equal to 0 in the integrand, then $K(0) = \pi/2$ for $0 < s \leq 1$. Anyway, when s too vanishes, then the argument of K may approach 1 (*e.g.*, if r and s vanish with the same law), so that $K(1) = \infty$. In other words, the integrand may behave as a Dirac δ in the vicinity of $r = 0$, where it deviates from its value $\pi/2$ to become

unbounded, its singularity possibly producing a finite contribution to the value of the integral. In other words, the substitution of K with $\pi/2$ (and the imposition $r = 0$ in the following fraction) may not be licit in the evaluation of (6.4.5.4), since it is not always permitted to interchange limit and Riemann integration operations (Oden (1979), p. 171). On the other side, it can be shown that the same results of (6.4.5.4) are actually obtained by substituting K with $\pi/2$, so that the interchange of limit and integration produces a correct answer for these integrals. The corresponding results — equivalent to (6.4.5.4) — are :

$$\int_0^1 \sqrt{1 - s^2}\, ds = \frac{\pi}{4}$$

$$\int_0^1 s^2 \sqrt{1 - s^2}\, ds = \frac{\pi}{16}$$

$$\int_0^1 s^4 \sqrt{1 - s^2}\, ds = \frac{\pi}{32} \qquad (6.4.5.5)$$

The final expression for the indentation, δ, as a function of the kernel series expansion coefficients, α_{ij} , of the contact radius, a, of the sphere radius, R, and of the contact radius to layer thickness ratio, β (the elastic constants do not explicitly appear in this equation, but they affect α_{ij} coefficients) is :

$$\delta = \frac{2\,a^2}{\pi\,R}\left(\frac{\pi}{2} + \beta\,\frac{2\,\alpha_{0}}{3} + \beta^3\,\frac{2\,\alpha_{20}}{5} + \beta^4\,\frac{4\,\alpha_{0}\,\alpha_{20}}{9\,\pi} + \beta^5\,\frac{76\,\alpha_{40} + 21\,\alpha_{22}}{630} + \right.$$

$$\beta^6\,\frac{8\,\alpha_{0}\,\alpha_{42} + 2\,\alpha_{0}\,\alpha_{22} + 12\,\alpha_{20}^2}{45\,\pi} + \beta^7\,\frac{33\,\pi^2\,\alpha_{60} + 15\,\pi^2\,\alpha_{42} + 280\,\alpha_{0}\,\alpha_{20}^2}{945\,\pi^2} +$$

$$\beta^8 \frac{810\pi\alpha_0\alpha_{60} + 342\pi\alpha_0\alpha_{42} + (2350\pi + 350)\alpha_{20}\alpha_{40} + 693\pi\alpha_{20}\alpha_{22}}{14175\pi^2} +$$

$$\beta^9 \frac{\alpha_{20}\left[(224\pi + 64)\alpha_0\alpha_{40} + 72\pi\alpha_0\alpha_{22} + 216\pi\alpha_{20}^2\right]}{1215\pi^3} +$$

$$\beta^{10} \frac{360\pi^2\alpha_{20}\alpha_{60} + 117\pi^2\alpha_{20}\alpha_{42} + 140\pi^2\alpha_{40}^2 + 27\pi^2\alpha_{22}\alpha_{40} + 8400\alpha_0\alpha_{20}^3}{42525\pi^3} +$$

$$\beta^{11} \frac{\alpha_{20}^2\left[(964\pi + 320)\alpha_{40} + 252\pi\alpha_{22}\right]}{42525\pi^3} +$$

$$\beta^{12} \frac{(11718\pi^2\alpha_{40} + 693\pi^2\alpha_{22})\alpha_{60} + 2750\pi^2\alpha_{40}\alpha_{42} + 129360\alpha_{20}^4}{6548850\pi^3} +$$

$$\beta^{13} \frac{\alpha_{20}\left[90\pi\alpha_{20}\alpha_{60} + (336\pi + 160)\alpha_{40}^2 + 108\pi\alpha_{22}\alpha_{40}\right]}{127575\pi^3} +$$

$$\beta^{14} \frac{6237\pi^2\alpha_{60}^2 + 2067\pi^2\alpha_{42}\alpha_{60} + 80080\alpha_{20}^3\alpha_{40}}{28378350\pi^3} +$$

$$\beta^{15} \frac{\alpha_{20}\alpha_{60}\left[(616\pi + 320)\alpha_{40} + 198\pi\alpha_{22}\right]}{2} +$$

$$\beta^{16} \frac{4\alpha_{20}^3\alpha_{60}}{8505\pi^3} \Bigg] \qquad (6.4.5.6)$$

Encouragingly, the β^0 term coincides with the Hertzian solution for the half space.

The expression for the resultant load is computed below. By exploiting integrals (6.4.5.3), the following force terms referring to the various perturbation

orders are obtained :

$$P_0 = \frac{4\,a^3}{3\,\alpha\,R} \tag{6.4.5.7}$$

$$P_2 = \frac{8\,\alpha_{20}\,\beta\,a^3}{9\,\pi\,\alpha\,R} \tag{6.4.5.8}$$

$$P_4 = \frac{4\,a^3\,\beta}{27\,\pi\,\alpha\,R}\left[\frac{4}{3}\,\alpha_{40}\left(1+\frac{4}{5}\right)+\frac{3}{5}\,\alpha_{22}+\frac{4}{\pi}\,\alpha_{20}^2\,\beta\right] \tag{6.4.5.9}$$

$$P_6 = \frac{4\,a^3\,\beta}{9\,\pi\,\alpha\,R}\left[\frac{8}{875}\,\alpha_{60}+\frac{2}{5}\left\{\frac{16}{27\,\pi^2}\,\alpha_{20}\,\alpha_{40}\,\beta+\frac{4}{25}\,\alpha_{60}+\frac{4}{45}\,\alpha_{42}\right\}+\right.$$

$$\left.\left\{\frac{3}{25}\,\alpha_{60}+\frac{23}{315}\,\alpha_{42}+\frac{112}{135\,\pi}\,\alpha_{20}\,\alpha_{40}\,\beta+\frac{4}{15\,\pi}\,\alpha_{20}\,\alpha_{22}\,\beta+\frac{8}{9\,\pi^2}\,\alpha_{20}^3\,\beta^2\right\}\right] \tag{6.4.5.10}$$

Finally, the total load is obtained by combining the various perturbed components according to (6.4.2.5).

6.4.6 Critical remarks on some integration formulae involving elliptic integrals

Formula (6.4.5.1) indicates that the evaluation of the indentation depth for an imposed pressure profile requires the computation of an integral whose integrand is essentially the known pressure, multiplied by the elliptic integral function K , and by the integration variable. Gladwell (1980) reports on p. 83 a useful results due to Popov (1962), which can be expressed as follows :

$$\int_0^1 \frac{s}{(r+s)} K\left(\frac{2\sqrt{r\,s}}{r+s}\right) \frac{P_{2n}[\sqrt{1-s^2}]}{\sqrt{1-s^2}}\, ds = \frac{\pi^2}{4}[P_{2n}(0)]^2\, P_{2n}[\sqrt{1-r^2}] \quad (6.4.6.1)$$

where P_{2n} represent modified Legendre polynomials ($n = 0 , 1 . .$) . The same expression is quoted by Jaffar (1988) in his formula after (8). These results are confirmed by formulae (6.4.5.4) for the case $r = 0$.

An alternative source for comparable integration expressions is the book of Johnson (1985), who on p. 116 quotes a result due to Steuermann (1939), which can be formulated as follows ($n = 1 , 2 . .$) :

$$\int_0^1 \frac{s}{(r+s)} K\left(\frac{2\sqrt{r\,s}}{r+s}\right) n\left[\frac{2\cdot 4\ldots 2n}{1\cdot 3\ldots(2n-1)}\right]^2 \cdot$$

$$\left[s^{2n-2} + \tfrac{1}{2}\, s^{2n-4} + \ldots + \frac{1\cdot 3\ldots(2n-3)}{2\cdot 4\ldots(2n-2)}\right]\sqrt{1-s^2}\; ds =$$

$$\frac{\pi^2}{4}\left[\frac{2\cdot 4\ldots 2n}{1\cdot 3\ldots(2n-1)} - r^{2n}\right] \quad (6.4.6.2)$$

(It should be noted that formula (5.21) of Johnson (1985) contains two differences with respect to the original Steuermann (1939) formulae (4,5). First, the denominator of the first bracketed, squared expression in (5.21) of Johnson (1985) reads : $1 \cdot 4 \ldots (2n - 1)$, whereas in Steuermann (1939) it reads : $1 \cdot 3 \ldots (2n - 1)$. Secondly, the first fraction in formula (5.21) of Johnson (1985) contains expression a^{2n-2} , while Steuermann (1939) reports p^{2n-1} , where both a and p denote the contact radius. It is believed that these differences are due to typing mistakes in Johnson (1985) book, so that formula (6.4.6.2) has been amended accordingly.)

Expression (6.4.6.1) furnishes the *surface deflection of* an *infinite* space loaded by an axisymmetric pressure profile of polynomial type with respect to the radial coordinate, r, and divided by $(1 - r^2)^{0.5}$. Formula (6.4.6.2), instead, treats an axisymmetric pressure curve again of polynomial kind, but this time multiplied by $(1 - r^2)^{0.5}$.

In the following the integrals of (6.4.6.1) are computed for $r \rightarrow 0$ and for $n = 0$, 1 and 2, respectively :

$$\lim_{r \rightarrow 0} \int_0^1 K\left(\frac{2\sqrt{r\,s}}{r+s} \right) \frac{1}{\sqrt{1-s^2}}\, ds = \frac{\pi^2}{4}$$

$$\lim_{r \rightarrow 0} \int_0^1 K\left(\frac{2\sqrt{r\,s}}{r+s} \right) \frac{2 - 3\,s^2}{2\sqrt{1-s^2}}\, ds = \frac{\pi^2}{16} \qquad (6.4.6.3)$$

$$\lim_{r \rightarrow 0} \int_0^1 K\left(\frac{2\sqrt{r\,s}}{r+s} \right) \frac{35\,s^4 - 40\,s^2 + 8}{8\sqrt{1-s^2}}\, ds = \frac{9\,\pi^2}{256}$$

The first integral agrees with result (3.36) on p. 60 of Johnson (1985). In addition, by putting $K = \pi/2$ (as commented with regard to formulae (6.4.5.4)) the same expressions as in (6.4.6.3) are obtained, a result which confirms the exactness of (6.4.6.3).

In the following the integrals of (6.4.6.2) are computed for $r \rightarrow 0$ and for $n =$ 1 and 2 , respectively :

$$lim_{\,|\,r \rightarrow 0} \int_0^1 K\left(\frac{2\sqrt{r\,s}}{r+s} \right) \sqrt{1-s^2}\; ds = \frac{\pi^2}{8}$$

$$lim_{\,|\,r \rightarrow 0} \int_0^1 K\left(\frac{2\sqrt{r\,s}}{r+s} \right) (1+2\,s^2) \sqrt{1-s^2}\; ds = \frac{3\,\pi^2}{32} \qquad (6.4.6.4)$$

The first integral agrees with result (3.41a) on p. 61 of Johnson (1985). By putting $K = \pi/2$, the first formula of (6.4.6.4) supplies the same expression as in (6.4.6.4) , while the second integral furnishes $3\,\pi^2/32$, which implies that the second result in (6.4.6.4) is wrong and, consequently, some misprint - not easy to localize - must be present in (6.4.6.2).

The observations which follow aim at comparing the expressions contained in (6.4.6.3) and (6.4.6.4) for some cases, so that additional checks on their exactness, or otherwise, can be effected. The following identity holds true :

$$\frac{1}{3}\,\frac{1}{\sqrt{1-s^2}} + \frac{2}{3}\,\frac{2-3\,s^2}{2\sqrt{1-s^2}} = \sqrt{1-s^2} \qquad (6.4.6.5)$$

and, therefore, the first result of (6.4.6.4) can be obtained by combining the first two results of (6.4.6.3), that is, by attributing the same coefficients as in (6.4.6.5) to the right hand-sides of the first two results of (6.4.6.4), and by summing the corresponding terms. Since :

$$\frac{1}{3}\,\frac{\pi^2}{4} + \frac{2}{3}\,\frac{\pi^2}{16} = \frac{\pi^2}{8} \qquad (6.4.6.6)$$

where the right hand-side of (6.4.6.6) agrees with that of the first formula of (6.4.6.4), it is concluded that the first two equations of (6.4.6.3) and the first expression of (6.4.6.4) are likely to be correct.

In a similar fashion it is possible to combine the three results of (6.4.6.3) to obtain the second result of (6.4.6.4). The following identity holds :

$$\frac{3}{5}\frac{1}{\sqrt{1-s^2}} + \frac{6}{7}\frac{2-3s^2}{2\sqrt{1-s^2}} - \frac{16}{35}\frac{35s^4-40s^2+8}{8\sqrt{1-s^2}} = (1+2s^2)\sqrt{1-s^2} \tag{6.4.6.7}$$

whereas the corresponding combination of the right hand-sides of (6.4.6.3) furnishes :

$$\frac{3}{5}\frac{\pi^2}{4} + \frac{6}{7}\frac{\pi^2}{16} - \frac{16}{35}\frac{9\pi^2}{256} = \frac{3\pi^2}{16} \tag{6.4.6.8}$$

a result which confirms the presence of an error in the second integral of (6.4.6.4), which should equal $3\pi^2/16$.

6.4.7 Selected numerical results

This Section reports selected perturbation forecasts, aimed at a) clarifying the peculiarities of the layer configuration and its differences with respect to a purely Hertzian situation ; b) validating the solution obtained.

Fig. 6.4.7.1 presents the plane counterpart of Fig. 4.3.5.1 of Chapter 4 . Various pressure profiles of increasing perturbation order are compared in the case of incompressible layer and for $a/h = 0.8$. Since the sixth order pressure differs moderately from the fourth one, it can be concluded - similarly to the plane strain analogue - that the sixth order solution represents a good trade-off between accuracy and simplicity. A method for estimating the convergence radius of a perturbation series is mentioned by Kwok (1991).

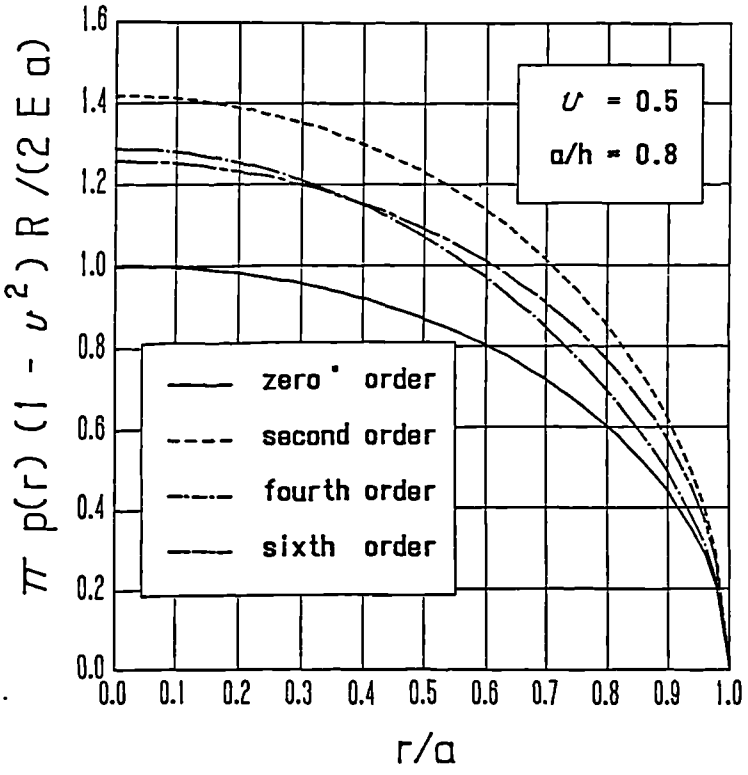

Fig. 6.4.7.1 : The contact pressure profile for various perturbation orders.

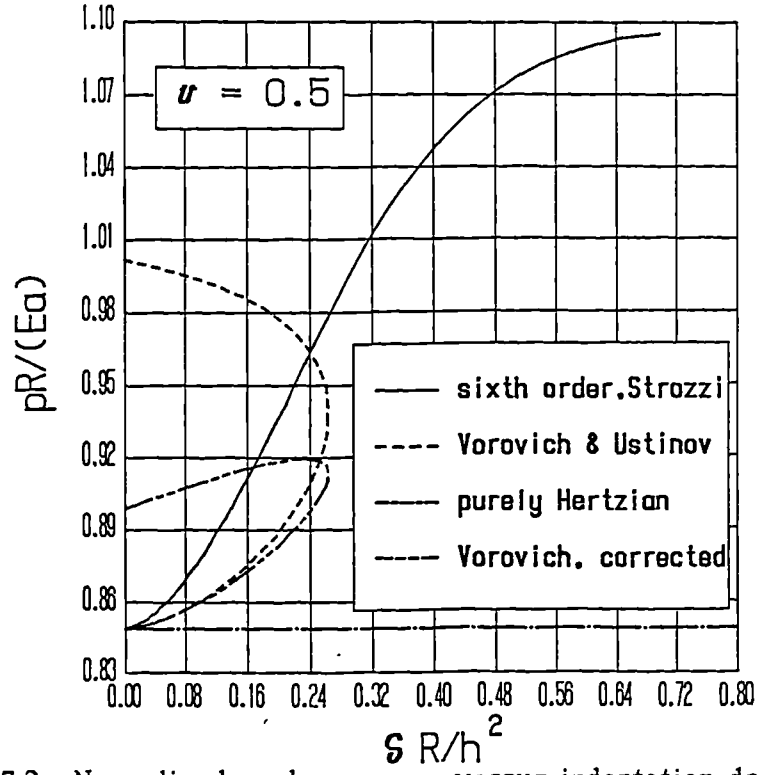

Fig 6.4.7.2 : Normalized peak pressure versus indentation depth for $\nu = 0.5$.

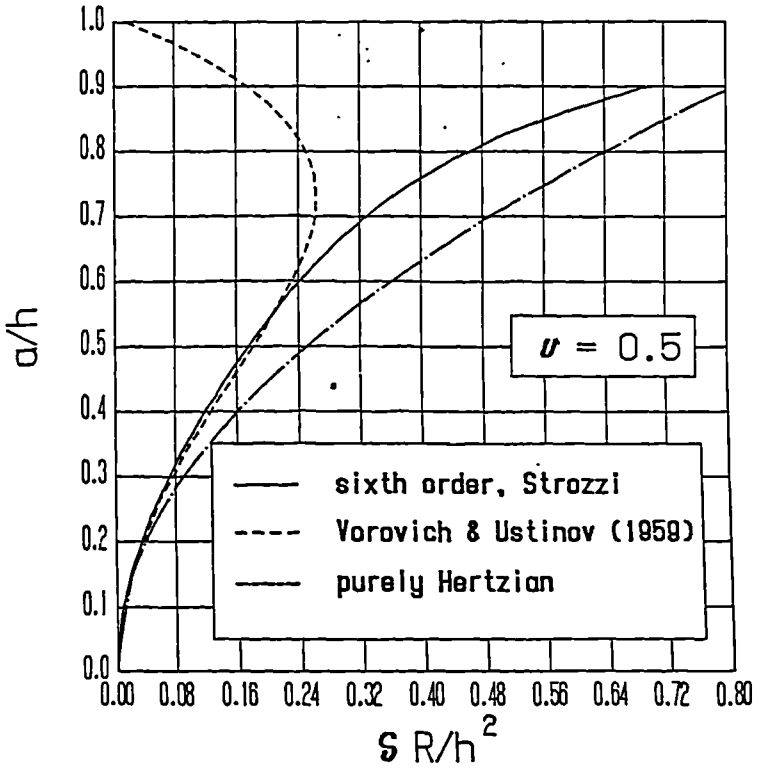

Fig 6.4.7.3 : Normalized contact radius versus indentation depth for $\nu = 0.5$.

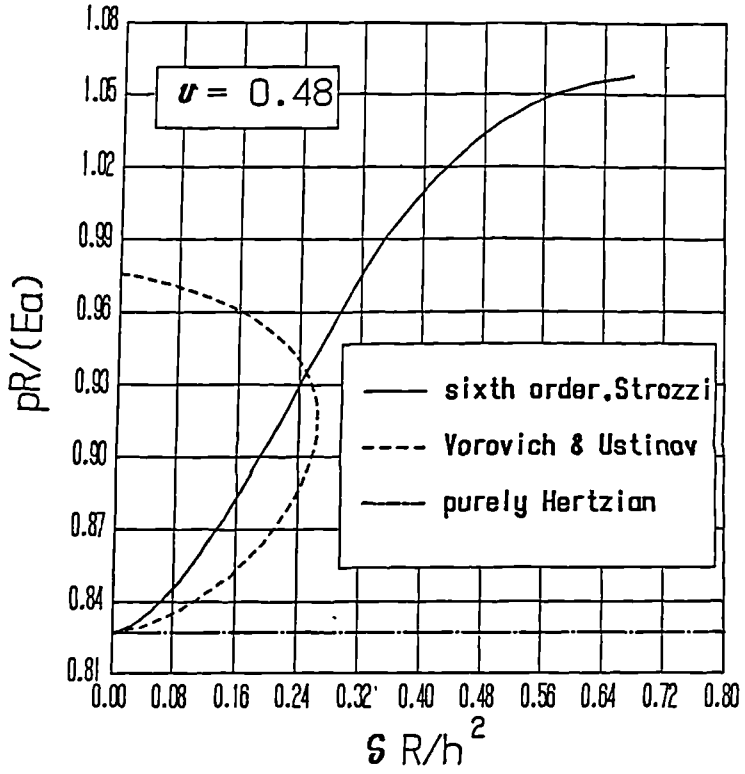

Fig 6.4.7.4 : Normalized peak pressure versus indentation depth for ν = 0.48 .

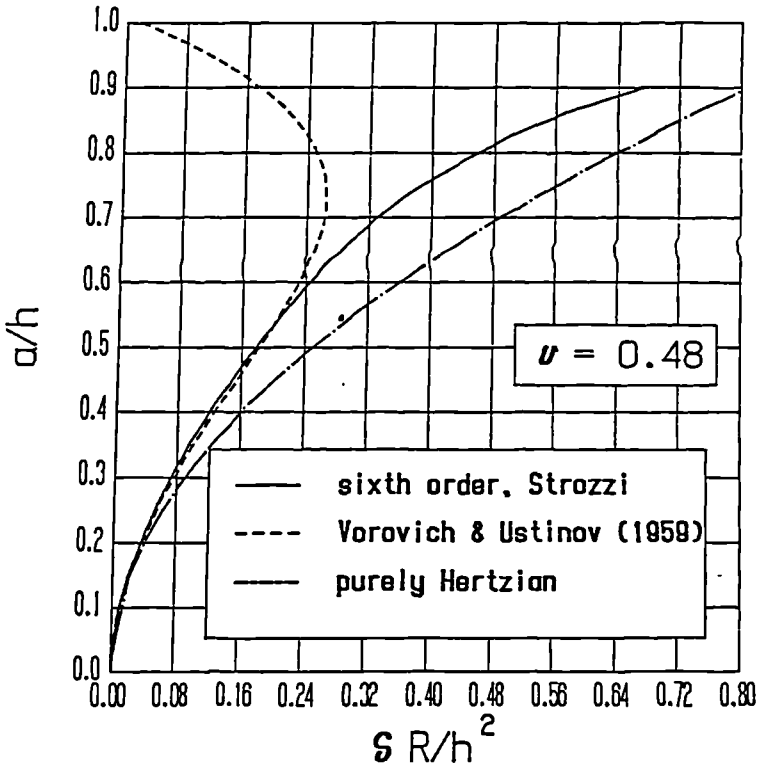

Fig 6.4.7.5 : Normalized contact radius versus indentation depth for ν = 0.48 .

Figs 6.4.7.2,3 display normalized peak pressure and contact radius as functions of the normalized indentation depth, for $\nu = 0.5$, whereas Figs 6.4.7.4,5 refer to $\nu = 0.48$. The Vorovich and Ustinov (1959) analytical predictions are also included, as well as the purely Hertzian forecasts. In a purely Hertzian context, variable $p\ R/(Ea)$ equals $2/(\pi(1 - \nu^2))$. In Figs 6.4.7.2 and 6.4.7.4 , this Hertzian value is represented by a horizontal line, in order to permit a clearer representation of the Hertzian result, and to indicate that this figure does not depend upon x-axis variable. However, it must be admitted that x and y variables of Figs 6.4.7.2,4 are not ideal to represent clearly the Hertzian results by themselves, so that some compromise is inevitable in displaying them. From the previous Figures it appears that the Hertzian results are not applicable to the layer configuration unless the contact radius is very small. From a comparison between Figs 6.4.7.2 and 6.4.7.4 , as well as between Figs 6.4.7.3 and 6.4.7.5 , it appears that, similar to their plane counterparts, the axisymmetric results too do not heavily depend upon the Poisson's ratio, for limited a/h ratios. Figs 6.4.7.2,3,4,5 show that for both figures of the Poisson's ratio, namely 0.48 and 0.5 , there is a noticeable disagreement between the normalized perturbed peak contact pressure and that due to Vorovich and Ustinov (1959). Conversely, the above mentioned accordance is good with regard to the normalized contact radius, at least up to $a/h < 0.6$, a limit in conformity with the value 1/1.5 suggested by the Russian authors. It was decided to investigate the possible sources of this disagreement. First, it was tested if the first formula of (5.9) of Vorovich and Ustinov (1959), expressing the normalized contact radius, a/H, as a function of its Hertzian counterpart, a_o/H, and the third equation of (5.9), reporting the peak pressure, q_{max} , as a function of the same Hertzian variable (the nomenclature of Vorovich and Ustinov (1959) is partially adopted here), were consistent with their formula (5.5), expressing the pressure profile as a function of a/H . The first expression of (5.9) was therefore introduced into (5.5), and the following peak pressure in terms of a_o/H up to the eighth degree was obtained :

$$q_{max} = \frac{4\ a\ H}{\pi\ R}\left[\frac{a_o}{H} + 0.224\left(\frac{a_o}{H}\right)^4 - 0.152\left(\frac{a_o}{H}\right)^6 - 0.013324\left(\frac{a_o}{H}\right)^7 + 0.02\left(\frac{a_o}{H}\right)^8\right] \qquad (6.4.7.1)$$

This formula differs slightly from the third expression of (5.9) in Vorovich and Ustinov (1959), quoted also by Finkin (1972), his expression (3), which reads :

$$q_{max} = \frac{4\,a\,H}{\pi\,R}\left[\frac{a_o}{H} + 0.225\left(\frac{a_o}{H}\right)^4 - 0.018\left(\frac{a_o}{H}\right)^6 - 0.0126\left(\frac{a_o}{H}\right)^7 + 0.013\left(\frac{a_o}{H}\right)^8\right]$$

(6.4.7.2)

The results (8) of Keer (1964) are not immediately useful for a comparison among analytical expressions, since they are presented in a different fashion. It should be noted that group $q_o\,R\,(1-\nu^2)/(Ea^2)$, qualified as "dimensionless loading" by Keer (1964), is in fact dimensional and, therefore, dubious. In addition, the pressure term q_1 depends in eqn (8) upon term $(1+\rho^2)^{0.5}$, which is also improbable.

Fig. 6.4.7.2 includes the "corrected" Vorovich and Ustinov (1959) expression (6.4.7.1), but the corresponding curve is even more distant from the present perturbed solution. In order to assess the exactness of the perturbed solution, it was decided to use as benchmarks the finite element forecasts of Ihara, Shaw and Bhushan (1986), referring to $\nu = 0.49$. Their Table 1 reports 14 configurations defined by x-axis variable $\delta R/h^2$ (See Figs 6.4.7.6,7), and by the corresponding total load, P . Then, the contact radius, a, was computed from their eqn (1) and from the latter piece of information, so that y-axis variable of Fig. 6.4.7.7 could be computed. (In fact, eqn (1) furnishes the Hertzian contact radius, but the results of Fig. 8 of Ihara, Shaw and Bhushan (1986) plus their comments of on p. 531 : "The Hertz value for a (a_o) represents a good approximation for all values of H" (for an imposed load, as suggested by the caption of their Fig. 12(b)) support the above approximation.) The results of Fig. 6.4.7.7 show a satisfactory agreement between the perturbation solution and the numerical forecasts of Ihara, Shaw and Bhushan (1986), so that the perturbed solution referring to the contact radius seems to be sufficiently validated. The y-axis variable of Fig. 6.4.7.6 , that is, $pR/(Ea)$, was derived from Fig. 11 of Ihara, Shaw and Bhushan (1986). (Fig. 11 reports σ_z/q_o for the 14 cases of Table 1, as well as the corresponding q_o , so that the peak contact pressure and, consequently, variable $pR/(Ea)$ can be computed.) Fig. 6.4.7.6 shows that the numerical predictions are spread over too wide an interval to constitute a

reliable benchmark. It is here noted that in Fig. 8 of Ihara, Shaw and Bhushan (1986), cases 3 and 6 exhibit the same a/H . Since these two configurations possess the same $H = 2$ (see Table 1), they must evidence (essentially) the same a . Conversely, the two indentations reported in Table 1 are considerably different, being $\delta_3 = 0.2$ and $\delta_6 = 0.4$, so that some misprint is suspected in Table 1.

To explore further the correctness of the perturbed normalized pressure solution, the data presented in Fig. 4 of Li and Dempsey (1990), referring to $\nu = 0.5$, were resorted to. A combination of the data of their Fig. 4 permits the axis variables of Figs 6.4.7.8,9 to be obtained. This time the agreement between perturbed and Li and Dempsey (1990) solution is acceptable with regard to both normalized contact pressure (Fig. 6.4.7.8) and contact radius (Fig. 6.4.7.9) variables. The validity limits for the perturbed solution appear to be $a/h < 0.7$.

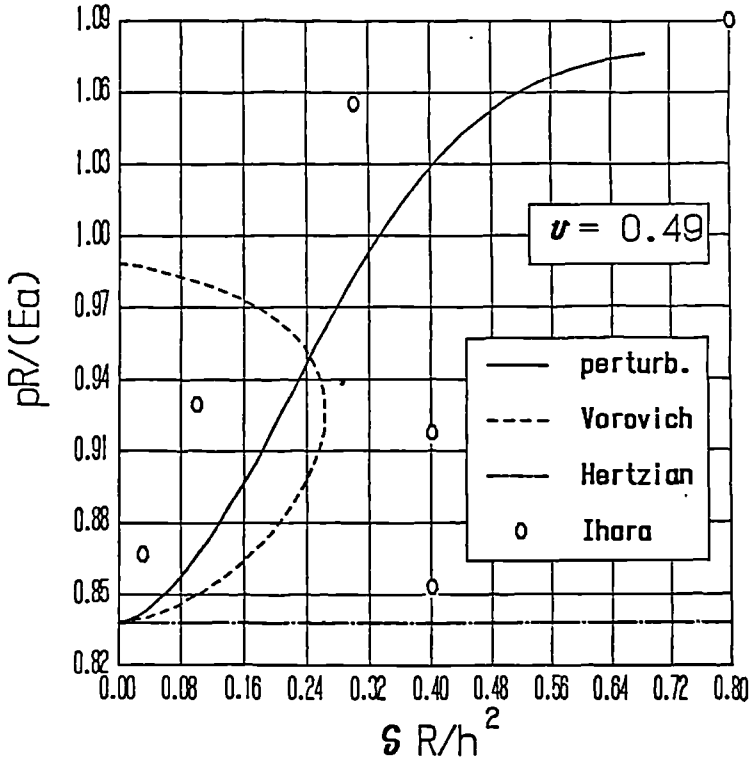

Fig 6.4.7.6 : Normalized peak pressure versus indentation depth for $\nu = 0.49$.

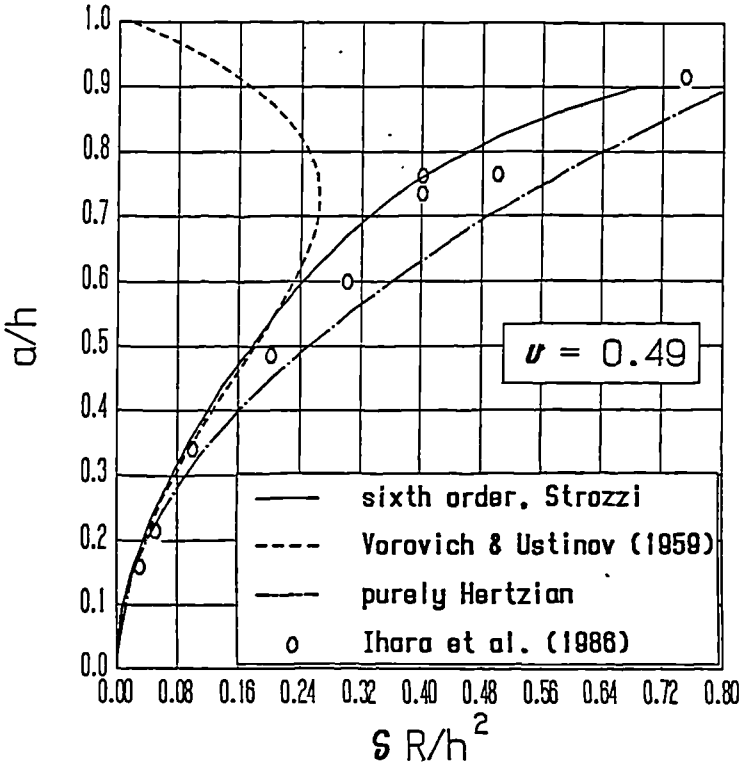

Fig 6.4.7.7 : Normalized contact radius versus indentation depth for ν = 0.49 .

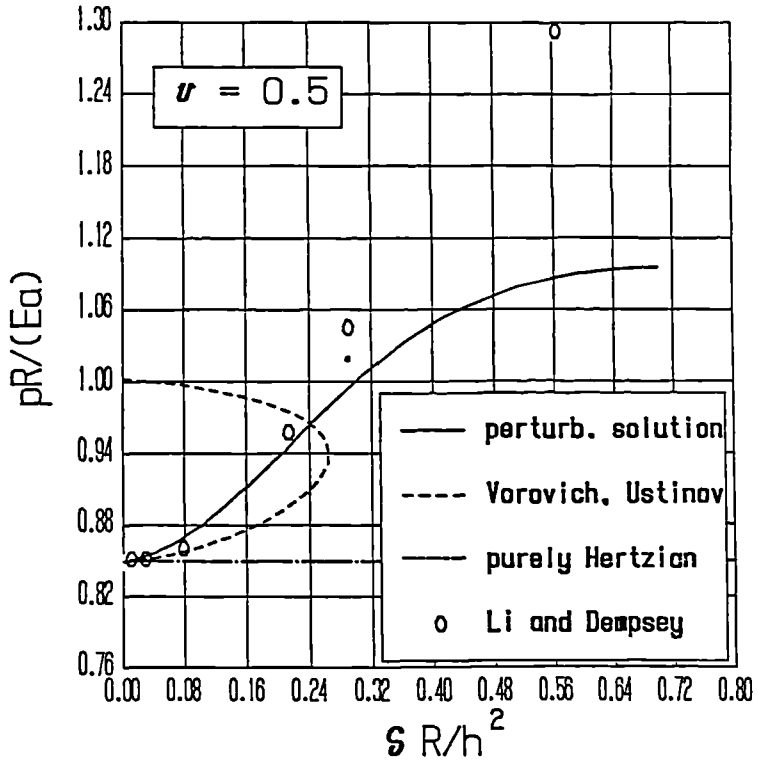

Fig 6.4.7.8 : Normalized peak pressure versus indentation depth for ν = 0.5 .

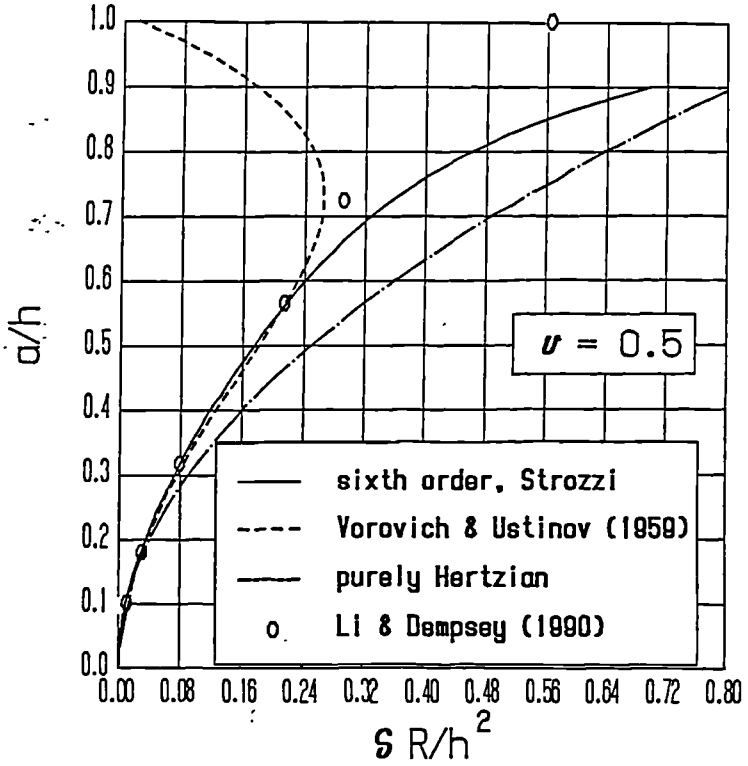

Fig 6.4.7.9 : Normalized contact radius versus indentation depth for $\nu = 0.5$.

6.5 NUMERICAL RESULTS

This Section addresses the peak pressure and contact radius as functions of the indentation depth and Poisson's ratio for a deformable cortex underlain by a rigid basement and indented by a rigid sphere, and for a spectrum of $\delta\ R/h^2$ values which cannot be covered by the perturbation solution of Section 6.4 . The commercial, powerful, finite element program ABAQUS has been exploited in this study. Section 6.5.1 briefly describes the package potentialities, whereas Section 6.5.2 presents the numerical forecasts in normalized form.

6.5.1 ABAQUS finite element program

The package ABAQUS (1989) includes a release specially addressed to the mechanical analysis of elastomeric units. The non-linearities connected to finite deformations, stress-strain relationships and unilateral contact problems - all aspects frequently encountered in the study of rubber components - are covered by ABAQUS. A brief introduction to the main finite elasticity aspects is reported in Chapter 2 , to which the interested reader is referred.

The strain energy function for hyperelastic materials, closely related to the stress - strain link, is expressed in ABAQUS as a series expansion in terms of the first and second strain invariants (commented in Section 2), plus a correction term depending upon the third strain invariant to account for the (moderate) compressibility of the elastomer (see ABAQUS User's Manual (1989), p. 4.7.5-1). In the present biomechanical application a compressible neo-Hookean law is adopted, where such a choice is rationalized in the following. In Prati and Strozzi (1984) , Fig. 13 , a comparison is presented between two stress-strain laws (namely a compressible neo-Hookean strain energy function and a more complex relationship, where the same figure for the bulk modulus is employed), from which it appears that their influence on the contact pressure profile is moderate. In Dragoni and Strozzi (1988) , Fig. 10 , it is shown that, for situations where the hydrostatic part of stress prevails, a perturbation of Poisson's ratio affects the stress field much

more dramatically than a modification of the Young's modulus. For the present application, characterized by high hydrostatic stress levels (Matthewson (1981)), it was decided to pay more attention to the Poisson's ratio influence that to that connected to the deviatoric part of stress. In other words, a simple neo-Hookean constitutive relation was adopted, while various cubic compressibilities were mimicked to retrieve information on their impact on the contact pressure profile and contact radius. More comments on this aspect are included in Section 2.2.3 .

Aspects connected to the unilateral contact problem were briefly treated in Chapter 4.

6.5.2 Influence of Poisson's ratio

Similar to Section 4.4.4 , a selection of Poisson's ratios close to the incompressibility figure 0.5 is systematically examined, and the normalized y-parameters $pR/(Ea)$ and a/h are diagrammatically reported as functions of x-variable $\delta R/h^2$ (where p denotes the peak contact pressure, R represents the equivalent radius of the paraboloidal indenter, a indicates the contact radius, h symbolizes the layer thickness, δ means the indentation depth, and E is the Young's modulus). In particular, the practically relevant Poisson's ratio figures 0.5 , 0.4999 , 0.4997 , 0.499 , 0.49 , 0.48 were studied. A paraboloidal indenter was adopted for consistency with most of the available results. Section 7.3.6 examines the errors incurred in mimicking a spherical indented via a paraboloidal punch for realistic geometries. Section 5.3.4 refers to the parallel, plane strain, curved layer situation and to the indenter parabolic approximation consequences. Finally, Dowson, Fisher, Jin, Auger, and Jobbins (1991) observe that "At higher [indentation] values the model applied to a sphere on a plane becomes less accurate."

Figs 6.5.2.1,2,3,4,5,6 report as y-variable a parameter closely related to the peak contact pressure, whereas Figs 6.5.2.7,8,9,10,11,12 address the normalized contact radius. The mesh for the layer description was formed by 2000 square elements, ten elements located along the axial direction (the layer thickness was assumed of 10 mm) and 200 elements aligned along the radial direction (the radius of the deformable disk was 200 mm). The equivalent radius of the rigid parabolic indenter was 10000 mm . This high value was employed to limit the non linear geometric and material effects (Chapter 2), since elevated pressures (connected to the essentially hydrostatic stress state) take place with moderate compressions, which scarcely involve finite deformation consequences and non linear stress-strain effects.

Four noded, bilinear displacement, constant pressure elements suitable for applications in the field of almost incompressible materials were adopted (see ABAQUS User's Manual (1989) , p. 3.2.6-1). In addition to the finite element forecasts, all Figures report the asymptotic incompressible predictions (Jaffar (1989)):

$$\frac{p\,R}{E\,a} = \frac{1}{4}\left(\frac{\delta\,R}{h^2}\right)^{1.5} \quad ; \quad a/h = 2\sqrt{\frac{\delta\,R}{h^2}} \quad ; \quad P = \frac{2\,\pi\,E\,\delta^3\,R^2}{3\,h^3} \tag{6.5.2.1}$$

while Figs 6.5.2.6 and 6.5.2.12 , which refer to the relatively low figure $\nu = 0.48$, include also the Winkler-type, laterally constrained column model forecasts :

$$\frac{p\,R}{E\,a} = \sqrt{\frac{\delta\,R}{h^2}}\;\frac{(1-\nu)}{\sqrt{2}\,(1+\nu)\,(1-2\nu)} \quad ; \quad \frac{a}{h} = \sqrt{2}\,\sqrt{\frac{\delta\,R}{h^2}} \quad ;$$

$$P \doteq \frac{(1-\nu)}{(1+\nu)\,(1-2\nu)}\;\frac{\pi\,E\,\delta^2\,R}{h} \tag{6.5.2.2}$$

Finally, Figs 6.5.2.1 and 6.5.2.7 - referring to perfect incompressibility - include some results derived from Fig. 4 of Li and Dempsey (1990).

It is here noted that the following observation of Dowson, Fisher, Jin, Auger, and Jobbins (1991) "For any particular contact width, peak normal stresses increased by a small amount for a reduced layer thickness." agrees with solution (6.5.2.1) , which suggests that the peak contact pressure is inversely proportional to the cube of the layer thickness, for an imposed contact radius.

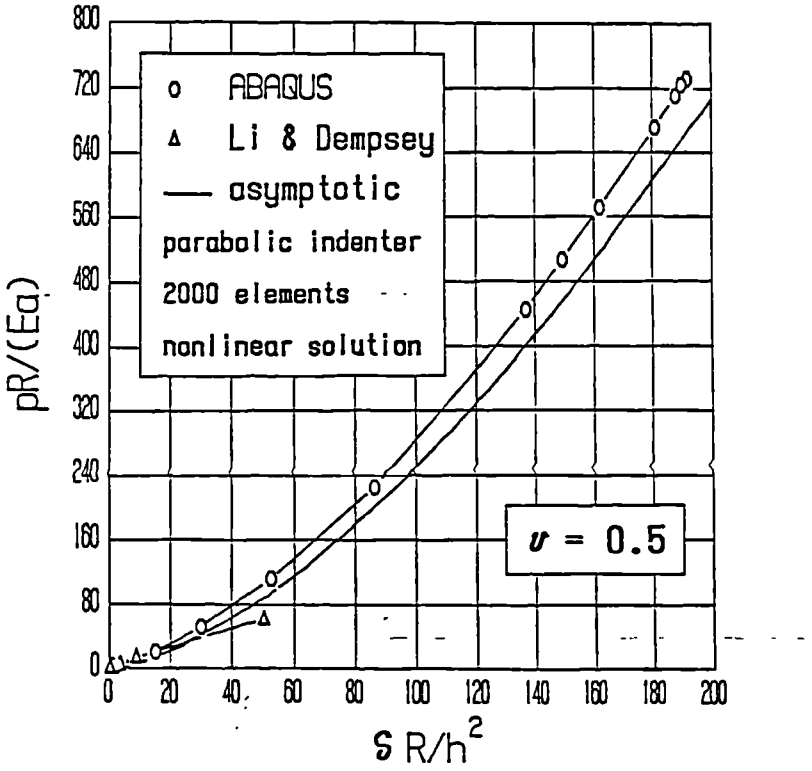

Fig 6.5.2.1 : Normalized peak pressure versus indentation depth for ν = 0.5 .

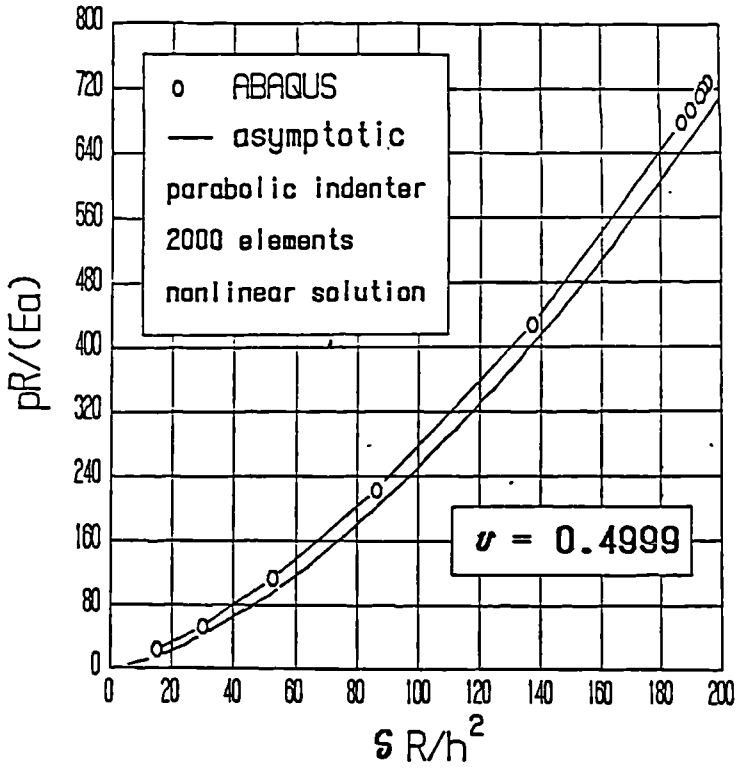

Fig 6.5.2.2 : Normalized peak pressure versus indentation depth for ν = 0.4999 .

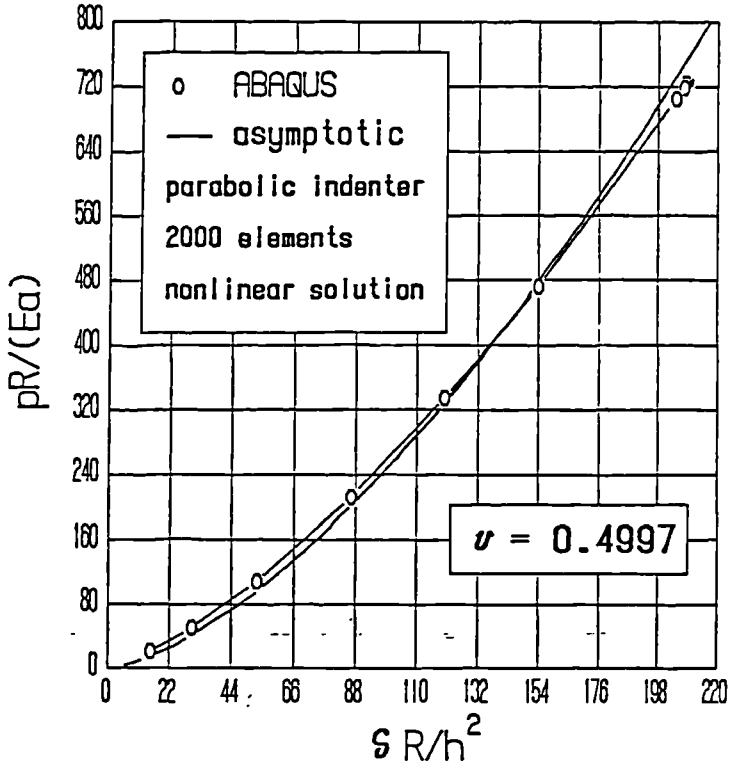

Fig 6.5.2.3 : Normalized peak pressure versus indentation depth for ν = 0.4997 .

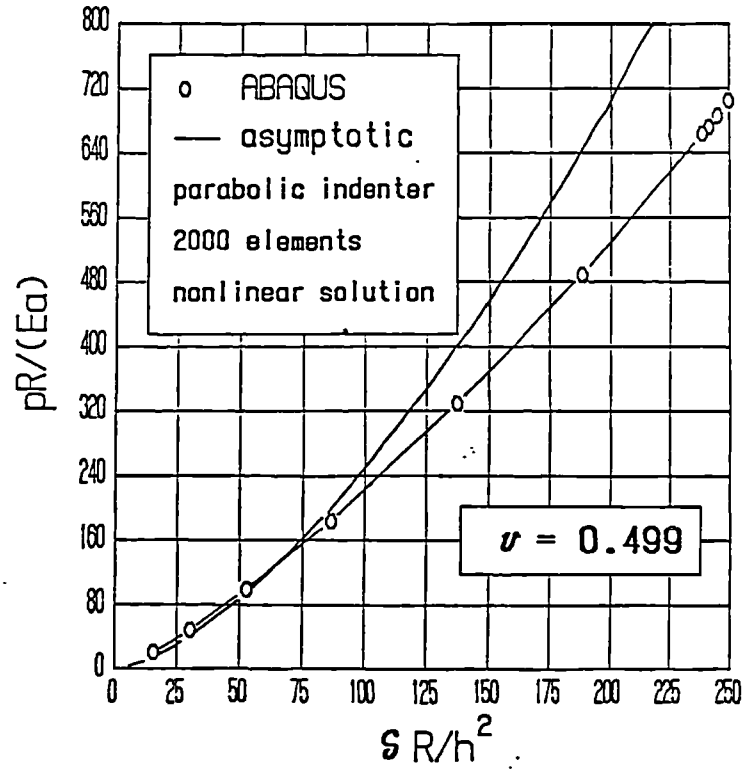

Fig 6.5.2.4 : Normalized peak pressure versus indentation depth for ν = 0.499 .

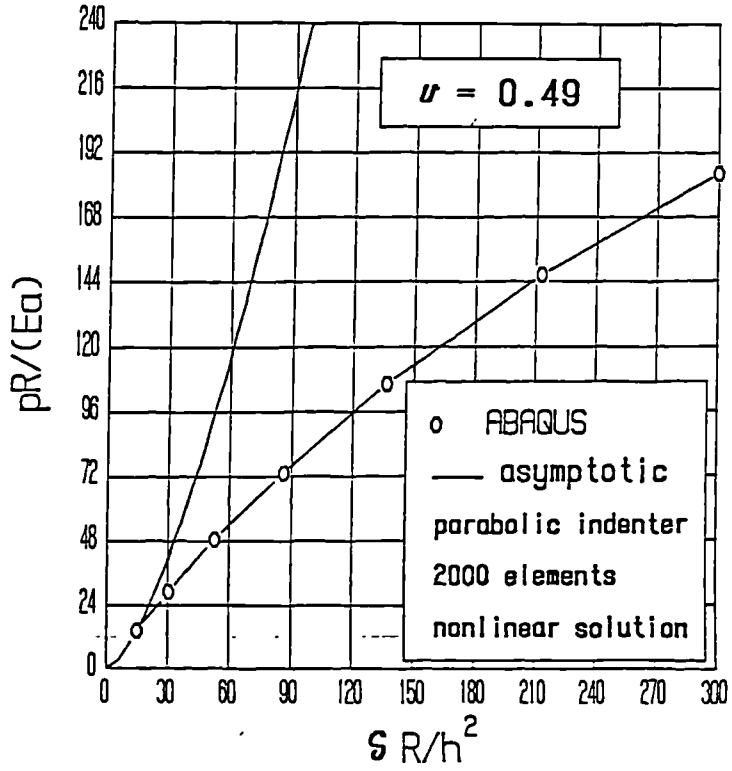

Fig 6.5.2.5 : Normalized peak pressure versus indentation depth for ν = 0.49 .

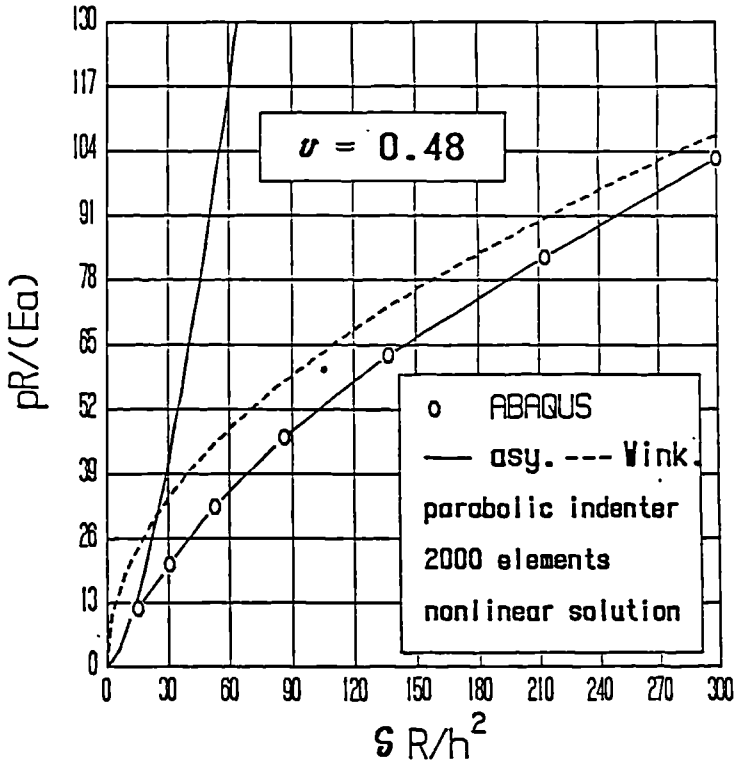

Fig 6.5.2.6 : Normalized peak pressure versus indentation depth for ν = 0.48 .

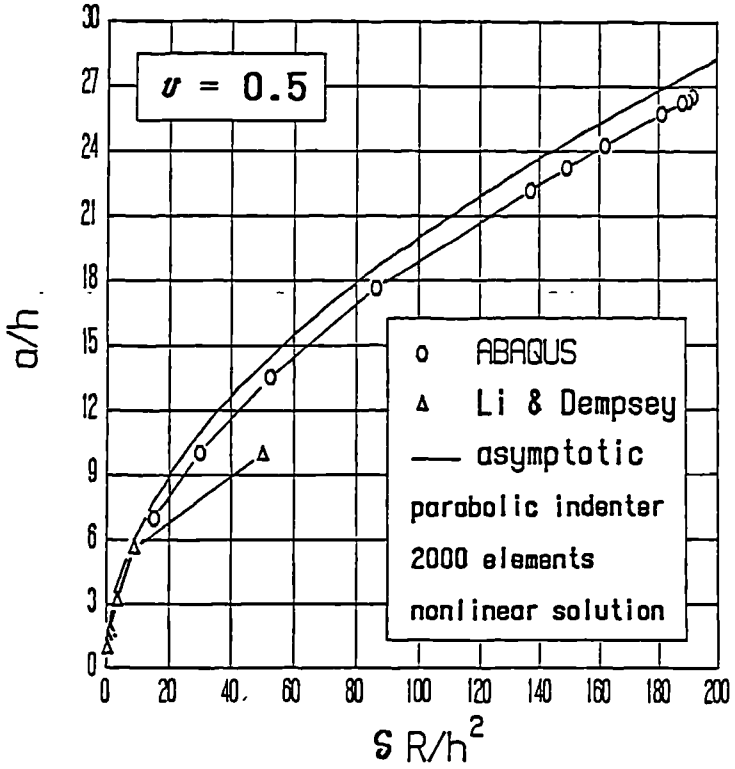

Fig 6.5.2.7 : Normalized contact radius versus indentation depth for ν = 0.5 .

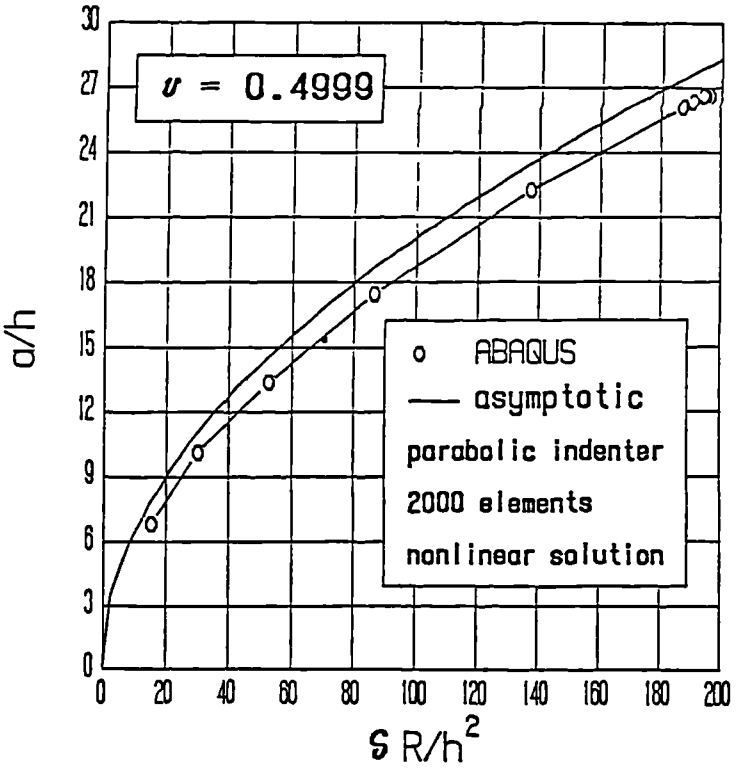

Fig 6.5.2.8 : Normalized contact radius versus indentation depth for ν = 0.4999 .

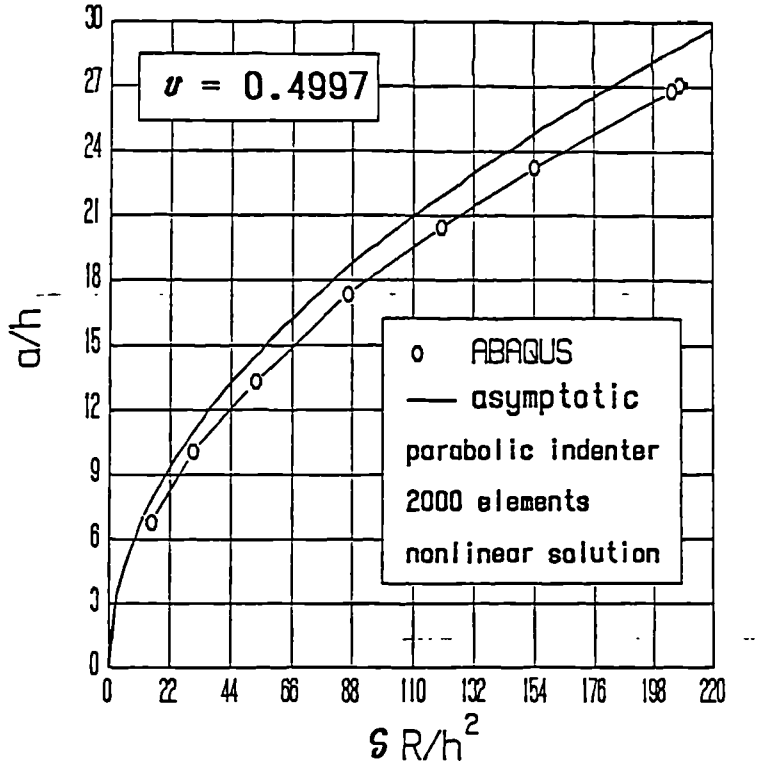

Fig 6.5.2.9 : Normalized contact radius versus indentation depth for ν = 0.4997 .

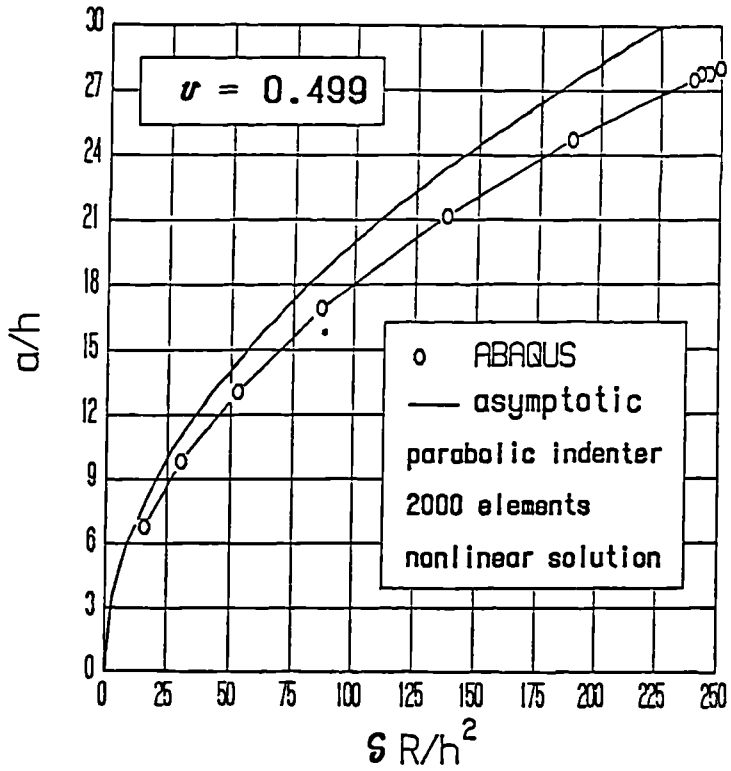

Fig 6.5.2.10 : Normalized contact radius versus indentation depth for ν = 0.499 .

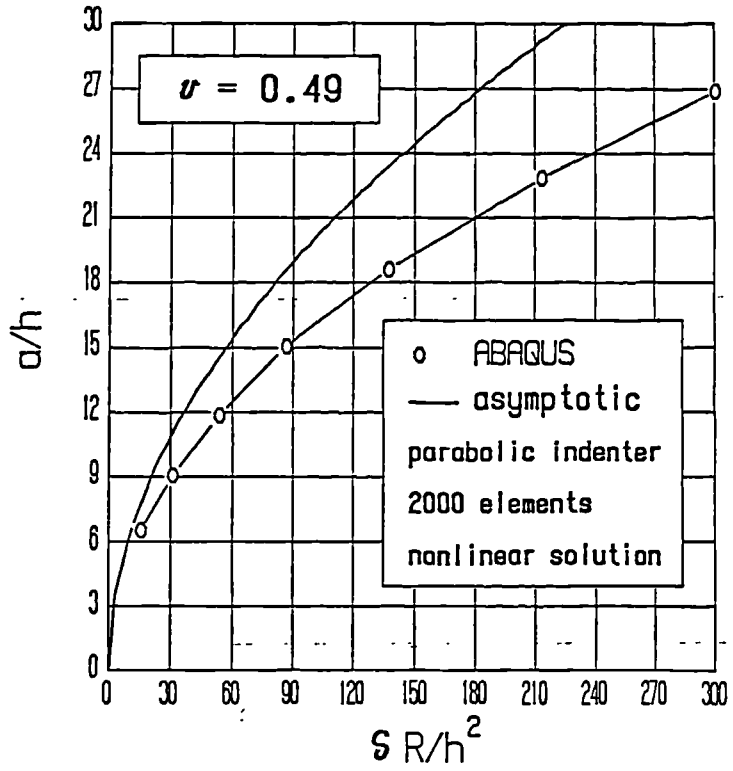

Fig 6.5.2.11 : Normalized contact radius versus indentation depth for ν = 0.49 .

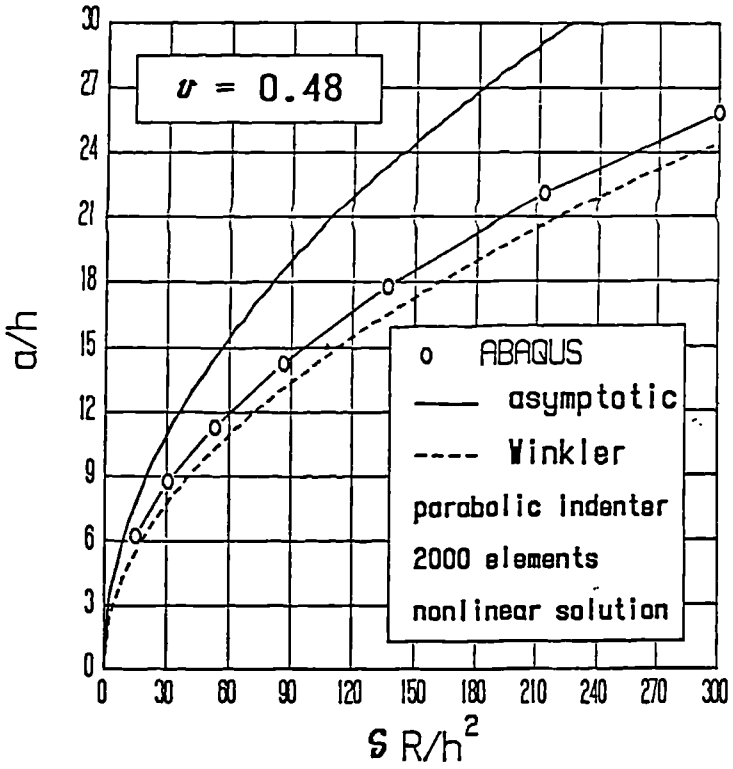

Fig 6.5.2.12 : Normalized contact radius versus indentation depth for ν = 0.48 .

It is noted that in Figs 6.5.2.1 and 6.5.2.7 the asymptotic incompressible forecasts agree reasonably well with the incompressible finite element forecasts, but not so well as for the corresponding plane situation of Fig. 4.3.4.1 , which was examined with a numerical program based on linear elasticity. The corresponding deviation may be imputable to nonlinear effects in the treatment of the stress-strain law and strain tensor and/or to inaccuracies in defining the contact radius (see Fig. 7 of Ihara, Shaw and Bhushan (1986), and the related text). As already commented in Section 4.2 with reference to Björkman (1991) paper, the non linear effects are likely to stiffen the layer, thus producing a higher peak contact pressure for a prescribed indentation depth, a trend visible in Fig. 6.5.2.1 . It must be admitted, however; that lower discrepancies are met between the finite element forecasts of the following Section 6.6 and the corresponding theoretical linear solutions, so that some doubts remain on the main causes of the mismatch between incompressible finite element forecasts and incompressible asymptotic predictions. This point is further commented in Section 6.6 .

The Li and Dempsey (1990) predictions cover only a limited part of the diagram, in which they substantially agree with the two previous results. The last value (along x-axis) according to Li and Dempsey (1990) appreciably deviates from the previous results, but it must be confessed that the corresponding reading from Fig. 4 is difficult, and seemingly affected by a considerable error. It also appears from Fig. 6.5.2.1 that ABAQUS program does not converge for x- variable exceeding about 200.

Moving to ν = 0.4999 (Figs 6.5.2.2 and 6.5.2.8), the differences in terms of central pressure with respect to the incompressible finite element forecasts are perceivable (about 4 percent for x-variable = 180), whereas the corresponding contact radii are hardly distinguishable. For the plane counterpart of Fig. 4.3.4.2 , the sensitivity of the central pressure to a Poisson's ratio perturbation appears to be higher, in the region of 8 percent.

The following decreasing Poisson's ratios 0.4997, 0.499 , 0.49 , 0.48 show an appreciable diminution of the peak contact pressure for the same value of x-variable, where the lower figure ν = 0.48 (Fig. 6.5.2.6) produces a good agreement between finite element predictions and the Winkler-type forecasts of eqns 6.5.2.2 .

The corresponding degree of agreement for the plane counterpart of Fig. 4.3.4.6 is similar (in both cases the Winkler solution overestimates the numerical forecasts), even if the two error trends with respect to x-variable are opposite. The variation in contact radius with ν is in all cases much less dramatic. It is observed that Dowson, Fisher, Jin, Auger, and Jobbins (1991) adopt the figure $\nu = 0.499$ without performing specific measurements and without assessing the sensitivity of the mechanical response of the elastomeric layer to perturbations of the Poisson's ratio. The following computations aim at estimating parameter $\delta R/h^2$ for the configuration of the above paper, to examine the relevance of ν . Dowson, Fisher, Jin, Auger, and Jobbins (1991) suggest in their Table 3 a tentatively optimized configuration for the cushion form bearing, defined by $h = 2$ mm , $R = 1000$ mm , $a = 16$ mm , $E = 20$ MPa , $P = 2500$ N (this figure for the load is reported in the caption to their Fig. 2). The asymptotic incompressible solution (6.5.2.1) expressing the normalized contact radius suggests $\delta \simeq 0.064$ mm , so that $\delta R/h^2 \simeq 16$. The accuracy of the asymptotic solution for low values of parameter $\delta R/h^2$ is questionable, as discussed in Sections 4.3.5 and 6.6 , so that the above parameter can be estimated only approximately. In any case, in Section 6.6 situations are analyzed in which variable $\delta R/h^2$ falls below 15 , and for which the *effects of a perturbation of the Poisson's* ratio (see Fig. 6.6.4) are found to be modest. It is concluded that for the above geometry and loads the Poisson's ratio is not a vital parameter. Anyway, it is anticipated that for higher loads the contact pressure may become very sensitive to perturbations of ν , see Section 7.3.4 , so that in general situations it becomes essential to perform an accurate measurement of the cubic compressibility of the elastomer adopted (Chapter 3).

It is also noted that the finite element forecasts produce a central contact pressure which, at the highest compressions imposed, becomes slightly lower than its adjacent nodal values (some central oscillations are visible in Fig. 7.3.2.15 , referring to a comparable configuration). This physically unjustified result is seemingly attributable to the ABAQUS internal numerical tolerance in imposing the boundary conditions. A very small extrusion beyond the symmetry axis is in fact tolerated which, due to the moderate compressibility of the elastomeric layer, may slightly, but appreciably, reduce the central contact pressure with respect to the contiguous

zones.

A comparison is made in the following between plane strain and axisymmetric cases with regard to maximum contact pressures and contact radii as functions of the indentation depth. For large indentation depths, the axisymmetric peak contact pressure is about three times lower than its plane strain counterpart of Chapter 4 (see Figs 4.3.4.1 and 4.3.5.5 for the plane case, and Figs 6.5.2.1 and 6.4.7.3 for the axisymmetric configuration), whereas the axisymmetric and plane contact radii are comparable (see Figs 4.3.4.7 and 6.5.2.7). For small penetrations, the plane and axisymmetric results are more similar, the former supplying moderately lower central pressures (see Figs 4.3.5.4,5 and 6.4.7.2,3). These findings in terms of pressure can be rationalized as follows. For moderate indentations, the circumstance that an infinite cylinder compressing a half space obliges the half space surface points aligned with respect to the cylinder axis to inflect uniformly releases the peak pressure with respect to the compression by a sphere. On the other side, when the higher indentations imposed produce larger contact widths, the plane strain state does not permit any lateral flow of the half space, thus resulting in a stiffer foundation with respect to its axisymmetric analogue, which is responsible for the higher plane strain peak contact pressure. Figs 4.3.5.4 and 6.4.7.2 demonstrate that the first aspect prevails for very low contact radii, whereas Figs 4.3.4.1 and 6.5.2.1 (as well as Figs 4.3.5.4 and 6.4.7.2) indicate that the second mechanism predominates for high contacts.

6.6 APPRAISAL OF O'CARROL *et al.* (1990) PAPER

The recent paper by O'Carrol, Jin, Dowson, Fisher and Jobbins (1990) reports various experimental results concerning a silicone disk firmly anchored to a rigid support and compressed by a spherical lens. Three disk thicknesses were examined, namely 3.15, 2.08 and 1.21 mm . The disk radius adopted is not indicated in the paper. The indenter radius was 104 mm . The Young's modulus for the elastomer was measured and found to be 3.04 MPa , whereas the Poisson's ratio was assumed as 0.4998 without performing specific measurements. Various diagrams are presented which report the measured total load versus the contact radius, together with theoretical forecasts obtained by applying the theory of Hayes, Keer, Herrmann and Mockros (1972), for the three available layer thicknesses. Consistent with Fig. 10 of Matthewson (1981), it is generally found in this paper that the force experimental readings overestimate the theoretical forecasts for a given contact radius, especially at the higher loads. Since the total load was imposed in the experiments rather than the penetration depth, the above result can be re-expressed by stating that the experimental contact radius was found to be lower than the theoretical predictions. In addition, consistent with Dragoni and Strozzi (1988), the loading of a dry contact produced a smaller contact radius than the lubricated contact. The sources of this disagreement are attributed in the above paper to : a) non linear elastic properties, to b) viscoelastic aspects, and to c) frictional effects. To these sources of errors, other plausible causes can be added : d) the influence of Poisson's ratio ; e) the fact that the theoretical indenter is assumed as paraboloidal, whereas the experimental profile is spherical ; f) the finiteness of the radial extent of the deformable disk.

To try and clarify these problems, it was decided to run ABAQUS for the three geometries under scrutiny. Figs 6.6.1,2,3 refer to the disk thicknesses 3.15 , 2.08 and 1.21 mm , respectively. They include the experimental and theoretical results from the above paper, as well as the ABAQUS nonlinear forecasts (2000 elements) referring to a deformable disk having a radius of 150 mm and the three above thicknesses, to ν = 0.4998 , and to a circular indenter of radius 104 mm . Since from Figs 6.6.1,2,3 it appears that the nonlinear ABAQUS predictions agree

with the theoretical linear predictions for all disk thicknesses, it can be concluded that the non-linear effects cannot be responsible for the disagreement between experimental readings and linear theoretical forecasts noted in the above paper (point a). Fig. 6.6.4 studies the effects of Poisson's ratio on the total load, as well as those related to the indenter profile. It appears from this Figure that a perturbation of ν between 0.5 and 0.499 does not significantly affect the total load in the physical range studied, nor does a modification of the indenter profile from circular to paraboloidal curves, since the corresponding results are essentially superimposed. As a consequence, the Poisson's ratio effects (point d) and the indenter profile choice (point e) cannot have caused the above deviations. In Fig. 9 of the paper under examination both loading and unloading loads are reported, and they both overestimate the theoretical predictions. As a consequence, it seems to the writer that the viscoelastic effects are not sufficient by themselves to explain the noted mismatch (point b). Similarly, Fig. 8 of the above paper reports dry and lubricated loads, which are both higher than the frictionless results. So, the frictional effects cannot justify the disagreement (point c). With regard to the consequences of the disk radial dimension (which is unknown), it can be observed that, if this dimension were comparable to the contact radius, the disk would become more deformable (since the layer lateral flow would be eased) and, therefore, the experimental total load would be lower than due, while it can be surmised that the effects on the contact radius would be less important. (In fact, in the Hertzian case of an infinitely deep layer, the contact radius depends only marginally on perturbations of the Poisson's ratio for an imposed load (Johnson (1985)). Modifications of ν alter the layer compliance, an effect somewhat comparable to a change in the disk radius, which also influences its deformability. Another source of information is Hanson and Keer (1989) paper, where in their Fig. 4 the indentation of a parabolic punch into a half plane in the vicinity of its corner is studied. The essentially Hertzian contact pressure profile even for punches very close to the quarter plane apex indicates that the foundation border effects on the contact width are modest. These comments suggest that the contact radius should be scarcely modified by a variation of the disk radius, provided that the contact is a fraction of the disk radius.) Since from the above paper it appears that the experimental load is higher than expected, it is concluded that the mismatch cannot

be convincingly attributed to the disk radial dimension adopted (point f).

Matthewson (1981) reports difficulties in the penetration readings, and shows in his Fig. 10 that a small offset in the indentation depth may significantly alter the results so that a much better agreement between experiments and theory is achieved. Analogously, Goodman and Keer (1965) note that "the measurement of relative approach is at a minimum accuracy" "for the lowest loads". Problems in the penetration depth measurements are signalled in Section 5.4 . In conclusion, it is here proposed that the mismatch noted in the paper under appraisal may be attributed to reading accuracy problems, possibly connected to the deformability of the loading device.

As a final observation, an apparent contradiction between the results of this Section and those of Section 6.5 is discussed in the following. It has been shown in this Section that the nonlinear elasticity effects are limited, since the nonlinear finite element forecasts agree with the linear elasticity theory predictions. In Section 6.5 , instead, the mismatch between the ABAQUS predictions of Fig. 6.5.2.1 and the asymptotic, linear elastic forecasts was ascribed to nonlinear elasticity effects. Aimed at clarifying this contradiction, the following TABLE reports the numerical penetration depth, δ , for the maximum numerical load, P, as a function of the layer thickness, h , with reference to Figs 6.6.1,2,3 , and it specifies the values of the corresponding normalized variable $\delta R/h^2$:

TABLE of penetrations δ

	h = 3.15 mm	h = 2.08 mm	h = 1.21 mm
δ [mm]	0.82	0.60	0.22
P [N]	1805	2179	524.7
$\delta R/h^2$	8.59	14.42	15.62

According to the asymptotic, incompressible solution (eqn 6.5.2.1) :

$$a/h = 2\sqrt{\delta\ R/h^2} \tag{6.6.1}$$

The asymptotic solution in terms of contact width is applicable provided that the contact radius, a , is much greater than - say ten times or more, as suggested by the high gradient of the (corresponding plane strain) contact width curve in the vicinity of the origin in Fig. 4.4.4.6 , which implies high deviations between asymptotic and real curves - the layer thickness, h. From (6.6.1), this condition requires that $\delta\ R/h^2 > 25$. The previous TABLE shows that the maximum value of this normalized variable is considerably lower than 25 , so that the asymptotic solution is not reliable for this physical range. As a consequence, the mismatch noted in Fig. 6.5.2.1 between nonlinear and (linear) asymptotic solutions can be attributed to nonlinear effects only within the range where the asymptotic solution is applicable, that is, when x-variable exceeds, say, 25 . For lower x-values, no conclusion can be drawn from Fig. 6.5.2.1 on the non linear effects. In fact, for low x-values, Figs 6.6.1,2,3 suggest that the non linear effects are negligible. It is concluded that the non linear elasticity effects become appreciable for the range of x-variable for which the asymptotic solution of eqn 6.5.2.1 is applicable.

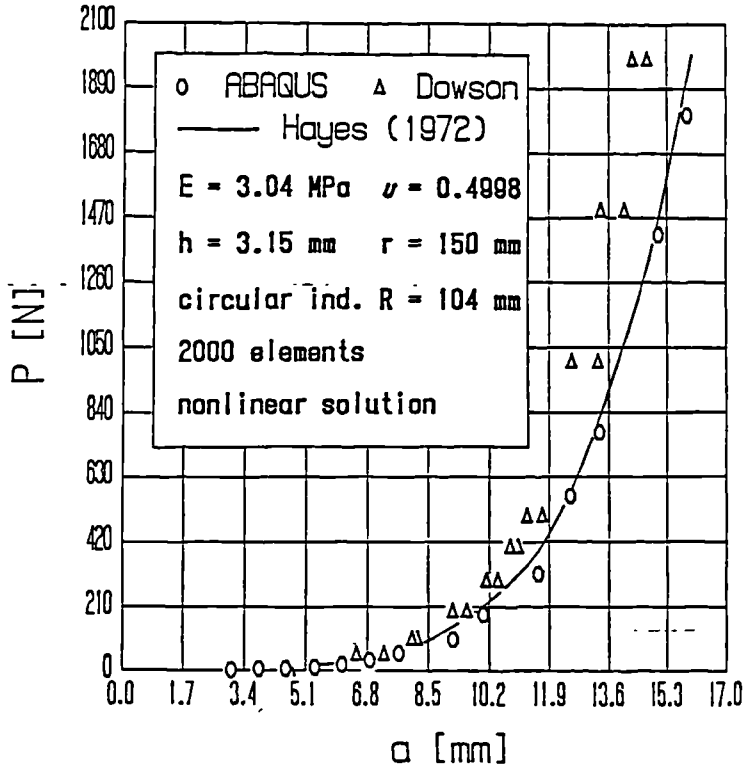

Fig 6.6.1 : Total load versus contact radius for h = 3.15 mm .

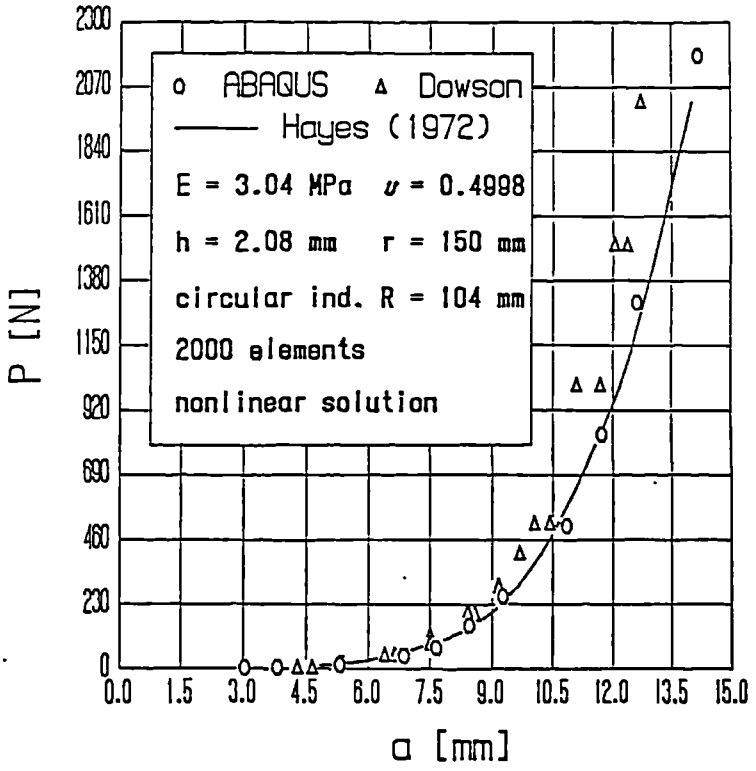

Fig 6.6.2 : Total load versus contact radius for h = 2.08 mm .

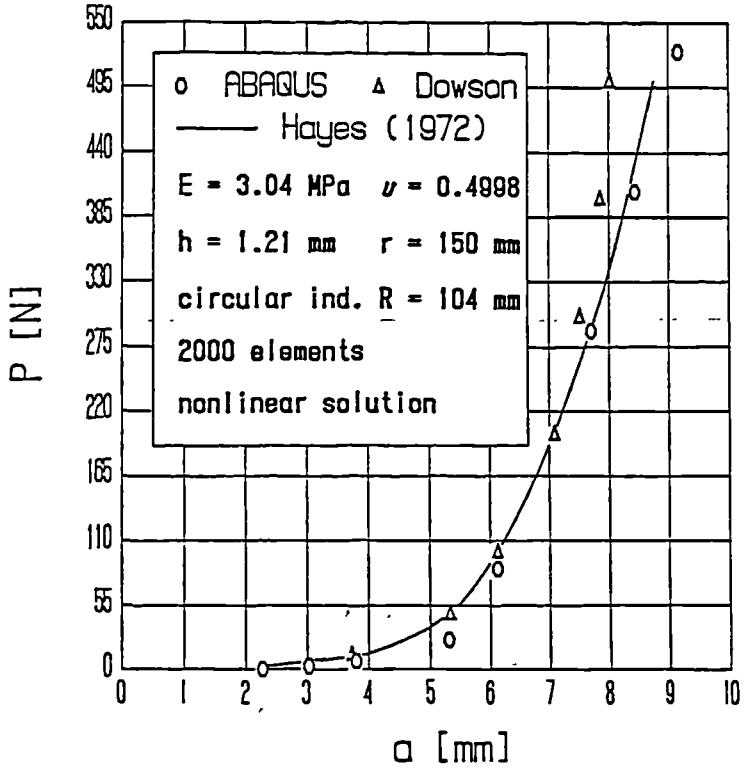

Fig 6.6.3 : Total load versus contact radius for h = 1.21 mm .

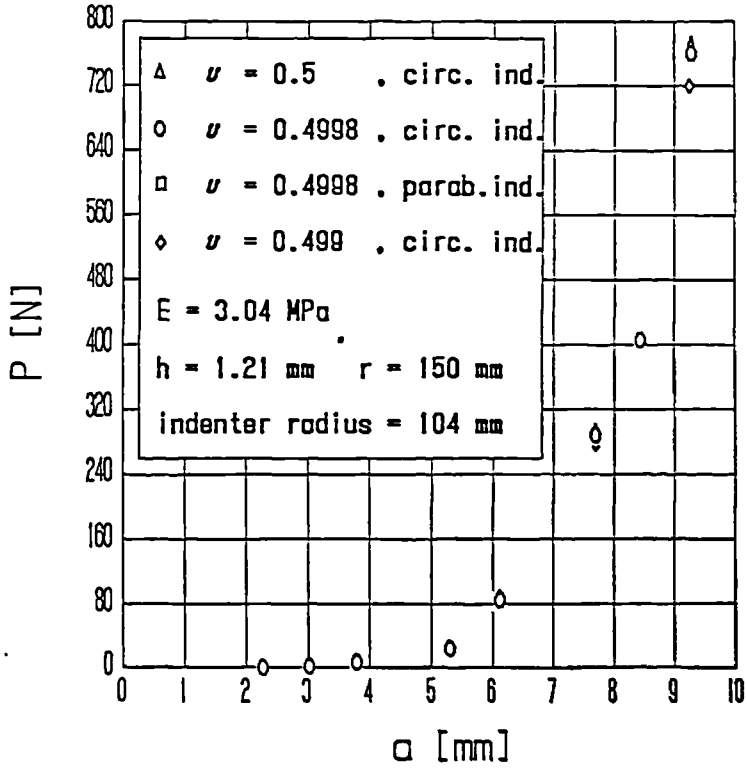

Fig 6.6.4 : Total load versus contact radius for various Poisson's ratios .

6.7 CONCLUSIONS

A perturbation solution of the problem of a deformable layer indented by a rigid sphere has been obtained. This solution is valid for ratios of contact radius to layer thickness up to 0.7 . Finite element forecasts have been achieved for higher compressions, and the sensitivity of the results to perturbations of Poisson's ratio has been clarified. For large contact radii, the axisymmetric peak contact pressure is about three times lower than its plane strain counterpart of Chapter 4, whereas the axisymmetric and plane contact radii are comparable. For small contact radii, the plane and axisymmetric results are more similar.

CHAPTER 7 . THE SPHERICAL, AXISYMMETRICALLY LOADED, ELASTOMERIC LAYER : NUMERICAL STUDY

7.1 INTRODUCTION

7.2 LITERATURE REVIEW

7.3 NUMERICAL STUDY

7.3.1 General remarks on the finite element approach

7.3.2 The four basic configurations for the hip replacements

7.3.3 Effects of the initial gap between head and layer loaded surface

7.3.4 Effects of perturbations of the Poisson's ratio

7.3.5 Effects of the angular extent of the elastomeric layer

7.3.6 Effects of the indenter profile

7.3.7 Considerations of the selection of the layer thickness

7.4 CONCLUSIONS

7.1 INTRODUCTION

The previous Chapter 6 addresses the axisymmetric problem of a flat layer indented by a spherical punch. This Chapter, instead, deals with a spherical layer anchored to a rigid backing and compressed by a rigid spherical indenter, Fig. 7.1.1 . This geometry mimics the hip replacements possessing an elastomeric layer firmly bondend to the cup (Unsworth, Pearcy, White, and White, (1987)).

Due to the complexity of this geometry, characterized by a curved layer of finite thickness and extent, the corresponding mechanical analysis was performed via a finite element package. The forecasts retrieved supply suggestions about the proper selection of the elastomeric layer thickness.

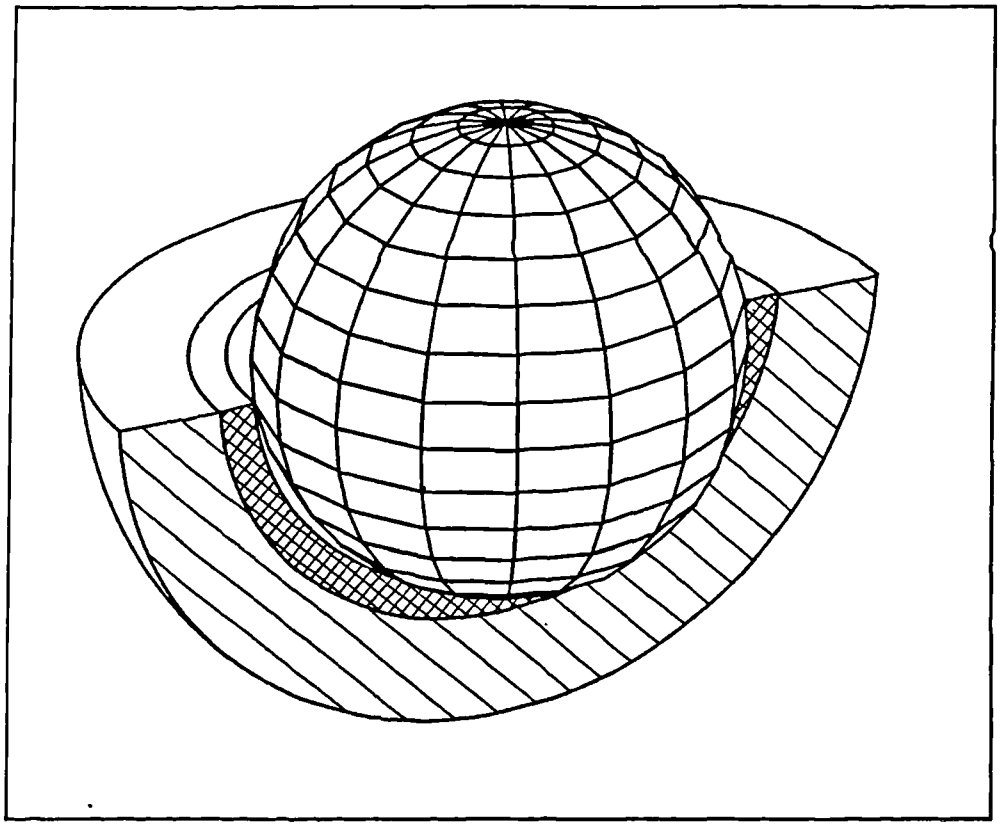

Fig. 7.1.1 : A spherical layer indented by a sphere.

7.2 LITERATURE REVIEW

In this Section the papers referring to the axisymmetric case of a deformable, spherical layer, anchored to a rigid backing and compressed by a rigid spherical indenter are reviewed. Comparable geometries, still pertinent to this literature review, are also considered.

Sternberg, Eubanks and Sadowsky (1951) treat the problem of a spherical layer under imposed axisymmetric pressure profiles at the inner and outer surfaces. The develop their theory on the basis of pioneering studies of Somigliana (1887), Fichera (1949), and Aquaro (1949). A series solution in explicit form, involving Legendre polynomials, is obtained (see also Timoshenko and Goodier (1970), p. 384). Unfortunately, the case of prescribed (vanishing) surface displacements along the outer surface of the spherical layer and of mixed boundary conditions for the inner profile, more pertinent to the hip replacement configuration, is not developed in detail. Abramian and Babloian (1962) study a torque problem similar to the elastic layer configuration. A hollow hemisphere is subject to imposed shear stresses at its inner and outer surfaces, and to known displacements along part of the annular surface of the hemisphere, so that a torsion is in fact imposed on the spherical shell. A series solution is obtained. Goodman and Keer (1965) apply Sternberg, Eubanks and Sadowsky (1951) formulation to describe the compliance of a spherical cavity in an infinite medium, which is compressed by a deformable sphere. The integral equation describing the contact problem is solved numerically. Some experimental results are also presented, which show a good agreement with the spherical cavity theory, and a certain deviation from a purely Hertzian solution. Gladwell and England (1975) solve analytically the problem of a deformable, hollow sphere frictionlessly compressed between two parallel, rigid planes. Based on the work of Bartel, Burstein, Toda and Edwards (1985), Fricker (1991) develops a Winkler-type model of a metal-backed, deformable spherical layer, an approach which looks very close to that proposed by Yao (1990), p. 231 . The Poisson's ratio employed by Fricker (1991) is 0.4 , a figure for which the column model according to Winkler is accurate (see Fig. 6.5.2.6 of Chapter 5). Fricker (1991) employs the constrained column model to predict the frictional moment during head spin and

sliding motions.

The contributions dealing with a deformable solid sphere loaded by known pressure profiles (or shear stresses), compressed by rigid planes or by variously shaped punches, are examined hereinafter. The solution of this problem is comparable to that of the hip configuration, in the sense that spherical coordinates are involved. Abramian, Arutiunian and Babloian (1964) consider an elastic sphere indented by two antipodal punches possessing a concave profile coinciding with the undeformed spherical surface. Arutiunian and Abramian (1964) examine the compression of a deformable sphere partially resting on a rigid hemispherical cavity and antipodally loaded by a uniform radial pressure, via a series solution. They also treat the similar case of a sphere attached to the two stamps and subject to torque. Bondareva (1969) solves in closed form two cases : a) a weighted deformable sphere equilibrated by a concentrated, radial force ; b) an elastic sphere compressed by two antipodal radial forces. Bondareva (1970) extends case a) of Bondareva (1969) to the situation of a weighted sphere resting on a concave rigid support of higher radius, and compares its predictions with the Hertzian theory. Karpenko (1973) extends Abramian, Arutiunian and Babloian (1964) paper to cover the case of punches whose concavity possesses a radius larger than that of the undeformed sphere, showing the differences between the present solution and the Hertzian approach. Unsworth (1978) examines experimentally the effects of lubricant viscosity in various hip replacements. In particular, Charnley prostheses were considered, where the cup is covered with an ultra high molecular weight polyethylene. Durelli and Chen (1979) examine experimentally a deformable sphere compressed between two rigid, parallel planes. Tatara (1991) develops an analytical theory for the case of a deformable sphere compressed by two parallel, flat, rigid planes, by accounting for large elastic deformations, non linear material relationship and unilateral contact aspects. The experimental readings of Tatara, Shima and Lucero (1991) exhibit a good agreement with the theoretical forecasts of Tatara (1991) up to compressions of 20 percent.

As a final remark, Gladwell (1980), p. 509 , shows the existing link between plane and axisymmetric problems, which permits the Green function for the axisymmetric case to be derived from its plane counterpart. This correlation is valid for Cartesian coordinates, and in fact it was used in Section 6.3 of Chapter 6

to check the displacement function at the surface of an infinite flat layer loaded by a concentrated transverse force. It is not known to the present author if a similar connection exists for polar coordinates. If an expedient could be devised to pass from polar to spherical coordinates, expression (5.3.7) of Chapter 5 could be used to construct the Green function for the spherical layer. More exactly, the resulting spherical cortex would be the analogue of that in Fig. 5.3.2 for the plane situation, which might supply simpler results than an actual spherical shell, without significant losses in precision.

7.3.1 General remarks on the finite element approach

The finite element program ABAQUS (1989), already employed in Sections 3.3.3.2 and 6.5.1 , was here used to describe a spherical deformed layer indented by a spherical rigid head. This package accounts for geometrical non-linearities deriving from finite deformations and from progressive contact aspects, as well as for material non-linearities, connected to the complexities of the stress-strain link. In the case of nearly incompressible elastomers, a sensitivity of the mechanical response to perturbations of the Poisson's ratio is expected, so that the program must be reliable under this aspect. Dragoni (1990,1991) specifically checks the sensitivity of ABAQUS to variations of the Poisson's ratio, and he finds this program to be accurate. Current research of Dragoni is devoted to the finite element analysis of the axisymmetric geometry analytically studied by Moghe and Neff (1971), noting again a refreshingly good degree of agreement between numerical and theoretical forecasts. Lau and Jeans (1989) report a good correlation between experimental and ABAQUS numerical deflections for and elastomeric dome. (It must be however remembered that a comparison on deflections is generally much less indicative than a confrontation on stresses, which is often more problematic, especially in the case of nearly hydrostatic stress states.) Two test cases on ABAQUS versus Hertzian problems are performed by Kanters (1990), who finds that "the ABAQUS program performed well for both test problems" in forecasting the contact pressure. It can be concluded that ABAQUS package is reliable in dealing with variations of the Poisson's ratio in the vicinity of incompressibility.

Version 4.8-4 of ABAQUS was used for the present study, running on the DEC MicroVAX 3500 System available at the Laboratory for Computational Mechanics (LAMC) of the University of Bologna, Italy.

7.3.2 The four basic configurations for the hip replacements

The four geometries for the rigid spherical head and for the elastomeric layer firmly bonded to a rigid foundation and forming a spherical cavity, as indicated by Prof. A. Unsworth, Durham University, Britain, are reported in the following TABLE :

TABLE

reporting the dimensions of head and layer for the four basic cases

	head radius, mm	layer inner radius, mm	layer outer radius, mm
Case 1	15.875	16.125	16.625
Case 2	15.875	16.125	17.125
Case 3	15.875	16.125	18.125
Case 4	15.875	16.125	19.125

The initial diametrical gap between head and layer inner surface is kept the same for the four cases, and equal to 0.5 mm . Conversely, the layer thickness is increased from 0.5 mm to 3 mm in passing from Case 1 to Case 4 .

In all four cases, the angular extent for the elastomeric layer was assumed as π , that is, a half spherical layer was considered. A numerical study concerning the sensitivity of the joint mechanical behaviour to alterations of this parameter is presented in Section 7.3.5 .

Only axisymmetric loadings were examined. Although cup and head remain reasonably coaxial in normal gait, the maximum resultant joint force acts at an angle of about 30° to their common axis (Paul (1976)). However, since the main aim of this

study is the comparison between different geometries, a purely axial loading was still adopted as a reference condition.

The following figures for the elastic constants were adopted : E = 8.506 MPa , ν = 0.49942 , which are the results of measurements presented in Chapter 3 for a polyurethane elastomer actually employed in this application, named "Estane" 5714F1 . More exactly, from Chapter 3 it appears that the Poisson's ratio slightly increases with pressure (from ν = 0.49915 for $p \simeq$ 20 MPa up to ν = 0.49942 for $p \simeq$ 80 MPa). The ABAQUS package can handle a bulk modulus non linearly varying with the hydrostatic pressure. However, in the interest of greater simplicity, it was decided to employ a constant value for the Poisson's ratio. The figure ν = 0.49942 pertains to a pressure of about 80 MPa (Section 3.3.4), and a comparable peak pressure of about 63 MPa is reached for Case 1 at the top indentation (Fig. 7.3.2.2), so that the most severe stress state is properly mimicked. (In fact, in a rigorous solution a slightly lower Poisson's ratio should be used in the vicinity of the contact ends, where the pressure diminishes.) (It is noted that pressures higher than 80 MPa , up to 130 and 260 MPa , are met in Figs 7.3.3.2 and 7.3.4.8 , respectively.) For the remaining cases, characterized by higher layer thicknesses and lower maximum contact pressures (about 10 MPa in Fig. 7.3.2.11), the Poisson's ratio adopted constitutes a first approximation, which on the other side permits a better comparison among the various forecasts obtained in this study. Section 7.3.4 examines the stress variation when ν passes from 0.49942 to 0.5 , so that provisional reassuring indications about the relative smallness of the stress alteration when ν changes from 0.49942 to 0.49915 can be formulated even for the configurations examined in this Chapter. A neo-Hookean constitutive law incorporating E = 8.506 MPa and ν = 0.49942 was adopted (Section 2.2.3).

In all cases, the head-layer contact was assumed as frictionless, due to the usual presence of the synovial fluid. The effects of a Coulomb friction have been accounted for by Jaffar (1991b) for a plane case. A number of 2000 four noded, isoparametric, reduced integration elements were adopted for all cases.

Figs 7.3.2.1,12 report various practically relevant mechanical parameters for these four cases, as functions of the indentation depth. In particular, Fig. 7.3.2.1 displays the total load as a function of the penetration depth, Fig. 7.3.2.2 depicts

the maximum contact pressure between head and layer as well as the peak shear stress at the interface between layer and foundation, while Fig. 7.3.2.3 reproduces the contact angular extent and the angular coordinate of the peak shear stress. In a similar fashion, the following Figs 7.3.2.4,12 address the remaining three cases according to the previous TABLE.

With regard to Figs 7.3.2.1,4,7,10 , the maximum total load practically applied to a hip joint can reach values of twice the body weight during walking (Kilvington and Goodman (1981)) and as much as ten times during running (Paul (1976)). The maximum loads considered here reach 10000 N (Figs 7.3.2.1,4) , a figure in line with the indications by Paul (1976). It is appreciated that running is not performed by patients with hip replacements. Anyway, loads higher than those encountered during walking can mimic overloads due to accidents or falls. It appears that the load increases more than linearly with the indentation depth, as suggested by the Hertzian-type character of the contact.

With reference to Figs 7.3.2.2,5,8,11 , the central contact pressure between head and layer is compared to the maximum shear stress at the interface between layer and backing. Since the peak shear stress is expected to be of the order of 1/10 times the central pressure (see Section 5.4.2 for the equivalent plane case), the units adopted for τ_{max} are MPa/10 (that is, the τ figure , once divided by 10, is to be understood as expressed in MPa), so that peak pressure and shear stress should be comparable in all diagrams. It is found that for small layer thicknesses (Cases 1 and 2) the maximum shear stress is lower than 1/10 times the peak pressure, whereas for the higher thicknesses (Cases 3 and 4) the shear stress tends to approach 1/10 times the top pressure. It can be concluded that a conservative estimate for the maximum shear stress is 1/10 times the peak contact pressure for a wide spectrum of layer geometries and indentation depths. The shear stress is relevant when considering the possible occurrence of debonding phenomena between layer and foundation (Matthewson (1981)).

The following observations aim at comparing the numerical findings, suggesting a maximum contact pressure to peak shear stress ratio of about 10 , to the corresponding asymptotic, incompressible, flat layer forecasts of eqn (6.5.2.1), according to the following development. According to Jaffar (1989), his formulae (20)

and (23) (see also Love (1944), p. 283), the maximum interface shear stress occurs for the following radial distance r :

$$r = \frac{2\sqrt{\delta R}}{\sqrt{3}} \tag{7.3.2.1}$$

The maximum value for the interface shear stress is :

$$\tau_{max} = \frac{2E\delta\sqrt{\delta R}}{3\sqrt{3}h^2} = \frac{E a^3}{12\sqrt{3}h^2 R} \tag{7.3.2.2}$$

where r is the radial distance, R the equivalent radius, δ the indentation depth, h the layer thickness, and E the Young's modulus.

The ratio between maximum contact pressure and peak shear stress is :

$$\frac{p_{max}}{\tau_{max}} = \frac{3\sqrt{3}}{4}\frac{\sqrt{\delta R}}{h} \tag{7.3.2.3}$$

In the configuration of Case 1 (Figs 7.2.3.2.1,2,3), $E = 8.506$ MPa , $R = 1023.9375$ mm . When $\delta = 50$ μm , then p_{max} / τ_{max} according to (7.3.2.3) equals 18.59 , where the numerical forecasts of Fig. 7.3.2.3 suggest $p_{max} / \tau_{max} \simeq 20$, whi represents a sufficiently accurate forecast. Anyway, it must be underlined that Fig. 7.3.2.3 refers to $\nu = 0.49942$, whereas the asymptotic forecasts are based upon an assumption of incompressible layer. The distinct asymptotic incompressible predictions for p_{max} and τ_{max} according to (6.5.2.1) are 87.0961 MPa and 4.6852 MPa , respectively, which exhibit considerable deviations from the numerical values, in the region of 40 $\div$ 50 percent. Such mismatches are attributable to Poisson's ratio effects and to errors in the description of the indenter profile (which is spherical in the finite element study and paraboloidal in the asymptotic solution). It is here

observed that, in the case examined, $\delta\ R/h^2 = 204.79 >> 100$, so that perturbations of the Poisson's ratio are expected to modify significantly the layer stress state (Section 7.3.4). Conversely, the contact angle (Section 7.3.6) is in the region of 0.89 rad $<$ 1 rad (the asymptotic incompressible contact radius is 14.3104 mm , according to eqn (6.5.2.1)), so that the errors ascribable to the indenter profile description should be small (Section 7.3.6).

The following expression of τ_{max} a a function of the load, P , is obtained by combining (7.3.2.2) with the expression for the load in (6.5.2.1) :

$$\tau_{max} = \frac{1}{3}\sqrt{\frac{2\,E\,P}{\pi\,R\,h}} \qquad (7.3.2.4)$$

which indicates that the maximum shearing stress increases with E for a fixed load. This indication seems to disagree with the results of Dowson, Fisher, Jin, Auger, and Jobbins (1991), who observe that "both the normal and shear stress distributions are primarily dependent on contact area. Reduction in elastic modulus would produce an increase in strain and an increased likelihood of fatigue failure." and that "a . . . reduction in modulus will produce increased shear strains." The obscure point in comparing the above sentences to the forecasts implicit in (7.3.2.4) is that it is not evident which parameter has been kept constant by Dowson, Fisher, Jin, Auger, and Jobbins (1991) in examining the effects of modifications of the Young's modulus. It is felt that this parameter is the imposed load, since a) this is the physically assigned parameter ; b) Fig. 2 of Dowson, Fisher, Jin, Auger, and Jobbins (1991) refers to a fixed load. If, on the other side, the contact radius is kept constant, as suggested by y-axis variable of Fig. 2 of the above paper, the last formula of (7.3.2.2) still suggests a diminution of the peak shear stress with E , still in contrast with the above study.

Encouragingly, the following observation of Dowson, Fisher, Jin, Auger, and Jobbins (1991) "For any particular contact width, peak normal stresses increased by a small amount for a reduced layer thickness" agrees with the asymptotic, incompressible, flat layer forecasts of eqn (6.5.2.1), as already commented in Section

6.5.2 .

With relation to Figs 7.3.2.3,6,9,12 , the expression "contact angle" denotes the angle between the layer symmetry axis and any point of the circle defining the end of the head-layer contact. The vertex of the contact angle coincides with the centre of the sphere defining the undeformed inner (or outer) surface of the layer. The angle defining the position of the maximum shear stress is to be interpreted in a similar fashion. It appears that the angular location of the top shear stress is often of the order of half the contact angle. The total load being kept the same, the contact angle increases with the layer thickness. Properly interpreted, this result is in line with the Hertzian theory, which strictly applies only for infinitely deep foundations. In fact, the Hertzian results indicate that, for a given load, the contact radius is inversely proportional to the equivalent Young's modulus to the exponent 1/3 . Now, an increase in layer thickness augments the foundation compliance, an effect similar to a decrease in the Young's modulus which, according to Hertz, suggests an increment in the contact width. Comparable conclusions are reached with the asymptotic, incompressible, flat layer forecasts of eqn (6.5.2.1), which imply the following relationship between contact radius, a , and Young's modulus, E , for an imposed load, P :

$$a = \sqrt[6]{\frac{96\ P\ R\ h^3}{\pi\ E}} \qquad (7.3.2.5)$$

which suggests that for a layer of finite thickness the contact radius is still inversely proportional to the Young's modulus, but this time the exponent becomes 1/6 .

Finally, three Figures addressing the whole stress-strain field in the elastomeric layer are included. Fig. 7.3.2.13 reports the layer deformed mesh for Case 4 and for the maximum indentation according to Fig. 7.3.2.10 , that is, δ = 0.3 mm . The end of the contact is visible. Fig. 7.3.2.14 displays the corresponding maximum shear stress pattern, indicating the presence of a maximum at the layer-cup interface, and at an angle from the vertical axis of about $\pi/4$. Fig 7.3.2.15

reproduces the contact profile. The x-coordinate represents the linear distance from the head symmetry axis along its generic meridian. An elliptic approximation starting and ending at the actual values is also included, to underline the noticeable deviation of the actual pressure profile from the Hertzian curve, a result in line with Fig. 3 of O'Carrol, Jin, Dowson, Fisher and Jobbins (1990).

The following Sections address the effects of alterations imparted to the geometrical and material parameters on the mechanical behaviour of the hip replacement with reference to the stress field in the elastomeric layer. In particular, the initial gap between head and layer loaded surface has been modified and the repercussions on the mechanical behaviour of the hip replacement have been quantified. In addition, the Poisson's ratio has been perturbed, to mimic the effects possible inaccuracies in its experimental measurement. Finally, the relevance of the angular extent of the elastomeric layer as well as of the indenter profile has been explored, to get indications about the validity of simplified modellings. The hip response to modifications of the Young's modulus has not explored in this thesis, since it is predictable, at least qualitatively, with simplified models. This point has been investigated by Dowson, Fisher, Jin, Auger, and Jobbins (1991).

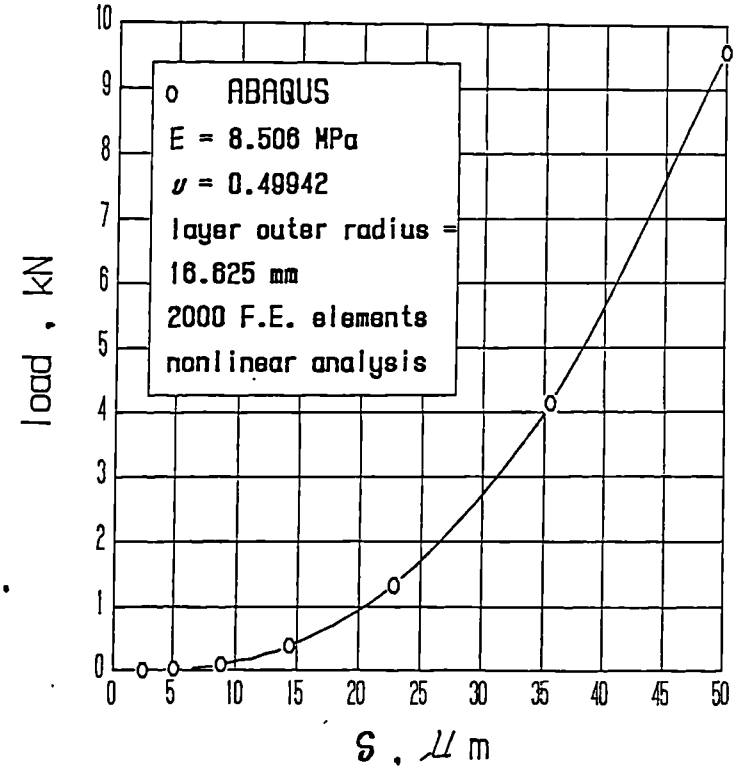

Fig 7.3.2.1 : Total load versus indentation depth for Case 1 .

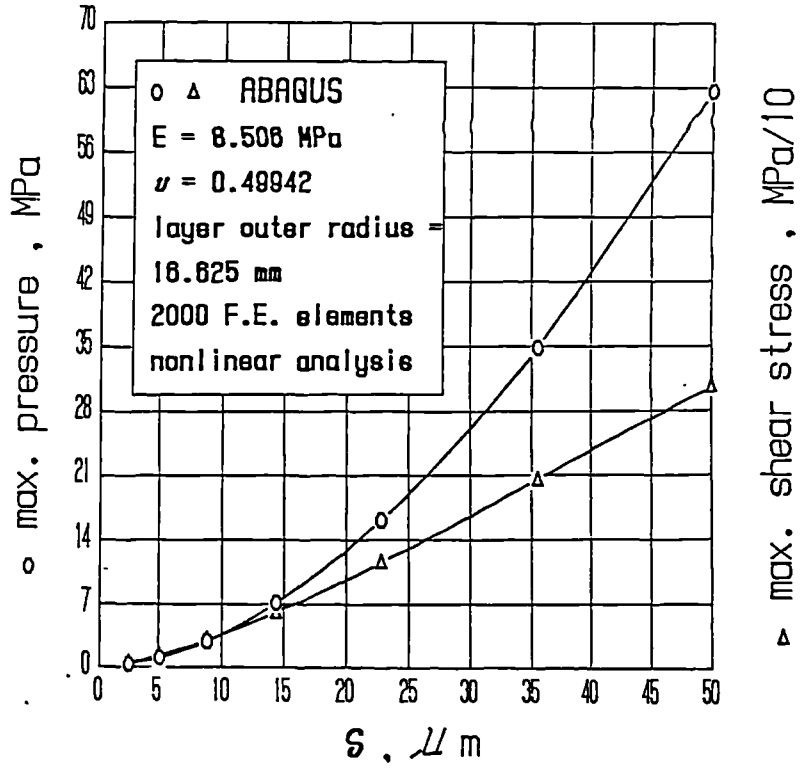

Fig 7.3.2.2 : Maximum pressure and shear stress versus indentation depth for Case 1 .

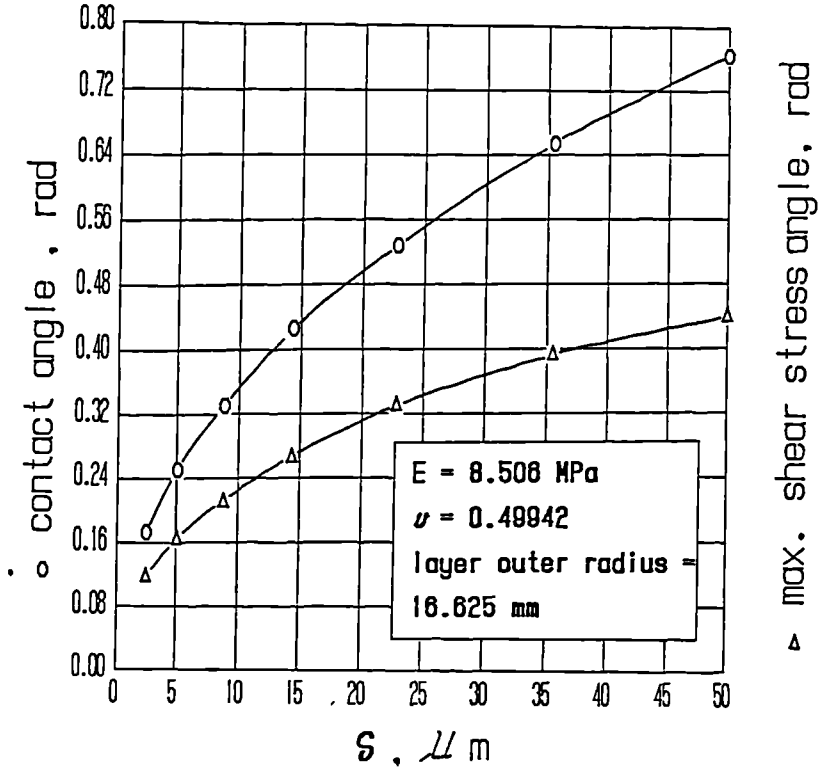

Fig 7.3.2.3 : Contact and shear stress angles versus indentation depth for Case 1 .

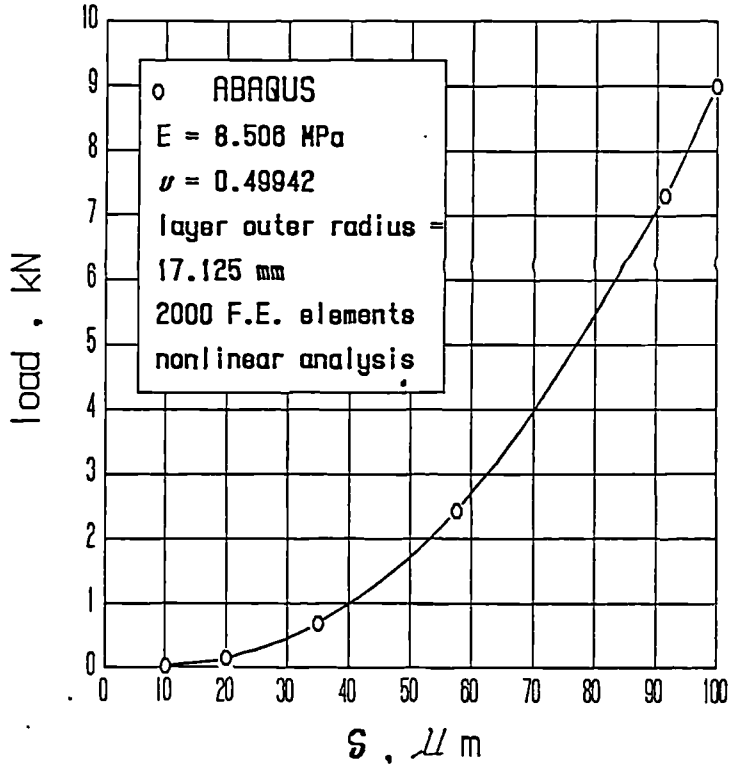

Fig 7.3.2.4 : Total load versus indentation depth for Case 2 .

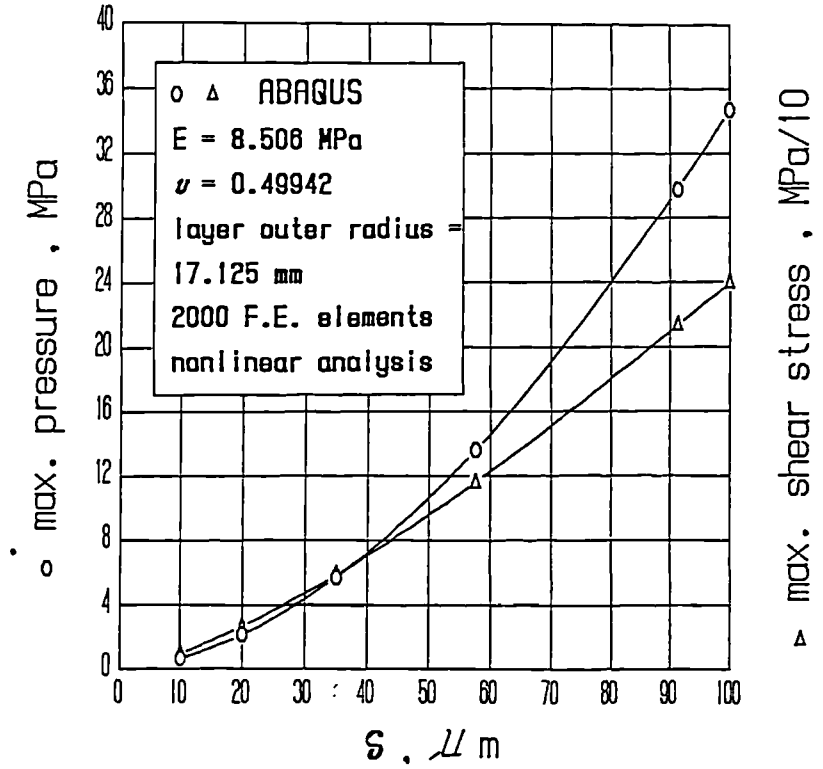

Fig 7.3.2.5 : Maximum pressure and shear stress versus indentation depth for Case 2 .

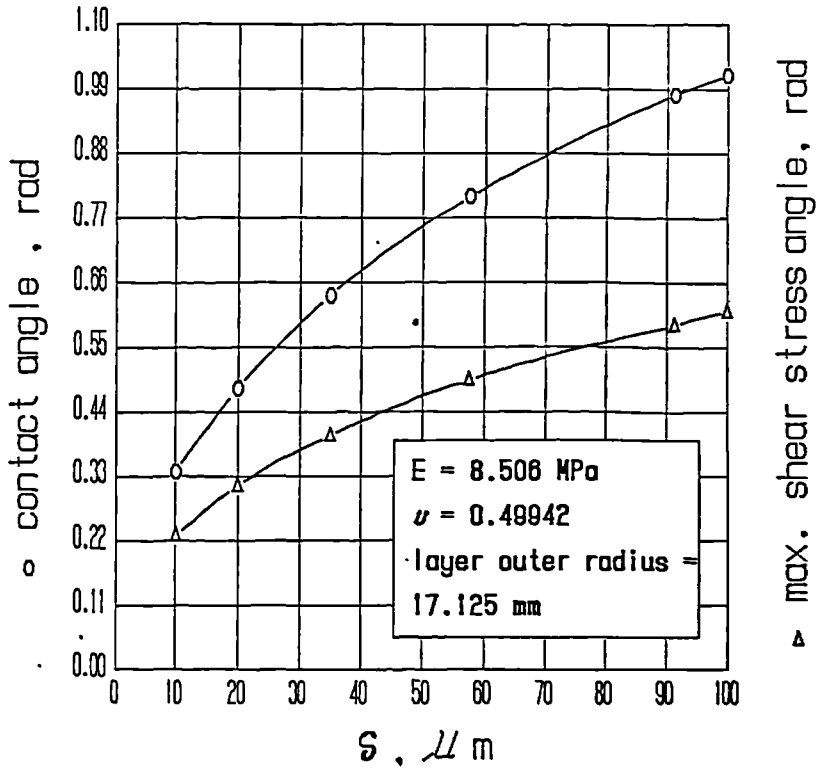

Fig 7.3.2.6 : Contact and shear stress angles versus indentation depth for Case 2 .

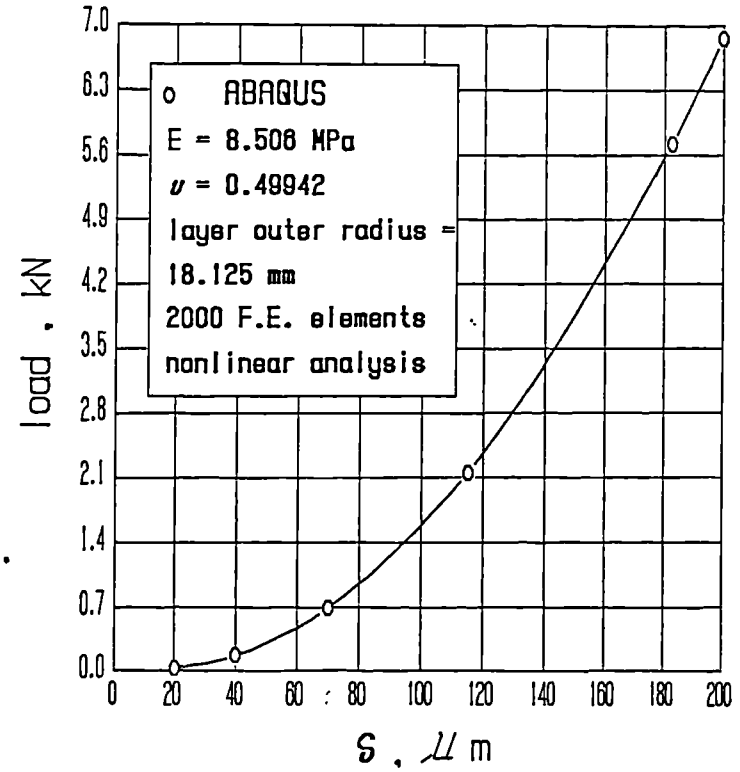

Fig 7.3.2.7 : Total load versus indentation depth for Case 3 .

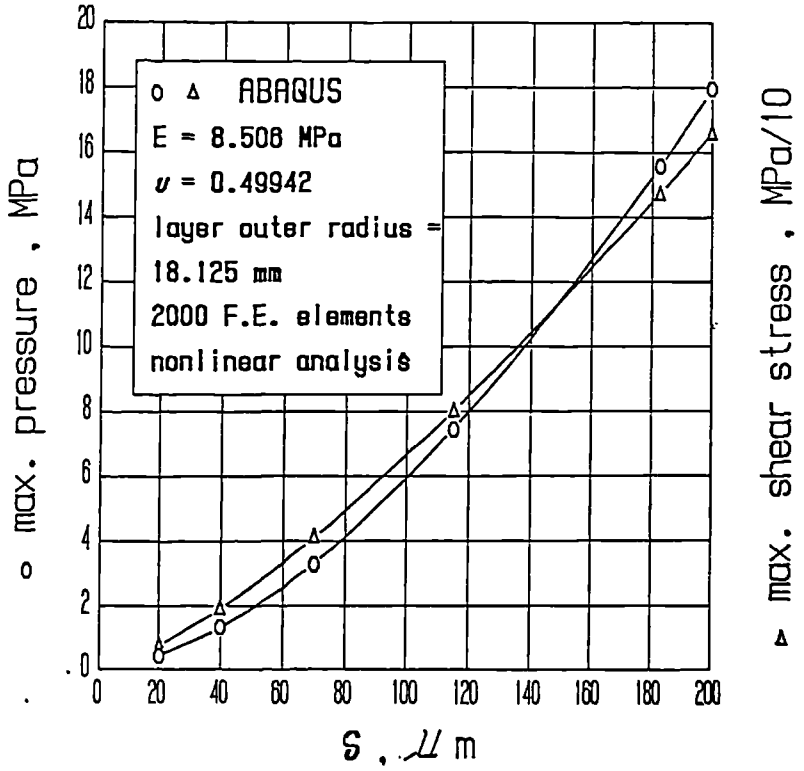

Fig 7.3.2.8 : Maximum pressure and shear stress versus indentation depth for Case 3 .

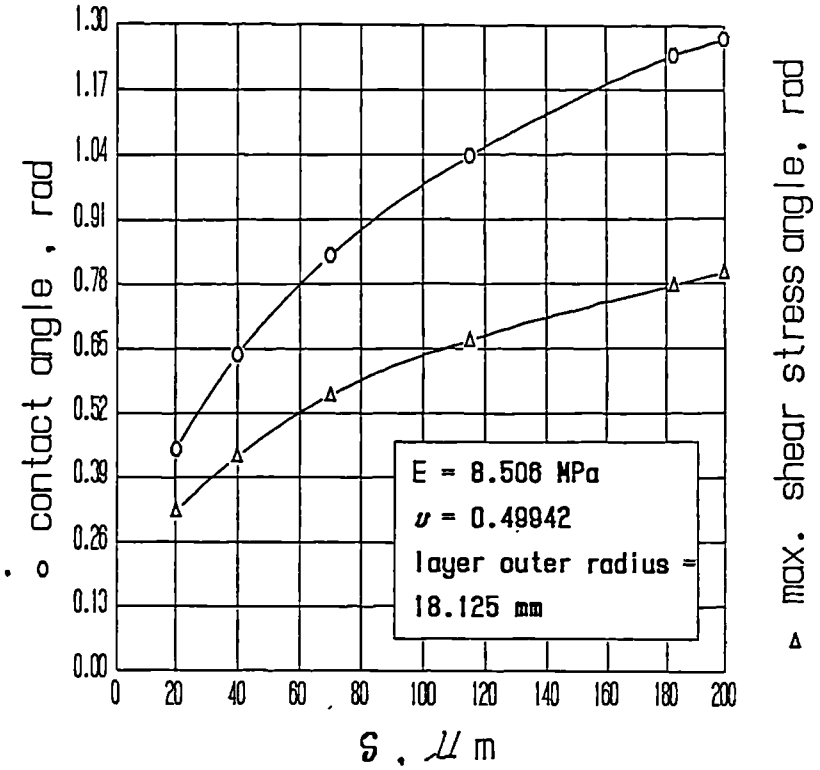

Fig 7.3.2.9 : Contact and shear stress angles versus indentation depth for Case 3 .

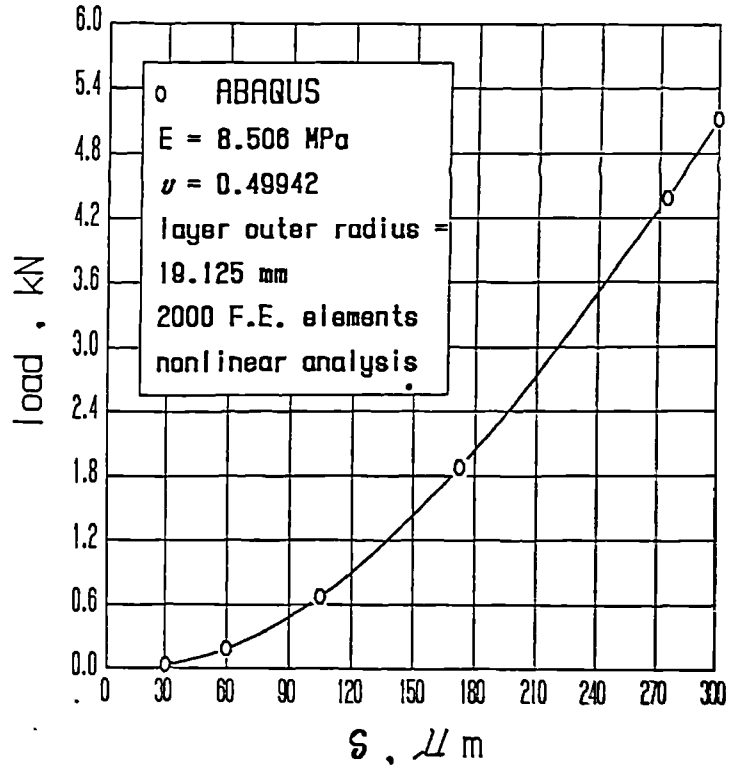

Fig 7.3.2.10 : Total load versus indentation depth for Case 4 .

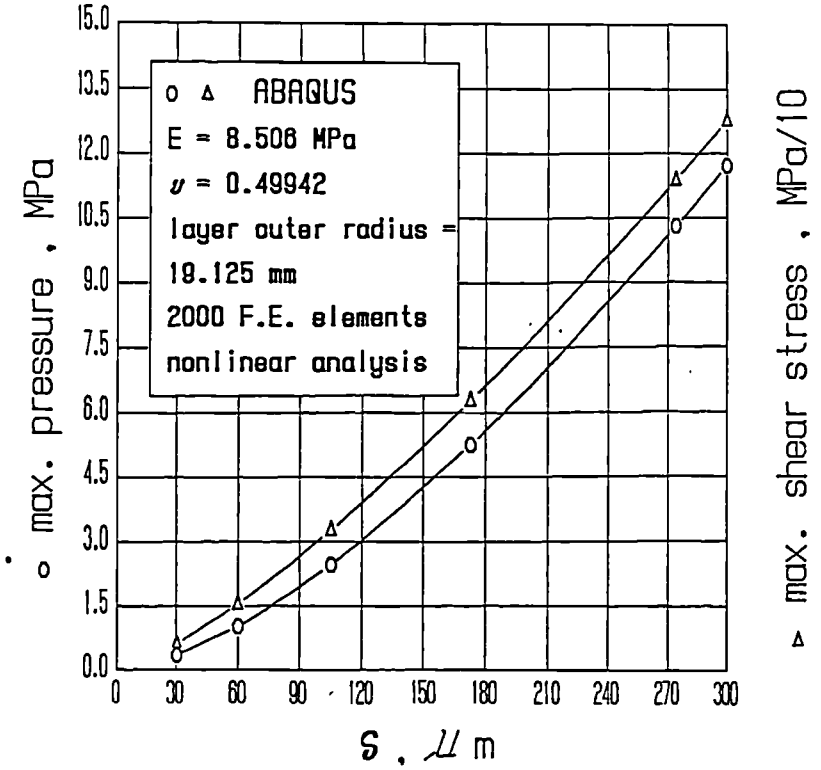

Fig 7.3.2.11 : Maximum pressure and shear stress versus indentation depth for Case 4 .

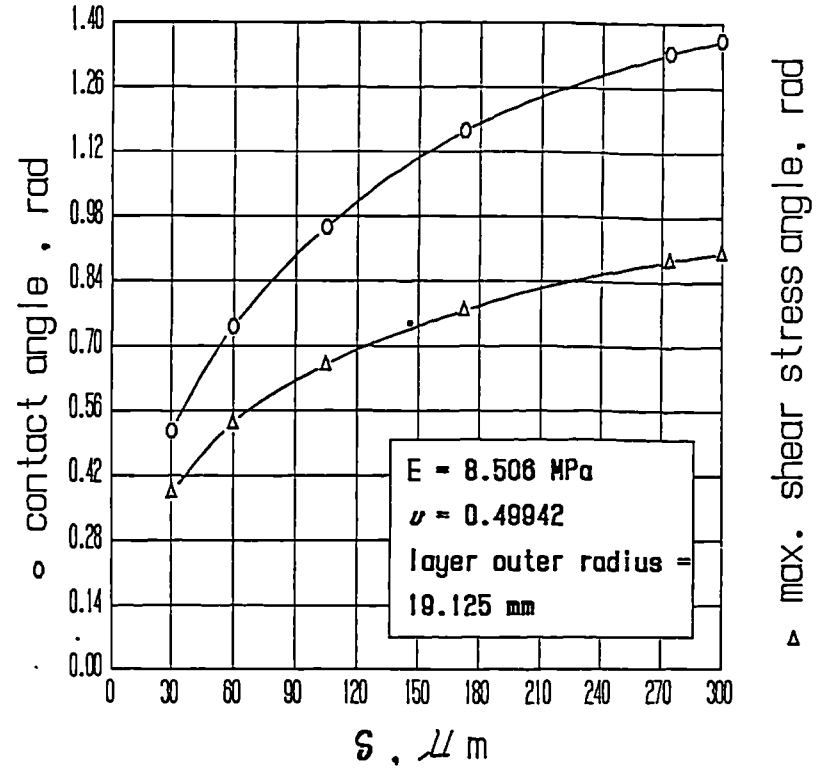

Fig 7.3.2.12 : Contact and shear stress angles versus indentation depth for Case 4 .

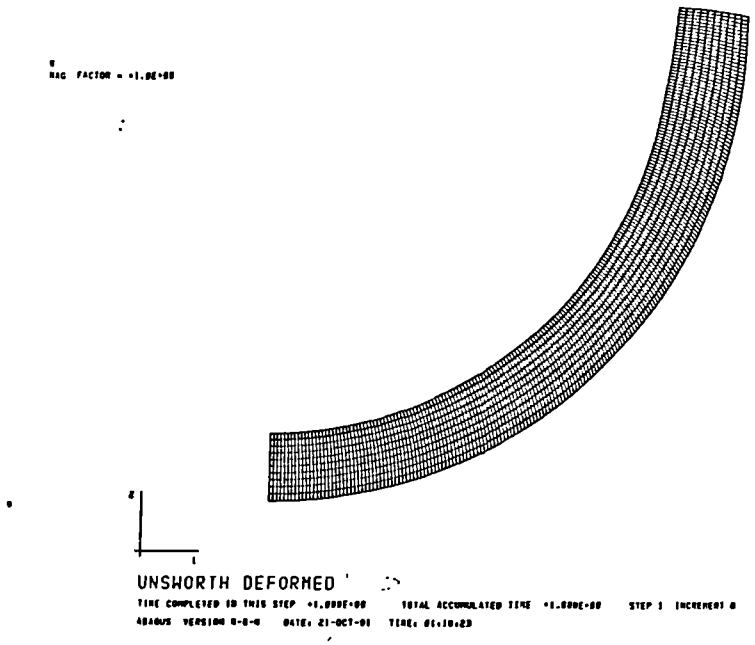

Fig 7.3.2.13 : The deformed mesh for Case 4 and for an indentation of 0.3 mm .

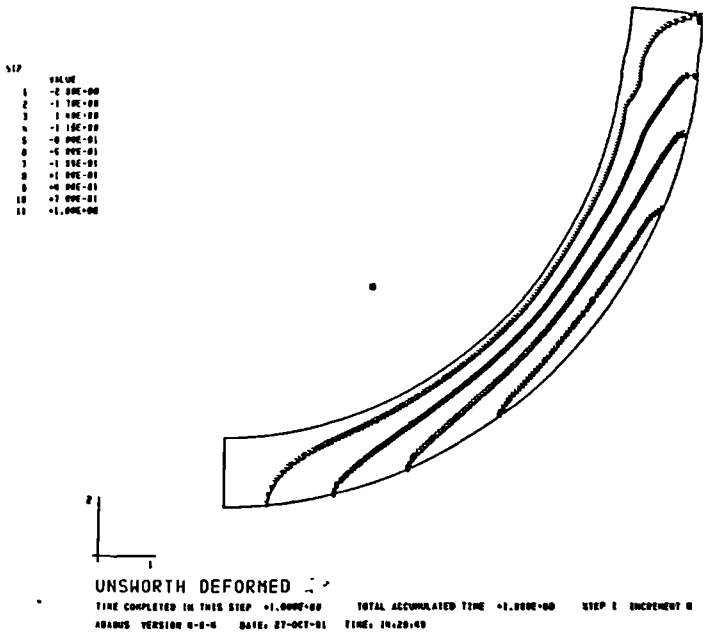

Fig 7.3.2.14 : The maximum shear stress pattern for Case 4 for δ = 0.3 mm .

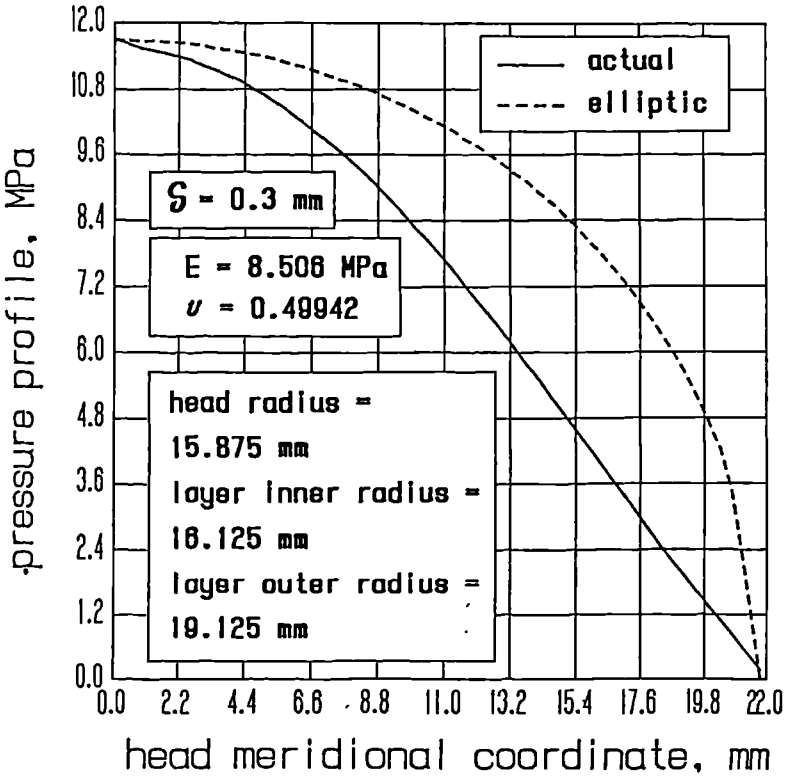

Fig 7.3.2.15: The pressure profile for Case 4, $\delta = 0.3$ mm, and an elliptic approximation.

7.3.3 Effects of the initial gap between head and layer loaded surface

The clearance between the ball and socket of the hip joint can vary enormously from joint to joint and manufacturer to manufacturer *(Unsworth (1981))*. Dowson, Fisher, Jin, Auger, and Jobbins (1991) examine in detail the dependence of the contact radius on the radial clearance for a selection of Young's moduli and for a given load and a single Poisson's ratio. An equivalent flat layer model compressed by a paraboloidal punch in linear elasticity is employed. In this thesis it was decided to investigate numerically the clearance effects on the joint load, peak pressure and shear stress, and contact extent and location of the maximum shear stress, versus the head indentation depth and for an imposed Young's modulus and Poisson's ratio, by referring to the real hip configuration. The finite element forecasts of the present study account for the curved lining consequences, for the actual punch profile, as well as for non linear elasticity effects.

If the initial gap is altered between head and layer with respect to the data reported in the TABLE of Section 7.3.2 , the equivalent radius according to the Hertzian theory (Johnson (1985), Appendix 3) changes substantially, and so does the contact compliance. More precisely, a reduction of the initial gap will result in higher loads and pressures for a prescribed head penetration depth. These predictions are quantified in Figs 7.3.3.1,2,3 which refer to total load, contact pressure plus maximum shear stress, and contact and shear stress angles, respectively. Each diagram addresses essentially Case 1 of the TABLE of Section 7.3.2 , but in addition it examines two other head geometries, characterized by increasingly conforming conjugate surfaces. More precisely, the first head configuration is that of Case 1 (when the radial head-layer clearance is 0.25 mm), while the second and third head radii considered produce decreasing radial gaps of 0.15 mm and 0.05 mm , respectively. The elastic constants are kept unchanged, that is, E = 8.506 MPa , ν = 0.49942 . The total load (Fig. 7.3.3.1), the peak pressure (Fig. 7.3.3.2) and the contact and shear stress angles (Fig. 7.3.3.3) increase dramatically for a prescribed indentation depth as the head-layer gap diminishes whereas, interestingly, the maximum shear stress is much less dependent upon to the initial clearance (Fig. 7.3.3.2). In fact, the shear stress level is connected to the

layer distortions consequent upon its lateral flow, which in turn mainly depend on the head penetration and only marginally on the Poisson's ratio, provided that ν is sufficiently close to the incompressibility figure 0.5 .

The asymptotic formulae (7.3.2.2) confirm this limited dependence of the interface peak shear stress on the initial clearance between head and layer loaded surface, even if the shear stress asymptotic, incompressible values differ from those of Fig. 7.3.3.2 , which refer to a compressible elastomer with $\nu = 0.49942$. For the three configurations described in the inset of Fig. 7.3.3.2 , and for $\delta = 50$ μm , the first asymptotic expression for the peak interface shear stress of (7.3.2.2) gives the values 4.68 , 6.06 , 10.54 MPa , respectively, which exhibit a moderate dependence upon the three very different equivalent radii 1023.94 , 1717.31 , 5184.19 mm , respectively, even if the asymptotic figures markedly disagree with the shear stress values of Fig. 7.3.3.2 .

While the radial gap does not appear to be a factor critically influencing the maximum interface shear stress, the results of Section 7.3.4 suggest not to adopt very small head-layer gaps in practical applications, since the dependence of the stress field on ν, a parameter difficult to measure accurately, becomes too high. Dowson, Fisher, Jin, Auger, and Jobbins (1991) suggest in their Table 3 a head diameter of 32 mm and an equivalent radius of 1000 $\div$ 1500 mm , which implies a radial clearance of 0.17 $\div$ 0.26 mm , a gap consistent with the TABLE of Section 7.3.2 .

The sensitivity of Cases 2 , 3 and 4 to the initial head-layer gap has not been explored in this study.

As already mentioned, Dowson, Fisher, Jin, Auger, and Jobbins (1991) examine in their Fig. 2 the effects of a change of head-layer clearance via a flat layer model. The results of Section 7.3.6 indicate that for small clearances the modelling of the hip replacement via a flat layer indented by a paraboloidal punch declines. It is noted in the above paper that the paraboloidal description for the punch becomes less accurate for high contacts. When the head-layer clearance decreases, the contact radius augments for a fixed load. As a consequence, a word of caution should be expressed on the accuracy of the curves of Fig. 2 of the above paper, at

least for small head-layer clearances.

It is finally noted that the data presented in Fig. 2 by Dowson, Fisher, Jin, Auger, and Jobbins (1991), which express the contact radius as a function of the radial clearance for a fixed load and Poisson's ratio, and for a selection of Young's moduli (top diagram) and of layer thicknesses (bottom diagram), could have been more effectively presented in a normalized fashion. Eqn (6.4.5.7) suggests that a suitable non-dimensionalized x-variable is $PR/E\ a^3$, where P is the total load, R represents the equivalent radius, E indicates the Young's modulus, and a denotes the contact radius, and that the proper y-variable is a/h , where h symbolizes the layer thickness. The computations which follow prove this point. With reference to the top diagram of Fig. 2 of the previous paper, the most left value of the bottom curve is characterized by $a \simeq 14.915$ mm and by $h = 2$ mm , so that $a/h = 7.4576$, and by a radial clearance of 0.05 mm , which implies $R = 5136$ mm . The other variables are $P = 2500$ N and $E = 100$ N/mm^2 , so that $PR/E\ a^3 \simeq 38.6966$. Again with regard to the top diagram of Fig. 2 of the previous paper, the most right value of the top curve is characterized by $a \simeq 14.915$ mm and by $h = 2$ mm , so that $a/h = 7.4576$ (the same figure as before), and by a radial clearance of 1 mm , which implies $R = 272$ mm . The other variables are $P = 2500$ N and $E = 5$ N/mm^2 , so that this time $PR/E\ a^3 \simeq 40.9871$, a figure very close to 38.6966 found in the previous computations for a considerably different configuration exhibiting the same a/h parameter. The above mismatch is imputable to inaccuracies in extracting the values from the diagram. These results confirm that the top diagram of Fig. 2 of Dowson, Fisher, Jin, Auger, and Jobbins (1991) could have been expressed in normalized variables.

Moving to the bottom diagram of Fig. 2 of the previous paper, the most left value of the top curve is characterized by $a \simeq 24.0678$ mm and by $h = 3$ mm , so that $a/h = 8.0226$, and by a radial clearance of 0.05 mm , which implies $R = 5136$ mm . The other variables are $P = 2500$ N and $E = 20$ N/mm^2 , so that $PR/E\ a^3 \simeq 46.0496$. Again with reference to the bottom diagram of Fig. 2 , the most right value of the bottom curve is characterized by $a \simeq 8.8136$ mm and by $h = 1$ mm , so that $a/h = 8.8136$ (a figure reasonably close to 8.0226 previously encountered), and by a radial clearance of 1 mm , which implies $R = 272$ mm . The other variables

are $P = 2500$ N and $E = 5$ N/mm^2 , so that $PR/E\ a^3 \simeq 49.6614$, a figure reasonably close to 46.0496 previously found for a considerably different configuration possessing a similar a/h parameter. The above mismatch is this time mainly assignable to the circumstance that the two a/h values are similar but not identical. It can be concluded that also the bottom diagram of Fig. 2 of Dowson, Fisher, Jin, Auger, and Jobbins (1991) could have been expressed in non-dimensionalized variables.

The fact that in the bottom diagram of Fig. 2 of Dowson, Fisher, Jin, Auger, and Jobbins (1991) and for low clearances the second curve from bottom exhibits a shape completely different from the adjacent curves has not been understood.

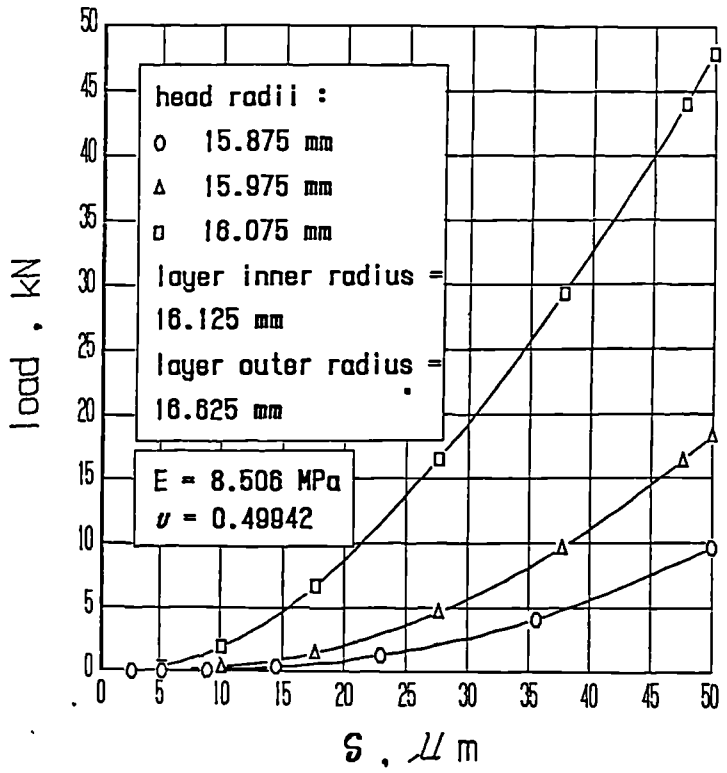

Fig 7.3.3.1 : Total load versus indentation depth for Case 1 and its variations .

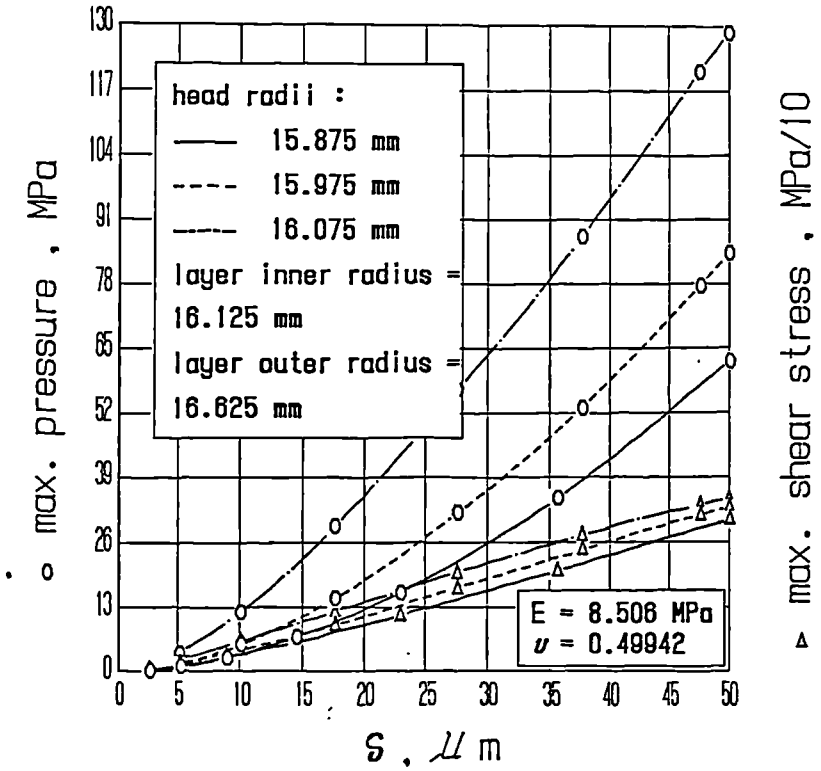

Fig 7.3.3.2 : Pressure & shear stress versus compression for Case 1 and its variations.

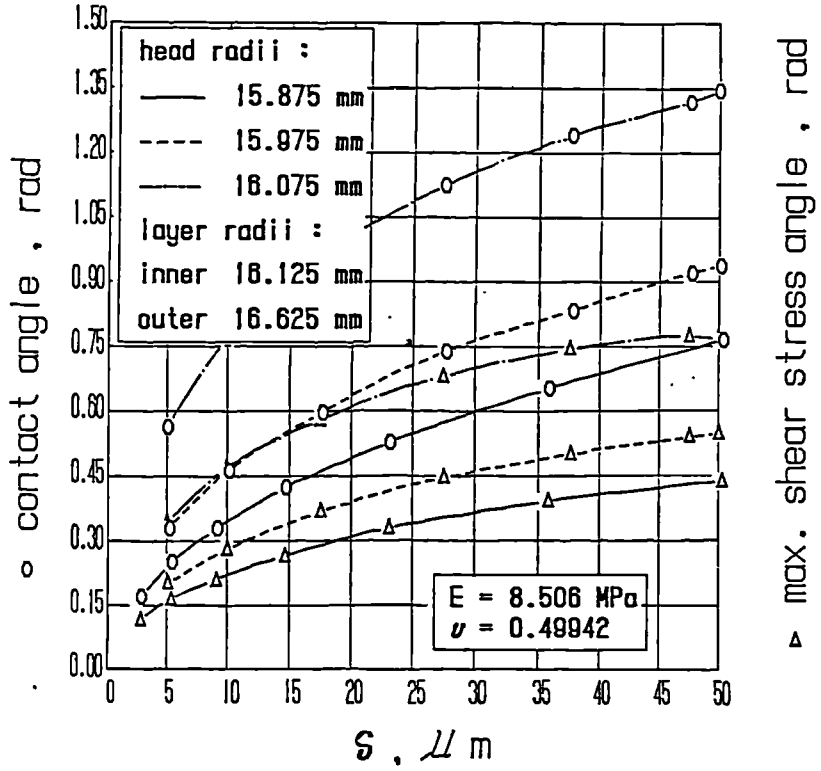

Fig 7.3.3.3 : Contact and shear angles versus compression for Case 1 and its variations.

7.3.4 Effects of perturbations of the Poisson's ratio

The whole of the results of Section 4 shows that perturbations of the Poisson's ratio influence the peak pressure especially when the contact width is high, that is, when the stress state is nearly hydrostatic (Matthewson (1981)), while such dependence is considerably lower for limited contact widths (Section 4.3.5), when the elastomer can easily flow laterally, thus preventing the build-up of nearly hydrostatic stresses. In the walking cycle the force across the joints in the lower limb drops to a very low level during the swing phase (Dowson, Fisher, Jin, Auger, and Jobbins (1991)), while the highest load levels during walking reach twice the body weight (Kilvington and Goodman (1981)) and as much as ten times during running (Paul (1976)). It is, therefore, advisable to analyze the mechanical behaviour of the hip replacement for a wide spectrum of loads.

In this numerical study the three configurations already examined in Figs 7.3.3.1,2,3 are revisited with reference to a perturbation of the Poisson's ratio. The effects of alterations of this mechanical parameter are not explored by Dowson, Fisher, Jin, Auger, and Jobbins (1991). The two figures ν = 0.49942 (experimental measurement, Section 3.3.4) and ν = 0.5 (ideal incompressibility) are here examined. Figs 7.3.4.1,2,3 refer to Case 1 of the TABLE of Section 7.3.2 (head radius = 15.875 mm) and to the two above reported Poisson's ratios, Figs 7.3.4.4,5,6 deal with the same layer geometry but with a head of radius 15.975 mm (already accounted for in Figs 7.3.3.1,2,3), whereas Figs 7.3.4.7,8,9 address a head radius of 16.075 mm . The whole of the results retrieved shows an appreciable sensitivity of the stress field to perturbations of the Poisson's ratio especially for the lowest head-layer clearances (compare Figs 7.3.4.1 , 7.3.4.4 and 7.3.4.7) and for the highest compressions, so that an accurate experimental measurement of ν becomes particularly relevant for the configurations of the TABLE of Section 7.3.2 . The sensitivity to ν of geometries characterized by small initial clearances is rationalized by observing that an imposed indentation depth produces higher contact widths and, consequently, increasingly hydrostatic stress states, as the head-layer gap diminishes. It has already been observed that a hydrostatic stress state is particularly sensitive to perturbations of the Poisson's ratio.

The incompressible finite element forecasts of Figs 7.3.4.1,2 are compared in the following to the incompressible asymptotic forecasts of eqns (6.5.2.1) and (7.3.2.2). For E = 8.506 MPa , R = 1023.94 mm , h = 0.5 mm , and δ = 25 μm (so that $\delta R/h^2$ = 102.39 , a value for which the asymptotic solution is applicable, see Section 6.6) , the asymptotic total load is 2334.75 N (a force encountered in practical situations, Kilvington and Goodman (1981)), the asymptotic peak contact pressure is 21.774 MPa , and the asymptotic maximum interface shear stress is 1.66 MPa . For δ = 50 μm ($\delta R/h^2$ = 204.79), the total load becomes 18678.02 N , the peak contact pressure is 87.10 MPa , and the maximum interface shear stress is 4.68 MPa . The agreement between incompressible asymptotic forecasts and finite element, incompressible predictions is good in terms of peak pressure (see the finite element values in Fig. 7.3.4.2), is modest in terms of interface shear stress (Fig. 7.3.4.2), and becomes poor in terms of total load (Fig. 7.3.4.1). This decline of accuracy is seemingly imputable to the curved profile of the conjugate surfaces. The peak contact pressure mainly depends upon the indentation mechanism regarding the central zone of the contact, which is accurately described by a paraboloidal surface, thus rationalizing the good results of the asymptotic, incompressible model. The peak shear stress occurs at a certain distance from the contact centre, eqn (7.3.2.5), where the paraboloidal approximation declines. Similarly, the curvature effects reduce the axial resultant of the contact pressures, that is, the total load, with respect to the flat, asymptotic, incompressible model.

It is also noted that the critical appraisal presented in Section 6.6 and concerning the experimental and analytical results of O'Carrol, Jin, Dowson, Fisher, and Jobbins (1990) shows that, at least for that configuration, the Poisson's ratio is not a critical factor (Fig. 6.6.4). The contradiction between that result and the indication of the present study with regard to the sensitivity of the mechanical behaviour of the hip replacement to perturbations of the Poisson's ratio is only apparent. In fact, Section 6.6 refers to small values of parameter $\delta R/h^2$ (< 16 , TABLE of Section 6.6) , while this time the maximum $\delta R/h^2$ value reaches 204.79 (according to the asymptotic predictions). In fact, the equivalent radius adopted by O'Carrol, Jin, Dowson, Fisher, and Jobbins (1990) is 104 mm , a value much smaller than the realistic range 1000 $\div$ 1500 mm (Dowson, Fisher, Jin, Auger, and Jobbins

(1991), their Table 3). It has been shown in Sections 4.3.5 and 6.4.7 that for very small contact radius to layer thickness ratios (say $a/h < 0.7$, Figs 6.4.7.2 and 6.4.7.4)) the peak pressure does not appreciably depend on ν. In addition, Section 6.6 indicates that for $\delta R/h^2$ up to 16 , that is, for a/h up to 8 (see eqn (6.6.1)) the Poisson's ratio is not yet a critical factor (Poisson's ratios ranging from 0.499 to 0.5 are considered in Fig. 6.6.4). Figs 6.5.2.1 and 6.5.2.4 , referring to $\nu = 0.5$ and $\nu = 0.499$, respectively (these two values of Poisson's ratio are analogous to the two figures analyzed in Fig. 7.3.4.2), show that for $\delta R/h^2 = 50$, the two normalized peak pressures are still comparable, whereas for $\delta R/h^2 = 100$ the two results differ appreciably, consistently with Fig. 7.3.4.2 . It is believed that an estimate of the transitional $\delta R/h^2$ value beyond which a perturbation of the Poisson's ratio appreciably modifies the contact pressure is 100 . As a consequence, the transitional value for a/h is 20 .

As it appears from Figs 7.3.4.2,5,8 , the peak pressure and shear stress curves follow trends similar to the total load as the radial gap diminishes, even if the variation with clearance of the shear stress is always smaller (Section 7.3.3). In addition, a new aspect appears for the maximum shear stress, namely the occurrence of a plateau at the higher head compressions and for $\nu = 0.5$, visible in Figs 7.3.4.5 and 7.3.4.8 .

Moving to the contact angle and to the maximum shear stress angle, Figs 7.3.4.3,6,9 , the dependence of the contact angle on the Poisson's ratio for an imposed penetration depth is always limited. This agrees with the findings of Dragoni and Strozzi (1988) referring to an elastomeric O-Ring seal. Conversely, the maximum shear stress angle exhibits a decreasing trend with increasing indentation, for $\nu = 0.5$, for low radial gaps and at the highest penetrations, which contrasts with its behaviour for lower penetration depths, Figs 7.3.4.6 and 7.3.4.9 , and also disagrees with the asymptotic forecasts of eqn (7.3.2.1), which suggest a maximum shear stress angle continuously increasing with δ . It was decided to examine more thoroughly this latter feature. Figs 7.3.4.10 and 7.3.4.11 report the shear stress angle of Figs 7.3.4.6 and 7.3.4.9 , as well as the maximum shear stress of Figs 7.3.4.5 and 7.3.4.8 and, in addition, they underline the presence of two local maxima for the shear stress, occurring at different angular coordinates. (Only the global maximum

was reported in Figs 7.3.4.5,8 .) The two shear stress maxima are very similar, so that the two curves are hardly distinguishable in Figs 7.3.4.10 and 7.3.4.11 . Conversely, the bifurcation of the shear stress angle curve at the higher head compressions expresses the occurrence of these two maxima at two different angular locations. For head indentations just smaller than those at which the bifurcation begins, the shear stress profile becomes very flat in the region of its maximum, that is, the shear stress assumes nearly uniform values, all close to its maximum, along an sizeable angular extent. The bifurcation phenomenon occurs only when $\nu = 0.5$, and is more appreciable for small head-layer gaps.

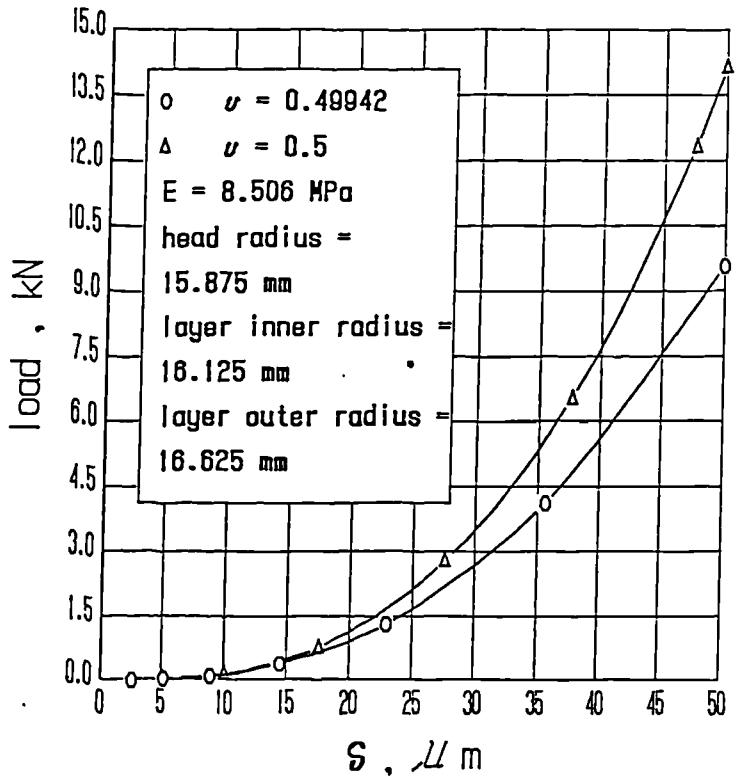

Fig 7.3.4.1 : Total load versus indentation depth for Case 1 and its variations .

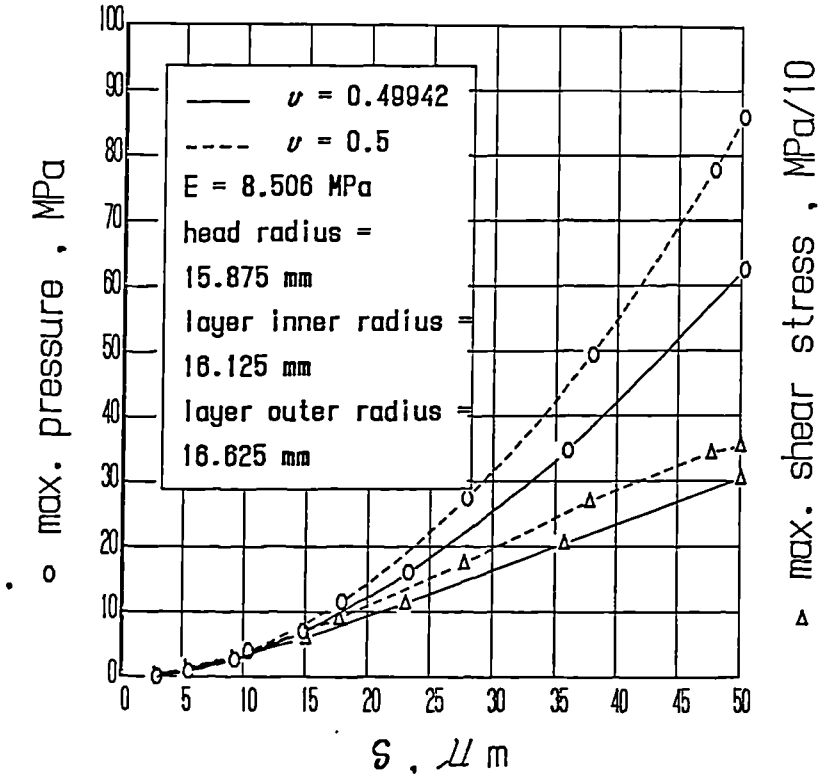

Fig 7.3.4.2 : Pressure & shear stress vs compression for Case 1 and its variations .

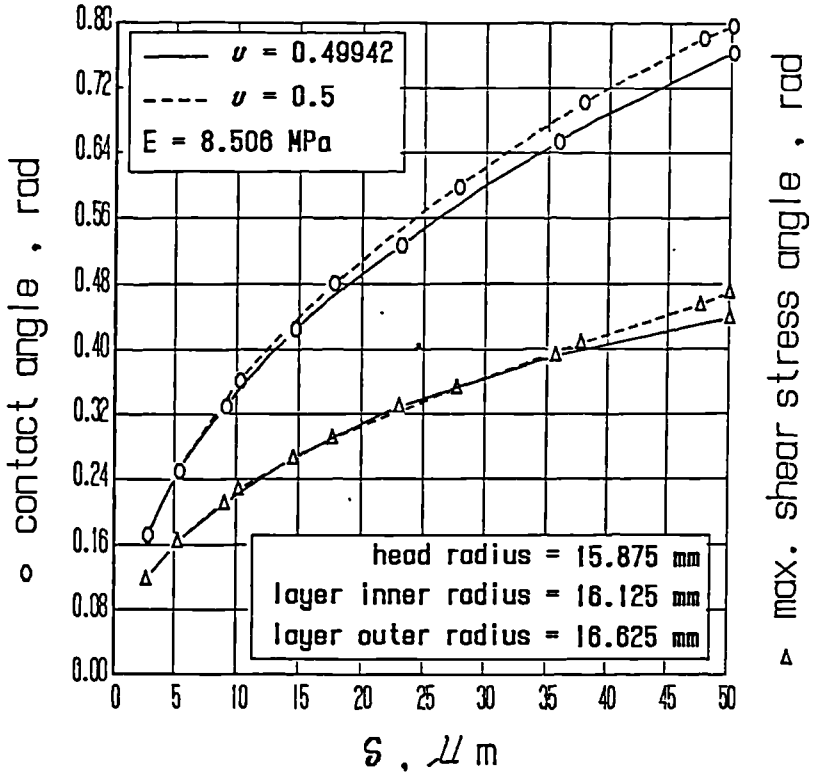

Fig 7.3.4.3 : Contact and shear angles vs compression for Case 1 and its variations.

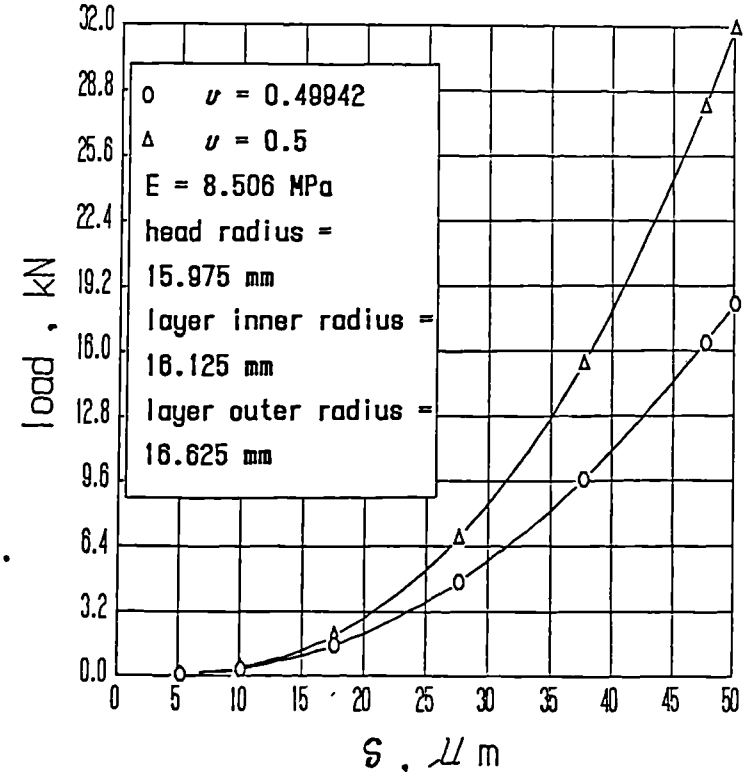

Fig 7.3.4.4 : Total load versus indentation depth for modifications of Case 1 .

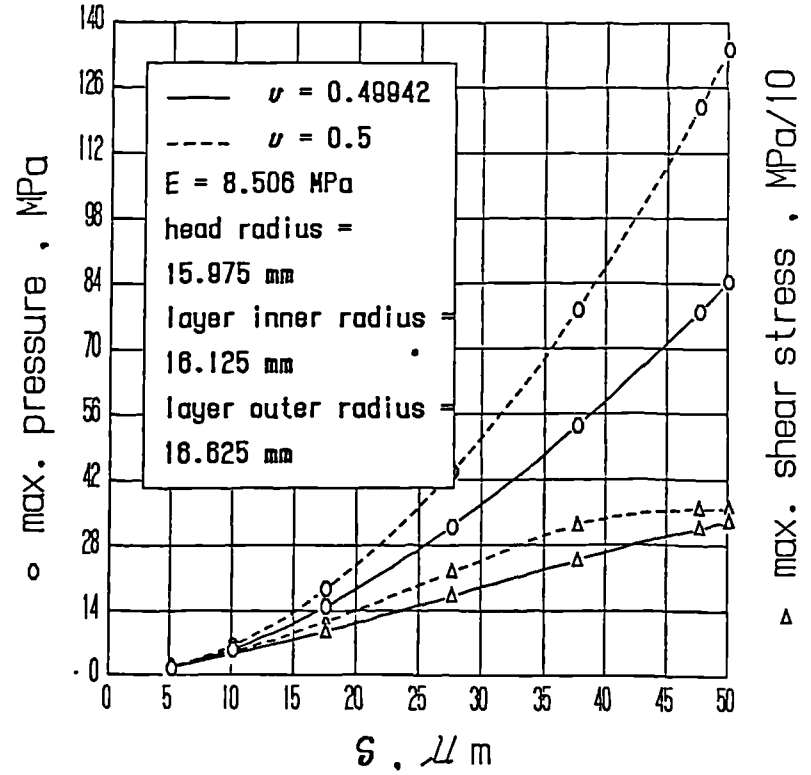

Fig 7.3.4.5 : Pressure & shear stress vs compression for modifications of Case 1 .

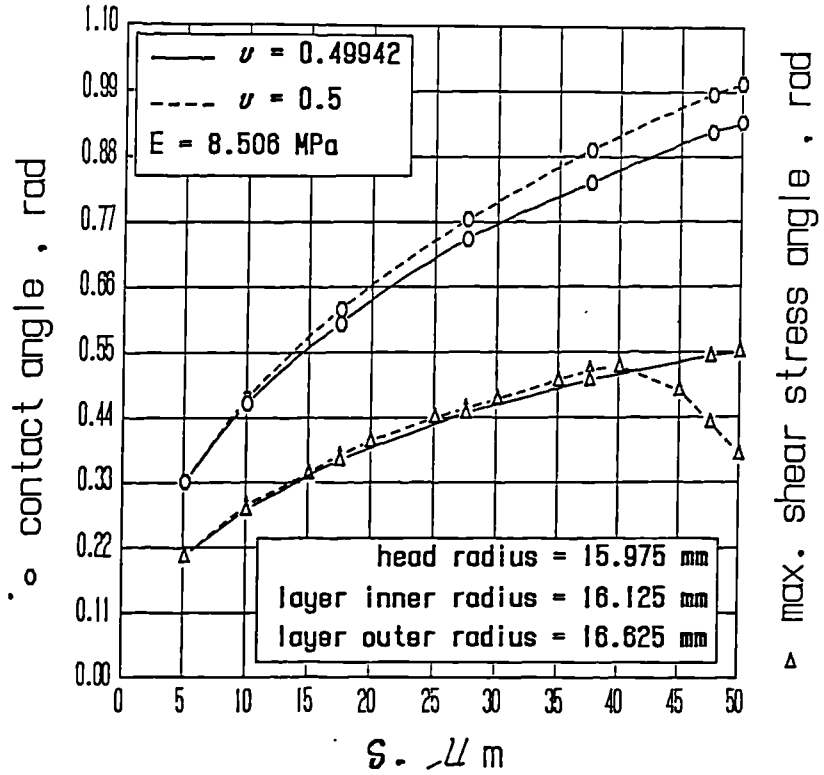

Fig 7.3.4.6 : Contact and shear angles vs compression for modifications of Case 1.

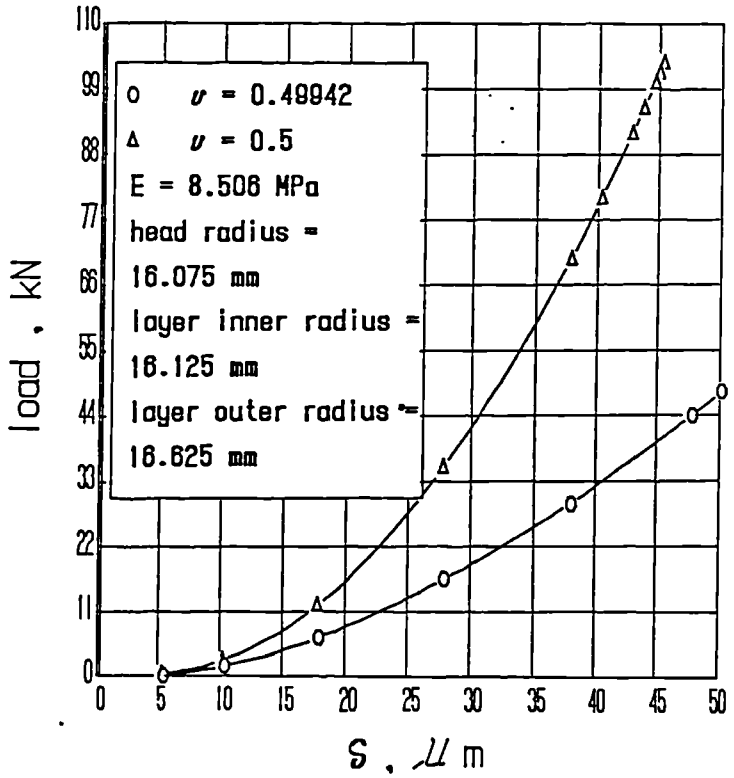

Fig 7.3.4.7 : Total load versus indentation depth for modifications of Case 1 .

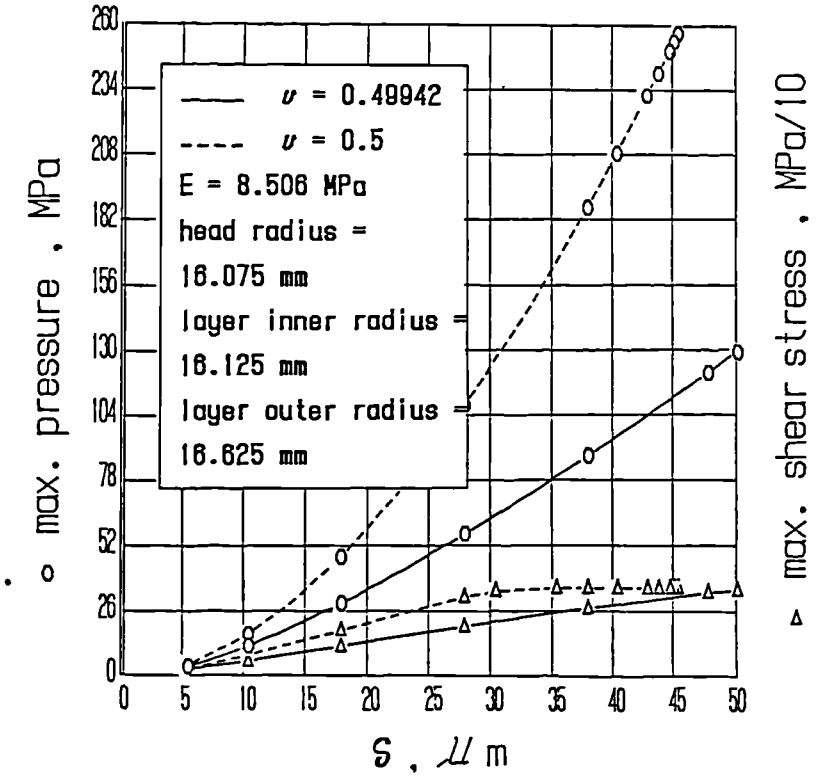

Fig 7.3.4.8 : Pressure & shear stress vs compression for modifications of Case 1 .

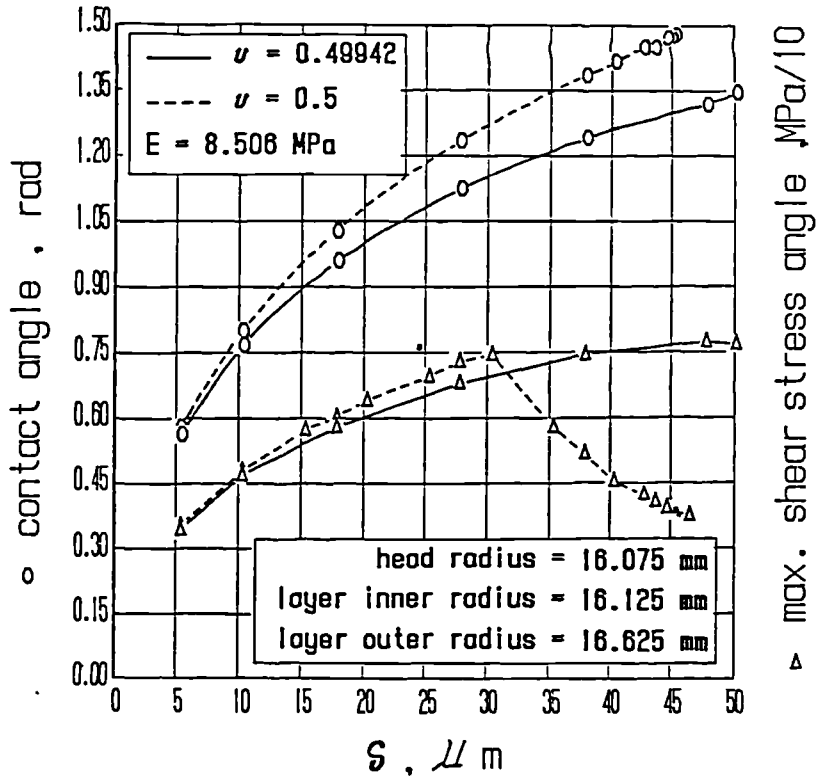

Fig 7.3.4.9 : Contact and shear angles vs compression for modifications of Case 1.

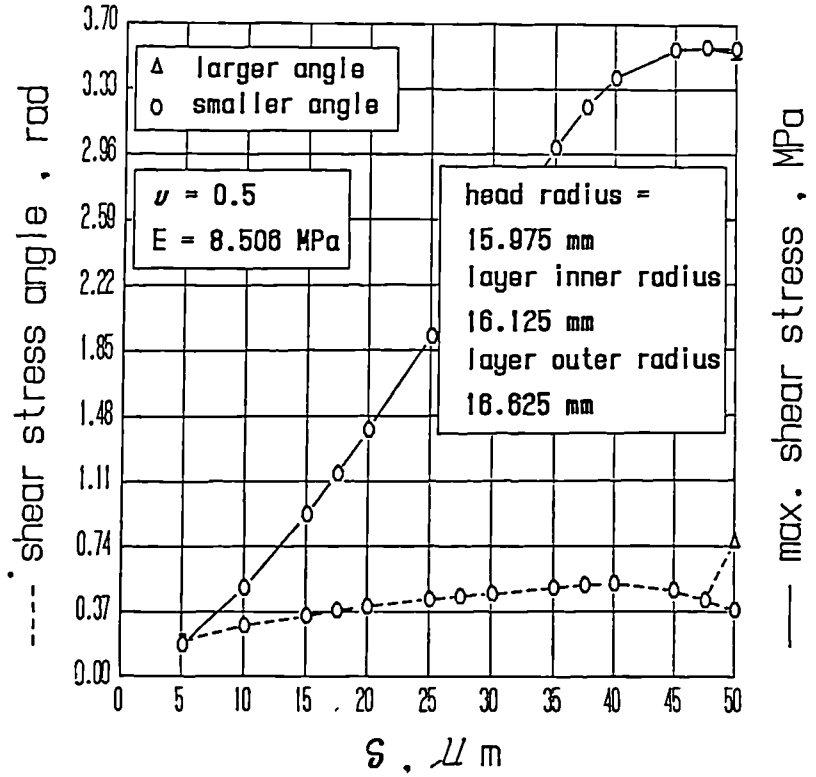

Fig 7.3.4.10 : Enlargement of shear stress and shear angle from Figs 7.3.4.5,6 .

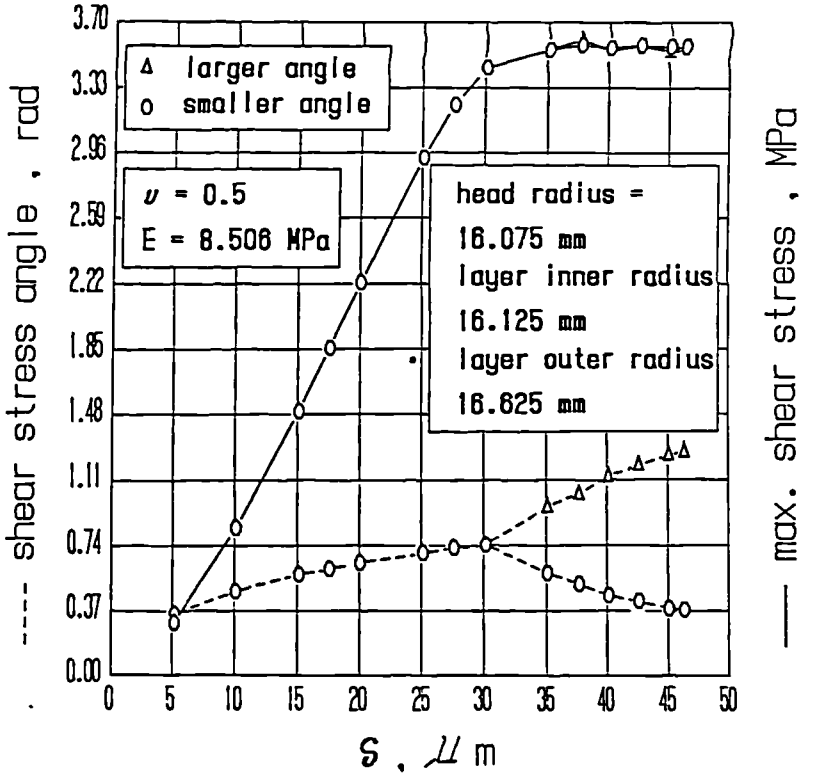

Fig 7.3.4.11 : Enlargement of shear stress and shear angle from Figs 7.3.4.8,9 .

7.3.5 Effects of the angular extent of the elastomeric layer

It appears from Fig. 7.3.2.3,6,9,12 that, the total load being kept the same, the contact end gets nearer to the layer extremity for the higher layer thicknesses (Fig. 7.3.2.12). As a consequence, the effects of the angular extent of the elastomeric layer were tested numerically only for Case 4 of Section 7.3.2 , for E = 8.506 MPa , ν = 0.49942 . Figs 7.3.5.1,2,3 present the results in terms of total load, contact pressure and shear stress, and contact and shear angles, for the geometry of a half spherical layer (see Fig. 7.1.1) and, alternatively, for the ideal configuration of a complete spherical shell. Moderate differences in terms of total load (Fig. 7.3.5.1) are perceivable only at the higher compressions, when the contact end approaches the layer end in the case of a half spherical cup, without actually encroaching upon the layer edge (Fig. 7.1.1). The two peak contact pressures referring to a spherical cup and to a half spherical cup are not distinguishable in Fig. 7.3.5.2 , while small differences appear between the two peak shear stresses. Finally, in Fig. 7.3.5.3 the two shear stress angle curves are superimposed, while the two contact angles are still distinguishable. It can be surmised that the effects of the angular extent of the elastomeric layer are smaller for the other geometries of the TABLE of Section 7.3.2 , since the corresponding contact ends are more distant from the layer extremities than in Case 4 for a given load. It can be concluded that the effects of the angular extent of the elastomeric layer are not relevant in practical situations. The relevance of this conclusion is connected to the fact that, during walking, the head oscillates within the cup (Dowson, Fisher, Jin, Auger, and Jobbins (1991)). As a consequence of the above conclusion, the contact pressure is not appreciably influenced by the relative angular position of the head with respect to the cup.

The end effects were discussed in Section 5.4.2 with reference to measurements on a plane model of the hip replacement. It was noted that these end effect may be responsible for a diminution of peak pressure for an imposed penetration depth. Fig. 7.3.5.2 confirms this trend, even if the corresponding end effects appear to be noticeably smaller than those visible in Fig. 5.4.2.12 .

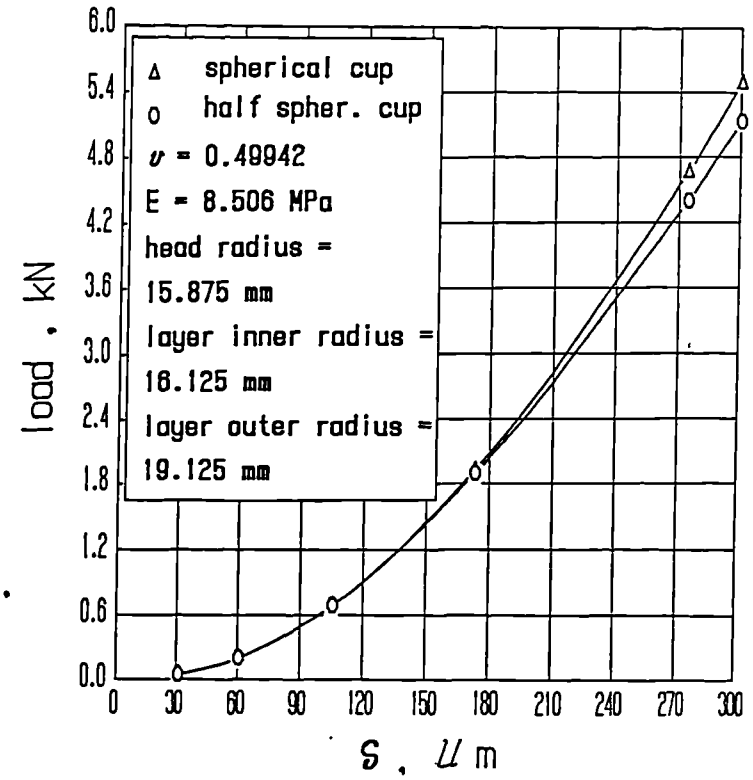

Fig 7.3.5.1 : Total load versus indentation depth for Case 1 and its modifications .

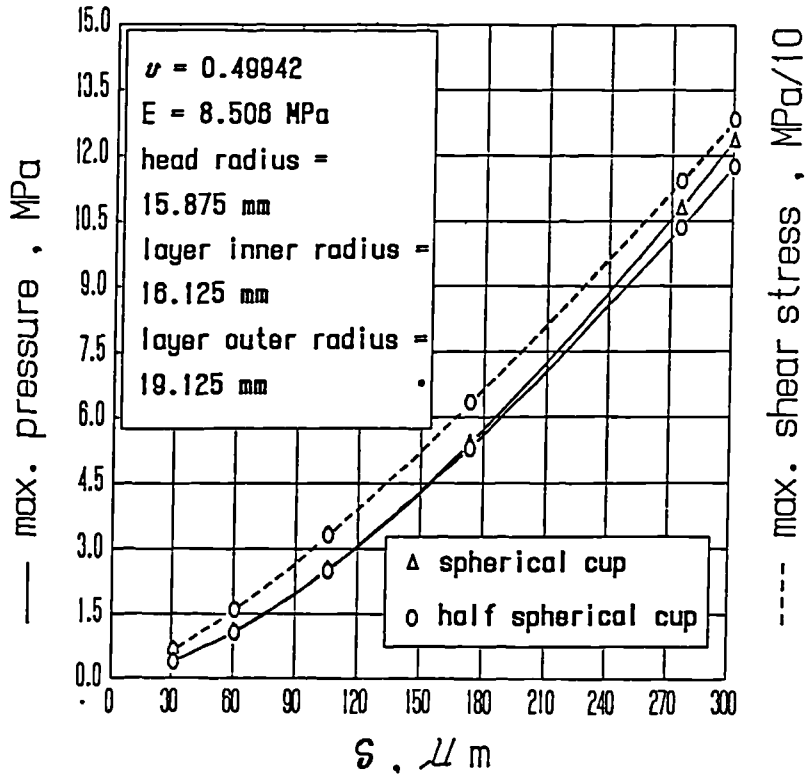

Fig 7.3.5.2 : Peak pressure and shear stress for Case 1 and its modifications .

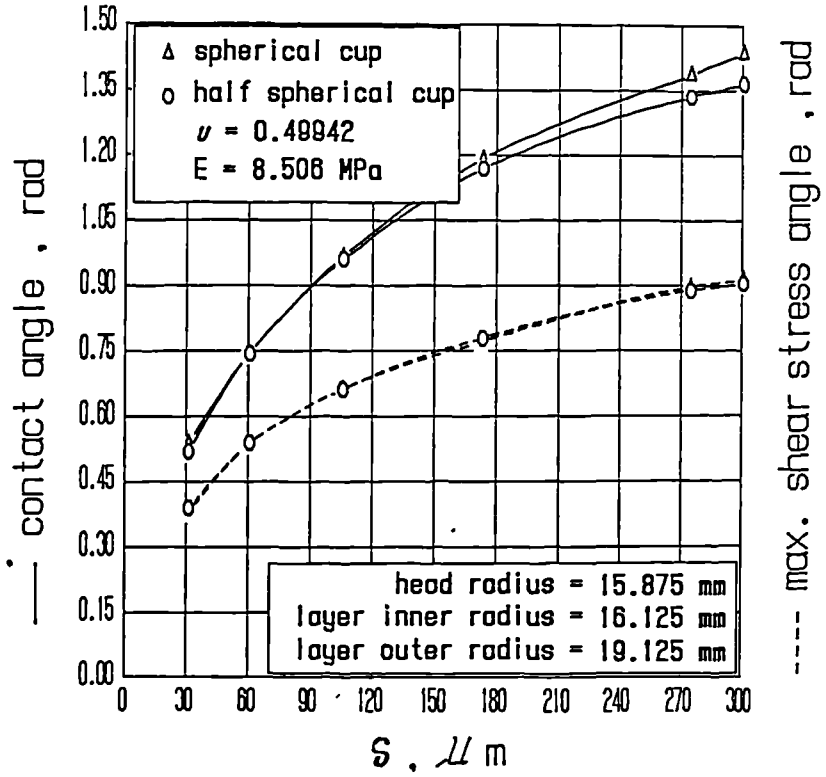

Fig 7.3.5.3 : Contact and shear stress angles for Case 1 and its modifications .

7.3.6 Effects of the indenter profile

According to the Hertzian theory, the contact between two spherical surfaces can be likened to the contact between a flat surface and a paraboloidal punch whose equivalent radius is expressed in Appendix 3 of Johnson (1985). Applied to the hip configuration, this assimilation implies that the head-layer contact may be studied by referring to a flat, deformable layer and to a rigid, paraboloidal indenter of equivalent radius. As noted by Matthewson (1981), this parabolic approximation for the head profile is sufficiently accurate only if the contact width is limited. Matthewson (1981) reports a geometric error lower than 1 percent for contact width to equivalent radius ratios below 0.2 . More precisely, Matthewson (1981) refers to the inaccuracy of a paraboloidal indenter in mimicking a spherical punch, while the other contacting surface is already initially flat. In the hip replacement geometry, instead, both contacting surfaces (that is, the head and the layer profiles) are curved, so that the error analysis of Matthewson (1981) does not strictly apply, since this time the inaccuracies made in describing the indenter profile are coupled with the errors of considering a curved layer as flat. Despite this uncertainty, the error analysis of Matthewson (1981) suggests that for the hip geometry too the geometrical deviations connected with the parabolic approximation diminish with the contact width. This decline of accuracy is underlined by Dowson, Fisher, Jin, Auger, and Jobbins (1991), who employ the flat layer model to mimic the spherical shell, and note that "At higher values the model applied to a sphere on a plane becomes less accurate."

It was decided to analyze numerically the effects of the parabolic approximation for the head profile and, inevitably superimposed, the layer curvature consequences, by referring essentially to Case 1 of the TABLE of Section 7.3.2 and, in addition, to a second case characterized by a smaller head-layer initial gap, in which the layer geometry is kept unchanged, but the head radius becomes 16.075 mm (as in Figs 7.3.4.7,8,9). In addition, E = 8.506 MPa , while ν = 0.5 , so that the results for the paraboloidal indenter could be simply extracted from Figs 6.5.2.1 and 6.5.2.7 of Chapter 6 , which refer to incompressible elastomers.

Figs 7.3.6.1,2 address the first configuration mentioned above, and report

peak pressure and contact arc (that is, the arc subtended by the contact angle (see Section 7.3.2) and related to the layer undeformed inner profile) as functions of the head indentation depth. From Fig. 7.3.4.1 it appears that the total load corresponding to the maximum penetration depth of 50 μm is about 15 kN , thus exceeding by a factor of two the maximum physically realistic load of ten times the body weight.

For compressions below 40 μm (corresponding to a realistic maximum load of 7.5 kN) the curved layer and spherical head forecasts in terms of peak contact pressure and contact arc closely agree with the predictions regarding a paraboloidal indenter compressing a flat layer. It can be concluded that for the hip geometry of Figs 7.3.6.1,2 both the curvature effect and the parabolic indenter consequences must be negligible (it is unlikely that the two effects are compensatory). The hip replacement can thus be properly mimicked by a flat layer compressed by a paraboloidal indenter of equivalent radius.

Figs 7.3.6.3 and 7.3.6.4 concern the second geometry mentioned above, characterized by a smaller initial head-layer gap. From Fig. 7.3.4.7 it appears that a total load of 7 kN (that is, ten times the body weight) requires an indentation of about 15 μm for $\nu = 0$. The penetration referring to a flat layer compressed by a paraboloidal head, as extracted from Fig. 6.5.2.1 , covers a range up to about 10 μm (convergence problems preclude the analysis of higher compressions), so that a complete comparison between real and idealized geometries is not possible. Despite this shortcoming, Figs 7.3.6.3,4 show the beginning of a certain deviation between the two models, which would have seemingly increased for indentations in the region of 15 μm . In conclusion, from Figs 7.3.6.3,4 it appears that the actual peak pressures and contact widths for a given indentation depth become higher than their flat analogues (where the punch curvature has been computed according to the Hertzian theory), especially at the highest indentation depths.

A disagreement somewhat similar in absolute value but opposite in sign was signalled by Goodman and Keer (1965), who examined the comparable problem of a deformable spherical cavity in an infinite medium, compressed by a deformable sphere. Contrary to the forecasts of Figs 7.3.6.3,4 , for an imposed indentation depth they found, with the spherical cavity theory, higher total loads and contact

widths than with the Hertzian approach. A possible explanation of this contradiction lies in the fact that in the present study the layer thickness is finite and the indenter is rigid, whereas in Goodman and Keer (1965) the spherical cavity is made in an infinite medium and the indenter is deformable. Another observation is that the actual pressure profile is no longer elliptical (see Fig. 7.3.2.15), so that the circumstance that, for a given penetration, the actual peak pressure is lower that its Hertzian counterpart at a first sight does not necessarily imply that a similar relationship holds for the total load. Anyway, it must be observed that the actual and Hertzian contact widths are in any case similar (see Fig. 7.3.6.4), while the shape of the real pressure profile (see Fig. 7.3.2.15) suggests that a lower peak pressure necessarily implies a smaller total load. In conclusion, despite the fact that Goodman and Keer (1965) compare actual and Hertzian total loads while in the present study real and Hertzian peak pressures are confronted (so that a direct comparison between the two analyses is not possible), these two studies show contradictory trends.

It can be however concluded that in the case of small initial head-layer clearances the simplified model of a flat layer compressed by a paraboloidal indenter does not mimic thoroughly the real geometry. The numerical results retrieved do not clarify whether the above deviation is mainly imputable to curvature effects or to indenter profile approximations, but the corresponding plane strain analysis of Section 5.5 indicates that the curvature effects should be much smaller than the parabolic indenter approximations. In addition, the idealized model holds better when the initial head-layer gap is larger, and this is seemingly ascribable to the fact that in this case the contact width is smaller for a prescribed load.

Curvature and indenter profile effects have already been studied in Section 5.3.4 for the plane strain counterpart of the spherical layer indented by a sphere. In that case too it was found that the parabolic approximation declines when the contact width becomes too large. In particular, from Fig. 5.3.4.8 it emerges that the real and idealized geometries supply similar results for indentations up to 0.3 mm , which implies an angular semicontact width in the region of 1 rad (see Fig. 5.3.4.9). Similarly, for the axisymmetric configuration of Figs 7.3.6.3,4 , the real and idealized geometries produce diverging peak pressures for indentations beyond 7 μm

(see Fig. 7.3.6.3), when the contact arc is about 11 mm (see Fig. 7.3.6.4), which corresponds to a contact angle of 0.7 rad , a figure in reasonable agreement with the plane strain indications.

Dowson, Fisher, Jin, Auger, and Jobbins (1991) examine in their Fig. 2 the effects of a change of head-layer clearance via a flat layer model. The results of this Section indicate that for small clearances the modelling of the hip replacement via a flat layer indented by a paraboloidal punch declines. As a consequence, a word of caution should be expressed on the accuracy of the curves of Fig. 2 of the above paper, for small head-layer clearances.

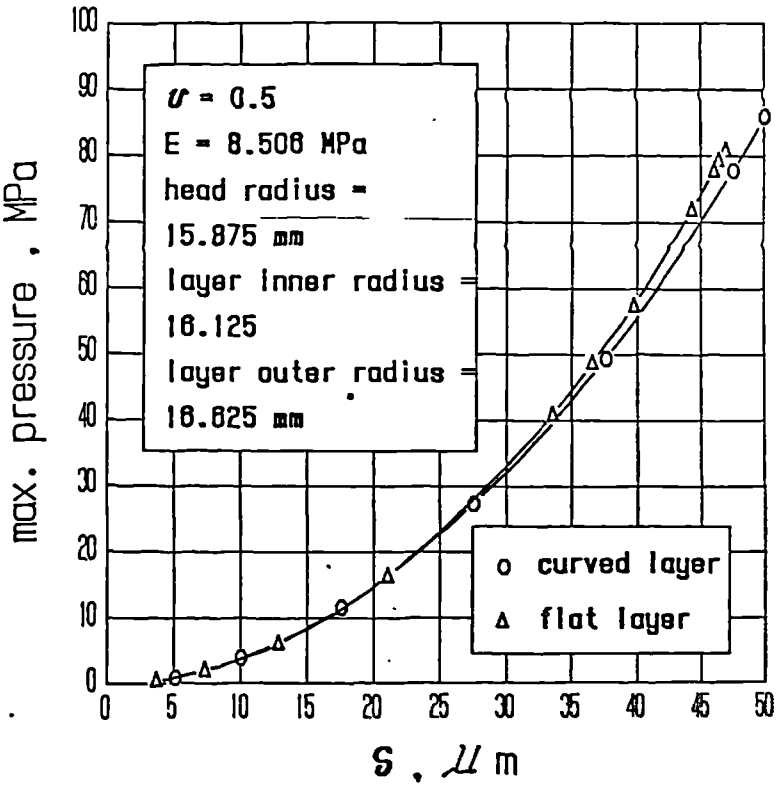

Fig 7.3.6.1 : Peak pressure versus indentation depth for Case 1 and its modification.

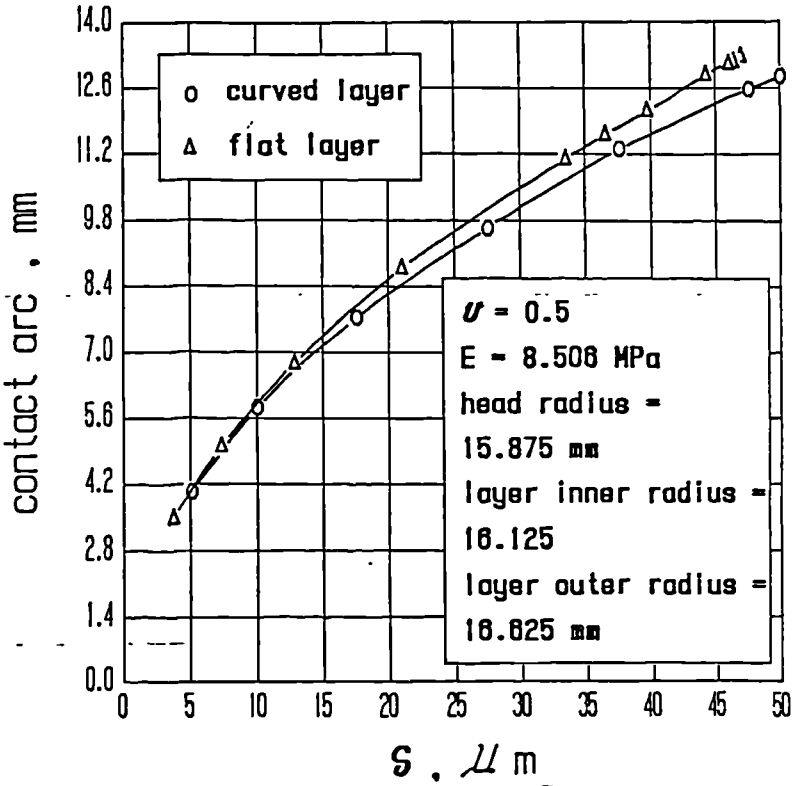

Fig 7.3.6.2 : Contact arc for Case 1 and its modification .

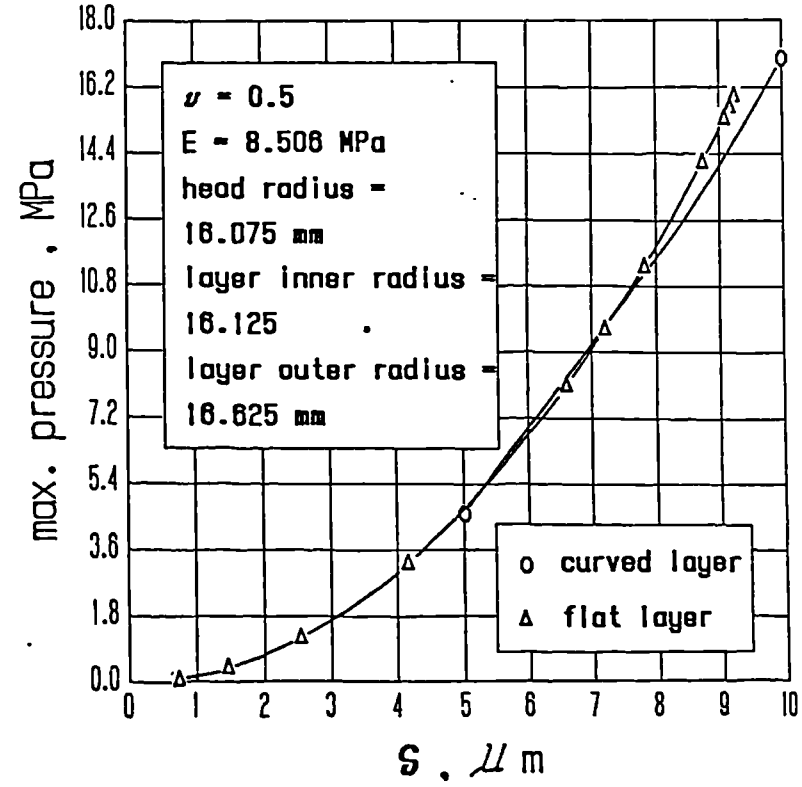

Fig 7.3.6.3 : Peak pressure versus indentation depth for Case 1 and its modification.

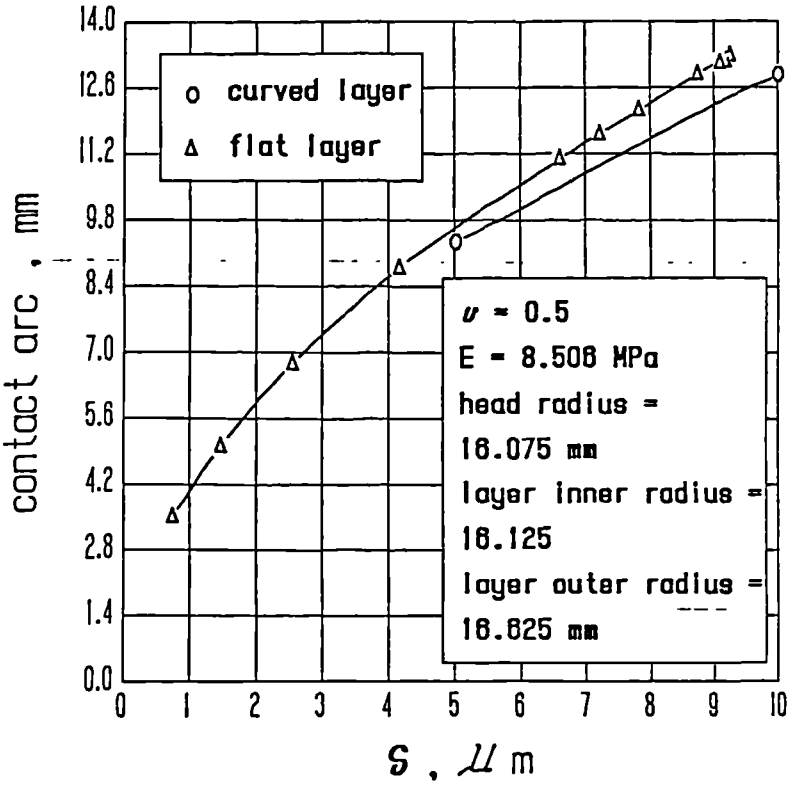

Fig 7.3.6.4 : Contact arc for Case 1and its modification .

7.3.7 Considerations about the selection of the layer thickness

A mechanical optimization of the hip replacement, and in particular of its elastomeric layer, would require a detailed knowledge of the mechanical response of the elastic lining to modifications of geometric (*e.g.* layer thickness, initial head-layer clearance) and mechanical (*e.g.* E and ν elastic constants) parameters, coupled with a lucid perspective of the aims to be pursued. Dowson, Fisher, Jin, Auger, and Jobbins (1991) investigate the effect of variations in the thickness and elastic modulus of the layer, the radial clearance and head diameter on the contact stresses and lubricating film thickness in a design analysis of cushion form bearings, by referring to the approximate modelling of a rigid sphere compressing a flat, deformable layer, and by adopting a fixed Poisson's ratio. The parameters examined are the minimum film thickness generated by elastohydrodynamic lubrication, the squeeze film thickness after one second, the maximum dry contact pressure and the elastic deformation of the surface asperities during microelastohydrodynamic lubrication.

In this thesis a realistic numerical modelling is adopted which incorporates the curvature effects and allows the relevance of perturbations of ν to be explored. Due to the implicit complexity of such optimization studies, the sensitivity analysis performed in this thesis is inevitably incomplete, and confined to some parameters recognized as crucial. In particular, this Section examines the dependence of the peak contact pressure, of the maximum interface shear stress and of the contact width, upon the layer thickness, for a prescribed total load and for the actual elastic constants. This information is particularly relevant from a technical standpoint. The maximum contact pressure and contact width are fundamental parameters connected to lubrication aspects (Chapter 8), whereas the peak shear stress at the interface between layer and foundation permits predictions to be formulated on the possible occurrence of undesired debonding phenomena. The practical consequences of perturbations of the Poisson's ratio, mimicking inevitable errors in its experimental measurement or a lack of information on its actual value, are also commented in this Section. Another problem, only marginally covered in this thesis, is the possible outcome of tensile stresses in the elastomeric layer (possibly

by the contact ends), which may promote detrimental cracks. Also, microelastohydrodynamic lubrication aspects are controlled by mechanical parameters (Dowson, Fisher, Jin, Auger, and Jobbins (1991)), but this aspect is not covered here. Finally, squeeze film thickness considerations, included in the previously quoted paper, are ignored in this thesis.

The above mentioned sensitivity study is effected for a fixed load, since this imposition closely mimics the physical loading of the joint, compressed by the body weight. The reference total load was assumed as 5 kN , in the region of ten times the body weight. (This figure was chosen because it is covered by all the pertinent diagrams presented in this Chapter.) The relevant variables, extracted from the TABLE and from the Figures of Section 7.3.2 , are collected in the following TABLE (the figures reported have been rounded off) :

TABLE

reporting the peak pressure and shear stress, the contact angle and the indentation depth for the four basic cases of Section 7.3.2 and for a total load of 5 kN

	Case 1	Case 2	Case 3	Case 4
layer thickness, mm	0.5	1.	2.	3.
equivalent radius, mm	1023.94	1023.94	1023.94	1023.94
peak pressure, MPa	40.	23.	14.5	11.5
peak shear stress, MPa	23.	18.	13.5	13.
contact angle, rad	0.7	0.9	1.25	1.35
indentation depth, μm	38.	77.	170.	300.
$\delta R/h^2$	155.	78.	43.	34.

It emerges from the previous TABLE that the indentation depths are very small for all four Cases, so that the finite elasticity effects, included in the finite element package ABAQUS, should be negligible.

It appears that for a total load of 5 kN both peak pressure and maximum interface shear stress diminish as the layer thickness is increased. This decrease is particularly desirable, since wear is reduced (as a consequence of the diminished peak contact pressure, in the case of mixed lubrication regime) and, in addition, debonding phenomena are less likely to occur (in relation to the decrease of the

peak interface shear stress).

The increase in the contact width with the layer thickness is also positive. In fact this trend, coupled with the decrease in the peak pressure, implies that the dry contact pressure gradient by the contact ends diminishes as the layer thickness is augmented. More exactly, the corresponding plane strain results of Meijers (1968) indicate, at the contact ends, for $\nu \neq 0.5$ and for high (mathematically infinite) contact widths, the existence of a finite gradient which is proportional to the peak contact pressure, which is inversely proportional to the contact width, and otherwise independent of ν (see observations of Meijers (1968) at p. 377). When the head-layer contact is lubricated, the fluid pressure essentially equals the dry contact pressure over most of the contact (an assumption typical of the inverse hydrodynamic lubrication approach, Blok (1963)), whereas some modifications occur at the inlet and outlet (Blok (1963)), where the fluid pressure vanishes together with its first derivative (this latter condition is not respected by the dry contact pressure, and this fact signals the presence of a modification). In other words, an inflexion point exists at the inlet for the fluid pressure profile. According to the inverse hydrodynamic lubrication theory, the fluid film thickness where the pressure gradient vanishes (which constitutes a reference fluid film thickness) is inversely proportional to the square root of the pressure gradient at the inlet inflexion point (Prati and Strozzi (1984)) which, according to the previous observations, diminishes as the contact width augments and the peak pressure decreases. In conclusion, an increase in layer thickness favours the formation of a desired thicker fluid film thickness, which in turn reduces wear. Dowson, Fisher, Jin, Auger, and Jobbins (1991) also find that "the film thicknesses were primarily dependent on contact half-width." and that "The film thickness increased as the contact area increased."

The possible occurrence of tensile stresses, which can promote cracks in the elastomer (Medri and Strozzi (1986), Stevens (1988), Dragoni and Strozzi (1988)), is another aspect to be taken into account in selecting the optimum layer thickness. The tensile stress level was not specifically examined in this study, but it must be observed that the stress field in the vicinity of the layer symmetry axis is essentially hydrostatic (Matthewson (1981)) and compressive, so that no tensile

stresses appears in this central region. The stress field becomes more deviatoric by the contact ends, so that the presence of tensile stresses cannot be excluded there. In any case, the contact pressure declines in the vicinity of the contact ends, and so does the whole stress field. In other words, it seems unlikely that appreciable tensile stresses occur in this biomechanical application, characterized by large contact widths. This point is further discussed at the end of this Section. In any case, it is believed that this aspect should deserve more attention.

It also emerges from the previous TABLE that the decrease in contact pressure and shear stress with an increase of layer thickness becomes less noticeable for higher cortex thicknesses, so that 2 mm and 3 mm thick coatings produce comparable results. It is concluded that it is convenient to employ relatively thick layers in this biomechanical application, but that an excessive increase in stratum thickness becomes only moderately beneficial. Dowson, Fisher, Jin, Auger, and Jobbins (1991) express a similar concept when they write "However, there is little benefit to be achieved by further reduction in the elastic modulus."

Dowson, Fisher, Jin, Auger, and Jobbins (1991) report in their Table 3 a tentatively optimized hip configuration characterized by a head radius of 16 mm , a layer inner radius of 16.2602÷16.1725 (derived from the reported equivalent radius, and implying a radial clearance of 0.1725÷0.2602 mm), a layer thickness of 1÷2 mm , a Young's modulus of 20 MPa , and a contact radius of 16 mm (implying a contact angle of 0.9840÷0.9893 radians). The Poisson's ratio adopted is 0.499, but it does not seem to have been directly measured. Such suggestions substantially agree with Case 3 of the previous TABLE , where the head radius is 15.875 mm , the layer inner radius is 16.125 mm (thus implying a radial clearance of 0.25 mm), the suggested layer thickness is 2 mm , and the angular contact radius is 1.22 radians (see Fig. 7.3.2.7 , which indicates $\delta \simeq 122$ μm for a load of 2.5 kN ; Fig. 7.3.2.9 reports for $\delta = 122$ μm a contact angle of about 1.08 radians. It is here assumed that Table 3 of Dowson, Fisher, Jin, Auger, and Jobbins (1991) refers to a load of 2.5 kN , as suggested by the caption of their Fig. 2 .) Conversely, the Young's modulus related to the previous TABLE is lower than that suggested by Dowson, Fisher, Jin, Auger, and Jobbins (1991); in the present study $E = 8.506$ MPa and, in addition, $\nu \simeq 0.49942$.

The previously noted increase in fluid film thickness with contact radius suggests to adopt small initial head-layer clearances, which promote large contacts for limited loads (Section 7.3.3). Unfortunately, small clearances enhance an undesired sensitivity of the contact pressure to perturbations of the Poisson's ratio (Section 7.3.4) which is an elastic constant difficult to measure (Chapter 3). In Section 7.3.4 it was shown that the transitional $\delta R/h^2$ value beyond which a perturbation of the Poisson's ratio appreciably modifies the contact pressure is 100, and that the corresponding transitional figure for a/h is 20 . For Case 3 of the previous TABLE, which refers to a load of 5 kN , $\delta R/h^2 = 43$, so that the Poisson's ratio is not a key variable. For the optimized configuration of Table 3 of Dowson, Fisher, Jin, Auger, and Jobbins (1991) (which possibly refers to a load of 2.5 kN), $a/h = 8 \div 16$, so that in this case too the Poisson's ratio is not a salient parameter. On the other side, if the head-layer gap is smaller (compare Fig. 7.3.4.1 and 7.3.4.7), or the load is higher (*e.g.* Fig. 7.3.4.1), the mechanical response of the hip replacement is increasingly dependent upon the Poisson's ratio adopted, so that it becomes necessary to measure ν experimentally with great accuracy. In conclusion, it seems wise not to adopt too small head-layer clearances.

The effects of a variation of E have not been explored in this thesis. Dowson, Fisher, Jin, Auger, and Jobbins (1991) write "The elastic modulus of the compliant layer should be low enough to produce effective microelastohydrodynamic lubrication and flattening of asperities" and "Both the normal and shear stress distributions are primarily dependent on contact area. Reduction in elastic modulus would produce an increase in strain and an increased likelihood of fatigue failure." This last sentence has already been criticized in Section 7.3.2 , where its validity has been questioned.

It is finally observed that in different applications of elastomeric coatings, aimed at protecting aircraft surfaces from damage by impact and abrasion (Matthewson (1981)), thinner layers are preferable. In fact, in this case the cortex thickness is chosen so that, under the impact of small particles, the outcome of tensile stresses, which can promote cracks in the coating, is prevented. Contrary to the biomechanical case, a minimum thickness criterion is the optimum solution for this latter application, characterized by much smaller contact widths.

7.4 CONCLUSIONS

A finite element mechanical analysis has been performed for a hip replacement possessing an elastomeric layer. Four basic geometries have been analyzed, and the total load, peak pressure and contact width, maximum interface shear stress and its location have been diagrammatically reported versus the head indentation depth. Then, modified geometries and situations have been explored, by altering the initial head-layer gap, the Poisson's ratio, the angular extent of the elastomeric layer, and by approximating with a paraboloidal profile the spherical shape of the rigid indenter penetrating a spherical, deformable layer. The results retrieved suggest that for a given load the peak pressure and the maximum shear stress diminish as the layer thickness is increased, thus providing practically relevant indications about the selection of the optimal layer thickness. In addition, the marked sensitivity of peak contact pressure to Poisson's ratio perturbations evidences the need for an accurate experimental measurement of ν . In any case, as a consequence of the above reported sensitivity to ν, it seems wise not to adopt very small head-layer gaps in practical applications.

CHAPTER 8 . SOME ANALYTICAL TOOLS FOR THE ELASTOHYDRODYNAMIC LUBRICATION PROBLEM

8.1 INTRODUCTION

8.2 ON THE CONSTRUCTION OF CLOSED FORM SOLUTIONS FOR THE EHL PROBLEM

8.2.1 Literature review

8.2.2 The construction of exact test cases

8.2.3 On the existence of infinite pressure peaks

8.3 THE ELASTOHYDRODYNAMIC PROBLEM EXPRESSED IN TERMS OF EXTENDED VARIATIONAL FORMULATION

8.3.1 Introduction and motivation

8.3.2 Mathematical aspects

8.3.3 Numerical aspects

8.3.4 Results

8.3.5 Conclusions

8.4 ON THE OUTCOME OF SPURIOUS NUMERICAL UNDULATIONS AFFECTING THE FLUID FILM THICKNESS

8.4.1 Literature review

8.4.2 Mathematical aspects

8.4.3 Numerical schemes

8.4.4 Results

8.4.5. Conclusions

8.5 GENERAL CONCLUSIONS

8.1 INTRODUCTION

The lubrication mechanism in artificial hip joints is being currently studied both experimentally (*e.g.* Unsworth, Pearcy, White and White (1987)) and numerically (*e.g.* Dowson and Jin (1986)). Only analytical-numerical aspects are considered in this Chapter. Reference books for the lubrication problem are those of Szeri (1980) and of Gohar (1988). The results of current international research show that it is now possible to mimic numerically the elastohydrodynamic lubrication (EHL) regime activated by soft layers in the case of a) plane (unidimensional) models which account for transient micro-elastohydrodynamic (that is, the walking mechanism and the profile roughness are incorporated) lubrication (Jin (1988)) and in the case of b) two-dimensional (quasi elliptic) descriptions in stationary conditions (Yao (1990)). The two-dimensional lubricated contact in hip replacements subject to walking conditions does not seem to have been treated so far. In fact, the concomitant accumulation of formidable analytical difficulties precludes its analytical-numerical solution with reasonable computing resources. To this aim, it would be important to devise numerical solution methods which are both reliable and fast. It would also be useful to produce exact solutions against which to assess the numerical forecasts, at least for particular cases.

This Chapter addresses a limited aim : to introduce some robust analytical tools developed by the present author and restricted, for the time being, to plane situations, which are useful in the numerical solution of the EHL problem and which are reliable and/or fast. The analytical tools reported here have already been published by the present writer, and the pertinent papers are quoted in due course. Such tools do not specifically address the hip joint lubrication, but they deal with the more general field of lubricated soft contacts. The numerical experiments here presented generally refer to lubricated elastomeric seals.

Each following subsection is dedicated to a particular aspect, and it includes a brief review of the pertinent literature.

8.2 ON THE CONSTRUCTION OF CLOSED FORM SOLUTIONS FOR THE EHL PROBLEM

This Section addresses the existence of exact solutions for the EHL problem, to be used as test cases in the validation of numerical programs and in the estimate of their accuracy. It is strongly underlined that this Section does lot look for a rather ambitious, general, analytical solution to the EHL problem, but much more modestly an analytical tool is developed which permits a series of significant test cases to be produced.

8.2.1 Literature review

Papers are reviewed in the following which quote the impossibility of obtaining analytical solutions to the EHL problem and, in addition, the difficulty in constructing analytical solutions to be used as test cases in the validation of numerical programs for the EHL problem. In plane configurations, it is well known that exact solutions exist for the hydrodynamic (as opposed to elastohydrodynamic) case, provided that the rigid, lubricated profile is simple enough so that some integrations can be performed analytically (Field and Nau (1975), Strozzi (1985)). Moving to the considerably more complex EHL problem, Oh and Rohde (1977) note that "a closed form solution . . . is almost always difficult to obtain." Hamrock and Tripp (1984) write: "Hitherto several approaches to the elastohydrodynamic lubrication problem have been considered, each of which finds application in some regime of the operating parameters contained in the model equations. However, since none of the methods produce a solution (i.e., a compatible pressure distribution and film shape) in closed mathematical form, questions of convergence and stability of the various results assume considerable importance. Moreover, in arriving at an acceptable solution, it should not be overlooked that while uniqueness of solutions is generally assumed, it has never been rigorously demonstrated in the case of the particular nonlinearities presented by the elastohydrodynamic lubrication problem." More recent and mathematically advanced research based upon variational inequalities has in fact shown that at least a solution exists for the EHL problem

incorporating cavitation phenomena and Boussinesq-type foundation models. The following papers employing functional analysis concepts are pertinent : Rohde and McAllister (1975), Rohde and Oh (1975), Cimatti (1980), Kostreva (1984), Oden and Wu (1985), Cimatti (1986), Wu and Oden (1987).

Moving to the papers specifically dealing with the difficulties encountered in performing an analytical test in the EHL regime, so that the validations effected are confined to the hydrodynamic situation, Rohde and Oh (1975) assess their finite element program in the case of a rigid slider. Similarly, Oh (1984) writes : "The application to journal bearing mentioned above offered an opportunity for partial validation of the computer codes. Cases were run with the compliance matrix set to zero, and the results agreed well with those obtained by a different computer program written for analyzing rigid journal bearing." To set the compliance matrix to zero simply means to treat exclusively the hydrodynamic problem. Analogously, Ruskell (1980) develops a finite element solution to the EHL problem and writes with regard to its validation : "A rigid inclined slider bearing ($\mathcal{L} = 0$) lubricated by an isoviscous fluid was used as a test case."

From the previous literature review it emerges that closed form solutions are too difficult to achieve for technically relevant situations. The next best is therefore to develop analytical solutions of simplified situations to be used as test cases in the assessment of numerical packages. The following Section presents a systematic way of constructing such test cases.

8.2.2 The construction of exact test cases

The considerations which follow are mainly extracted from the following papers : Strozzi (1984c), Strozzi (1987a), Strozzi (1987b). The relevant equations describing the steady, unidimensional, isothermal, isoviscous, elastohydrodynamic problem are :

$$\frac{d}{d\,x}\left[\frac{h^3}{\eta}\frac{d\,p}{d\,x} - 6\,U\,h\right] = 0 \qquad (8.2.2.1)$$

$$h = L\left[p - p_c\right] \qquad (8.2.2.2)$$

$$p\,(x_i) = p_i \;\; ; \;\; p\,(x_o) = p_o \qquad (8.2.2.3)$$

where h is the fluid film thickness, p the fluid pressure, p_c the dry contact pressure, U the sliding velocity, η the fluid viscosity, p_i and p_o are the inlet and outlet pressures, and x_i and x_o are the inlet and outlet coordinates. In addition, L is a linear, positive-definite, integral operator expressing the lubricated profile compliance.

In technically significant situations, p_c , p_i and p_o are usually known, while p and h are the unknowns. They are a solution to the elastohydrodynamic problem if they satisfy the previous equations (8.2.2.1,2,3) simultaneously. Exact solutions for the EHL problem stated as above are too difficult to achieve, and therefore a different treatment is proposed in the follow-up.

By integrating twice equation (8.2.2.1) with respect to x, by imposing the boundary conditions expressed by (8.2.2.3) and by introducing the symbol :

$$I_n\,(x) = \int_{x_i}^{x} \frac{d\,y}{h^n} \qquad (8.2.2.4)$$

pressure p can be explicitly expressed as a function of h (Field and Nau (1975)) :

$$p(x) = 6\,\eta\,U\left[\, I_2(x) - \frac{I_2(x_o)}{I_3(x_o)}\, I_3(x)\,\right] + p_i\left[1 - \frac{I_3(x)}{I_3(x_o)}\right] + p_o\left[\frac{I_3(x)}{I_3(x_o)}\right]$$

(8.2.2.5)

Cases of piezoviscous lubricants can be treated by resorting to the "fictitiously isoviscous pressure" concept (Blok (1963), p. 16).

Equation (8.2.2.5) is equivalent to (8.2.2.1), provided that curve h satisfies the regularity requirements imposed by (8.2.2.1). If h were chosen to be piecewise linear, integral I_n in (8.2.2.4) could be computed exactly, and therefore an analytical expression for p could be derived. Anyway, if such p and h curves were introduced in (8.2.2.1), they would not satisfy it, since dh/dx would not exist at the nodes of the piecewise linear fluid film profile. This example clarifies that (8.2.2.1) and (8.2.2.5) are equivalent only if the film curve h employed in (8.2.2.5) is supposed to be differentiable along the whole sealing length. Also, this example shows that, if h is selected among sufficiently regular and simple curves, and if the inlet and outlet pressures are known, the corresponding fluid pressure profile p can be computed exactly.

Moreover, operator L of (8.2.2.2) , being positive-definite, is always invertible. In addition, if the foundation model is chosen to be reasonably simple, operator L may be inverted in closed form. Thus, (8.2.2.2) becomes :

$$p_c = p - L^{-1}\,h \qquad (8.2.2.6)$$

As already mentioned, once h has been chosen, p can be computed. Consequently, an exact expression for p_c can be derived from (8.2.2.6). In so doing, a dry contact pressure profile, p_c , is obtained for which the imposed curve of the fluid film thickness, h , and the derived fluid pressure, p , are exact solutions of the EHL problem, so that a complete formal solution has been achieved. The proposed procedure permits a set of analytical solutions to be obtained for foundations ranging from soft to hard contact, and therefore it produces

particularly suitable test cases.

A key point in this treatment is the fact that, if h is reasonably simple, integrals I_n in (8.2.2.5) can be computed exactly for a variety of fluid film profiles, despite the fact that the relationship between fluid pressure and film thickness of (8.2.2.5) is highly nonlinear.

If the film thickness is described in terms of a polynomial expression up to the fourth degree included, then the corresponding roots can be computed exactly, and the integrands of integrals I_n in (8.2.2.5), being proper rational functions, can be decomposed into partial fractions and integrated exactly. From the numerical solutions (*e.g.* Ruskell (1980)) it appears that a fourth degree fluid film profile can describe with reasonable accuracy many practically significant situations. If h is expressed by higher order polynomials, it is convenient to formulate $h\,(x)$ as follows :

$$h\,(x) = C\,(x - x_1)\,(x - x_2)\,(x - x_3)\,\ldots \qquad (8.2.2.7)$$

so that its coefficients are already initially expressed in terms of its roots and, consequently, $1/h^2$ and $1/h^3$ are still integrable in closed form.

A slightly different approach consists in expressing $1/h$ (and not h) via a polynomial expansion of a however high degree. As a consequence, functions $1/h^2$ and $1/h^3$ appearing in (8.2.2.5) are polynomial themselves and, therefore, they are easily integrable in closed form, where the corresponding computations can be performed with an algebraic manipulator. From (8.2.2.5) it also appears that $p\,(x)$ too is polynomial. The counterpart to this alternative approach is that the calculations contained in (8.2.2.6) may become impossibly complex ($1/h$ and not h is polynomial), unless a simple Winkler foundation model is adopted.

Considerations concerning some foundation models are presented hereinafter. Among the theoretical foundations (Kerr (1964)), the Winkler and the Pasternak models are easily invertible in closed form, as requested by (8.2.2.6). The Winkler foundation describes a local interaction between the film thickness and the pressure

variation, and therefore it is often referred to as "independent linear column model" :

$$h\,(x) = K\left[p(x) - p_c(x)\right] \tag{8.2.2.8}$$

It is appreciated that in some cases such a foundation can lead to physically unrealistic results (Strozzi (1984d)). On the other side, this foundation model generates test cases particularly suitable in assessing the physical likeliness of numerical undulations in the pressure profile (Strozzi (1987a)). In fact, since each column in the Winkler foundation behaves individually, such a model does not prevent the outcome of pervasive numerical undulations and, therefore, it is regarded as particularly suitable for assessing the regularity of the numerical fluid film profile.

The Pasternak model is the most natural generalization of (8.2.2.8), since in addition it assumes the existence of shear interactions between two subsequent columns :

$$h\,(x) = K_1 \int_{x_i}^{x_o} e^{-\kappa_2|x-y|}\left[p\,(y) - p_c\,(y)\right] dy \tag{8.2.2.9}$$

The Boussinesq-type foundation has been studied in Chapter 4, and the analytical difficulties inherent in this model transpire from the perturbation solution developed in Section 4.3.5 .

Having examined the main analytical aspects, the next task is to apply the proposed procedure to a practical case, and to develop in detail the corresponding calculations. In the following, only a linear fluid film profile and a Winkler foundation model are considered. This choice permits integrals I_n to be computed exactly, and equation (8.2.2.6) to be handled easily.

The published numerical fluid film profiles for soft contacts are of nearly uniform thickness over most of the lubricated zone. A typical nip occurs in the vicinity of the outlet, while the profile by the inlet can be complex in shape (Prati

and Strozzi (1984)). Thus, a linear fluid film profile can properly describe the central lubricated zone, while it cannot cope with the local deviations from the film thickness constancy by the leading and trailing edges.

In the case of a (rigid) linear slider (Fig. 8.2.2.1) , the pressure profile, p , is obtained from eqn (8.2.2.5), see Strozzi (1983) :

$$p(x) = \frac{6\,\eta\,U\,(x_o - x_i)}{(h_o - h_i)\,(h_i + h_o)} \left[1 - \frac{h_i}{h}\right] \left[1 - \frac{h_o}{h}\right] +$$

$$p_i \frac{1 - \left[\frac{h_o}{h}\right]^2}{1 - \left[\frac{h_o}{h_i}\right]^2} + p_o \frac{1 - \left[\frac{h_i}{h}\right]^2}{1 - \left[\frac{h_i}{h_o}\right]^2} \qquad (8.2.2.10)$$

where h_i and h_o are the inlet and outlet film thicknesses, respectively.

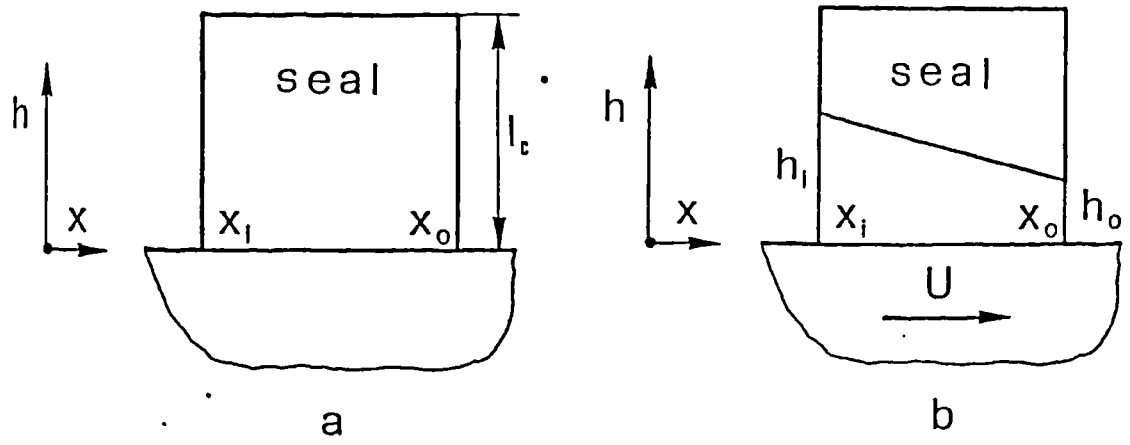

Fig. 8.2.2.1 : The meaning of symbols x_i , x_o , h_i , h_o , U , l_c .

The next aim is to compute the dry contact pressure profile. To do so, it is necessary to evaluate the Winkler coefficient K in (8.2.2.8). While K , in the limits of a linear analysis, is constant with the deformation imposed to the individual columns, it is not necessarily constant from one column to the next. In other words, K can be a function of the axial coordinate, x . If in every column the x-oriented deformation is negligible , then the link between the dry contact pressure, p_c , the column free length, l (which corresponds to a vanishing fluid pressure), and the column length in the deformed configuration, l_c (Fig. 8.2.2.1), is (see equation (4.4.2.1.13)) :

$$p_c = \frac{E\,(1 - \nu)}{(1 + \nu)(1 - 2\,\nu)} \frac{l - l_c}{l} \tag{8.2.2.11}$$

where E is the Young's modulus and ν is the Poisson's ratio of the deformable, lubricated layer. By comparing (8.2.2.8) with (8.2.2.11), the expression for K is derived :

$$K = \frac{l\,(1 + \nu)\,(1 - 2\,\nu)}{E\,(1 - \nu)} \tag{8.2.2.12}$$

and, therefore, K varies with the column free length l. Since p (and not p_c) is available from (8.2.2.10), it is necessary to modify (8.2.2.8). Since :

$$K\,p_c = l - l_c \tag{8.2.2.13}$$

equation (8.2.2.8) becomes :

$$K\,p = l - l_c + h \tag{8.2.2.14}$$

By combining (8.2.2.12) and (8.2.2.14), it follows :

$$l = \frac{l_c - h}{1 - p \dfrac{(1 + \nu)(1 - 2\nu)}{E(1 - \nu)}} \qquad (8.2.2.15)$$

where p is expressed by (8.2.2.10), which in turn depends essentially upon the choice of p_i and p_o . (The way in which p_i and p_o can be fixed is examined later on.) Having imposed l_c (which is the height of the column under dry contact, and generally known from the shape of the rigid indenter), the free column length can be computed from (8.2.2.15) as a function of p_i and p_o .

Equation (8.2.2.15) defines the shape of the undeformed lubricated profile which would produce the desired fluid pressure curve, p , in the case of a Winkler foundation model. Equation (8.2.2.15) shows that for certain combinations of E, ν and p , the denominator may vanish, in which case such a linear foundation model would become no longer physically realistic.

Then, the value of K can be computed for every x-coordinate from (8.2.2.12).

Finally, the dry contact pressure profile, p_c , is obtained from (8.2.2.8) as :

$$p_c = p - \frac{h}{K} \qquad (8.2.2.16)$$

It may be desirable to attain a vanishing dry contact pressure profile by the seal inlet and outlet. This situation occurs in hip prostheses. In this case, $l = l_c$ at the seal edges and, consequently, it follows from (8.2.2.14) :

$$p_i = \frac{h_i}{K} \quad ; \quad p_o = \frac{h_o}{K} \qquad (8.2.2.17)$$

By performing the suggested computations, the explicit expressions for p_i and p_o as functions of h_i , h_o , $l_c\,(x_i)$, $l_c\,(x_o)$, E and ν are :

$$p_i = \frac{h_i\,E\,(1-\nu)}{l_c\,(x_i)\,(1+\nu)\,(1-2\,\nu)} \quad ; \quad p_o = \frac{h_o\,E\,(1-\nu)}{l_c\,(x_o)\,(1+\nu)\,(1-2\,\nu)} \qquad (8.2.2.18)$$

In summary, the parameters to be initially imposed are h_i , h_o , x_i , x_o , η and U . From (8.2.2.10) an analytical expression for $p\,(x)$ is obtained which depends upon p_i and p_o . Having additionally imposed the values of curve l_c (which is not necessarily constant, and related to the punch shape) and of the elastic constants E and ν , and knowing already h from the previous imposition of h_i and h_o , the analytical expression of the free column length, l , is derived from (8.2.2.15) as well as the curve for K from (8.2.2.12), as functions of x-coordinate. It is noted that both l and K curves are functions of p_i and p_o . Then, the boundary fluid pressures p_i and p_o are computed from (8.2.2.18), which impose that the dry contact pressure vanishes at the contact ends. As a consequence, p , l and K are now completely known. Finally, the dry contact pressure, p_c , is analytically derived from (8.2.2.16).

Conversely, if the dry contact pressure possesses the above shape, if to the boundary pressures the above values are imposed and if the foundation model is of Winkler type where K varies as previously indicated, then the fluid film shape is linear with inlet and outlet widths h_i and h_o , respectively, and the fluid pressure possesses the form of equation (8.2.2.10). In other words, the analytical solution for the fluid pressure and fluid film thickness is known, and it can be used to assess numerical packages.

As a final remark, it might be argued that the employ of a variable Winkler coefficient K is little justified, since it does not substantially improve the limited accuracy of the Winkler model. As a matter of fact, this choice retains some of the difficulties inherent in more complex foundation models. Consequently, the numerical methods capable of handling a variable Winkler coefficient can be extended to deal with foundations of integral type.

The above approach characterized by a linear fluid film profile was employed in Strozzi (1986c) and in Strozzi (1987b) to validate a numerical program dealing with the lubrication of soft contacts. In Strozzi (1987a), instead, a polynomial expansion for $1/h$ up to the fourth degree included was adopted for a similar task. Figs 8.2.2.2,3,4 and 8.2.2.5 refer to these two situations, respectively. Fig. 8.2.2.2 shows fluid film profile, h , dry and lubricated contact pressures, p and p_c , and dry profile, l , for $h_i = 2.5$ μm , $h_o = 2.3$ μm , $x_i = 0.$, $x_o = 4.83$ mm , $E = 7.58$ N/mm^2 , $U = 127$ mm/s , $\eta = 0.43 \times 10^{-6}$ N s/mm^2 . (The Winkler model employed in this Figure presupposes vanishing stresses in the direction parallel to x-axis, so that eqn (8.2.2.11) becomes slightly different (see Strozzi (1987b)), and $\nu = 0.5$ can be imposed.) Fig. 8.2.2.3 uses similar data, but this time the elastomer becomes harder, where $E = 100$ N/mm^2 . Following the same trend, Fig. 8.2.2.4 refers to $E = 1000$ n/mm^2 . Finally, moving to a polynomial expansion for $1/h$, Fig. 8.2.2.5 presents an experimentally measured fluid film thickness taken from Field and Nau (1973) together with its analytical approximation via a fourth degree polynomial for $1/h$.

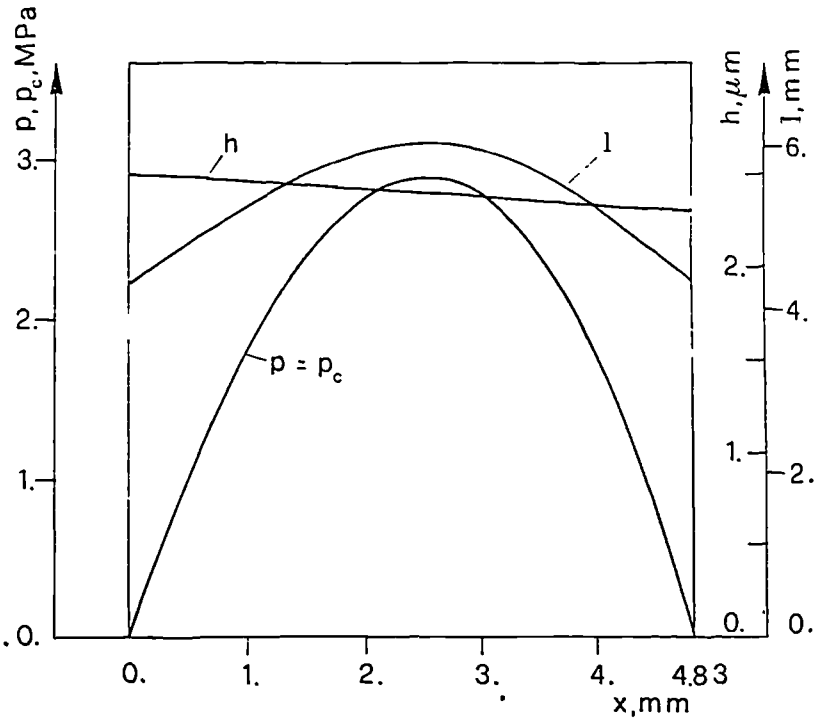

Fig. 8.2.2.2 : Exact test case for $h_i = 2.5$ μm , $h_o = 2.3$ μm , $E = 7.58$ N/mm^2 , $U = 127$ mm/s and $\eta = 0.43 \times 10^{-6}$ Ns/mm^2 .

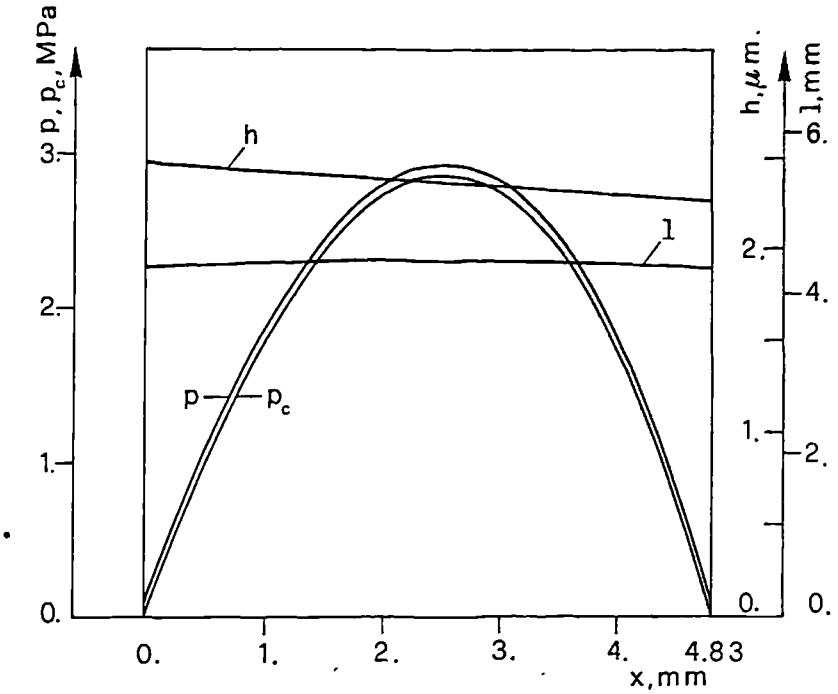

Fig. 8.2.2.3 : Exact test case for $h_i = 2.5$ μm , $h_o = 2.3$ μm , $E = 100$ N/mm^2 , $U = 127$ mm/s and $\eta = 0.43 \times 10^{-6}$ Ns/mm^2 .

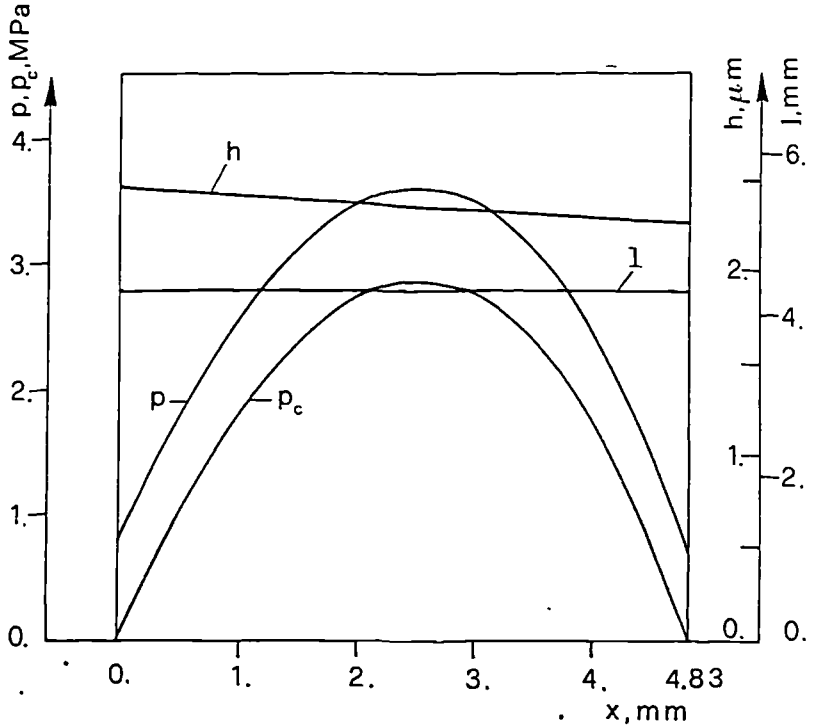

Fig. 8.2.2.4 : Exact test case for $h_i = 2.5$ μm , $h_o = 2.3$ μm , $E = 1000$ N/mm^2 , $U = 127$ mm/s and $\eta = 0.43 \times 10^{-6}$ Ns/mm^2 .

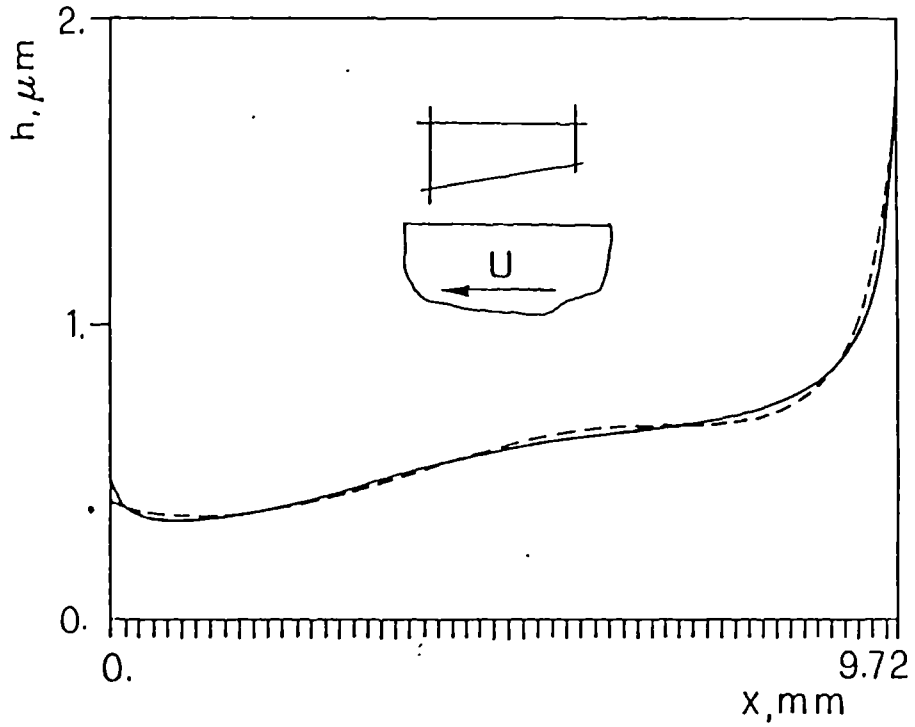

Fig. 8.2.2.5 : Experimental (--------) and analytical (- - - -) fluid film profiles.

8.2.3 On the existence of infinite pressure peaks

An open problem regarding the elastohydrodynamic lubrication regime is whether the pressure spike often encountered in the lubricated contacts (*e.g.* Blok (1963)) is mathematically finite or infinite. A conspicuous technical literature exists on this controversy, partially asserting the finiteness of the pressure spike, and partially favouring an infinite peak. The first class includes the work of Herrebrugh (1968), who concludes that no pressure spike occurs for constant viscosity. Wu (1986) investigates the continuity of the pressure derivative, and concludes that the pressure profile is smooth in the isoviscous or closely isoviscous case. Wierzcholski (1986) studies the lubricated Hertzian contact in the presence of a non Newtonian, pseudoplastic lubricant, and he notes that "the pressure peak in the pressure distribution non appears because in the . . . region . . . near the exit of the film . . . the non-Newtonian properties of the lubricant are taking into account (*sic*)". Bisset and Glander (1988) find numerically that the spike is smooth for the situations examined. They note that "a proof that the pressure derivative is continuous for general problems, not requiring near-constant viscosity, is still a very worthwhile goal." Hamrock, Pan, and Lee (1988) also support numerically the conclusion that the pressure peak "did not exist for the isoviscous solution but did exist for the viscous solution", so that they conclude that "the pressure spike is viscosity driven." In any case, the spike is found to be finite, where its amplitude depends on the fluid compressiblity. Hall (1990) favours a "mathematical weakness of the spike", even if "the pressure distribution is closely logarithmic on both sides of the pressure spike" , "although it is not a logarithmic singularity." His numerical results indicate that "no computed pressures were greater than about 2.2 p_o", where p_o denotes the peak Hertzian pressure. Hall (1990) observes that "it is now generally accepted that the isoviscous case . . . does not exhibit a spike under even the most extreme loading conditions."

The papers favouring an infinite pressure spike include Kostreva (1984b), who shows that the hydrodynamic pressure corresponding to a strictly parallel section of piezoviscous film possesses a logarithmic singularity, which can be avoided if some conditions are satisfied. Kostreva (1984b) observes that "these conditions do

occur in most practical instances. Hence only a finite segment of the log function (and not the infinite arc of the singularity) enters the solution $p(x)$ as a pressure spike."

The observations which follow demonstrate that an infinite pressure spike is consistent with the Reynolds equation for the plane, stationary, piezoviscous case, but not with the isoviscous situation. Configurations where the pressure spike is infinite are analytically developed by exploiting methods similar to those developed in Section 8.2.2 . It is, however, underlined that the results here obtained do not necessarily conflict with the above-quoted papers (*e.g.* with the above observations of Bisset and Glander (1988)). In particular, the previous studies refer to realistic situations, mainly to lubricated Hertzian contacts, while the configurations here explored are very particular, and purposely constructed to evidence peculiar aspects, which may never be encountered in practical problems.

The integrated form of Reynolds equation (Bisset and Glander (1988)) is :

$$\frac{h^3}{\eta}\frac{d\,p}{d\,x} - 6\,U\,h = Q \qquad . \tag{8.2.3.1}$$

where h is the fluid film thickness, p the fluid pressure, U the sliding velocity, η the fluid viscosity, and Q is the fluid flow. It is assumed that the pressure spike occurs, if it does, for $x = 0$, where x is the conjunction zone coordinate.

In the isoviscous case, η is constant. If h is assumed as continuous ($h \in C^0$) (a however concentrated pressure distribution cannot produce a discontinuity in the free border of a half space describing the elastic foundation of the lubricated conjunction), then $6\,U\,h$ is the same for $x = 0^+$ and $x = 0^-$. Similarly, the flow Q remains the same for $x = 0^+$ and $x = 0^-$. If a (positive) pressure spike occurs at $x = 0$, then in a sufficiently small neighbourhood of $x=0$ $dp/dx > 0$ for $x < 0$, while $dp/dx < 0$ for $x > 0$ (Fig. 8.2.3.1) . As a consequence, term $(h^3/\eta)(dp/dx)$ would change its sign when passing from $x = 0^-$ to $x = 0^+$. It is concluded that a pressure spike cannot exist in isoviscous circumstances.

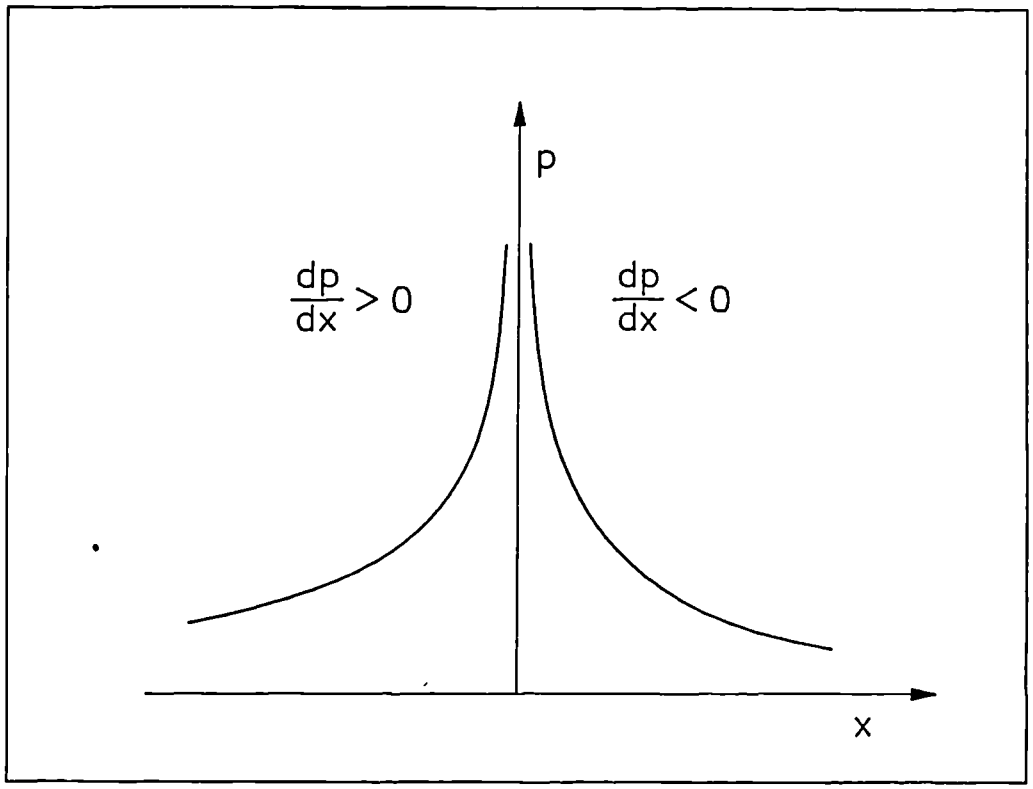

Fig. 8.2.3.1 : The pressure peak in the vicinity of $x = 0$.

Moving to the piezoviscous situation, the usual pressure-viscosity dependence equation is adopted *in this study* :

$$\eta = \eta_0 \, e^{\alpha \, p} \tag{8.2.3.2}$$

Following schemes similar to the isoviscous case, the existence of an infinite pressure peak for $x = 0$ requires that :

$$\lim|_{x \to 0^-} \quad \frac{\frac{dp}{dx}}{e^{\alpha \, p}} \quad = \quad \lim|_{x \to 0^+} \quad \frac{\frac{dp}{dx}}{e^{\alpha \, p}} \tag{8.2.3.3}$$

Since term dp/dx changes its sign when passing from $x = 0^-$ to $x = 0^+$, while term $e^{\alpha \, p}$ is always positive, equation (8.2.3.3) requires :

$$\lim|_{x \to 0^-} \frac{\frac{dp}{dx}}{e^{\alpha p}} = \lim|_{x \to 0^+} \frac{\frac{dp}{dx}}{e^{\alpha p}} = 0 \qquad (8.2.3.4)$$

and (8.2.3.1) shows that :

$$Q = -6 U h_p \qquad (8.2.3.5)$$

where h_p denotes the fluid thickness by the pressure spike.

By accounting for (8.2.3.5), eqn (8.2.3.1) becomes :

$$\frac{h^3}{\eta} \frac{d p}{d x} = 6 U (h - h_p) \qquad (8.2.3.6)$$

If $U > 0$, since physically $h > 0$, $\eta > 0$, and since the existence of an infinite pressure peak for $x = 0$ requires that in a sufficiently small neighbourhood of $x = 0$, $dp/dx > 0$ for $x < 0$ and $dp/dx < 0$ for $x > 0$, then from (8.2.3.6) it follows that $h > h_p$ for $x < 0$, and $h < h_p$ for $x > 0$, that is, the clearance is convergent by the pressure spike. This conclusion does not exclude that dh/dx may vanish for $x = 0$. These results contrast with Kostreva (1984b), who assumes a constant film thickness in the vicinity of the pressure spike.

The following observations examine if condition (8.2.3.4) is verified by the singular pressure profile found by Kostreva (1984b). His pressure curve is :

$$p(x) = p(x_c) - \frac{1}{\alpha} \ln \left[1 - \alpha \frac{d p}{d x} |_{x=x_c} (x - x_c)\right] \qquad (8.2.3.7)$$

where x_c denotes a point to the left of the pressure singularity. In addition, following again Kostreva (1984b) :

$$\frac{d\,p\,(x)}{d\,x} = \frac{1}{\frac{1}{\frac{d\,p\,(x_c)}{d\,x}} - \alpha\,(x - x_c)} \tag{8.2.3.8}$$

where the pressure singularity occurs when :

$$x = x_c + \frac{1}{\alpha \frac{d\,p}{d\,x}\,|x = x_c} \tag{8.2.3.9}$$

If the singularity has to appear for $x = 0$, then :

$$x_c = -\frac{1}{\alpha \frac{d\,p}{d\,x}\,|x = x_c} \tag{8.2.3.10}$$

which implies $p'(x) > 0$, since x_c is to the left of $x = 0$, that is, $x_c < 0$.

By employing (8.2.3.7) and (8.2.3.8), condition (8.2.3.4) becomes for the Kostreva (1984b) case :

$$\lim|_{x \to 0} \frac{\frac{dp}{dx}}{e^{\alpha p}} =$$

$$\lim|_{x \to 0} \frac{\frac{1}{\frac{1}{\frac{d\,p\,(x_c)}{d\,x}} - \alpha\,(x - x_c)}}{e^{\alpha\,p\,(x_c) - \ln\left[1 - \alpha \frac{d\,p}{d\,x}\,|_{x=x_c}\,(x - x_c)\right]}} =$$

$$\frac{\frac{d\,p(x_c)}{d\,x}}{e^{\alpha\,p\,(x_c)}} \text{ for } x = 0^- \quad \text{and} \quad -\frac{\frac{d\,p(x_c)}{d\,x}}{e^{\alpha\,p\,(x_c)}} \text{ for } x = 0^+ \tag{8.2.3.11}$$

(where conditions $\alpha > 0$, $p'(x_c) > 0$ have been exploited), which vanishes only if d $p(x_c)/dx = 0$, thus implying from (8.2.3.9) that $x - x_c = \infty$ (that is, the pressure peak occurs at an infinite distance from the reference point x_c , that is, the lubricated contact is infinitely long), or if $p(x_c) = \infty$, which presupposes two pressure singularities along the lubricated contact. It is concluded that the singular pressure profile proposed by Kostreva (1984b) does not generally satisfy condition (8.2.3.3) and, therefore, its validity is questionable. In other words, the limit value (8.2.3.11) indicates that the Kostreva fluid flow does not remain constant when passing through the $x = 0$ coordinate at which the spike occurs. It is finally observed that the Kostreva solution satisfies (8.2.3.6) if there is a discontinuity in the film thickness. Another possibility is that the singular pressure of Kostreva does not equally hold for the two sides of the pressure peak.

The following observations present singular pressure profiles which respect condition (8.3.2.4). Observations about the film thickness shape in the vicinity of the spike are also derived. If, for instance :

$$\frac{d\,p}{d\,x} = e^{\,\alpha p/2} \quad \text{for } x < 0 \quad \text{and} \quad \frac{d\,p}{d\,x} = -\,e^{\,\alpha p/2} \quad \text{for } x > 0 \qquad (8.2.3.12)$$

then :

$$\lim|_{x \to 0^-} \quad \frac{\frac{dp}{dx}}{e^{\alpha\, p}} = \frac{1}{e^{\,\alpha p/2}}$$

$$\lim|_{x \to 0^+} \quad \frac{\frac{dp}{dx}}{e^{\alpha\, p}} = -\frac{1}{e^{\,\alpha p/2}} \qquad (8.2.3.13)$$

which both vanish as $p \to \infty$. As a consequence, the singular pressure profile (8.2.3.12) satisfies condition (8.2.3.4).

Condition (8.2.3.12) implies that :

$$p(x) = -\frac{2}{\alpha}\ln\left[e^{-\alpha p_c/2} + \frac{\alpha}{2}(x_c - x)\right] \quad \text{for } x < 0$$

$$p(x) = -\frac{2}{\alpha}\ln\left[e^{-\alpha p_c/2} + \frac{\alpha}{2}(x - x_c)\right] \quad \text{for } x > 0 \qquad (8.2.3.14)$$

The following observations analyze the properties of the fluid film shape in the vicinity of the pressure spike. Form (8.2.2.1) it follows :

$$3h^2\frac{dh}{dx}\left[\frac{\frac{dp}{dx}}{\eta}\right] + h^3\frac{d}{dx}\left[\frac{\frac{dp}{dx}}{\eta}\right] = 6U\frac{dh}{dx} \qquad (8.2.3.15)$$

According to (8.2.3.13), the first term in (8.2.3.15) vanishes by the pressure spike. By employing (8.2.3.13), the second term of (8.2.3.15) equals $-\alpha h_p^3/(2\eta_o)$, where h_p denotes the fluid thickness by the pressure spike. If U is positive, eqn (8.2.3.15) becomes for $x = 0^-, 0^+$:

$$-\frac{\alpha h_p^3}{2\eta_o} = 6U\frac{dh}{dx} \qquad (8.2.3.16)$$

which implies that the film thickness is convergent for $x = 0$.

Cases characterized by :

$$\frac{dp}{dx} = x^n e^{\alpha p/2} \quad \text{for } x < 0 \quad \text{and} \quad \frac{dp}{dx} = -x^n e^{\alpha p/2} \quad \text{for } x > 0 \qquad (8.2.3.17)$$

where n is a positive, integer number, can be studied in the same way, and they show that the corresponding film thickness gradient may vanish by the pressure spike.

Situations are now examined in which the fluid profile, h , is imposed, and information on the pressure profile is retrieved. If eqn (8.2.3.1) is integrated in the case of piezoviscous fluids between coordinates x and 0 (the pressure spike is thought to occur for $x = 0$), then :

$$e^{-\alpha p(x)} = \alpha \eta_o \left[6 U \int_x^0 \frac{d y}{h^2} + Q \int_x^0 \frac{d y}{h^3} \right] \qquad (8.2.3.18)$$

which implies that the parenthetical term is positive. Finally :

$$p(x) = -\frac{1}{\alpha} \ln \left[\alpha \eta_o \left(6 U \int_x^0 \frac{d y}{h^2} + Q \int_x^0 \frac{d y}{h^3} \right) \right] \qquad (8.2.3.19)$$

Eqn (8.2.3.19) is a generalization of (8.2.2.5). The condition of infinite pressure for $x = 0$ has been used in deriving (8.2.3.19). Employing condition (8.2.3.5), expression (8.2.3.19) becomes :

$$p(x) = -\frac{1}{\alpha} \ln \left[6 \alpha \eta_o U \left(\int_x^0 \frac{d y}{h^2} - h_p \int_x^0 \frac{d y}{h^3} \right) \right] \qquad (8.2.3.20)$$

where h_p denotes the fluid film thickness by the pressure spike. It can be shown that (8.2.3.20) satisfies condition (8.2.3.4) referring to the left branch of the pressure spike (here x coordinate is to the left of the spike, that is, it is negative). If h is constant and equal to h_p , then $p(x) \equiv \infty$ everywhere, a results in contrast with the Kostreva (1984b) conclusions. In addition, it is now shown that a convergent film profile is consistent with the condition implicit in equation (8.2.3.18) (see also (8.2.3.20)), and there commented. In fact, if the fluid film shape is convergent between x and 0 , then :

$$\frac{h_p}{h} \leq 1 \rightarrow \left[\frac{h_p}{h}\right]^2 \geq \left[\frac{h_p}{h}\right]^3 \rightarrow \int_x^0 \left[\frac{h_p}{h}\right]^2 dy \geq \int_x^0 \left[\frac{h_p}{h}\right]^3 dy \rightarrow$$

$$\int_x^0 \frac{dy}{h^2} - h_p \int_x^0 \frac{dy}{h^3} \geq 0 \qquad (8.2.3.21)$$

It would be possible to select a sufficiently general expression for the fluid film thickness (Section 8.2.2), *e.g.* :

$$\frac{1}{h} = a + b\,x + c\,x^2 + d\,x^3 \qquad (8.2.3.22)$$

and to introduce (8.2.3.22) into (8.2.3.19), to study the conditions which the coefficients of (8.21.3.22) must satisfy to produce an infinite pressure peak as $x \rightarrow 0$.

In conclusion, it has been shown in this Section that an infinite pressure peak is mathematically consistent with Reynolds equation even in the case of piezoviscous fluids. No result here obtained leads one to exclude that this pressure spike might appear even in the case of soft lubricated contacts, even if the present author is unaware of works exhibiting such pressure peaks.

8.3 THE ELASTOHYDRODYNAMIC PROBLEM EXPRESSED IN TERMS OF EXTENDED VARIATIONAL FORMULATION

In this Section the stationary, plane, elastohydrodynamic problem is revisited in terms of an extended variational formulation, where the corresponding functional exhibits minimum properties in the solution neighborhood. Such features are exploited in the development of a relaxation-type solver. The numerical results indicate that the convergence rate of the proposed relaxation scheme becomes increasingly poor as the solution of the elastohydrodynamic problem is approached. A polyâlgorithm based on a combination between relaxation-type and Newton-type schemes is proposed. The numerical experiments referring to various sealing profiles of decreasing foundation compliance show that the proposed procedure is particularly advantageous in the case of soft lubricated contacts.

Most of this Chapter is extracted from Strozzi (1986c), while the initial examples of Section 8.3.4 are unpublished.

8.3.1 Introduction and motivation

The last decade has witnessed the application of sophisticated analytical tools to elastohydrodynamic lubrication (EHL) problems. Most times such tools have been borrowed from the area of traditional structural mechanics, where they have initially been developed and validated.

Significant examples encompass the finite element formulation coupled with a functional linearization of the EHL problem (Rohde and Oh (1975)). Similarly, the concept of complementarity, which was initially applied to the mechanical analysis of units subject to unilateral contacts (*e.g.* Cannarozzi (1980)) , has recently been extended to the cavitation problem (Kostreva (1984), Oh (1984), Oh and Goenka (1985)), as well as to mixed lubrication and to tangential velocity slip situations (Strozzi (1985)). Quite recently, a more exhaustive modelling of the cavitation problem has been achieved by resorting to a formulation in terms of variational inequalities (Oden and Wu (1985)), which enables conditions on the existence and uniqueness of the solution to be achieved. Stability *considerations on* the elastohydrodynamic solution are developed by Kostreva (1984), by extending to EHL situations basic concepts which are familiar to mechanics. Finally, a preliminary variational formulation of the classical EHL problem is presented in Alliney, Strozzi, and Tralli (1985) together with exploratory numerical results.

Although it would be injudicious to rely entirely on numerical results, the current direction of engineering practice is one in which computer simulations are employed to make design decisions, while experiments are used to gain better insight into basic physical phenomena and to validate numerical results. The analytical tools mentioned above have undoubtedly enabled various EHL problems to be properly formulated, as well as they have frequently spurred the development of novel numerical strategies. For instance , specialized techniques have permitted the numerical solution of the classical EHL problem to be attained more rapidly (Rohde and Oh (1975), Oh and Goenka (1985), Ruskell (1980)) and, therefore, they have led to substantial savings in computer time.

In this Section the classical EHL problem is revisited in terms of an extended variational approach. As it will emerge from Section 8.3.2 , such a modelling enables

a locally convex functional to be obtained, the minimum points of which are solutions to the original problem. Extended variational principles can be used to underpin the finite element method in a more general context. In addition, they provide a mathematical basis for the application - in the solution of the classical EHL problem - of relaxation-type algorithms exhibiting good global convergence. This latter property makes the proposed variational formulation a valid alternative to continuation methods, which also can be employed to improve convergence (Strozzi (1987a)). In this latter approach an initial solution is achieved for a problem which is similar to the real one but in which the deformability of the sealing profile is fictitiously stiffened (Oh and Rohde (1977) employ a continuation method in solving heavily loaded point contacts). Then, the foundation is gradually softened until the actual value of the Young's modulus is approached, where the solution referring to the previous, higher Young's modulus is used as a starting point for the subsequent, softened case.

The observations which follow address the question whether the extended variational formulation is useful in treating the EHL problem in hip replacements. From the previous considerations, and from the results of this Subsection, it emerges that convergence problems are encountered particularly in the case of very compliant foundations. This circumstance occurs *especially in elastomeric seals* (Prati and Strozzi (1984)). In the case of hip replacements characterized by cups covered by an elastomeric layer, the question arises whether this foundation is more or less compliant with respect to an elastomeric seal. The whole of the results of Chapters 6 and 7 shows that the stress state in the elastomeric stratum is mainly hydrostatic when the contact width is much larger than the layer thickness (as it occurs under nearly static loading due to the body weight), so that the foundation is more rigid than its seal analogue, and seemingly stiff enough to avert convergence problems. Conversely, when the load imparted to the joint declines as a result of the walking load cycle, the contact width diminishes in comparison to the elastomeric stratum thickness, and the cortex stress state becomes more deviatoric, so that the elasticity of the foundation increases and convergence problems may arise in treating the EHL aspect. In addition, an augment in the layer thickness is equivalent to a relative diminution in the contact width, so that thicker elastomeric

strata are more likely to originate convergence problems than their thinner counterparts. Specific numerical tests to assess such predictions have not been effected.

8.3.2 Mathematical aspects

The mathematical modelling of a particular physical problem can often be stated in two different ways. The first description relies upon pointwise equations, which express the relationship among the physical variables associated with a particular point and those related to the adjacent ones. Ordinary differential and, in general, functional equations fall into this category. The second way consists in describing the physical modelling in a global sense, where the mathematical formulation expresses an interaction which simultaneously involves all the points of the physical domain. Variational formulations fall into this category, where those based on a functional with extremum properties are particularly desirable.

In the first description a solution must satisfy the functional equation in every point and, therefore, it is required that the residual of the functional equation vanishes over the whole physical domain. In other words, the first modelling relies upon an equality sign. Conversely, in the second formulation a solution must minimize (or, alternatively, maximize or make stationary) the corresponding functional, and therefore such a modelling involves an inequality sign (Milne (1980)).

When the physical problem is stated in terms of a functional, it is nearly always possible to transform it into a set of equivalent functional (Euler-Lagrange) equations. In other words, the second modelling can be modified into the first description. This poser is called the direct problem of the calculus of variations. On the other side, if the first modelling is available, the development of a suitable functional the minimum points of which are solutions to the initial problem is not generally straightforward. This stumper is called the inverse problem of the calculus of variations.

The classical results concerning the inverse problem of the calculus of variations are summarized in the following. In the case of a linear, self-adjoint operator A, the problem :

$$A(u) = 0 \qquad (8.3.2.1)$$

admits a classical variational formulation, where the corresponding functional has the stationary point where equation (8.3.2.1) is satisfied (Mitchell (1971)). In the case of a nonlinear operator A, a classical variational formulation exists provided that it satisfies the so-called Vainberg-Volterra condition :

$$< A'_u \ \phi \ , \psi > \ = \ < A'_u \ \psi \ , \phi > \qquad (8.3.2.2)$$

where $< . \ , \ . >$ denotes the inner product, A' indicates the Gateaux differential of operator A at u with direction ϕ , and ϕ and ψ are a generic couple of functions for which (8.3.2.2) is meaningful (Alliney and Tralli (1984)). In this case the functional the stationary points of which are solutions to the original problem (8.3.2.1) is given in Mitchell (1971).

When operator A is Gateaux differentiable but does not satisfy the symmetry condition (8.3.2.2), a classical variational formulation is not available. Remarkably, it has recently been demonstrated that an extended variational formulation can still be achieved (Tonti (1984)). According to Tonti theory, the initial equation (8.3.2.1) can be modified into an equivalent potential equation :

$$A'^{*}_u \ K \ (\ A \ (u) \ ) \ = \ 0 \qquad (8.3.2.3)$$

(where the star apex denotes the adjoint operator), whose extended functional $\overline{F} \ [u]$:

$$\overline{F} \ [u] \ = \ \frac{1}{2} < A \ (u) \ , \ K \ A \ (u) > \qquad (8.3.2.4)$$

vanishes at the critical points, and exhibits local convexity properties in each solution neighborhood (Alliney and Tralli (1984), Tonti (1984)). Operator K of

(8.3.2.3) and (8.3.2.4) must satisfy the following five conditions (Alliney and Tralli (1984), Tonti (1984)) :

1) $D(K) \supset R(A)$ and $R(K) \subset D(A'^{*})$
2) it is linear;
3) it is invertible;
4) it is symmetric;
5) it is positive-definite.

Equation (8.3.2.3) is not particularly useful from a numerical viewpoint, since "we cannot expect any improvement in the computed solution" (Alliney and Tralli (1985)) with respect to a standard Galerkin method. Conversely, the minimum properties of the extended functional (8.3.2.4) at the critical points are particularly appealing from a numerical standpoint, since the minimization of the functional can be used for numerical calculations (Tonti (1984) and Szeri (1980), p. 307). Functional (8.3.2.4) can be interpreted as a generalization of the least square functional (which is recovered for $K \equiv I$, Alliney and Tralli (1984), Tonti (1984)), but, similar to the Galerkin method, it permits a weak formulation to be obtained by means of suitable integrations by parts. While operator K is not unequivocally defined by Tonti's theory, it can be selected according to the available numerical experience in the numerical applications (Alliney and Tralli (1984)) (see Section 8.3.3).

The extended variational formulation was first applied to structural problems by Alliney and Tralli (1984). In Vecile (1984) an extended variational characterization of Navier-Stokes equation was developed. Finally, in Alliney, Strozzi, and Tralli (1985) a preliminary application of such a formulation to lubrication problems was presented.

The mathematical equations describing the quasisteady, unidimensional, isothermal, isoviscous, elastohydrodynamic problem (cavitation and slippage phenomena being ignored) have already been presented in eqns (8.2.2.1,2,3), and for convenience they are repeated here :

$$\frac{d}{d x}\left[\frac{h^3}{\eta}\frac{d p}{d x} - 6 U h\right] = 0 \qquad (8.3.2.5)$$

$$h = L\left[p - p_c\right] \qquad (8.3.2.6)$$

$$p(x_i) = p_i \;\; ; \;\; p(x_o) = p_o \qquad (8.3.2.7)$$

where p is the fluid pressure, p_c is the dry contact pressure, h is the film thickness, η is the fluid viscosity, U is the sliding velocity, p_i and p_o are the inlet and outlet pressures, and x_i and x_o are the inlet and outlet coordinates. In addition, L is a linear, positive-definite, integral operator, which expresses the foundation compliance (Strozzi (1985)). Following Rohde (Rohde and Oh (1975), Ruskell (1980), Prati and Strozzi (1984)), it is possible to introduce equation (8.3.2.6) into equation (8.3.2.5), to obtain a single integrodifferential equation in p :

$$\frac{d}{d x}\left[\left\{L\{p(x) - p_c(x)\}\right\}^3 \frac{d p(x)}{d x} - 6\eta U L\{p(x) - p_c(x)\}\right] = 0 \qquad (8.3.2.8)$$

Equation (8.3.2.8) can be likened to equation (8.3.2.1), where operator A is easily identifiable. Operator A is nonlinear and it does not generally satisfy condition (8.3.2.2). While it cannot be excluded that particular choices of the key physical parameters and of operator L would enable classical variational formulations to be achieved, they do not appear to be available for the general case. In Milne (1980), p. 417 , it reads : " Variational principles exist for certain problems in fluid mechanics but have not yet been developed for the most general case.". In Tonti (1984) it reads : " The [Tonti] method seems particularly promising for the equations of fluid-dynamics".

Before formulating functional $\overline{F}$ $[p]$ according to expression (8.3.2.4), it is necessary to choose a particular form for operator K. Following Alliney, Strozzi, and Tralli (1985), Alliney and Tralli (1984), and Tonti (1984), an integral expression is adopted for K :

$$K\ (\ u\ (x)\ ) = \int_{x_i}^{x_o} k\ (x,y)\ \ u\ (y)\ dy \qquad (8.3.2.9)$$

where $k\ (x,y)$ is a symmetric function of its arguments. By choosing K according to equation (5.5) of Tonti (1984), the 5 conditions previously mentioned can be fulfilled. In fact, by performing in equation (8.3.2.8) a change of variable which renders its boundary conditions homogeneous (Castelli and Pirvics (1968)), its domain is assumed to be $C_o^2\ [\ x_i\ ,\ x_o\ ]$. If the kernel of the integral foundation model (8.3.2.6) and $k\ (x,y)$ of (8.3.2.9) are sufficiently regular, the range of (8.3.2.8) is included in the domain of (8.3.2.9) and the domain of the adjoint operator of that embedded in the Gateaux linearization of equation (8.3.2.8) (after the proper change of variable) includes the range of (8.3.2.9).[1] Consequently, the first condition is fulfilled. Linearity and symmetry of (8.3.2.9) are obvious. Invertibility is implicit in positive-definiteness (Milne (1980)), which is demonstrated in (5.5) of Tonti (1984). Anyway, in the numerical applications an expression for $k\ (x,y)$ exhibiting a more local support is preferred, which, conversely, does not strictly guarantee positive-definiteness. This point is discussed in the next section.

The extended functional $\overline{F}\ [p]$ of equation (8.3.2.3) becomes (in Alliney, Strozzi, and Tralli (1985) the case of a Winkler support (Strozzi (1984)) is treated) :

$$\overline{F}\ [p] = \frac{1}{2} \int_{x_i}^{x_o} \int_{x_i}^{x_o} \frac{d}{d\ x} \left(\left\{ L\ \{\ p\ (x) - p_c\ (x)\ \} \right]^3 \frac{\mathrm{d}\ p\ (x)}{\mathrm{d}\ x} - 6\ \eta\ U\ L\ \{\ p\ (x) - p_c\ (x)\ \} \right) \cdot$$

$$k\ (x,y)\ \frac{d}{d\ y} \left(\left[L\ \{\ p\ (y) - p_c\ (y)\ \} \right]^3 \frac{\mathrm{d}\ p\ (y)}{\mathrm{d}\ y} - 6\ \eta\ U\ L\ \{\ p\ (y) - p_c\ (y)\ \} \right) dx\ dy = 0$$

(8.3.2.10)

---

[1] If the kernel of (8.3.2.6) is sufficiently regular, both h and dh/dx are continuous, and the range of (8.3.2.8) is $C\ [\ x_i\ ,\ x_o\ ]$. If $K\ (x,y)$ of (8.3.2.9) belongs to L_1, then the range of (8.3.2.8) is included in the domain of (8.3.2.9). The domain of the adjoint operator of that embedded in the Gateaux linearization of equation (8.3.2.8) (after the proper change of variable) is $C_o^2\ [\ x_i\ ,\ x_o\ ]$. It includes the range of (8.3.2.9), provided that $K\ (x,y)$ of (8.3.2.9) belongs to H_o^2.

One of the advantages of the presence of operator K is that, if $k\ (x,y)$ is selected to be sufficiently smooth, the higher order derivatives can be removed from the extended functional by integrating by parts, where kernel $k\ (x,y)$ absorbs the derivatives (Tonti (1984)) :

$$\overline{F}\ [p] = \frac{1}{2} \int_{x_i}^{x_o} \int_{x_i}^{x_o} \left(\left(L\ \{\ p\ (x) - p_c\ (x)\ \} \right)^3 \frac{d\ p\ (x)}{d\ x} - 6\ \eta\ U\ L\ \{\ p\ (x) - p_c\ (x)\ \} \right) \bullet$$

$$\frac{\partial^2\ k\ (x,y)}{\partial\ x\ \partial\ y} \left(\left(L\ \{\ p\ (y) - p_c\ (y)\ \} \right)^3 \frac{d\ p\ (y)}{d\ y} - 6\ \eta\ U\ L\ \{\ p\ (y) - p_c\ (y)\ \} \right) dx\ dy = 0 \qquad (8.3.2.11)$$

Remarkably, only first order derivatives of pressure p appear in expression (8.3.2.11). As a matter of fact, the extended variational formulation inherits the benefits of the least-square method and those of Galerkin-type procedures, since the potential extremum properties are combined with a weakening of the regularity requirements for the unknown function p .

In expression (8.3.2.11) the boundary terms arising from integrations by parts are zero provided that both k and its first derivatives vanish at the boundary of its domain.

8.3.3 Numerical aspects

A piecewise-linear interpolation for p satisfies the regularity requirements embodied in equation (8.3.2.11). Thus, $p \in H^1$, exactly as it would occur in Galerkin-type models. The remaining variable p_c could be chosen to be piecewise-constant, since it is not subject to differentiation. In the interest of greater consistency, p_c too is selected to be piecewise-linear. Similarly, according to equation (8.3.2.9), kernel k can be chosen to be bilinear within each square subdomain in the x-y plane. Only the nodal values of k at the four corners of each square subdomain need to be defined. If a vanishing nodal value is chosen at the nodes lying on the periphery of the whole domain, then both k and its first derivatives vanish along the entire domain boundary. This peculiarity avoids the outcome of boundary terms in expression (8.3.2.11).

The k nodal values can be advantageously stored in a square matrix K , where its generic entry k_{ij} defines the corresponding k-value for node i along x-axis and for node j along y-axis. In Alliney and Tralli (1984)) it is shown that matrix K can be favourably chosen to be (apart from the boundary nodes) symmetrical, tridiagonal, and diagonally dominant. Because of the previous observations on the boundary nodes, the entries k_{11} , k_{12} , k_{21} must be set equal to zero together with the corresponding terms referring to the opposite corner in the whole x-y domain. In Fig. 8.3.3.1 the nodes where kernel k does not vanish are denoted with a dot, while the square elements where k is not entirely null are shaded. For such elements, term $(\partial^2 k\ (x,y))/\partial x\ \partial y)$ in equation (8.3.2.11) is constant, as $k\ (x,y)$ is bilinear.

The numerical difficulties encountered in dealing with positive-definiteness of the numerical operator K based upon kernel k just described are discussed in the following. If the numerical kernel $k\ (x,y)$ and a generic function $u\ (x)$ are analytically expressed as :

$$K\ (x,y) = \boldsymbol{\phi}^T(x)\ K\ \boldsymbol{\phi}\ (y)\ ;\ u\ (x) = \boldsymbol{\psi}^T(x)\ \boldsymbol{u} \qquad (8.3.3.1)$$

where vectors $\boldsymbol{\phi}$ and $\boldsymbol{\psi}$ collect suitable basis functions referring to the N nodes,

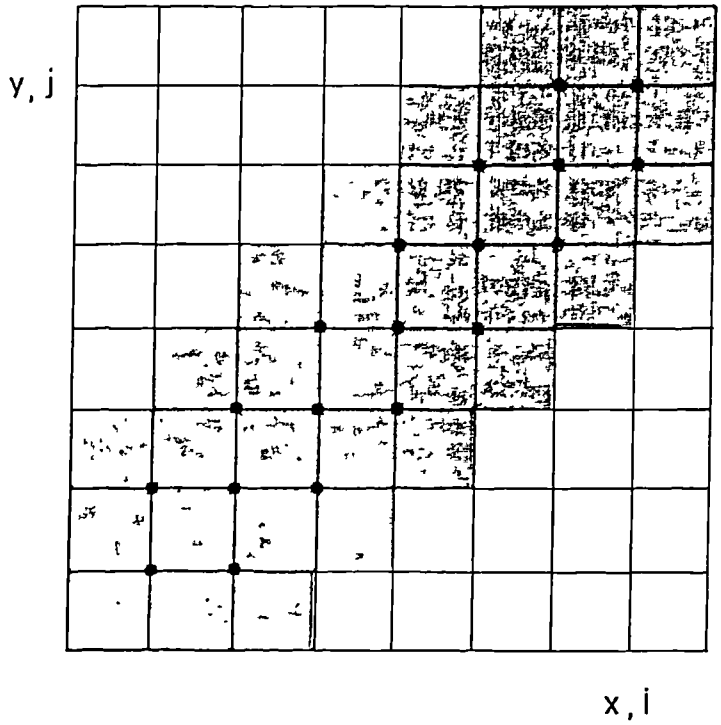

Fig. 8.3.3.1 : The nodes where kernel k does not vanish are denoted with a dot, while the square elements where k is not entirely null are shaded.

while matrix K and vector u express the nodal values of k (x,y) and u (x), respectively, then, by employing (8.3.2.9) and (8.3.3.1), positive-definiteness of operator K requires that :

$$< K\,u\,,\,u > \;=\; u^{T}\left[\int_{x_i}^{x_o} \psi\,(x)\;\phi^{T}\,(x)\;dx\right] K \left[\int_{x_i}^{x_o} \phi\,(y)\;\psi^{T}\,(y)\;dy\right] u \;\geq\; 0$$

$$(\;=\;0 \text{ iff } u\;=\;0\;) \qquad (8.3.3.2)$$

If $\phi \equiv \psi$, the two parenthetical terms are square Gram matrices (Mitrinovic (1970)), and therefore they are positive-definite. Consequently, if matrix K is positive-definite, so is operator K. If $\phi \neq \psi$, operator K is in general only positive-semidefinite, a fact which might results in spurious solutions being added to the Tonti functional. In other words, a non-vanishing vector u (to be interpreted as

a description of the residual of equation (8.3.2.8)) might exist for which the inner product in (8.3.3.2) vanishes. For instance, in Fig. 8.3.3.2 two functions ϕ and ψ are depicted whose product may exhibit a vanishing integral over interval [-1 , 1]. In technical applications, condition $\phi \equiv \psi$ is often impractical. Anyway, as the number of elements adopted in the discretization process is increased, function u (interpreted as previously mentioned) is approached by a piecewise-linear curve exhibiting the same nodal values, and positive-definiteness is recovered in the limit. Consequently, situations like that of Figure 8.3.3.2 are unlikely to take place for a sufficiently high number of elements, and this is in agreement with the experience that spurious solutions never occurred in the numerical tests performed. In addition, the Tonti functional tends to the least-square functional (for which local convexity properties hold) as kernel k tends to a Dirac-type function. Despite these encouraging observations, positive-definiteness of K cannot be proved rigorously for a given number of nodes. This drawback is the counterpart of the numerical advantages discussed with reference to Figure 8.3.3.3.

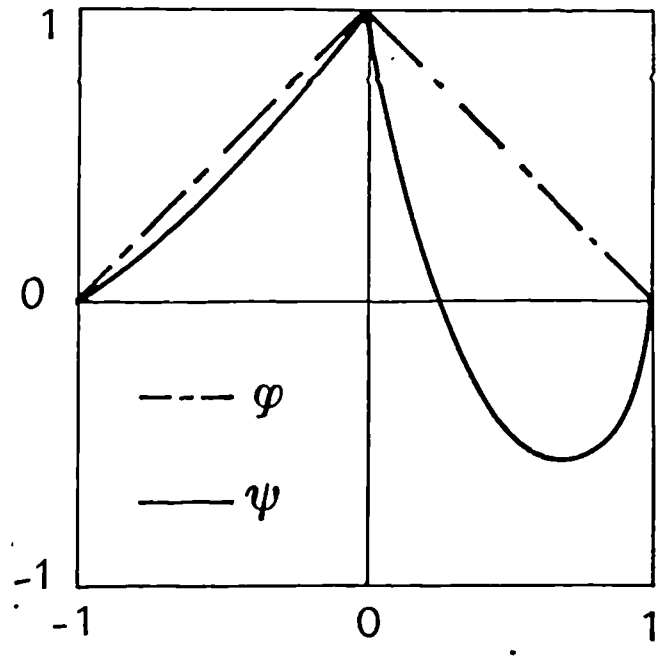

Fig. 8.3.3.2 : The product of two functions ϕ and ψ may exhibit a vanishing integral over interval [-1 , 1].

Positive-definiteness of matrix K is discussed in the sequel. Since the diagonal entries of K by the domain corner nodes vanish (see Figure 8.3.2.1), matrix K cannot be positive-definite in itself. Anyway, it should be noted that, since the inlet and outlet fluid pressures are imposed, the first and last entries of the vector describing the nodal pressure values must not be considered in the constrained minimization process of the Tonti functional. Similarly, the first and last degrees of freedom of the generic function u , expressed via its nodal values and the corresponding basis functions, must be disregarded in checking for positive-definiteness of operator K in (8.3.2.10). Matrix K , once its boundary rows and columns are deleted, becomes positive-definite, as it is symmetric, strictly diagonally dominant, and with positive diagonal elements.

Since a relaxation-type solver is planned, it is fundamental to clarify which partial integrals must be actually computed to evaluate the effects of a perturbation of the fluid pressure p at the generic node i on the whole extended functional. At most the elements with non vanishing kernel second derivative must be accounted for. Because of the symmetry features inherent in the extended variational formulation, only the diagonal and above-diagonal elements need to be considered.

If a Winkler foundation model (Strozzi (1984)) is adopted, a nodal pressure modification affects only the fluid film thickness at that node, while the remaining film thickness nodal values do not change. Also, the perturbation of p at node i along x-axis is inevitably coupled with an identical modification of p at node $j = i$ along y-axis. Consequently, such a perturbation affects the elements contacting the two crossed solid lines (shown in Fig. 8.3.3.3) referring to nodes i and to $j = i$, respectively. As a result, only the elements shaded in Fig. 8.3.3.3 need to be considered. These observations permit noticeable savings in computer time with respect to non optimized programs (Alliney, Strozzi, and Tralli (1985)).

If a non local foundation is adopted, all the diagonal and above-diagonal elements should be considered. Anyway, the computing time can be appreciably reduced by observing that the effects of a pressure perturbation at node i on the film profile generally diminish at the nodes far from i. Consequently, the effects of a nodal pressure modification on the extended functional can be estimated by

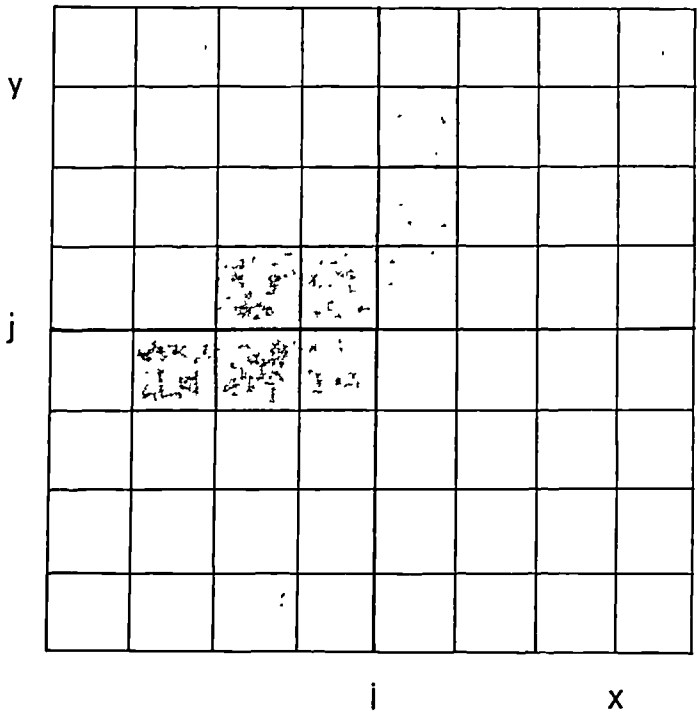

Fig. 8.3.3.3 : In the case of a local foundation model, only the shaded elements need to be considered in the minimization process.

considering only the elements in the vicinity of node i (Cook (1981), p. 425). Whether a sufficient number of elements has been accounted for can be verified by computing occasionally the Tonti functional over the whole x-y domain and by checking for its decrease.

All the numerical tests were performed by adopting a Winkler foundation model. It is appreciated that such a support model can lead to physically unrealistic results (Strozzi (1984)). On the other side, with such a support equation (8.3.2.8) retains its differential (as opposed to the more complex integrodifferential) character, and therefore it is particularly suitable for numerical experiments.

As already mentioned, the local convexity properties of the extended functional provide a mathematical foundation for the development of relaxation algorithms. The relaxation solver is organized as follows. A fractional value p_i / M

is computed for the generic node i , where appropriate values for M range from 5 to 10. A series of perturbed nodal pressure values included in the interval $[\, p_i - p_i /2M\,,\; p_i + p_i /2M]$ are considered. In particular, Q equispaced p_q pressures ($q = 1,.,.,Q$) are examined, where the extremum values coincide with those of the closed interval mentioned above. Q can be advantageously chosen to be odd, so that the initial pressure estimate coincides with the central pressure value p_q for $q = (Q + 1)/2$. A felicitous choice for Q is 9. Then, the nodes defining the film profile length are examined sequentially. For every node, the extended functional is computed for the p_q values mentioned above, and the p_q pressure which minimizes the extended functional is attributed to that node. The sequential examination and updating of the nodal pressure values along the lubricated profile length constitutes a relaxation iteration. After a certain number of iterations, the extended functional reaches a stagnation value, since the discrete character of the minimizing process explained above precludes the resolution of the correct nodal pressure values. This conundrum can be overcome by increasing the value of M when a plateau is faced for the extended functional. In particular, M can be doubled, and the relaxation process restarted.

It is known that Newton-type solvers exhibit quadratic convergence if the starting point is within the sphere of attraction, otherwise they may diverge. Conversely, relaxation-type solvers applied to variational formulations with extremum properties show good global convergence, but poor local convergence (Prati and Strozzi (1984)). Thus, a polyalgorithm which combines relaxation-type and Newton-type schemes can be advantageously developed (Milne (1980), p. 405), where the relaxation method may be adopted to reach the sphere of attraction of the Newton method, which in turn can be employed to approach the solution more efficiently. A similar strategy was successfully used in Prati and Strozzi (1984) in the case of structural problems.

For the purpose of this paper, which is to explore the merits of the extended functional concept, a simpler strategy was adopted. In particular, the selection between the two solvers was not made automatically, whereas a preassigned number of relaxation iterations was performed, followed by Newtonian loops. Alternatively, the Newton method was applied directly to the starting point, in order to retrieve

qualitative indications about the extent of its sphere of attraction.

As a final remark, it should be mentioned that relaxation-type solvers require much less computer memory than Newton-type schemes, since only vectors and not square matrices are involved.

8.3.4 Results

An appraisal of the numerical schemes under examination requires the knowledge of exact solutions to the EHL problem to be used as test cases. The first part of this section deals with the development of analytical solutions. In the second part, the numerical results according to the extended variational formulation and referring a) to qualitative examples and b) to three configurations of increasing foundation compliance are presented and compared to a more conventional Newtonian solver.

Exact solutions to the EHL problem against which to check the numerical results can be achieved as thoroughly discussed in Section 8.2 . For the sake of completeness, a brief summary of this methodology is repeated here. A fluid film profile is selected among sufficiently simple and regular curves. By integrating twice equation (8.3.2.5), p can be expressed in terms of h and of known parameters (Strozzi (1985)). If the selected h curve is introduced in this expression, and if proper boundary conditions (discussed in the sequel) are chosen, an exact expression for the fluid pressure p can be derived. Then, the corresponding contact pressure p_c is computed by introducing in the foundation compliance equation (8.3.2.6) the selected h curve and the computed p profile. So doing, a contact pressure curve p_c is achieved for which the analytical h and p profiles satisfy simultaneously equation (8.3.2.5-7), and therefore they constitute an exact solution to the EHL problem. Such a method for obtaining analytical solutions to the EHL problem does not appear to have been exploited previously, since the numerical codes are usually validated in hydrodynamic situations (rigid profile assumption) (Rohde and Oh (1975), Oh (1984), Ruskell (1980)). In particular, a linear fluid film profile and a Winkler foundation as in Strozzi (1987b) have been considered. Also, the inlet and outlet fluid pressures have been chosen so that the contact pressure profile vanishes by the tracing and trailing edges.

Some qualitative results are produced below, aimed at showing the merits of the extended variational formulation and at comparing it to a more traditional Newton solver. A linear fluid film profile defined by four nodes and of varying foundation compliance is considered (Section 8.2), Fig. 8.3.4.1 . The exact values

adopted for the physical parameters are omitted, since these examples are purely qualitative. The two extreme nodes are kept fixed, while the two central nodes are movable vertically. The corresponding extended functional depends only on two variables, namely the heights of the two central nodes, so that it is possible to represent it graphically. Fig. 8.3.4.2 reproduces a perspective view of this functional in the case of soft foundations, where the central point of x-y platform is the exact solution (that in which the four nodes of Fig. 8.3.4.1 are aligned to form a linear profile), to which a minimum corresponds for the extended functional. Fig. 8.3.4.3 displays the corresponding contour lines in the case of a rigid foundation, while Fig. 8.3.4.4 reports the contour lines for a soft configuration. In all cases, the functional minimum is clearly visible, even if in the hard situation the contour lines are more regular. The presence of a clear minumum confirms the validity of the proposed formulation. In particular, a solution method based upon a search for the potential minimum (Section 8.3.3) would converge regardless of the starting point.

Fig. 8.3.4.5 studies the convergence of a standard Newton solver (Ruskell (1980)) for the same configuration of Fig. 8.3.4.1 . It includes indications concerning which starting points in terms of fluid film thickness are successful, and which fail to converge. The x-variable reports the vertical distance of node 2 of Fig. 8.3.4.1 from a linear profile, while y-variable reproduces the corresponding distance of node 3 . In other words, x and y variables indicate the deviations of the starting point for the fluid film profile from the exact solution. (The x and y axes of Figs 8.3.4.2,3,4 are to be interpreted in the same sense, and in the same scale.) The asterisks indicate divergence, while the dots (scarcely visible) denote convergence. Fig. 8.3.4.6 displays a schematic version of Fig. 8.3.4.6 , which shows that the x-y portion defining converging starting points is reminiscent of a four leafed clover, where the top-right and bottom-left leaves are much smaller than the remaining two leaves. This means that a starting point in which one node is higher than the right value, and the other node is lower, behaves more favourably than a starting point where both nodes 2 and 3 are higher (or lower) than their correct values. In addition, Fig. 8.3.4.6 shows that the Newton method fails to converge for starting points for which a solution method based upon the extended functional still converges.

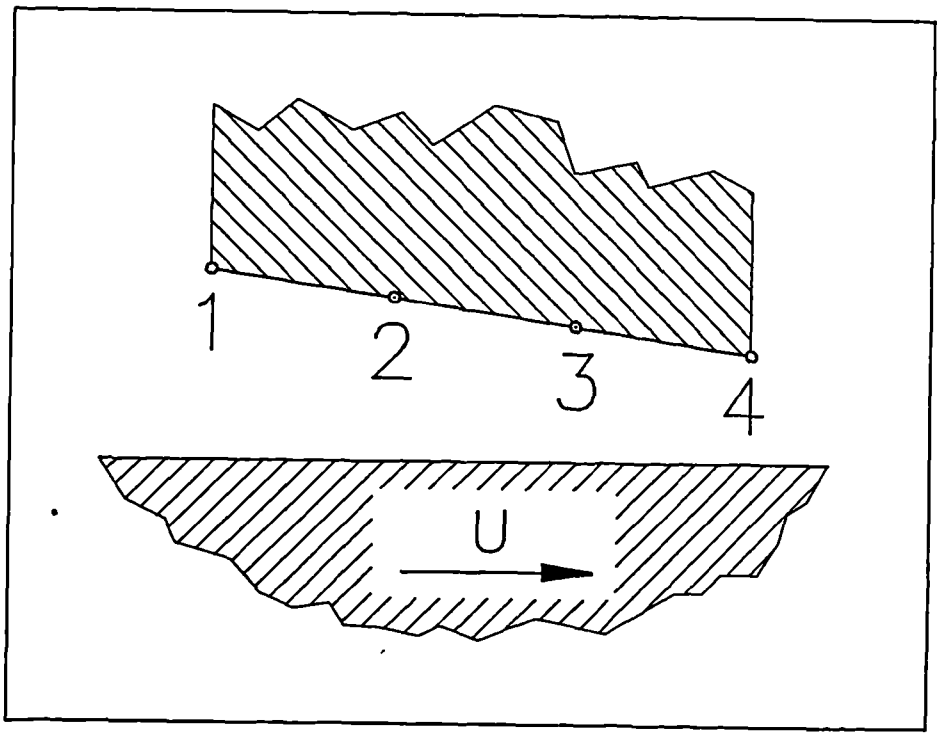

Fig. 8.3.4.1 : The linear fluid film profile defined by four nodes.

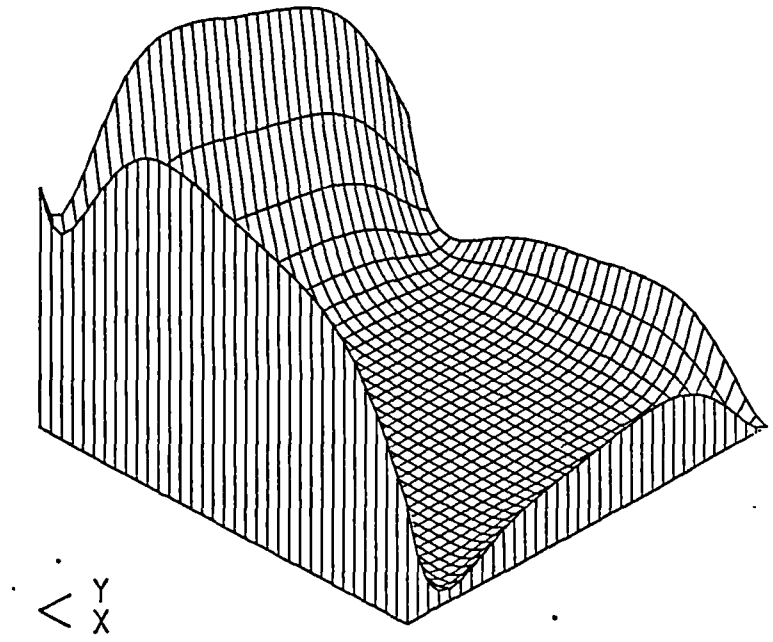

Fig. 8.3.4.2 : A perspective view of the extended functional.

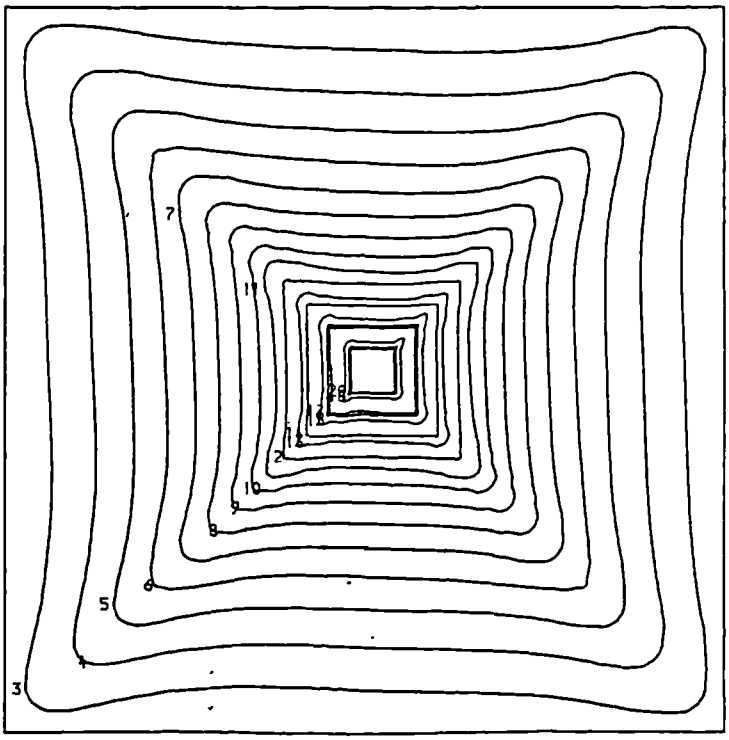

Fig. 8.3.4.3 : The extended functional contour lines for a rigid foundation.

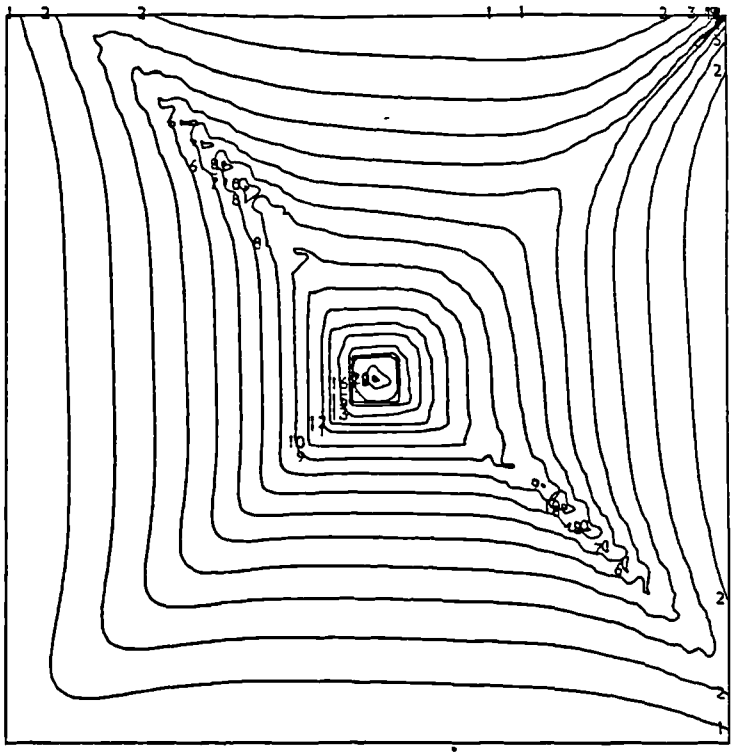

Fig. 8.3.4.4 : The extended functional contour lines for a soft foundation.

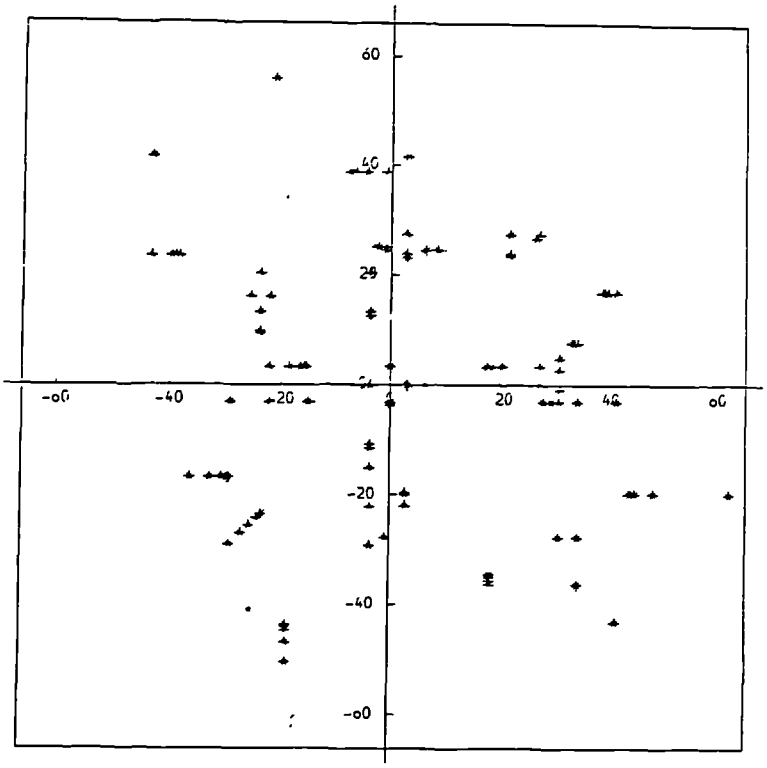

Fig. 8.3.4.5 : The convergence of a Newton solver.

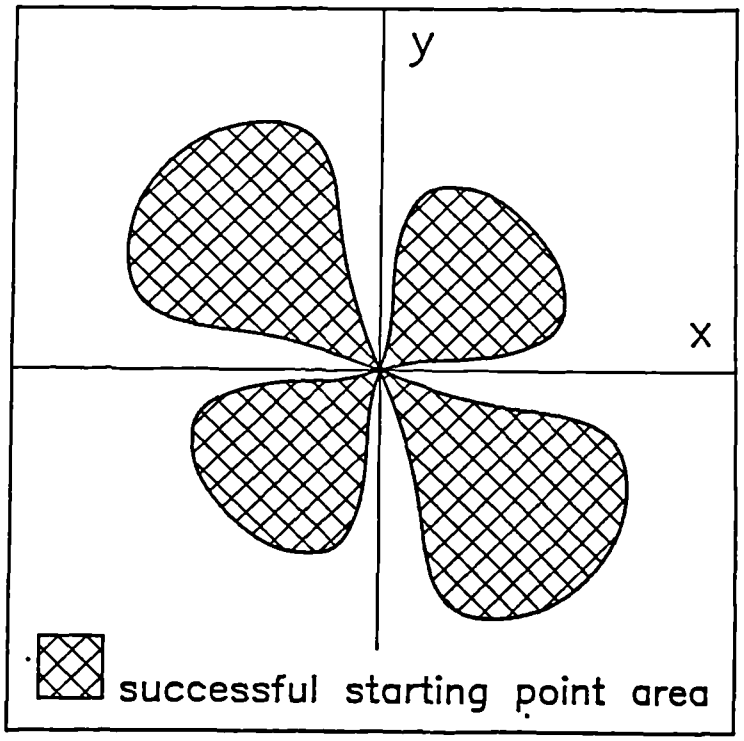

Fig. 8.3.4.6 : A schematic version of Fig. 8.3.4.5 .

The following results still deal exclusively with linear profiles, but they contain more qualitative information. The following values, mainly borrowed from Ruskell (1980), have been attributed to the corresponding physical variables in all cases : fluid film thickness at the inlet : 2.5 μm ; fluid film thickness at the outlet : 2.3 μm ; sliding velocity : 127 mm/s; fluid viscosity : 0.43 x 10^{-6} Ns/mm^2 ; sealing length : 4.83 mm ; compressed seal radial depth : 4.32 mm.

In addition, 30 nodes have been used in the discretization process in all cases. The diagonal and off-diagonal entries of the tridiagonal matrix K (see Section 8.3.3) were set equal to 10 and to 3, respectively, similar to Alliney and Tralli (1984). Three cases referring to decreasing Young's moduli were considered. The first value to be studied was E = 210000 MPa (case of steel-like materials). In Fig. 8.3.4.7 the exact solution is displayed in terms of fluid pressure $\bar{p}$, dry contact pressure p_c , fluid film thickness h and undeformed seal radial depth l .

Then, the exact fluid pressure profile was modified by introducing a noticeable spurious pressure perturbation at node 12 and the effectiveness of the proposed approach in reducing the spurious pressure modification towards the exact solution was tested. Fig. 8.3.4.8 shows that 20 relaxation iterations produce a considerable reduction in the pressure irregularity, together with a spreading of the initially localized perturbation along a wider lubricated profile portion as the relaxation process proceeds. Interestingly, but not unexpectedly, it appears from Figure 8.3.4.8 that the convergence rate becomes poorer as the exact solution is approached.

Figure 8.3.4.9 displays the results obtained with a standard Galerkin method coupled with a Newtonian iteration scheme (Rohde and Oh (1975), Ruskell (1980), Prati and Strozzi (1984)) applied to the same perturbed starting point of Figure 8.3.4.8. After 6 - 7 Newton loops the exact solution is recovered. Consistent with the available results (Rohde and Oh (1975)), the sphere of attraction of the Newton method in the case of hard contacts is sufficiently extended, that is tantamount to saying that the convergence of this iterative process is good even in the presence of severely misjudged starting points. In this case a traditional Newton solver is generally preferable to the extended variational formulation.

Different results are obtained with a lower Young's modulus E = 100 MPa. Indeed, in this case a Newton procedure applied to an analogously perturbed starting point diverges dramatically. Conversely, the perturbed pressure profile is improved by the proposed relaxation scheme to such an extent that it becomes a successful starting point for the Newtonian iterations. Such results are too voluminous to present in the limited space available, and therefore they are omitted. Instead, the analogous findings referring to the more deformable foundation characterized by E = 7.58 MPa (rubber-like materials) are presented in detail.

Fig. 8.3.4.10 displays the fluid pressure curve affected by a noticeable perturbation imposed to node 12, together with the effects of 100 relaxation iterations. Remarkably, the proposed variational formulation ensures a good global convergence even in the case of soft foundations, for which the less mathematically sound direct iterative method can fail to converge (Rohde and Oh (1975)). Because of the high foundation compliance, the pressure perturbation produces a magnified fluid film profile modification. Fig. 8.3.4.11 displays the initial and final fluid film profiles. While the imposed perturbation is considerably reduced, some pervasive undulations appear along the sealing profile. They are shown in an enlarged h-scale in Fig. 8.3.4.12 together with the exact linear profile. If a Newton solver is applied to this configuration, the exact solution is approached in 5-6 Newton iterations. Conversely, the Newton method applied to the perturbed pressure profile of Fig. 8.3.4.10 diverges dramatically, where the first four loops are displayed in Fig. 8.3.4.13 together with the initial pressure profile. This feature can be attributed to the contraction of the sphere of attraction of the Newton method as the foundation becomes softer.

For more compliant foundations, spurious undulations tend to appear in the fluid film profile. The interpretation and, possibly, the control of such wiggles are beyond the scope of this paper.

Finally, in Fig. 8.3.4.14 the value of the extended functional referring to the starting point and to 100 subsequent relaxation iterations is displayed. Fig. 8.3.4.14 confirms that the convergence rate becomes increasingly poor as the solution is approached. The convergence rate of Fig. 8.3.4.14 is not appreciably modified by setting the diagonal value of matrix K equal to 100, whereas it can be conjectured

that a more extended support for K might affect more perceivably the minimization procedure performance.

The proposed procedure was not tested in the case of nonlocal foundation models. Anyway, the numerical divergences which occur especially in the case of soft contacts are mainly attributable to the fact that limited pressure perturbations result in considerable modifications of the film profile, more than to a particular expression of the foundation model. Consequently, the usefulness of the Tonti functional should not be undermined by integral foundation models.

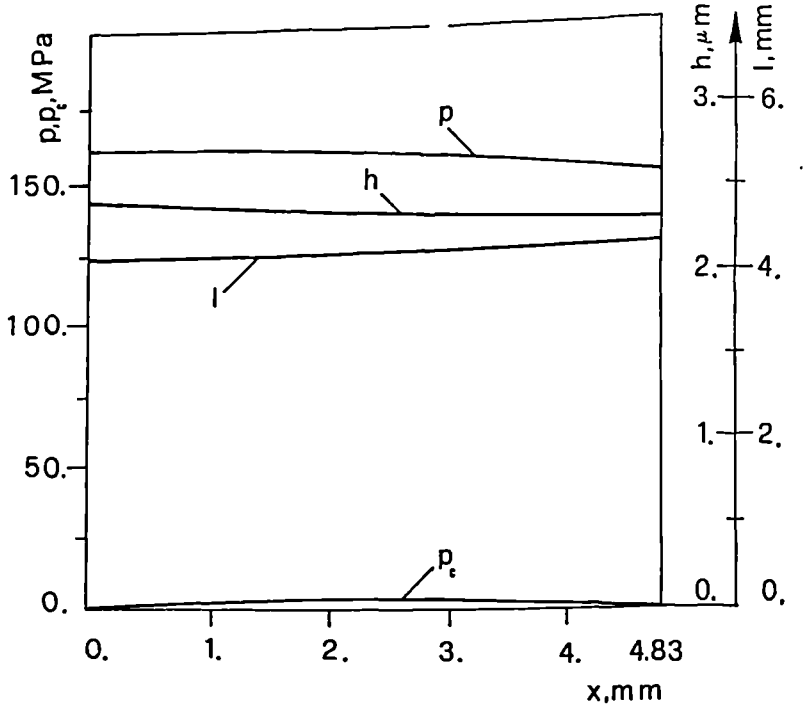

Fig. 8.3.4.7 : The exact solution of the EHL problem in terms of fluid pressure p , dry contact pressure p_c , fluid film thickness h , and undeformed profile radial depth, l .

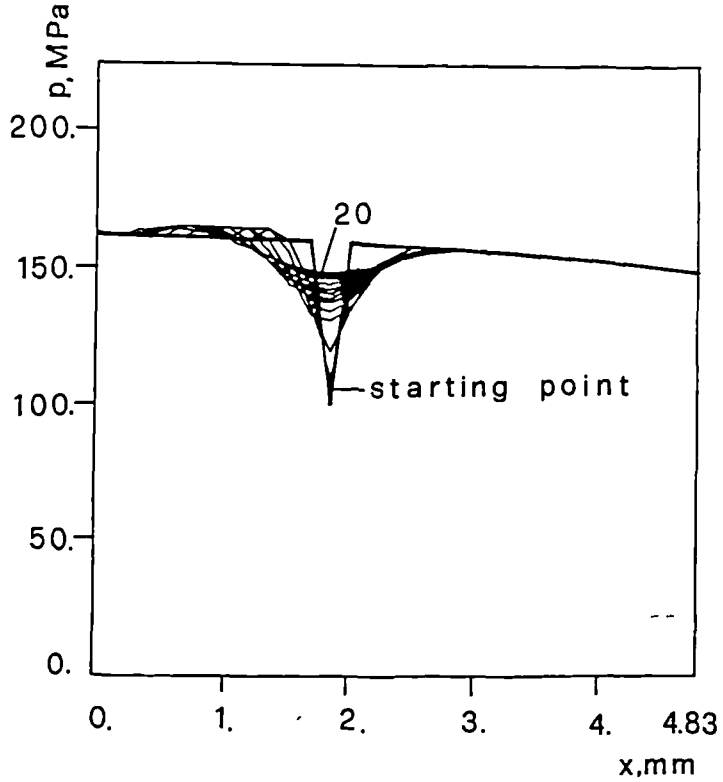

Fig. 8.3.4.8 : 20 relaxation iterations reduce considerably the initial spurious pressure modifications.

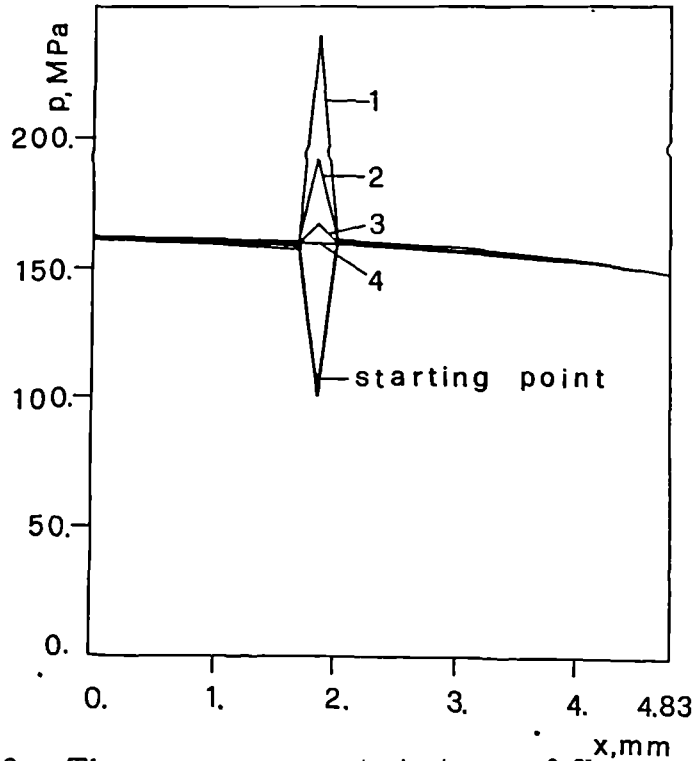

Fig. 8.3.4.9 : The convergence rate in terms of fluid pressure for a standard Newton-Galerkin solver is good in the case of stiff foundations.

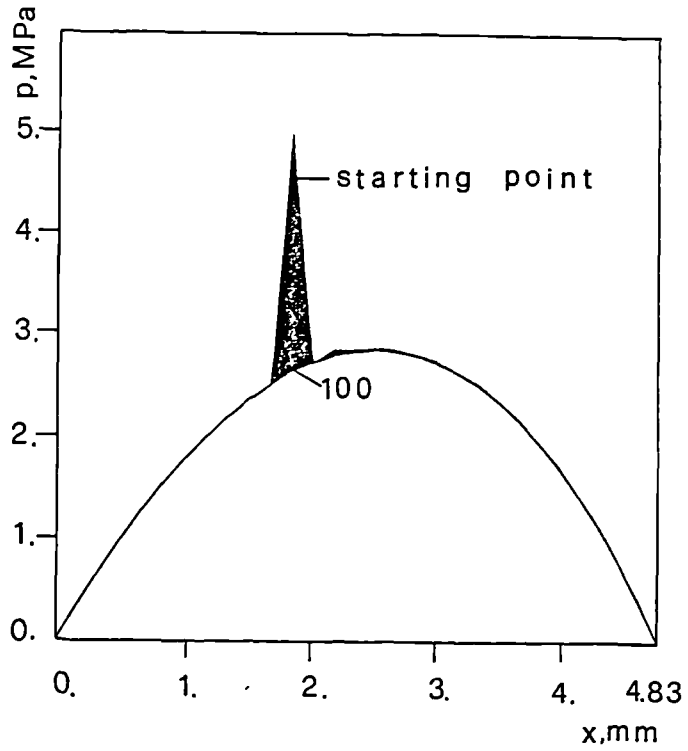

Fig. 8.3.4.10 : The effects of 100 relaxation iterations on the initially perturbed pressure profile.

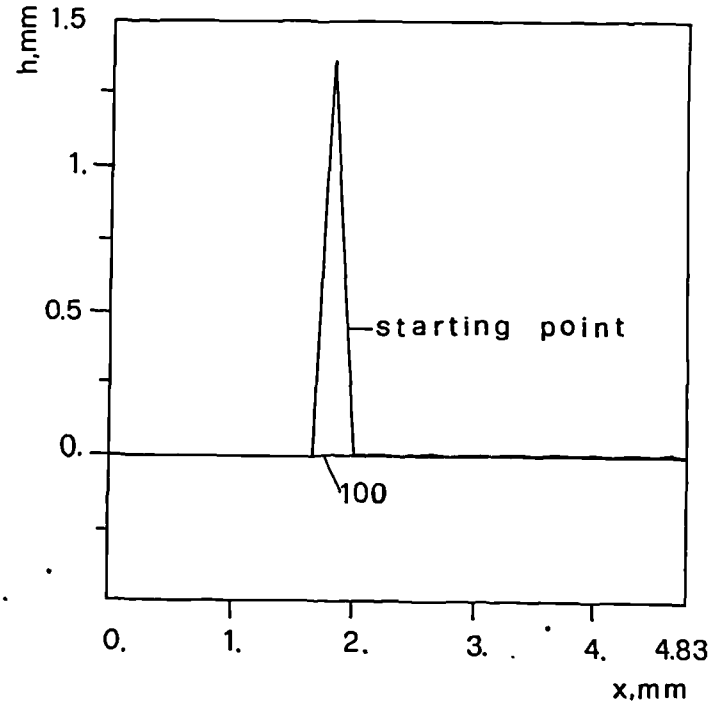

Fig. 8.3.4.11 : The initial and final fluid film profiles corresponding to Fig. 8.3.4.4 .

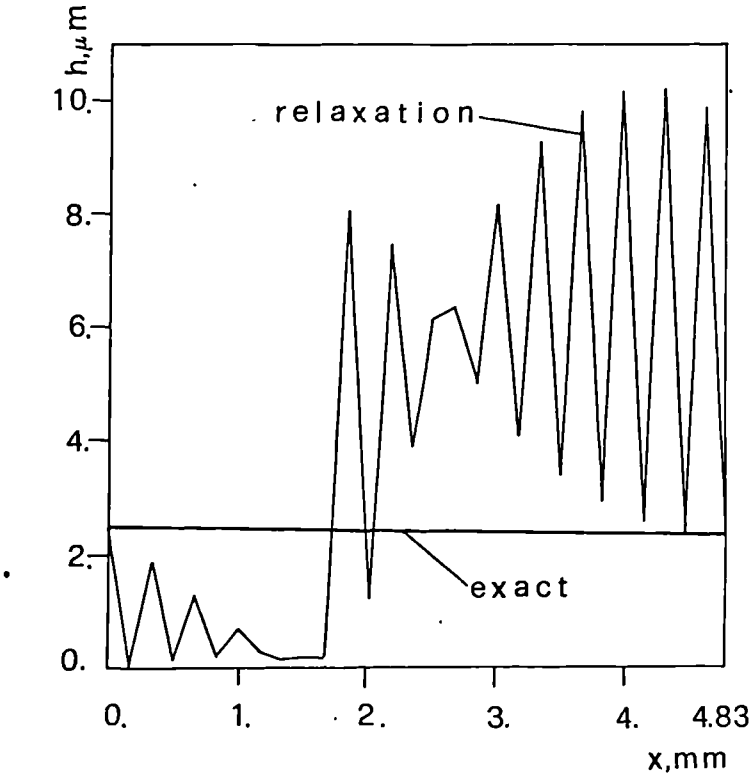

Fig. 8.3.4.12 : The final fluid film profile of Fig. 8.3.4.5 , together with the exact solution.

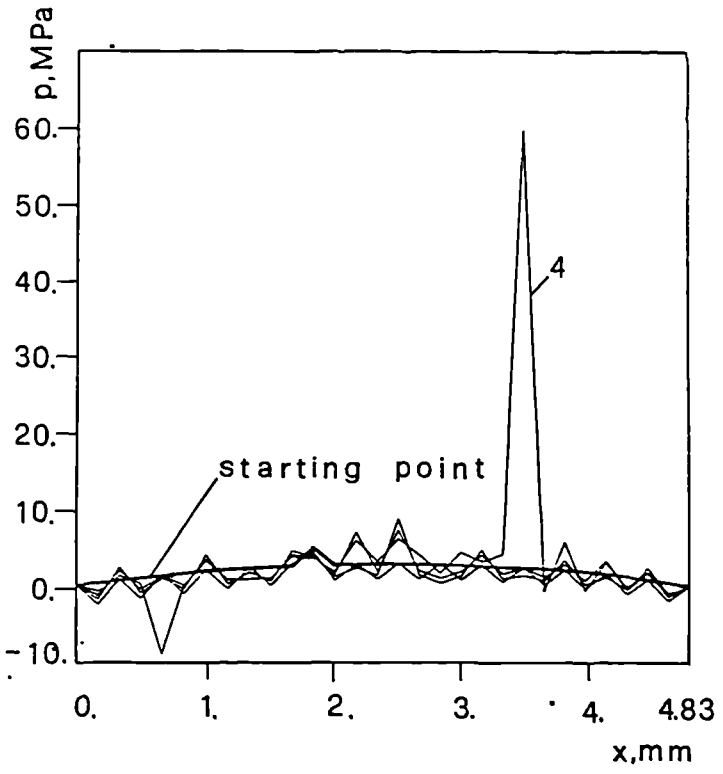

Fig. 8.3.4.13 : As the foundation becomes softer, the Newton method may diverge easily.

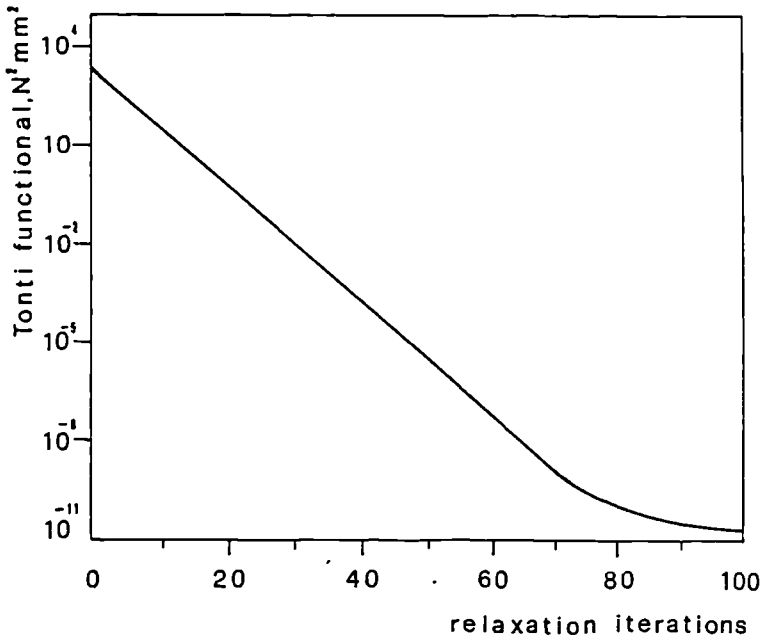

Fig. 8.3.4.14 : The convergence rate of the relaxation method based upon the extended functional becomes increasingly poor as the solution is approached.

8.3.5 Conclusions

An extended variational approach with local extremum properties has been formulated for the EHL problem. The numerical difficulties encountered in respecting the analytical requirements have been discussed. A variety of numerical experiments have shown that such formulation provides a mathematical basis for the development of a relaxation-type solver with good global convergence properties. It has been shown that the convergence rate of this relaxation method becomes increasingly poor as the solution is approached. As a consequence, the proposed iterative procedure cannot be employed by itself in achieving the numerical solution of EHL problems. Instead, this relaxation method can be advantageously used for improving the approximate pressure profile until it falls within the sphere of attraction of the Newton method, which in turn permits a rapid refinement of the solution to be achieved. In other words, the proposed formulation supplies a mathematical foundation for the development of a polyalgorithm based upon a combination between relaxation-type and Newton-type solvers. It has been shown that such a solution scheme is particularly advantageous in the case of soft foundations, for which the direct iterative method as well as the Newton method can fail to converge. Consequently, the proposed procedure should prove to be particularly useful in studying the development of EHL conditions in elastomeric seals.

8.4 ON THE OUTCOME OF SPURIOUS NUMERICAL UNDULATIONS AFFECTING THE FLUID FILM THICKNESS

In this Section the possible outcome of spurious undulations in the numerical description of the fluid film profile in soft lubricated contacts is rationalized. A numerical procedure which can placate the outcome of spurious oscillations in the film curve is illustrated. Such tools are applied to the analysis of lubricated elastomeric seals. The possible application to the lubrication regime in hip joints with soft layers is also discussed.

8.4.1 Literature review

The accurate evaluation of the fluid film thickness in lubricated soft contacts is often of the utmost relevance from an engineering viewpoint. For instance, in the case of elastomeric seals, the fluid film thickness must be small in order to limit the leakage of the fluid to be sealed, but not so small as to permit an extended, direct interaction between the elastomer and the shaft asperities (Theyse (1967)). In the case of artificial human joints, the solution of the EHL problem would help to define the optimal design for the mating surfaces.

Unfortunately, the numerical solution of the EHL problem for soft contacts appears to be more troublesome than that for hard contacts. In fact, regularity problems may manifest themselves in oscillatory fluid film profiles as the foundation becomes softer (Field and Nau (1975)). Such spurious undulations are attributable to limited pressure perturbations resulting in magnified film thickness fluctuations (Okamura (1982)).

Undesired spurious undulations in terms of fluid film profile are evident in many numerical results concerning soft contacts and, in particular, lubricated elastomeric seals for reciprocating motion. For instance, the numerical fluid film thicknesses in rubber seals presented by Field and Nau (1975) exhibits pronounced oscillations as the contact becomes softer. Many diagrams of Fig. 14 in Austin,

Flitney, and Nau (1977), who examine again elastomeric seals, exhibit pervasive undulations. The film profiles presented by Ruskell (1980) for rectangular elastomeric seals are oscillation-free, but in some unpublished situations such irregularities appeared (Ruskell, personal communication). Medley, Dowson and Wright (1984) recognize the stiff character of the differential equation describing the lubrication of the human ankle joint, especially for high loads. Some undulations affect the fluid film profiles of Prati and Strozzi (1984), who study again a rectangular seal. A Runge-Kutta scheme produced undulation-free film profiles for a similar problem in Yang and Huges (1984). Being of integral type, this method is expected to supply regular solutions, but its accuracy should be checked against the existing solutions. Some wiggles in the film shape appear at the inlet in Alliney, Strozzi and Tralli (1985). In this case the iterative process aimed at determining the solution of the non-linear problem was limited to four loops and the numerical convergence was not reached, so that definitive conclusions about the outcome of undulations are difficult to draw. Stakenborg, van Leeuwen, and ten Hagen (1990), and van Leeuwen and Stakenborg (1990) examine the visco-elastohydrodynamic lubrication regime in elastomeric, radial lip seals. Fig. 6 of van Leeuwen and Stakenborg (1990) shows some wiggles at the highest frequencies. These authors observe that "If the static pressure component is very high, [the] differential equation . . . becomes rather stiff . . . Therefore, the problems encountered could equally well be of numerical origin." Finally, adjustments of the Young's modulus to mimic via a Poisson's ratio of 0.4 the actual cases characterized by ν closer to 0.5 , recently proposed by Dowson, Fisher, Jin, Auger, and Jobbins (1991), betray the difficulties encountered in treating directly incompressible layers.

In the case of hard contacts, the undulations appear sporadically, and they are generally restricted to a limited portion of the lubricated length. On the other side, they tend to affect both h and p curves. For instance, in Rohde and Oh (1975) the possible presence of oscillatory numerical solutions is mentioned. Fig. 6 of Oh and Rohde (1977) is affected by pressure undulations in the vicinity of the pressure spike. Some catastrophic results are presented by Okamura (1982). Some wiggles appear both in the pressure and in the fluid profile for a limited range of key physical variables in Oh (1984). Wu (1986) finds a vibrating fluid film profile, visible

in his Fig. 3. Finally, Oh (1986) notes that "for higher load levels, the solutions for pressure and film gap in the hydrodynamic region . . . become oscillatory . . . This problem . . . is related to the choice of interpolation function, and worsens for increasing loads. Hence, more research is needed to develop an ideal interpolation method."

The presence of spurious numerical undulations is particularly detrimental, since it obscures the actual solution. Also, it would inevitably produce numerical instabilities in the treatment of more complex situations, as are those concerning mixed lubrication (but Oh (1986) notes that his solution is not oscillatory in the solid-to-solid contact region).

Moving to the experimentally measured fluid film thicknesses, Field and Nau (1976) present optically retrieved oscillatory fluid film thicknesses in elastomeric seals for reciprocating motion. In addition, Kalshi (1981) measures an oscillatory lubricated film profile in an O-Ring. These experimental results suggest that oscillatory film thicknesses may be physically realistic. In fact, Nau (1968) notes : "One possibility which might account for the ability of a rectangular seal to function in practice is the existence of an undulating seal profile, i.e. a form of dynamic instability. This certainly seems a possibility at low speeds where "stick-slip" occurs and might extend to speeds at which the characteristic judder is not evident in practice. If dynamic instability occurs then it should be very dependent on the form of construction of the seal, rubber seals would, for instance, be likely to behave differently from seals made of rubberised-fabric." In addition, Kostreva (1984a) writes : "The generalized derivatives used in the above also allow for 'spikiness' and mild singularities in the functions $p\ (x)$, $h\ (x)$ and their derivatives. Features such as these have been observed in some numerical solutions and measured experimentally, and they are physically justifiable."

On the other side, recent experimental readings via fluorescence techniques of the lubricated conjunction zone in elastomeric seals for rotating shafts exhibit smooth profiles (Binnington (1991), Poll, Gabelli, Binnington, and Qu (1992)).

Oscillatory solutions are endemic to a variety of engineering situations. Diffusion-convection problems (Heinrich, Huyakorn, Mitchell, and Zienkiewicz

(1977)), the mechanical analysis of slightly compressible units (Prati and Strozzi (1984)) and the treatment of non-linear dynamic situations (Schulz (1985)) are significant examples. These cases exhibit mathematical analogies which are responsible for the similar numerical instabilities. The terms hourglassing, keystoning, zero energy modes and kinematic modes have also been used in the literature to describe oscillatory results.

This brief and inevitably incomplete review of the numerical difficulties encountered in dealing with lubricated soft contacts shows that there is a need for numerical techniques capable of producing oscillation-free results. In addition, the improvement in the solution regularity should be achieved without compromising the solution accuracy. In this Subsection it is shown that the outcome of oscillations can be placated by employing suitable finite-element schemes which do not affect the solution accuracy. An initial Section deals with the basic equations and the mathematical justification of the appearance of spurious oscillations. There follows a Section devoted to a numerical procedure, namely the Petrov-Galerkin method, which can partially placate the outcome of spurious oscillations. Finally, numerical results are developed and compared to exact test cases, to demonstrate that there are cases in which the numerical undulations are undoubtedly spurious.

These concepts are applied to relatively simple situations, but they may be extended to more complex and realistic configurations with particular regard to soft lubricated contacts.

8.4.2 Mathematical aspects

The relevant equations describing the steady, unidimensional, isothermal, isoviscous, elastohydrodynamic problem have already been reported in eqns (8.2.2.1,3), and they are repeated here for convenience :

$$\frac{d}{d x}\left[\frac{h^3}{\eta}\frac{d p}{d x} - 6 U h\right] = 0 \qquad (8.4.2.1)$$

$$h = L\left[p - p_c\right] \qquad (8.4.2.2)$$

$$p(x_i) = p_i \;;\; p(x_o) = p_o \qquad (8.4.2.3)$$

where h is the fluid film thickness, p is the fluid pressure, p_c is the dry contact pressure, U is the sliding speed, η is the fluid viscosity, p_i and p_o are the inlet and outlet pressures, and x_i and x_o are the inlet and outlet coordinates. In addition, L is a linear, positive-definite, integral operator expressing the lubricated profile compliance.

In the following, the previous basic lubrication equations are manipulated at an analytical level, to obtain expressions capable of justifying the outcome of spurious numerical undulations in the case of soft foundations. Following Rohde's formulation (Rohde and Oh (1975)), it is possible to incorporate equation (8.4.2.2) into equation (8.4.2.1), to obtain a unique operatorial equation in p (see eqn (8.3.2.8)), thus reducing the number of unknown functions from two (p and h) to one (p alone) :

$$\frac{d}{d x}\left[\left[L\{p(x) - p_c(x)\}\right]^3 \frac{d p(x)}{d x} - 6\eta U L\{p(x) - p_c(x)\}\right] = 0 \qquad (8.4.2.4)$$

Equation (8.4.2.4) can be linearized by resorting to Gateaux differentiation Rohde and Oh (1975), Milne (1980)), where ϵ is the analogue of Δx in a usual differentiation. In fact, the expression which follows supplies the analogue of a

Newton-Raphson iteration scheme, where unknown ϵ is a function which, added to the previous starting point, produces a hopefully improved p solution for the next iteration :

$$\frac{d}{d x}\left[\frac{h^3}{\eta}\frac{d \epsilon}{d x}+\left[3\frac{h^2}{\eta}\frac{d p}{d x}-6 U\right] L \epsilon\right]=-\frac{d}{d x}\left[\frac{h^3}{\eta}\frac{d p}{d x}-6 U h\right] \qquad (8.4.2.5)$$

Equation (8.4.2.5) exhibits a certain analogy with the convection-diffusion, second order, ordinary differential equation with constant coefficients (Heinrich, Huyakorn, Mitchell, and Zienkiewicz (1977), Barret and Morton (1980)) :

$$\frac{d}{d x}\left[\frac{d \epsilon}{d x}-P \epsilon\right]=f(x) \qquad x \in [0,1] \qquad (8.4.2.6)$$

In equation (8.4.2.6), P is the Péclet number, which controls the relative importance of the first and second order terms.

In Heinrich, Huyakorn, Mitchell, and Zienkiewicz (1977) it is shown that spurious numerical undulations appear as the Péclet number is increased. In fact, by approximating in eqn (8.4.2.6) the first and second ϵderivatives with respect to x-coordinate according to the usual central difference scheme (Δ represents the distance between two adjacent nodes in a uniform discretization (*e.g.* $(x_{i+1}-x_i)$)), see Timoshenko and Goodier (1970), p. 515 :

$$\frac{d \epsilon(x)}{d x} \simeq \left[\epsilon(x_{i+1})-\epsilon(x_{i-1})\right]/(2\Delta)$$

$$\frac{d^2 \epsilon(x)}{d x^2} \simeq \left[\epsilon(x_{i+1})-2\epsilon(x_i)+\epsilon(x_{i-1})\right]/\Delta^2 \qquad (8.4.2.7)$$

equation (8.4.2.6) can be written as a linear difference equation :

$$\epsilon\,(x_{i+1})\,(1\,-\,\frac{P\,\Delta}{2}\,)\,-\,2\,\epsilon\,(x_i)\,+\,\epsilon\,(x_{i-1})\,(1\,+\,\frac{P\,\Delta}{2}\,)\,\simeq\,\Delta^2\,f\,(x)\qquad x\in[\,0\,,\,1\,]$$

(8.4.2.8)

While a particular solution to equation (8.4.2.8) is difficult to determine for a generic $f\,(x)$ (Padovan and Patuzzo Grego (1981), p. 30), the general solution to the associated homogeneous difference equation to equation (8.4.2.8) is known, and it is based upon the solution of the following characteristic algebraic equation (Bender and Orszag (1984), p. 36 , Hemker (1970)), p. 19) :

$$(1\,-\,\frac{P\,\Delta}{2}\,)\,y^2-\,2\,y\,+\,\,(1\,+\,\frac{P\,\Delta}{2}\,)\,=\,0 \tag{8.4.2.9}$$

whose roots are :

$$y_1\,=\,1\quad;\quad y_2\,=\,\frac{(1\,+\,\frac{P\,\Delta}{2}\,)}{(1\,-\,\frac{P\,\Delta}{2}\,)} \tag{8.4.2.10}$$

so that the general solution to the associated homogeneous difference equation to (8.4.2.8) is :

$$\epsilon_n\,=\,C_1\,\Big[\,1\,\Big]^n\,+\,C_2\,\Big[\,\frac{1\,+\,\frac{P\,\Delta}{2}}{1\,-\,\frac{P\,\Delta}{2}}\,\Big]^n \tag{8.4.2.11}$$

where C_1 and C_2 are two generic constants, and n represent the generic index of the discretization nodes.

As already noted, a particular solution to (8.4.2.8) is difficult to determine for a generic $f\,(x)$ and, therefore, its influence on the mathematical character of

the complete solution to (8.4.2.8) cannot be examined in detail. It is only observed that $f(x)$ is likely to be closely approximated by a polynomial expression in n, say $f(x) \simeq p_0 n^s + p_1 n^{s-1} + p_2 n^{s-2} + \ldots + p_{s-1} n + p_s$ (pressure spikes are unlikely to occur in soft contacts, so that $f(x)$, which corresponds to the right hand-side in (8.4.2.5), should be regular), a case for which a particular solution to (8.4.2.8) possesses the form $n(A_0 n^s + A_1 n^{s-1} + A_2 n^{s-2} + \ldots A_{s-1} n + A_s)$ (since a root of the characteristic algebraic equation (8.4.2.9) is 1, see Padovan and Patuzzo Grego (1981), p. 30), and this particular solution does not evidence an oscillatory character. Instead, the behaviour of the homogeneous solution (8.4.2.11) is thoroughly discussed in the following.

When P is increased (case of soft foundations, see below), root y_2 approaches -1 and, therefore, the ϵ_n solution (8.4.2.11) assumes an undesired oscillating character with respect to the part multiplying coefficient C_2. This negative trend may be limited by the imposition of the boundary conditions, which influence the values of C_1 and C_2. Also, a mesh with an odd number of nodes is more prone to develop oscillations than an analogue discretization with an even number of nodes, since in the first case the undulations are less restrained by the boundary conditions, as it appears from Fig. 9 of Strozzi (1987b). Unfortunately, it is not always possible to use an even number of nodes. A pertinent example can be found in the case of lubricated contacts subject to cavitation when a complementarity approach is adopted for the definition of the pressurized and cavitated profile portions. According to this methodology, a generous estimate of the lubricated contact length is discretized, and a complementarity routine decides which nodes are cavitated, or otherwise (Kostreva (1984a)). In this case it is not possible to know *a priori* whether the pressurized zone is described by an even or by an odd number of nodes.

Going back to the analogy between eqns (8.4.2.5) and (8.4.2.6), this similarity is impaired by the presence of non constant coefficients and of the integral operator L in (8.4.2.5). In fact, due to the lack of constancy of the coefficients of eqn (8.4.2.5), it is difficult to define its equivalent of the Péclet number. (Anyway, variable coefficients are examined *e.g.* by Barret and Norton (1980).) In addition, to recover the simpler, purely differential character in eqn (8.4.2.5), the foundation

operator L , which is usually of integral type as in eqn (8.2.2.9), should be likened to an algebraic operator consisting of a coefficient, K , multiplying function ϵ of equation (8.4.2.5). This assimilation is rigorously feasible only if a Winkler (local) foundation model (see eqn (8.2.2.8)) is adopted, whereas such an expression becomes approximate in the case of integral support models. By accepting a Winkler description for the foundation, so that $L\ \epsilon \simeq K\ \epsilon$, where K is a constant (or a function of x-coordinate, but no longer an integral operator), the equivalent of the Péclet number for equation (8.4.2.5) is essentially obtained as the negative of the ratio between the coefficients of ϵ and of $d\epsilon/dx$:

$$P = K\, l_c \left(\frac{6\,\eta\, U}{h^3} - \frac{3}{h}\,\frac{d\,p}{d\,x} \right) \tag{8.4.2.12}$$

where l_c represents the lubricated contact length, and it appears in (8.4.2.12) as the result of a normalization procedure, since in eqn (8.4.2.6) $x \in [\,0\,,\,1\,]$, whereas in (8.4.2.5) $x \in [\,0\,,\,l_c\,]$.

Aspects connected to the lack of constancy of (8.4.2.12) are examined in the following. Many published numerical fluid film profiles for soft contacts are nearly constant in shape (*e.g.* Ruskell (1980)), so that h in expression (8.4.2.12) can be assumed as essentially constant. It emerges from expression (8.4.2.12) that a decrease in the mean film thickness would generally result in a deleterious increase in the Péclet number. Contrary to the fluid film thickness, dp/dx varies considerably along the lubricated length (in quasi-elliptical pressure profiles, as are those encountered in hip joints, dp/dx changes its sign when proceeding along the lubricated contact), so that a meaningful value of the analogue of the Péclet number is difficult to estimate for a generic situation, since it changes considerably along the sealing length.

Additional uncertainties derive from the evaluation of the Winkler coefficient K . In those plane strain situations for which the elastomeric stratum can easily flow laterally, the Winkler constant of eqn (8.2.2.8) is estimated as (see eqn (11) of Strozzi (1987b)) :

$$K = \frac{h\,(1 - \nu^2)}{E} \qquad (8.4.2.13)$$

where h represents the stratum height.

Conversely, in plane strain cases where the lateral flow is prevented, the Winkler constant of eqn (8.2.2.8) assumes the following expression (see eqn (4.4.2.1.13)) :

$$K = \frac{h\,(1 + \nu)\,(1 - 2\nu)}{E\,(1 - \nu)} \qquad (8.4.2.14)$$

Equation (8.4.2.13) describes for instance rectangular seals whose lateral sides are free to expand, or the elastomeric layer of a hip joint in the case of small contact widths. Conversely, equation (8.4.2.14) applies to rubber cortices of hip replacements in the situation of high contact widths. (The decrease of its accuracy when ν approaches the incompressibility figure 0.5 is discussed in Chapter 4.)

The role of the Poisson's ratio in affecting the Péclet number is examined in the following. It is noted that in eqn (8.4.2.13) constant K does not vanish in the case of incompressible elastomers characterized by $\nu = 0.5$, whereas K of eqn (8.4.2.14) does. This in turn implies that, when scarcely compressible elastomers are employed (a realistic figure for ν is 0.4997), the foundation with restrained lateral movements is much stiffer (*i.e.* K small) than that with free lateral expansions, so that the Péclet number for the first case is considerably smaller than that for the second situation. It can therefore be surmised that, in hip replacements with elastomeric layers, oscillating fluid film profiles are more likely to occur for the lower contact widths and loads. Medley, Dowson and Wright (1984) note the stiff character of the differential equation describing the lubrication of the human ankle joint, especially for high loads. Due to a certain similarity between natural and artificial joints, the above results confirm the suspicion that undulating fluid film profiles may be encountered in the analysis of hip replacements in particular situations.

The role of the Young's modulus is considered hereinafter. Despite the uncertainties in the selection between eqns (8.4.2.13) and (8.4.2.14), the above-mentioned Winkler constant, K , is in any case inversely proportional to the Young's modulus. As a consequence, a decrease in the Young's modulus would result in a detrimental increase in the Péclet number. The circumstance of a low E occurs in soft lubricated contacts, characterized by elastomeric foundations.

In conclusion, despite the above examined uncertainties, expression (8.4.2.12) supplies a mathematical justification for the possible appearance of spurious numerical oscillations in the case of lubricated soft contacts.

It is finally noted that in Strozzi (1987b) a more compact expression of the maximum Péclet number is proposed by resorting to classical results of the inverse hydrodynamic theory (Theyse (1967)).

It should be also underlined that the possible occurrence of undulations refers to eqn (8.4.2.5) which, as already noted, describes a functional Newton iteration. In other words, the previous observations show that, in the case of soft foundations, every Newton iteration solution and, consequently, the converged solution, should be affected by oscillations. Conversely, Rohde and Oh (1975) explicitly observe that "The 'wiggles' disappear as the iteration process continues.", a numerical finding which does not fit with the above theoretical observations. In addition, it is observed that eqn (8.4.2.5) can be simply interpreted as a linearization of eqn (8.4.2.4), so that the above discussed relationship between the Péclet number and the outcome of oscillations should be valid independently of the solution method employed.

8.4.3 Numerical schemes

This Section aims at briefly illustrating the salient aspects of the numerical procedure adopted, more than at presenting the computational details.

The numerical scheme to be analyzed in this work is based on the Petrov-Galerkin procedure. Contrary to the more conventional Galerkin approach, in the more flexible Petrov-Galerkin method the test and the trial functions (Becker, Carey, and Oden (1981)) are not necessarily selected from the same finite-dimensional space. For instance, the trial functions are chosen to be piecewise-linear, while the test functions can be selected among piecewise-quadratic polynomials (Heinrich, Huyakorn, Mitchell, and Zienkiewicz (1977)). Linear and quadratic test functions are compared in Fig. 8.4.3.1 . If the test functions degenerate into a conventional piecewise-linear profile, the corresponding finite element method supplies the analogue of the central difference in a finite difference scheme (Heinrich, Huyakorn, Mitchell, and Zienkiewicz (1977)). As the degree of asymmetry of the test functions is increased (which consequently assume a sail-shaped profile), the corresponding finite element method becomes the equivalent of the upwind finite difference scheme. Anyway, the finite element method is more general than the finite difference approach, since intermediate solutions between the central difference and the upwind schemes can be easily obtained (Heinrich, Huyakorn, Mitchell, and Zienkiewicz (1977)), while they can be hardly rationalized if finite-difference descriptions are used (Okamura (1982)). Computational details on the asymmetric test functions can be found in Strozzi (1987b).

According to a central difference approximation, the oscillatory curve of Figure 8.4.3.2 is very regular, since angles φ_i , which represent the first derivatives at nodes i , change smoothly from one node to the next. What is considerably irregular is the second derivative, but its relative importance in the numerical treatment of Reynolds equation for soft contacts is limited with respect to the first derivative component. In fact, the latter component is amplified by the presence of the Péclet number, which is particularly high in soft contacts. An asymmetry of the test function will result in situations like that depicted in Figure 8.4.3.2 no longer being interpreted as regular from the first derivative viewpoint. Since the

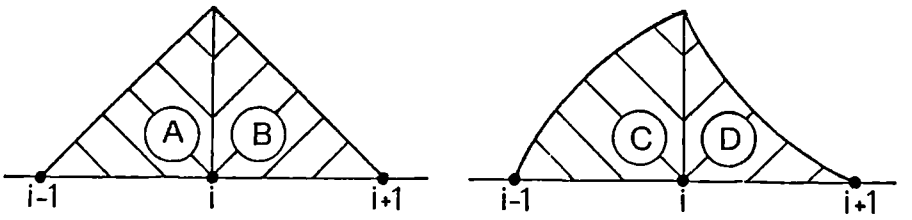

Fig. 8.4.3.1 : Piecewise-linear (left) and piecewise-quadratic (right) test functions referring to node i.

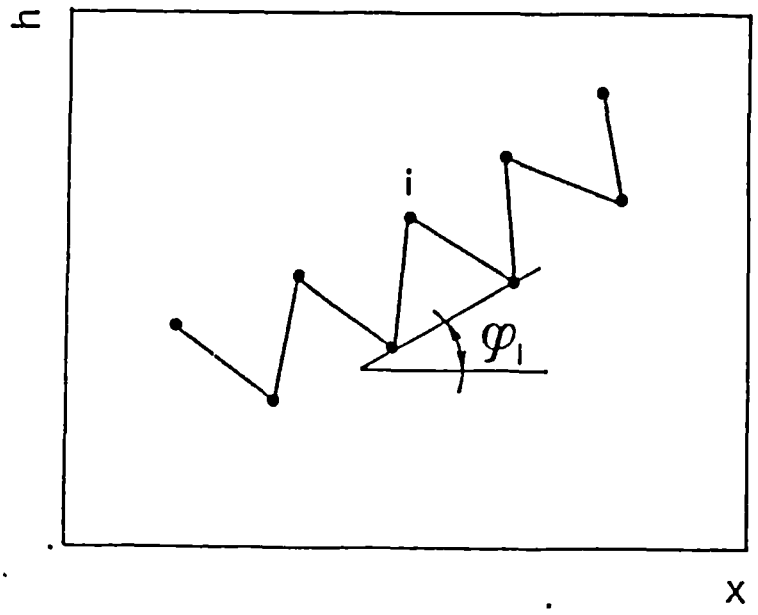

Fig. 8.4.3.2 : The oscillatory curve is very regular according to the central difference scheme.

regularity of the first and second derivatives is embedded in the analytical description of the EHL problem, curves as irregular as that of Fig. 8.4.3.2 are less likely to be produced by a Petrov-Galerkin scheme based on asymmetric test functions. On the other side, if an unduly high asymmetry is adopted for the test functions, the consequence will be a spurious tendency of the solution towards an unrealistic, nearly straight profile. In other words, the more asymmetric the test functions, the stiffer the solution is expected to become (Heinrich, Huyakorn, Mitchell, and Zienkiewicz (1977)). It can be speculated that in some cases a suitable value of the asymmetry of the test functions will exist which permits the receipt of regular profiles in terms of fluid film thickness without compromising the solution accuracy. The next Subsection examines the effects of different degrees of asymmetry on the solution regularity in terms of fluid film thickness, and compares the numerical forecasts to theoretical solutions obtained according to Section 8.2 .

For the time being, only degrees of asymmetry which are kept constant along the lubricated contact have been tested in the following Section.

8.4.4 Results

A series of numerical results concerning lubricated elastomeric seals are presented in this Subsection. They are compared to the exact solutions according to Section 8.2 , to retrieve indications about the ability of the proposed approach to prevent the above spurious undulations without compromising the solution accuracy. To limit numerical convergence problems (See Section 8.3), the exact solution was always assumed as the starting point for the Newton-Raphson process.

The first case examined is that of a nearly straight fluid film profile defined between inlet and outlet coordinates $x_i = 0$ and $x_o = 6$ mm, depicted in Figure 8.4.4.1 . In addition, $E = 10$ MPa, $\eta = 0.43 \times 10^{-6}$ Mpa s , $U = 400$ mm/s , while the deformed seal radial height is 6 mm. In addition, 100 nodes are employed in the discretization process. In this case the numerical film profile is oscillation-free even when the standard Galerkin method (Prati and Strozzi (1984)) is used .

Different results are obtained in the case of the film profile of Figure 8.4.4.2 , which is considerably more inclined than the previous one. This circumstance suggests that in this case spurious undulations are more prone to occur. In fact, the numerical results of Okamura (1982) and of Barret and Morton (1980) indicate that the oscillations of the solution are somewhat fomented by high gradients and by rapid variations of the curve slope. Also, the mean film thickness is lower than that of Figure 8.4.4.1 , and this fact is responsible for the analogue of the Péclet number assuming higher values (See Section 8.4.2). This is qualitatively confirmed by the numerical results of Fig. 6a of Field and Nau (9175), where the amplitude of the film profile undulations remains essentially the same as the reciprocating speed diminishes, that is, as the mean film thickness decreases. As a consequence, the relative importance of the film profile oscillations increases as the mean film thickness diminishes in the paper by Field and Nau (9175). The remaining variables are as in the previous example. Consistent with the increase of the Péclet number, in the case of Figure 8.4.4.2 a conventional Galerkin method produces an oscillatory fluid film profile. Despite this fact, the convergence rate is still very good.

The spurious undulations of Figure 8.4.4.2 are fully eliminated by assuming

asymmetric test functions. The degree of asymmetry used in Figure 8.4.4.3 is taken as constant and equal to 0.5 , that is, a first derivative definition which is the mean between the finite element analogue of an upwind and a central difference scheme is adopted. Interestingly, Figure 8.4.4.3 demonstrates that the spurious undulations of Figure 8.4.4.2 are fully removed without compromising the solution accuracy.

The third example aims at simulating an experimentally measured film profile (Field and Nau (1973)). Such a curve was interpolated via a fourth-degree polynomial describing the inverse of the analytical film curve (see Section 8.2.2). In Figure 8.4.4.4 , which coincides with Fig. 8.2.2.3 and is here repeated for convenience, analytical and experimental film profiles are compared. This is a particularly complex film shape. In fact, the curve gradient is very high by the inlet and, contrary to the numerical results characterized by a nearly constant film profile, in this experimental curve the highest film thickness exceeds the lowest value by a factor of 5. This circumstance implies that the Péclet number varies considerably along the sealing profile. The remaining variables, borrowed from Field and Nau (1973), are $x_i = 0$, $x_o = 9.72$ mm , $\eta = 0.026\ 10^{-6}$ MPa s , $U = 152.4$ mm/s, while the compressed seal radial height is 6.223 mm. The pressure profile corresponding to the film thickness mentioned above is displayed in Figure 8.4.4.5 , in which the inlet and outlet sealed pressures are chosen so that the dry contact pressure vanishes for $E = 100$ MPa (see Section 8.2.2). Anyway, for low values of the Young's modulus, the fluid pressure of Figure 8.4.4.5 is scarcely affected by E.

In the case of a relatively stiff foundation model (E ranging from 210000 MPa to 500 MPa), the solution in terms of film thickness is very regular and superimposed to the exact solution, and therefore the corresponding results are omitted.

If a less stiff support is adopted ($E = 200$ MPa), some wiggles appear by the inlet when a conventional Galerkin method is used (Figure 8.4.4.6). This agrees with Fig. 6c of Field and Nau (1975), which shows a worsening of the solution regularity as the foundation becomes softer. No improvement in the solution regularity is achieved by employing a constant asymmetry factor of 0.01 - 0.05 , while with higher factors (0.2) the solution iterative scheme diverges.

Finally, in the case of a soft foundation model (E = 20 MPa , Field and Nau (1973)), a standard Galerkin scheme produces highly oscillatory results (Figure 8.4.4.7). As already noted, the numerical results of Okamura (1982) and of Barret and Morton (1980) suggest that the undulations are promoted by high gradients and by rapid variations of the curve slope. Interestingly, the wiggles become more pronounced in a plateau region for the film thickness. Also, in this case the convergence of the numerical procedure is somewhat undefined, since during the Newton iterations the pressure curve is very stable, while the film profile changes appreciably.

Then, asymmetric test functions (with an asymmetry factor of 0.2) were introduced (Figure 8.4.4.8). In this case, part of the solution becomes oscillation-free, but also stiffer, since it tends to a nearly straight curve. Unfortunately, the more pronounced oscillations of Figure 8.4.4.7 explode, and they are not represented in detail in Figure 8.4.4.8 . This anomalous behaviour is possibly ascribable to the presence of an extended second derivative inflection zone for the fluid pressure profile. Anyway, such a behaviour could not be properly rationalized, and further numerical experiments are necessary to clarify the connection between spurious, pronounced oscillations in terms of film thickness and extended inflection zones for the fluid pressure curve. In addition, this example suggests that, consistent with the pronounced lack of constancy of the Péclet number along the sealing profile, a non constant asymmetry factor should be employed, where the higher values should be used where the fluid film undulations tend to be more pronounced.

Moving to the specific problem of lubricated hip joints, the geometry examined in Chapter 7 exhibits the presence of an elastomeric layer adherent to a rigid backing forming the cup. The Young's modulus of the elastomer employed is low (typically of the order of 3 - 50 MPa (O'Carrol, Jin, Dowson, Fisher, and Jobbins (1991)), which suggests to classify this foundation as very soft. On the other side the rubber, at least in the case of high contact widths and in the vicinity of the hip symmetry axis, undergoes an essentially hydrostatic compression. As a consequence of a Poisson's ratio approaching.the incompressibility figure 0.5 , the elastomer behaves as stiff, so that the foundation as a whole should not be too soft. It is felt that, in the case of high contact widths, that is, of highly loaded

joints, the elastomeric support should behave as sufficiently rigid to prevent the outcome of spurious numerical undulations in terms of fluid film profile. In fact, the numerical results of Jin (1988) do not show vibrating film thicknesses. Conversely, when the load diminishes during walking, and the consequent diminution of the contact width does not prevent the rubber lateral flow, the foundation should become softer and regularity problems might appear.

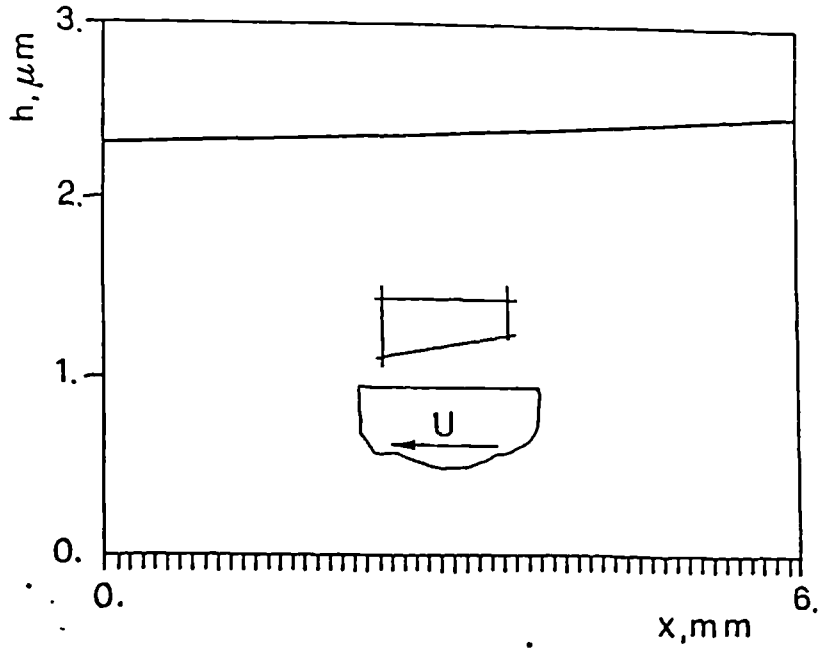

Fig. 8.4.4.1 : The case of a nearly straight fluid film profile.

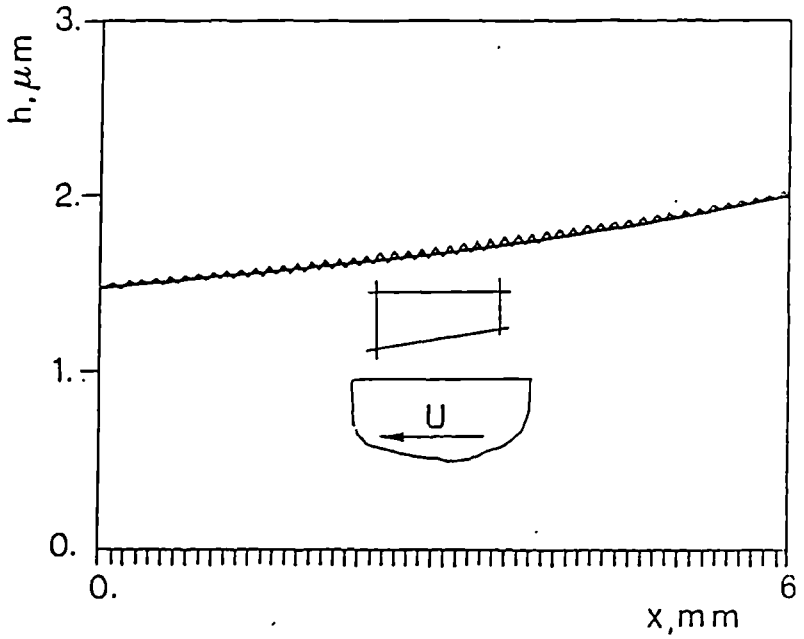

Fig. 8.4.4.2 : The exact fluid film profile and the numerical, oscillatory curve for a convergent profile.

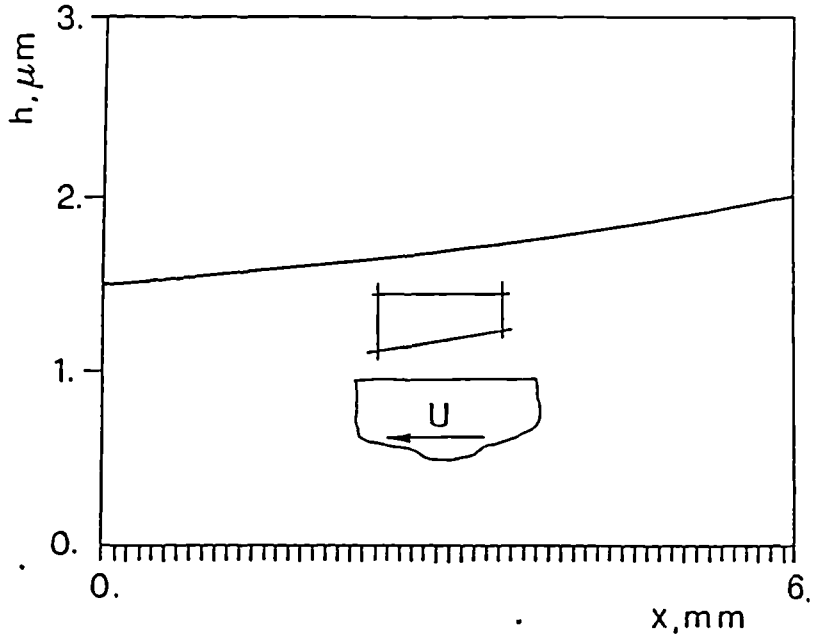

Fig. 8.4.4.3 : The numerical oscillations of Figure 8.4.4.2 are eliminated by using asymmetric test functions.

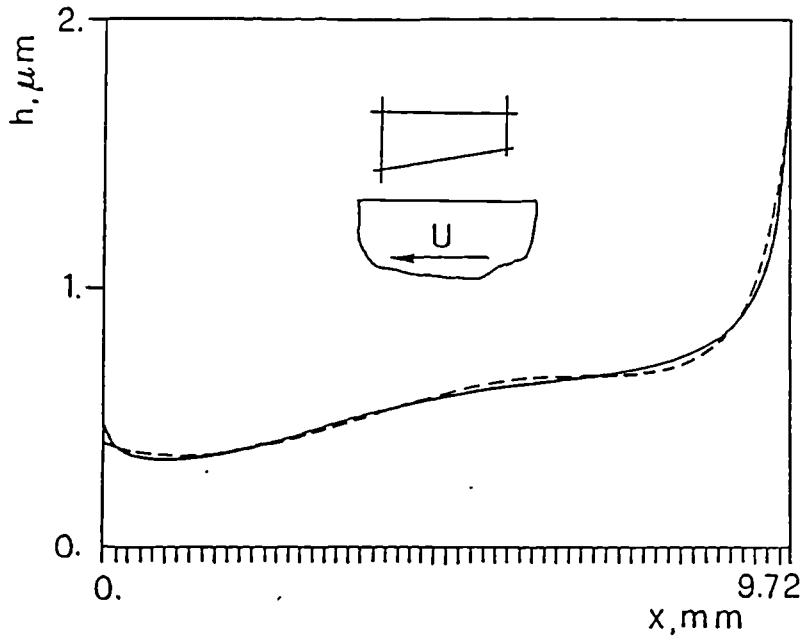

Fig. 8.4.4.4 : Experimental (-----) and analytical (- - - -) fluid film profiles.

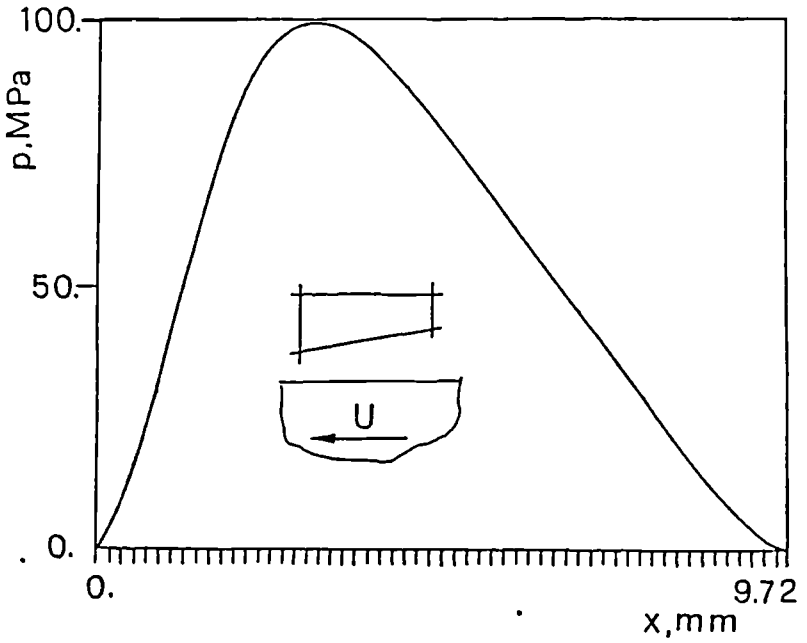

Fig. 8.4.4.5 : The pressure profile corresponding to the film thickness of Figure 8.4.4.4.

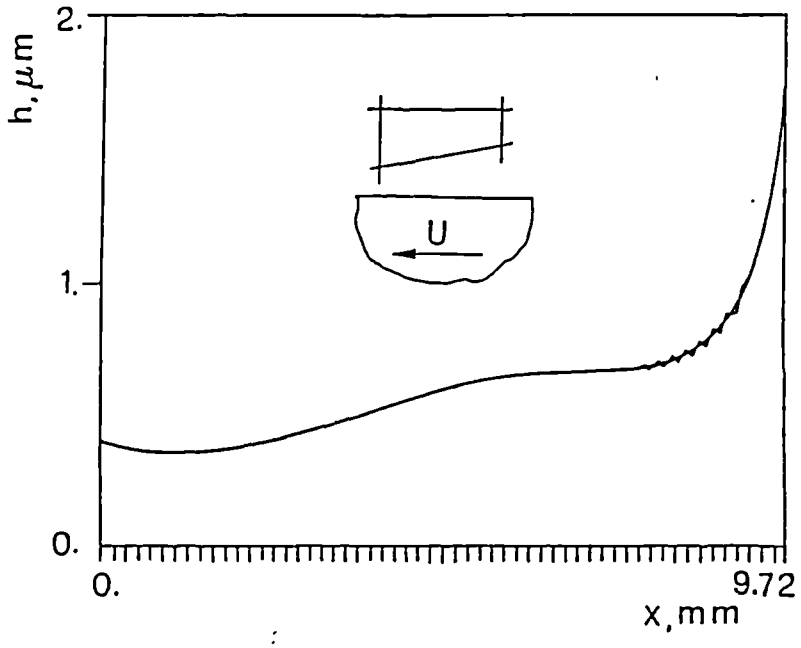

Fig. 8.4.4.6 : Some wiggles appear at the inlet for E = 200 MPa.

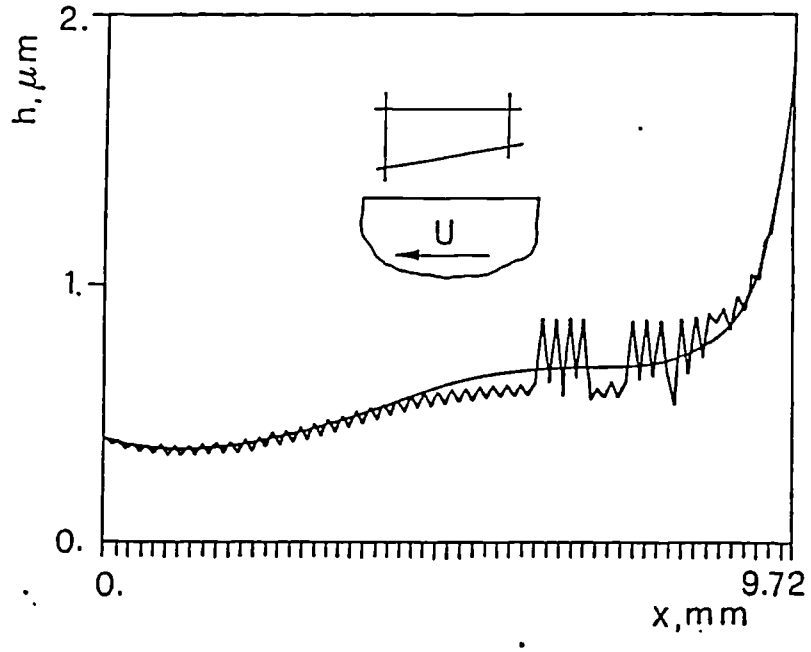

Fig. 8.4.4.7 : The solution is very irregular for E = 20 MPa.

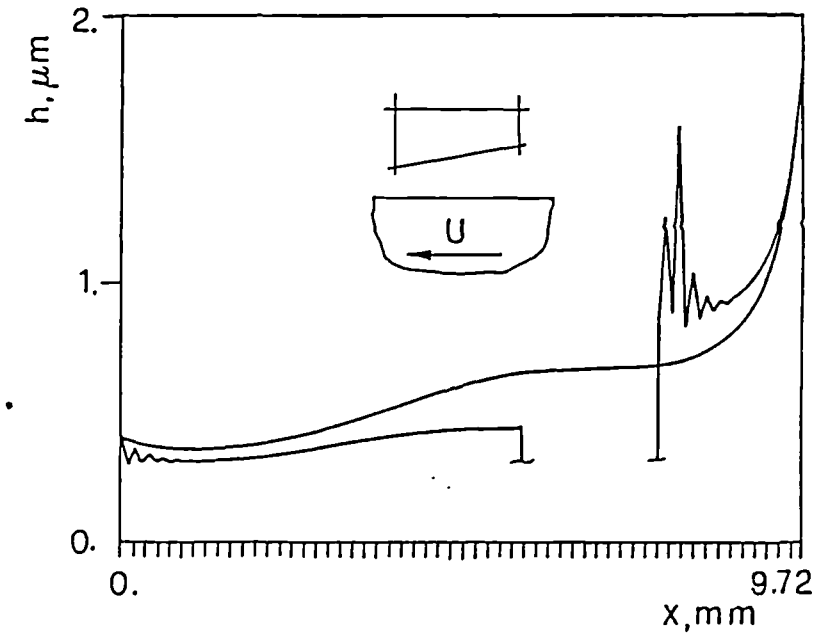

Fig. 8.4.4.8 : The use of asymmetric test functions improves part of the solution, but it worsens the other part.

8.4.5. Conclusions

A method which permits the obtaining of closed form solutions to be used as test cases has been presented. The possible outcome of spurious undulations in the numerical description of the fluid film profile has been rationalized by introducing the analogue of the Péclet number. It is shown that spurious undulations are prone to occur when the Péclet number is particularly high.

The numerical tests performed refer to lubricated rubber seals, but speculations are also presented concerning the applicability of the procedures developed to hip replacements. These numerical tests show how to limit the outcome of spurious numerical oscillations. When the analytical fluid film profile does not substantially deviate from constancy, the numerical oscillations can be placated by employing a numerical procedure based upon the Petrov-Galerkin method with a constant asymmetry factor in the test functions. When high gradients occur in the analytical fluid film curve, the performance of the proposed numerical method is unsatisfactory. In these cases, the numerical results achieved suggest that asymmetric test functions with a variable asymmetry factor along the sealing profile may be advantageous.

8.5 GENERAL CONCLUSIONS

Some robust analytical tools have been presented, which are useful in the numerical solution of the EHL problem and which are reliable and/or fast. In particular, a method has been developed for constructing closed form solutions to the stationary EHL problem in plane cases, to be used as test cases in validating numerical codes. Secondly, an extended variational formulation for the stationary EHL problem in plane situations, which possesses local minimum properties in the solution neighbourhood, has been developed, and a relaxation solver which exploits the mihimum properties has been implemented and tested numerically. Third, a mathematical justification of the possible appearance of spurious numerical undulations in the fluid film thickness has been derived, *and numerical schemes* acting as palliatives on the film undulations have been tested numerically, obtaining satisfactory results in simple cases.

Most of the numerical tests presented in this Chapter refer to soft lubricated contacts mimicking elastomeric seals. Anyway, some speculations about the possible usefulness of such tools if applied to the lubrication of hip joints with soft layers have also been formulated.

CHAPTER9 . OVERALL CONCLUSIONS

9.1 INTRODUCTION

9.1.1 On the experimental measurement of the Poisson's ratio in elastomers

9.1.2 On the geometry of a deformable, flat layer indented by a rigid cylinder

9.1.3 On the geometry of deformable, curved layer indented by a rigid cylinder

9.1.4 On the geometry of deformable, flat layer indented by a rigid sphere

9.1.5 On the geometry of deformable, spherical layer indented by a rigid sphere

9.1.6 On the validity range of some approximations

9.1.7 On the elastohydrodynamic lubrication problem in hip joints

9.1 INTRODUCTION

A comprehensive theoretical and partially experimental mechanical analysis has been presented for a particular type of hip replacements, possessing an elastomeric layer firmly bonded to a rigid cup, and indented by a rigid head. Various models of increasing adherence to the actual geometry have been mechanically analyzed, namely : a) a cylinder compressing a flat covering ; b) a cylinder penetrating a curved stratum ; c) a sphere indenting a flat cortex ; d) a sphere squeezing a spherical lining. In addition, the Poisson's ratio for the elastomer adopted has been experimentally measured. Some theoretical-numerical tools useful in tackling the lubrication of hip joints have also been developed. Finally, a complementary introduction to the theory of elasticity in finite deformations has been included.

The following conclusions have been drawn from the present study :

9.1.1 On the experimental measurement of the Poisson's ratio in elastomers

A piston device has been built to measure the Poisson's ratio of elastomeric materials. Theories have been developed to correct the experimental measurements by accounting for elastic distortions of the device and possible extrusions of the elastomeric specimen. In particular, an existing theory for predicting the deformations of a hollow cylinder subject to an axisymmetrical radial pressure along part of its inner contour has been corrected and further extended. Apparent and compensated values of the cubic compressibility have been obtained for two elastomers, which indicate the relative importance of such corrections.

9.1.2 On the geometry of a deformable, flat layer indented by a rigid cylinder

An existing integral-type, perturbation solution for cylindrical indenters and small contact widths has been corrected with the aid of an algebraic manipulator, and extended to include higher-order perturbation terms. It has been shown that a sixth order perturbation theory is a good trade-off between simplicity and accuracy. Similarly, and existing differential approach for cylindrical indenters and large contact widths has been further developed to cover higher order terms, and its limits when dealing with very large contact lengths have been explored and attributed to the circumstance that the imposed boundary conditions become questionable for high perturbation orders.

An analytical approximate Green function has been developed which forms the basis of an integral formulation solved via a finite element approach, capable of treating a generic indenter profile. Comparisons with other methods have shown that this approach is accurate. The results retrieved indicate that the contact pressure for an imposed contact penetration depth is very sensitive to perturbations of the Poisson's ratio especially when the following situations occur simultaneously: a) the Poisson's ratio is close to its incompressibility figure 0.5 ; b) the contact width is considerably larger than the layer thickness. The modifications in the contact pressure when passing from a cylindrical indenter to a parabolic approximation have been explored numerically and found to be negligible in biomechanical applications.

9.1.3 On the geometry of deformable, curved layer indented by a rigid cylinder

A series solution has been developed with the aid of an algebraic manipulator for a deformable annulus firmly bonded to a rigid substrate along one periphery and subject to a concentrated radial force acting at the other contour. Series acceleration techniques have been developed. .Contrary to the previous treatments, this solution does not degenerate for Poisson's ratios equal to half. This Green function has been exploited to treat numerically the biomechanically relevant case

of a deformable annulus indented by a rigid cylinder. The effects of curvature and Poisson's ratio perturbations have been explored numerically, and they have been found to become significant in geometries of interest in biomechanical problems. More exactly, the effects of layer curvature have been examined separately from those referring to the circumstance that the actual indentation curve of the cylinder is not precisely described by a cylindrical or parabolic profile. It has been found that the pure curvature effects are modest, whereas those deriving from the approximations in the description of the indenter profile are appreciable. As a consequence, a reliable mechanical model of a curved layer can be achieved by considering a flat layer approximation compressed by an indentation curve recreating the actual gap between the layer loaded border and the indenting cylinder.

The shear stress at the interface between layer and foundation has been examined analytically, and it has been clarified that, for an imposed load, the maximum interface shear stress decreases as the layer thickness is increased.

Finally, four configurations have been examined experimentally in terms of pressure profile and contact width versus indentation, and they have been found to agree reasonably with the theoretical forecasts, where the possible causes of errors have been discussed.

9.1.4 On the geometry of deformable, flat layer indented by a rigid sphere

A perturbation solution of the problem of a deformable layer indented by a rigid sphere has been obtained with the aid of an algebraic manipulator. This solution is valid for ratios of contact radius to layer thickness up to 0.7 . Inaccuracies in an existing analytical iterative solution have been signalled. Finite element forecasts have been achieved for higher compressions, and the sensitivity of the numerical previsions to perturbations of Poisson's ratio has been explored. For an imposed indentation and for large contact radii, the axisymmetric peak contact pressure is about three times lower than its plane strain counterpart,

whereas the axisymmetric and plane contact radii are comparable. For small contact radii, the plane and axisymmetric results are more similar.

9.1.5 On the geometry of deformable, spherical layer indented by a rigid sphere

A finite element mechanical analysis has been performed for a sphere indenting a half-spherical layer, a geometry which mimics hip replacement possessing an elastomeric lining. Four basic geometries have been analyzed in the idealized situation of axial loading, and the total load, peak pressure, maximum interface shear stress as well as their locations have been diagrammatically reported versus the head indentation depth. Then, modified geometries and situations have been explored, by altering the initial head-layer gap, the Poisson's ratio, the angular extent of the elastomeric layer, and by approximating the spherical shape of the indenter with a paraboloidal profile. The results retrieved suggest that for a given load the peak pressure and the maximum shear stress diminish as the layer thickness is increased, thus providing practically relevant indications about the selection of the optimal layer thickness. In addition, the marked sensitivity of peak contact pressure to Poisson's ratio perturbations, especially when the head-layer initial gap diminishes, evidences the need for an accurate experimental measurement of ν . In any case, as a consequence of the above reported sensitivity to ν, it seems wise not to adopt very small head-layer gaps in practical applications.

9.1.6 On the validity range of some approximations

Validity intervals of simplified modellings are extracted from the various results obtained in this thesis. The applicability fields here reported are inevitably qualitative.

The asymptotic, incompressible solution (eqns (4.4.2.2.8) and (4.4.2.2.11) for the plane case, and (6.5.2.1) for the axisymmetric case) holds when $\delta\ R/h^2 > 25$,

that is, $a/h > 10$ (Sections 4.3.5 and 6.6). Within this range, the asymptotic solution holds when a) the elastomer is essentially incompressible ($\nu > 0.4999$, Section 4.4.4) ; b) the indenter is parabolic (or paraboloidal).

The Winkler solution applies when $\nu < 0.48$ and the ratio of contact semiwidth (or radius) to layer thickness > 10 (Section 4.4.4)

The parabolic approximation for the circular indenter profile is acceptable when the contact semiwidth (or radius) is defined by an angle < 1 radians (Section 7.3.6), which often corresponds to a ratio of contact radius to head radius (or, to layer curvature radius, the clearance between head and layer being small) in the region of 0.7 (Section 7.3.6).

When $\delta R/h^2 > 100$, that is, $a/h > 20$, the stress field is particularly sensitive to perturbations of the Poisson's ratio (Section 7.3.4).

The maximum shear stress at the interface between elastomeric layer and rigid backing is of the order of 1/10 the maximum contact pressure between head and layer (Section 7.3.2).

9.1.7 On the elastohydrodynamic lubrication problem in hip joints

Some robust analytical tools have been presented, which are useful in the numerical solution of the EHL problem and which are reliable and/or fast. In particular, a method has been developed for constructing closed form solutions to the stationary EHL problem in plane cases, to be used as test cases in validating numerical codes. Secondly, an extended variational formulation for the EHL problem in plane situations, possessing local minimum properties in the solution neighbourhood, has been developed, and a relaxation solver which exploits the minimum properties has been implemented and tested numerically. Third, a mathematical justification of the possible appearance of spurious numerical undulations in the fluid film thickness has been derived, and numerical schemes

acting as palliatives on the film undulations have been tested numerically, obtaining satisfactory results in simple cases. Most of the numerical tests have dealt with soft lubricated contacts mimicking elastomeric seals. Anyway, some speculations about the possible usefulness of such tools if applied to the lubrication of hip joints with soft layers have also been formulated.

CHAPTER 10. REFERENCES

ABAQUS *User's Manual* (1989), Hibbitt, Karlsson and Sorensen, Inc.

Abramian, B. L., Arutiunian, N. Kh. and Babloian, A. A. (1964). "On two-contact problems for an elastic sphere." *J. Math. Mech* (*PMM*), 28 (4), pp. 622-629 .

Abramian, B. L., Babloian, A. A. (1962). "On a contact problem connected with the torsion of a hollow semisphere." *J. Math. Mech* (*PMM*), 26 (3), pp. 471-480 .

Abramowitz, M., and Stegun, I.A. (1972) . *Handbook of Mathematical Functions*. Dover Publ., New York.

Ahmadi, N., Keer, L.M., and Mura, T. (1983). "Non-hertzian contact stress analysis for an elastic half space - normal and sliding contact.", *Int. J. Solids Struct.*, 19, pp. 357-373.

Alblas, J.B., and Kuipers, M. (1969). "Contact problems of a rectangular block on an elastic layer of finite thickness. Part I: the thin layer." *Acta Mech.* 8, pp. 133-145.

Alblas, J.B., and Kuipers, M. (1970). "Contact problems of a rectangular block on an elastic layer of finite thickness. Part II: the thick layer." *Acta Mech.* 9, pp. 1-12.

Alblas, J.B., and Kuipers, M. (1970). "On the two dimensional problem of a cylindrical stamp pressed into a thin elastic layer. " *Acta Mech.* 9, pp. 292-311.

Alexander, H. (1968). "A constitutive relation for rubber-like materials." *Int. J. Engng Sci.*, 6, pp. 549-563 .

Aleksandrov, V.M. (1962). "On the approximate solution of a certain type of integral equations." *J. Math. Mech.* (*PMM*), 26 (5), pp. 934-943.

Aleksandrov, V.M. (1963a). "Some contact problems for the elastic layer." *J. Math. Mech.* (*PMM*), 27 (4), pp. 1165-1174.

Aleksandrov, V.M. (1963b). "On the solution of certain contact problems of the theory of elasticity." *J. Math. Mech.* (*PMM*), 27 (5), pp. 970-972 .

Aleksandrov, V.M. (1967). "On the approximate solution of some integral equations of the theory of elasticity and mathematical physics." *J. Math. Mech.* (*PMM*), 31 (6), pp. 1117-1131.

Aleksandrov, V.M. (1969). "Asymptotic solution of the contact problem for a thin elastic layer." *J. Math. Mech.* (*PMM*), 33 (1), pp. 61-73.

Aleksandrov, V.M. (1970). "On plane contact problems of the theory of elasticity in the presence of adhesion or friction." *J. Math. Mech.* (*PMM*), 34 (2), pp. 246-257 .

Aleksandrov, V.M. (1975). "On a method of reducing dual integral equations and dual series equations to infinite algebraic systems." *J. Math. Mech.* (*PMM*), 39 (2), pp. 324-332 .

Aleksandrov, V.M. , and Babeshko, V.A. (1972). "On the pressure of an elastic half-space by a wedge-shaped stamp." *J. Math. Mech.* (*PMM*), 36 (1), pp. 88-93 .

Aleksandrov, V.M. , Babeshko, V.A., and Kucherov, V.A. (1966). "Contact problems for an elastic layer of slight thickness." *J. Math. Mech.* (*PMM*), 30 (1), pp. 124-142 .

Aleksandrov, V.M. , and Chebakov, M.I. (1980). "On am method of solving dual integral equations." *J. Math. Mech.* (*PMM*), 37 (6), pp. 1087-1097 .

Aleksandrov, V.M. , and Karpenko, V.A. (1980). "Torsion of a spherical layer by a spherical annular stamp." *J. Math. Mech.* (*PMM*), 44 (1), pp. 143-150 .

Aleksandrov, V.M., and Vorovich, V.M. (1960). "The action of a die on an elastic layer of finite thickness." *J. Math. Mech.* (*PMM*), 24 (2), pp. 323-333 .

Aleksandrov, V.M., and Vorovich, V.M. (1964). "Contact problems for the elastic layer of small thickness." *J. Math. Mech. (PMM)*, 28 (2), pp. 350-351 .

Alexander (1968). "A constitutive relation for rubber-like materials." *Int. J. Engng Sci.*, 6, pp. 549-563 .

Alliney, S., Strozzi, A., and Tralli, A. (1985). "Extended variational formulations and finite element models for the elastohydrodynamic lubrication problem." *Engineering Computations*, 2, pp. 145-151 .

Alliney, S., and Tralli, A. (1984). "Extended variational formulations and F.E. models for nonlinear beams under nonconservative loading." *Comp. Methods Appl. Mech. Engng*, 46, pp. 177-194 .

Alliney, S., and Tralli, A. (1985). " 'Extended variational formulations and F.E. models for nonlinear non-conservative mechanical problems." *Comp. Meth. Appl. Mech. Engng*, 51, pp. 209-219 .

Al-Qureshi, H.A., and Das, M.K. (1976). "Thin-walled cropping using elastomer." *Int. J. Mach. Tool Des. Res.*, 16, pp. 77-85 .

Aquaro, G. (1949). "Sul calcolo delle deformazioni di uno strato sferico elastico." *Atti dell'Accademia Nazionale dei Lincei, Classe di Scienze Fisiche, Matematiche e Naturali*, 7, pp. 289-297 .

Armstrong, C.G. (1985). "Stress analysis of a thin layer of soft tissue over a bony support." *Material Properties and Stress Analysis in Biomechanics (Proceedings)*, Institute of Physics, Brunel University, Paper 14, pp. 74-79 .

Armstrong, C.G. (1986). "An analysis of the stresses in a thin layer of articular cartilage in a synovial joint." *Engineering in Medicine*, 15 (2), pp. 55-61.

Armstrong, C.G. (1988). Private communication.

Arutiunian, N. Kh., Abramian, B. L. (1964). "On the impression of a rigid die into an elastic sphere." *J. Math. Mech (PMM)*, 28 (6), pp. 1101-1105 .

Auger, D. D., Medley, J. B., Fisher, J. and Dowson, D. (1990). "A preliminary investigation of the 'cushion bearing' concept for joint replacement implants." *Mechanics of Coatings*, Elsevier, N.Y. , pp. 251-269 . *Proceedings of the 16th Leeds-Lyon Symposium on Tribology*, Lyon, France, 5th-8th September 1989.

Austin, R.M., Flitney, R.K., and Nau, B.S. (1977). *Research into factors affecting reciprocating rubber seal performance.* RR 1449, BHRA, December 1977.

Babeshko, V.A. (1966). "On an asymptotic method applicable to the solution of integral equations in the theory of elasticity and in mathematical physics." *J. Math. Mech. (PMM)*, 30 (4), pp. 732-741 .

Bandera, C., and Strozzi, A. (1991). "Integrazione di metodologie computer aided: esperienze didattiche." 7° *Convegno Nazionale Associazione Disegno di Macchine*, Trento, 2 - 4 Ottobre 1991, pp. 579-589 (in Italian).

Bapat, C., and Batra, R.C. (1982). "Indentation of a viscoelastic rubber covered roll by a rigid plane surface." *Mech. Res. Communications*, 9 (4), pp. 265-272.

Bapat, N.C., and Batra, R.C. (1984). "Finite plane strain deformations of nonlinear rubber-covered rolls." *Int. J. Num. Methods in Engng*, 20, pp. 1911-1927 .

Barber, J.R. (1990). "Contact problems for the thin elastic layer." *Int. J. Mech. Sci.*, 32 (2), pp. 129-132 .

Bariani, P. (1977). "Stresses and displacements in the finite hollow circular cylinders under axisymmetric loading." *Vth Italian National Meeting AIAS, Bari, Italy*, pp. 1-20 (in Italian).

Bariani, P. (1983a). "Elastic behaviour of shrink-fitted forming die assemblies. Part I: development of an analytical solution." *Meccanica*, 18, *pp.* 21-29 .

Bariani, P. (1983b). "Elastic behaviour of shrink-fitted forming die assemblies. Part II: numerical applications and results." *Meccanica*, 18, *pp.* 97-106 .

Barret, J.W., and Morton, K.W. (1980). "Optimal finite element solutions to diffusion-convection problems in one dimension." *Int. J. Num. Methods Engng*, 15, pp. 1457-1474 .

Barret, J.W., and Morton, K.W. (1981). "Optimal Petrov-Galerkin methods through approximate symmetrization." *IMA J. Numer. Anal.*, 1, pp. 439-468 .

Barret, J.W., and Morton, K.W. (1984). "Approximate symmetrization and Petrov-Galerkin methods for diffusion-convection problems." *Computer Methods in Applied Mechanics and Engng*, 45, pp. 97-122 .

Bartel, D. L., Burstein, A. H., Toda, M.D. and Edwards, D. L. (1985). "The effect of conformity and plastic thickness on contact stresses in metal-backed plastic implants." *ASME J. Biomech. Eng.*, 107 (3), pp. 193-199 .

Barton, M.V. (1941). "The circular cylinder with a band of uniform pressure on a finite length of the surface." *J. Appl. Mech.*, 10, pp. A173-175 .

Bathurst, R.J., and Rothenburg, L. (1988). "Note on a random isotropic granular material with negative Poisson's ratio.", *Int. J. Engng Sci.*, 26 (4), pp.373-383 .

Batra, R.C. (1977). "Cold sheet rolling, the thermoviscoelastic problem, a numerical solution." *Int. J. Num. Methods Engng*, 11, pp. 671-682.

Batra, R.C. (1978). "Cold rolling of a laminated composite sheet-a numerical solution." *Int. J. Num. Methods in Engng*, 12, pp. 429-435 .

Batra, R.C. (1980 a). "Rubber covered rolls - the nonlinear elastic problem." *ASME J. Appl. Mech.*, 47, pp. 82-86.

Batra, R.C. (1980b). "Finite plane strain deformations of rubberlike materials." *Int. J. Num. Methods in Engng*, 15, pp. 145-160 .

Batra, R.C. (1980c). "Contact of a rubberlike roll cover with a rigid plane surface." *Proceedings 2nd Int. Congress on Numerical Methods for Engineering*, Paris, France.

Batra, R.C. (1981). "Quasistatic indentation of a rubber-covered roll by a rigid roll." *Int. J. Num. Methods in Engng*, 17, pp. 1823-1833 .

Batra, R.C., Levinson, M. and Betz, E. (1976). "Rubber covered rolls-the thermoviscoelastic problem. A finite element solution." *Int. J. Num. Methods in Engng*, 10, pp. 767-785 .

Batra, R.C., Levinson, M., and Betz, E. (1980). "Rubber covered rolls - the thermoviscoelastic problem." *Int. J. Num. Methds in Engng*, 10, pp. 767-785.

Bazarenko, N.A., and Vorovich, I.I. (1965). "Asymptotic solution of the elasticity problem for a hollow, finite length, thin cylinder." *PMM*, 29 (6), pp. 1035-1052 .

Beatty, M.F. (1987). "Topics in finite elasticity: hyperelasticity of rubber, elastomers, and biological tissues — with examples." *Appl. Mech. Rev.*, 40, (12), pp. 1699-1735 .

Becker, E.B., Carey, G.F., and Oden, J.T. (1981). *Finite elements, an introduction, Vol.1, Prentice Hall.*

Bellman, R. (1964). *Perturbation Techniques in Mathematics, Physics, and Engineering.* Holt, Rinehart and Winston, Inc., New York.

Bender, C.M., and Orszag, S.A. (1984). *Advanced mathematical methods for scientists and engineers*. McGraw-Hill, London.

Bentall, R.H., and Johnson, K.L. (1967). "Slip in the rolling contact of two dissimilar elastic rollers." *Int. J. Mech. Sci.*, 9, pp. 389-404.

Bentall, R.H., and Johnson, K.L. (1968). "An elastic strip in plane rolling contact." *Int. J. Mech. Sci.*, 10, pp. 637-663.

Bernasconi, G. (1971). "Tensioni elastiche in cilindri di lunghezza finita forzati con interferenza variabile assialmente." *I National Congress AIMETA*, 3 (1), pp. 131-175 .

Billington, E.W. (1971). "Mechanical properties of various polymeric solids tested in compression." *Int. J. Mech. Science*, 13, pp. 531-545 .

Binnington, P.G. (1991). *The Measurement of Rotary Shaft Seal Film Thickness*. PhD Thesis, School of Engng, Durham.

Biot, M.A. (1937). "Bending of an infinite beam on an elastic foundation." *ASME J. Appl. Mech.* , 59, pp. A1-A7.

Bisset, E.J, and Glander, D.W. (1988). "A highly accurate approach that resolves the pressure spike of elastohydrodynamic lubrication." *ASME J. Tribology*, 110, pp. 241-246 .

Björkman, G. (1991). "The solution of large displacement frictionless contact problems using a sequence of linear complementarity problems." *Int. J. Num. Methods in Engng*, 31, pp. 1553-1556 .

Blatz, P.J., and Ko, W.L. (1962). "Application of finite elasticity theory to the deformation of rubbery materials." *Transactions of the Society of Rheology*, 6, pp. 223-251 .

Blok, H. (1963). "Inverse problems in hydrodynamic lubrication and design directives for lubricated flexible surfaces." *Proc. Int. Symp. on Lubrication and Wear*, Houston, TX. , pp. 1-151 .

Bondareva, V.F. (1969). "On the effect of an axisymmetric normal loading on an elastic sphere." *J. Math. Mech. (PMM)*, 33 (6), pp. 1029-1033 .

Bondareva, V.F. (1971). "Contact problems for an elastic sphere." *J. Math. Mech. (PMM)*, 35 (1), pp. 61-70 .

Bosson (1939). "The flexure of an infinite elastic strip on an elastic foundation." *Phil. Mag,*. 27, pp. 37-50.

Brighton, D.K., Hooke, C.J., and O'Donoghue, J.P. (1967-68). "A theoretical and experimental investigation of the effect of elastic distortions on the performance of journal bearings." *Proc. Instn. Mech. Engr.*, 182, pp. 194-202 .

Brothers, P.W., and Sinclair, G.B. (1977). "Uniform indentation of the elastic half-space by a rigid rectangular punch." *Int. J. Solids Struct.* , 13 (11) pp.1059-1072.

Budiansky, B. and Kimmel, E. (1991). "On the shear modulus of polyhedron-cell liquid foam." *ASME J. Appl. Mech.*, 58, *pp.* 289-290 .

Burchett, O., and Bert, C.W. (1972). "The effect of specimen geometry and lateral constraint on the isothermal compressibility of low-strength polymeric materials", *Exp. Mech.*, 12, pp. 328-331 .

Burmister, D.M. (1945). "The general theory of stresses and displacements in layered systems." *J. Appl. Phys.*, 16, pp. 89-94 .

Byrd, P.F., and Friedman, M.D. (1954). *Handbook of Elliptic Integrals for Engineers and Physicists*. Springer-Verlag, Berlin.

Cannarozzi, A.A. (1980). "On the resolution of some unilaterally constrained problems in structural engineering." *Computer Methods Appl. Mech. Engng*, 24, pp. 339-357 .

Cappello, F., And Nigrelli, V. (1987). "Analisi teorica di stati di deformazione assialsimmetrici in cilindri cavi di lunghezza finita." Rapporto n. 23 dell'Istituto di Costruzione di Macchine dell'Universita' di Palermo, Italy (in Italian).

Cappello, F., And Nigrelli, V. (1989). "Calcolo dello stato di tensione e degli spostamenti in cilindri circolari cavi di lunghezza finita deformati assialsimmetricamente." Rapporto n. 29 dell'Istituto di Costruzione di Macchine dell'Universita' di Palermo, Italy (in Italian).

Cappello, F., And Nigrelli, V. (1990). "Accoppiamenti forzati mozzo-albero con distribuzione assialsimmetrica dell'interferenza." Atti del convegno in onore di A. Dornig, Politecnico di Milano, 7 Giugno 1990, Italy, pp.59-79. (in Italian).

Castelli, V., and Pirvics, J. (1968). "Review of numerical methods in gas bearing film analysis." *ASME J. Lubrication Technology*, 90, pp. 777-792 .

Chen, W.T. (1971). "Computation of stresses and displacements in a layered elastic medium." *Int. J. Engng Sci.*, 9, pp. 775-800 .

Chen, W.T., and Engel, P.A. (1972). "Impact and contact stress analysis in multilayer media." *Int. J. Solids Structures*, 8, pp. 1257-1281 .

Christensen, R.M. (1980). "A nonlinear theory of viscoelasticity for application to elastomers." *ASME J. Appl. Mech*, 47, pp. 762-768 .

Cicala, P. (1985). "Analytic solutions of axisymmetric problems in elastic cylinders." *Meccanica*, pp. (incomplete reference).

Cimatti, G. (1980). "A free boundary problem in the theory of lubrication." *Int. J. Engng Sci.* 18, pp. 703-711 .

Cimatti, G. (1980). "Existence and uniqueness for nonlinear Reynolds equation." *Int. J. Engng Sci.* 24 (5), pp. 827-834 .

Civelek, M.B., and Erdogan, F. (1976). "Interface separation in a frictionless contact problem for an elastic layer." *ASME J. Appl. Mech.*, 43, pp. 175-177.

Coker, E.G. and Filon, L.N.G. (1957). *A treatise on photoelasticity*. Cambridge University Press, Cambridge. (see p. 436).

Conway, H.D. and Farnham, K.A. (1967a). "The contact stress problem for indented strips and slabs under conditions of partial slipping." *Int. J. Eng. Sci*, 5, pp. 145-154 .

Conway, H.D. and Farnham, K.A. (1967b). "Contact stresses between cylindrical shafts and sleeves." *Int. J. Eng. Sci*, 5, pp. 541-554 .

Conway, H.D., and Engel, P.A. (1969). "Contact stresses in slabs due to round rough indenters." *Int. J. Mech. Sci.*, 11, pp. 709-722.

Conway, H.D., and Farnham, K.A. (1968a). "The relationship between load and penetration for a rigid, flat-ended punch of arbitrary cross section." *Int. J. Eng. Sci.*, 6, pp. 489-496 .

Conway, H.D., and Farnham, K.A. (1968b). "Slabs and shafts compressed by circular indenters." *Int. J. Mech. Sci.*, 10, pp. 981-987.

Conway, H.D., Vogel, S.M., and Farnham, K.A. (1966). "Normal and shearing contact stresses in indented strips and slabs." *Int. J. Eng. Sci.*, 4, pp. 343-359.

Cook, R.D. (1981). *Concepts and applications of finite element analysis*, Wiley, New York .

Coumans, W.J., and Heikens, D. (1980). "Dilatometer for use in tensile tests." *Polymer*, 21, pp. 957-961 .

Craggs, J.W., and Roberts, A.M. (1967). "On the motion of a heavy cylinder over the surface of an elastic solid." *ASME J. Appl. Mech.*, 34, pp. 207-209.

Cudworth, C.J. (1974). *Fluid lubrication of soft surface layers*, PhD Thesis, School of Engng, Durham.

Cudworth, C.J. (1978). "Finite element solution of the elastohydrodynamic lubrication of a compliant layer in pure sliding." *Proceedings 5th Leeds-Lyon Symposium on Tribology*, Leeds, pp.375-377.

Cudworth, C.J. and Higginson, G.R. (1976). "Friction of lubricated soft surface layers." *Wear*, 37, pp. 299-312.

Da Rios, G., and Rinelli, S. (1980). "Definizione speditiva delle caratteristiche meccaniche di una terra mediante prove triassiali." *Le strade*, 1188, pp. 45-53 (in Italian).

Dempsey, J.P., Zhao, Z.G., and Li, H. (1991). "Axisymmetric indentation of an elastic layer supported by a Winkler Foundation." *Int. J. Solids Structures*, 27 (1), pp. 73-87 .

Dempsey, J.P., Zhao, Z.G., Minnetyan, L., and Li, H. (1990). "Plane contact of an elastic layer supported by a Winkler foundation." *ASME J. Appl. Mech.*, 57, pp. 974-980 .

de Mul, J.M., Kalker, J.J., and Fredriksson, B. (1986). "The contact between arbitrarily curved bodies of finite dimensions." *ASME J. Tribology*, 108, pp. 140-148 .

Dhaliwal, R.S. (1970). "Punch problem for an elastic layer overlying an elastic foundation." *Int. J. Engng Sci.* 8, pp. 273-288 .

Dhaliwal, R.S., and Rau, I.S. (1970). "The axisymmetric Boussinesq problem for a thick elastic layer under a punch of arbitrary profile." *Int. J. Engng Sci.* 8, pp. 843-856 .

Dimnikov, S.I., Sniegs, M.I., and Erdmanis, A.G. (1984). "Models of near incompressible medium in the calculations of rubber elements." *International Rubber Conference*, Vol. 1, Moscow.

Dornig, A. (1965). "Effetto della distribuzione assial-simmetrica dell'interferenza negli accoppiamenti forzati mozzo-albero." *Ingegneria Meccanica*, 12, pp. 35-48 (in Italian).

Dowson, D., Fisher, J., Jin, Z.M., Auger, D.D., and Jobbins, B. (1991). "Design considerations for cushion form bearings in artificial hip joints." *J. Engng in Medicine*, 205, pp. 59-68 .

Dowson, D., Fisher, J., Jobbins, B., O'Carrol, S., and Jin, Z.M. (1990). "Contact mechanics of low elastic modulus layers in 'cushion form' bearings for artificial hip joints." *7-th Meeting of the European Society of Biomechanics*, Aarhus, July 8-11 , paper C.19 .

Dowson, D. and Jin, Z. (1986). "Micro-elastohydrodynamic lubrication of synovial joints."*Engng in Medicine*, 15 (2), pp. 63-65 .

Dowson, D., and Yao, J. (1990). "A full solution to the problem of film thickness prediction in natural synovial joints." *Mechanics of Coatings*, Elsevier, N.Y. , pp. 91-102 . *Proceedings of the 16th Leeds-Lyon Symposium on Tribology*, Lyon, France, 5th-8th September 1989.

Dragoni, E. (1990). "Modelling elastomeric units by 'ABAQUS' : a case study." *III ABAQUS User's Cong.*, Newport, Rhode Island, U.S., May 30-June 1, 1990, pp. 165-174 .

Dragoni, E. (1991). "Checking ABAQUS' sensitivity to variations of the Poisson's ratio in linear elasticity." *IV ABAQUS User's Cong.*, Oxford, UK, September 11-13, 1991, pp. 175-181 .

Dragoni, E., and Strozzi, A. (1986). "Analysis of a split ring inserted into a circular housing." *J. Strain Analysis*, 21, pp. 59-70 .

Dragoni, E., and Strozzi, A. (1987). "Design of an end face seal assembly for lubricated rotary joints.." *J. Strain Analysis*, 22, pp. 37-47 .

Dragoni, E., and Strozzi, A. (1988). "Analysis of an unpressurized, laterally restrained, elastomeric O-Ring seal." *ASME J. Tribology*, 110, pp. 193-200 .

Dragoni, E., and Strozzi, A. (1989). "Theoretical analysis of an unpressurized elastomeric O-ring seal inserted into a rectangular groove." *Wear*, 130 (1), pp. 41-51.

Drutowski, R.C. (1968). "Contact elasticity of seal elastomers." *ASME J. Lubrication Technology*, 90, pp. 478-483 .

Durelli, A.J., and Chen, T.L. (1973). "Displacement and finite-strain fields in a sphere subjected to large deformations." *Int. J. Non-Linear Mech.*, 8, pp. 17-30 .

Emery, A.F., and Segedin, C.M. (1973). "A numerical technique for determining the effect of singularities in finite difference solutions illustrated by application to plane elastic problems." *Int. J. Num. Methods Engng*, 6, pp. 367-380.

England, A.H. (1971). *Complex Variable Methods in Elasticity.* Wiley Interscience, London.

Fabrikant, V.I. (1986). "Inclined flat punch of arbitrary shape on an elastic half-space." *ASME J. Appl. Mech.*, 53, pp. 798-806 .

Fabrikant, V.I. (1988). "Elastic field around a circular punch." *ASME J. Appl. Mech.*, 55, pp. 604-610 .

Fabrikant, V.I. (1990). "An arbitrary tangential load underneath a smooth circular punch." *ASME J. Appl. Mech.*, 57, pp. 596-599 .

Fabrikant, V.I., Selvadurai, A.P.S., and Xistris, G.D. (1985). "Elastic field around a circular punch." *ASME J. Appl. Mech.*, 52, pp. 681-685 .

Favretti, G. (1966). "Indentation of a rigid punch on a plastically non-homogeneous material." *Meccanica*, 1, (3/4), pp. 83-94 .

Fichera, G. (1949). "Sul calcolo delle deformazioni, dotate di simmetria assiale, di uno strato sferico elastico." *Atti dell'Accademia Nazionale dei Lincei, Classe di Scienze Fisiche, Matematiche e Naturali*, 6, pp. 582-589 (in Italian).

Field, G.J., and Nau, B.S. (1973). "The lubrication of rectangular rubber seals under conditions of reciprocating motion, Part 3." *RR* 1200, *British Hydromechanics Research Association, Cranfield, Beds.*

Field, G.J., and Nau, B.S. (1975). "A theoretical study of the elastohydrodynamic lubrication of reciprocating rubber seals." *ASLE Transactions*, 18 (1), pp.48-54 .

Field, G.J., and Nau, B.S. (1976). "An optical interference method of studying the lubrication of a compliant bearing." *ASME J. Lubr. Techn.*, 98, pp.486-490 .

Finkin, E.F. (1972). "The determination of Young's modulus from the indentation of rubber sheets by spherically tipped indentors." *Wear*, 19, pp. 277-286 .

Fisher, J., and Dowson, D. (1991). "Tribology of total artificial joints." *J. Engng in Medicine*, 205, pp. 73-79 .

Forster, M. (1955). "Unilateral compression of rubber." *J.Appl. Phys.*, 26 (9), pp. 1104-1106 .

Fricker, D.C. (1991). "Friction when femoral prosthesis heads slide in acetabular cups." Ceramics in substitutive and reconstructive surgery. Elsevier Science Publ. B.V., Amsterdam. Proceedings of the Satellite Symposium 3 on Ceramics in Substitutive and Reconstructive Surgery of the 7th International Meeting on Modern Ceramics Technologies (7th CIMTEC - World Ceramics Congress), Montecatini Terme, Italy, 27-30 June 1990 .

Fritzsche, C. (1974). "Die Poissonzahl als Umrechnungsgröße zwischen Elastizitäts- und Torsionsmodul." *Kunststoffe - Plastics* 6, pp. 19-22 .

Gabelli, A. (1991). *Deformation, Stresses and Elastohydrodynamic Film Formation in Soft Contacts*. Ph. D. Thesis, Machine and Vehicle Design, Chalmers University of Technology, Göteborg, Sweden.

Gabelli, A., Jacobson, B. (1990). "Finite element analysis of EHD lubrication of rubber layers." *Mechanics of Coatings*, Elsevier, N.Y. , pp. 103-110 . *Proceedings of the 16th Leeds-Lyon Symposium on Tribology*, Lyon, France, 5th-8th September 1989.

Gabelli, A., Ponson, F., and Poll, G. (1992). "Computation and Measurement of the Contact Stress and its role in rotary lip seal design." To be presented at the 13th International Conference on Fluid Sealing, 7-9 April, Brugge, Belgium.

Gadala, M.S. (1990). "Unified numerical treatment of hyperelastic and rubber-like constitutive laws." *Communications in Applied Numerical Methods*, 7, pp. 581-587.

Galin, L.A. (1961). *Contact Problems in the Theory of Elasticity*. Sneddon Editor, North Carolina State College.

Gent, A.N., Henry, R.L. and Roxbury, M.L. (1974). "Interfacial stresses for bonded rubber blocks in compression and shear." *ASME J. Appl. Mech.*, 41 , pp. 855-859 .

George, A.F. (1984). "The effect of high pressure carbon dioxide on silicone and fluorocarbon seal materials." 10*th Int. Conf. Fluid Sealing*, Innsbruck, Austria, pp. 173-188 .

George, A., Strozzi, A. and Rich, J. (1987). "Stress fields in a compressed unconstrained elastomeric O-Ring seal and a comparison of computer predictions and experimental results." *Tribology International*, 20, pp. 237-247 .

Gilmour, I., Trainor, A., and Haward, R.N. (1974). "The determination of the Bulk Modulus in a constrained solid." *J. Polymer Science*, 12, pp. 1939-1940 .

Gladwell, G.M.L. (1974). "Unbonded contact between a circular plate and an elastic half-space." *J. Elasticity*, 4 (2), pp. 115-130 .

Gladwell, G.M.L. (1976). "On some unbonded contact problems in plane elasticity theory." *ASME J. Appl. Mech.*, 43, pp. 263-267.

Gladwell, G.M.L. (1980). *Contact problems in the classical theory of elasticity*. Sijthoff & Noordhof, Alphen aan den Rijn, The Netherlands.

Gladwell, G.M.L., and England, A.H. (1975). "Contact problems for the spherical shell." *Proceedings* 12*th Annual Meeting Soc. Eng. Sci.*, Univ. Texas at Austin.

Gladwell, G.M.L., and Iyer, K.R.P. (1974). "Unbonded contact between a circular plate and an elastic half-space." *J. Elasticity*, 4, pp. 115-130 .

Gohar, R. (1988). *Elastohydrodynamics*. Ellis Horwood Limited, John Wiley & Sons, N.Y. .

Goodman, L.E., and Keer, L.M. (1965). "The contact stress problem for an elastic sphere indenting an elastic cavity." *Int. J. Solids Structures*, 1, pp. 407-415 .

Gorelik, B.M., Bukhina, M.F. and Ratner, A.V. (1961). "Variation of the contact area in the deformation of rubber cylinders and rings." *Soviet Rubber Technology*, 1, pp. 10-14 .

Gradshteyn, I.S., and Ryzhik, I.M. (1979). *Table of integrals, series, and products*. Academic Press Inc., N.Y.

Greenberg, M.D. (1978). *Foundations of Applied Mathematics*. Prentice-Hall, Englewood Cliffs, New Jersey.

Guarnieri, G. (1965). *Somme di series*, Levrotto & Bella, Turin (in Italian).

Gueury, M., Bagur, P., Rezakhanlou, R. and von Stebut, J. (1990). "Elasto-plastic finite element analysis of axisymmetric indentation using a simple personal computer." *Mechanics of Coatings*, Elsevier, N.Y. , pp. 295-301 . *Proceedings of the 16th Leeds-Lyon Symposium on Tribology*, Lyon, France, 5th-8th September 1989.

Gupta, P.K., and Walowit, J.A. (1974). "Contact stresses between and elastic cylinder and a layered elastic solid." *ASME J. Lubr. Techn.*, 96, pp. 250-257.

Hahn, H.T., and Levinson, M. (1974a). "Indentation of an elastic layer(s) bonded to a rigid cylinder - I. Quasistatic case without friction." *Int. J. Mech. Sci.*, 16, pp. 489-502 . .

Hahn, H.T. and Levinson, M. (1974 b). "Indentation of an elastic layer bonded to a rigid cylinder. II. Unidirectional slipping with Coulomb friction." *Int. J. Mech. Sci.*, 16, pp. 503-514.

Hall, R.W. (1988). "The numerical solution of some singular contact problems using a Hilbert transform." *J. Strain Analysis*, 23 (3), pp. 129-135.

Hall, R.W. (1989). "Pressure spikes in elastohydrodynamics - some elastic considerations." *Wear*, 131 (1), pp. 151-161 .

Hamrock, B.J, Pan, P, and Lee, R.T. (1988). "Pressure spikes in elastohydrodynamically lubricated conjunctions." *ASME J. Tribology*, 110, pp. 279-284 .

Hamrock, B.J., and Tripp, J.H. (1984). "Numerical methods and computers used in elastohydrodynamic lubrication." in *Proc. 10th Leeds-Lyon Symp. on Tribology*, Lyon, September 1983, Butterworths, London; Dowson D., Taylor, C.M., Godet, M. and Berthe, D. eds., pp. 11-19 .

Hannah, M. (1951). "Contact stress and deformation in a thin elastic layer." *Quart. J. Appl. Math.*, 4, pp. 94-105.

Hanson, M.T., and Keer, L.M. (1989). "Stress analysis and contact problems for an elastic quarter-plane." *Jl Mech. Appl. Math.*, 42 (3), pp. 363-383

Harper, D (1989). *An introduction to Maple.* The University of Liverpool, Liverpool.

Hartnett, M.J. (1979). "The analysis of contact stresses in rolling element bearings." *ASME J. Lubr. Techn.*, 101, pp.105-109.

Hartnett, M.J. (1980). "A general numerical solution for elastic body contact problems." *Solid Contact and Lubrication, the Winter Annual Meeting of the ASME*, Chicago, IL, pp. 51-66.

Hayes, X.C., Keer, L.M., Herrmann, G., and Mockros, L.F. (1972). "A mathematical analysis for indentation tests of articular cartilage." *J. Biomechanics*, 5, pp. 541-551 .

Heinrich, J.C., Huyakorn, P.S., Mitchell, A.R., and Zienkiewicz, O.C. (1977). "An upwind finite element scheme for two-dimensional convective transport equation." *Int. J. Num. Methods Engng*, 11, pp. 131-143 .

Heydemann, P.L.M., and Howck, J.C. (1972). "Bulk modulus and density of polyethylene to 30 Kbar." *J. Polymer Sci.*, 10, pp. 1631-1672 .

Hemker, P.W. (1970). *A Numerical Study of Stiff Two-Point Boundary Problems*. Mathematisch Centrum, Amsterdam 1970.

Hencky, H. (1933). "The elastic behaviour of vulcanized rubber." *ASME J. Appl. Mech.*, 1 (2), pp. 45-53 .

Herrebrugh, K. (1968). "Solving the incompressible and isothermal problem in elastohydrodynamic lubrication through an integral equation." *ASME J. Lubr. Techn.*, 90, pp. 262-270 .

Hetenyi, M. (1960). "A method of solution for the elastic quarter-plane." *ASME J. Appl. Mech.*, 27, pp. 289-296 .

Hoheisel, G. (1967). *Integral Equations*. F. Ungar Publ., New York.

Holownia, B.P. (1971). "Compression of bonded rubber blocks." *J. Strain Analysis*, 6 (2), pp. 121-123 .

Holownia, B.P. (1972). "Effect of Poisson's ratio on bonded rubber blocks." *J. Strain Analysis*, 7 (3), pp. 236-242 .

Holownia, B.P. (1974). "Effect of carbon black on the elastic constants of elastomers." *J. Inst Rubber Ind.*, 8 (4), pp. 246-253 .

Holownia, B.P. (1977). "Temperature buildup in bonded rubber blocks due to hysteresis." *Rubber Chemistry and Technology*, 50 (1), pp. 186-193 .

Holownia, B.P. (1980). "Effect of different types of carbon black on elastic constants of elastomers." *Plastics and Rubber: Materials and Applications*, pp. 129-132 .

Holownia, B.P. (1979). "Rubber hysteresis in biaxial and triaxial loadings", *Elastomers: Criteria for Engineering Design, Chapter 8, Appl. Sci. Publ.*, England, pp. 111-125 .

Holownia, B.P. (1985a). "Experimental measurement of dynamic Bulk Modulus using holography." *Rubber Chemistry and Technology*, 58, pp. 258-268 .

Holownia, B.P. (1985b). "Comparison between finite element and finite difference methods for stress analysis of elastomers." *Plastics Rubber Processing and Applications*, 5, pp. 379-380 .

Holownia, B.P. (1986). "Measurement of dynamic Bulk Modulus and phase angle using ESPI." *Rubber Chemistry end Technology*, 59 (2), pp. 223-232 .

Hooke, C.J. (1986). "The elastohydrodynamic lubrication of a cylinder on an elastomeric layer." *Wear*, 111, pp. 83-99.

Hooke, C.J. (1986). "The lubrication of soft contacts." *13th Leeds-Lyon Symposium on Tribology*, Leeds, pp. 299-305 .

Hooke, CJ. Brighton, D.K., and O'Donoghue, J.P. (1966-67) "The effect of elastic distortions on the performance of thin shell bearings." *Proc. Instn. Mech. Engr.*, 181, pp. 63-69.

Hooke, C.J., and O'Donoghue, J.P. (1972). "Elastohydrodynamic lubrication of soft, highly deformed contacts." *J. Mech. Engng Sci.*, 14 (1), pp. 34-48 .

Hooper, J.A. (1974). "Analysis of a circular raft in adhesive contact with a thick elastic layer." *Geotechnique*, 24 (4), pp. 561-580 .

Huyakorn, P.S., Mitchell, A.R., and Zienkiewicz, O.C. (1977). "An upwind finite element scheme for two-dimensional convective trasport equations", *Int. J. Num. Meth. Engng*, 11, pp.131-143 .

Ihara, T., Shaw, M.C., and Bhushan, B. (1986a). "A finite element analysis of contact stress and strain in an elastic film on a rigid substrate-part I : zero friction." *J. Tribology*, 108, pp. 527-533 .

Ihara, T., Shaw, M.C., and Bhushan, B. (1986b). "A finite element analysis of contact stress and strain in an elastic film on a rigid substrate-part II : with friction." *J. Tribology*, 108, pp. 534-539 .

Jaffar, M.J. (1988). "A numerical solution for axisymmetric contact problems involving rigid indenters on elastic layers." *J. Mech. Phys. Solids*, 36 (4), pp. 401-416.

Jaffar, M.J. (1989). "Asymptotic behaviour of thin elastic layers bonded and unbonded to a rigid foundation." *Int. J. Mech. Sci.*, 31 (3), pp. 229-235.

Jaffar, M.J. (1991a). "Pressure-viscosity effect on the solutions of a lubricated thick elastic bonded strip." *Tribology International*, 24 (2), pp. 91-94 .

Jaffar, M.J. (1991b). "Elastic strips in sliding contact." *J. Strain Analysis*, 26 (3), pp. 193-199 .

Jaffar, M.J., and Savage, M.D. (1988). "On the numerical solution of line contact involving bonded and unbonded strips.", *J. Strain Analysis*, 23 (2), pp. 67-77.

Jana, M.K., Renganathan, K., and Venkateswara Rao, G. (1987). "Effect of Bulk Modulus variation with pressure in propellant grain elastic stress analysis." *Computers & Structures*, 26 (5), pp. 761-766 .

Jin, Z. (1988). *Micro-elastohydrodynamic lubrication of synovial joints*. Ph. D. Thesis, Institute of Tribology, Dept. Mech. Engng, The University of Leeds.

Johannesson, H. (1980). *On the optimization of hydraulic cylinder seals*, Doctoral Thesis, University of Lulea .

Johnson, K. L. (1985). *Contact Mechanics*, Cambridge University Press, Cambridge.

Johnson, R.L. (1969). Discussion to "Separation of principal stresses" by A. Kuske, in *Experimental Mechanics*, September, p. 432 .

Kalandiya, A.I. (1975). *Mathematical Methods of Two-dimensional Elasticity*. Mir Publishers, Moscow.

Kalshi, M.S. (1981). "Elastohydrodynamic lubrication of offset O-Ring rotary seal." *ASME J. Lubr. Techn.*, 103, pp. 414-427 .

Kanters, A. F. C. (1990). *On the Calculation of Leakage and Friction of Reciprocating Elastomeric Seals*. Ph. D. Thesis, Eindhoven, Denmark.

Karpenko, V. A. (1976). "Axisymmetric impression of two stamps into an elastic sphere." *J. Math. Mech. (PMM)*, 40 (4), pp. 763-766 .

Kawahara, Y., Ohtake, Y., and Hirabayashi, H. (1964). "Oil film formation of oil seals for reciprocating motion." *Ninth Int. Conf. on Fluid Sealing, BHRA, Cranfield*, pp. B2/13-28 .

Keer, L.M. (1964). "The contact stress problem for an elastic sphere indenting an elastic layer." *ASME J. Appl. Mech.*, 31, pp. 143-145 .

Keer, L.M., and Miller, G.R. (1983). "Smooth indentation of a finite layer." *ASCE J. of Engineering Mechanics*, 109, pp. 706-717 .

Keer, L.M., and Sve, C. (1969). "Indentation of an elastic layer by an array of punches moving with steady velocity." *ASME J. Appl. Mech.*, 38, pp. 92-98.

Key, S.W. (1974). "A finite element procedure for the large deformation dynamic response of axisymmetric solids." *Comp. Methd. in Appl. Mech. and Engng*, 4, pp. 195-218 .

Kerr, A.D. (1964). "Elastic and viscoelastic foundation models." *ASME J. Appl. Mech.*, 31, pp. 491-498.

Kilvington, M. and Goodman, R.M.F. (1981). "*In vivo* hip joint forces recorded on a strain gauged 'English' prosthesis using an implanted transmitter." *Engng Med.*, 10, pp. 175-187 .

King, R.B. (1987). "Elastic analysis of some punch problems for a layered medium." *Int. J. Solids Structures*, 23 (12), pp. 1657-1664.

King, R.B., and O'Sullivan, T.C. (1987). "Sliding contact stresses in a two-dimensional layered elastic half-space." *Int. J. Solids Structures*, 23 (5), pp. 581-597 .

Knopp, K. (1928). *Theory and application of infinite series*. Blackie & Sons, London.

Komvopoulos, K. , Saka, N., and Suh, N.P. (1987). "The role of hard layers in lubricated and dry sliding." *ASME J. Tribology*, 109, pp. 223-231 .

Komvopoulos, K. (1988). "Finite element analysis of a layered elastic solid in normal contact with a rigid surface." *ASME J. Tribology*, 110, pp. 477-485 .

Komvopoulos, K. (1989). "Elastic-plastic finite element analysis of indented layered media." *ASME J. Tribology*, 111, pp. 430-439 .

Kostreva, M. M. (1984a). "Elasto-hydrodynamic lubrication: a non-linear complementarity problem." *Int. J. Num. Methods in Fluids*, 4, pp. 377-397 .

Kostreva, M.M. (1984b). "Pressure spikes and stability considerations in elastohydrodynamic lubrication models." *ASME J. Tribology*, 106, pp. 386-395 .

Krasnov, M.L. (1983). *Equazioni Integrali*. Mir, Mosca (in Italian).

Kreyszig, E. (1988). *Advanced Engineering Mathematics*. John Wiley & Sons, N.Y.

Kuske, A. (1968). "Separation of principal stresses in the freezing method." *Exp. Mech.*, August, p. 384 .

Kuznetsov, A.I. (1962). "Penetration of rigid dies into a half-space with power-law strain-hardening and with nonlinear creep of the material." *J. Math. Mech (PMM)*, 26 (3), pp. 481-491 .

Kwok, Y.K. (1991). "Location and structure of the nearest singularity of a perturbation series." *Communications in Applied Numerical Methods*, /, pp.19-28 .

Lanczos, C. (1964). *Applied Analysis*. Pitman, London.

Lanczos, C. (1966). *Discourse on Fourier Series*. Oliver & Boyd, Edimburgh.

Langhaar, H. L. (1951). *Dimensional analysis and theory of models*. Wiley & Sons, New York-

Latta, G.E. (1956). "The solution of a class of integral equations." *J. Rational Mech. Anal.*, 5(5), pp. 821-834 .

Lau, J. H., and Jeans, A. H. (1989). "Nonlinear analysis of elastomeric keyboard domes." *ASME J. Appl. Mech.*, 56, pp. 751-755 .

Lebedev, N. N., and Ufliand, Ia. S. (1958). "Axisymmetric contact problem for an elastic layer." *J. Math. Mech. (PMM)*, 22 (3), pp. 320-326 .

Levinson, M., and Burgess, I. (1971). "A comparison of some simple constitutive relations for slightly compressible rubber-like materials." *Int. J. Mech. Sci.*, 13, pp. 563-572 .

Li, H., and Dempsey, J.P. (1988). "Unbonded contact of finite Timoshenko beam on elastic layer." *ASCE J. of Engng Mech.*, 114 (8), pp.1265-1284.

Li, H., and Dempsey, J.P. (1990). "Axisymmetric contact of an elastic layer underlain by rigid base." *Int. J. Num. Methods in Engng*, 29, pp.57-72 .

Lindley, P.B. (1967). "Poisson's ratio and the incompressibility of rubber." *Bull. Mech. Engng Educ.*, 6, pp. 186-187 .

Lindley, P.B. (1980). Private Communication.

Ling, F. F. (1973). *Surface Mechanics*. John Wiley & Sons, New York.

Ling, F. F. (1959). "A quasi-iterative method for computing interface temperature distributions." *Zeitshrift für Angewandte Mathematik und Physik*, 10, pp.461-474 .

Litovchenko, S.I., and Nuller, B.M. (1973). "On the bending of an elastic cylinder by rigid bands." *PMM*, 37 (3), pp. 515-523 .

Loss, F.J., Weinstein, A.S. and Zorowski, C.F. (1966). "Elastic behaviour in cold strip rolling at the onset of plasticity." J. Inst. Metals, 92 (104), pp. 104-110 .

Love, A.E.H. (1944). *A Treatise on the Mathematical Theory of Elasticity*. Dover, N.Y.

Lubliner, J. (1985). "A model of rubber viscoelasticity." *Mechanics Research Communications*, 12 (2), pp. 93-99 .

Luke, Y.L. (1962). *Integrals of Bessel Functions*. McGraw-Hill, New York.

Lur'e, A.I., McVean, D.B., and Radok, J.R. (1964). *Three-dimensional problems of the theory of elasticity*. Interscience Publishers, John Wiley, New York.

MACSYMA *Reference Manual* (1983). Symbolics Inc., Cambridge, MA .

Maguerre, K. (1931). "Druckverteilung durch eine elastische Schicht auf starrer rauher Unterlage." *Ingenieur Archiv*, 2 (1), pp. 108-117.

Maguerre, K. (1933). "Spannungverteilung und Wellenausbreitung in der kontinuierlich gestützen Platte." *Ingenieur Archiv*, 4 (4), pp. 332-353.

Margetson, J. (1970). "The indentation of elastic and viscoelastic strips by rigid or elastic cylinders." *Zeitschrift für Angewandte Mathematik und Physik*, 21, pp. 1040-1052 .

Mase, G.E. (1970). *Continuum Mechanics*. Shaum's Outline Series, McGraw-Hill, New York.

Mattewson, M.J. (1981). "Axi-symmetric contact on thin compliant coatings." *J. Mech. Phys. Solids*, 29 (2), pp. 89-113.

May, E.M. (1957). "Pressure drop across a packing." *Appl. Hydr.*, pp. 110-114 .

McCormick, J.A. (1978). "A numerical solution for a generalised elliptical contact of layered elastic solids." *MTI Report N. 78TR52, Mechanical Technology, Latham, New York* .

Mead, D.J. and Joannides, R.J. (1991). "Measurement of the dynamic moduli and Poisson's ratios of a transversely isotropic fibre-reinforced plastic." *Composites*, 22 (1), pp. 15-29 .

Medley, J.B., Dowson, D., and Wright, V. (1984). "Transient elastohydrodynamic lubrication models for the human ankle joint." *Engng Med.*, 13 (3), pp. 137-151 .

Medri, G. (1982a). "Caratterizzazione meccanica di un elastomero per pneumatici." *X National Congress AIAS*, Italy, pp. 299-309 (in Italian).

Medri, G. (1982b). "Mechanical characterization of elastomers." *Plastics and Rubber Processing and Applications*, 2 (4), pp. 293-296 .

Medri, G. (1984a). "Analysis of a case of rubber pad forming." *Plastics and Rubber Proceedings and Applications*, 4, pp.115-120 .

Medri, G. (1984b). "Elastic modelling of rubber-like materials." *Int. Rubber Conf.*, Moscow.

Medri, G. and Strozzi, A. (1984). "Mechanical analysis of elastomeric seals by numerical methods", *I&C Product Research & Development*, 23, pp. 596-600 .

Medri, G. and Strozzi, A. (1986). "Stress-strain fields in compressed elastomeric seals and their extension to fracture mechanics.", *Rubber Chemistry and Technology*, 59 (5), pp. 709-721 .

Meijers, P. (1968). "The contact problem of a rigid cylinder on an elastic layer.", *Appl. Sci. Res.* 18, pp. 353-383.

Myers, T.G. (1991). "A *series solution method for sharp asymmetric dry contact* problems." *J. Strain Analysis*, 26 (1), PP. 39-45 .

Miklin, S.G. (1964). *Integral Equations*. Pergamon Press, Oxford.

Miller, R.D.W. (1964). "Variations of line pressure and rolling speed with indentation of covered rollers." *British J. Appl. Phys.*, 15, pp. 1423-1435.

Miller, R.D.W. (1966). "Some effects of compressibility on the indentation of a thin elastic layer by a smooth rigid cylinder." *Appl. Sci. Res.* 16, pp. 405-424.

Miller, R.D., and Poulter, S.R.C. (1962). "Pressure and speed effects of cylinder covering during printing." *Advances in Printing Science and Technology*, 2, pp. 35-52 .

Milne, R.D. (1980). *Applied Functional Analysis*. Pitman, London .

Milne-Thompson, L.M. (1960). *Plane Elastic Systems*. Springer Verlag, Berlin.

Mitchell, A.R. (1971). "Variational principles and the finite-element method in partial differential equations." *Proc. R. Soc. London*, Ser. A, 323, pp. 211-217 .

Mitrinovic, D.S. (1970). *Analytical Inequalities*, Springer-Verlag, Berlin .

Moghe, S.R. and Neff, H.F. (1971). "Elastic deformations of constrained cylinders." *ASME J. Appl. Mech.*, 38, pp. 393-398 .

Morman, K.N. (1984). *Rubber Viscoelasticity - A Review of Current Understanding*. Ford Motor Company, Dearborn, Michigan.

Mossakowskii, V. I. (1958). "Pressure of a circular die [punch] on an elastic half-space, whose modulus of elasticity is an exponential function of depth." *J. Math. Mech. (PMM)*, 22 (1), pp. 123-125 .

Mozarovsky, V.V., Shylkc, S.V., and Starzynsky, V.E. (1986). "Contact stress and strains in elastic layer." *Second Int. Symp. INSYCONT, Krakow, Poland, 24-26 September* 1986 , pp.373-382 .

Mrowczynski, Z., and Bezinski, R. (1973). "Lane elastomery uretanowe w zastosowaniu do elastoptycznych badan modelowych.", *Ploimery-Tworzywa Wielkoczasteczkowe*, pp. 403-404 .

Mukhopadhyay, J. (1982). "Effect of non-homogeneity on yield stress in a thick-walled cylindrical tube under pressure." *Int. J. Engng Sci.*, 20 (8), pp. 963-968 .

Muki, R. and Dong, S.B. (1980). "Elastostatic far-field behavior in a layered half space under surface pressure." *ASME J. Appl. Mech.*, 47, pp. 504-512 .

Najak, L., and Johnson, K.L. (1979). "Pressure between elastic bodies having a slender area of contact and arbitrary profiles." *Int. J. Mech. Sci.*, 21, pp. 237-247.

Nayfeh, Ali (1973). *Perturbation Methods*. Wiley & Sons, New York.

Nau, B.S. (1968). *Leakage and friction measurements on reciprocating square-section seals*. RR 938, BHRA, Cranfield, Britain .

Noble, B., and Hussain, M. (1969). "A variational method for inclusion and indentation problems." *J. Maths Applics*, 5, pp. 194-205 .

Nowell, D., and Hills, D.A. (1988). "Contact problems incorporating elastic layers." *Int. J. Solids Structures* 24 (1), pp. 105-115.

O'Carrol, S., Jin, Z.M., Dowson, D., Fisher, J. , and Jobbins, B. (1990). "Determination of contact area in 'cushion form' bearings for artificial hip joints." *J. Engng in Medicine*, 204, pp. 217-223 .

Oda, J., Shibahara, M., and Miyamoto, H. (1972). "On shrink-fit stresses between an infinite cylinder and a finite hollow cylinder." Bulletin of JSME, 15 (88), pp. 1147-1155 .

Oden, J.Y. (1972). *Finite Elements of Nonlinear Continua*. McGraw-Hill Book Co., N.Y.

Oden, J.Y. (1979). *Applied Functional Analysis*. Prentice-Hall. New Jersey.

Oden, J.Y. and Wu, S.R. (1985). "Existence of solutions to the Reynolds' equation of elastohydrodynamic lubrication." *Int. J. Engng Sci.*, 23 (2), pp. 207-215 .

O'Donoghue, J., Brighton, D.K., and Hooke, C.J. (1967). "The effect of elastic distortions on journal bearing performance." *ASME, J. Lubr. Techn.*, 89, pp. 409-416 .

Ogden R.W. (1972). "Large deformation isotropic elasticity - on the correlation of theory and experiment for incompressible rubberlike solids." *Proc. R. Soc. Lond.* , Ser. A, 326, pp. 565-584 .

Ogden R.W. (1976). "Volume changes associated with the deformation of rubber-like solids." *J. Mech. Phys. Solids*, 24, pp. 323-338 .

Ogden R.W. (1984). *Non-Linear Elastic Deformations*. Ellis Horwood, John Wiley & sons, N.Y.

Oh, K.P. (1984). "The numerical solution of dynamically loaded elastohydrodynamic contact as a nonlinear complementarity problem." ASME *J. Tribology*, 106, pp. 88-95 .

Oh, K.P. (1986). "The formulation of the mixed lubrication problem as a generalized nonlinear complementarity problem." ASME *J. Tribology*, 108, pp. 598-604 .

Oh, K.P. , and Goenka, P.K. (1985). "The elastohydrodynamic solution of journal bearings under dynamic loading." *ASME J. Tribology, 107, pp. 389-395* .

Oh, K.P. , and Rohde, P.K. (1977). "Numerical solution of the point contact problem using the finite element method." *Int. J. Num. Methods Engng* , 11, pp. 1507-1518.

Okamura, H. (1982). "A contribution to the numerical analysis of isothermal elastohydrodynamic lubrication." in *Tribology of Reciprocating Engines, Proceedings of the 9th Leeds-Lyon Symposium on Tribology*, Leeds, 7-10 September 1982, Butterworths, London; Dowson, D., Taylor, C.M., Godet, M., and Berthe, D. eds., pp. 313-320 .

Okubo, H. (1951). "On the two-dimensional problem of a semi-infinite elastic body compressed by an elastic plane." *Quart. J. Mech. and Appl. Math.*, 4 (3), pp. 260-270 .

Okubo, H. (1952). "The stress distribution in a shaft press-fitted with a collar." *Z. angew. Math. Mech.*, 32 (6), pp. 178-186 .

Ol'khovik, O.Ye., and Grigoryan, E.S. (1974). "Apparatus for measuring compressibility of polymers.", *Polymer Science U.S.S.R.*, 16, pp.2501-2506 .

O'Neill, G. (1976). "Compression of elastomeric seal materials at pressures up to 3.5 GNm^{-2} ." *NPL Report Chem*, 54, August .

Ortali, M. (1991). *Dipendenza dalla Frequenza delle Caratteristiche Meccaniche dei Materiali Isotropi.* Thesis for the Italian title of Engineer, Udine University, Italy (in Italian).

Padovan, G., and Patuzzo Grego, P. (1981). *Equazioni e Sistemi di Equazioni alle Differenze Finite.* CLEUP, Padova (in Italian).

Pampillo, C.A., and Davis, L.A. (1971). "Volume change during deformation and pressure dependence of Yield stress." *J. Appl. Physics*, 42 (12), pp. 4674-4679 .

Pao, Y.C., Wu, T.S., and Chiu, Y.P. (1971). "Bounds on the maximum contact stress of an indented elastic layer." *ASME J. Appl. Mech.*, 38, pp. 608-614.

Parish, G.J. (1955). "Measurement of the pressure distribution between rollers in contact." *British J. Appl. Phys.*, 6, pp. 256-261.

Parish, G.J. (1958). "Measurement of pressure distribution between metal and rubber covered rollers." *British J. Appl. Phys.*, 9, pp. 158-161.

Parish, G.J. (1961). "Calculation of the behaviour of rubber-covered pressure rollers." *British J. Appl. Phys.*, 12, pp. 333-336.

Parks, V.J., and Durelli, A.J. (1969). "Natural stress." *Int. J. Non-Linear Mechanics*, 4, pp. 7-16 .

Parton, V., and Perline, P. (1983). *Equations Integrales de la Theorie de L'Elasticite'.* Mir, Moscou.

Parton, V., and Perlin, P.I. (1984). *Mathematical Methods of the Theory of Elasticity.* Mir, Moscou.

Paul, J.P. (1976). "Force actions transmitted by joints in the human body." *Proc. Royal Soc. London*, Ser. B, 192, pp. 163-172 .

Paul, B., and Hashemi, J. (1981). "Contact pressures on closely conforming elastic bodies." *ASME J. Appl. Mech.*, 48, pp. 543-548 .

Paul, J. P. (1976). "Force actions transmitted by joints in the human body." *Proc. R. Soc. Lond.*, Ser. B, pp. 163-172 .

Pearson, C.E. (1957). "On the finite strip problem." *Quarterly Applied Mathematics*, 15(2), pp.203-211 .

Penn, R.W. (1970). "Volume changes accompanying the extension of rubber." *Transactions of the Society of Rheology*, 14, pp. 509-517 .

Piragino, R. (1945). "Determinazione del modulo elastico volumetrico della gomma", *Relazione n.* 1497, RIV (in Italian).

Poll, G., Gabelli, A., Binnington, P.G., and Qu, J. (1992). "Dynamic mapping of rotary lip seal lubricant films by fluorescent image processing". To be presented at the 13th International Conference on Fluid Sealing, 7-9 April, Brugge, Belgium.

Polvara, O. (1978). "Determinazione del modulo a compressione volumica." *Rapporto Tecnico n.* 4, Industrie Pirelli, Divisione Pneumatici (in Italian).

Popov, G. Ia. (1962). "The contact problem of the theory of elasticity fro the case of a circular area of contact." *J. Math. Mech. (PMM)*, 26 (1), *pp.* 152-164 .

Posfalvi, Ö. (1982). "Zur Bestimmung der Poissonshen Zahl von gummielastischen Stoffen." *Kautshuk + Gummi Kunststoffe* 35 (11), pp. 940-941 .

Poulos, H.G. (1968). "The behaviour of a rigid circular plate resting on a finite elastic layer." *Civil Engng Transactions*, pp. 213-219 .

Prati, E., and Strozzi, A. (1984). "A study of the elastohydrodynamic problem in rectangular elastomeric seals." *ASME J. Tribology*, 106, pp. 505-512 .

Pupyrev, V. A., and Ufliand, Ia. S. (1960). "Certain contact problems for an elastic layer." *J. Math. Mech. (PMM)*, 24 (4), pp. 683-690 .

Ramachandra Rao, B.S., Kandya, A.K., and Gopalacharyulu, S. (1976). "Axial eigenfunctions for the axisymmetric problem of an elastic circular cylinder." *Int. J. Engng Sci.* 14, pp. 99-112 .

REDUCE (1987). *The Rand Corporation*, Santa Monica, California.

Rice, J.R. (1983). *Numerical Methods*, McGraw-Hill, New York.

Rigbi, Z. (1969). "A strain energy function for swollen crosslinked elastomers." *Int. J. Engng Sci.* 7, pp. 1163-1165 .

Rightmire, G.K. (1970). "An experimental method for determining Poisson's ratio of elastomers." *J. Lubrication Technology*, 92, pp. 381-388 .

Rohde, S. M. and McAllister, G.T. (1975). "A variational formulation for a class of free boundary problems arising in hydrodynamic lubrication." *Int. J. Engng Sci.*, 13, pp. 841-850 .

Rohde, S.M. and Oh, K.P. (1975). "A unified treatment of thick and thin film elastohydrodynamic problems by using higher order element methods." *Proc. R. Soc. London*, Ser. A , 343, pp. 315-331 .

Röntgen, W.C. (1876). "Uber das Verhältnis der Quercontraction zur Längendilatation bei Kautshuk." *Ann. Physik*, 159, pp. 601-616 .

Ruskell, L.E. (1980): "A rapidly converging theoretical solution of the elastohydrodynamic lubrication problem for rectangular rubber seals." *J. Mech. Engng Sci.*, 22 (1), pp. 9-16 .

Rvachev, V.L. (1959). "The pressure on an elastic half-space of a stamp with a wedge-shaped planform." *J. Math. Mech. (PMM)*, 23 (1), pp. 169-171 .

Scheid, F. (1968). *Theory and Problems of Numerical Analysis.* Schaum's Outline Series, McGraw-Hill Co., New York.

Segedin, C.M. (1957). "The relation between load and penetration for a spherical punch." *Mathematika*, 4, pp. 156-161 .

Sekiguchi, H., Kakiuchi, M., Morimoto, T., Fujimoto, K. and Yoshimura, N. (1969). "Poisson's ratio for stretched vulcanized natural rubber." *Rubber Chem. and Techn.*, 42, pp. 547-556 .

Sharma, M.G. (1966). "Failure of polymeric materials under biaxial stress fields." *Polymer Engng and Science*, January, pp. 30-35 .

Shelest, L.A. (1975). "Distribution of stresses and displacements in a foundation bed of finite thickness beneath a circular rigid foundation." *Soil Mech. Found. Eng.*, 17, pp. 404-407 .

Shibahara, M, and Oda, J. (1968). "Problems on the finite hollow cylinder under the axially symmetrical deformations." *Bulletin of JSME*, 11 (48), pp. 1000-1014 .

Shield, T.W. (1991). "Contact of a smooth flat indenter on a layered elastic half-space: beam on an elastic foundation model." *ASME J. Appl. Mech.*, 58, *pp.* 855-857 .

Shield, T.W. and Bogy, D.B. (1989a). "Multiple region contact solutions for a flat indenter on a layered elastic half space: plane-strain case." *ASME J. Appl. Mech.*, 56, *pp.* 251-262 .

Shield, T.W. and Bogy, D.B. (1989b). "Some axisymmetric problems for layered elastic media: part I - multiple region contact solutions for simply-connected indenters." *ASME J. Appl. Mech.*, 56, *pp.* 798-806 .

Shield, T.W. and Bogy, D.B. (1989c). "Some axisymmetric problems for layered elastic media: part II - solutions for annular indenters and cracks." *ASME J. Appl. Mech.*, 56, *pp.* 807-813 .

Shinbrot, M. (1959). "A generalization of Latta's method for the solution of integral equations." *Quarterly Applied Mathematics*, 16(4), pp. 415-421 .

Schulz, J.C. (1985). "Finite element hourglassing control." *Int. J. Num. Methods Engng*, 21, pp. 1039-1048 .

Sierakowski, R.L., and Sun, C.T. (1968). "An exact solution to the elastic deformation of a finite length hollow cylinder." *J. Franklin Institute*, 286 (2), pp. 99-113 .

Singh, K.P., and Paul, B. (1974). "Numerical solution of non-hertzian elastic contact problems." *ASME J. Appl. Mech.*, 41 (2), pp.484-490.

Smith, S.F. (1964). "On a flat punch indenting an elastic layer in plane strain." *Quart. J. Math. Oxford, second series*, 15, pp. 223-237 .

Smith, D.R. (1985),. *Singular Perturbation Theory*. Cambridge University Press, Cambridge.

Smith, T.J., and Medley, J.B. (1987). "Development of transient elastohydrodynamic models for synovial joint lubrication.", *Fluid Film Lubrication - Osborne Reynolds Centenary, Proc. 13th Leeds-Lyon Symp. on Trib., D. Dowson, C.M. Taylor, M. Godet, D. Berthe, eds.*, Elsevier, Amsterdam, pp. 369-374 .

Sneddon, I.N. (1946). "The elastic stresses produced in a thick plate by the application of pressure to its free surfaces." *Proc. Cambridge Phil. Soc.*, 42, pp. 260-271. .

Sneddon, I.N. (1965). "The relation between load and penetration in the axisymmetric Boussinesq problem for a punch of arbitrary profile." *Int. J. Engng. Science*, 3, pp. 47-57 .

Solecki, R. (1986). "In-plane indentation and separation of a flat, or rounded rigid stamp from an elastic, finite layer." *ASME J. Appl. Mech.*, 53, pp. 785-790 .

Solecki, R., and Ohgushi, Y. (1984). "Contact stresses between layered elastic cylinders." *ASME J. Tribology*, 106, pp.396-404 .

Somigliana, C. (1887). "Sopra l'equilibrio di un corpo elastico isotropo limitato da una o due superficie sferiche." *Annali della Scuola Normale Superiore di Pisa, Scienze Fisiche e Matematiche*, Serie 1, pp. 100-172 (in Italian).

Soong. T.C. and Li, C. (1980). "On the unbounded contact between plates and layered cylinders." *ASME J. Appl. Mech.*, 47, pp. 841-846.

Soong, T.C. and Li, C. (1981). "The steady rolling contact of two elastic layer bonded cylinders with a sheet in the nip." *Int. J. Mech. Sci.*, 23, pp. 263-273.

Spengos, A.C. (1965). "Experimental investigation of rolling contact." *ASME J. Appl. Mech.*, 32, pp. 859-864.

Spiegel, M.R. (1968). *Mathematical Handbook*. McGraw-Hill Book Co., New York.

Spillers, W.R. (1964). "A shrink fit problem." *J. Mathematics and Physics*, 43, pp. 65-71 .

Stakenborg, M.J.L. , van Leeuwen, H.J. , and ten Hagen, E.A. (1990). "Visco-elastohydrodynamic (VEHD) lubrication in radial lip seals : part 1 - steady-state dynamic viscoelastic seal behaviour." *ASME J. Tribology*, 112, pp. 578-583 .

Steven, G.P. (1973). "The eigenvalue problem for hollow circular cylinders. " *Int. J. Engng Sci.* 11, pp. 795-810 .

Stevens, C.A. (1988). *Fracture and Ageing of Elastomeric O-Ring Seals.* PhD Thesis, Unversity of Bath.

Strozzi, A. (1973). *Introduzione allo Studio del Comportamento Elastico, nel Campo delle Grandi Deformazioni, di Corpi Soggetti a Grandi Spostamenti.* Thesis for the Italian title of Engineer, Bologna University, Italy (in Italian).

Strozzi, A. (1983). "Elastohydrodynamic lubrication in elastomeric reciprocating seals. Numerical Methods." *Plast. Rubber Process. Appl.*, 3, pp. 4-8 .

Strozzi, A. (1984a). "On the cubic compressiblity of rubber-like materials." *International Rubber Conference*, Vol. 1, Moscow .

Strozzi, A. (1984b). "Theoretical analysis of a segmented locking ring for shell-bottom connection in pressure vessels." *J. Strain Analysis*, 19 (3), pp. 153-160 .

Strozzi, A. (1984c). "Formulation of the mixed lubrication problem for elastomeric reciprocating seals in terms of complementarity." *VII National Congress AIMETA*, Trieste 2nd-5th October, pp. III 157-167 .

Strozzi, A. (1984d). "On the elastohydrodynamic lubrication in soft seals." *Wear*, 97, pp. 107-109 .

Strozzi, A. (1985). "Formulation of three lubrication problems in terms of complementarity." *Wear*, 104, pp. 103-119 .

Strozzi, A. (1986a). "Static stresses in an unpressurized, rounded, rectangular, elastomeric seal." *ASLE Transactions*, 29, pp. 558-563 .

Strozzi, A. (1986b). "Experimental stress-strain field in elastomeric O-Ring seals." *Proceedings of the VIIIth Int. Conf. on Experimental Stress Analysis*, Amsterdam, pp. 613-622 .

Strozzi, A. (1986c). "The elastohydrodynamic problem expressed in terms of extended variational formulation." *ASME J. Tribology*, 108, pp. 557-564 .

Strozzi, A. (1986d). "An assessment of the inverse hydrodynamic theory." *Zagadnienia Eksploatacji Maszyn*, 1 (65), pp. 123-134 .

Strozzi, A. (1987a). "An assessment of the numerical solution of the elastohydrodynamic problem for soft contacts." *Wear*, 115, pp. 53-61 .

Strozzi, A. (1987b). "Numerical solution of the elastohydrodynamic problem in soft reciprocating seals." *Engng Computations*, 4, pp. 199-206 .

Strozzi, A. (1989). "Mechanical analysis of an annular plate subject to a transverse concentrated load.", *J. Strain Analysis*, 24 (3), pp. 139-149 .

Sve, C., and Keer, L.M. (1969). "Indentation of an elastic layer by moving punches." *Int. J. Solids Structures*, 5, pp.795-816.

Szeri, A.Z. (1980). *Tribology : Friction, Lubrication and Wear*. McGraw-Hill Book Co. , N.Y. .

Tang, R., and Erdogan, F. (1984). "Stress intensity factors in a reinforced thick-walled cylinder." *Int. J. Engng Sci.*, 22 (7), *pp.* 867-879 .

Tarasov, L.A., and Tyutekin, V.V. (1960). "Method of measuring the shear and compression moduli of a rubber at small deformations." *Soviet Rubber Technology*, 9, pp. 36-38 .

Tatara, Y. (1991). "On compression of rubber elastic sphere over a large range of displacements - part 1 : theoretical study." *J. Engng Materials and Technology*, 113, pp. 285-291 .

Tatara, Y., Shima, S. and Lucero, J.C. (1991). "On compression of rubber elastic sphere over a large range of displacements - part 2 : comparison of theory and experiments." *J. Engng Materials and Technology*, 113, pp. 292-295 .

Theocaris, P.S., and Philippidis, T.P. (1992). "True bounds on Poisson's ratios for transversely isotropic solids." *J. Strain Analysis*, 27 (1), pp. 43-44 .

Theyse, F.H. (1967). "The inverse hydrodynamic theory and its application in the design of controlled leakage seals between moving parts." *3rd Int. Conf. on Fluid Sealing*, BHRA, Cranfield, pp. F2/17-32 .

Thomas, T.R. (1982). *Rough Surfaces*. Longman, London.

Thornton Coe, R. (1938). "The bending of a beam on elastic foundations." *Phil. Mag.*, 25, pp. 49-65 .

Tiffen, R. and Semple, H.M. (1965). "An investigation of the elastic strip and the annulus." *Mathematika*, 12, pp. 193-200 .

Timoshenko, S.P., and Goodier, J.N. (1970). *Theory of Elasticity*. McGraw-Hill Book Co, New York.

Tonti, E. (1984). "Variational formulation for every nonlinear problem.", *Int. J. Engng Sci.*, 22, pp. 1343-1371 .

Treloar, L.R.G. (1948). "Stress and birefringence in rubber subjected to general homogeneous strain." *Proc. Phys. Soc.*, 60 (2), pp. 134-144 .

Treloar, L.R.G. (1975). *The Physics of Rubber Elasticity*. Clarendon Press, Oxford.

Tu, Y.H. (1967). "A numerical solution for an axially symmetric contact problem." *ASME J. of Applied Mechanics*, 34, pp. 283-286 .

Tu, Y.H., and Gazis, D.C. (1964). "The contact problem of a plate pressed between two spheres." *ASME J. of Applied Mechanics*, 31, pp. 659-666 .

Tuncel, O. (1964). "Circular ring plates under partial arc loading." *ASME J. Appl. Mech.*, 31, pp. 340-341 .

Tuomala, M., Owen, D., and Zienkiewicz, O., (1981). "A penalty function finite element method in nonlinear elasticity." *Numerical Methods for Coupled Problems*, Swansea, pp. 466-477 .

Unsworth, A. (1978). "The effects of lubrication in hip joint prostheses." *Phys. Med. Biol.*, 23 (2), pp. 253-268 .

Unsworth, A. (1981). "Lubrication of joints: B. artificial joints." In : *An Introduction to the Bio-mechanics of Joints and Joint Replacement*. Dowson, E. & Wright, V. editors, MEP, London.

Unsworth, A., Pearcy, M.J., White, E.F.T., and White, G. (1987). "Soft layer lubrication of artificial hip joints." *Proc. Inst. Mech. Engr., Int. Conf. : Tribology - Friction, Lubrication and Wear, Fifty Years on*, London, pp. 715-724.

Valov, G.M. (1962). "On the axially-symmetric deformations of a solid circular cylinder of finite length." *PMM*, 26 (4), pp. 650-667 .

van Leeuwen, H.J. , and Stakenborg, M.J.L. (1990). "Visco-elastohydrodynamic (VEHD) lubrication in radial lip seals : part 2 - fluid film formation." *ASME J. Tribology*, 112, pp. 584-592 .

Varga, O.H. (1966). *Stress-Strain Behaviour of Elastic Materials.* Interscience Publishers, Wiley & Sons, N.Y.

Varnam, C.J., and Hooke, C.J. (1977). "Non-Hertzian elastohydrodynamic contacts: an experimental investigation." *J. Mechanical Engineering Science*, 19 (7), pp. 189-192 .

Vecile, C. (1984). "Extended variational formulation of Navier-Stokes complete equation." *Engineering Analysis*, 1, pp. 211-214 .

Vorovich, I. I., and Ustinov, Iu. A. (1959). "Pressure of a die on an elastic layer of finite thickness." *J. Math. Mech. (PMM)*, 23 (3), pp. 445-455 .

Warfield, R.W. (1980). "Static high-pressure measurements on polymers." *Methods of Exp. Phys.*, 160, *pp.* 91-116 .

Warfield, R.W., Cuevas, J.E., and Barnet, F.R. (1968). "Simple specimen determination of Young's and Bulk Moduli." *J. Appl. Polymer Sci.*, 12, pp. 1147-1149 .

Warren, W.E. and Kraynik, A.M. (1991). "The nonlinear elastic behavior of open-cell foams." *ASME J. Appl. Mech.*, 58, *pp.* 376-381 .

Wendt, G. (1971). "Investigation of rubber O-Rings and X-Rings. 1: stress distributions, service life and groove design." T1115, BHRA, Cranfield .

Wheelon, A.D. (1968). *Tables of Summable Series and Integrals involving Bessel Functions.* Holder Day, London.

Wierzcholski, K. (1986). "A numerical solution of EHD-problem for non-Newtonian pseudoplastic lubricant between two cooperating cylinders." *Second Int. Symp. INSYCONT, Krakow, Poland,* 24-26 *September* 1986 , pp.145-154 .

Williams, J.G. (1973). *Stress Analysis of Polymers.* Longman, N.Y.

Wylie, C.R. (1975). *Advanced Engineering Mathematics*. McGraw-Hill Co., New York.

Wood, L.A., and Martin, G.M. (1964). "Compressibility of natural rubber at pressures below 500 Kg/cm^2." *Journal of Research of the National Bureau of Standards - A. Physics and Chemistry*, 68 (3), pp. 259-268. .

Wu, S.R. (1986). "A penalty formulation and numerical approximation of the Reynolds-Hertz problem of elastohydrodynamic lubrication." *Int. J. Engng Sci.*, 24 (6), pp. 1001-1013 .

Wu, S.R. and Oden, J.T. (1987). "A note on some mathematical studies on elastohydrodynamic lubrication." *Int. J. Engng Sci.* 25 (6), pp. 681-690 .

Wu, T.S. and Chiu, Y.P. (1967). "On the contact problem of layered elastic bodies." *Quarterly of Applied Mathematics* 25 (3), pp. 233-242 .

Yang, Y., and Huges, W.F. (1984). "An elastohydrodynamic analysis of preloaded sliding seals." *ASLE Transactions*, 27 (3), pp. 197-202 .

Yao, J.Q. (1990). *A study of the deformation and the lubrication of synovial joints*. Ph.D. Thesis, Leeds, England.

Yogananda, C.V. (1967). "A symmetric solution for a cylindrical shell enclosed in an elastomeric casing." *Int. J. Engng Sci.* 5, pp. 681-688 .

Youngdahl, C. K. (1969). "On the completeness of a set of stress functions appropriate to the solution of elasticity problems in general cylindrical coordinates." *Int. J. Engng Sci.* 7, pp. 61-79 .

Zagorskii, M.V., Balashow, A.P., Roginskaya, G.F., and Surdutovich, L.I. (1976). "Study of compressibility of rubbers in the regions of moulding pressures." *Int. Polymer Sci. and Techn.*, 3 (8), pp. T/104-T/106 .

Zapas, L.J. (1981). "The strain-energy function for rubber-like materials." *Proc. IUTAM Symp. on Finite Elasticity*, Leigh Univ., August 10-15 1980, pp. 445-455 .

Zhang, Y. (1987). "Linear deformation of a journal bearing and its relationship to hydrodynamic pressure." *Wear*, 115, pp. 41-52.

Zhang, Y. (1989). "Dynamic properties of flexible journal bearings of infinite width considering oil supply position and pressure." *Wear*, 130, pp. 53-68 .